UNCLASSIFIED

AD 276 747

Reproduced
by the

ARMED SERVICES TECHNICAL INFORMATION AGENCY
ARLINGTON HALL STATION
ARLINGTON 12, VIRGINIA

UNCLASSIFIED

NOTICE: When government or other drawings, specifications or other data are used for any purpose other than in connection with a definitely related government procurement operation, the U. S. Government thereby incurs no responsibility, nor any obligation whatsoever; and the fact that the Government may have formulated, furnished, or in any way supplied the said drawings, specifications, or other data is not to be regarded by implication or otherwise as in any manner licensing the holder or any other person or corporation, or conveying any rights or permission to manufacture, use or sell any patented invention that may in any way be related thereto.

MEASUREMENT OF TEMPERATURE, SALINITY, AND VELOCITY OF WATER THROUGH ELECTROLYTIC CONDUCTIVITY MEASUREMENTS

by L.L. Higgins

Technical Report No. 8609-01000-RU-000

15 March 1962

276 747

Prepared Under Office of Naval Research
Contract Nonr 3474 (00), NR 062 276

SPACE TECHNOLOGY LABORATORIES, INC.
A SUBSIDIARY OF THOMPSON RAMO WOOLDRIDGE INC.
8433 FALLBROOK AVENUE · CANOGA PARK, CALIFORNIA

TABLE OF CONTENTS

			Page
1.	INTRODUCTION		
2.	CONDUCTIVITY DETECTOR		
	2.1	Concept	2.1
	2.2	Related Techniques	2.3
	2.3	Description and Theory	2.4
3.	TEMPERATURE DETECTOR		
	3.1	Description	3.1
	3.2	Separation of Variables	3.7
	3.3	Resistance-Wire Thermometer	3.11
	3.4	Comparison of Methods	3.13
4.	SALINITY DETECTOR		
	4.1	Description	4.1
	4.2	Separation of Variables	4.4
	4.3	TS-Meter	4.5
5.	VELOCITY DETECTOR		
	5.1	Concept	5.1
	5.2	Electrochemical Methods	5.4
	5.3	Description and Theory	5.7
	5.4	Hot-Wire Anemometer	5.14
	5.5	Comparison of Methods	5.25
6.	SIGNAL PHENOMENA		
	6.1	Electrode Effects	6.1
	6.2	Differential Relations	6.7
	6.3	Correlated Signals	6.11
7.	CONDUCTING MEDIUM		
	7.1	Medium Variables	7.1
	7.2	Physical Data	7.4
	7.3	Ocean Environment	7.21
8.	DETECTION THEORY		
	8.1	Intrinsic (S/N) Ratio	8.1
	8.2	Background Noise	8.9
	8.3	Minimum Detectable Signal	8.11
	8.4	(S/N) Ratio	8.22
	8.5	Mode of Operation	8.30

9. ELECTRODES

9.1	General Considerations	9.1
9.2	Eye-Type Electrode	9.5
9.3	Other Electrodes	9.15
9.4	Polarization Impedance	9.20
9.5	Induction Probe	9.25
9.6	CP-Electrode	9.28
9.7	Electrode Measurements	9.35
9.8	Design and Construction	9.63

10. RESISTANCE CALCULATION

10.1	Potential Theory	10.1
10.2	Axisymmetric Potential	10.8
10.3	Homogeneous Volume	10.12
10.4	Inhomogeneous Volume	10.17
10.5	Homogeneous Surface	10.23

11. DETECTOR HEAD

11.1	General Considerations	11.1
11.2	Rankine Probe	11.2
11.3	Cylinder	11.14
11.4	Wedge	11.19
11.5	Electrode Position	11.27

12. HEATING EFFECT

12.1	Elementary Heating	12.1
12.2	General Electrode	12.3
12.3	Internal Heat Generation	12.13
12.4	Boundary Layer Heating	12.17
12.5	Heat Transfer Equation	12.25
12.6	Non-Linear Heating	12.36

13. CONDUCTIVITY RESPONSE

13.1	Temperature Fluctuations	13.4
13.2	Boundary Layer Response	13.14
13.3	Drift	13.25
13.4	Response to Bubbles	13.35
13.5	Differential Probe	13.39

14. VELOCITY RESPONSE

14.1	Isotropic Turbulence	14.1
14.2	One-Dimensional Case	14.9
14.3	Proportional Fluctuating Flow	14.10
14.4	Boundary Layer Response	14.12
14.5	Mode of Operation	14.27

15. ELECTRONICS ANALYSIS

15.1 Wheatstone Bridge	15.1
15.2 Optimum Bridge Network	15.9
15.3 Balance Problem	15.23
15.4 Low-Noise Techniques	15.30
15.5 Advanced Systems	15.35

16. DETECTION EQUIPMENT

16.1 General Description	16.1
16.2 Electronics Design	16.5

17. LABORATORY EXPERIMENTS

17.1 Electrode Experiments	17.1
17.2 Water Tunnel Experiments	17.5
17.3 Detection Equipment Experiments	17.36

ADDENDUM

REFERENCES

1. INTRODUCTION

A measurement of the electrical resistance between electrodes immersed in flowing water containing dissolved salts depends on the temperature of the water, the concentration of the electrolyte solution, and under certain conditions, on the velocity of the water flowing between the electrodes. The techniques considered in this Report take advantage of the dependence of the electrical conductivity of the water on these variables to make simultaneous, independent and continuous measurements of the temperature, concentration (salinity) and velocity at a point in the conducting fluid medium. In order to separate the contributions of these three quantities, the electrolytic conductivity measurements must be supplemented by a measurement of the dielectric constant of the medium and the use of artificial heating of the water flowing between the electrodes. Water media of most interest for the application of these techniques are sea water and tap water.

A brief description of the principles of measurement with the instrumentation covered in this Report is the following. The sensitive element of the detector consists of a probe comprised of small electrodes exposed to flowing water of finite electrolytic conductivity. The electrode resistance depends on the conductivity which, in turn, is a function of the temperature and salinity of the water. Thus, variations in these quantities give rise to electrode resistance variations which are measurable with electronic equipment. This method of measurement is analogous to the resistance-wire technique of temperature measurement, but uses the water itself as the sensitive element instead of a thin wire. The temperature coefficient of electrode resistance is about five times that of typical metalic resistance wires and is comparable with that of thermistor temperature sensors. The probe resistance depends on water velocity if the water is heated appreciably by the electrical current. The resultant temperature rise of the water as it passes between the electrodes depends on its duration in the vicinity of the electrodes and, therefore, on the fluid velocity. This mode of operation is analogous to that of the hot-wire anemometer. The salinity is determined independent of the temperature by measuring simultaneously the dielectric constant of the medium which depends differently on the salinity and temperature than does the electrical conductivity. The sensitivity of the detector is higher than that of conventional methods because the temperature sensitivity coefficient is higher, and because higher applied power may be used before the occurrence of adverse effects. The response time of the probe is limited only by its physical size since the thermal inertial effects due to a cooling process are not operative in the new device. Also, the probe is relatively easy to construct, even in very small sizes, in a simple and rugged configuration. The direct measurement of the properties of the medium by purely electrical means, through an intrinsic measurement of the conductivity and dielectric constant, enjoys the convenience and extreme sensitivity of electronic measurements not possible with mechanical or other means.

Best Available Copy

very high power where the velocity signal dominates. Signals due to bubbles are characterized by their pulse shape. Temperature and salinity signals are separated effectively by operating at ultra-high frequency where the capacity of the electrode is important. Two frequencies exist where either specific temperature or specific salinity measurements may be made. This is a consequence of the differences in temperature and salinity dependence of the conductivity and dielectric constant of the medium.

(d) The factors which determine the ultimate differential sensitivity of the detector to variations in temperature, salinity and velocity have been determined. These limiting sensitivities depend on the operating conditions; for example, in the ocean it is possible to measure temperature variations of the order of 10^{-6} °C, salinity variations of the order of 10^{-6} ‰ and velocity variations of the order of 10^{-5} knots. Comparison with conventional measuring techniques indicates a superiority, in this respect, of one or two order of magnitude.

(e) The frequency response of the probe is determined primarily by its physical size. Theoretical studies of the power sensitivity spectrum of the electrode to temperature, salinity, and velocity variations as determined by its geometrical configuration have been made. The limitations due to boundary layer flow have also been included.

(f) The electrical properties of the electrode sensing elements have been investigated theoretically and experimentally. The potential field of a given electrode and the associated function which determines the sensitivity at a point in the electrode volume has been analyzed and related to the overall resistance of the electrode. Measurements with contact electrodes have been made of the electrode impedance as a function of temperature, salinity, size and shape, frequency, surface condition, as well as other factors. Numerous practical electrode designs have been fabricated. Theoretical studies have been made of the induction and capacitive type probes which show promise of being superior to contact electrodes with respect to stability. Different methods of mounting the electrodes to measure the fluid flow without adverse effects due to the velocity boundary layer have been studied.

(g) Electronic equipment has been designed and constructed to measure temperature, salinity, and velocity variations with high sensitivity. The optimization of the electronics for this purpose involves analysis of the bridge network, techniques for balancing the bridge to a high degree, choice of operating frequency, phase detection, and low noise amplification systems. The existing equipment is capable of detecting velocity variations and temperature (or salinity) independently.

(h) Laboratory experiments have been performed in a small water tunnel to investigate the response of small probes to a known laminar

or turbulent velocity field. Other experiments with the high sensitivity detection equipment have been performed to measure very small temperature variations in a well stirred tank of water.

The Report is divided into seventeen main sections, with subsections, figures, tables and pages numbered sequentially in each of the main sections. For example, the Fifth Figure in Section Twelve is numbered 12.5.

2. CONDUCTIVITY DETECTOR

The measurement of the electrolytic conductivity of a flowing conducting medium, such as an aqueous salt solution, is discussed in this Section. Electronic instrumentation which performs such a measurement will be termed a "C-meter" for brevity sake.

2.1 Concept

The electrolytic conductivity of a solution is ordinarily measured by placing a sample in a vessel which has two electrodes in contact with the solution. If the properties of this "conductivity cell" are known, a measurement of the electrical resistance between the electrodes is a measure of the conductivity of the solution. The conductivity of a flowing solution is obtained continuously in the same way simply by making provisions for the inlet and outlet of the solution through the conductivity cell. The resistance measurement is frequently made with a bridge network operating at some convenient frequency. A simplified diagram of such an arrangement is shown in Figure 2.1 ; an oscillator supplies a signal to a bridge in which the resistance of the cell constitutes one element of the four-arm bridge. The output signal from the bridge is indicated on an ac voltmeter and may be used as a measure of the variation of electrode resistance from some reference value. The electrode resistance may also be measured by the settings on the adjustable arms of the bridge which are required to produce a null output.

The continuous measurement of the conductivity of a solution is of particular interest in the case of an extended conducting medium such as sea water. The variation of the conductivity of the medium from point to point is obtained by moving the electrodes through the water and observing the resultant variations in the voltmeter readings of the bridge output. Accurate absolute measurements of the conductivity requires a single electrode cell with stable characteristics, stable reference resistances in the bridge network, and/or a well calibrated voltmeter. Differential measurements of the conductivity of reasonable accuracy but high sensitivity are best made by using <u>two</u> electrode cells in the bridge arrangement instead of one. The other electrode replaces one of the other fixed arms of the bridge, and the two electrode cells are physically separated from each other by a distance comparable to, or larger than, the size of the largest conductivity structure to be measured in the medium. The conductivity cells, themselves, should be comparable to, or smaller than, the smallest conductivity structure that is to be measured.

The electrolytic conductivity of a solution is a function of the temperature and salinity. The temperature coefficient of most electrolyte solutions is approximately 2 % per ^{o}C and the conductivity is roughly proportional to the concentration or salinity of the solution. As a consequence, a measurement of the conductivity structure of the medium depends

Best Available Copy

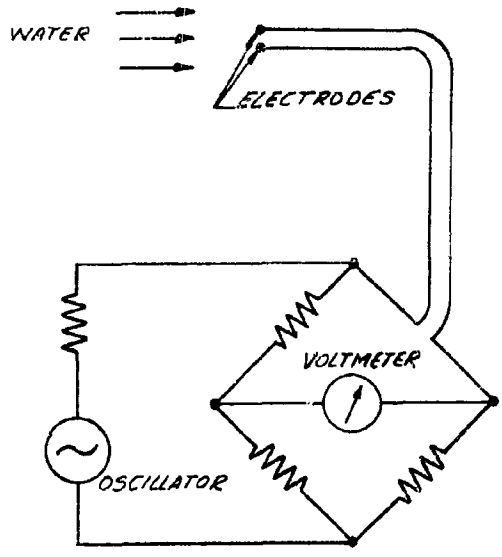

Figure 2.1 . Continuous Flow Conductivity Bridge

on an unspecified combination of these variables which are inhomogeneous over the (small) distances of interest. While, in some cases, it is of interest to separate the relative contributions of temperature and salinity to the conductivity variations, there are cases when a direct determination of the conductivity of the medium is useful. For example, if one is interested in the way in which a certain turbulent field mixes a scalar quan·.y in the medium, the measurement of the random conductivity field in the medium suffices to answer this question. This is valid provided the scale of the structure which is measured is not so small that thermal diffusion and/or ionic diffusion processes are operative.

The refinement of the direct conductivity measurement, in order to determine the values of the other properties of the medium, is the primary purpose of this Report. We shall see that the temperature, salinity, velocity and bubble content of the medium are measurable independently by techniques involving the electrolytic conductivity measurement. If δR is a small change in electrode resistance of average resistance R, it may

be shown that small changes in temperature, δT, salinity, δS, and velocity, δU, of the medium moving at speed U relative to the electrode are related by

$$\left(\frac{\delta R}{R}\right) = -\beta_T \delta T - \beta_S \delta S + \beta_T \overline{\Delta T} \left(\frac{\delta U}{U}\right),$$

where β_T is the temperature coefficient of conductivity, β_S is the salinity coefficient of conductivity, and $\overline{\Delta T}$ the average temperature rise due to heating of the medium as it flows through the electrodes. The development and consequences of this equation are the object of a large part of the analysis of this Report.

2.2 Related Techniques

The measurement of electrolytic conductivity has been used for many years as a means of determining the concentration of aqueous solutions of known temperature, and more recently as a means of measuring the temperature of a solution of known concentration. Examples of these are now given.

A stable electrolytic sensing element for measuring temperature for direct current operation is described by Craig (1). It consists of a solution of cuprous chloride, hydrochloric acid, and ethyl alcohol in a capillary tube with 1 mm bore. The electrodes are made of copper. The temperature coefficient of resistance is of the order of -2 % per ^{o}C. Temperature measurements obtained with this element are accurate to within 1^{o}C. This type of electrolytic resistance thermometer can be used with other electrolytes, most of which have a resistance coefficient of the order of -2 % per ^{o}C, but which can be as high as -8.9 % per ^{o}C for a 42.7 % NaOH solution. Polarization effects, the development of gas, and instabilities are likely to cause troubles. The use of ac equipment is effective in reducing polarization effects. It is important to note in this electrolytic resistance thermometer that it measures temperature specifically since concentration (salinity) variations are eliminated by always measuring the same mass of well mixed solution. Such a measurement is, in general, not specific for a continuously flowing electrolyte solution past the electrodes.

A technique quite similar to the conductivity sensor of this Report is described by Prausnitz and Wilhelm (2). The authors describe an electrical conductivity fluctuation measuring instrument. A small conductivity cell consisting of two platinum wires about 1.0 mm apart and 1.2 mm in length is immersed in a turbulent conducting solution in which concentration microstructure is maintained by mixing dissimilar solutions at the same temperature. The variations in electrical resistance between the electrodes was used to measure the turbulent concen-

Best Available Copy

tration fluctuations in the flowing medium. The experiments were so designed that the concentration gradients were, relatively, much larger than the temperature gradients in the solution. Thus, the measurements were essentially specific to salinity. The instrument operates with a 10 kc carrier and solutions of .001 N - .050 N hydrochloric acid.

A very important example of a related instrument is the salinometer based on the technique of a temperature compensated conductivity measurement. A conductivity bridge instrument for this purpose was first successfully used by Wenner (3) and recently modified and improved by Schleicher and Bradshaw (4). Composite instruments based on this principle for simultaneously measuring salinity, and temperature as a function of depth have been developed (5). The compensation and regulation of temperature are a serious source of difficulty for high precision salinity measurements by this means due to the large temperature coefficient of conductivity of sea water. A powerful method to eliminate much of the temperature problem is temperature compensation, in which a compensating resistor or conductivity cell forming one arm of the wheatstone bridge is exposed to the same temperature as that of the sea water under measurement. The ultimate accuracy of salinometers based on a conductivity measurement rests on the tables of conductivity of sea water as a function of temperature and salinity. A general review of this type of salinometer is given by Paquette and Hersey (6,7,8).

2.3 Description and Theory

A more detailed description of instrumentation for measuring the conductivity of a flowing medium is given below.

Electrolytic Conductivity

The conduction of electric currents in electrolyte solutions is due to the motion of the disolved ions rather than electrons as in the case of metalic conductors, hence, the term "ionic conductivity" or "electrolytic conductivity." The conductivity of metalic and electrolytic conductors are greatly different; for example, the conductivity of copper and sea water are in the ratio 10^7 to 1. Ohm's Law applies to electrolytic conductors, e.g., aqueous solutions, but here the relation is less straight forward to apply in practice because the electrolysis accompanying the passage of a current may cause both the appearance of insulating films on the electrodes and an increased electrolytic resistance due to removal of ions from the solution (polarization). These effects are large for direct currents and progressively smaller at higher alternating currents.

The electrical conduction of an electrolyte depends on the nature and number of ions present. Generally speaking, the greater the concentration of ions the higher the electrical conductivity. The conductivity is also

strongly dependent on the temperature of the solution. It increases at higher temperature because of the increased mobility of the ions responsible for electrical conduction. For most electrolyte solutions the temperature coefficient of conductivity is about 2 % per ^{o}C. As an example of this temperature dependence, the conductivity of sea water as a function of temperature from 0 ^{o}C to 100 ^{o}C is shown in Figure 2.2 . A five fold increase in conductivity is experienced over this temperature range and this is typical for most electrolyte solutions. The variation of conductivity with concentration is illustrated in Figure 2.3 for the two common and important electrolyte solutions of sodium chloride (NaCl) and sodium hydroxide (NaOH)(9). The conductivity of NaCl increases with concentration up to the saturation point, but NaOH has the interesting property that a maximum in the conductivity occurs at a certain concentration (15 %) which is well below the saturation point for that solution. The conductivity of sea water is also shown in that Figure as a basis for comparison. Reference will be made frequently to sea water as an example of an aqueous electrolyte solution, which primarily consists of about a 3.3 % sodium chloride (NaCl) solution, since it represents one of the most important waters in which the instrumentation described in this Report finds application.

Electrode Resistance

The resistance, R, of a uniform conductor is directly proportional to its length, ℓ, and inversely proportional to its cross-sectional area, A. The constant of proportionality is the resistivity, ρ, or the conductivity, σ:

$$R = \frac{\rho \ell}{A} = \frac{\ell}{\sigma A} = \frac{1}{\sigma h}$$

where $h^{-1} = (\ell/A)$ is the "cell constant." The resistivity represents the resistance between opposite faces of a centimeter cube of the conductor and has the units ohm-cm. Correspondingly, the units of conductivity are $ohm^{-1}cm^{-1}$. The resistance between electrodes immersed in an electrolyte solution is, in general, a complicated function of the shape of the electrode configuration and container of the solution. Rather than construct conductivity cells in which the cell constant is known accurately from the geometry, it is much simpler to calibrate each conductivity cell by making measurements using an electrolyte of known conductivity to obtain the cell constant.

A typical electrode cell arrangement frequently found in use in electrochemical measurements is shown in Figure 2.4 (10). The electrodes consist of discs of platinum with platinum black surfaces sealed in a vessel in which the quantity of electrolyte is measured. A cell arrangement of interest to the present detection techniques is one which allows the continuous flow of the electrolyte solution through the field

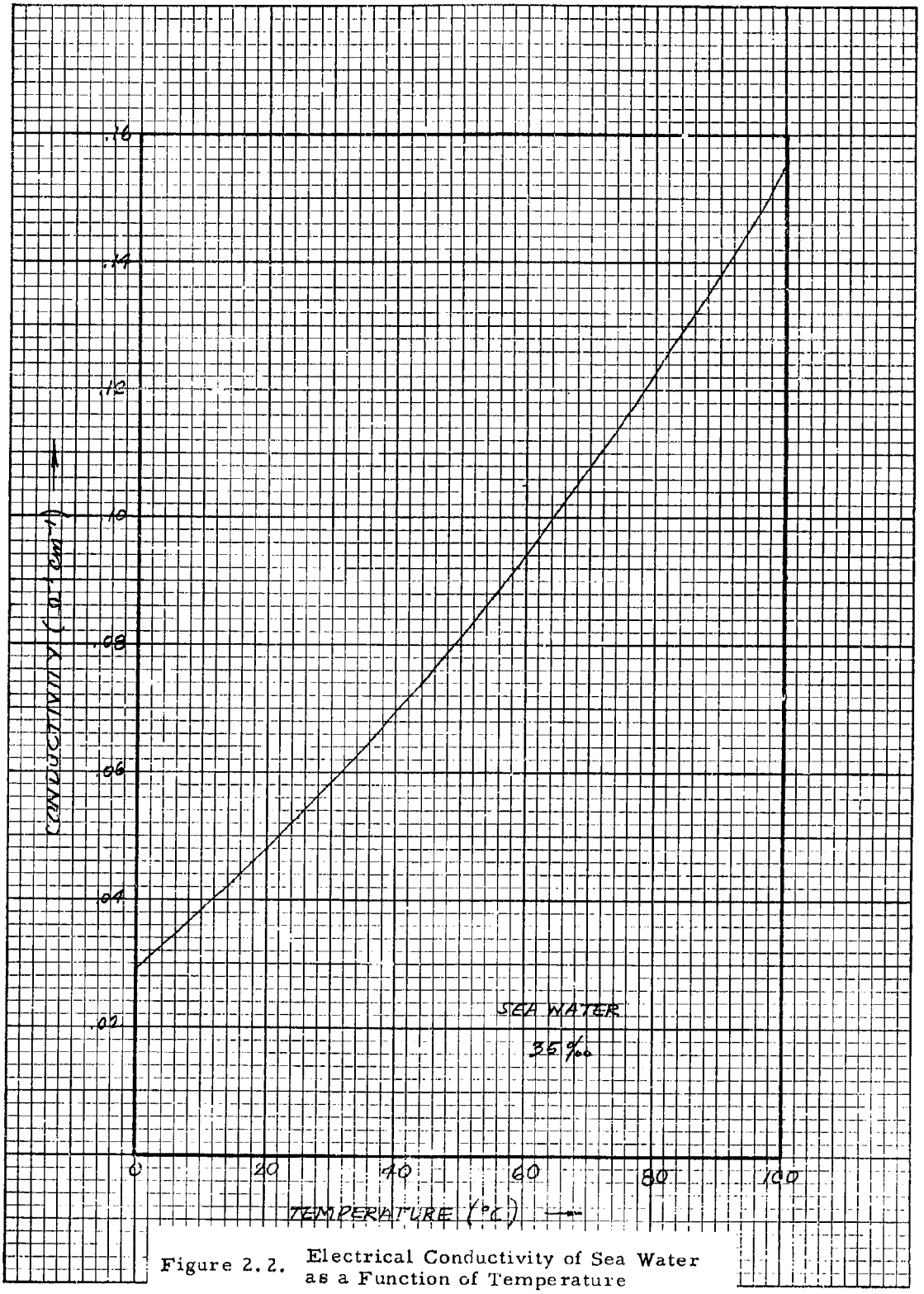

Figure 2.2. Electrical Conductivity of Sea Water as a Function of Temperature

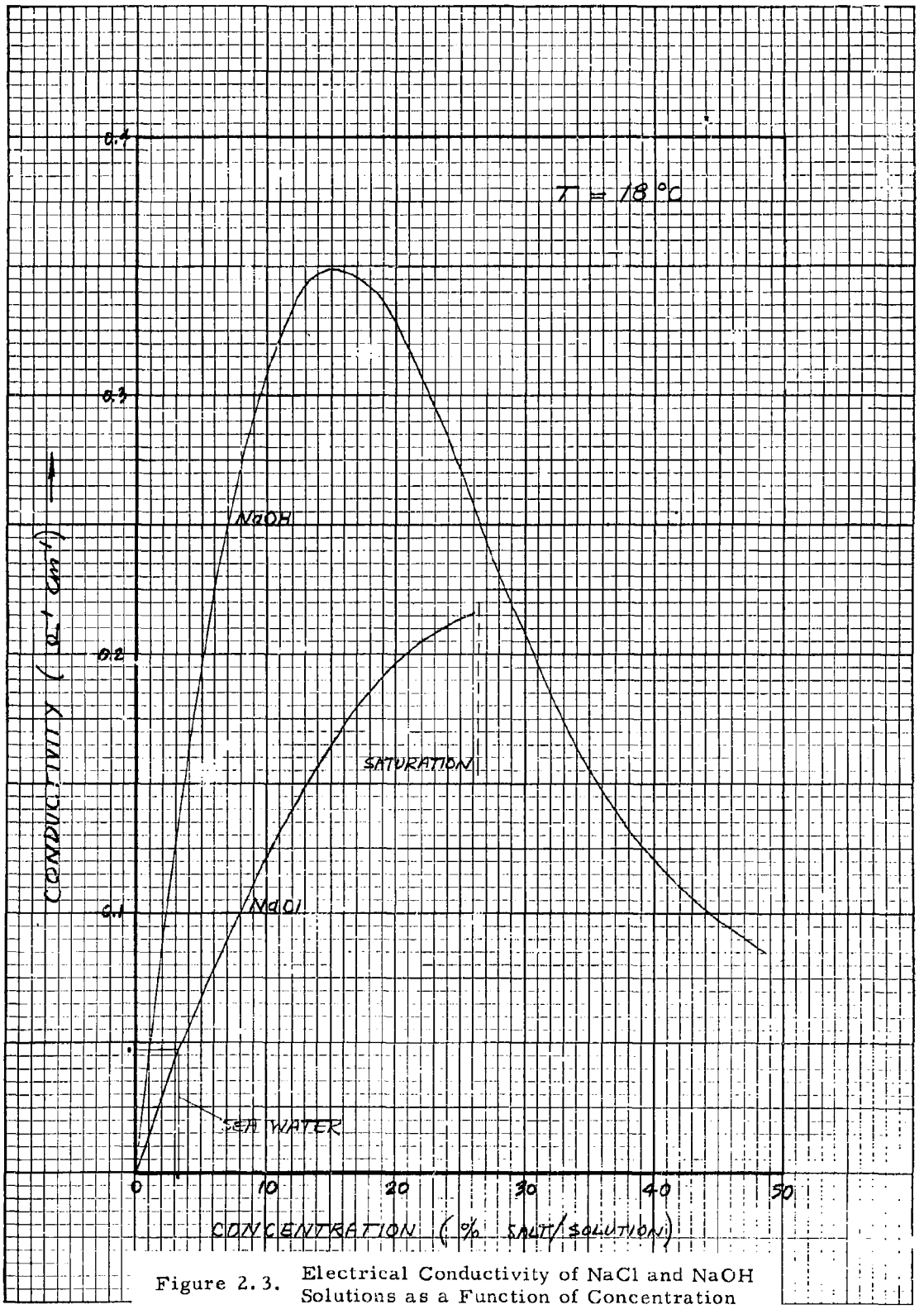

Figure 2.3. Electrical Conductivity of NaCl and NaOH Solutions as a Function of Concentration

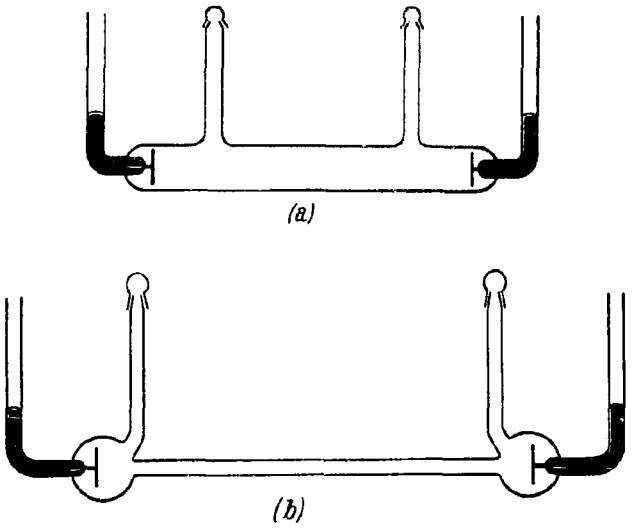

Figure 2.4 . Typical Conductivity Cell Design

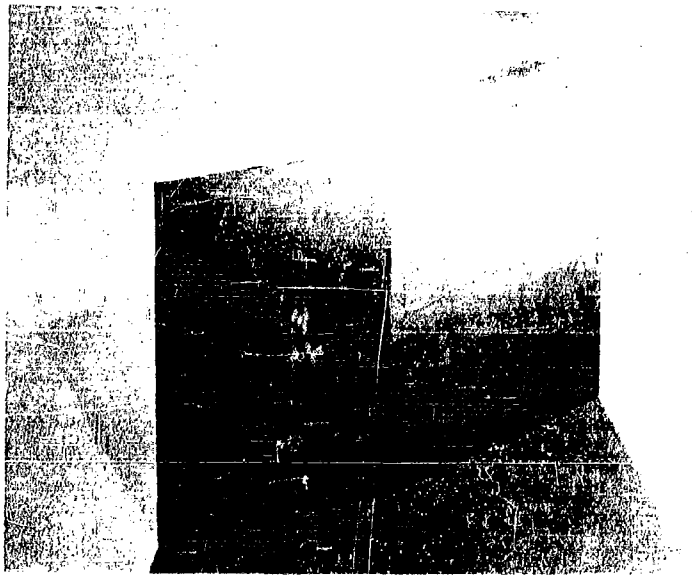

Figure 2.5 . Hydrodynamic Conductivity Cell Design

of the electrodes. Such an arrangement must also take in consideration the hydrodynamic porperties of the flow through the conductivity cell. An arrangement of this type is shown in Figure 2.5 where both the electrodes are in the same plane, thus, presenting a smooth flat surface to the fluid flow. The electrodes consist of the central metal disc and the outer metal region both separated by the flush electrical insulator. The electrical wires leading to the electrodes are not shown in the photo; one goes to the main stock and one to the central disc. The fluid flow is from the left to right over the wedge shaped structure. For spacial differential measurements two conductivity cells are located in close proximity with a given separation distance. This situation applies in Figure 2.5 where an identical electrode cell is also located on the other face of the wedge not visible in the photograph.

The dependence of the conductivity, σ, of a solution on small changes in temperature and concentration (or salinity) can be expressed as

$$\sigma = \sigma_0 \left[1 + \beta_T (T - T_0) + \beta_S (S - S_0) \right] ,$$

where σ_0 is the conductivity at temperature T_0 and salinity S_0, and β_T and β_S are the coefficients of temperature and salinity, respectively. The convention will be adopted in this Report of expressing salinity in units of grams of salt to 1000 gms of solution (‰). With the notation

$$\Delta\sigma = \sigma - \sigma_0$$

$$\Delta T = T - T_0$$

and

$$\Delta S = S - S_0 ,$$

the above expression becomes

$$\left(\frac{\Delta\sigma}{\sigma_0}\right) = \beta_T \Delta T + \beta_S \Delta S .$$

In general, the temperature and salinity coefficients of conductivity for aqueous electrolyte solutions are positive; e.g., for sea water at 20 °C

$$\beta_T = +2.1 \text{ \% per } ^\circ C$$

and

$$\beta_S = +2.5 \text{ \% per ‰} .$$

As mentioned above, the resistance between electrodes immersed in a

solution is

$$R = \frac{1}{\sigma h}$$

where h^{-1} is the cell constant and σ the conductivity of the solution. A small change in electrode resistance, ΔR, is related to a small change in conductivity simply by

$$\frac{\Delta R}{R_o} = -\left(\frac{\Delta \sigma}{\sigma_o}\right) ,$$

where R_o is the electrode resistance at temperature T_o and salinity S_o. In terms of the coefficients of conductivity

$$\frac{\Delta R}{R_o} = -\beta_T \Delta T - \beta_S \Delta S .$$

Since sea water is one of the most important electrolyte solutions of interest in this Report, it is of interest to look more closely at its electrical properties. In Figure 2.6 the resistivity of sea water is plotted as a function of temperature and salinity over the range of these variables found in most of the world's oceans (11). The resistance of an electrode configuration in sea water with a cell constant of 1 cm^{-1} is numerically equal to the resistivity given in Figure 2.6 . At a temperature of 20 °C and a salinity of 35 ‰ the resistivity is about 21 ohm-cm which corresponds to a conductivity of about .048 $ohm^{-1}cm^{-1}$. The corresponding electrical conductivity varies non-linearly with both temperature and salinity, increasing with increasing temperature and increasing salinity. The conductivity ranges from approximately zero at river outlets to about .060 $ohm^{-1}cm^{-1}$ for sea water of high salinity and temperature. The fact that the resistivity (or conductivity) of sea water is a sensitive measure of its thermochemical state in the oceans is a consequence of the two fold change in this variable over the range of temperature and salinity found in the oceans, whereas the temperature and salinity variables themselves experience a far smaller fractional change over the same range (a fractional change of about 1/10 for both)*. The temperature and salinity coefficients of conductivity for sea water are shown in Figures 2.7 and 2.8 over the range of these variables of interest in the oceans. It will be noticed that these coefficients are largest in the deeper waters where the temperature and salinity are low. The large temperature coefficient of sea water (or any electrolyte solution) is compared in Figure 2.9 with that of typical metals used in resistance-wire thermometers. The magnitude of the resistance of a wire or electrode relative to the resistance at zero degrees is plotted in this graph;

---

*The fractional temperature change is with respect to absolute temperature, e.g., 20 °C is 293 °K.

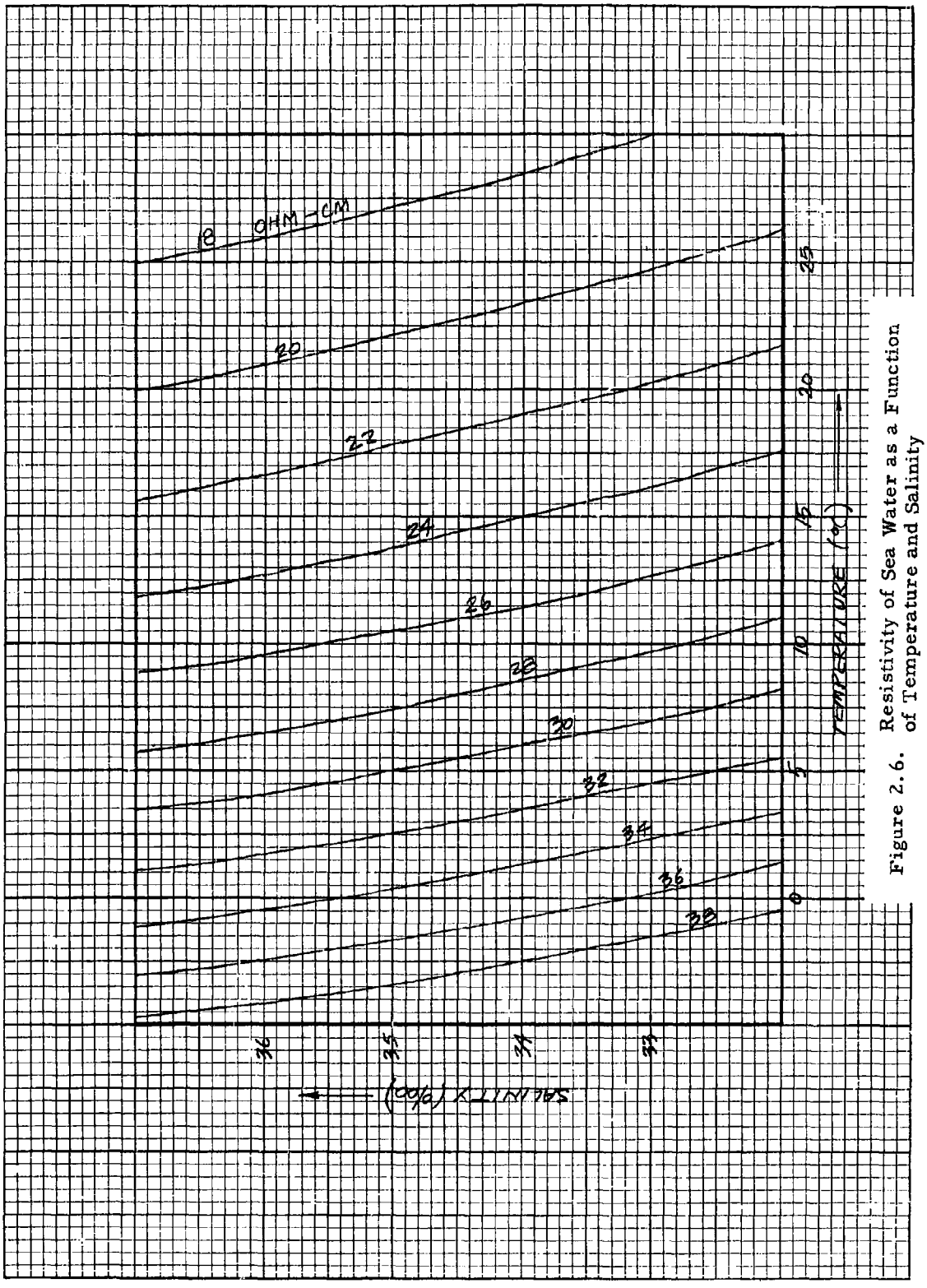

Figure 2.6. Resistivity of Sea Water as a Function of Temperature and Salinity

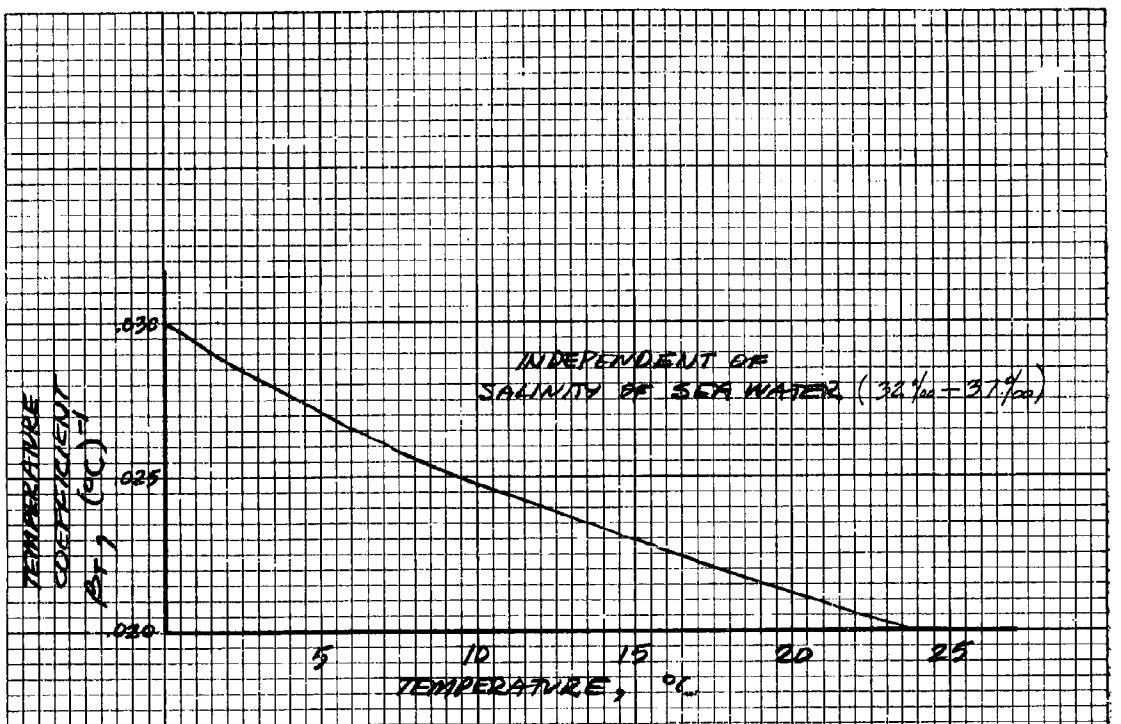

Figure 2.7. Temperature Coefficient of Conductivity of Sea Water

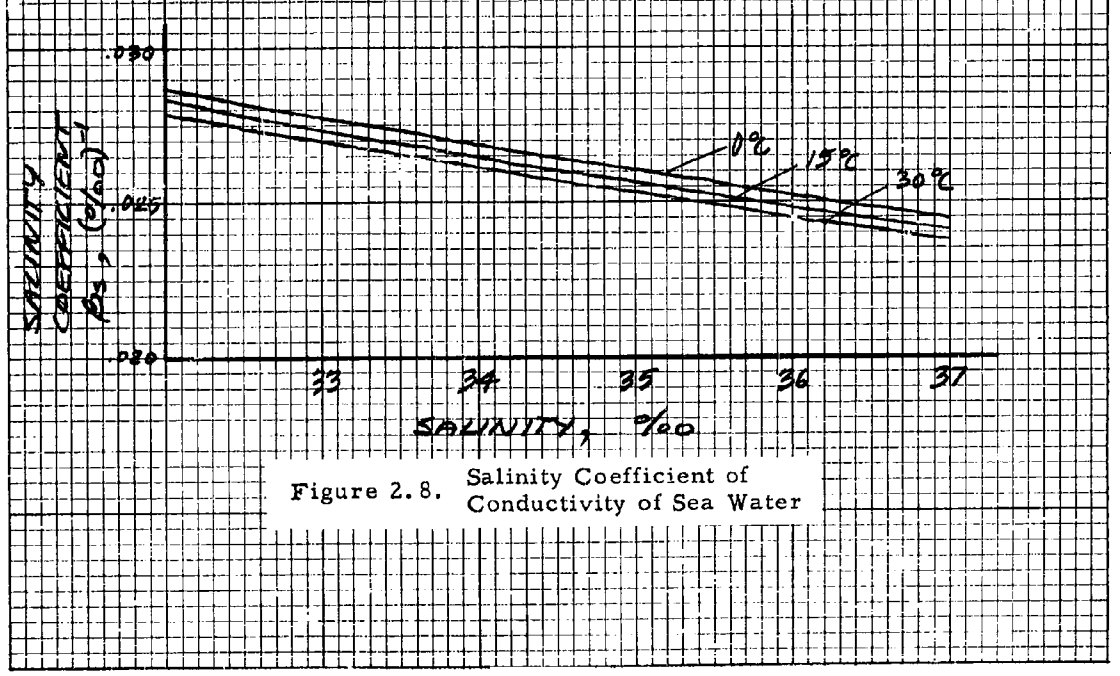

Figure 2.8. Salinity Coefficient of Conductivity of Sea Water

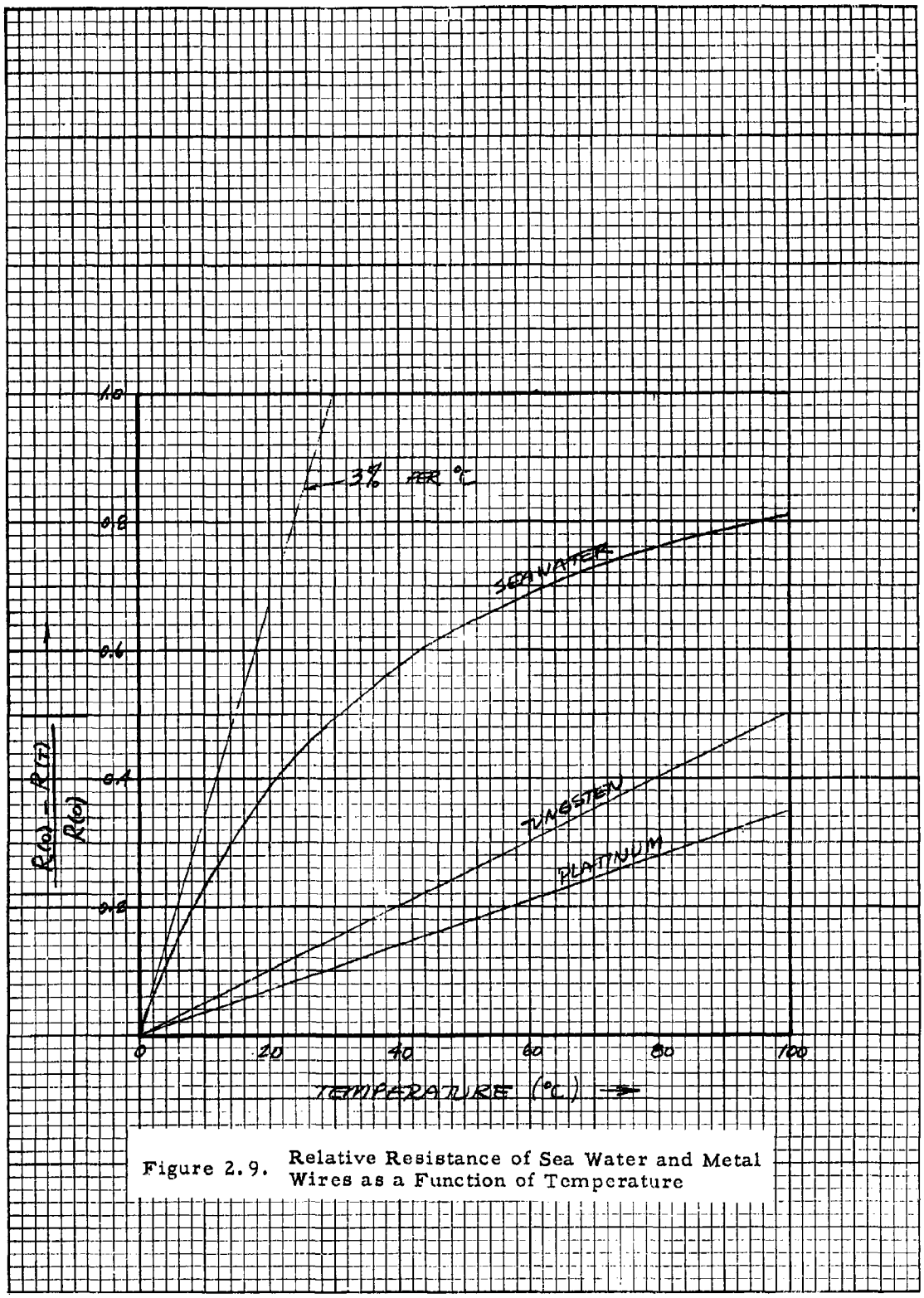

Figure 2.9. Relative Resistance of Sea Water and Metal Wires as a Function of Temperature

it should be remembered, however, that the resistance of wires increases with increasing temperature whereas the electrode resistance decreases with increasing temperature. The temperature coefficient of wires is of the order of 0.4 % per ^{o}C in comparison with 2 % per ^{o}C for aqueous solutions.

Electronic Equipment

A simplified electronic arrangement for measuring conductivity variations in flowing water is shown in Figure 2.1 . Two electrodes of suitable design are immersed in the water and the resistance between them is arranged so that it represents one arm of a wheatstone bridge. A bridge arrangement is well suited to the measurement of small changes in the value of an electrical element about its average value. Variations in electrode resistance due to conductivity changes caused by temperature and salinity changes gives rise to a voltage across the voltmeter, thus providing a means for measuring the combined temperature and salinity variations. The source of electrical power indicated in this diagram is an oscillator since it is necessary to use a source of high frequency (e.g., 40 kc) electrical power to avoid electrochemical polarization effects at the metal electrodes. A great variety of instrumentation is in use today for electrolytic conductivity bridge measurements to determine the absolute salt concentrations in solutions of known temperature (12).

Although the absolute measurement of the conductivity of the water is important, the present instrumentation finds its greatest value in measuring small changes of conductivity in space and time. That is, interest is centered on a differential conductivity measurement. Differential measurements in time are performed by comparing the instantaneous signal with the average signal over a given time interval. This is accomplished in practice by an appropriate electronic filter; a simple single stage high pass filter with a given time constant is an example. Differential measurements in space can be performed by two sensing elements spaced a given distance apart which is comparable or larger than the scale of conductivity microstructure which it is desired to measure. Such an arrangement is shown in Figure 2.10 . The equipment consists basically of a source of alternating electrical current to drive the bridge network; the double conductivity cell wheatstone bridge; electronic detection equipment consisting of amplifiers, detector and filters; and display equipment for recording and measuring the resultant output signal induced by the conductivity differences between the two electrodes.

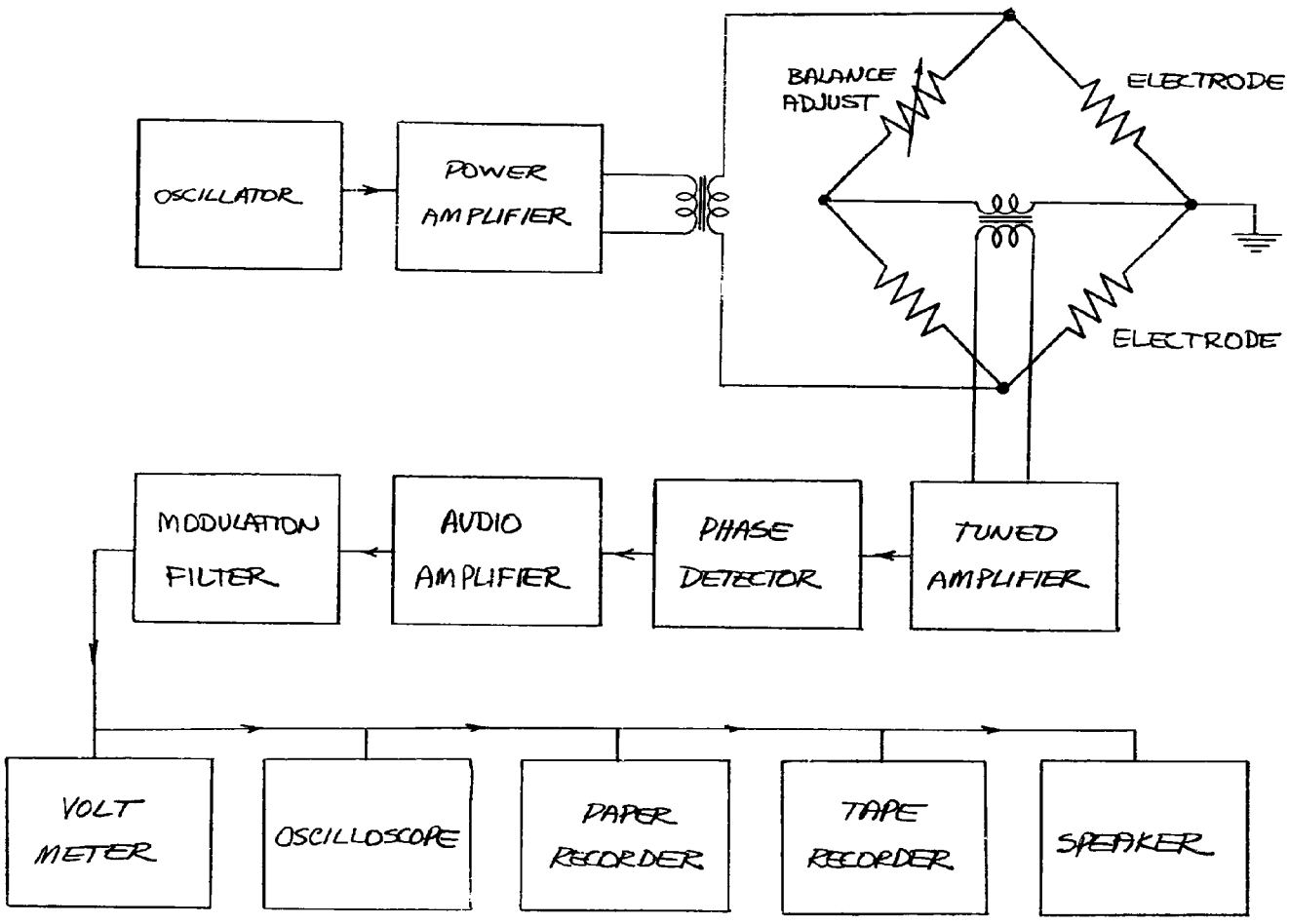

Figure 2.10. Differential Conductivity Microstructure Detection Electronics

3. TEMPERATURE DETECTOR

The use of a measurement of electrolytic conductivity to determine, specifically, the temperature of a solution is investigated in this Section. Instrumentation based on this principle for a temperature measurement will be termed a "T-meter" for brevity sake. The characteristics of a T-meter are compared with those of a resistance-wire thermometer at the end of this Section in order to evaluate the relative merits of the new technique of temperature measurement.

3.1 Description

Temperature measurement by means of a conductivity measurement is now studied in more detail. The key problem of making specific temperature measurements without errors due to salinity variations is set off for special consideration in Section 3.2 . The outstanding property of the present method of detecting temperature fluctuations is its relatively high sensitivity and rapid response time.

Sensitivity

The original motivation for the development of the present detection techniques was based on the fact that, from elementary considerations, extremely small temperature fluctuations were potentially measurable. The reasoning was based on the following analysis. Consider a pair of electrodes immersed in a flowing medium of conductivity σ. The resistance, R, of the electrodes is related to the conductivity of the fluid medium by

$$R = \frac{1}{\sigma h} ,$$

where h^{-1} is the cell constant; h is comparable with the size of the electrode volume. Assume that the measurement of the resistance of an electrode is ultimately limited by the Johnson noise voltage which appears across the resistance. Suppose a voltage, V, is applied to the electrode for the purpose of measuring its resistance, R:

$$V = IR ,$$

where I is the electrode current. For a constant current, small variations in resistance, δR, cause small variations in voltage, δV, across the resistance given by

$$\frac{\delta V}{V} = \frac{\delta R}{R} .$$

The smallest detectable resistance change is set by the condition that

Best Available Copy

δV is equal to the random Johnson noise voltage (1)

$$\delta V = \sqrt{4kT\Delta fR} ,$$

where k is Boltzmann's constant, T the absolute temperature ($kT = 4 \times 10^{-21}$ joule), and Δf is the bandwidth over which the temperature fluctuations occur. Rewriting the above relations we obtain

$$\frac{\delta R}{R} = \sqrt{\frac{4\ kT\Delta f}{P}}$$

and

$$P = \frac{V^2}{R} ,$$

where P is the electrical power dissipated in the electrode resistance. If δT is the rms temperature fluctuation of the electrode resistance, then

$$\frac{\delta R}{R} = \beta_\tau \delta T ,$$

where β_τ is the temperature coefficient or the electrical conductivity of the fluid medium. The minimum detectable temperature fluctuation is given by

$$\delta T = \frac{1}{\beta_\tau} \sqrt{\frac{4kT\Delta f}{P}} .$$

We illustrate the very small magnitude of this temperature variation for an electrode moving at velocity, U, through sea water. The bandwidth, Δf, is limited by the physical size of the electrode. If λ is the physical wavelength of the smallest scale of temperature microstructure in the sea water measured by the instrument, then the bandwidth is

$$\Delta f = \frac{U}{\lambda} .$$

The wavelength is related to the size of the electrode approximately by the condition*

$$\frac{\lambda}{2\pi} = h$$

and

$$\Delta f = \frac{1}{2\pi}\left(\frac{U}{h}\right) ,$$

*This condition is probably too severe, a more realistic one is $\lambda = 2h$ (see Sec. 13.1).

that is, the cutoff wavenumber is equal to the cell constant of the electrode.

The above expressions are illustrated by the following numerical example for electrodes in sea water:

$$\sigma = .048 \text{ ohm}^{-1} \text{ cm}^{-1}$$
$$\beta_T = .021 \text{ per } ^\circ\text{C}$$
$$h = 1 \text{ cm}$$
$$U = 12 \text{ knots}$$
$$V = 1 \text{ volt},$$

then

$$R = 21 \text{ ohms}$$
$$P = 48 \text{ milliwatts}$$
$$\Delta f = 100 \text{ cps}$$
$$\lambda = 6.3 \text{ cm},$$

and

$$\delta T = 3 \times 10^{-7} \, ^\circ\text{C}.$$

Thus, this elementary analysis indicates that extremely small temperature variations are detectable by this method with relatively fast response time (1.6×10^{-3} sec). The analysis of the sensitivity is again carried out in detail in Section 8.3 and, though the results there are not as optimistic as above, it does not change our basic observation that the present instrumentation is capable of high sensitivity with rapid response time.

Background Noise

The minimum detectable temperature variation found above assumed background noise due only to Johnson noise associated with the thermal agitation of the carriers of electrical charge in the electrode resistance. If there is a random salinity variation, δS, present in the medium, the minimum detectable temperature variation is given simply by

$$\delta T = \left(\frac{\beta_s}{\beta_T} \right) \delta S \quad ,$$

where β_s is the salinity coefficient of the electrical conductivity. This limit of detectability is usually much larger than that given previously for Johnson noise. The reduction or removal of this source of background noise for the temperature measurements is discussed in Section

3.2 , below.

Another source of background noise is associated with the temperature rise of the water caused by the electrical power, P, dissipated in the water. The average temperature rise, $\overline{\Delta T}$, of the water passing through the electrodes is (Sec. 12.1)

$$\overline{\Delta T} = \frac{P}{2cAU} ,$$

where c is the heat capacity per unit volume of the fluid and A is the "frontal area" of the electrode volume. For simplicity we assume here that the frontal area is approximately

$$A = h^2 .$$

If the flow velocity, U, experiences random fluctuations, δU, (turbulence) then the temperature rise fluctuates and appears as a false temperature signal. The rms value of these temperature fluctuations sets the minimum detectable signal as

$$\delta T = \overline{\Delta T} \left(\frac{\delta U}{U} \right) .$$

As a numberical example of this noise limitation, we assume the values of the previous numerical example, and in addition :

$$\delta U = .01 \text{ knot}$$
$$c = 4.09 \text{ joule/cm}^3/^\circ\text{C} ,$$

then

$$\left(\frac{\delta U}{U} \right) \approx 10^{-3}$$
$$\overline{\Delta T} \approx 10^{-5} \, ^\circ\text{C}$$
$$P \approx 50 \text{ mw}$$

and

$$\delta T \approx 10^{-8} \, ^\circ\text{C}.$$

Thus, this source of noise associated with electrode self heating and turbulence of the medium is a small but not negligible effect in comparison with Johnson noise for the example given.

The ultimate temperature sensitivity, when turbulence is the limiting factor, occurs when the Johnson noise limitation equals that due to tur-

bulence, i.e., when

$$\overline{\Delta T}\left(\frac{\delta U}{U}\right) = \delta T = \frac{1}{\beta_T}\sqrt{\frac{4kT\Delta f}{P}} \quad .$$

Rewriting this expression with the forms given previously for the bandwidth and temperature rise, we obtain the ultimate temperature sensitivity according to this simplified analysis:

$$\delta T = \left[\frac{kT}{\pi h^3 c \beta_T^2}\left(\frac{\delta U}{U}\right)\right]^{1/3} .$$

For the numerical values given previously, this amounts to a temperature sensitivity of about 10^{-7} °C. The above expression shows the general dependence of the sensitivity on the electrode size and relative turbulence level, viz.,

$$\delta T \sim h^{-1}\left(\frac{\delta U}{U}\right)^{1/3} ,$$

that is, the sensitivity increases as the size of the electrode increases, and decreases (slowly) as the turbulence level increases. The electrode, thus, should be as large as possible provided it is not larger than the smallest scale of microstructure to be detected; and should be moved at high speed through the random temperature field. The above analysis is again carried out in Section 8.3 in more detail and confirms the results obtained here indicating a high temperature sensitivity even in the presence of a turbulent velocity field.

Effective Temperature

In the event that it is not possible to separate the temperature and salinity variations in their effect on the measured conductivity variations, it is convenient to introduce the concept of "effective temperature," δT^*, given by

$$\delta T^* = \delta T + \left(\frac{\beta_S}{\beta_T}\right)\delta S \quad .$$

That is, the effective temperature is equal to that temperature variation which would cause the same conductivity variation that the actual temperature and salinity variations did cause. The sensitivity theory given above applies strictly to effective temperature. If the salinity variations, δS, are small relative to the temperature variations, δT, (as is the case in most of the oceans) the effective temperature is approximately

equal to the actual temperature:

$$\delta T^* \simeq \delta T$$

when

$$\left(\frac{\beta_s}{\beta_T}\right)\left(\frac{\delta S}{\delta T}\right) << 1 \quad .$$

Frequency Response

Since the measurement of the temperature of the medium does not depend on the cooling of a sensing element (as is the case with the resistance-wire thermometer) but depends only on the mechanical transport of the fluid through the sensitive volume of the electrode, the frequency response is determined only by the physical size of the electrode. It was pointed out earlier that the bandwidth, Δf, set by this condition was given approximately by

$$\Delta f = \frac{1}{2\pi}\left(\frac{U}{h}\right) \quad .$$

This formula assumes that the velocity is essentially uniform over the electrode volume. The boundary layer at the surface of the electrodes, where the velocity falls to zero, must therefore represent only a small portion of the electrode volume if the above formula is to be valid. Assuming the typical dimension of the electrode is h, the boundary layer thickness is of the order of

$$\sqrt{\frac{h\nu}{U}} \quad ,$$

where ν is the kinematic viscosity of the fluid. We require that the electrode dimensions are large in comparison with the above boundary layer thickness:

$$h \geqslant M\sqrt{\frac{\nu h}{U}} \quad ,$$

where M is a number of the order of ten. Rewriting the above relations we have

$$h \geqslant \left(\frac{\nu}{U}\right)M^2$$

and

$$\Delta f \leqslant \frac{U^2}{2\pi\nu M^2} \quad .$$

As a numerical example, assume the following:

$$\nu = .01 \text{ cm}^2/\text{sec}$$
$$U = 12 \text{ knots} = 620 \text{ cm/sec}$$
$$M = 10$$

and, therefore

$$h \geq 1.6 \times 10^{-3} \text{cm}$$
$$\Delta f \leq 61 \text{ kc.}$$

Thus, a very small electrode may be used, corresponding to a very wide bandwidth, before the limitations of boundary layer thickness become important. These matters are discussed in more detail in Section 13.2 .

3.2 Separation of Variables

The fundamental quantity measured in the present instrumentation is the conductivity of an electrolyte solution and its variations. These variations are caused by corresponding changes in temperature and salinity if we neglect the miscellaneous other effects, such as pressure changes and bubbles in the water as considered in detail in Section 6.1 . Although one can argue, as we have done in Section 2.3 , that a conductivity measurement, of itself, is a significant parameter to measure in the water, it is also of interest to measure specifically and independently the associated changes in temperature and salinity. Conventionally, this is done by instrumentation which is specific to the particular variable under consideration, e.g., a resistance-wire thermometer for temperature and (at a much slower rate) a salinometer based on a temperature compensated conductivity measurement for salinity. In this Section we discuss a number of situations in which the conductivity measurement is essentially a specific measurement of temperature.

Low Background

The first and simplest example of this is when, as a result of natural circumstances, the variations of salinity happen to be much smaller than those due to temperature. As shown in Section 7.3 this situation pertains to some degree in most of the world's oceans. Typically, the variations in conductivity due to salinity microstructure in the ocean are about ten times smaller than those due to natural temperature microstructure. On the average, then, the signal from a detector based on a conductivity measurement operating in the ocean measures temperature variations and the contribution due to salinity is about 20 db below that due to temperature. This fact is of great practical importance in the application of such instrumentation to oceanographic research problems.

Another experimental situation where this simple principle of temperature dominance applies is where a great deal of heat energy can be generated in the experimental region as, for example, in the turbulence field behind a heated wire mesh or in a jet of hot water issuing into a volume of cold water.

Well Mixed Solutions

Another situation where conductivity variations are due almost entirely to temperature variations occurs when the solution is completely contained in a vessel which is well stirred and not in contact with undissolved quantities of the salt in solution. In this case, there is no source or sink for solute or solvent. The salinity microstructure dies out relatively quickly due to mixing and is, to a very high degree, eliminated from the measurement. The ease with which this is achieved in the laboratory, and even in large water tunnels, is a very important factor in the application of conductivity measurements to temperature measurements in these situations. This principle does not, of course, apply to the temperature microstructure in the water because many sources of heat energy are present in or about the stirred solutions. As a matter of fact, any form of energy, e.g., the mechanical energy of the flowing water, must ultimately be converted to heat energy and consequently give rise to temperature microstructure. A steady state equilibrium situation is reached in which temperature structure is present but salinity structure is completely absent.

Zero Salinity Coefficient

Another technique for removing the effects of salinity microstructure is applicable in laboratory experiments where the concentration of the solution may be varied at the discretion of the experimenter. By referring to Figure 2.3 it is seen that sodium hydroxide (NaOH) has a maximum in the curve of conductivity vs. concentration. If a solution of such an electrolyte were to be adjusted to a concentration corresponding to this maximum, then slight variations in concentration cause only small second order changes in conductivity. If the conductivity of the solution is expanded about this point, the leading term is

$$\frac{\Delta\sigma}{\sigma_\Lambda} = \frac{m}{2}\left(\frac{\Delta S}{S_\Lambda}\right)^2 ,$$

where m is a pure number and σ_Λ is the maximum conductivity corresponding to the salinity S_Λ. For the NaOH solution of Figure 2.3 ,

$$\sigma_\Lambda = 0.35 \text{ ohm}^{-1}\text{cm}^{-1}$$
$$S_\Lambda = 15\ \%$$
$$m \approx 2.0 .$$

As an illustration, suppose that, because of a process outside the experimenter's control, a 1 % variation in NaOH concentration about S_A is continuously present, then the corresponding variation in conductivity is only one part in 10^4. This method constitutes either an additional reduction of salinity background over the last method or one which would be applicable in the case where a source of the dissolved salt is always exposed to the solution under measurement. The constant m may possibly be significantly reduced by an appropriate choice of a mixture of two salts for example, NaOH and NaCl as is suggested by the curves of Figure 2.3 .

Dielectric Loss in Water

The conduction of electricity in electrolyte solutions discussed so far has been attributed solely to the motion of charged ions. This conduction is characterized by the resistance of the medium to the flow of electricity, which, in turn, implies a dissipation of energy in the solution, i.e., electrically speaking, the medium is "lossy." This source of dissipation of electrical energy is the dominant one over a very wide range of the frequency of electrical oscillations. In aqueous solutions, however, at very high frequencies of the order of, or greater than, 10 kmc (radar frequencies) another mechanism of absorption of electrical energy becomes important and is the dominant contribution to the resistive component of the medium. This phenomenon has its origin in the dipole relaxation absorption by the water molecules themselves (2). The consequence of this is that the conductivity of the water at this high frequency is independent of the salinity of the water (3). For example, sea water and fresh water have essentially the same electrical properties above 20 kmc. This phenomenon immediately suggests making the conductivity measurements at radar frequencies so that the measurements are independent of salinity. The temperature coefficient of conductivity is still quite appreciable (2 % per $^{\circ}$C) at these frequencies and is due to the temperature dependence of the water molecule dipolar conductivity.

Correlated Signals

A measurement of conductivity variations is a specific indication of corresponding temperature variations, even in a medium where there are also salinity variations, if these two variables are linked by some relation, i.e., if they are directly correlated. All that need be known in this use is the average relation between temperature and salinity. An example of this is found in the ocean where it has been known for some time that masses of ocean water are characterized by a fixed relation between its temperature and salinity, i.e., the so-called "TS-diagram" (4). Assuming this to be the case, if a small change in salinity, ΔS, is related to a small change in temperature, ΔT, by the equation

$$\Delta S = \gamma_0 \Delta T \ ,$$

then a change in conductivity is given by

$$\frac{\Delta\sigma}{\sigma_0} = \beta_T \Delta T + \beta_S \gamma_0 \Delta T = \left(\beta_T + \gamma_0 \beta_S\right) \Delta T.$$

Thus, the conductivity is specific to temperature (or salinity, for that matter) and the only thing that need otherwise be known about the medium is the average value of the parameter γ_0 which is the slope of the TS-diagram. In Section 7.3 it is shown that in the ocean the typical value of γ_0 is about 0.1 ‰ per ^{o}C. If we let

$$\gamma_1 = \frac{\beta_S}{\beta_T}$$

and

$$\gamma = \gamma_0 \gamma_1$$

then

$$\frac{\Delta\sigma}{\sigma_0} = \beta_T \Delta T(1 + \gamma) \quad .$$

For average ocean water $\gamma \approx 0.1$. This principle represents a refinement over the first mentioned technique applicable to solutions with relatively small salinity microstructure. The correlation between temperature and salinity variations is valid approximately for large scale masses of water in the ocean but, obviously, it cannot hold down to the smallest scale microstructure because of the great difference in the diffusion constants for temperature and salinity. At the smallest scales no correlation between temperature and salinity should be found and this principle of the separation breaks down.

Salinity Compensation

The conventional means for correcting a measurement of a quantity for variations in a spurious variable is to make a measurement of the spurious variable and compensate the original measurement with this additional data. Unfortunately no instrumentation presently exists for rapidly measuring the salinity on a continuous basis for this means of compensating the conductivity measurement. This technique can be generalized to apply in the case where two non-specific measurements of temperature and salinity by two instruments with different response to two variables are combined appropriately to obtain measures of the temperature and salinity separately. Compensation is most effective if one instrument responds predominantly to salinity* This principle is enlarged on in some detail in Section 4.3 and appears as a promising new method for making continuous and simultaneous measurements of temperature and salinity microstructure in water.

*and the other predominantly to temperature.

Temperature Dependent Coefficients

If the temperature and salinity sensitivity coefficients depend on temperature, these variables may be separated by operating the electrode at two different temperatures. One measurement could be performed at ambient temperature and the other at a higher temperature obtained by electrically heating the water between the electrodes. In this way, two equations based on the two measurements are obtained with two unknowns (temperature, and salinity), which may be solved. This method is discussed in detail in Section 4.3 along with a class of other such compensation techniques. The method as described above is difficult in practice because the temperature dependence of the sensitivity coefficients is small. Some aspects of this double type of measurement are discussed in References (8,9).

3.3 Resistance-Wire Thermometer

One of the most reliable and widely used temperature sensors is the resistance-wire thermometer. Such an instrument is potentially capable of a sensitivity of the order of 100 μ ^{o}C and is capable of accurate absolute temperature measurements due to its stability. Temperature measurements in water present some added practical problems over those in air.

The resistance wire thermometer consists of a fine wire which is exposed to the medium whose temperature is being measured. The resistance of the wire depends on its temperature and, therefore, on the temperature of the medium. Variations in temperature of the medium give rise to resistance variations which are measured by electronic equipment.

The earliest measurements of temperature by a resistance thermometer were those of Siemens in 1871, but it was left to Callendar some years later (1887) to develop the science of precision resistance-wire thermometry (5,6). A recent innovation in the use of resistance thermometers in water is the metal film type element introduced by Ling (7).

The properties of resistance wire thermometers for practical use are described by Mueller (10) and Lion (11). Some of the salient features of these instruments are discussed briefly below. The development of the basic theory of the operation of the wire element is put off to Section 5.4 where it is treated in connection with the extension of this instrument to the measurement of fluid velocity, i.e., the hot-wire anemometer.

Wire Resistance

In general, the resistivity of metals increases with increasing

temperature (positive resistance temperature coefficient), whereas the resistivity of electrolytes and semiconductors decreases with increased temperature (negative coefficient). Over the range of temperature where the wire resistance is essentially a linear function of temperature, the resistance may be expressed as

$$R = R_0\left(1 + \beta \Delta T\right)$$

where $\Delta T = T - T_0$, R_0 is the resistance at temperature T_0, and β is the temperature coefficient. R_0 is the so-called "cold resistance." At room temperature this coefficient is 0.39 % per ^{o}C for pure platinum and 0.48 % per ^{o}C for tungsten.

Sensitivity

The sensitivity of a resistance-wire thermometer is defined as the change in voltage, ΔV, across the wire due to a temperature, ΔT. For a constant current I through the wire, we have

$$\Delta V = I \Delta R = I R_0 \beta \Delta T \quad .$$

or the sensitivity is

$$\frac{\Delta V}{\Delta T} = I R_0 \beta \quad .$$

This quantity is large if the three quantities β, I, and R_0 are large. Aside from the choice of wire material which determines β, this calls for a long thin wire which carries a large current. The practical limitation to these extremes is set by the physical size of the region whose temperature is to be measured and the fact that high currents cause excess heating of the wire resulting in a self-induced temperature signal. This effect relates to the heat transfer from the medium to the wire and is treated later in Section 5.4 . The temperature sensitivity of conventional resistance-wire thermometers can be as high as 100 $\mu^{o}C$ in air as well as water.

Response Time

The temperature of the wire and medium are the same only if the changes in temperature of the medium take place slowly enough for a complete heat exchange between the wire and the medium. The rate of change of wire temperature depends in a relatively simple way on the heat capacity of the wire, the heat transfer characteristic, and the temperature difference between the wire and the medium. It is shown in Section

5.4 that the wire responds to temperature changes like a series resistance-capacitance circuit with a time constant

$$\text{time constant} = \frac{c_w d^2}{4 K N}$$

where d is the wire diameter, c_w the heat capacity per unit volume of the wire, K the thermal conductivity of the fluid medium (water in this case) and N is the Nusselt number for the wire in the flowing medium. A rapid response to temperature variations calls for a wire of small diameter.

Errors and Compensation

Spurious signals are generated in a resistance wire thermometer because of a) the strain-gauge effect in the thin wire due to the dynamic pressure of the flowing medium (water) on the wire, b) self-heating of the wire by the electrical current which generates a false temperature reading dependent on the flow about the wire, and c) variations in shunt resistance when the wire is immersed in a conducting medium such as sea water. These effects can be reduced in a medium when the velocity is uniform over two sensing wires in a symmetrical bridge but the temperature microstructure is not uniform over the separation distance between the wires. Double wire techniques provide some advantages which are not possible with single wire measurements (12,13,14). The resistance-wire technique may be used to measure several variables of the medium besides temperature (8,9).

3.4 Comparison of Methods

The relative performance of the T-meter and resistance-wire thermometer operating in water is now considered. This comparison is carried out in more detail in Section 5.5 along with the comparison of the U-meter and hot-wire anemometer. It is shown in that Section that the temperature snesitivity of the T-meter is considerably greater than that of the resistance-wire thermometer because of the former's higher temperature coefficient of resistance and ability to dissipate greater power in the sensing element before the limitations of electrode heating are appreciable. The general utility of the T-meter is also superior because of the ruggedness of the sensor itself. The stability of calibration probably is not as good as that of the resistance-wire thermometer and, because of the dependence on the salinity of the water, the T-meter, in general, does not measure temperature specifically whereas the resistance-wire thermometer does. The response frequency of both instruments, for operation in water, is limited by the physical size of the sensors. It is shown in Section 5.5 that electrode sensors can be made much

smaller than wire sensors, thus, the T-meter is capable of a higher frequency response than the resistance-wire thermometer.

4. SALINITY DETECTOR

The use of a measurement of electrolytic conductivity to determine, specifically, the salinity of a solution is investigated in this Section. Instrumentation based on this principle of salinity measurement will be termed an "S-meter" for brevity sake. A comparison of the S-meter with other conventional electronic means of measuring salinity is not possible since there are none (the conventional salinometer is a type of S-meter). The instrumentation described in Section 4.3 is of interest since it represents, it is believed, the first example of an instrument which measures salinity specifically by electronic means.

4.1 Description

The measurement of the salinity of water by means of a conductivity measurement is now considered in more detail. The primary limitation to making a specific salinity measurement by this means is the temperature background. In situations where a specific measurement is possible, the salinity detector is capable of high sensitivity and rapid response. The following analysis closely parallels that for the temperature detector in Section 3.1 .

Sensitivity

The ultimate sensitivity of the detector to salinity fluctuations follows directly from the simplified analysis for the temperature detector, but with a change in the β-coefficient:

$$\delta S = \frac{1}{\beta_S} \sqrt{\frac{4kT\,\Delta f}{P}} \quad ,$$

where β_S is the salinity coefficient of conductivity, Δf is the bandwidth of the salinity fluctuations, P is the electrical power dissipated in the water and $kT = 4 \times 10^{-21}$ joule. Under the conditions assumed in Section 3.1 , this corresponds to a salinity sensitivity of about

$$\delta S \approx 1.1 \times 10^{-7} \text{ ‰}$$

where

$$\beta_S = 2.5 \text{ \% per ‰} \quad .$$

This extremely high sensitivity to salinity variations is not realizable in terms of a specific measurement unless conditions are such that the temperature is low or can be compensated for in some way. This matter is

studied qualitatively in Section 4.2 and in detail in Section 4.3 .

Background Noise

The above salinity sensitivity is based on the limitation imposed by Johnson noise. If, in fact, the background noise is due to temperature fluctuations, δT, in the band of interest, then the sensitivity to salinity fluctuations is simply

$$\delta S = \left(\frac{\beta_T}{\beta_S}\right) \delta T \quad .$$

If the temperature background of this type is negligible, consideration must be given to noise associated with fluctuating electrode heating due to velocity fluctuations, δU. Following the corresponding analysis of this effect for the temperature detector, we find that the ultimate salinity sensitivity is

$$\delta S = \frac{1}{\beta_S} \left[\frac{k T \beta_T}{\pi h^3 C}\left(\frac{\delta U}{U}\right)\right]^{1/3}$$

$$= \left(\frac{\beta_T}{\beta_S}\right) (\delta T)_{min} \quad .$$

where $(\delta T)_{min}$ is the ultimate temperature sensitivity subject to the same background noise. The ultimate salinity sensitivity is of the order of 10^{-7} ‰.

Zero Temperature Coefficient

A notable case of interest is when the sensing element has a zero (first order) temperature coefficient. Such a case is studied in Section 4.3 , where the resistive component of a complex impedance sensing element is found to be independent (to first order) of temperature at a certain frequency. This fortunate circumstance has the advantage that the salinity measurement becomes, to a high degree, independent of temperature background noise. The second order temperature coefficient of the sensing element is, however, finite.

Suppose that the resistance variations, ΔR, of the sensing elements satisfy the equation

$$\frac{\Delta R}{R} = \beta \Delta S + \eta \Delta T^2 \quad ,$$

where β is the salinity coefficient of the resistance, ΔS and ΔT are salinity and temperature fluctuations about their respective average values, and γ is the second order temperature coefficient. The first order temperature coefficient is assumed to be zero. The limit of detectability for the salinity measurement, δS, occurs when:

$$\beta \delta S = \gamma \Delta T_{rms}^2$$

where ΔT_{rms} is the rms temperature fluctuation background. As a numerical example, assume

$$\beta = \frac{1}{10} \beta_S = 2.5 \times 10^{-3} \text{ per } ‰$$

$$\gamma = \frac{1}{10} \beta_T^2 = 4.0 \times 10^{-5} \text{ per } {}^{\circ}C^2$$

and $$\Delta T_{rms} = 10^{-3} \ {}^{\circ}C$$

then

$$\delta S = 2 \times 10^{-8} ‰ .$$

It is clear that if an instrument with a zero first order temperature coefficient could be obtained, salinity measurements to the limit of sensitivity set by Johnson noise could be made. An instrument with such a property is discussed in Section 4.3 . In addition, it should be mentioned that this type of instrument is not limited with respect to electrode power because of heating fluctuations which occur when velocity fluctuations are present. This suggests the potentiality of even greater salinity sensitivity than 10^{-7}‰ discussed earlier in this Section.

Frequency Response

Since the detector has no capacity for the measured variable (salinity), the response of the detector is determined by its physical size. As in the case of the temperature detector the bandwidth, Δf, of the detectable salinity fluctuations is approximately*

$$\Delta f = \frac{1}{2\pi} \left(\frac{U}{h}\right)$$

where h^{-1} is the cell constant of the electrode. This expression is valid within the constraints imposed by the finite thickness of the velocity

*A more realistic condition is $f = \frac{1}{2} \left(\frac{U}{h}\right)$ (see Sec. 13.1).

boundary layer discussed in Section 3.1 and in more detail in Section 13.2 .

4.2 Separation of Variables

Let us now consider the methods for making specific salinity measurements by means of a conductivity measurement in which variations in temperature represent a small background. Several of the methods to be mentioned are just the inverse of the methods utilized to make specific temperature measurements considered in Section 3.2 .

Low Background

The simplest situation in which specific salinity measurements can be performed is when, because of experimental design or natural processes, the salinity variations are much larger than those due to temperature. An example of this is the measurement of the flow characteristics of a jet of concentrated salt solution issuing into a volume of tap water at the same temperature.

Correlated Signals

If the temperature and salinity variations are directly correlated, as discussed before, a specific salinity (or temperature) measurement can be made through a conductivity measurement.

Temperature Compensation

The compensation technique involving two different measurements is also applicable to salinity as well as to temperature as described previously. The simplest example of this is to simultaneously measure temperature by some means in order to correct the conductivity measurement. Salinometers based on a conductivity measurement utilize this technique.

Diffusion Effect

An important technique for separating salinity and temperature signals is based on the 100 fold difference in their respective diffusion constants. Because of the relatively small diffusion constant for salinity, small scale temperature microstructure is removed by diffusion before the diffusion process is operative in smoothing out salinity microstructure. In the ocean one would expect to find small scale salinity microstructure present where temperature microstructure is absent because of this effect (1).

This principle may be applied even to large scale temperature and

salinity microstructure in the following way. The sensing electrodes are located on a surface in such a way that a small volume in the undisturbed fluid medium experiences a large distortion due to shear flow over the surface. For example, this situation is achieved in laminar flow in a pipe or at the stagnation point of a disc moving perpendicular to the direction of motion. A similar situation exists in the turbulently mixed region behind a wire mesh screen. After the fluid has experienced great distortion, the previously large scale temperature and salinity structure contains large gradients which preferentially remove, by diffusion, that component with the highest diffusion constant. With a proper choice of electrode size and position, the salinity microstructure could be measured at a point where the temperature variations are small.

Zero Temperature Coefficient

The most desirable case occurs when the sensing element has a finite salinity coefficient but a zero (first order) temperature coefficient. In this case a specific salinity measurement can be performed even in the presence of relatively large temperature background noise. A sensing element with this property is discussed next in Section 4.3 .

4.3 TS-Meter

A principle of measurement is described in this Section which allows the independent measurement of temperature and salinity. It is basically a generalization of the ordinary compensation technique in which a primary measurement is corrected by an independent secondary measurement. In the present case the two sensing elements may be functions of both temperature and salinity. The conductivity of sea water is an example of such a measurable variable. An instrument based on this principle for measuring temperature and salinity will be referred to as a "TS-meter."

Suppose there are two instruments which measure some parameter of the water which depend, in general, on both the temperature and salinity. If the dependence of the two instruments on these variables is distinct, then the two independent measurements provide sufficient information to solve for the unknown temperature and salinity (two equations, two unknowns). Examples of measurable quantities which depend differently on temperature and salinity are the conductivity, $\sigma(T,S)$, the density, $d(T,S)$, and the dielectric constant, $\kappa(T,S)$, as well as others. Our present interest would be with quantities which are directly measurable by electronic means, i.e., conductivity and dielectric constant. The TS-meter principle is most effective when applied to sensors which can be integrated essentially into one, for example, the real (resistive) and imaginary (reactive) parts of a complex impedance whose values depend differently on temperature and salinity. It is simplest if these two impedance measurements are performed at the same frequency, however, to obtain more distinct information, it may be more desirable to perform the respective

measurements at different frequencies. A practical example of the TS-meter principle will occupy our attention later in this Section. First we develop the theory of this principle, in particular an analysis of the resultant errors and calibration techniques.

Theory

The theory of the TS-meter is illustrated for an impedance whose real and imaginary parts depend differently on temperature and salinity.

The impedance of an electrode, z, immersed in a flowing aqueous electrolyte solution (e.g., sea water) consists of the resistive, R, and reactive, X, parts:

$$z = R + iX \ .$$

The resistive and reactive parts are both functions of the temperature and salinity. It is fundamental to the principle of the TS-meter that these functions of temperature and salinity are different. If ΔR is a small change in resistance about the average value R_o, and ΔX is a small change in reactance about the average value X_o, then

$$\left(\frac{\Delta R}{R_o}\right) = \beta_{TR}\,\Delta T + \beta_{SR}\,\Delta S$$

$$\left(\frac{\Delta X}{X_o}\right) = \beta_{TX}\,\Delta T + \beta_{SX}\,\Delta S \ ,$$

where ΔT and ΔS are small changes in the temperature and salinity of the solution, and the β-coefficients are given by

$$\beta_{TR} = \frac{1}{R_o}\left(\frac{\partial R}{\partial T}\right) \qquad \beta_{SR} = \frac{1}{R_o}\left(\frac{\partial R}{\partial S}\right)$$

and

$$\beta_{TX} = \frac{1}{X_o}\left(\frac{\partial X}{\partial T}\right) \qquad \beta_{SX} = \frac{1}{X_o}\left(\frac{\partial X}{\partial S}\right) .$$

To insure the independence of the two measurements, we require (2)

$$\beta_{TR}\beta_{SX} - \beta_{TX}\beta_{SR} \neq 0.$$

Let us simplify this notation to facilitate further analysis by introducing

$$y_1 = \frac{\Delta R}{R_0} \qquad y_2 = \frac{\Delta X}{X_0}$$

$$a_1 = \beta_{TR} \qquad b_1 = \beta_{SR}$$

$$a_2 = \beta_{TX} \qquad b_2 = \beta_{SX}$$

and

$$t = \Delta T \qquad s = \Delta S$$

In this notation

$$y_1 = a_1 t + b_1 s$$
$$y_2 = a_2 t + b_2 s,$$

with the requirement that the determinant, D, is non-zero:

$$D = a_1 b_2 - a_2 b_1 \neq 0.$$

According to the principle of the TS-meter, we measure the quantity y_1 and y_2 with electronic instrumentation and then form appropriate linear combinations of these signals to obtain a measure of the temperature (t) and salinity (s) which are completely independent of each other. Let the linear combinations of the directly measured quantitics, y_1 and y_2, be

$$t^* = A_1 y_1 + B_1 y_2$$
$$s^* = A_2 y_1 + B_2 y_2 ,$$

where t* and s* are signals which approximate, as closely as the coefficients of the linear combination will allow, the temperature, t, and salinity, s, of the medium. The choice of the above coefficients of y_1 and y_2 is based of the coefficients of t and s in the previous (inverse)

set of linear equations. This linear combination of signals is accomplished in practice by an appropriate electrical network of passive attenuator and adder circuits. The ideal choice of the above coefficients follows from the usual solution of the linear equations

$$y_1 = a_1 t + b_1 s$$

$$y_2 = a_2 t + b_2 s \ ,$$

namely (2):

$$t = \frac{\begin{vmatrix} y_1 & b_1 \\ y_2 & b_2 \end{vmatrix}}{\begin{vmatrix} a_1 & b_1 \\ a_2 & b_2 \end{vmatrix}} = y_1 \left(\frac{b_2}{D}\right) + y_2 \left(\frac{-b_1}{D}\right)$$

$$s = \frac{\begin{vmatrix} a_1 & y_1 \\ a_2 & y_2 \end{vmatrix}}{\begin{vmatrix} a_1 & b_1 \\ a_2 & b_2 \end{vmatrix}} = y_1 \left(\frac{-a_2}{D}\right) + y_2 \left(\frac{a_1}{D}\right) .$$

Thus, the ideal choice of the constants of the linear combination (distinguished by hats) are:

$$\hat{A}_1 = \frac{b_2}{D} \qquad \hat{B}_1 = -\frac{b_1}{D}$$

$$\hat{A}_2 = -\frac{a_2}{D} \qquad \hat{B}_2 = \frac{a_1}{D} \ ,$$

in which case, we have exactly

$$t^* = t$$

$$s^* = s \ .$$

Such a choice of coefficients would accomplish our goal, that is, specific and independent measurements of temperature and salinity.

The above ideal choice is obvious; the same solution could have been obtained directly by requiring $t = t^*$ and $s = s^*$ so that

$$t = t^* = A_1 y_1 + B_1 y_2 = A_1 (a_1 t + b_1 s) + B_1 (a_2 t + b_2 s)$$

$$= (A_1 a_1 + B_1 a_2) t + (A_1 b_1 + B_1 b_2) s$$

and

$$s = s^* = A_2 y_1 + B_2 y_2 = A_2 (a_1 t + b_1 s) + B_2 (a_2 t + b_2 s)$$

$$= (A_2 a_1 + B_2 a_2) t + (A_2 b_1 + B_2 b_2) s.$$

These equations are satisfied when

$$1 = A_1 a_1 + B_1 a_2$$

$$0 = A_1 b_1 + B_1 b_2$$

$$0 = A_2 a_1 + B_2 a_2$$

$$1 = A_2 b_1 + B_2 b_2 \quad .$$

These four equations in four unknowns have the solutions already given above.

The simplest example of a TS-meter is when one measurement (say, y_1) is almost exclusively a measurement of temperature, t, and the other (say, y_2) almost exclusively a measurement of salinity, s. In this fortuitous case

$$a_1 = a \qquad b_1 = 0$$

$$a_2 = 0 \qquad b_2 = b \qquad (D = ab)$$

and

$$y_1 = at \qquad y_2 = bs \quad .$$

It follows that $\hat{B}_1 = \hat{A}_2 = 0$, therefore, choose $B_1 = A_2 = 0$ so that

$$t^* = A_1 y_1 \qquad s^* = B_2 y_2 \, .$$

In this case the measurements of both temperature and salinity are specific even for non-ideal values of A_1 and B_2, however, errors may occur in the respective constants of proportionality (calibration factors). The ideal values of A_1 and B_2 are

$$\hat{A}_1 = \frac{b_2}{D} = \frac{b}{ab} = \frac{1}{a}$$

$$\hat{B}_2 = \frac{a_1}{D} = \frac{a}{ab} = \frac{1}{b}$$

In the analysis that follows we will tend to associate the y_1 - measurement with a temperature measurement and the y_2 - measurement with a salinity measurement (i.e., the subscript 1 is associated with t and the subscript 2 with s). This association is not fundamental, however. The test of the TS-meter principle is the accuracy with which t and s can be measured. This topic is the subject of the following paragraphs.

Error Analysis

Errors in the temperature and salinity measurements occur when the coefficients A_1, B_1, A_2, B_2 are not exactly equal to their respective ideal values due to spurious variations of the coefficients of each of the two measurements, viz., a_1, b_1, a_2, b_2. Let the average value of these quantities be indicated by a zero subscript. The instruments are operated with the coefficients of the linear combination of y_1 and y_2 fixed at the average values:

$$\hat{A}_{10} = A_{10} = \frac{b_{20}}{D_0} \qquad \hat{B}_{10} = B_{10} = -\frac{b_{10}}{D_0}$$

$$\hat{A}_{20} = A_{20} = -\frac{a_{20}}{D_0} \qquad \hat{B}_{20} = B_{20} = \frac{a_{10}}{D_0} \, ,$$

where $D_0 = a_{10}b_{20} - a_{20}b_{10}$. The signals, y_1 and y_2, are given at any instant by

$$y_1 = (a_{10}t + b_{10}s) + (\delta a_1 t + \delta b_1 s)$$

$$y_2 = (a_{20}t + b_{20}s) + (\delta a_2 t + \delta b_2 s) \, ,$$

where the coefficients are

$$a_1 = a_{10} + \delta a_1 \qquad b_1 = b_{10} + \delta b_1$$

$$a_2 = a_{20} + \delta a_2 \qquad b_2 = b_{20} + \delta b_2$$

Introduce the notation:

$$y_{10} = a_{10}\, t + b_{10}\, s$$

$$y_{20} = a_{20}\, t + b_{20}\, s$$

then

$$y_1 - y_{10} = \delta a_1\, t + \delta b_1\, s$$

$$y_2 - y_{20} = \delta a_2\, t + \delta b_2\, s \,.$$

The linear combinations of these signals are

$$t^* - t_o^* = A_{10}\,(t\,\delta a_1 + s\,\delta b_1) + B_{10}\,(t\,\delta a_2 + s\,\delta b_2)$$

$$s^* - s_o^* = A_{20}\,(t\,\delta a_1 + s\,\delta b_1) + B_{20}\,(t\,\delta a_2 + s\,\delta b_2)\,,$$

where the values of t* and s* for the average coefficients are denoted by t_o^* and s_o^* :

$$t_o^* = A_{10}\, y_{10} + B_{10}\, y_{20}$$

$$s_o^* = A_{20}\, y_{10} + B_{20}\, y_{20} \,.$$

Regrouping the above expressions

$$t^* - t_o^* = (A_{10}\,\delta a_1 + B_{10}\,\delta a_2)\,t + (A_{10}\,\delta b_1 + B_{10}\,\delta b_2)\,s$$

$$s^* - s_o^* = (A_{20}\,\delta a_1 + B_{20}\,\delta a_2)\,t + (A_{20}\,\delta b_1 + B_{20}\,\delta b_2)\,s,$$

where we see that the measurement of temperature is <u>not</u> specific unless

$$\delta b_1 = \delta b_2 = 0\,,$$

and the measurement of salinity is <u>not</u> specific unless

$$\delta a_1 = \delta a_2 = 0 \ .$$

In general, these conditions do not obtain and errors in the temperature and salinity will occur due to <u>two</u> effects: 1) variations in the constant of proportionality for each variable, i.e., the calibration factor, and 2) the occurrence of spurious signals due to the opposite variable because the measurements are not specific.

To simplify the error analysis, assume the rms fluctuations of all coefficients are equal to ϵ:

$$\frac{(\delta a_1)_{rms}}{a_{10}} = \frac{(\delta b_1)_{rms}}{b_{10}} = \frac{(\delta a_2)_{rms}}{a_{20}} = \frac{(\delta b_2)_{rms}}{b_{20}} = \epsilon .$$

In the following, assume no correlation between fluctuating quantities, and squared quantities are understood to be time averages:

$$(t^*-t_0^*)^2 \equiv (\delta t^*)^2 = (A_{10}^2 a_{10}^2 + B_{10}^2 a_{20}^2)\epsilon^2 t^2 + (A_{10}^2 b_{10}^2 + B_{10}^2 b_{20}^2)\epsilon^2 s^2$$

$$(s^*-s_0^*)^2 \equiv (\delta s^*)^2 = (A_{20}^2 a_{10}^2 + B_{20}^2 a_{20}^2)\epsilon^2 t^2 + (A_{20}^2 b_{10}^2 + B_{20}^2 b_{20}^2)\epsilon^2 s^2 .$$

Let the mean-square values of the temperature and salinity variations be related by the constant γ_0:

$$s^2 = \gamma_0^2 t^2$$

or

$$s_{rms} = \gamma_0 t_{rms} \ ,$$

then

$$\frac{1}{\epsilon^2}\left(\frac{\delta t^*}{t}\right)^2 = (A_{10}^2 a_{10}^2 + B_{10}^2 a_{20}^2) + (A_{10}^2 b_{10}^2 + B_{10}^2 b_{20}^2)\gamma_0^2$$

$$\frac{1}{\epsilon^2}\left(\frac{\delta s^*}{s}\right) = (A_{20}^2 a_{10}^2 + B_{20}^2 a_{20}^2)\frac{1}{\gamma_0^2} + (A_{20}^2 b_{10}^2 + B_{20}^2 b_{20}^2).$$

These are the expressions which give the resultant errors in the temperature and salinity measurements with the TS-meter. These relations are simplified using the following equations which hold for the average values

of the coefficients:

$$
\begin{aligned}
1 &= A_{10}a_{10} + B_{10}a_{20} \\
0 &= A_{10}b_{10} + B_{10}b_{20} \\
0 &= A_{20}a_{10} + B_{20}a_{20} \\
1 &= A_{20}b_{10} + B_{20}b_{20} \; .
\end{aligned}
$$

Squaring these equations we get

$$A_{10}^2 a_{10}^2 + B_{10}^2 a_{20}^2 = 1 - 2A_{10}B_{10}a_{10}a_{20}$$

$$A_{10}^2 b_{10}^2 + B_{10}^2 b_{20}^2 = -2A_{10}B_{10}b_{10}b_{20}$$

$$A_{20}^2 a_{10}^2 + B_{20}^2 a_{20}^2 = -2A_{20}B_{20}a_{10}a_{20}$$

$$A_{20}^2 b_{10}^2 + B_{20}^2 b_{20}^2 = 1 - 2A_{20}B_{20}b_{10}b_{20}$$

Let

$$\gamma_1 = \frac{b_{10}}{a_{10}} = -\frac{B_{10}}{B_{20}} = -\frac{\hat{B}_{10}}{\hat{B}_{20}}$$

$$\gamma_2 = \frac{a_{20}}{b_{20}} = -\frac{A_{20}}{A_{10}} = -\frac{\hat{A}_{20}}{\hat{A}_{10}}$$

and

$$\mu = \gamma_1\gamma_2 = \left(\frac{b_{10}a_{20}}{a_{10}b_{20}}\right)$$

and

$$\gamma = \gamma_0\gamma_1 \; .$$

Without loss of generality, we can choose the coefficients of the y_1 - and y_2 - measurements so that

$$0 \leq |\mu| \leq 1 \; . \qquad (a_{10}b_{20} \neq 0)$$

The quantity μ may be either positive or negative, and, we shall see, plays

a fundamental role in the error analysis. The (average) determinant is

$$D_0 = a_{10} b_{20} - a_{20} b_{10} = a_{10} b_{20} (1-\mu) \neq 0,$$

so that

$$\mu \neq 1 ,$$

or, with consideration of the range of values of μ, it follows that

$$\mu < 1 .$$

We will see that the errors become unworkably large when $\mu \rightarrow 1$; the errors are smallest when $\mu \rightarrow 0$ (either one or the other measurement is specific); and when $\mu \rightarrow -1$ an intermediate situation exists. In terms of the above notation

$$A_{10} B_{20} a_{10} b_{20} = \left(\frac{b_{20} a_{10}}{D_0}\right)^2 = (1-\mu)^{-2},$$

furthermore,

$$-2 A_{10} B_{10} a_{10} a_{20} = 2 \gamma_1 \gamma_2 A_{10} B_{20} a_{10} b_{20} = \frac{2 \gamma_1 \gamma_2}{(1-\mu)^2}$$

$$-2 A_{10} B_{10} b_{10} b_{20} = 2 \gamma_1^2 A_{10} B_{20} a_{10} b_{20} = \frac{2 \gamma_1^2}{(1-\mu)^2}$$

$$-2 A_{20} B_{20} a_{10} a_{20} = 2 \gamma_2^2 A_{10} B_{20} a_{10} b_{20} = \frac{2 \gamma_2^2}{(1-\mu)^2}$$

$$-2 A_{20} B_{20} b_{10} b_{20} = 2 \gamma_1 \gamma_2 A_{10} B_{20} a_{10} b_{20} = \frac{2 \gamma_1 \gamma_2}{(1-\mu)^2}$$

It follows that

$$\frac{1}{\epsilon^2}\left(\frac{\delta t^*}{t}\right)^2 = 1 + \frac{2\gamma_1\gamma_2}{(1-\mu)^2} + \frac{2\gamma_1^2\gamma_0^2}{(1-\mu)^2}$$

$$\frac{1}{\epsilon^2}\left(\frac{\delta s^*}{s}\right)^2 = 1 + \frac{2\gamma_1\gamma_2}{(1-\mu)^2} + \frac{2\gamma_2^2}{\gamma_0^2(1-\mu)^2}$$

or

$$\frac{1}{\epsilon^2}\left(\frac{\delta t^*}{t}\right)^2 = 1 + \frac{2\mu}{(1-\mu)^2} + \frac{2\gamma^2}{(1-\mu)^2}$$

$$= 1 + \frac{2\mu}{(1-\mu)^2}\left[1 + \frac{\gamma^2}{\mu}\right]$$

$$\frac{1}{\epsilon^2}\left(\frac{\delta s^*}{s}\right)^2 = 1 + \frac{2\mu}{(1-\mu)^2} + \frac{2\mu^2}{\gamma^2(1-\mu)^2}$$

$$= 1 + \frac{2\mu}{(1-\mu)^2}\left[1 + \frac{\mu}{\gamma^2}\right]$$

These are the error expressions that have been sought.

Three limiting cases of the above error formulas are now considered.

Case $\mu \approx 1$: In this case the errors are largest since the measurements are only slightly independent. We have, approximately,

$$\left(\frac{\delta t^*}{t}\right)_{rms} = \frac{\epsilon\sqrt{2(1+\gamma^2)}}{(1-\mu)} \approx \frac{\epsilon\sqrt{2}}{1-\mu}$$

$$\left(\frac{\delta s^*}{s}\right)_{rms} = \frac{\epsilon}{1-\mu}\sqrt{2\left(1+\frac{1}{\gamma^2}\right)} \approx \frac{\epsilon\sqrt{2}}{\gamma(1-\mu)},$$

where the latter approximation is valid for $\gamma << 1$ (e.g., in the ocean). As a numerical example, assume small variations in the coefficients, $\epsilon = .01$, but the unfavorable value $\mu = 0.9$, and $\gamma = 0.1$, then

$$\left(\frac{\delta t^*}{t}\right)_{rms} = 0.14 = 14\ \%\ \text{error}$$

$$\left(\frac{\delta s^*}{s}\right)_{rms} = 1.4 = 140\ \%\ \text{error}\ .$$

The temperature measurements are of fair accuracy, but the salinity measurements are completely confused unless long term averaging methods (correlation techniques) are applied. Thus, in this case the TS-meter is of no value in separating the salinity and temperature signals even though ϵ is small. This trouble lies in the poor characteristics of the y_1 - and y_2 - measurements in that they differ only slightly from each other, and measure almost the same quantities.

Case $\mu \approx 0$: In this case, either one of the other (or both) of the y_1- and y_2 - measurements are specific. We have approximately

$$\left(\frac{\delta t^*}{t}\right)_{rms} \approx \epsilon\sqrt{1+2\gamma^2} \approx \epsilon$$

$$\left(\frac{\delta s^*}{s}\right)_{rms} \approx \epsilon\sqrt{1+2\left(\frac{\mu}{\gamma}\right)^2} \approx \frac{\epsilon\mu\sqrt{2}}{\gamma}\ ,$$

where the latter approximation assumes $2\mu^2 \gg \gamma^2$. If $2\mu^2 \ll \gamma^2$ then the error of the salinity measurement is about ϵ. As a numerical example, assume fairly large instability in the coefficients: $\epsilon = 0.1$ and $\gamma = 0.1$, $\mu = 0.1$ then

$$\left(\frac{\delta t^*}{t}\right)_{rms} = 0.1 = 10\ \%\ \text{error}$$

$$\left(\frac{\delta s^*}{s}\right)_{rms} = 0.17 = 17\ \%\ \text{error}\ .$$

In this case, both the temperature and salinity measurements are meaningful although the salinity measurements suffer somewhat additionally from the lack of specificity of the measurements.

Case $\mu = -1$: This case illustrates the errors which occur when the characteristics of y_1 and y_2 are "orthogonal" as described in a later paragraph. This is the next best thing to specificity if the latter cannot be had in two instruments. The errors are approximately

$$\left(\frac{\delta t^*}{t}\right)_{rms} \approx \epsilon\sqrt{\frac{1+\gamma^2}{2}} \approx \frac{\epsilon}{\sqrt{2}}$$

$$\left(\frac{\delta s^*}{S}\right)_{rms} \approx \epsilon\sqrt{\frac{1}{2}\left(1+\gamma^{\frac{1}{2}}\right)} \approx \frac{\epsilon}{\gamma\sqrt{2}} \quad ,$$

where the latter approximations assume $\gamma \ll 1$. We observe, here, the interesting fact that, in the case of orthogonal measurements, the lack of specificity is somewhat of an aid in reducing calibration errors ($\sqrt{2}$ factor) for the temperature measurements. This suggests that there is an optimum μ-value for a given ϵ. As a numerical example, assume $\epsilon = .05$ and $\gamma = 0.1$, then

$$\left(\frac{\delta t^*}{t}\right)_{rms} = .035 = 4\ \%\ \text{error}$$

$$\left(\frac{\delta s^*}{s}\right)_{rms} = 0.35 = 35\ \%\ \text{error} \quad .$$

The temperature measurements are good in this case, but the salinity measurements suffer appreciably from the relatively large temperature fluctuations assumed in this example.

All the cases above indicate that, while relatively good temperature measurements can be made in the ocean, the salinity measurements, at best, are only of modest accuracy. In a later paragraph it is shown how this situation can be considerably improved upon by a simple and continuous calibration technique. First, let us consider a geometrical interpretation of the quantities considered so far.

Geometrical Interpretation

The quantities actually measured are y_1 and y_2:

$$y_1 = a_1 t + b_1 s$$

$$y_2 = a_2 t + b_2 s \quad .$$

For a given value of y_1 or y_2 there is a whole range of values of t and s which produce the same signal. Let us plot two of these characteristic lines over the t-s plane as in Figure 4.1* .

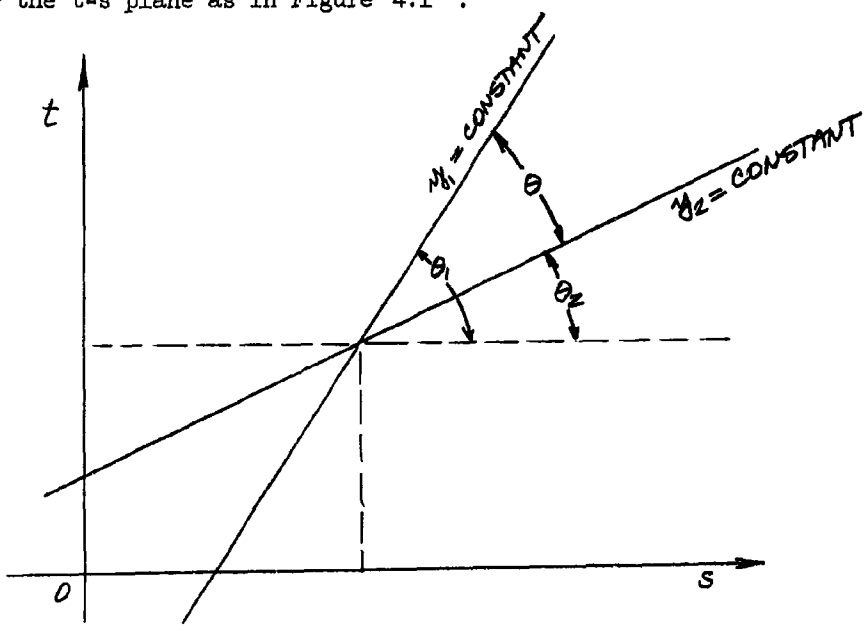

Figure 4.1 . Characteristic Lines of the TS-Meter

The average slope of the y_1 - characteristic line is

$$\frac{dt}{ds} = -\frac{b_{10}}{a_{10}} = \tan\theta_1 = -\gamma_1$$

and that of the y_2 - characteristic line is

$$\frac{dt}{ds} = -\frac{b_{20}}{a_{20}} = \tan\theta_2 = -\frac{1}{\gamma_2} \quad .$$

The y_1 - measurement is specific to temperature if $\theta_1 = 0$ ($b_1 = 0$), i.e., y_1 is independent of s. The y_2 - measurement is specific to salinity if $\theta = \pi/2$ ($a_2 = 0$), i.e., y_2 is independent of t. The parameter μ is

$$\mu = \left(\frac{a_{20}\, b_{10}}{a_{10}\, b_{20}}\right) = \gamma_1\gamma_2 = \frac{\tan\theta_1}{\tan\theta_2} \quad .$$

*The point of intersection of these two lines detemines the instantaneous t and s values.

This relation shows that if either y_1 is specific to temperature ($\theta_1 = 0$) or y_2 is specific to salinity ($\theta_2 = \pi/2$) or both, then $\mu = 0$, and conversely. The angle, θ, between the characteristic lines is $\theta = \theta_1 - \theta_2$, and

$$\tan(\theta_1 - \theta_2) = \frac{\tan\theta_1 - \tan\theta_2}{1 + \tan\theta_1 \tan\theta_2} = \tan\theta$$

or

$$\tan\theta = \frac{a_1 b_2 - a_2 b_1}{a_1 a_2 + b_1 b_2} = \frac{1-\mu}{\gamma_2 + \gamma_1}$$

If the two instruments are not independent $\mu = 1$, $\theta = 0$, and the characteristic curves intersect nowhere in the t-s plane. The characteristic lines are perpendicular if $\theta = \pi/2$ which occurs when

$$\gamma_1 = -\gamma_2 ,$$

in which case

$$\mu = -\gamma_1^2 = -\gamma_2^2 < 0 .$$

In this case the two measurements are said to be "orthogonal." The extreme case of orthogonal measurements occurs when

$$\mu = -1 ,$$

and

$$y_1 = a_1(t + s)$$

$$y_2 = b_2(s - t) .$$

Calibration Technique

A simple technique is available for calibrating the measurement with respect to temperature. A sharp pulse of electrical energy is dissipated in the water in the electrode volume. As a result, a known temperature rise occurs in the water. The coefficients of the linear combination of the measured signals are adjusted so that t^* exactly equals the known temperature rise and s^* shows zero response to the temperature pulse. This situation is illustrated in Figure 4.2 . The duration of the measured pulses in this Figure is of the order of the response time of the electrode. Adjustments are made to make the actual and ideal response coincide. The pulsing for calibration can be done occasionally in order not to interfere with the actual measurements, or, continuously and

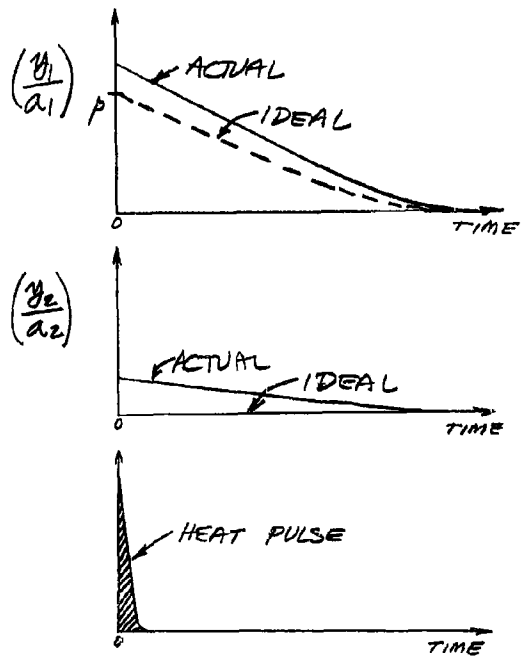

Figure 4.2 . Pulse Calibration

periodically at a frequency comparable with the cutoff frequency of the electrode (inverse response time). At the upper end of the pass band of the instrument the calibration signal would not interfere with the majority of the signals being observed. The heating can be in the form of repetative sharp pulses, but a simple sinusoidal heating signal is preferable.

A corresponding simple and direct method for calibration with respect to salinity is not available. The obvious method for calibrating, with respect to salinity, by injecting a solution of known salinity and temperature into the field of the electrode seems somewhat cumbersome for the class of instrumentation under discussion in this Report. This procedure may be used in precision salinometers based on a conductivity measurement for individual samples but is not suitable for continuous flow measurements.

This calibration technique is studied analytically as follows. Suppose the known pulse temperature rise is p. The corresponding outputs from the two instruments are

$$y_1 = a_1 p$$

$$y_2 = a_2 p \quad ,$$

where use has been made of the fact that this signal can be separated from those already occurring naturally, due to the t and s variations in the fluid medium, by appropriate filtering. Futhermore, the calibration temperature rise can be made much larger than the natural temperature variations. This is particularly true for differential microstructure measurements involving two sensing elements. The linear combination of the pulse signals are

$$t^* = A_1 a_1 p + B_1 a_2 p$$

$$s^* = A_2 a_1 p + B_2 a_2 p \quad .$$

The requirement is to adjust the coefficients (continuously) so that

$$t^* = p = \text{known}$$

and

$$s^* = 0 , \qquad \text{(null value)}$$

If the adjustments are made continuously, then, for all time, we know that the following equations hold

$$1 = A_1 a_1 + B_1 a_2$$

$$0 = A_2 a_1 + B_2 a_2 \ .$$

This being the case, we have

$$t^* = t + (A_1 b_1 + B_1 b_2) s$$

$$s^* = (A_2 b_1 + B_2 b_2) s \ .$$

This points up the important fact that now the s* output is specific to salinity, i.e., s* does not respond at all to changes in the temperature of the medium. It is important to note that specificity of the salinity measurement is insured even if only the later of the two conditions is valid (this condition is easier to achieve in practice since it requires a null measurement instead of an absolute measurement). The above calibration technique makes possible the measurement of salinity microstructure in the presence of relatively large temperature microstructure. Such a technique is well suited to measure small scale salinity microstructure in the ocean (with modest absolute accuracy) but probably not accurate enough for high quality absolute measurements of salinity.

The error analysis for measurements using this compensation technique is now given, but first we must decide how to adjust the four "knobs" to obtain the two condition equations given above. The two additional conditions on the coefficients of the linear combination will be chosen by requiring that the coefficients which experience the least variation will be set to their respective average ideal values. This, provided it does not conflict with the above condition equations (e.g., it is not possible to hold both A_2 and B_2 constant, or A_1 and B_1 constant). To calculate the mean-square variations in $\hat{A}_1 \hat{B}_1 \hat{A}_2 \hat{B}_2$, assume that the mean-square fractional variations in the coefficients $a_1 b_1 a_2 b_2$ are all the same and equal to ϵ. The corresponding variations of the ideal linear combination coefficients can be shown with some manipulation to be

($\epsilon << 1$)

$$\left(\frac{\delta\hat{A}_1}{\hat{A}_{10}}\right)_{rms} = \left(\frac{\delta\hat{B}_2}{\hat{B}_{20}}\right) = \frac{\epsilon\sqrt{3+\mu^2}}{1-\mu}$$

and

$$\left(\frac{\delta\hat{A}_2}{\hat{A}_{20}}\right)_{rms} = \left(\frac{\delta\hat{B}_1}{\hat{B}_{10}}\right) = \frac{\epsilon\sqrt{1+3\mu^2}}{1-\mu} .$$

For all values of $\mu(0 \leq \mu^2 \leq 1)$ the first of these expressions is the larger. Consequently, the conditions we impose are

$$A_2 = \hat{A}_{20} = A_{20} \quad \text{and} \quad B_1 = \hat{B}_{10} = B_{10} ,$$

i.e., these "knobs" are permanently set at the average ideal values. These conditions are compatible with the previous condition equations, which now become

$$1 = A_1 a_1 + B_{10} a_2$$

$$0 = A_{20} a_1 + B_2 a_2 .$$

Solving these equations for A_1 and B_2 we get

$$A_1 = \frac{1 - B_{10} a_2}{a_1}$$

and

$$B_2 = -\frac{A_{20} a_1}{a_2} .$$

The corresponding t* and s* signals are

$$t^* - t = \left(\frac{b_1 + D B_{10}}{a_1}\right) s$$

$$s^* = -\left(\frac{A_{20} D}{a_2}\right) s$$

or

$$t^* - t = \left(\frac{B_{10} - \hat{B}_1}{\hat{B}_1}\right) \cdot \left(\frac{\hat{B}_1}{\hat{B}_2}\right) s$$

$$s^* - s = \left(\frac{A_{20} - \hat{A}_2}{\hat{A}_2}\right) s \quad .$$

Taking mean-square values and using previous expressions we get

$$\left(\frac{\delta t^*}{t}\right)_{rms} = \frac{\epsilon\gamma\sqrt{3+\mu^2}}{1-\mu}$$

$$\left(\frac{\delta s^*}{s}\right)_{rms} = \frac{\epsilon\sqrt{1+3\mu^2}}{1-\mu} \quad .$$

It is important to note that, as a result of this calibration process, no γ appears in the errors for s*, i.e., temperature fluctuations of the medium do not produce spurious s* signals. As a numerical example, take $\gamma = 0.1$, $\mu = 0.4$ and $\epsilon = .05$, then

$$\left(\frac{\delta t^*}{t}\right)_{rms} = .015 = 2\ \%\ \text{error}$$

$$\left(\frac{\delta s^*}{s}\right)_{rms} = 0.1 = 10\ \%\ \text{error} \quad .$$

The errors in the salinity measurement are due only to fluctuations in the constant or proportionality and contains no error (to first order) associated with the temperature variations of the medium.

The means for improving on the above accuracy of the salinity measurement is, as mentioned before, to expose the electrode volume to a solution of known salinity and temperature. One consequence of the heat pulse calibration scheme is, however, that now the condition on the calibration solution that its temperature be known can be relaxed. Since s* does not now respond to temperature changes, this condition is no longer necessary. This greatly improves the prospects of a practical method for also calibrating with respect to salinity, in which case the above errors in s* can be improved upon.

TS-Meter at Radar Frequency

As a practical example of an instrument based on the TS-meter principle, let us consider the impedance of an electrode at very high frequency where the shunt volume capacity has an impedance of the order of the volume resistance. It is shown that it is possible, by operating at a certain frequency, to make a specific measurement of either salinity or temperature because of the particular behavior of the salinity and temperature coefficients of the electrode impedance.

The electrode impedance has the equivalent circuit shown in Figure 4.3 at very high frequency. The impedance, z, is given by

$$z = R + iX$$

where the resistive part, R, is

$$R = \frac{r}{1 + k^2} ,$$

and the reactive part, X, is

$$X = \frac{-kr}{1 + k^2}$$

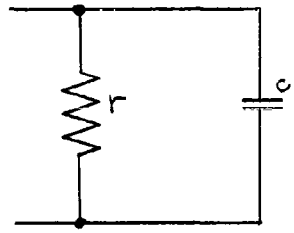

Figure 4.3 .
Electrode Impedance

and $k = r\omega c$. The impedance phase angle, ϕ, is

$$\tan \phi = \frac{X}{R} = -k = -r\omega c .$$

Suppose the resistance and capacity depend on a variable, ξ, such as temperature and/or salinity. The fractional derivatives of R and X are

$$\beta_R \equiv \frac{1}{R}\left(\frac{\partial R}{\partial \xi}\right) = \beta_r - \left(\frac{2k^2}{1+k^2}\right)(\beta_r + \beta_c)$$

and

$$\beta_X \equiv \frac{1}{X}\left(\frac{\partial X}{\partial \xi}\right) = \beta_r + \left(\frac{1-k^2}{1+k^2}\right)(\beta_r + \beta_c) ,$$

where

$$\beta_r = \frac{1}{r}\left(\frac{\partial r}{\partial \xi}\right) \quad \text{and} \quad \beta_c = \frac{1}{c}\left(\frac{\partial c}{\partial \xi}\right).$$

It is apparent from these relations that the salinity and temperature coefficients of the resistive and reactive components of the electrode impedance are functions of the frequency dependent phase factor k.

The temperature and salinity fluctuations of the fluid medium are measured by means of measurements of the fluctuations of the resistance, R, and reactance, X. Is there a value of k for which these measurements are specific? To evaluate whether such a situation exists, let us assume we are dealing with sea water which has the following coefficients at 20°C and 35 ‰ (Sec. 2.3)

$$\beta_{rT} = \frac{1}{r}\left(\frac{\partial r}{\partial T}\right) = -2.14\% \text{ PER °C} \qquad \beta_{rs} = \frac{1}{r}\left(\frac{\partial r}{\partial s}\right) = -2.55\% \text{ PER ‰}$$

$$\beta_{cT} = \frac{1}{c}\left(\frac{\partial c}{\partial T}\right) = -0.51\% \text{ PER °C} \qquad \beta_{cs} = \frac{1}{c}\left(\frac{\partial c}{\partial s}\right) = -0.27\% \text{ PER ‰}$$

To find if such a condition exists for the reactive component (for either temperature or salinity changes) set

$$\beta_x = \frac{1}{x}\left(\frac{\partial x}{\partial \xi}\right) = 0$$

or

$$-\left(\frac{1-k^2}{1+k^2}\right) = \left(\frac{\beta_r}{\beta_r+\beta_c}\right).$$

If such a value of k exists, this group of coefficients must lie between ± 1. For temperature and salinity, respectively, this group is

$$\frac{\beta_{rT}}{\beta_{rT}+\beta_{cT}} = \frac{2.14}{2.14+0.51} = 0.807$$

$$\frac{\beta_{rs}}{\beta_{rs}+\beta_{cs}} = \frac{2.55}{2.55+0.27} = 0.905 .$$

Thus, values of k exist for which specific measurements of both temperature and salinity may be made. The corresponding values of k are

$k_{xs} = 3.06$ (independent of temperature)

$k_{xT} = 4.48$ (independent of salinity) .

The salinity coefficient of the reactance in the first case ($k = k_s$) is

$$\beta_{xs} = \frac{1}{X}\left(\frac{\partial X}{\partial S}\right) = \frac{\beta_{rs}\beta_{cT} - \beta_{rT}\beta_{cs}}{\beta_{rT} + \beta_{cT}} = -0.27\% \text{ PER } ‰ .$$

The temperature coefficient of reactance in the latter case ($k = k_T$) is

$$\beta_{xT} = \frac{1}{X}\left(\frac{\partial X}{\partial T}\right) = \frac{\beta_{rT}\beta_{cs} - \beta_{rs}\beta_{cT}}{\beta_{rs} + \beta_{cs}} = -0.26\% \text{ PER } ^\circ C .$$

We now seek values of k for which the coefficients of the resistance satisfy

$$\beta_R = \frac{1}{R}\left(\frac{\partial R}{\partial S}\right) = 0$$

or

$$\frac{2k^2}{1+k^2} = \frac{\beta_r}{\beta_r + \beta_c} .$$

If such a value of k exists, this group of coefficients must lie between zero and two. We saw above that this is the case. The corresponding values of k are

$k_{RS} = 0.821$ (independent of temperature)

$k_{RT} = 0.909$ (independent of salinity) .

The salinity coefficient of resistance in the first case ($k = k_s$) is

$$\beta_{RS} = \frac{1}{R}\left(\frac{\partial R}{\partial S}\right) = \left(\frac{\beta_{rs}\beta_{cT} - \beta_{rT}\beta_{cs}}{\beta_{rT} + \beta_{cT}}\right) = -0.27\% \text{ PER } ‰$$

The temperature coefficient of resistance in the latter case ($k = k_T$) is

$$\beta_{RT} = \frac{1}{R}\left(\frac{\partial R}{\partial T}\right) = \frac{\beta_{rT}\beta_{cs} - \beta_{rs}\beta_{cT}}{\beta_{rs} + \beta_{cs}} = -0.26\% \text{ PER } ^\circ\text{C}.$$

These are precisely the same as the corresponding coefficients of reactance at k_{cx} and $k_{T,x}$. The relation between the values of k for resistance and reactance is

$$k_R^2 = \frac{k_X^2 - 1}{k_X^2 + 3}.$$

The requirement of a certain value for k is really a condition on the operating frequency of the instrument

$$k = r\omega c = \left(\frac{\omega K K_0}{\sigma}\right),$$

where K is the dielectric constant of the water, K_0 is the dielectric constant of free space ($K_0 = 8.85 \times 10^{-12}$ farad/meter) and σ is the conductivity of water. It is important to note that this is independent of the electrode geometry but it <u>is</u> dependent on the properties of the medium (which, in turn, depend on the temperature and salinity). The operating frequency, f, is

$$f = \frac{k\sigma}{2\pi K K_0} = kf_0$$

where

$$f_0 = \frac{\sigma}{2\pi K K_0}.$$

For sea water at 20°C and 35 ‰ the dielectric constant and conductivity are (Sec. 7.2)

$$K = 73.8$$
$$\sigma = 4.79 \text{ ohms}^{-1}\text{meter}^{-1}$$

and

$$f_0 = 1.17 \text{ kmc}.$$

The operating frequencies, corresponding to these values, for the respective values of k are listed in Table 4.1 .

Table 4.1 . TS-Meter Operating Frequencies in Sea Water

k / f	Measure Temperature	Measure Salinity
Measure Resistance	0.909 1062 mc	0.821 961 mc
Measure Reactance	4.48 5.24 kmc	3.06 3.58 kmc

These are well separated, from the practical standpoint, and correspond to ordinary radar frequencies. The availability of electronic components is good at this frequency because of the developments of radar equipment.

The operating frequencies in tap water with conductivity about 1/100 that of sea water and dielectric constant of about 80 lie in the radio frequency range:

$$f_o \approx 11 \text{ mc} .$$

A word of caution concerning the fact that the electrode element can be made specific to either temperature or salinity is necessary. This technique involves the same errors as were considered before in the error analysis for the general TS-meter since the β-coefficeints of the electrode also vary with the properties of the medium. We may look on this technique as an intrinsic example of the TS-meter principle applied to the sensing element itself, without the addition of external and auxiliary electrical networks to perform the desired linear combinations to obtain pure temperature and/or salinity signals. The intrinsic μ-value of the sensing element may be defined as

$$\mu_{INTRINSIC} = \left(\frac{\beta_{RT}\,\beta_{CS}}{\beta_{RS}\,\beta_{CT}}\right) = 0.445 ,$$

where the numerical value corresponds to that of sea water.

A fundamental problem lies in establishing exactly at what fre-

quency the measurements are independent of either temperature (f_s) or salinity (f_T). Continuous adjustments are required since these discrete values of frequency change with the salinity and temperature of the medium:

$$f = \frac{k(T,S)\,\sigma(T,S)}{2\pi K_0\, k(T,S)}$$

For the measurement of salinity, it is clear that the simplest and most effective way of locating f_s precisely and continuously is by means of the heat pulse calibration technique outlined previously.

It is a novel feature of this instrumentation that by just merely tuning the frequency of the electrical power one can change from a temperature measuring device (at f_T) to a salinity measuring device (at f_S). Thus, by an appropriate automatic time sharing procedure, in which the operating frequency is very rapidly switched between f_T and f_S, the one instrument provides simultaneously independent measures of the temperature and salinity fluctuations.

5. VELOCITY DETECTOR

The measurement of the flow velocity of water by means of an electrolytic conductivity measurement is studied in this Section. Instrumentation based on this principle of velocity measurement will be termed a "U-meter" for brevity sake. The characteristics of a U-meter are compared with those of a hot-wire anemometer in water at the end of this Section in order to evaluate the relative merits of the new technique of velocity measurement.

5.1 Concept

A more detailed description of the basic concepts underlying the operation of the U-meter is appropriate. The process of measurement consists of three steps: 1) velocity dependent temperature rise due to heating, 2) electrical heating of the conducting medium, and 3) temperature dependence of the electrical conductivity. These three processes take place simultaneously at one and the same location, i.e., in the water itself.

The first of these processes was used by Thomas (1) for the measurement of gas flow velocity but the method applies equally well to the measurement of any fluid flow. The method is illustrated in Figure 5.1 where a gas is shown flowing in a pipe past an input thermometer, a heating element, and an output thermometer, in that order.

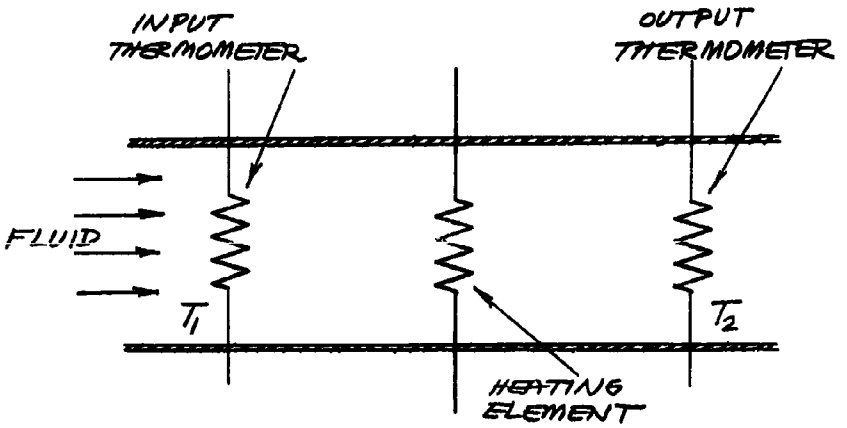

Figure 5.1 . Thomas Method of Velocity Measurement

The gas enters at a temperature T_1, is then heated by a source which is dissipating heat energy at a rate, P, and then leaves at a temperature, T_2, after being heated. If the input and output temperatures are measured by thermometers, and the amount of input heating power is known, then the flow rate of the gas can be determined from the relation

$$P = cAU(T_2 - T_1) \quad ,$$

where c is the heat capacity per unit volume of the gas, A is the cross sectional area of the pipe, and U is the average flow velocity. The volumetric flow rate is just AU. For a given input power the measured temperature rise $(T_2 - T_1)$ varies inversely with velocity, thus, the temperature increases as the velocity decreases. The Thomas method illustrates the basic idea of measuring fluid velocity by measuring a known and artificially produced temperature rise in the flowing medium.

The second process involves the means of heating the flowing medium. Instead of heating the fluid by its contact with a heated surface, as done by Thomas, the medium may be heated internally by Joule electrical heating if it has an appreciable electrical conductivity. Such a method was devised by Rein (2) for measuring the flow velocity of blood in animal experiments. This method of based on that of Thomas, however, the flowing medium can be heated approximately uniformly without using heating elements which obstruct the flow. This situation is illustrated in Figure 5.2 . The steady state temperature rise is measured by means of

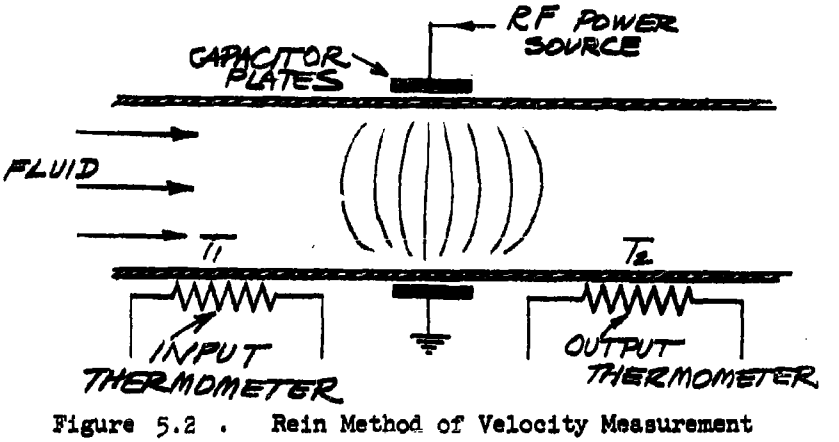

Figure 5.2 . Rein Method of Velocity Measurement

temperature sensitive elements in contact with the walls of the tube. Heat is supplied to the conducting fluid by the RF field generated between

the plates of a capacitor which surround the tube. The response time of such a system is poor as a consequence of the long time required for heat to be transferred by conduction through the walls of the tube to the thermometers. Electrical heating can also be accomplished by direct electrical conduction by placing electrodes on the inner walls of the tube where it is in electrical contact with the flowing medium. Induction coupling may be used (induction heating).

The third process pertains to the fact that the electrical conductivity of an electrolyte solution depends on its temperature. This fact has been taken advantage of by Craig (3) in order to measure temperatures in a way analogous to the resistance-wire thermometer but uses the temperature coefficient of an electrolyte rather than that of a wire. This idea was discussed in detail in Section 2.3 where it was found that the temperature of a flowing liquid of finite conductivity could be measured by means of electrodes in contact with the fluid. It was shown there that, the resistance, R, of the electrode is related to the temperature, T, of the fluid by

$$R = R_o \left\{ 1 - \beta_T (T - T_o) \right\} \quad ,$$

where R_o is the resistance at the temperature T_o, and β_T is the temperature coefficient of conductivity of the medium.

The essence of the concept of the U-meter is that the above three processes can be combined into a single sensing electrode which simultaneously heats the fluid, measures its temperature and hence determines the fluid velocity. This situation is shown in Figure 5.3 . The fluid enters at temperature T_1 and leaves at temperature T_2 after being heated at a rate, P, by electrical currents which flow in the medium from the immersed electrodes. The resistance of the electrodes is measured simultaneously by means of a bridge network.

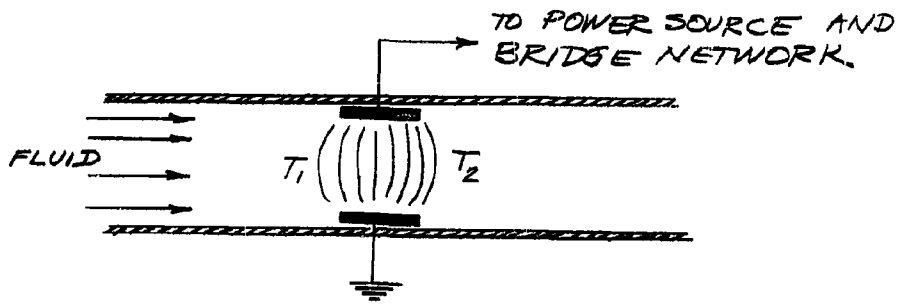

Figure 5.3 . U-Meter Method of Velocity Measurement

The temperature rise and velocity are related, as with the Thomas method, by

$$P = cAU(T_2 - T_1) \quad .$$

The average temperature of the fluid in the electrode volume is

$$T_1 + \frac{T_2 - T_1}{2} \quad ,$$

and the electrode resistance is

$$R = R_o \left\{ 1 - \beta_T \left(\frac{T_2 - T_1}{2} \right) - \beta_T (T_1 - T_o) \right\} \quad .$$

Combining the above relations we obtain

$$\left(\frac{R - R_o}{R_o} \right) = - \frac{\beta P}{2cAU} - \beta_T (T_1 - T_o) \quad .$$

This method differs from the previous one discussed in one important respect, viz., only one temperature measurement is made. As a consequence, the velocity measurement is subject to errors due to temperature fluctuations of the medium.* This effect is reduced by operating at high power in order to cause a large temperature rise in the electrode volume. Neglecting temperature fluctuations of the medium, resistance-velocity relation becomes

$$\left(\frac{R - R_o}{R_o} \right) = - \frac{\beta_T P}{2cAU} \quad .$$

There is considerable similarity between this type of sensor and the hot-wire anemometer. The similarity lies in the use of electrical techniques to measure resistance changes of a temperature sensitive element which is heated electrically. The major dissimilarities are: 1) the medium itself is used as the sensing element instead of a wire, and 2) heat transfer is by direct transport of the medium instead of cooling. The latter difference is responsible for an improved response time of the U-meter.

5.2 Related Electrochemical Methods

Several methods are described below which make use of electrolytic conductivity to measure the velocity of solutions. These methods, however,

---

*An identical unheated electrode located upstream is suitable for measuring T_1 to avoid this problem.

depend for their operation on special electrochemical effects, whereas the present detector is based on the simple mechanism of Joule heating by an electric current in a conducting medium.

It has long been known that the direct current resistance of an electrode immersed in an electrolyte varies with the movement of the electrolyte. Apparently the first attempt to measure fluid velocities by means of an electrolytic conductivity measurement was reported in 1917 by Cleverdon (4) - he asked "Can the velocity of water be measured by passing an electric current through it?" It was observed that the resistance between two electrodes immersed in water increased as the flow of water increased as shown in Figure 5.4 . Direct current was used in these tests and it was emphasized that the results of the measurement were very erratic and changed in an unpredictable way with experimental conditions. The explanation of these results is not clear. If the effect is due to an electrochemical effect based on velocity dependent electrolyte concentration gradients, then the resistance should have decreased with increasing velocity. If a heating effect is operative, the resistance should increase with increasing velocity as observed, however, the electrical currents and voltages involved seem to be too low (about a milliwatt) to account for the observed effect.

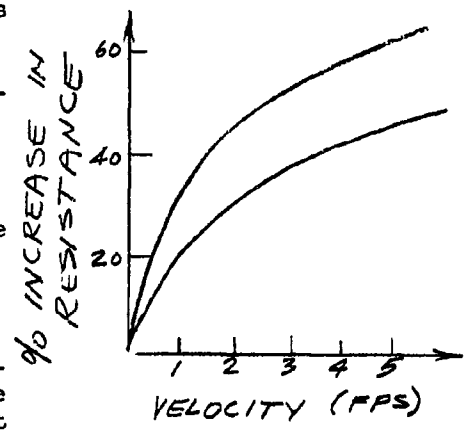

Figure 5.4 . Cleverdon Velocity Measurement

Boyer and Lonsdale (5,6) studied a probe for measuring low water velocities (fraction of a knot) by electrolytic means. The current flowing between small electrodes with an applied dc voltage is shown to vary as the square root of the velocity of the fluid. An example of the velocity characteristic of the probe is shown in Figure 5.5 . The electrical power involved in these measurements amounts to a fraction of a milliwatt. The authors ascribe the operation of the sensor to an unknown combination of complex electromechanical phenomena, presumably the main one being a dissolved oxygen reaction at the cathode.

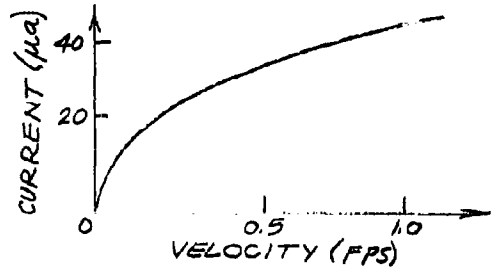

Figure 5.5 . Boyer and Lonsdale Velocity Measurement

Ranz (7) describes an electrolytic method for measuring water velocities. The operation of the sensor is based on a convection-controlled mass transfer process in which the rate of mass transfer results in an electrical signal across the probe. It is also stated that the response time seems to be comparable with, or better than, hot-wire detectors because "the measuring probe has no capacity for the transferred quantity." In water, these processes are possible whenever electrolysis occurs under conditions of concentration polarization (8,9), and they exist in relatively uncomplicated form as the limiting currents in polarographic analysis (10).

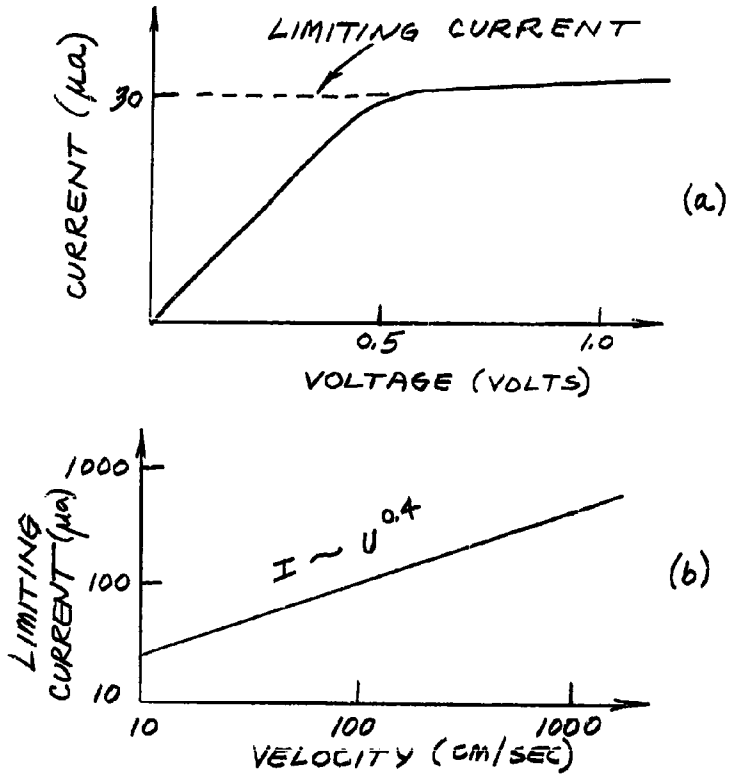

Figure 5.6 . Ranz Velocity Measurement

The typical dc current-voltage characteristic of a probe as shown in Figure 5.6a and Figure 5.6b illustrates the observed current - velocity characteristic. The power dissipated at the electrode is of the order of a small fraction of a milliwatt.

Eskinazi (11) describes the results of velocity measurements based on an electrolytic conductivity measurement. A dc current flows between

two small closely spaced electrodes and the resultant voltage across the electrodes shows the following velocity dependence: voltage = velocity^2 + constant. The electrode power amounts to only a small fraction of a milliwatt (20μa at 1 volt). The following statement was made concerning the origin of the effect: "The narrow electrical passage in the electrode gap is distorted by the velocity of the medium that flows through the gap. The velocity of the medium increases the length of the electrical path between the electrodes and consequently increases the overall resistance of the gap." It will be remembered that Cleverdon (4) also found an increase in electrode resistance with an increase in fluid velocity.

The topic of the variation of limiting direct currents in electrolyte solutions which is associated with the rate of mass transfer at electrodes is studied in detail in the book by Delahay (12).

5.3 Description and Theory

In this Section the operation of the U-meter is studied in greater detail.

The sensing element of the U-meter is the water itself. Water of finite electrical conductivity is heated by the electrical current which flows in it as it passes through the field of a small electrode. The resultant temperature rise of the water depends on its duration in the vicinity of the electrodes and, therefore, on the fluid velocity. The electrical resistance between the electrodes and/or the conductivity of the flowing medium depends on its temperature and, consequently, on the velocity of the water. Thus, velocity variations give rise to electrode resistance variations which are measurable by electronic equipment.

Electrode Resistance

The electrical resistance of electrodes immersed in an electrolyte solution depends on the temperature of the solution and provides the basic means for translating the velocity dependent temperature of the flowing aqueous solution into an electrically measurable quantity. The electrode resistance may be expressed as follows over the practical range of interest from 0° C to 100° C (boiling):

$$R = R_o \left\{ 1 - \beta(T - T_o) + \gamma (T - T_o)^2 \right\} ,$$

where R_o is the electrode resistance at the reference temperature T_o, and β and γ are the linear and quadratic temperature coefficients of the conductivity of the solution*. For most electrolyte solutions β is of the order of 2 % per °C. For sea water of 35 ‰ salinity at 20° C:

$$\beta = .021\ ^{\circ}C^{-1} \quad \text{and} \quad \gamma = 3.9 \times 10^{-4}\ ^{\circ}C^{-2} .$$

*See Addendum No. 1.

A rough measure of the non-linearity of the temperature dependence of the electrode resistance is that temperature rise $(T_N - T_o)$ where the changes of resistance of the linear and quadratic terms are equal:

$$T_N - T_o = \frac{\beta}{2\gamma} \approx 28\ ^{\circ}C\ ,$$

which for sea water occurs at about 28 °C. Actually, the non-linearity is appreciable for temperature changes considerably less than this. The non-linearity is, thus, not small and must be considered for large temperature changes. In particular, it is much larger than the non-linearity of typical resistance wires.

For small temperature changes $\Delta T = T - T_o$, where only the linear term is important

$$R = R_o \left[1 - \beta \Delta T\right]$$

or

$$\frac{\Delta R}{R_o} = -\beta \Delta T = -\alpha\ ,$$

where $\Delta R = R - R_o$ and $\alpha = \beta \Delta T$. If the non-linearity of the resistance is included, this expression becomes

$$\frac{\Delta R}{R_o} = -\alpha\left(1 - \frac{\gamma}{\beta^2}\alpha\right).$$

For sea water the coefficient of the non-linear term is approximately

$$\frac{\gamma}{\beta^2} = 0.86\ .$$

The average value of ΔT termed the "over temperature" and $T_o + \Delta T$ the "operating temperature."

Heat Transfer Equation

Fundamental to the operation of the U-meter is the relation between the rate at which heat is generated by electrical energy and the fluid velocity. The heat transfer takes place primarily by forced convection of the internally heated fluid, and transfer by conduction, free convection and radiation are usually small. The heat transfer equation is discussed in detail in Section 12.5 . The forced convection term is

$$P = 2cAU\sqrt{\Delta T}\ ,$$

where P is the input in electrical power to the water, c is the heat capacity per unit volume of the water, A is the "frontal area" of the electrode, U is the fluid velocity, and $\overline{\Delta T}$ is the average temperature rise throughout the electrode volume (Sec. 12.1). This expression is approximately valid over the range of Péclet number greater than ten ($P_R > 10$).

If I is the (rms) current to the electrode, the heat transfer equation is

$$I^2R = 2cAU\overline{\Delta T} \quad .$$

Combining this with the (linear) resistance equation, we obtain

$$\frac{I^2R}{R - R_o} = -BU \quad .$$

where

$$B = \frac{2cA}{\beta R_o} \quad .$$

This expression is analogous to the corresponding equation for the hot-wire anemometer but with a different velocity dependence. Because of the difficulty of calculating the frontal area of a given electrode, the parameters of the above equation are best obtained by experimental calibration. The velocity dependence of the above equation is shown in Figure 5.7 along with the same quantity for the hot-wire anemometer. The dynamic pressure as measured by a pitot tube is included for comparison.

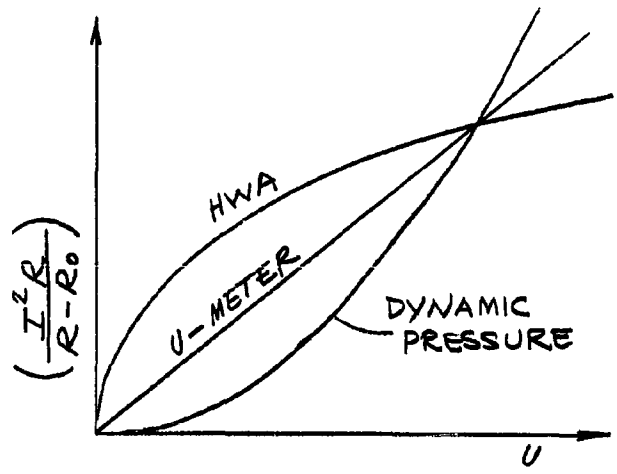

Figure 5.7 . Velocity Calibration Curves

Electronic Equipment

A simplified electronic arrangement for the U-meter is shown in Figure 2.1 . The electrode sensing element constitutes one arm of a wheatstone bridge. Variations of resistance due to velocity variations produces a voltage across the voltmeter, thus, providing a means for measuring the changes of velocity. A source of alternating current is utilized to heat the water because of troublesome problems associated with electrolysis at the electrodes when direct current is used. As with the hot-wire anemometer, the associated electronics of the velocity detector may be operated in several ways, two of the most important being a) constant current operation (CCO) shown in Figure 5.8 and b) constant-temperature operation (CTO) shown in Figure 5.9 . In the CCO mode the current is held constant and the resultant resistance variations are detected as voltage fluctuations across the electrodes. In the CTO mode, which also implies constant-resistance-operation (CRO), the heating current is automatically adjusted to hold the temperature (or resistance) constant and the resultant heating current fluctuations reflect the changes in velocity.

Sensitivity

The sensitivity to velocity variations is defined as the magnitude of the factor of proportionality between the velocity fluctuations, ΔU, and the consequent fluctuations in voltage, ΔV, across the electrode resistance.

In the constant-current mode, differentiation of the following equations for constant current, I:

$$\frac{I^2 R}{R - R_0} = - \frac{2cAU}{\beta R_0}$$

$$V = IR$$

yields the sensitivity

$$\left(\frac{\Delta V}{\Delta U}\right) = \alpha^2 \left(\frac{2cAU}{\beta I^2 R_0}\right) \cdot \left(\frac{I R_0}{U_0}\right) .$$

Expressing I in terms of α, it follows that

$$\left(\frac{\Delta V}{\Delta U}\right) \sim \alpha^{3/2} \sqrt{1 - \alpha} .$$

In the constant-temperature mode, the sensitivity is obtained in a similar manner, but, with the resistance held constant. The sensitivity

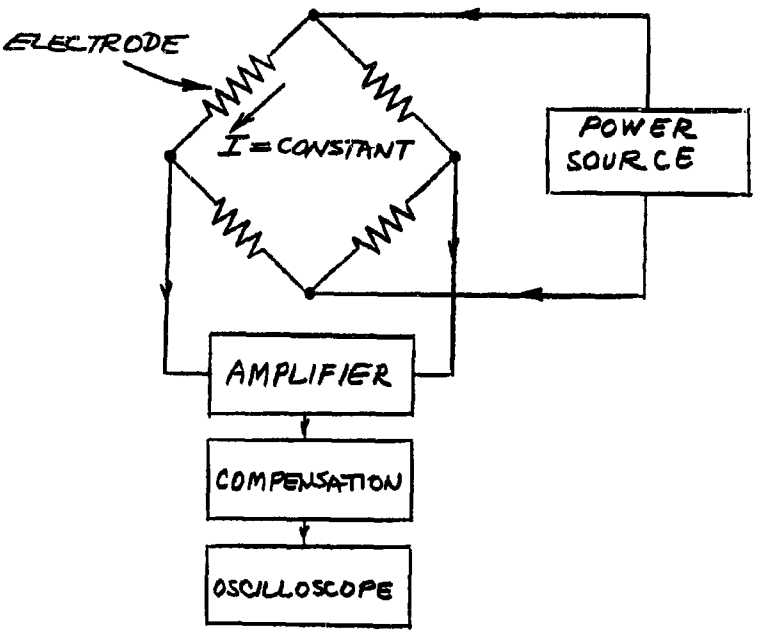

Figure 5.8 . Constant-Current-Operation

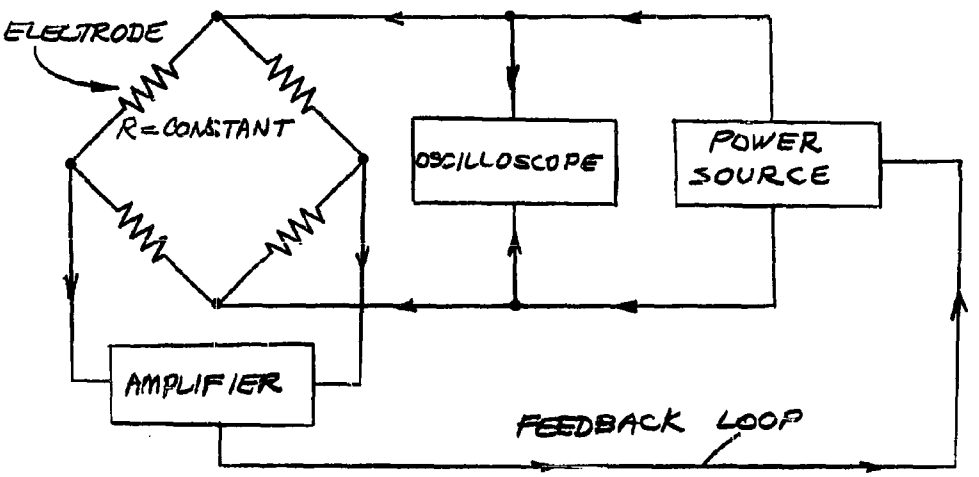

Figure 5.9 . Constant-Temperature-Operation

in this case is

$$\left(\frac{\Delta V}{\Delta U}\right)_{CTO} = \frac{1}{2}\alpha\left(\frac{2CAU_o}{\beta I^2 R_o}\right)\left(\frac{IR_o}{U_o}\right)$$

and the dependence on α is

$$\left(\frac{\Delta V}{\Delta U}\right)_{CTO} \sim \sqrt{\alpha(1-\alpha)}$$

or

$$2\alpha\left(\frac{\Delta V}{\Delta U}\right)_{CTO} = \left(\frac{\Delta V}{\Delta U}\right)_{CCO}$$

Since α is, at best, about 0.4 for typical aqueous electrolyte solutions (without boiling at the electrodes) it follows that the sensitivity in the CCO mode is always less than that in the CTO mode.

Constant Power Operation

The above analysis adheres to the customary analysis for hot-wire anemometer. Frequently it is necessary to operate the U-meter at very high power where the efficient transfer of electrical energy from the power source to the electrode is important. This is achieved when the source resistance equals the electrode resistance, i.e., the source is matched to the electrode. This arrangement corresponds to constant-power-operation. This case is analysed below and includes the correction for the non-linearity of the resistance which was not included in the above sensitivity formulas.

The electrode resistance is

$$R = R_o\left\{1 - \beta\Delta T + \gamma\Delta T^2\right\} \quad ,$$

and the small change in resistance δR caused by a small change $\delta\Delta T$ in the average electrode temperature rise is given by

$$\frac{\delta R}{R_o} = -\beta\,\delta\Delta T + 2\gamma\,\Delta T\cdot\delta\Delta T$$

$$= -\alpha\left(1 - \frac{2\gamma\alpha}{\beta^2}\right)\left(\frac{\delta\Delta T}{\Delta T}\right)$$

where $\alpha = \beta\Delta T$. The average electrode temperature is related to the

electrode power, P, by

$$\Delta T = \frac{P}{2c\lambda U} ,$$

and a small change in this temperature due to a change, δU, in the velocity satisfies

$$\frac{\delta \Delta T}{\Delta T} = -\left(\frac{\delta U}{U}\right) .$$

Combining the above relations, and retaining only terms to the 2nd order in α

$$\frac{\delta R}{R_o} = +\alpha \left(\frac{\delta U}{U}\right) \cdot \left(\frac{1-2k\alpha}{1+\alpha}\right)$$

where for sea water

$$k = \frac{\nu}{\beta^2} \approx 0.86 .$$

Frequency Response

Since the velocity measurement does not depend on a cooling effect, as with the hot-wire anemometer, the frequency response is determined primarily by the physical size of the electrode. This topic is considered in detail in Section 14 . It was pointed out in an earlier Section that the bandwidth, Δf, of the velocity measurement is approximately*

$$\Delta f = \frac{1}{2\pi}\left(\frac{U}{h}\right) ,$$

where h^{-1} is the cell constant of the electrode. An electrode with a typical dimension of 1 mm (h = 0.1 cm) moving at 10 knots (U = 514 cm/sec) measures velocity fluctuations over an 820 cps bandwidth.

Additional Effects

Several other aspects of the U-meter are now mentioned briefly. The presence of the velocity and thermal boundary layers at the electrode surfaces modifies the response characteristics of the velocity detector.

*A more realistic condition is $\Delta f = \frac{1}{2}\left(\frac{U}{h}\right)$. See Section 14.

This effect is similar to the "end effect" in the case of the hot-wire anemometer and is studied in detail in Section 14.4 . The problem of errors in the velocity measurements due to temperature fluctuations in the medium is analysed in Section 8.3 . The non-linearity of the resistance-temperature characteristic is studied in Section 12.6 and the response of the U-meter to non-uniform velocities over the sensing volume of the electrode is analysed in Section 14.1 .

5.4 Hot-Wire Anemometer

In this Section a review of the hot-wire anemometer (HWA) will be made both as background information which is particularly useful because of the similarity with the U-meter and to develop formulas which will allow direct comparisons with the U-meter. Practically all of the concepts of the hot-wire anemometer carry over directly to the electrode velocity detector. This review is based primarily on the excellent general introductory articles by Hinze (13) and Kovasznay (14). Several others may be consulted for references to all aspects of the hot-wire anemometer (15,16,17,18).

The hot-wire anemometer is the principal tool for turbulence research today. The detecting element of a hot-wire anemometer consists of a fine wire which is heated by an electrical current and cooled by the flowing medium. The resistance of the wire depends on its temperature which, in turn, is determined by the fluid velocity. Thus, velocity variations give rise to resistance variations which are measured by electronic instrumentation.

The earliest work (1894) on the hot-wire concept for air velocity measurement appears to be due to Weber (19) and Oberbeck (20). It was not for almost two decades that a number of investigators turned to the development of this instrument for air flow measurements in aerodynamic research (1912). The first systematic study (1914) of the basic principle of the hot-wire anemometer, i.e., the loss of heat from wires (cylinders) in a flowing fluid, was carried out both theoretically and experimentally by King (21). The realization that the response time of the detector could be improved artificially by electronic compensation techniques was first accomplished (1928) by Dryden and Kuethe (22,23). The idea and advantages of maintaining the wire at a constant temperature by a feedback system was advocated in 1934 by Ziegler (24). Since that time the hot-wire anemometer has been widely developed in all aspects of its use, and has found application in airflow measurements from the very lowest velocities (25) to supersonic speeds (26). The use of this instrument in water has been slow to develop since the work in 1929 of Richardson (27); the first application was made about 1947. A similar device, using a hot-film instead of a hot-wire, was advanced by Ling in 1955 and has been found more useful for measurements in water (28).

The properties of the hot-wire anemometer are analysed in the following paragraphs.

Wire Resistance

The electrical resistance of a wire depends on its temperature as follows:

$$R = R_o \left\{ 1 + \beta(T - T_o) + \gamma (T - T_o)^2 \right\} \quad ,$$

where R_o is the resistance at temperature T_o, T is the temperature of the wire, and β and γ are the linear and quadratic temperature coefficients of resistance of the wire. For tungsten:

$$\beta = 5.2 \times 10^{-3} \, {}^{o}C^{-1} \quad , \quad \gamma = 7.0 \times 10^{-7} \, {}^{o}C^{-2}$$

and for platinum

$$\beta = 3.5 \times 10^{-3} \, {}^{o}C^{-1} \quad , \quad \gamma = -5.5 \times 10^{-7} \, {}^{o}C^{-2} \quad .$$

The quadratic term is appreciable relative to the linear term for temperatures of the order of

$$\frac{\beta}{2\gamma} \approx 5000 \, {}^{o}C \quad .$$

Since hot-wires are ordinarily operated at temperatures of the order of 100°C, the non-linearity is usually small.

Assuming linearity we have

$$R = R_o \left[1 + \beta \Delta T \right]$$

or

$$\frac{\Delta R}{R_o} = \beta \Delta T = \alpha \quad ,$$

where $R - R_o = \Delta R$ and $T - T_o = \Delta T$. The average value of the temperature difference, ΔT, is termed the "operating temperature" or "over temperature."

Heat Loss Equation

For an incompressible fluid, in which the heat transfer does not

modify the flow, King (21) it is found that the rate of heat loss, P, from a circular cylindrical wire in steady flow is

$$P = \ell \Delta T \left(\kappa + \sqrt{2\pi \kappa c d U} \right),$$

where ℓ and d are the length and diameter of the wire, κ is the thermal conductivity of the medium, and c is the heat capacity per unit volume of the medium. This can be transformed into non-dimensional form by the usual dimensionless groups:

$$N = \frac{P}{\pi \ell \kappa \Delta T} \qquad \text{Nusselt number}$$

$$R = \frac{Ud}{\nu} \qquad \text{Reynolds number}$$

$$P = \frac{\nu c}{\kappa} \qquad \text{Prandtl number ,}$$

where ν is the kinematic viscosity of the fluid medium. King's theoretical law becomes

$$N = \frac{1}{\pi} + \sqrt{\frac{2}{\pi} PR}$$

This law has been superseded by the empirical relation (29,30):

$$N = 0.42 P^{0.20} + 0.57 P^{0.33} R^{0.50},$$

which is valid for both air and water.

For thermal equilibrium conditions between the wire and flowing medium in steady state flow, the heat loss from the wire, P, is just equal to the Joule heat generated in the wire by the passage of the electrical current, I, through the wire resistance R:

$$P = I^2 R = \pi \kappa \ell \Delta T N ,$$

or

$$I^2R = \pi K \ell \Delta T \{.42 P^{1/5} + 0.57 P^{1/3} R^{1/2}\},$$

where the temperature dependent parameters K, P, and R are evaluated at the "film temperature," T_f, defined by:

$$T_f = T_0 + \frac{\Delta T}{2} \quad .$$

The average temperature, $\overline{\Delta T}$, in the vicinity of the wire is defined to be

$$\overline{\Delta T} = T_f - T_0 = \frac{\Delta T}{2} \quad ,$$

i.e., half the wire over-temperature. It is usual to write the above relation in the form

$$\frac{I^2R}{R-R_0} = A + B\sqrt{U}$$

where

$$A = 0.42 \left(\frac{\pi K \ell}{\beta R_0}\right) P^{1/5}$$

$$B = 0.57 \left(\frac{\pi K \ell}{\beta R_0}\right)\left(\frac{d}{\nu}\right)^{1/2} P^{1/3} \quad .$$

Constant-Current-Operation

The sensitivity of the hot-wire in constant-current-operation is found by differentiation of the following relations

$$\frac{I^2R}{R-R_0} = A + B\sqrt{U} \qquad \text{(I = constant)}$$

and

$$V = IR \quad ,$$

with the result:

$$\left(\frac{\Delta V}{\Delta U}\right)_{cco} = -\frac{\alpha^2}{2}\cdot\left(\frac{B\sqrt{U_o}}{I^2}\right)\cdot\left(\frac{IR_o}{U_o}\right).$$

Expressing I in terms of α we find

$$\left(\frac{\Delta V}{\Delta U}\right)_{cco} \sim -\alpha^{3/2}\sqrt{1+\alpha}\ .$$

The response of the wire to rapid velocity fluctuations is limited by its thermal inertia. This effect is calculated by equating the rate of change of the heat content of the wire to the input electrical power minus the heat loss to the flowing medium:

$$c_w\left(\frac{\pi}{4}d^2\ell\right)\frac{d\Delta T}{dt} = I^2R - (R-R_o)\left(A+B\sqrt{U}\right),$$

where c_w is the heat capacity per unit volume of the wire material, and $(\pi/4)\,d^2\ell$ is the wire volume. Combining the above dynamic equation with the resistance equation

$$R = R_o(1+\beta\Delta T)\ ,$$

and considering only small increments in resistance and velocity about their respective average values R_1 and U_o:

$$r = \left(\frac{R-R_1}{R_1}\right) \qquad |r| << 1$$

$$u = \left(\frac{U-U_o}{U_o}\right) \qquad |u| << 1\ ,$$

then we obtain the following simple differential equation

$$M\left(\frac{dr}{dt}\right) + r = -Ku$$

where

$$M = \frac{c_w(1+\alpha)d^2}{4KN\ell}$$

and

$$K = 0.29 \left(\frac{D^{1/3} R^{1/2}}{\nu} \right) \alpha .$$

The quantity M is the "time constant" and indicates the response time of the hot-wire anemometer. The response time of the resistance-wire thermometer corresponds to the case $\alpha = 0$. The above differential equation has the following solution for periodic velocity variations:

$$r = \frac{-nK}{(1+i\omega M)} = \frac{-nK e^{-i\psi}}{\sqrt{1+\omega^2 M^2}}$$

where $\tan \psi = \omega M$. The detector response falls off at high frequencies ($\omega M > 1$) and the resistance variations lag the velocity fluctuations by a phase angle ψ.

The attenuation and phase shift due to the thermal inertia of the wire may be corrected automatically by means of a (passive) compensation network with inverse transfer characteristics. By this means, the response time of the hot-wire in the CCO mode may be increased by more than a factor of ten.

Constant-Temperature-Operation

The sensitivity in constant-resistance-operation is found in a manner similar to that for CCO:

$$\left(\frac{\Delta V}{\Delta U} \right)_{CTO} = \frac{1}{4} \alpha \left(\frac{B\sqrt{U_0}}{I^2} \right) \cdot \left(\frac{IR_0}{U_0} \right)$$

or

$$-2\alpha \left(\frac{\Delta V}{\Delta U} \right)_{CTO} = \left(\frac{\Delta V}{\Delta U} \right)_{CCO} .$$

In water the over-temperature is limited by boiling effects to about 20°C, thus, the maximum value of α is about

$$\alpha = .005 \times 20 = 0.1 ,$$

and it follows that the sensitivity in the CCO mode is always less than in the CTO mode. Expressing I in terms of α we find

$$\left(\frac{\Delta V}{\Delta U} \right)_{CTO} \sim \sqrt{\alpha(1+\alpha)} .$$

The response of the wire in the CTO mode is improved over that in the CCO mode. Assume the automatic feedback circuit which holds the resistance constant does so with a small but finite error δR. The increment in feedback current, ΔI, which holds the temperature constant and which also represents the fluctuating output signal, is related to the small resistance fluctuation by

$$\Delta I = -g_m I \delta R \quad ,$$

where g_m is the transconductance of the feedback loop. Substituting this relation in the heat loss and resistance equation we find after some manipulation that the time constant in the CTO mode is

$$M_{CTO} = \frac{M}{1 + 2\alpha(1+\alpha) R_o g_m} \quad ,$$

where M is the time constant in the CCO mode. Thus, if the transconductance is large the CTO time constant is smaller than that in the CCO mode. The improvement is of the order of 100 in practice.

Sensitive Volume

The dimensions of the volume in space which the hot-wire senses is determined by the length and response time of the wire. For measurements in an isotropic homogeneous turbulence field, the largest dimension of the sensitive volume determines the overall response of the velocity detector. For measurements in water, the length of the wire usually sets the limitation, rather than the time constant of the wire. Let $k_c(\ell)$ be the cutoff wavenumber associated with the wire length where the detector response begins to fall off. Let $k_c(M)$ be the corresponding cutoff wavenumber associated with the wire time constant. Suppose we require that the wire length be the determining dimension of the sensitive volume:

$$k_c(M) \geq k_c(\ell)$$

where

$$k_c(\ell) \approx \ell^{-1}$$

$$k_c(M) \approx \frac{1}{UM} \, .$$

Substituting the expression for M (with $\alpha = 0$) we find

$$R = \frac{Ud}{\nu} \leq \frac{4KN}{\nu C_W} \left(\frac{\ell}{d}\right) ,$$

which is a condition on the wire Reynolds number for a given wire and medium. With the expression for the Nusselt number this condition is approximately

$$R^{1/2} \leq \left(\frac{4K}{2c_w}\right)\left(\frac{\ell}{d}\right) .057\, P^{1/3} .$$

For a tungsten wire in sea water:

$$K = .006 \text{ watt/cm/}^{\circ}\text{C}$$

$$\nu = .01 \text{ cm}^2\text{/sec}$$

$$c_w = 2.6 \text{ joule/cm}^3\text{/}^{\circ}\text{C}$$

$$\ell = 300\, d$$

$$P \approx 4.7$$

the condition is

$$R \leq 30{,}000 ,$$

or

$$U\ell \leq 10^5 \text{ cm}^2\text{/sec} .$$

This condition is satisfied for essentially all experiments in water. Thus, the wire length is the determining factor of the sensitive volume (resolution) for operation of the hot-wire in (locally) isotropic turbulent water.

Typical Values

For comparison with the U-meter, typical values for the operation of a tungsten hot-wire anemometer in sea water are listed in Table 5.1 . These numbers may be compared with those for the U-meter in Section 5.5 . A graph of the wire Nusselt number as a function of velocity and wire diameter is shown in Figure 5.10 .

Table 5.1 . Typical Values for Operation of a Tungsten Hot-Wire Anemometer in Sea Water at 3 Knots (154 cm/sec)

Property	Value
Diameter (d)	3 microns
Length (ℓ)	1 mm
Length/Diameter (ℓ/d)	330
Resistivity	5.5×10^{-6} ohm-cm
Resistance (R)	8 ohms
Temperature Coefficient (β)	.0051 per ^{o}C
Over-Temperature ($\overline{\Delta T}$)	$20^{o}C$
$\alpha = \beta\overline{\Delta T}$	0.10
Time Constant (M)	3.4×10^{-6} sec
Wire Heat Capacity (c_w)	2.6 joule cm^{-3} $^{o}C^{-1}$
Wire Thermal Conductivity (K_w)	2.0 watt cm^{-1} $^{o}C^{-1}$
Reynolds Number (R)	6.4
Nusselt Number (N)	3.0
Prandtl Number (P)	4.7
Kinematic Viscosity (ν)	.0072 cm^{2} sec^{-1}
Water Thermal Conductivity (K)	.0063 watt cm^{-1} $^{o}C^{-1}$
Wire Temperature	$60^{o}C$
Current (I)	0.17 amp
Voltage (V)	1.4 volts
Power (P)	0.24 watt

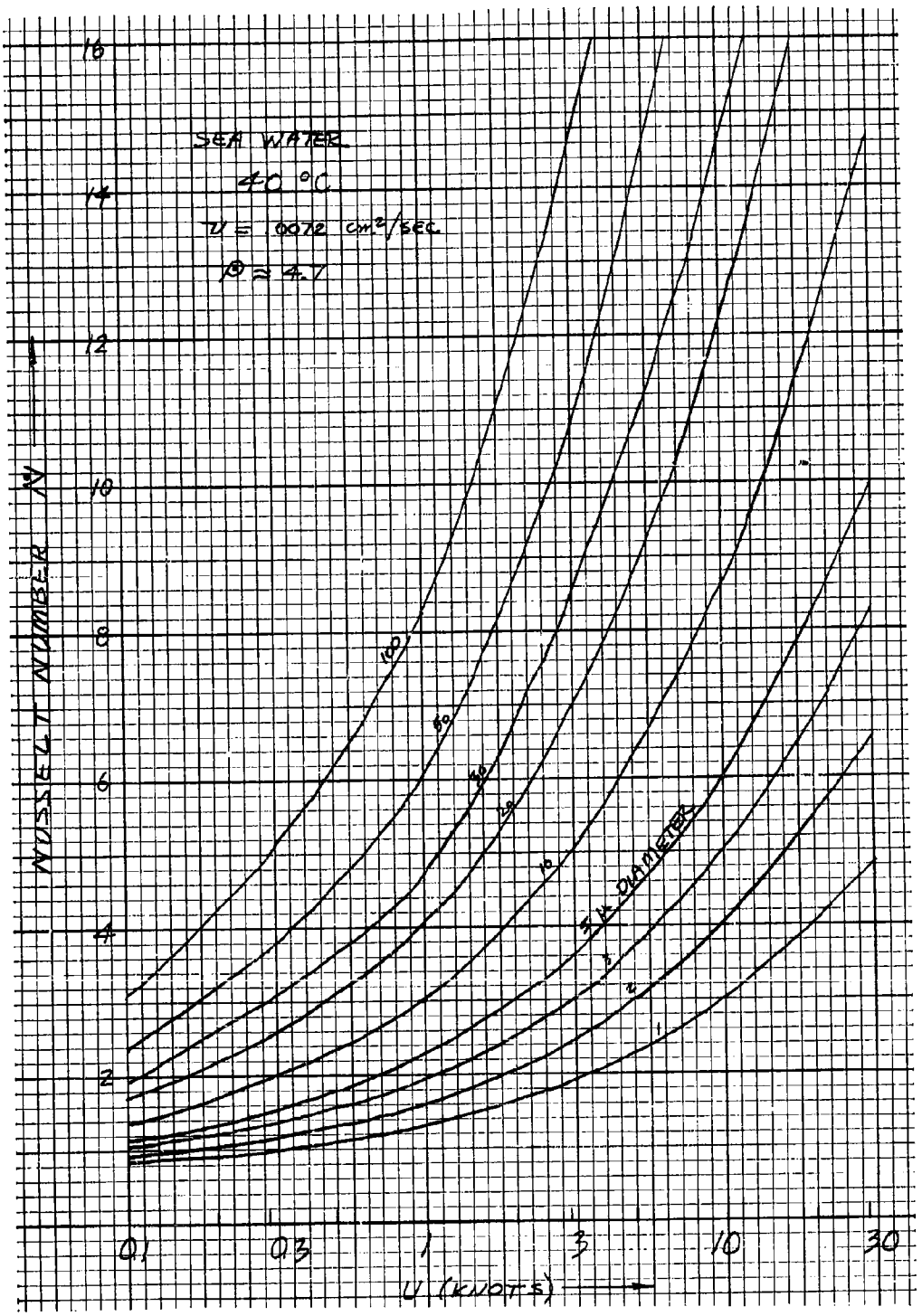

Figure 5.10. Nusselt Number of a Hot-Wire as a Function of Velocity and Diameter

Measurements in Water

The measurement of water flow velocity by means of a hot-wire began in earnest in about 1947 although measurements at low fluid velocities (convection cooling) had been performed by Davis (31) in 1924. Literature on hot-wire measurements in water are listed in References (31-46).

The hot-wire anemometer for use in water has not experienced as much development and successful application as it has for measurements in air. This fact is due in part to some of the problems and characteristics which are listed below for operation in water:

a) Electrolysis - the use of direct current to heat the wire sets up a potential difference along the length of the wire which gives rise to electrolysis effects associated with the dissolved salts in the water. This results in gas bubbles forming and sticking to the wire, thus, changing its heat transfer characteristics. This problem is largely overcome by the use of alternating current which greatly reduces the electrolysis process.

b) Corrosion - in tap water and sea water it is found that the bare wire material quickly develops a surface film due to the corrosive action of the electrolyte. Similar adverse effects take place if dissimilar metals are present at the probe due to galvanic currents between the metals. The use of a very thin non-conducting coating or film on the wire reduces the problems due to corrosion. The coating reduces the response of the wire, however, at high frequencies.

c) Contamination - the hot-wire has a tendency to accumulate gas bubbles, dirt, lint and surface contaminents when operating in all but the very purest water. This causes changes in the calibration of the wire and produces erratic and non-reproducible results. This is overcome somewhat by slanting the wire to the direction of flow and by avoiding protuberances at the wire mounts which might accumulate foreign matter. A regular wire cleaning procedure is advisable.

d) Calibration - as a result of the above effects it is necessary to frequently calibrate a hot-wire instrument to overcome its instability. Dynamic calibration techniques, such as exposing it to a known turbulence field, have also been suggested.

e) Operating Temperature - the temperature in the vicinity of the wire must not exceed the boiling point of water, thus, large over-temperatures are not possible as is the case in the air. This results in a lower sensitivity to velocity fluctuations.

f) Background Noise - the background noise due to temperature fluctuations in the water are relatively larger as a consequence of the low operating temperature.

g) Conductivity of Water - precautions in the choice of wire parameters and mounting posts must be taken to avoid the possibility of the elec-

trolytic conductivity of the medium providing an appreciable current path (resistance) which shunts the wire and which is also subject to temperature, and salt concentration variations. This effect is largest in sea water.

h) Strength - the hydrodynamic force of the water on the wire is about 1000 times the force experienced in air at the same velocity. A thicker wire is called for to withstand this force at high velocity.

i) Power - the power required to heat the wire in water is much higher than that in air because of the high thermal conductivity and heat capacity of water.

j) Time Constant - as a consequence of the above properties of water, the cooling of the wire is more efficient in water. This results in a more rapid response than in air, under the same conditions.

An instrument very similar to the hot-wire anemometer which seems to be better suited to instruments in water is the hot-film anemometer introduced by Ling (28,44). The sensing element consists of a very thin platinum film fused to a glass surface supporting the film. It is rugged, less subject to contamination than the hot-wire and apparently has a favorable thermal response time.

5.5 Comparison of Methods

The properties and performance of the U-meter (UM) and hot-wire anemometer (HWA) for operation in water are now compared. The comparison will cover the velocity sensitivity, frequency response, and general utility of each of the sensors. The temperature sensitivity of the instruments when operated as the T-meter and resistance-wire thermometer is also analysed.

As a basis for comparison of the minimum detectable velocity variation, the following criterion is assumed: require that both velocity detectors must a) operate at the same average over-temperature, $\overline{\Delta T}$, and b) possess the same cutoff wavenumber, k_c, in a homogeneous isotropic turbulent velocity field. Of course, the same flowing medium under identical conditions is also required for the comparison. In the case of the electrode sensor, the average over-temperature is defined as

$$\overline{\Delta T}_{UM} = \int (T - T_0)\, w\, dv$$

where the integration is carried over the entire electrode volume, and w is the sensing distribution function of the electrode (Sec. 12.2). In the case of the wire sensor the average temperature simply refers to the "film temperature" rise, $T_f - T_0$, which is just half (by definition) of the wire temperature rise, $T_w - T_0$:

$$\overline{\Delta T}_{HWA} = T_f - T_0 = \frac{T_w - T_0}{2},$$

The criterion for comparison requires

$$\overline{\Delta T_{UM}} = \overline{\Delta T_{HWA}} = \overline{\Delta T}.$$

The quantities we will want to compare are, for example, the sensitivity, signal-to-noise ratio, or resistance, etc. If ψ is one of these parameters then we will be interested in the ratio

$$\psi_\lambda = \frac{\psi(UM)}{\psi(HWA)} \quad ,$$

where the subscript, λ, simply means that a comparative ratio is formed for the parameter ψ.

As we shall see later in Section 9.3 , there are very few electrode geometries which readily allow mathematical analysis. For this reason we choose a simple electrode geometry which is mathematically tenable, though admitedly idealized. An electrode of uniform current density which is completely confined in a circular cylinder as shown in Figure 5.11 is assumed. The average fluid flow is perpendicular to the axis of the cylinder and the electrodes are represented by discs on the top and bottom of the cylindrical volume. Fringe fields are neglected and the velocity boundary layer on the disc electrode surfaces is assumed to be of zero thickness. This type of U-meter probe is to be compared with a hot-wire of length ℓ and wire diameter d as shown in Figure 5.12 . The corresponding electrode probe for UM will be taken to be a "square" cylinder with the diameter equal to its height and length, which will be called the dimension of the cylindrical electrode. This dimension must be chosen so that the electrode has the same cutoff wavenumber, k_c, of the hot-wire detector. The cutoff wavenumber is some multiple of ℓ^{-1}:

$$k_c = \frac{\text{CONST.}}{d} = \frac{\text{CONST.}}{m\ell}$$

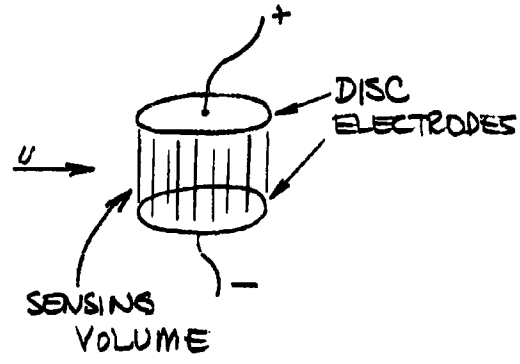

Figure 5.11 . Cylinder Electrode

The magnitude of m is of the order of unity; its actual value has been calculated in Section 14.1 for a square cylinder:

$$m = 0.67^*$$

*This is incorrect. The proper value is m = 1.29. This number is more favorable for the U-meter in the comparison with HWA.

This idealized electrode structure is shown in Figure 5.13 to the same scale as Figure 5.12 .

In numerical calculations we will assume the properties of the hot-wire anemometer listed in Table 5.1 operating in sea water.

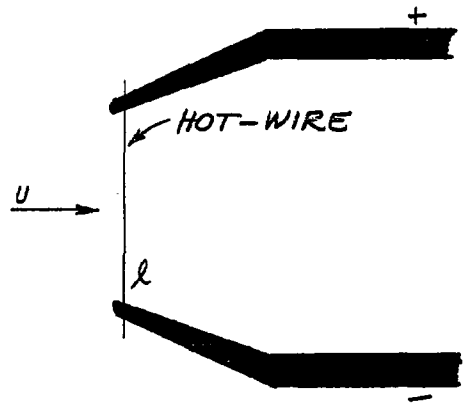

Figure 5.12 . Hot Wire

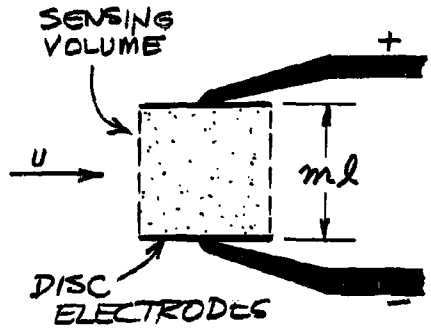

Figure 5.13 . Electrode Velocity Probe

Resistance

The resistance of the wire and the resistance between the electrodes are not greatly different for use in sea water in spite of the great difference in their respective conducting volumes. This is due to the fact that the conductivity of typical wire materials is many orders of magnitude greater than that of sea water. The ratio of UM and HWA resistances is

$$R_\lambda = \frac{R(UM)}{R(HWA)} = \frac{\left(\frac{m\ell}{\sigma \frac{\pi}{4}(m\ell)^2}\right)}{\left(\frac{\rho \ell}{\frac{\pi}{4} d^2}\right)} = \frac{1}{m \sigma \rho}\left(\frac{d}{\ell}\right)^2 ,$$

where ρ is the resistivity of the wire material and σ is the conductivity of sea water. For a tungsten wire in sea water at 20°C (i.e., "cold" conditions)

$$\sigma\rho = (.048)(5.5 \times 10^{-6}) = 2.6 \times 10^{-7} ,$$

and for a typical hot-wire the (cold) resistance ratio is

$$R_\lambda \approx 63$$

Thus, the electrode resistance is larger than the wire resistance by a factor of 63, for example

$$R(HWA) = 8 \text{ ohms}$$
$$R(UM) = 500 \text{ ohms} .$$

For operation in tap water the ratio is about 100 times larger ($R_\lambda \approx 6300$).

The temperature coefficient of resistance

$$\frac{1}{R_o}\left(\frac{\partial R}{\partial T}\right)$$

is of opposite sign and different magnitude for the hot-wire resistance and electrode resistance. The hot-wire resistance increases with increasing temperature, whereas the electrode resistance decreases at higher temperature (i.e., the conductivity of the water increases with temperature). The ratio of the temperature coefficients for the UM and HWA detectors is approximately

$$\left[\frac{1}{R_o}\left(\frac{\partial R}{\partial T}\right)\right]_\lambda = \frac{-.020}{+.005} = -4.0 .$$

The coefficient of electrode resistance is 4 times as large as that for the hot-wire.

Power

The steady state electrical power dissipated in the velocity probes depends on their respective heat transfer equations. For the U-meter:

$$P = 2cAU\overline{\Delta T} ,$$

where c is the heat capacity per unit volume of the water, A is the frontal area of the electrode, and U is the flow velocity. For the cylindrical electrode configuration, the frontal area is (Sec. 12.2)

$$A = \left(\frac{3\pi^2}{32}\right)(m\ell)^2 = 0.415\,\ell^2 .$$

The heat transfer equation for the hot-wire is (Sec. 5.4)

$$P = 2\pi K \ell N \overline{\Delta T} ,$$

where κ is the thermal conductivity of the water, and $\mathcal{N}$ is the Nusselt number of the wire (which depends on the velocity U). The ratio of these is

$$R_\lambda = \frac{P(UM)}{P(HWA)} = \left(\frac{3\pi}{32}\right) \frac{m^2 c \ell U}{K \mathcal{N}} = \left(\frac{3\pi}{32}\right) m^2 \left(\frac{\ell}{d}\right) \frac{PR}{\mathcal{N}} ,$$

where P is the Prandtl number of the water, and R is the Reynolds number based on the wire diameter (the Péclet number is PR):

$$P = \frac{c\nu}{K}$$

$$R = \frac{Ud}{\nu} .$$

For a 3μ diameter hot-wire in water at 40°C and 3 knots

$$P = 4.7 \quad , \quad R = 6.4 \quad , \quad \mathcal{N} = 3.0 .$$

Under these conditions the power ratio is (ℓ = 300 d)

$$R_\lambda \approx 400$$

Thus, 400 times as much power is dissipated in the U-meter electrodes as in the hot-wire.

Frontal Area

A greater swept volume of water is involved in the measurement with the U-meter compared with the hot-wire anemometer. It is for this reason that a higher power level may be used with the U-meter. The frontal area, A, of the electrode sensor satisfies the equation

$$P = 2cAU\overline{\Delta T} .$$

The corresponding frontal area of the wire, A_w, may be defined by the relation

$$P = 2cA_w U \overline{\Delta T} = 2\pi K \ell \mathcal{N} \overline{\Delta T}$$

or

$$A_w = (\ell d)\left(\frac{\pi K N}{c_d U}\right)$$

$$= (\ell d)\left(\frac{\pi N}{P R}\right).$$

At large Reynolds number, we have

$$\frac{PR}{\pi N} \approx 0.56\, P^{2/3} R^{1/2}$$

thus, the frontal area of the wire decreases with increasing velocity and wire length (i.e., with increasing R). For 3 micron wire at 3 knots in sea water

$$A_w = 0.31\ (\ell d).$$

The power ratio, P_λ, is

$$P_\lambda = \frac{A}{A_w} = \left(\frac{3\pi^2}{32}\right)\left(\frac{\ell}{d}\right)\left(\frac{PR}{\pi N}\right) m^2.$$

This ratio is roughly equal to (ℓ/d).

Signal-to-Noise Ratio

The intrinsic signal-to-noise ratio, Λ, is more basic than the sensitivity of a detector. A comprehensive expression* has been obtained for, Λ, in Section 8.3 for all modes of operation and both types of detectors. In that Section we found that the intrinsic signal-to-noise ratio is

$$\Lambda = \left(\frac{P}{4kT\Delta f}\right) E^2 n^2$$

where E is a parameter given in Section 8.3 which depends on the type of detector and mode of operation. The ratio of signal-to-noise ratios, Λ_λ, for the two velocity detectors is

---

*We take H = 1 in that expression and drop the asterisk notation.

$$\Lambda_\lambda = P_\lambda E_\lambda^2$$

where the other variables are assumed equal for the two detectors. This ratio is illustrated for the constant-power-operation (CPO) mode:

$$E_\lambda^2 = 93 \qquad (+20 \text{ db})$$

$$P_\lambda = 400 \qquad (+26 \text{ db})$$

and

$$\Lambda_\lambda = 37{,}000 \; . \qquad (+46 \text{ db})$$

Thus, the minimum detectable velocity variation in the case of the U-meter is considerably less than that of the hot-wire anemometer; in terms of amplitudes the relative detectability is

$$\sqrt{37{,}000} = 190 \; .$$

This remarkable increase in detectability is attributable to the greater power dissipated in the electrode and the more favorable temperature coefficient of electrode resistance. If the velocity measurements by means of both detectors is subject to temperature noise as the primary background noise, the difference in detectability of both detectors is, of course, reduced. In the extreme case of high background noise there would be no difference in detectability between the two.

The theory given above refers to an electrode with a temperature uniformity of 50 % (Sec. 12.2). We shall see in Section 12.4 that boundary layer effects frequently lower the temperature uniformity of an electrode thereby lowering the maximum average electrode temperature rise $\overline{\Delta T}$. The non-uniformity of the temperature distribution in the vicinity of a hot-wire is of no importance since the wire is placed at the hottest point anyway. Thus, in the above comparison, consideration should be given to this effect which acts unfavorably in the case of the U-meter in comparison with HWA. If m_5 is the temperature uniformity of the electrode, the velocity sensitivity is proportional to m_5. For example, if m_5 = 10 % instead of the 50 % assumed above, the relative detectability of the U-meter is only $40 \approx 190/5$ times superior to that of the HWA.

Frequency Response

In the comparative analysis of the sensitivity of the U-meter and hot-wire anemometer above, the cutoff frequencies of the two probes were

assumed equal. In this paragraph this constraint is removed in order to make a comparative analysis of the frequency response of the two detectors. It was shown in Section 5.4 that the response of the hot-wire anemometer in water is determined solely by its length in an isotropic turbulent field. A similar conclusion was drawn in Section 12.5 with respect to the U-meter and the physical size of the electrode volume. Thus, in a comparison of the response of these detectors, it reduces to the question of the practical limitation to how small the respective probes can be made. The smallest practical hot-wire detectors are believed to be about 3 microns in diameter and 0.5 mm in length ($\ell \approx 150\ d$). A U-meter probe constructed from a small hypodermic needle described in Section 9.8 has an electrode volume of less than 0.3 mm typical dimension. It appears that, if necessary, this can be improved on for this type of probe design. Thus, electrode sensors can be made comparable or smaller than the smallest hot-wire sensor. By the use of a special cross-wire electrode described below, it is possible to construct essentially a point velocity sensor of very small dimensions (.01 mm).

Consider the probe structure shown in Figure 5.14a and 5.14b consisting of two crossed wires which are separated at the point of crossing by a distance comparable with the wire diameter. The sensitive volume of this electrode configuration is in the immediate vicinity of the crossing in spite of the fact that the entire wire length is exposed to the conducting fluid (assume the supports are insulated, however). If d is the wire diameter, the cutoff wavenumber is estimated to be, roughly,

$$k_c \approx \frac{2}{d} \quad .$$

The length, ℓ, of the wires need not be very large in comparison with the wire diameter as is the case with the hot-wire sensor. Experience with hot-wire construction enables us to estimate the smallest practical limit to this type of electrode structure, viz., d = 3μ. Thus, the cutoff wavenumber is about

$$k_c \approx 6000\ \text{cm}^{-1} \quad .$$

This represents an improvement in this respect by a factor of about 50 over the wire sensor. At a velocity of 3 knots the corresponding bandwidth, Δf, is

$$\Delta f \approx \frac{k_c U}{2\pi} = 150\ \text{kc}$$

and the Reynolds number of the wire is about 5. Modifications of the above electrode structure allows operation in a boundary layer near a wall and with an additional wire or wires, differential spacial (double or triple) measurements may be made.

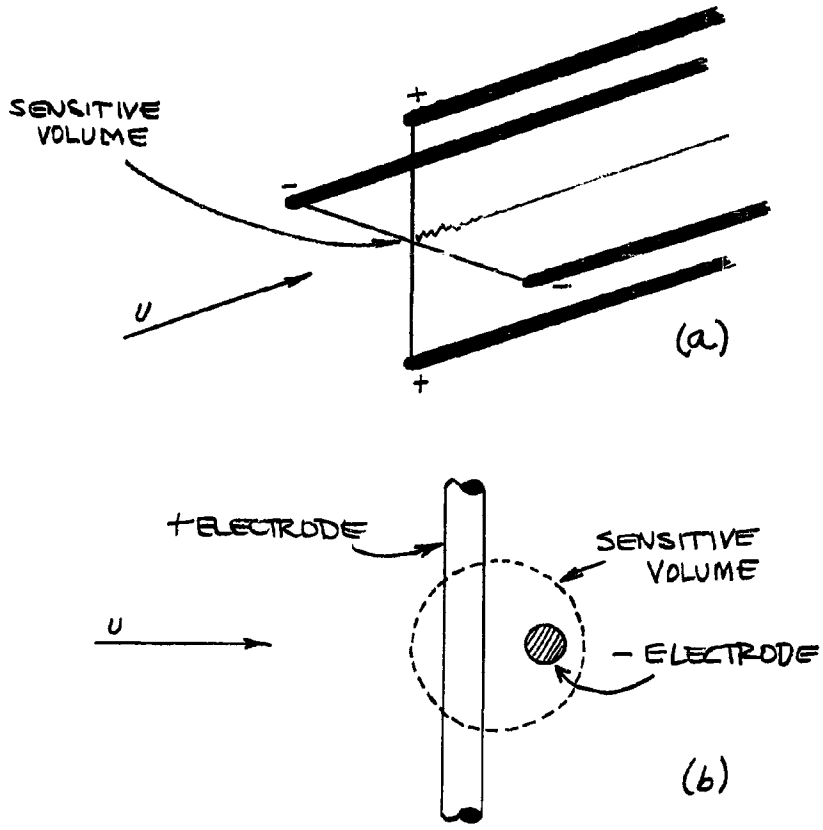

Figure 5.14 . Cross-Wire Electrode

The above discussion indicates that, in all cases, it is possible to construct electrode sensors with a smaller sensitive volume than hot-wire sensors.

Utility

The comparison of the sensitivity and frequency response of the U-meter with the hot-wire anemometer indicates the potential usefulness of the former in fluid velocity measurements. The general utility of the electrode velocity sensor for such measurements is now considered. Because of the shape and structure of the probe type electrodes, the sensor

is intrinsically rugged. This property facilitates the general handling of the instrument and it is not subject to impact damage by bits of matter in the flowing medium. The durability of U-meter sensing elements is, thus, superior to that of the fragile hot-wire detector. The stability of calibration of the U-meter for absolute velocity measurements, however, is probably not as good in this respect as the hot-wire anemometer.

Temperature Sensitivity

It has been necessary to delay the analysis of the temperature sensitivity of the T-meter (TM) and resistance-wire thermometer (RWT) until now because of the need of formulas which had to be developed beforehand. The intrinsic signal-to-noise ratio, Λ , for temperature measurements is (Sec. 8.3)*

$$\Lambda = \left(\frac{P}{4kT\Delta f}\right) E^2\theta^2$$

where θ is the relative temperature variation, and the other quantities are defined in Section 8.3 . We are interested in the ratio

$$\Lambda_\lambda = \frac{\Lambda(TM)}{\Lambda(RWT)} = R_\lambda E_\lambda^2 = R_\lambda \left(\epsilon'/\beta_T\right)_\lambda^2$$

This ratio is

$$P_\lambda \approx 400 \qquad (+26 \text{ db})$$

$$\left(\epsilon'/\beta_T\right)^2 = 16 \qquad (+12 \text{ db})$$

and

$$\Lambda_\lambda \approx 6{,}400 \qquad (+38 \text{ db})$$

Thus, the minimum detectable temperature variation is

$$\sqrt{6400} = 80$$

times smaller for the T-meter relative to the resistance-wire thermometer.

---

*We assume $H \ll 1$ in that equation and write $P = P^*H$.

6. SIGNAL PHENOMENA

In this Section, a study of the physical effects which cause measurable changes in electrode impedance is made. This includes the effects already considered in earlier Sections as well as others. The differential relations which exist between changes in electrode impedance and the independent variables, temperature, salinity and pressure, are also developed. The consequences of correlated independent variables on the impedance measurements are considered at the end of this Section.

6.1 Electrode Effects

We wish to make a detailed study of all physical effects which cause a measurable change in the impedance of an electrode. One can regard these effects, on one hand, as mechanisms for producing useful signals for measuring the properties of the medium, or on the other hand, as effects which cause background noise tending to mask the desired signal. The electrode impedance includes contributions from both volume and surface properties and consists of resistive and reactive components. The detection of the resultant changes in impedance are performed with electronic instruments operating at a given frequency. For several reasons it is desirable to make these impedance measurements at relatively high frequencies (greater than 1000 cps). The only effects we consider here are ones which produce changes in impedance occuring and measurable in the passband of the detection equipment. Phenomena not considered here are active electrode effects which cause a potential to appear across the electrode impedance, for example; a) A magnetic induction effect in which a strong magnetic field present at the electrode coupled with the flowing conducting fluid induces a potential (1,2,3,), b) An electrokinetic effect associated with the relative motion of the ions at the electrolyte/electrode interface in which a "streaming potential" is developed (4), c) The potential caused by variations in the inhomogeneity of the electrical properties of the medium which induces a space charge in the electrode volume (5), or d) Velocity dependent limiting direct currents in a solution determined by mass transfer rates at the electrode (6,7,8,9). Though these effects can, and have been used to measure the velocity of a fluid, we will not consider them here because the resulting potentials produce no effective change in the electrode impedance at the (high) frequency of the impedance measurement.

There are many electrode effects, but any given one produces changes only if there is a corresponding change in the thermodynamic variables, viz., temperature, pressure, salinity, chemical composition and the relative velocity of the fluid with respect to the sensing electrode. The magnitude of effect considered below will be with respect to small relative fluctuations in these variables such as $(\delta T/T)$ or $(\delta U/U)$. We begin with the two main effects of interest in the present measuring techniques.

Conductivity

The electrode impedance consists primarily of the resistance associated with the volume conductivity of the electrolyte. The conductivity is a relatively strong function of temperature and salinity of the water. In sea water, a 1 % change in temperature (relative to 293° K) at 20° C gives rise to a 6 % change in conductivity and electrode resistance; a 1 % change in salinity at 35 ‰ causes about a 1 % change in conductivity. If β_T is the temperature coefficient of conductivity (about 2 % per °C) and β_S the salinity coefficient (about 2.5 % per ‰), the change in electrode resistance is

$$\frac{\delta R}{R} = -\beta_S \delta S - \beta_T \delta T ,$$

where δS, and δT are the changes in salinity and temperature, respectively.

Heating Effect

The electrical energy developed in a resistive load is dissipated in that load as Joule heating resulting in a temperature rise. The electrical power dissipated in the resistance of an electrode immersed in a flowing conducting medium heats the medium and causes a temperature rise in the fluid as it passes through the field of the electrode. It may be shown that the average temperature rise, $\overline{\Delta T}$, of the fluid which is flowing at velocity, U, through an electrode of frontal area A is given by

$$\overline{\Delta T} = \frac{P}{2cAU} ,$$

where c is the heat capacity per unit volume of the fluid, and P is the electrical power dissipated in the electrode. Since the conductivity of the medium is a function of temperature, this causes a change in the electrode resistance. Differentiating this relation and combining it with the one above, we find that fluctuations in the flow velocity cause the following changes in electrode resistance:

$$\frac{\delta R}{R} = -\beta_T \overline{\Delta T} \left(\frac{\delta U}{U} \right) .$$

This velocity dependence of the electrode resistance goes to zero if the temperature rise, $\overline{\Delta T}$, is small, i.e., if the applied power is small. For an average electrode temperature rise of $\overline{\Delta T} = 20°C$, a 1 % change in velocity causes a 0.4 % change in electrode resistance.

Dielectric Constant

Just as the resistance between the electrodes can be calculated from

the geometry and the conductivity of the medium, so can the capacity be calculated from the geometry and the dielectric constant of the medium. The resulting resistance and capacity satisfy a relation which is independent of the electrode geometry and dependent only on the properties of the flowing medium

$$RC = \frac{\kappa \kappa_0}{\sigma},$$

where C is the (volume) electrode capacity, κ is the dielectric constant of the fluid, κ_0 is the permittivity of free space, and σ is the conductivity of the medium. Thus, if the electrode resistance is known, the capacity may be calculated. The electrode capacity and resistance are in parallel. If, as is the case in many instances, the reactance, X, due to the electrode capacity is small in comparison with the electrode resistance, R, the reactance is given approximately by

$$X = -R(R\omega C) ,$$

where ω is the angular frequency at which the impedance is measured. The quantity $R\omega C$ is independent of electrode geometry and is comparable to unity only at very high frequency, e.g., in sea water (35 ‰, 20°C)

$$R\omega C = 1 \quad \text{at} \quad f = \frac{\omega}{2\pi} = 1.2 \text{ kmc} .$$

In tap water the corresponding frequency is about 10 mc. The dielectric constant of the fluid is a function both of temperature and salinity; the temperature coefficient is about 0.5 % per °C and the salinity coefficient is about 0.2 % per ‰ . Thus, in sea water, a 1 % change in temperature causes a 1.5 % change in electrode reactance, and a 1 % change in salinity causes a .07 % change in reactance.

Impurities

If a localized inhomogeneity or a foreign particle in the medium passes through the electrode volume a change in resistance is observed. Examples of such impurities are gas bubbles, bits of matter, oil traces, and marine organisms such as plankton. Ordinarily these impurities are non-conductors and produce the same effect as a gas bubble of the same shape; in general, however, any impurity with a conductivity different from that of the medium will cause a small change in electrode resistance. If δv is the volume of a (spherical) non-conducting bubble, the resulting average resistance change is (Sec. 10.4)

$$\frac{\delta R}{R} = \frac{1}{2} \left(\frac{\delta v}{v_0} \right) ,$$

where v_o is the effective volume of the electrode field. Thus, a bubble with a volume 1 % of that of the electrode (about 20 % the size in linear dimensions) produces a 0.5 % change in electrode resistance. Since the bubble volume varies as the cube of its diameter, the resistance change becomes quite small for relatively small bubbles.

Magneto-Hydrodynamic Effect

The electrical currents which flow in the fluid medium induce a (weak) magnetic field which interacts with the conducting medium producing an auxiliary current which varies periodically with the frequency of the applied alternating current. As a consequence, a virtual change in electrode impedance occurs. This effect occurs at the operating frequency whereas that produced by a strong static magnetic field occurs at zero frequency. The effective electric field strength produced in the electrode volume is

$$\vec{U} \times \vec{B} ,$$

where $\vec{B}$ is the magnetic field produced by the currents flowing in the medium and is of the order of (10)

$$B = \frac{\mu\mu_o\sigma V}{4\pi} ,$$

where V is the voltage applied to the electrode, μ is the permeability of the medium and μ_o is the permeability of free space. The power developed in the electrode due to this effect is of the order of

$$\delta P \approx \sigma \left[\frac{U\mu\mu_o V\sigma}{4\pi}\right]^2 b^3 ,$$

where δR is the effective change in electrode resistance associated with this effect, and b is the typical electrode dimension. Re-arranging terms, we find that a small change in velocity, δU, causes an effective change in electrode resistance of the order of

$$\frac{\delta R}{R} \approx (R\sigma b)^3 \left(\frac{\mu\mu_o U}{4\pi R}\right)^2 \left(\frac{\delta U}{U}\right) .$$

This magneto-hydrodynamic effect is very small. An electrode of 30 ohms resistance with a cell constant such that $R\sigma b \approx 1$, experiences a 30×10^{-17} % change in resistance for a 1 % change in velocity at 3 knots in sea water ($\mu \approx 1$).

Adiabatic Temperature Rise

If a body moves through a fluid, a temperature rise, ΔT, over ambient temperature is experienced at the stagnation point due to the adiabatic compression of the medium given by

$$\Delta T = \frac{dU^2}{2c} ,$$

where d is the density of the medium, and c is the heat capacity per unit volume. A similar temperature rise is experienced due to friction heating caused by viscous forces acting at the surface of the body. If an electrode is located at a point where such a temperature rise takes place, the conductivity will be changed due to the temperature rise. As a consequence, the electrode resistance becomes velocity sensitive. The resultant change in resistance due to a change in velocity is

$$\frac{\delta R}{R} = \beta_T \left(\frac{dU^2}{c}\right)\left(\frac{\delta U}{U}\right)$$

a 1 % change in velocity causes a 10^{-5} % change in resistance in sea water at 3 knots velocity – a very small effect.

Electrochemical Surface Effects

Complicated electrochemical processes take place at the electrolyte/electrode interface and give rise to additional contributions to the electrode impedance which are both resistive and reactive. This surface impedance is associated with the capacity of the electric double layer, the reaction resistance of the electrochemical process, and the concentration polarization impedance associated with the diffusion rates of the ions involved in the conduction processes (Sec. 9.4). These phenomena are critically dependent on the chemical constitution of the electrolyte and metal electrode, the condition of the electrode surface, and operating frequency as well as the fundamental variables of temperature, pressure, and velocity. Because of the complexity of these processes and since their actual properties must, in each case, be determined experimentally, it is not worth while to give approximate formulas for these effects. Briefly, let it be mentioned that by the appropriate choice of operating conditions, a 1 % change in temperature, salinity or velocity can cause a change in electrode impedance (mostly reactance) of the order of 1 %. Also by another choice of operating conditions these effects can be made quite small, for example, by operating at high frequencies with platinum black electrodes.

Geometric Distortion

The resistance of an electrode configuration immersed in an elec-

trolyte depends on the size and shape of the electrode system. Variations in temperature cause a distortion of this geometry due to the thermal expansion of the materials with which the electrode conductivity cell is constructed. Differential pressures over the electrode volume can also distort the electrode. For example, the electrode geometry is changed by acoustic vibration fields much like the operation of a capacity microphone. The pressure effect is negligibly small in practically all situations in comparison to other effects. Concerning the thermal expansion of the conductivity cell (11), the effect is dependent on the expansion coefficients of the cell materials; typically a 1 % change in temperature causes only about a 3×10^{-3} % change in electrode resistance. The response time of the electrode system depends on the constitution of the cell, and the heat capacity and heat transfer properties of the electrode cell materials.

Spectrum Dilation

If a random distribution of some scalar variable, such as temperature or salinity, exists in the medium to which the electrode is responsive, it is possible to measure the velocity by means of the spectral distribution of the scalar variables. This is done by spectrum analysing the detected signal and thereby determining the width of the distribution which is proportional to the average velocity. If λ_c is the physical wavelength of some component of the distribution which is easily determined by the spectrum analysis (e.g. where spectral distribution falls off rapidly), then the width of the spectrum in the frequency domain is, Δf, where

$$\Delta f = \frac{U}{\lambda_c} .$$

If the turbulence field is in an equilibrium condition, λ_c is a constant and the bandwidth, Δf, is proportional to velocity. This means of measuring velocity is statistical in nature and the accuracy of the measurement is determined by the product of the bandwidth and smoothing time, t, (or response time) of the measurement. If λ_v is the physical wavelength of the turbulent velocity fluctuation, δU, then the smallest value of this velocity fluctuation which is just measurable is

$$\left(\frac{\delta U}{U}\right) = \sqrt{\frac{\lambda_c}{\lambda_v}} .$$

For example, if the scalar field cutoff wavelength is $\lambda_c = 0.2$ cm, and the velocity field being measured is $\lambda_v = 20$ cm, a velocity measurement of 10 % accuracy is possible.

Summary

In summary, the largest effects to be considered are those due to conductivity variations, the heating effect, impurities, and spectrum

dilation. All of these effects are considered and exploited in this Report. The variations in dielectric constant and electrochemical effects can either be minimized or optimized, as the case may be, to facilitate the physical measurements of the conducting medium. The effects due to geometric distortion, adiabatic and friction heating and magneto-hydrodynamic effects are all quite negligible.

6.2 Differential Relations

This Section deals with expressions which relate changes in electrode impedance to small increments in the independent variables such as temperature or velocity. Coefficients which indicate the sensitivity of the electrode impedance to changes in these physical variables are introduced. Reference should be made to Section 7.1 for a description of the three types of variables, viz., independent property and system variables.

Let $\{\xi_i\}$ be the set of n independent (signal) variables where $i = 1,2,\ldots,n$. These variables are, of course, independent of each other. Let $\{\psi_j\}$ be the least set of property variables which are necessary to completely describe the value of the electrode impedance, z. Suppose this set consists of m variables and $j = 1,2,\ldots,m$. These variables depend only on the independent variables. Let $\{\lambda_k\}$ be a set of p system variables or parameters where $k = 1,2,\ldots,p$. The variables are independent of each other and the independent variables. The electrode impedance is completely determined if the independent and the system variables are specified, however, mathematical expressions for the impedance usually involve explicitly only the property and system variables

$$z = z(\psi_1, \psi_2, \cdots \psi_m; \lambda_1, \lambda_2, \cdots, \lambda_p).$$

The total differential of the electrode impedance, dz, with respect to the independent variables, $d\xi_i$, is given by

$$\begin{aligned} dz &= \frac{\partial z}{\partial \xi_1} d\xi_1 + \frac{\partial z}{\partial \xi_2} d\xi_2 + \cdots + \frac{\partial z}{\partial \xi_n} d\xi_n \\ &= \sum_{i=1}^{n} \left(\frac{\partial z}{\partial \xi_i}\right) d\xi_i \end{aligned}$$

The partial derivatives of the impedance, z, with respect to the independent variables, ξ_i, are given, in turn, by

$$\frac{\partial z}{\partial \xi_{i'}} = \sum_{j=1}^{m} \left(\frac{\partial z}{\partial \psi_j}\right)\left(\frac{\partial \psi_j}{\partial \xi_{i'}}\right)$$

Consider a small but finite increment, Δz, in the electrode impedance; the fractional change in the impedance is, to first order in finite increments, $\Delta \xi_i$,

$$\frac{\Delta z}{z} = \sum_{i=1}^{n} \left(\frac{\partial z}{\partial \xi_i}\right) \frac{1}{z} \Delta \xi_i \ .$$

The coefficient of $\Delta \xi_i$ in this equation is denoted by β_i and is called "the ξ_i -sensitivity coefficient" (of the impedance):

$$\beta_i = \frac{1}{z}\left(\frac{\partial z}{\partial \xi_i}\right) .$$

The units of β_i are the inverse of ξ_i. These coefficients are given by the expression

$$\beta_i = \sum_{j=1}^{m} \left(\frac{1}{z}\frac{\partial z}{\partial \psi_j}\right)\left(\frac{\partial \psi_j}{\partial \xi_i}\right)$$

$$= \sum_{j=1}^{m} \left[\frac{\psi_j}{z}\left(\frac{\partial z}{\partial \psi_j}\right)\right]\cdot\left[\frac{1}{\psi_j}\left(\frac{\partial \psi_j}{\partial \xi_i}\right)\right]$$

$$= \sum_{j=1}^{m} \zeta_j \, \beta_{ji}$$

where

$$\zeta_j = \frac{\psi_j}{z}\left(\frac{\partial z}{\partial \psi_j}\right)$$

$$\beta_{ji} = \frac{1}{\psi_j}\left(\frac{\partial \psi_j}{\partial \xi_i}\right) .$$

The quantity, ζ_j , is the "ψ_j - sensitivity exponent of the impedance"* and β_{ji} is the "ξ_i - sensitivity coefficient of ψ_j ." The property ψ_j in these coefficients is evaluated at that value corresponding to the reference values of the independent variables, ξ_i. The quantity ζ_j is dimensionless, and β_{ji} has dimensions of inverse - ξ_j .

As an example of these coefficients, consider an electrode with the equivalent circuit shown in Figure 6.1 . We seek the temperature coefficient, β_T, of this impedance. The resistance, R, is due to the volume conductivity, σ, of the solution and the capacity, C, is due to the volume

---

* IF $y = k x^{\alpha}$, THEN $\frac{x}{y}\left(\frac{dy}{dx}\right) = \alpha$.

dielectric constant, K, of the solution. If h^{-1} is the cell constant of the electrode then, the resistance and capacity are given by:

$$R = \frac{1}{\sigma h} \quad \text{and} \quad C = K K_0 h.$$

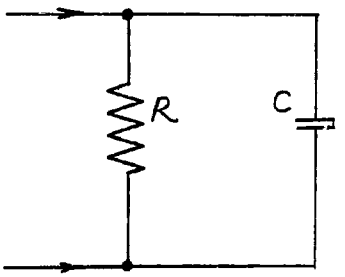

Figure 6.1 . Electrode Impedance

We assume that the capacity is small so that

$$RwC = \frac{wKK_0}{\sigma} << 1$$

at the operating frequency $\omega/2\pi$. In this case, the electrode impedance is approximately

$$z = R - i\,R(RwC) = \frac{1}{\sigma h} - i\,\frac{wKK_0}{\sigma^2 h}.$$

The σ - and K - sensitivity exponents of the impedance are

$$\zeta_\sigma = \frac{\sigma}{z}\left(\frac{\partial z}{\partial \sigma}\right) = -1 + i\,2(RwC)$$

$$\zeta_K = \frac{K}{z}\left(\frac{\partial z}{\partial \sigma}\right) = -i\,(RwC).$$

The temperature - sensitivity coefficients of the conductivity and dielectric constant of sea water at 20°C and 35 ‰ (Sec. 7.2) are

$$\beta_{\sigma T} = \frac{1}{\sigma}\left(\frac{\partial \sigma}{\partial T}\right) = +.021 \quad \text{PER °C}$$

$$\beta_{KT} = \frac{1}{K}\left(\frac{\partial K}{\partial T}\right) = -.0045 \quad \text{PER °C}.$$

The temperature coefficient of the electrode impedance is

$$\beta_T = \zeta_\sigma \beta_{\sigma T} + \zeta_K \beta_{KT} = \left[-.021 + i\,(RwC)\,.047\right] \text{ PER °C}$$

which consists of real and imaginary parts.[9] The fractional impedance change ($\Delta z/z$) can also be written in terms of other dimensionless quantities, viz.,

$$\alpha_{j\lambda} = \beta_{ji}\,\xi_{i\lambda} = \frac{\xi_\lambda}{\psi_j}\left(\frac{\partial \psi_j}{\partial \xi_{i\lambda}}\right)$$

which is "the ξ_λ - sensitivity exponent of ψ_j ," and

$$\alpha_{i\lambda} = \beta_{i\lambda}\,\xi_\lambda = \frac{\xi_{i\lambda}}{z}\left(\frac{\partial z}{\partial \xi_{i\lambda}}\right),$$

which is "the ξ_i - sensitivity exponent of the impedance" in this notation:

$$\left(\frac{\Delta Z}{Z}\right) = \sum_i \sum_j \zeta_j \alpha_{ji} \left(\frac{\Delta \xi_i}{\xi_i}\right) = \sum_i \alpha_i \left(\frac{\Delta \xi_i}{\xi_i}\right)$$

and

$$\alpha_i = \sum_{j=1}^{m} \zeta_j \alpha_{ji} .$$

For example, the temperature-sensitivity exponent of conductivity of sea water at 20°C (293°K) is

$$\alpha_{\sigma T} = \frac{T}{\sigma}\left(\frac{\partial \sigma}{\partial T}\right) = +6.2 .$$

The α_{ji} - sensitivity exponents for the properties of sea water under standard conditions are listed in Table 6.1 . The References for this data are given in brackets; if none appear, the data is taken from Section 7.2 . The pressure-sensitivity exponents are all quite small and for this reason pressure effects have not been studied for detection purposes in this Report. Since the dependence of the electrical conductivity of sea water is of primary importance to this work, the temperature and salinity coefficients of conductivity (denoted simply by β_T and β_S , respectively) are shown in Figures 2.7 and 2.8 for the range of temperature and salinity found in the oceans (12).

Table 6.1 . Absolute Sensitivity Exponents of Physical Properties of Sea Water

$T = 293^{\circ}K$ $S = 35$ ‰ $P = 1$ Atm Property (ψ)	Temperature Sensitivity Exponent $\alpha_{\psi T}$	Salinity Sensitivity Exponent $\alpha_{\psi S}$	Pressure Sensitivity Exponent $\alpha_{\psi P}$
Density (d)	-0.080	+0.026	$+4.3 \times 10^{-5}$ (13)
Conductivity (σ)	+6.2	+0.89	$+6.8 \times 10^{-5}$ (14,15)
Dielectric Constant (κ)	-1.5	-0.095	-
Heat Capacity (c)	-0.071	-0.020	-1.4×10^{-5} (16)
Kinematic Viscosity (ν)	-6.7	+0.027	-4.0×10^{-5} (17)
Prandtl Number (P)	-7.8	+0.043	-
Schmidt Number (S)	-12.8	+0.027	-

The sensitivity exponents of Table 6.1 indicate the relative magnitude of signals caused by temperature and salinity variations in the ocean

for the reference temperature (293°K) and salinity (35 ‰) used in the Table. As shown in Section 7.3 , the rms salinity and temperature variations are related by

$$\frac{\Delta S}{\Delta T} \approx 0.11 \text{ ‰ per } ^{\circ}C$$

so that

$$\left(\frac{\Delta S}{\Delta T}\right)\frac{T}{S} = 0.11 \times \frac{293}{35} \approx \text{unity} \quad .$$

6.3 Correlated Signals

The measured variables, temperature, salinity, and velocity are usually thought of as independent variables. In certain situations, however, these variables are coupled or correlated with each other so that a change in one implies a change in the other. The best example of this is the relation which exists between temperature and salinity of given large masses of sea water, i.e., the so-called "TS-diagram." We now analyze the consequences of this correlation between temperature and salinity microstructure on the measurement of the conductivity of sea water.

Fluctuations in conductivity of sea water are related to temperature and salinity variations by

$$\frac{\Delta\sigma}{\sigma} = \beta_T \Delta T + \beta_S \Delta S$$

where β_T and β_S are the temperature and salinity coefficients, respectively. Define a dimensionless parameter, γ, which indicates the relative magnitude of the salinity variations with respect to the temperature variations:

$$\gamma = \frac{\beta_S \ (\Delta S)_{rms}}{\beta_T \ (\Delta T)_{rms}} \quad .$$

Also, define the related parameters

$$\gamma_1 = \frac{\beta_S}{\beta_T} \qquad \text{and} \qquad \gamma_0 = \frac{(\Delta S)_{rms}}{(\Delta T)_{rms}}$$

where

$$\gamma = \gamma_0 \gamma_1 \quad .$$

The correlation between the temperature and salinity variations is determined by the correlation coefficient, ρ, which is defined by

$$\rho = \frac{(\Delta T \cdot \Delta S)_{rms}}{(\Delta T)_{rms} \ (\Delta S)_{rms}} \quad .$$

The rms value of the conductivity variations is

$$\left(\frac{\Delta\sigma}{\sigma}\right)^2_{rms} = \beta_T^2\,\overline{\Delta T^2}_{rms} + \beta_s\,\overline{\Delta S^2}_{rms} + 2\beta_T\beta_S\,(\overline{\Delta T\cdot\Delta S})_{rms}$$

or

$$\left(\frac{\Delta\sigma}{\sigma}\right)_{rms} = \beta_T\,\Delta T_{rms}\left\{1 + 2\rho\gamma + \gamma^2\right\}^{1/2}$$

If the correlation is very small ($\rho \ll 1$), then

$$\left(\frac{\Delta\sigma}{\sigma}\right)_{rms} = \beta_T\,\Delta T_{rms}\,\sqrt{1+\gamma^2}\;;$$

if the temperature and salinity are completely correlated ($\rho = \pm 1$), then

$$\left(\frac{\Delta\sigma}{\sigma}\right)_{rms} = \beta_T\,\Delta T_{rms}\,(1 \pm \gamma);$$

if the salinity variations are very small in comparison with the temperature variations, then

$$\left(\frac{\Delta\sigma}{\sigma}\right)_{rms} = \beta_T\,\Delta T_{rms}\,(1+\rho\gamma).$$

In the ocean γ is approximately 0.1 (small) and ρ is probably near +1.0 for large scale microstructure, and zero for microstructure smaller than the dissipation length (Section 13.) of the temperature structure. In any case, we see that, in the ocean, the conductivity variations on the average are due primarily to temperature variations:

$$\left(\frac{\Delta\sigma}{\sigma}\right)_{rms} \approx \beta_T\,\Delta T_{rms}.$$

Effective Temperature

The changes of conductivity in a solution are due to a combination of corresponding fluctuations in temperature and salinity. The magnitude of these conductivity fluctuations can be described in terms of a fractional change, ($\Delta\sigma/\sigma$), or in terms of an "effective temperature change," ΔT^*, which causes the same fractional change in conductivity. We could also speak of an "effective salinity change," ΔS^*, which produces the same fractional change in conductivity. If the conductivity change ($\Delta\sigma/\sigma$) is known, then we have

$$\beta_T\,\Delta T^* \equiv \left(\frac{\Delta\sigma}{\sigma}\right) \equiv \beta_s\,\Delta S^*$$

We will tend to talk more in terms of the effective temperature, ΔT^*, because in the water media of most interest, viz., in the ocean and water tunnel experiments, the conductivity fluctuations are due primarily to temperature fluctuations, i.e., the following inequality holds in several important cases

$$\beta_S (\Delta S)_{rms} << \beta_T (\Delta T)_{rms} .$$

Typically, in the ocean the conductivity variations due to salinity are about 1/10 those due to temperature (Sec. 7.3).

The effective temperature is related to the actual temperature and salinity variations as follows:

$$\beta_T \Delta T^* = \frac{\Delta\sigma}{\sigma} = \beta_T \Delta T + \beta_S \Delta S$$

or

$$\Delta T^* = \Delta T + \left(\frac{\beta_S}{\beta_T}\right)\Delta S = \Delta T + \gamma \Delta S$$

The rms value of the effective temperature is

$$\Delta T^*_{rms} = \Delta T_{rms} \sqrt{1+\gamma^2} ,$$

where the temperature and salinity fluctuations are assumed to be independent. If, on the other hand, these signals are correlated then,

$$\Delta T^*_{rms} = \Delta T_{rms} \sqrt{1+2\rho\gamma+\gamma^2}$$
$$\approx \Delta T_{rms} (1+\gamma\rho) ,$$

where the latter approximation assumes $\gamma << 1$ as is the case in the ocean where γ is about 1/10.

The fractional electrode resistance variations in terms of the effective temperature change is simply:

$$\frac{\Delta R}{R} = -\beta_T \Delta T^* .$$

7. CONDUCTING MEDIUM

The analysis of the detection instrumentation of this Report calls for the consideration of many variables and parameters which describe the phenomena under study in the conducting fluid medium. It is useful at the outset to list precisely what variables will be considered, it being assumed that those not mentioned will be of negligible importance to the analysis. The variables have been classed either as "medium variables" because they describe the physical state of the medium in which measurements are being made, or "system variables" because they describe the state of the instrumentation which is operative in the measurements. In the interest of illustrating the performance of properties of various aspects of the instrumentation, certain typical or standard values of the physical variables will be decided upon and used in numerical examples throughout the Report. The oceans represent one of the most important conducting media for the application of the present instrumentation, therefore some of the average properties of the ocean environment are presented in Section 7.3 for estimating the performance of the detection equipment. Tables of physical data are given in Section 7.2 for several conducting solutions which are of interest.

7.1 Medium Variables

The conducting medium under consideration, here, is assumed to be an aqueous electrolyte solution (liquid) which, in general, is inhomogeneous in concentration and may contain solid impurities. It is this medium which we wish to adequately and concisely describe by a set of variables which specify the physical state of the water. Simplifying assumptions will be made where necessary to make the problem subject to analysis. The thermodynamic properties of the water are described by a chosen set of "thermodynamic variables" and the other physical properties by so-called "property variables." Special reference will be made to the two important cases of sea water and tap water. Measurements performed by detection equipment refer to measurements of "independent variables," which, as we shall see, are taken to be the thermodynamic variables of temperature, pressure, and salinity. The volume of localized inhomogeneities such as bubbles is another independent variable of the medium. Also measured is the velocity of the water with respect to the sensing instrument. Velocity is a relative quantity and should properly be considered both as a medium variable and system variable.

Thermodynamic Variables

The description of the thermodynamic state of a medium involves the description of the thermodynamic state of each of its homogeneous phases. Each phase is specified by its content, i.e., the quantity of each chemical substance it contains, and a specification of two other thermodynamic quantities such as temperature and pressure. A property of the medium is uniquely determined by specifying the temperature, pressure, and content,

provided the relation between the property and these variables is known (1). If the property under consideration is the density, then this relation is called the equation of state; this relation is known to high accuracy for sea water and fresh water (2,3).

The content or phase description of the water media of interest, viz., sea water and tap water, must be considered in more detail. In the case of sea water, it has been found that regardless of the absolute concentration, the relative proportions of the different major constituents are virtually constant, except in regions of very low salinity where minor deviations may occur. Oceanographers have made use of this principle of constancy of ratios of the major constituents of sea water in order to utilize the measurement of a single component to determine the salinity, S(‰), of a sample. We will assume that sea water is of constant relative composition to the degree of accuracy with which we are presently concerned. Sea water may then be considered as a composite electrolyte solution whose properties are single-valued functions (unique) of temperature, T, pressure, P, and total salt content or salinity, S. The typical composition of sea water may be found in the Reference (4).

For tap water, the principle of the constancy of ratios of the component salt concentrations is not valid. The concentration of dissolved salts varies widely depending on the tap water used (5). In order to work with a single variable to describe the concentrations of salts in tap water, we will define an effective salinity, S, based on the electrical conductivity of the tap water sample. This is done in the following manner: if σ is the measured conductivity of the tap water sample, and S_o and σ_o are the adopted standard salinity of sea water (Sec. 7.2), then the effective salinity, S, of the tap water is defined by the equation

$$S = S_o \left(\frac{\sigma}{\sigma_o}\right).$$

The adopted standard values at 20° C are S_o = 35 ‰ and σ_o = .0479 $ohm^{-1}cm^{-1}$; typically the conductivity of tap water is about 1/100 times that of sea water so that S is typically about 0.3 ‰.

Random localized impurities in the water, for example bubbles, will be considered to be internally homogeneous and characterized by their volume v.

Property Variables

The dependent variables of the medium are those physical characteristics other than the temperature, salinity and pressure and will be termed "property variables." The electrical conductivity, dielectric constant and density are examples of property variables. The property variables are only functions of temperature, salinity and pressure; if ψ is a property of the medium, then it satisfies the equation

$$\psi = \text{function } (T,S,P).$$

The pressure dependence proves to be of negligible importance in the present research.

Numerous properties of the medium are of interest in the present analysis; not all of these properties are independent, however. For example, the kinematic viscosity is the ratio of dynamic viscosity and density. In this Report we will prefer to work with the least number of independent properties necessary for the analysis, and the most dimensionless properties as, for example, the Prandtl number (6). We chose the following list as the preferred set of medium properties:

Density (d)
Electrical Conductivity (σ)
Dielectric Constant (κ)
Heat Capacity per Unit Volume (c)
Prandtl Number (P)
Schmidt Number (S)
Kinematic Viscosity (ν).

These are functions only of

Temperature (T)
Salinity (S)
Pressure (P) .

In the analysis, work will be done with other property variables (e.g. resistivity) which are not independent of the above property variables as required to simplify the analysis, but will reduce most of the final results to the above minimal set of property variables. The dependence of these variables on temperature and salinity is covered in Section 7.2 and on pressure in Section 6.2 .

The parameters or variables which relate to the characteristics of the detection instrument are termed system variables. The most important of these, actually, is the quantity which is measured, that is the electrode impedance. Others are the electrode power, size and velocity in the water medium. The system variables have average values which are controllable by design. Their fluctuating values are dependent on the independent variables to be measured, viz., temperature, salinity, pressure, cavity volume and velocity.

Standard Conditions

The standard conditions for the thermodynamic variables which are assumed in this Report for sea water are the following:

Temperature	20°C (293 °K)
Salinity	35 ‰
Pressure	1 Atm

For calculations where reference to tap water is necessary, the same standard temperature and pressure will be used. A standard concentration of dissolved salts and gases is not as meaningful in the case of tap water as sea water because of the great variability in the composition of tap water from one location to another. It seems more useful to assume a standard electrical conductivity (a property variable) as a value for reference. The value assumed for tap water in this Report is 1/100 that of standard sea water;

$$4.8 \times 10^{-4} \quad \text{ohm}^{-1}\text{cm}^{-1} \quad ,$$

which corresponds to about 0.4 ‰ dissolved salts (in a variety of proportions) in pure water.

The assumed standard conditions for the property variables pertinent to this work follows immediately from the above standard conditions because of their unique dependence on temperature, pressure and concentration. These standard values for sea water and tap water (and/or fresh water) are given in Table 7.1 below. More detailed data is found in Section 7.2 at non-standard temperature, pressure and concentration.

Table 7.1. Physical Properties of Standard Sea Water and Tap Water at 20°C and 1 Atm.

Variable	Sea Water	Tap Water
Density (d, gm/cm^3)	1.0248	0.9982
Conductivity (σ, $ohm^{-1}cm^{-1}$)	.0479	.00048
Dielectric Constant (K)	73.8	80.1
Heat Capacity (c, $joule/cm^3/°C$)	4.092	4.174
Kinematic Viscosity (ν, cm^2/sec)	.0106	.01004
Prandtl Number ($\mathbb{P}$)	7.30	7.01
Schmidt Number ($\mathbb{S}$)	770	~700

7.2 Physical Data

The measurement of temperature, salinity and velocity of water by the principles of this Report requires that the water have a finite electrolytic conductivity. The water media of most interest for these measurements are sea water and tap water. Other electrolyte solutions of interest in experimental measurements are, e.g., sodium chloride and sodium hydroxide solutions. The electrical conductivity, under varying conditions,

of a number of aqueous solutions are given in this Section along with other physical properties which relate to the analysis of the detection techniques. Since many of these properties are approximately those of pure water, its characteristics are also listed (although its electrical conductivity is altogether too low for practical measurements by the present techniques).

This somewhat extensive compilation of physical data was felt to be worth while because of its present and future usefulness in the applications of these instruments. The aqueous solutions for which data and references are given are:

Sea Water
Artificial Sea Water
NaCl Solution
Tap Water
Pure Water
NaOH Solution
KCl Solution

For general information concerning the properties of water and aqueous solutions reference should be made to Dorsey (7) and the Physical and Chemical Handbooks (8,9,10). Because it is necessary to operate the velocity detector in a way which brings the water near boiling, it is of interest to know the physical properties over the range from 0 - 100°C, which will be done in as many cases as data is available. Much of the data presented in this Section has been processed so that it is in units convenient to the present analysis, (e.g., salinities (‰) instead of concentration (mole/liter)). No claims will be made for the accuracy of the data in this Section other than to say that its treatment was carried out with care and with consistency checks. In some cases the accuracy is not as good as the original data because some significant figures have been dropped in the interest of space and because very great precision in the values of the properties is not called for. In only a few cases the data has been smoothed from original data and may implicitly overstate the accuracy of the data. The differential coefficients with respect to temperature, salinity, and pressure of many of the properties considered here are given in Section 6.2 . For the purpose of making numerical calculations as examples throughout this Report, certain "standard conditions" have been defined as discussed in Section 7.1 and in the following paragraphs.

Sea Water

Sea water is of primary concern as an electrically conducting solution. The general physical properties and chemical composition of sea water may be found in the References (4,9,15). The experimental data on the conductivity of sea water (11,12) has been tabulated in Table 7.2 as a function of temperature and salinity. It is necessary to convert from the chlorinity, Cl, of the water to the salinity, S, by the accepted formula (13)

$$S = 0.03 + 1.805\ (Cl)\ ,$$

where both S and Cl are expressed in ‰ units. This data is shown in graphical form in Figure 2.6 of Section 2.3 over the range of temperature and salinity ordinarily found in the ocean. The temperature and salinity coefficients computed from this data are shown in Figures 2.7 and 2.8 of Section 2.3 . The electrical properties of sea water at very high frequencies in the radar range are treated by Saxton and Lane (14). For the calculation of numerical examples, it is useful to define a "standard sea water" corresponding to a standard salinity and temperature. The standard temperature will be taken as 20°C which is more like the temperatures found in the laboratory than in the average ocean temperature (15°C). Concerning the standard salinity, we use that of the so-called "normal water" prepared by the Hydrographical Laboratories in Copenhagen, Denmark (13). The chlorinity of normal water is 19.381 ‰ corresponding to a salinity of 35.02 ‰. The conductivity of this standard sea water is .04790 $ohm^{-1}cm^{-1}$, and the density is 1.0248 gm/cm^3. Although our interest in the properties of sea water extends over the temperature range from 0° - 100°C, data is not available over this range but covers only the range from 0° - 30°C. Furthermore, many of the physical properties of actual sea water have not been measured. It is customary where such gaps exist in the data to use as an approximation the properties of a corresponding sodium chloride (NaCl) solution. This procedure is adopted here; data on NaCl is given in a following Section. Some of the physical properties of standard sea water are shown in Table 7.3 as a function of temperature; the source references are given at the bottom of this Table. The variation of the density of sea water over the range of temperature and salinity ordinarily found in the oceans is shown in Figure 7.6 of Section 7.3 . Also in that Section are found data on the average values of the properties of sea water as a function of depth.

Table 7.2. Electrical Conductivity of Sea Water as a Function of Temperature and Salinity at Atmospheric Pressure (1 Atm)

σ ($ohm^{-1}m^{-1}$) ↘		S (‰) →					
		32	33	34	35	36	37
T (°C) ↓	0	2.667	2.749	2.827	2.904	2.979	3.016
	5	3.082	3.178	3.266	3.352	3.429	3.481
	10	3.498	3.617	3.711	3.804	3.906	3.968
	15	3.945	4.073	4.179	4.286	4.403	4.470
	18	4.207	4.367	4.454	4.566	4.679	4.773
	20	4.405	4.545	4.669	4.790	4.904	4.988
	25	4.988	5.043	5.168	5.316	5.432	5.556
	30	5.587	5.682	5.780	5.917	6.042	6.173

Table 7.3 . Properties of Normal Sea Water (35.02 ‰) as a Function of Temperature at Atmospheric Pressure.

T (°C)	Density (gm/cm^3)	Heat Capacity per Unit Volume (joule/cm^3/°C)	Electrical Conductivity (ohm^{-1} m^{-1})	Resistivity (ohm-cm)	Viscosity (.01 cm^2/sec)
0	1.0281	4.0971	2.955	33.84	1.83
5	1.0277	4.0964	3.403	29.39	1.57
10	1.0270	4.0956	3.855	25.94	1.36
15	1.0260	4.0937	4.337	23.06	1.19
18	1.0253	4.0927	4.617	21.66	1.11
20	1.0248	4.0920	4.790	20.88	1.06
25	1.0234	4.0883	5.367	18.63	0.94
30	1.0217	4.0860	5.968	16.76	0.85
Ref.	3,16	17	11	11	18

Artificial Sea Water

The relative chemical composition of sea water is found to be quite uniform over a wide range of salinity and contains a large number of constituents, the most abundant being common salt, NaCl. Formulas for mixing solutions which closely approximate that of sea water have been developed and can be used where it is important to simulate as closely as possible the actual conditions which exist in a sea water environment (20,21). The approximate quantities of the main components of one formula for artificial sea water solution is listed in Table 7.4 (19). Because of the complexity of working with these artificial sea water solutions in routine laboratory work and because the precise chemical composition of solutions used in experimental work is not germain to the present experiments, these solutions were not used. Only the simplest of approximations to sea water was used in the laboratory tests, namely the NaCl solution, discussed subsequently.

Table 7.4 . Composition of Artificial Sea Water

Salt	Salinity (‰)
NaCl	25.2
$MgCl_2$	5.3
Na_2SO_4	4.2
$CaCl_2$	1.2
KCl	0.7
$NaHCO_3$	0.2
KBr	0.1

NaCl Solution

A solution of sodium chloride (NaCl) of appropriate concentration (salinity) has physical properties which closely approximate those of sea water. This is of practical importance for experimental work in the laboratory because of the ease and simplicity of working with a solution of common salt instead of the more complicated artificial sea water solution discussed above. This electrolyte solution is probably the simplest and most commonly available, hence there is a considerable amount of data available on its physical properties. It is somewhat surprising that much of the data at higher concentration ($\sim 4\%$), of the order of that found in the oceans, has been measured only in the last decade. For use as a substitute for sea water, some convention must be established in order to be able to decide when sea water of given salinity and temperature is equivalent to a NaCl solution. The following convention is adopted: a standard NaCl solution is one which has the same electrical conductivity as sea water of 35.02 ‰ salinity at 20°C temperature. The conductivity of sea water at this temperature and salinity is 0.04790 $ohm^{-1}cm^{-1}$. A NaCl solution has the same conductivity at 20°C at a salinity of 32.84 ‰. A sodium chloride solution of this salinity has been used in laboratory experiments as the electrical equivalent of standard sea water. The adopted convention insures the equality of the electrical conductivity of these solutions, however, with respect to the other physical properties small differences exist. Since the NaCl solution is a convenient substitute for experiments which are intended to approximate sea water, some of the properties of NaCl solutions with a salinity covering the approximate range of sea water salinities have been computed at atmospheric pressure (1 Atm) and listed in Tables 7.5 to 7.11 . The electrical conductivity data was taken from References (22-26); the density from (27), and the molecular weight of NaCl is 58.45 gms. The electrical properties at high frequencies (radio and radar range) is found in References (28,14,

29,30). The physical properties of standard NaCl solution (32.84 ‰) have been computed as a function of temperature from 0° - 100°C and are listed in Table 7.12 ; the References to this data appear at the bottom of the Table. The diffusion coefficient was assumed to vary in proportion with the electrical conductivity over the temperature range in question (31, 32). The electrical conductivity of standard NaCl solution at temperatures above 100°C, listed in Table 7.13 and plotted in Figure 7.1 , are of interest in the operation of the velocity sensor at great depths in the ocean where because of the greater pressure the boiling point is increased (see Table 7.17a for pure water). The conductivity of NaCl solution as a function of concentration (mole/liter) is given in Table 7.14 .

Table 7.5 . Concentration (moles/liter) of NaCl Solution as a Function of Temperature and Salinity

(mole/liter)	S (‰) ⟶						
c	30	31	32	33	34	35	36
15	.5239	.5418	.5597	.5776	.5955	.6134	.6314
16	.5238	.5416	.5595	.5774	.5953	.6133	.6312
T 17	.5237	.5415	.5594	.5772	.5952	.6131	.6311
(°C) 18	.5235	.5413	.5592	.5771	.5950	.6129	.6309
↓ 19	.5234	.5412	.5591	.5770	.5949	.6128	.6307
20	.5233	.5411	.5589	.5768	.5947	.6126	.6306
21	.5231	.5410	.5588	.5767	.5946	.6125	.6304
22	.5230	.5408	.5586	.5765	.5944	.6123	.6303
23	.5229	.5407	.5585	.5764	.5943	.6122	.6301
24	.5228	.5406	.5584	.5762	.5941	.6120	.6300
25	.5226	.5404	.5583	.5761	.5940	.6119	.6298

Table 7.6 . Density (gm/cm^3) of NaCl Solution as a Function of Temperature and Salinity

(gm/cm^3) 1000(d-1)		S (‰) → 30	31	32	33	34	35	36
T (°C) ↓	15	20.77	21.51	22.26	22.98	23.66	24.39	25.13
	16	20.51	21.22	21.95	22.70	23.41	24.13	24.87
	17	20.29	20.90	21.70	22.41	23.15	23.86	24.59
	18	20.00	20.68	21.42	22.14	22.87	23.59	24.31
	19	19.77	20.45	21.14	21.90	22.62	23.34	24.06
	20	19.60	20.20	20.90	21.67	22.37	23.08	23.79
	21	19.24	19.96	20.63	21.40	22.11	22.82	23.53
	22	19.00	19.71	20.39	21.14	21.85	22.56	23.29
	23	18.78	19.40	20.17	20.90	21.59	22.30	23.03
	24	18.51	19.20	19.90	20.64	21.33	22.05	22.79
	25	18.28	18.98	19.67	20.38	21.08	21.81	22.54

Table 7.7 . Resistivity (ohm-cm) of NaCl Solution as a Function of Temperature and Salinity

(ohm-cm) ρ		S (‰) → 30	31	32	33	34	35	36
T (°C) ↓	15	25.39	24.64	23.94	23.28	22.66	22.08	21.52
	16	24.83	24.10	23.41	22.77	22.16	21.59	21.05
	17	24.29	23.57	22.90	22.28	21.68	21.11	20.58
	18	23.77	23.07	22.41	21.79	21.21	20.66	20.14
	19	23.26	22.57	21.93	21.32	20.76	20.22	19.71
	20	22.76	22.09	21.47	20.88	20.32	19.79	19.29
	21	22.29	21.63	21.02	20.44	19.89	19.38	18.89
	22	21.83	21.19	20.58	20.02	19.48	18.98	18.50
	23	21.39	20.76	20.17	19.61	19.08	18.59	18.13
	24	20.95	20.33	19.76	19.22	18.70	18.22	17.76
	25	20.53	19.93	19.36	18.84	18.33	17.86	17.41

Table 7.8 . Equivalent Conductance ($ohm^{-1}mole^{-1}cm^2$) of NaCl Solution as a Function of Temperature and Salinity

$\left(\frac{cm^2}{ohm\text{-}mole}\right)$		S (‰) →						
		30	31	32	33	34	35	36
	15	75.16	74.90	74.63	74.36	74.10	73.84	73.59
	16	76.88	76.61	76.33	76.06	75.79	75.53	75.27
T	17	78.62	78.34	78.06	77.78	77.51	77.24	76.97
(°C)	18	80.37	80.08	79.81	79.53	79.25	78.98	78.72
↓	19	82.16	81.86	81.57	81.28	80.99	80.71	80.43
	20	83.95	83.65	83.35	83.05	82.76	82.47	82.19
	21	85.76	85.45	85.15	84.84	84.55	84.25	83.96
	22	87.59	87.28	86.96	86.65	86.35	86.05	85.75
	23	89.43	89.11	88.79	88.47	88.17	87.86	87.56
	24	91.29	90.97	90.64	90.31	90.00	89.68	89.38
	25	93.18	92.83	92.50	92.16	91.83	91.51	91.19

Table 7.9 . Electrical Conductivity ($ohm^{-1}cm^{-1}$) of NaCl Solution as a Function of Temperature and Salinity

$(ohm^{-1}cm^{-1})$ $100\ \sigma$		S (‰) →						
		30	31	32	33	34	35	36
	15	3.938	4.058	4.177	4.295	4.413	4.529	4.646
	16	4.027	4.149	4.271	4.392	4.512	4.632	4.751
T	17	4.117	4.242	4.367	4.489	4.613	4.736	4.858
(°C)	18	4.207	4.335	4.463	4.590	4.715	4.841	4.966
↓	19	4.300	4.430	4.561	4.690	4.818	4.946	5.073
	20	4.393	4.526	4.658	4.790	4.922	5.052	5.183
	21	4.486	4.623	4.758	4.893	5.027	5.160	5.293
	22	4.581	4.720	4.858	4.995	5.133	5.269	5.405
	23	4.676	4.818	4.959	5.099	5.240	5.379	5.517
	24	4.773	4.918	5.061	5.204	5.347	5.488	5.631
	25	4.870	5.017	5.164	5.309	5.455	5.599	5.743

Table 7.10 . Salinity Coefficient of Conductivity (% per ‰) of NaCl Solution as a Function of Temperature and Salinity

(% per ‰) β_S		S (‰) ⟶						
		30	31	32	33	34	35	36
	15	3.043	2.949	2.854	2.763	2.675	2.594	2.521
	16	3.041	2.947	2.852	2.761	2.673	2.592	2.519
T	17	3.039	2.945	2.850	2.759	2.671	2.590	2.517
(°C)	18	3.037	2.943	2.848	2.757	2.669	2.588	2.515
↓	19	3.035	2.941	2.846	2.755	2.667	2.586	2.513
	20	3.033	2.939	2.844	2.753	2.665	2.584	2.511
	21	3.031	2.937	2.842	2.751	2.663	2.582	2.509
	22	3.029	2.935	2.840	2.749	2.661	2.580	2.507
	23	3.027	2.933	2.838	2.747	2.659	2.578	2.505
	24	3.025	2.931	2.836	2.745	2.657	2.576	2.503
	25	3.023	2.929	3.834	2.743	2.655	2.574	2.501

Table 7.11 . Temperature Coefficient of Conductivity (% per °C) NaCl Solution as a Function of Temperature and Salinity

(% per °C)		S(‰)
	β_T	30 - 36
	15	2.275
	16	2.249
T	17	2.224
(°C)	18	2.198
↓	19	2.173
	20	2.147
	21	2.121
	22	2.096
	23	2.070
	24	2.045
	25	2.019

Table 7.12 . Properties of Standard NaCl Solution (32.84 ‰) as a Function of Temperature

t (°C)	Density (gm/cm^3)	Dielectric Constant	Conductivity .01 (ohm^{-1} cm^{-1})	Resistivity (ohm-cm)	Equivalent Conductance (ohm^{-1} mole^{-1} cm^2)	Kinematic Viscosity .01 (cm^2/sec)	Diffusion Coefficient 10^{-5} (cm^2/sec)	Thermal Conductivity 10^{-5} (watt cm^{-2} °C^{-1})
0	1.0246	81.4	2.93	34.17	51.0	1.79	0.82	536
5	1.0243	79.5	3.37	29.68	58.7	1.53	0.94	546
10	1.0237	77.5	3.82	26.20	66.5	1.33	1.06	557
15	1.0228	75.6	4.27	23.42	74.4	1.16	1.19	568
18	1.0221	74.5	4.58	21.9	79.6	1.08	1.28	574
20	1.0216	73.8	4.79	20.88	83.1	1.03	1.34	578
25	1.0201	72.0	5.29	18.90	92.2	.920	1.474	587
30	1.0185	70.2	5.82	17.18	101.4	.828	1.62	595
35	1.0166	68.5	6.35	15.74	110.7	.751	1.77	602
40	1.0148	66.8	6.92	14.46	120.5	.685	1.93	609
45	1.0126	65.2	7.50	13.34	130.6	.628	2.09	616
50	1.0104	63.6	8.09	12.36	141.0	.578	2.25	622
55	1.0079	62.0	8.73	11.45	152.1	.536	2.43	628
60	1.0054	60.5	9.40	10.64	163.7	.497	2.62	633
65	1.0023	59.0	10.08	9.92	175.6	.464	2.81	637
70	0.9997	57.6	10.79	9.27	187.9	.435	3.0	642
75	0.9967	56.1	11.51	8.69	200.5	.409	3.2	646
80	0.9939	54.7	12.26	8.16	213.6	.385	3.4	649
85	0.9906	53.4	13.03	7.68	227.0	.364	3.6	651
90	0.9872	52.0	13.82	7.24	240.8	.345	3.9	654
95	0.9839	50.7	14.64	6.83	255.1	.327	4.1	656
100	0.9806	49.4	15.48	6.46	269.7	.312	4.3	658
Ref.	27	33	22-26	22-26	22-26	32	31, 35	34

Table 7.12 . Properties of Standard NaCl Solution (32.84 ‰) as a Function of Temperature

T (°C)	Thermal Diffusivity .001 (cm^2/sec)	Prandtl Number (P)	Schmidt Number (S)	Heat Capacity per Volume Unit (joule/cm^3/°C)
0	1.31	13.7	2180	4.109
5	1.33	11.5	1630	4.107
10	1.36	9.78	1250	4.107
15	1.39	8.35	975	4.104
18	1.40	7.71	844	4.103
20	1.41	7.30	769	4.102
25	1.44	6.39	624	4.097
30	1.46	5.67	511	4.095
35	1.47	5.11	424	4.092
40	1.49	4.60	355	4.088
45	1.51	4.16	300	4.085
50	1.53	3.78	257	4.079
55	1.54	3.48	221	4.074
60	1.56	3.19	190	4.068
65	1.57	2.96	165	4.061
70	1.59	2.74	145	4.054
75	1.60	2.56	127	4.047
80	1.61	2.39	113	4.037
85	1.62	2.25	101	4.030
90	1.63	2.12	88	4.021
95	1.64	1.99	80	4.012
100	1.65	1.89	73	4.003
Ref.	-	-	-	17,41

Table 7.13 . Electrical Conductivity of Standard NaCl Solution (32.84 ‰) at High Temperature

T (°C)	Conductivity $ohm^{-1}cm^{-1}$
100	0.155
120	0.181
140	0.209
160	0.232
180	0.252
200	0.269
220	0.285
240	0.299
260	0.310
280	0.319
300	0.328
320	0.336
340	0.344
360	0.350
Ref.	26

Table 7.14 . Electrical Conductivity of NaCl Solution as a Function of Concentration at 20°C

Concentration (moles/liter)	Equivalent Conductivity $(ohm^{-1}mole^{-1}cm^{2})$	Conductivity $(ohm^{-1}m^{-1})$
0.0	114	.0000
0.0005	112	.0056
0.001	111	.0111
0.005	108	.0541
0.01	106	.106
0.02	104	.208
0.05	100	0.500
0.1	95.9	0.959
0.2	91.4	1.83
0.5	84.3	4.22
1.	77.1	7.71
1.5	71.9	10.8
2.	67.3	13.5
3.	59.0	17.7
4.	51.4	20.6
5.	44.5	22.2

Reference (22)

Tap Water

In most respects tap water behaves very much like pure water. The main difference between these two waters is in their electrical conductivity. The conductivity of tap water is typically 500 times that of distilled water. The concentration of dissolved salts in tap water varies considerably from location to location; in Los Angeles water the salinity is about 0.50 ‰; in Washington, D.C. it is about 0.22 ‰ (5). The term salinity here refers to the grams of total filterable residue per liter

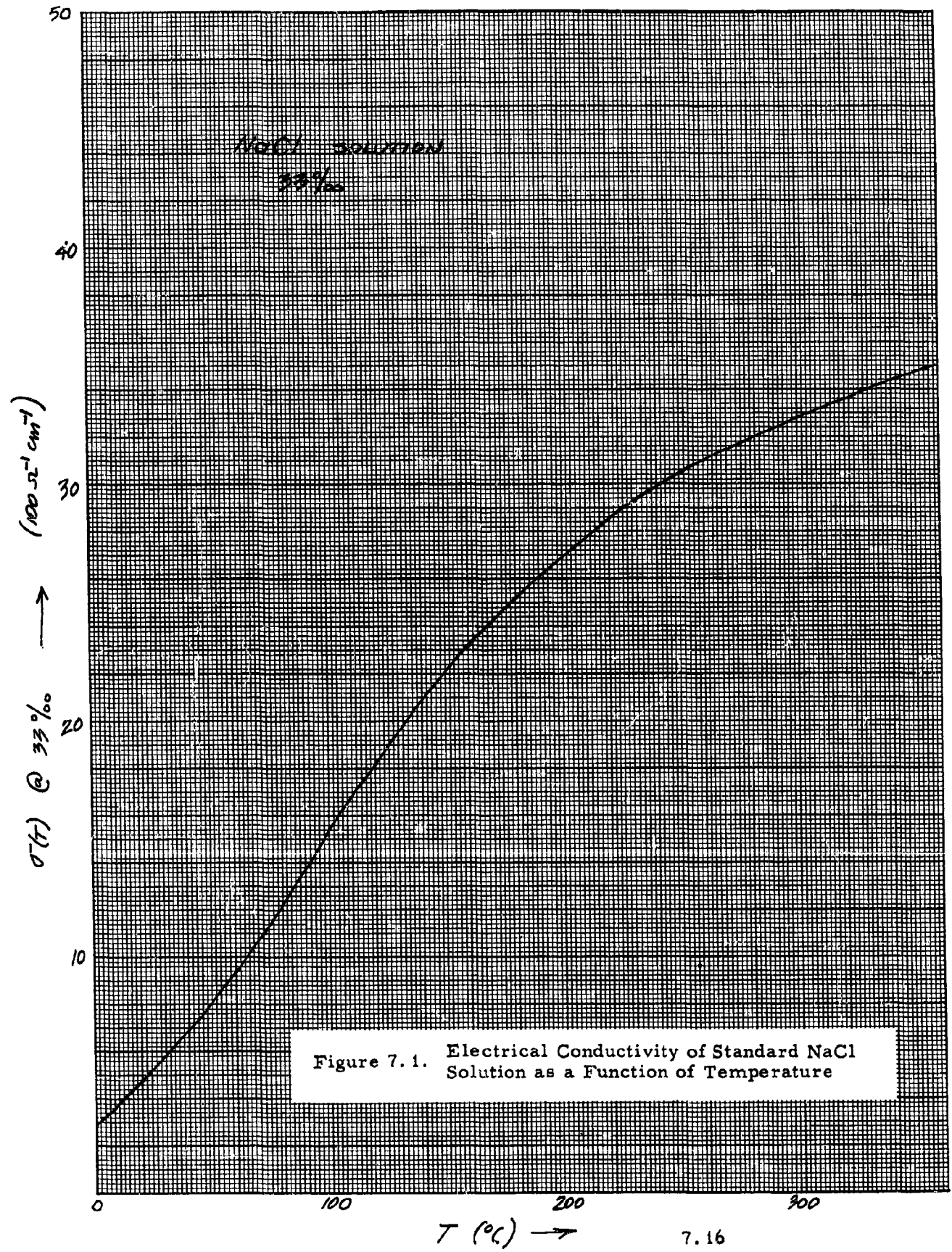

Figure 7.1. Electrical Conductivity of Standard NaCl Solution as a Function of Temperature

of solution which is very rarely equal to the same quantity per 1000 grams of solution (‰). The common unit used in water analysis is mg/liter or approximately 10^{-3} ‰. The conductivity of the water is related to the total concentration of the ionized substances. The amount of dissolved matter in a sample (in mg/liter) may often be estimated by multiplying the conductivity (in 10^{-6} ohm^{-1}cm^{-1}) by an empirical factor which varies from 0.55 to 0.9, depending on the soluble components of the particular water (36). The conductivity per unit concentration of the ions commonly found in tap water is listed in Table 7.15 for water with a conductivity of about 100 micro-ohm^{-1}cm^{-1} (5,37,38,39). This data was prepared from the values and behavior of the conductivity at infinite dilution (3). It is necessary to specify the concentration (or conductivity) because the conductivity of the water is not directly proportional to the concentration, although it is a rough approximation. As a rough estimate of the coefficient, Λ_i listed in Table 7.15 at a conductivity other than 100 micro-ohm^{-1}cm^{-1}, we have

$$\frac{\Lambda(\sigma)}{\Lambda(100)} = 1 + K - K\sqrt{\frac{\sigma}{100}} \quad , \quad (K \approx .06)$$

where σ is in units of micro-ohm^{-1}cm^{-1}. As an example of the conductivity of ordinary tap water, we list in Table 7.16 the concentration and conductivity of the individual and total ions according to the coefficients in Table 7.15 . Applying the above correction to the total conductivity for the two waters, we obtain the corrected conductivity at the bottom of this Table along with the conductivity/concentration ratio. This ratio falls within the range previously mentioned (.55 - .90).

The effective salinity with reference to sea water was defined in Section 7.1 as

$$S_{EFF} = S_o \left(\frac{\sigma}{\sigma_o}\right)$$

where σ_o, S_o are the standard conductivity and salinity of sea water at 20°C (.0479 ohm^{-1}cm^{-1}, 35 ‰). The values of S_{EFF} are listed at the bottom of Table 7.16 for Los Angeles and Washington, D.C. waters. This quantity has been defined to standardize tap water measurements by measuring only the conductivity and not the individual salt concentrations.

The variability of the conductivity from location to location is illustrated in Table 7.16 , but it also varies with time and water source in a given city. Laboratory measurements here usually give a conductivity of about 500 μ ohm^{-1}cm^{-1} instead of the 740 μ ohm^{-1}cm^{-1} listed in Table 7.16 taken from Reference (5).

For the other physical properties of tap water the values for pure water may be used with good accuracy.

Table 7.15. Conductance Factors of Ions Commonly Found in Water

Ion		Λ, Equivalent Conductivity (25°C) 10^{-6} ohm^{-1}cm^{-1}	
		Per me/l	Per mg/l
HCO_3^-	Bicarbonate	43.6	0.715
Ca^{++}	Calcium	52.0	2.60
CO_3^{--}	Carbonate	84.6	2.82
Cl^-	Chloride	75.9	2.14
Mg^{++}	Magnesium	46.6	3.82
NO_3^-	Nitrate	71.0	1.15
K^+	Potassium	72.0	1.84
Na^+	Sodium	48.9	2.13
SO_4^{--}	Sulfate	73.9	1.54

Table 7.16 Conductivity of Tap Water

Ion	Los Angeles		Washington, D.C.	
	Concentration mg/l	Conductivity 10^{-6} ohm^{-1}cm^{-1}	Concentration mg/l	Conductivity 10^{-6} ohm^{-1}cm^{-1}
Bicarbonate	215	154	79	56
Calcium	27	70	34	88
Carbonate	90	254	59	166
Chloride	44	94	5.2	11
Magnesium	12	46	1.9	7
Nitrate	1	1	1	1
Potassium	18	33	1.7	3
Sodium	56	119	5.1	11
Sulfate	39	60	34	52
TOTAL	502	831	221	395
Corr. Conductivity	740		372	
Ratio	0.68		0.60	
$S_{eff.}$	0.54 ‰		0.27 ‰	

Pure Water

In many respects the physical properties of pure water and tap water are almost identical. The main exception is the electrical conductivity. Because of the availability of data on pure water, its physical properties will be used and tabulated under the assumption that they can be used with accuracy for ordinary tap water. Tables for the properties of interest are listed in Table 7.17 as a function of temperature from 0°C to 100°C. This full range is of importance because the detection equipment is operated near boiling when water velocity is being measured. The sources of these data are listed at the bottom of the Table. Entries without references were computed from combinations of data with references. The data refers to atmospheric pressure (1 Atm). Vapor pressure data above 100°C shown in Table 7.17a is of interest in connection with boiling at great depths in the ocean (Sec. 12.6). The properties of water at high (radar) frequencies is found in References (30, 29, 45).

Table 7.17a. Vapor Pressure of Pure Water at High Temperature

(°C) T	Vapor Pressure (ATM)
100	1.00
120	1.96
140	3.57
160	6.10
180	9.90
200	15.3
220	22.9
240	33.0
260	46.3
280	63.3
300	84.8
320	111
340	144
360	184
Ref. (46)	

Table 7.17 . Properties of Pure Water as a Function of Temperature

T (°C)	Density (gm/cm^3)	Dielectric Constant	Kinematic Viscosity .01 (cm^2/sec)	Heat Capacity per Unit Volume (joule/cm^3/°C)	Thermal Conductivity 10^{-5} (watt/cm/sec)	Thermal Diffusivity .001 (cm^2/sec)	Prandtl Number
0	.9998	87.74	1.787	4.217	554	1.314	13.6
5	1.0000	85.76	1.516	4.203	565	1.344	11.3
10	.9997	83.83	1.306	4.191	576	1.374	9.51
15	.9991	81.95	1.139	4.183	587	1.403	8.12
18	.9986	80.84	1.055	4.178	593	1.419	7.44
20	.9982	80.10	1.004	4.174	598	1.433	7.01
25	.9970	78.30	.8929	4.168	607	1.456	6.13
30	.9957	76.55	.8010	4.160	615	1.478	5.42
35	.9940	74.82	.7237	4.153	622	1.498	4.86
40	.9922	73.15	.6582	4.146	630	1.520	4.33
45	.9902	71.51	.6022	4.139	637	1.539	3.91
50	.9880	69.91	.5533	4.131	643	1.557	3.55
55	.9857	68.34	.5117	4.123	649	1.574	3.25
60	.9832	66.81	.4746	4.114	654	1.590	2.99
65	.9806	65.32	.4428	4.106	659	1.605	2.76
70	.9778	63.86	.4141	4.097	664	1.621	2.56
75	.9749	62.43	.3886	4.088	668	1.634	2.38
80	.9718	61.03	.3657	4.078	671	1.645	2.22
85	.9686	59.66	.3453	4.069	673	1.654	2.09
90	.9653	58.32	.3269	4.059	676	1.665	1.96
95	.9619	57.01	.3103	4.050	678	1.674	1.85
100	.9584	55.72	.2952	4.040	680	1.683	1.75
Refs.	41,42	41,30	41	43	44	-	-

KCl Solution

The cell constant of a given conductivity cell is ordinarily determined by a measurement with an electrolyte solution of known conductivity rather than by a computation based on the geometry of the electrodes. The most common solution for this purpose is potassium chloride (KCl). The conductivity of this solution is known to very high accuracy for a number of concentrations (47). The specific conductivity at selected points is listed in Table 7.18 .

Table 7.18 . Conductivity of KCl Solution

Salinity (‰)	σ (ohm^{-1}cm^{-1})		
	0°C	18°C	25°C
71.1352	0.06518	0.09784	0.11134
7.41913	0.007138	0.011167	0.012856
0.745263	0.0007736	0.0012205	0.001409

NaOH Solution

Some of the physical properties of sodium hydroxide solution (NaOH) are given because of their rather remarkable electrical conductivity properties. Among these are: relatively high conductivity, large temperature coefficient, and a salinity coefficient which is either positive, negative, or zero. The use of solutions of caustic soda present some hazard in laboratory experiments and therefore care must be taken in handling such solutions. This compound is available and is quite inexpensive. It is not corrosive to iron containers. The curves of conductivity vs. salinity for several temperatures shown in Figure 7.2 were calculated from available data on the equivalent conductivity vs. concentration (48), and the density vs. concentration (27). The molecular weight of NaOH is 40.01 grams. Because of interest in a solution whose conductivity is independent of salinity variations ($\beta_S \approx 0$), the conductivity at a salinity of about 20 ‰ has been computed as a function of temperature as shown in Figure 7.3 . The temperature coefficient at 20°C is 4.1 % per °C; at 0°C this coefficient is as high as 8.9 % per °C at saturation ($\sim$30 %).

7.3 Ocean Environment

Data on the typical values and characteristics of the temperature, salinity and velocity in the oceans are useful to estimate the performance of the present instrumentation at sea. Both steady state and turbulence

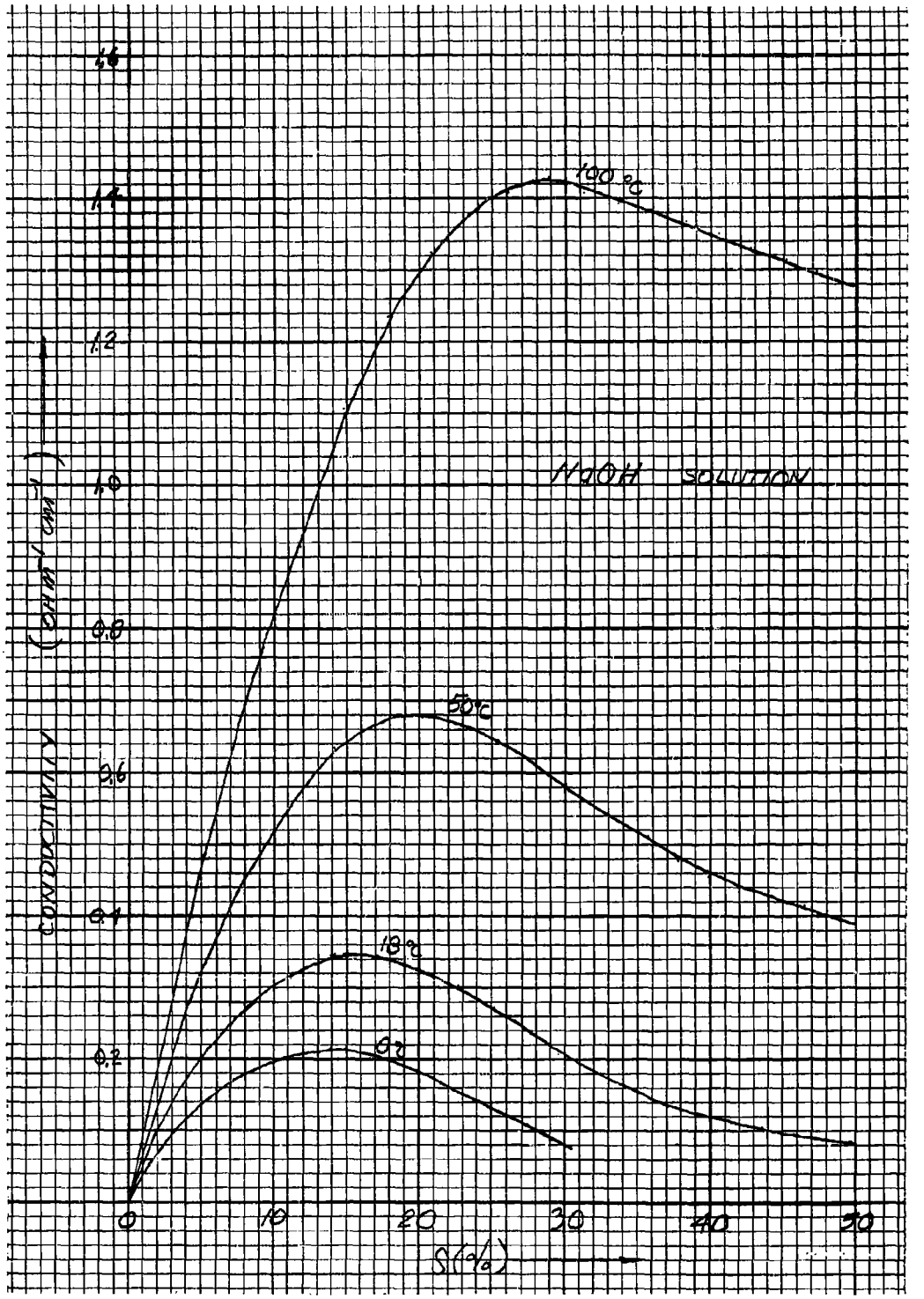

Figure 7.2. Electrical Conductivity of NaOH Solution as a Function of Salinity

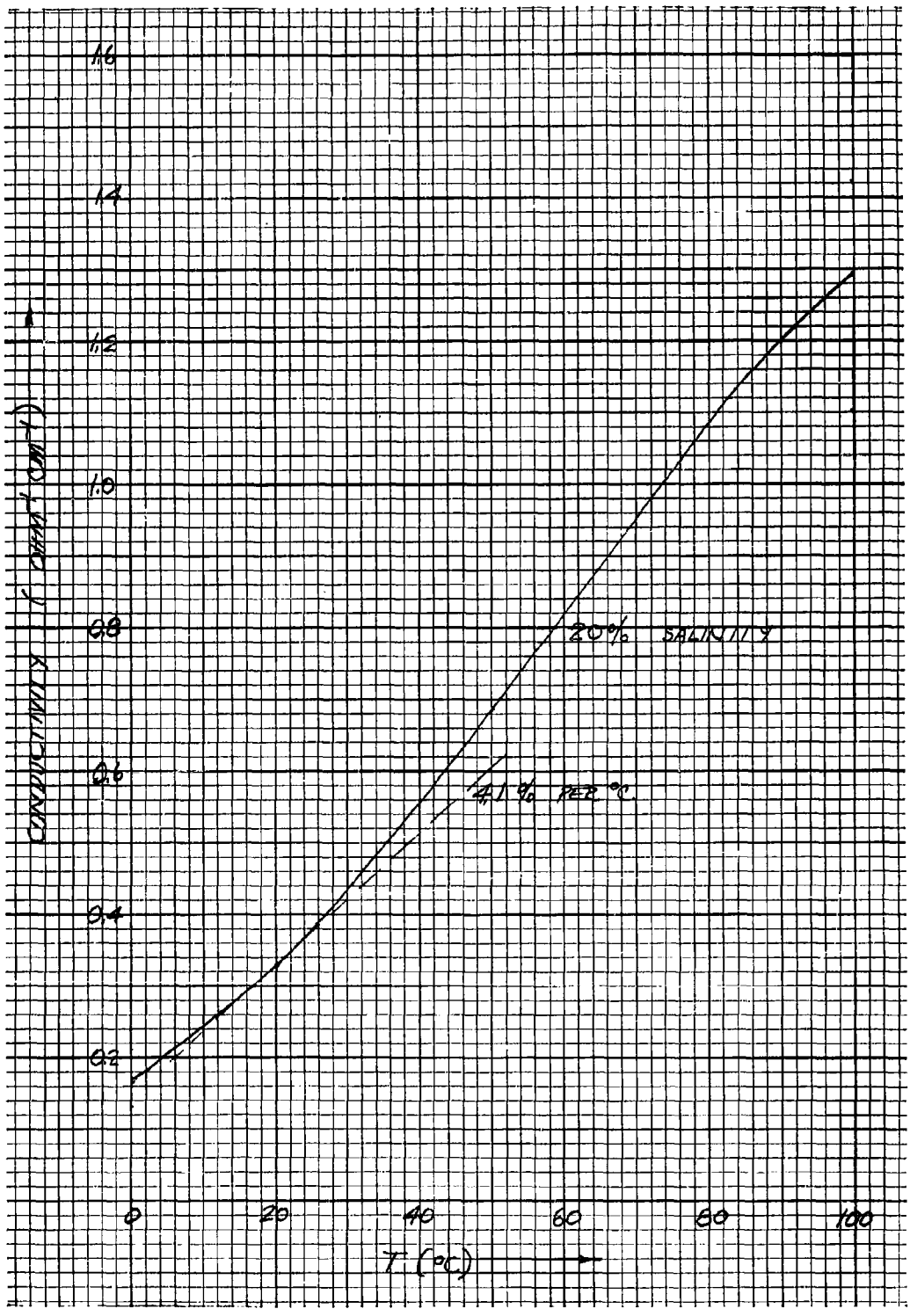

Figure 7.3. Electrical Conductivity of NaOH Solution as a Function of Temperature

data are of interest.

Great liberties have been taken in obtaining the typical or average characteristics of the ocean. It should be emphasized that this data has value only in making the most general predictions concerning oceanographic experiments. The average values quoted at a given depth represent the average for all oceans of the world and all time, i.e., a year-round time average. This average is called the "world-time-average." The data obtained refers to only the upper 500 meters or 1500 feet of the ocean depths. When an average in depth is taken it means an average only over this range of depths. The basic data on which the averages are based are obtained from The Oceans (49). Simple mathematical expressions are fitted to the data for steady state and turbulent quantities.

Temperature Distribution

The world wide temperature distribution in the ocean during the year (49) when averaged with respect to surface area and time yields the following data

Table 7.19 . Average Temperature of the Oceans

(Meters) Depth	Average (^{o}C) Temperature
0	23.3
200	14.5
400	10.6

A simple mathematical form which fits this world-time-average data is

$$T(y) = \left[T(0) - T(\infty)\right] e^{-\lambda y} + T(\infty)$$

where y is the depth, T(0) is the surface temperature, T(∞) is the hypothetical temperature at great depth (although the equation is valid only for y less than some maximum value y_{Λ}), and λ is a constant indicating the rate of temperature decrease with depth. Solving for the three parameters of this equation by means of the three data points above:

$$T(0) = 23.3\ ^{o}C$$
$$T(\infty) = 7.4\ ^{o}C$$
$$T(0) - T(\infty) = 15.9\ ^{o}C$$
$$\lambda^{-1} = 817 \text{ feet}$$

and for y_Λ = 1500 feet we have

$$\lambda y_\Lambda = 1.84 \ .$$

The resulting static temperature profile is shown in Figure 7.4 . The average temperature over depth from 0 to y_Λ , T_o, is derived from the formula by integration:

$$T_c = T(\infty) + \left[T(0) - T(\infty)\right] g(\lambda y_\Lambda)$$

where

$$g(\lambda y_\Lambda) = \frac{1 - e^{-\lambda y_\Lambda}}{\lambda y_\Lambda} \ .$$

substituting values we obtain

$$g(1.84) = 0.458$$
$$T_o = 14.7\ ^\circ C. \quad (\sim 15\ ^\circ C) \ .$$

This temperature is attained at a depth of about 640 feet where $e^{-\lambda y} = g(\lambda y_\Lambda)$. The root-mean-square temperature difference, ΔT_o, averaged over depths from 0 to y_Λ is again found by means of integration to be

$$\Delta T_o = \left[T(0) - T(\infty)\right] \left\{ g(2\lambda y_\Lambda) - g^2(\lambda y_\Lambda) \right\}^{1/2}$$

substituting values we have

$$\Delta T_o = 3.8\ ^\circ C. \quad (\sim 4\ ^\circ C) \ .$$

Combining the previous results it can be said that the world-time-depth average temperature in the ocean is

$$T = 15 \pm 4\ ^\circ C.$$

for $$0 < y < 1500 \text{ feet.}$$

The temperature gradient is found by differentiation to be

$$\left(\frac{dT}{dy}\right) = -\lambda \left[T(0) - T(\infty)\right] e^{-\lambda y} \ ,$$

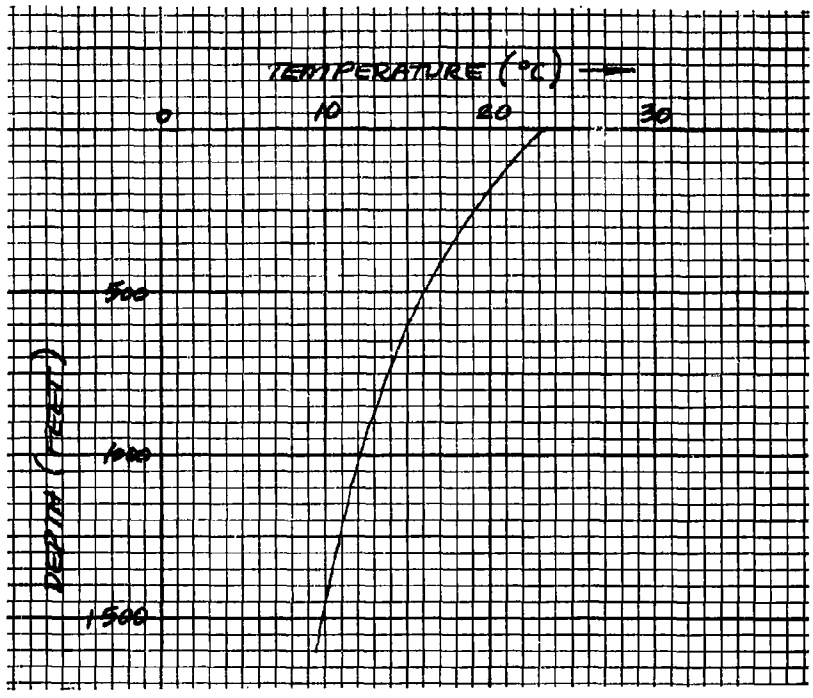

Figure 7.4. Average Ocean Temperature Distribution as a Function of Depth

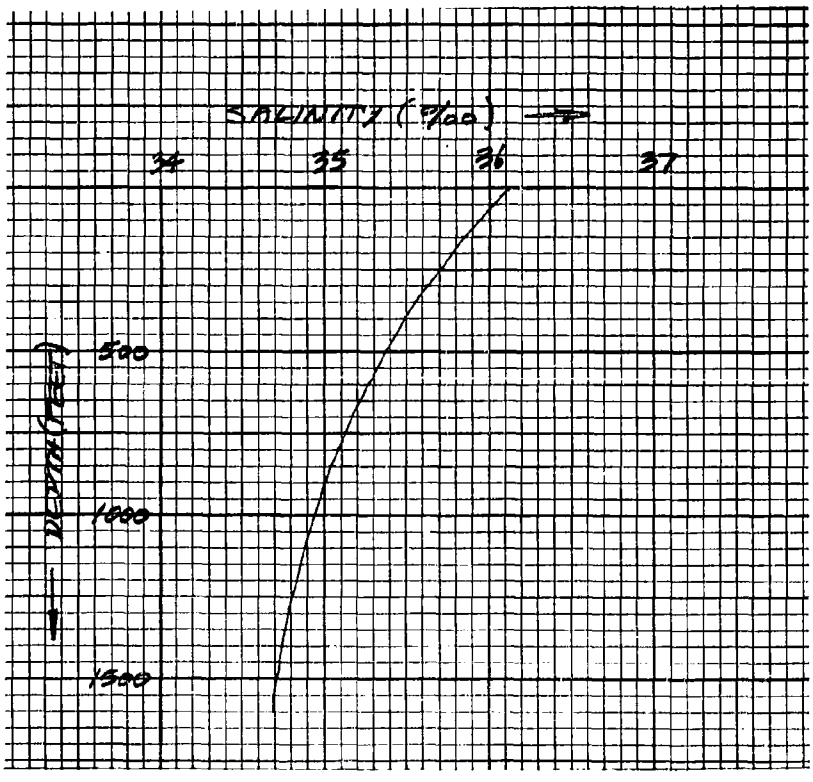

Figure 7.5. Average Ocean Salinity Distribution as a Function of Depth

and the average gradient is

$$\left(\frac{dT}{dy}\right)_0 = -\lambda\left[T(0) - T(\infty)\right] g(\lambda y_n) .$$

substituting values we get the world-time-depth average gradient:

$$\left(\frac{dT}{dy}\right)_0 = -.0089\ ^{\circ}C/ft.$$
$$\approx -.01\ ^{\circ}C \text{ per ft.}$$

Salinity Distribution

Lacking extensive data on world salinity distributions, as such, use can be made of the fact that there is a more or less fixed relation between temperature and salinity for a given mass of water. In the upper 500 meters of the ocean this TS-relation is roughly linear, except at the surface, for most waters of the world. A world-time-average has been taken of available data (50) and is presented in the next Section. In any case, this data provides information for determining the average salinity profile which is of the same form as that for temperature because of the linear relation between temperature and salinity:

$$S(y) = S(\infty) + \left[S(0) - S(\infty)\right] e^{-\lambda y} ,$$

where λ is the same as for the temperature distribution. Substituting the values found in the next Section we obtain

$$S(0) = 36.14\ ‰$$
$$S(\infty) = 34.45\ ‰$$
$$S(0) - S(\infty) = 1.69\ ‰$$

and

$$\lambda^{-1} = 817 \text{ feet.}$$

The salinity gradient profile has the same shape as that for temperature and is shown in Figure 7.5 . Following exactly the same procedures as in the last Section for temperature we obtain

$$S_0 = 35.22\ ‰ \qquad (\sim 35.2\ ‰)$$
$$\Delta S_0 = 0.40\ ‰ \quad .$$

Thus, we can say that the world-time-depth-average salinity in the oceans is

$$S = 35.2 \pm 0.4 \text{ ‰}$$

for $0 < y < 1500$ feet.

The salinity gradient at depth y is

$$\left(\frac{dS}{dy}\right) = -\lambda \left[S(0) - S(\infty)\right] e^{-\lambda y},$$

and the average over depths from 0 to y_1 is

$$\left(\frac{dS}{dy}\right)_0 = -\lambda \left[S(0) - S(\infty)\right] g(\lambda y_1).$$

Substituting values we get the world-time-depth-average salinity gradient:

$$\left(\frac{dS}{dy}\right)_0 = -.00095 \text{ ‰ per ft.}$$

$$\approx -.001 \text{ ‰ per ft.}$$

TS-Diagram

Given masses of ocean water show a characteristic relation between temperature and salinity. Typically this relation is linear in the upper 500 meters of the ocean except at the surface (less than 100 meters) where the TS-relation frequency becomes confused. The world-time-average of TS-curves based on available data (50) satisfies the linear relation in the depth range from 500 - 100 meters:

$$(S - S_0) = \gamma_0 (T - T_0)$$

where

$S_0 = 35.22$ ‰

$T_0 = 14.7$ °C

and

$\gamma_0 = 0.11$ ‰ per °C.

This average TS-diagram is shown in Figure 7.6 superimposed on the density curves of sea water taken from Reference (51). The dots on the straight line segment represent the situation at the surface (y = 0) and maximum depth considered (y = 1500'). The middle point is the average temperature and salinity which is at an intermediate depth (y = 640'). The slope of the TS-diagram is

$$\left(\frac{\partial S}{\partial T}\right) = \gamma_0$$

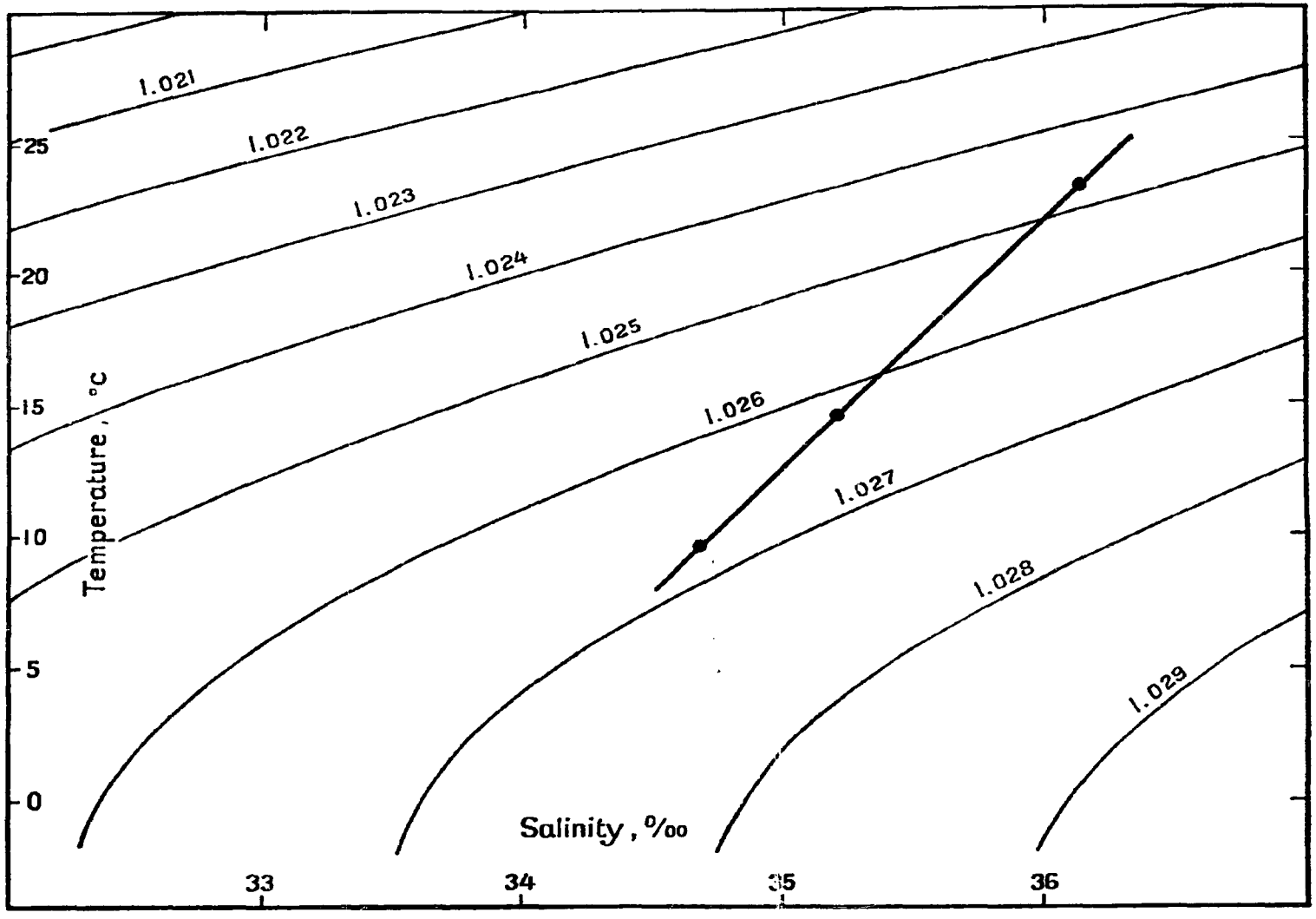

Figure 7.6. Average TS-Diagram for the Oceans

A statistical average of this slope and its rms variation obtained for the data mentioned above is

$$\gamma_0 = \left(\frac{\partial S}{\partial T}\right) = (11 \pm 4)\ 10^{-2}\ ‰\ \text{PER}\ ^\circ\text{C}.$$

This correlation between T and S is valid for relatively large regions of sea water but on a microscale it does not continue to hold because of diffusion processes which take place at different rates for thermal conduction and ionic diffusion.

Table 7.20 . Properties of Average Ocean Water as a Function of Depth

(Feet) Depth	($^\circ$C) T	(‰) S	(gm/cm^3) d	($joule/cm^3/^\circ C$) c	(ohm-cm) ρ	(% per $^\circ$C) β_T	(% per ‰) β_S	($ohm^{-1}-m^{-1}$) b
0	23.3	36.14	1.0247	4.089	19.0	2.02	2.46	5.28
200	19.8	35.77	1.0254	4.092	20.6	2.13	2.49	4.86
400	17.1	35.49	1.0259	4.093	22.0	2.22	2.52	4.55
600	15.0	35.26	1.0262	4.094	23.2	2.29	2.54	4.32
800	13.4	35.08	1.0264	4.094	24.2	2.35	2.57	4.14
1000	12.1	34.95	1.0266	4.095	25.0	2.40	2.58	4.00
1200	11.1	34.84	1.0267	4.095	25.6	2.44	2.59	3.90
1400	10.2	34.75	1.0267	4.096	26.3	2.47	2.60	3.80
1600	9.6	34.69	1.0268	4.096	26.8	2.49	2.60	3.74

Other Properties

With a knowledge of the average temperature and salinity as a function of depth, it is possible to calculate all of the other properties of sea water as a function of depth from known physical data tabulated in Section 7.2 . The world-time-averages of several useful properties are listed in Table 7.20 as a function of depth. The depth average of these data is the value at about 600 to 700 foot depth.

Turbulence Characteristics

The velocity in the ocean is a random function of position for the

smaller scale fluctuations and is amenable to analysis in the framework of homogeneous anisotropic (layered) turbulence theory. The velocity fluctuations give rise to the mixing of existing temperature and salinity gradients, thus, producing microstructure of these variables in the water (52,53,54). Measurements have been made which show the existence of temperature microstructure (55,56) but no measurements are yet available on salinity microstructure in the ocean. Over the velocity range where viscosity is not important (inertial subrange) the velocity spectrum varies as $k^{-5/3}$ (k wavenumber) (57,58); the wavenumber, k_d, where viscous dissipation becomes important (near the surface) is about $k_d = 2\ cm^{-1}$ (59,60,61), i.e., the smallest blobs of water in motion are about 5 mm in size. Temperature and salinity microstructure is expected to have a spectrum which also varies as $k^{-5/3}$ in the inertial subrange, if these fluctuations are thought of as being injected into the spectrum before the inertial range starts (58), and if the spectrum is due to the turbulent mixing of the existing ocean gradients, it varies as k^{-3} (54).

8. DETECTION THEORY

This Section deals with the factors which set limits on the detection of small variations of temperature, salinity and velocity in water. The theory developed here depends in part on results of later Sections, consequently familiarity with these Sections will facilitate the understanding of the present Section. The analysis below is carried out for temperature (T-meter) and velocity (U-meter) measurements, and with appropriate changes, the theory for temperature measurements is applicable to salinity measurements (S-meter). The ultimate sensitivity of these measurements is studied from the standpoint of the minimum detectable signal and the signal-to-noise ratio in the presence of given background noise. The operation of the instrumentation in modes suitable for velocity and temperature (and/or salinity) measurements is also included.

8.1 Intrinsic Signal-to-Noise Ratio

All electronic detection devices are limited, at least, by Johnson thermal noise which is developed across the resistance of the sensing element. The signal-to-noise ratio (intrinsic) of a detector relative to the Johnson noise is a useful dimensionless quantity of fundamental significance in connection with its sensitivity.

The velocity detector (U-meter) and temperature detector (T-meter), which are based on an electrolytic conductivity measurement, and the hot-wire anemometer (HWA) and resistance-wire thermometer (RWT) are now analysed in a general way to obtain their respective intrinsic signal-to-noise ratios. It is found that a single formula applies to all these instruments (with appropriate changes in parameters) in any of the modes of operation discussed in Section 8.5 .

The analysis begins by assuming the detecting element to be a pure resistance, R, at a temperature, T_o, which is operated in electronic equipment with a bandwidth Δf. The mean-square Johnson noise voltage, $\overline{n^2}$, across this resistor is (Sec. 15.4)

$$\overline{n^2} = 4kT_oR\Delta f \quad ,$$

where k is Boltzmann's constant. The intrinsic signal-to-noise ratio, Λ, for voltage fluctuations Δv across the sensing element is defined as

$$\Lambda = \left(\frac{\overline{\Delta V^2}}{\overline{n^2}} \right) .$$

In the instruments considered above, there exists a certain maximum power which can be dissipated in the resistance, R, in order that the temperature of the sensor not exceed some maximum value. Call this maximum power P*. Define the ratio

$$H \equiv \left(\frac{P_1}{P_*}\right) , \qquad (0 \leq H \leq 1)$$

where P_1 is the actual steady state power dissipated in the resistance. The signal-to-noise ratio is now

$$\Lambda = \frac{\overline{\Delta V^2}}{4kT_o R_1 \Delta f} = \frac{(V_1^2/R_1)}{4kT_o \Delta f} \left(\frac{\Delta V}{V_1}\right)^2$$

$$= \left(\frac{P_1}{4kT_o \Delta f}\right) v^2 = \left(\frac{P_*}{4kT_o \Delta f}\right) H v^2$$

where V_1 is the rms voltage across the element, and the fractional voltage fluctuation is

$$v = \left(\frac{\Delta V}{V_1}\right) .$$

Had we considered the signal as current fluctuations, ΔI, then

$$\Lambda = \left(\frac{P_*}{4kT_o \Delta f}\right) H i^2 ,$$

where

$$i = \left(\frac{\Delta I}{I_1}\right)$$

and

$$V_1 = RI_1 .$$

The resistance of the sensing element varies (we assume) linearly with its average temperature. For an electrode sensing element

$$R = R_o \left[1 - \beta \overline{\Delta T} - \beta \delta T\right] ,$$

where R_0 is the resistance at the average ambient temperature T_0, β is the temperature coefficient of the conductivity of the fluid, $\overline{\Delta T}$ is the average electrode temperature rise due to electrical heating, and δT is the temperature fluctuation of the medium averaged over the sensing volume of the electrode. For a wire sensing element, the corresponding equation is

$$R = R_0\left[1 + \beta\overline{\Delta T_w} + \beta\delta T\right] ,$$

where, here, β is the temperature coefficient of resistance of the wire, $\overline{\Delta T}_w$ is the wire over-temperature, and δT is the temperature fluctuation of the medium averaged over the length of the wire.

To put these equations on an identical basis, the maximum allowable temperature rise, $\overline{\Delta T}*$, must be qualified for both cases. The maximum temperature of a heated wire occurs <u>at</u> the wire surface. In the case of an electrode, the maximum temperature occurs in the downstream region of the electrode and is equal to the exit temperature. The average temperature of the medium in the case of the wire is the so-called "film temperature" which is half the wire temperature

$$\overline{\Delta T} = \frac{\overline{\Delta T_w}}{2} .$$

Utilizing this fact, the resistance equation may be put in the following form which is applicable to both electrode and wire sensors:

$$R = R_0\left[1 + \epsilon\beta\overline{\Delta T} + \epsilon'\beta\delta T\right] ,$$

where $\overline{\Delta T}$ is understood to be the average temperature rise of the fluid medium, and for the wire sensor

$$\epsilon = +2 \qquad \epsilon' = +1 ,$$

and for the electrode sensor

$$\epsilon = -1 \qquad \epsilon' = -1 .$$

Define the dimensionless quantity

$$\alpha* = \beta\overline{\Delta T}* ,$$

where $\overline{\Delta T}^*$ is the critical average temperature of the medium beyond which boiling sets a limitation.

The power dissipated in the sensing element is related to its average temperature rise, $\overline{\Delta T}$, at a certain velocity, U, by an equation of the form

$$P = \overline{\Delta T} \cdot \text{function (U)}$$

or

$$P = P_* \left(\frac{\overline{\Delta T}}{\overline{\Delta T}_*}\right) f\left(\frac{U}{U_o}\right),$$

where U_o is some reference velocity (for example, the steady state operating velocity) and f(x) has the form

$$f(x) = a + bx^m$$

and we require

$$f(1) = 1 = a + b \ .$$

This form is applicable to both the U-meter and HWA. In the case of the HWA, the heat loss equation is (Sec. 5.4)

$$P = 2\pi k l \, \overline{\Delta T} \, \mathcal{N}$$

where

$$\mathcal{N} = 0.42 \, P^{1/5} + 0.57 \, P^{1/3} R_o^{1/2} \left(\frac{U}{U_o}\right)^{1/2}$$

and

$$R_o = \frac{d U_o}{\nu} \ .$$

In terms of the above quantities

$$P_* = 2\pi k l \, \overline{\Delta T}_* \, \mathcal{N}_o ,$$

where $\mathcal{N}_o$ is the value of $\mathcal{N}$ at $U = U_o$, and

$$f\left(\frac{U}{U_o}\right) = \frac{\mathcal{N}}{\mathcal{N}_o} \ ,$$

or

$$a = \frac{0.42\, P^{1/5}}{\nu_0}$$

$$b = \frac{0.57\, P^{1/3} R_0^{1/2}}{\nu_0}$$

and m = 1/2. In the case of the U-meter the heating equation is (Sec. 12.1)

$$P = 2cAU\overline{\Delta T} \ ,$$

which applies for heat transfer by forced convection only. It follows that

$$P* = 2cAU_0\,\overline{\Delta T}*$$

and

$$f\left(\frac{U}{U_0}\right) = \left(\frac{U}{U_0}\right)$$

or

$$a = 0, \quad b = 1, \quad m = 1 \ .$$

Combining the equations for resistance, power and temperature, we get

$$\frac{R}{R_0} = 1 + \epsilon \alpha_* \left(\frac{P}{P_*}\right)\frac{1}{f} + \epsilon' \beta \delta T .$$

Small changes in the variables of this equation (resistance, power, velocity, and temperature) are related by the following equation which is obtained by differentiation and evaluated at steady state conditions ($U = U_0$, $P = P_1$):

$$\frac{\delta R}{R_0} = \epsilon \alpha_* \left(\frac{\delta P}{P_*}\right) - \epsilon \alpha_* \left(\frac{P_1}{P_*}\right) f'(1) \left(\frac{\delta U}{U_0}\right) + \epsilon' \beta \delta T$$

or

$$r\left(1 + \epsilon \alpha_* H\right) = \epsilon \alpha_* H p - \epsilon \alpha_* H\, bm\, u + \epsilon' \alpha_* \theta \ ,$$

where

$$r = \frac{\delta R}{R_1} \qquad u = \frac{\delta U}{U_0}$$

$$p = \frac{\delta P}{P_1} \qquad f'(1) = bm$$

and

$$\theta = \frac{\delta T}{\Delta \bar{T}_*} \quad .$$

Later, in Section 8.5 we find that, in a given mode of operation, the variables r, p, i, and v are related by

$$\begin{aligned} i &= -v \tan\varphi \\ r &= v(1 + \tan\varphi) \\ p &= v(1 - \tan\varphi) \ , \end{aligned}$$

where φ is the mode angle. For modes of operation where $0 \leq |\varphi| \leq \pi/4$ it is preferable to detect voltage fluctuations (v), and for $\pi/4 \leq |\varphi| \leq \pi/2$ it is preferable to detect current fluctuations (i). Substituting these equations into the one obtained above we get for voltage fluctuations:

$$v\left[(1+\tan\varphi) - \left(\frac{\epsilon\alpha_* H}{1+\epsilon\alpha_* H}\right)(1-\tan\varphi)\right] = -\left(\frac{\epsilon\alpha_* H}{1+\epsilon\alpha_* H}\right) bmu + \frac{\epsilon'\alpha_*\theta}{1+\epsilon\alpha_* H}$$

and for current fluctuations

$$i\left[\left(\frac{1+\tan\varphi}{-\tan\varphi}\right) - \left(\frac{\epsilon\alpha_* H}{1+\epsilon\alpha_* H}\right)\left(\frac{\tan\varphi - 1}{-\tan\varphi}\right)\right] = -\left(\frac{\epsilon\alpha_* H}{1+\epsilon\alpha_* H}\right) bmu + \frac{\epsilon'\alpha_*\theta}{1+\epsilon\alpha_* H} \ .$$

We are now in a position to write down the signal-to-noise ratio in the general case. We assume for simplicity, however, that the velocity fluctuations, u, and temperature fluctuations, θ, are uncorrelated. Correlated signals simply add another term to our final result. The above equations are the same on the right side, but differ on the left by the

complicated expression in square brackets which is a function only of the mode angle φ and the group $\epsilon\alpha_* H$. With reference to the earlier expressions for the intrinsic signal-to-noise ratio, Λ, we can now write a single expression for both cases of voltage and current fluctuations as follows:

$$\Lambda = \left(\frac{P_*}{4kT_0\Delta f}\right) H F^2 \left\{ \left(\frac{\epsilon\alpha_* H}{1+\epsilon\alpha_* H}\right)^2 b^2 m^2 n^2 + \left(\frac{\epsilon'\alpha_*}{1+\epsilon\alpha_* H}\right)^2 \theta^2 \right\}$$

where $F = F(\varphi, \epsilon\alpha_* H)$ is defined as follows:

$$F^{-1} = \begin{cases} (1+\tan\varphi) - \left(\frac{\epsilon\alpha_* H}{1+\epsilon\alpha_* H}\right)(1-\tan\varphi) , & \text{FOR } 0 \le |\varphi| \le \pi/4 \\ \left(\frac{1+\tan\varphi}{-\tan\varphi}\right) - \left(\frac{\epsilon\alpha_* H}{1+\epsilon\alpha_* H}\right)\left(\frac{\tan\varphi - 1}{\tan\varphi}\right) , & \text{FOR } \frac{\pi}{4} \le |\varphi| \le \frac{\pi}{2} . \end{cases}$$

The function $|F|$ is given in Table 8.1 for the main modes of operation and for temperature and velocity sensors of either the wire or electrode type. The values listed refer to sea water at 20°C and a velocity of 3 knots (154 cm/sec); the wire diameter is 3 microns (see Table 5.1); the maximum temperature, $\overline{\Delta T}_*$, is 20°C corresponding to an average water temperature of 40°C in the sensitive volume of the detector. The parameters of the wire and electrode are listed in Table 8.2 .

Table 8.1 . Values of the Function $|F|$

φ Mode Angle	T-Meter H = 0	RWT H = 0	U-Meter H = 1	HWA H = 1
0° (CCO)	1	1	0.60	1.2
45° (CPO)	0.50	0.50	0.50	0.50
90° (CVO)	1	1	3.0	0.86
-45° (CRO)	∞	∞	0.75	3.0

Table 8.2 . Parameters of Wire and Electrode Sensors

	a	b	m	ϵ	ϵ'	$\alpha*$	β (% per ^{o}C)
Electrode	0	1	1	-1	-1	0.4	2.0
Wire	0.19	0.81	1/2	2	1	0.1	0.5

Table 8.3 . Values of the Function $|E|$

ψ Mode Angle	T-Meter H = 0	RWT H = 0	U-Meter H = 1	HWA H = 1
0^{o} (CCO)	0.40	0.10	0.40	0.081
45^{o} (CPO)	0.20	0.05	0.33	0.034
90^{o} (CVO)	0.40	0.10	2.0	0.058
-45^{o} (CRO)	∞	∞	0.50	0.20

In the case where the velocity signal dominates (H→1)

$$\Lambda = \left(\frac{P_*}{4kT_o\Delta f}\right) H E^2 u^2$$

where

$$E = \frac{F b m \epsilon \alpha_* H}{1 + \epsilon \alpha_* H} .$$

When the temperature signal dominates (H→0)

$$\Lambda = \left(\frac{P_*}{4kT_o\Delta f}\right) H E^2 \theta^2$$

where, now

$$E = F\epsilon'\alpha_* .$$

The values of the function $|E|$ are listed in Table 8.3 for the assumed conditions. The apparent paradox of infinite signal-to-noise ratio in Table 8.1 and 8.3 for the CRO mode of the temperature detectors arises because noise in the feedback loop has been neglected. This is a special case of the "divergent mode" of operation when $\Lambda \rightarrow \infty$ which occurs when

$$-\tan\varphi = \frac{1}{1 + 2\epsilon\alpha_* H} \quad .$$

In any case, the active modes are of no use in connection with temperature detectors.

To compare the relative merits of the wire and electrode sensors, we are interested in the following ratios

$$\frac{\Lambda(\text{T-METER})}{\Lambda(\text{RWT})} = \frac{\left\{P_* (\epsilon' \alpha_*)^2\right\}_{\text{T-METER}}}{\left\{P_* (\epsilon' \alpha_*)^2\right\}_{\text{RWT}}} \qquad (H \rightarrow 0)$$

$$\frac{\Lambda(\text{U-METER})}{\Lambda(\text{HWA})} = \frac{\left\{P_* E^2\right\}_{\text{U-METER}}}{\left\{P_* E^2\right\}_{\text{HWA}}} \qquad (H \rightarrow 1)$$

These comparisons are considered in more detail in Section 5.5.

8.2 Background Noise

The desired signal at the output of a detector bridge network is accompanied by other signals which are classed as background noise. In the last Section one of these noise signals was considered, viz., the fundamental noise associated with the thermal agitation of the conducting element (Johnson noise). Other background signals are now considered in order to develop the theory of the minimum detectable signal in Section 8.3.

The (complex) output voltage at the wheatstone bridge output or detector input, Δv, is given by (Section 15.1)

$$\left(\frac{\Delta v}{v}\right) = m\left(\frac{\Delta z}{z}\right) ,$$

where v is the input voltage to the bridge, m is the bridge factor, and

Δz is the variation in the impedance z. The variations in impedance are due to variations in temperature, salinity, velocity and boiling in the sensitive volume of each electrode. The resultant signal at the detector input is

$$\Delta V = m v \sum_i \left(\frac{\Delta z}{z}\right)_i + v_n$$

where the summation extends over the different types of impedance fluctuations in each electrode, and the voltage v_n is due to Johnson noise. All of these terms are assumed to be statistically independent over the frequency band of interest. The mean-square, ΔV^2, of the net signal is

$$\Delta V^2 = M^2 V^2 \sum_i \left(\frac{\Delta z}{z}\right)^2 + (v_n)^2_{rms} \quad .$$

Each of these individual terms is discussed below.

Temperature $\quad \Delta V^2(\text{temperature}) = M^2 V^2 M_1 \beta^2 \delta T^2$,

where M is the magnitude of the bridge factor, V is the rms input voltage to the bridge, M_1 is the number of sensing elements (Sec. 15.2), β is the temperature coefficient of the electrode resistance, and δT is the rms temperature fluctuation.

Salinity The term associated with salinity variations is exactly the same as that for temperature but with the salinity coefficient resistance instead of that for temperature. In the analysis that follows, the salinity variations will be omitted and it will be understood that the temperature variations actually represent the "effective temperature" variations (Sec. 3.1).

Velocity $\quad \Delta V^2(\text{velocity}) = M^2 V^2 M_1 \beta^2 \overline{\Delta T}^2 \left(\frac{\delta U}{U}\right)^2$

where $\overline{\Delta T}$ is the average electrode temperature rise, and $(\delta U/U)$ is the rms relative velocity variation.

Boiling $\quad \Delta V^2(\text{boiling}) = M^2 V^2 M_1 K \left(\frac{P}{P_\Lambda}\right)^n$,

where K is a dimensionless constant determined empirically in Section 17.2 , P is the electrode power, P_Λ the power level where boiling noise becomes appreciable and the exponent n is found by experiment to be of the order of 10 to 25.

Johnson Noise $\quad (v_n)^2_{rms} = 4 M_3 R k T \Delta f F$,

where M_3R is the total resistance in parallel with the detector input (Sec. 15.2), R is the electrode resistance, and F is the overall noise factor* (Sec. 15.4) of the detection electronics.

The qualitative behavior of ΔV^2 as a function of electrode power is shown in Figure 8.1 . At low power the signal is due only to Johnson noise. As the electrode power increases the temperature (or salinity) variations are first detected. At still higher power the signal due to velocity variations dominates, and finally, at the highest power, boiling in the electrode volume produces a signal which masks all the others. The optimum power level for detecting temperature or velocity variations in the presence of the other background signals is considered in the next Section.

8.3 Minimum Detectable Signal

The analysis of the limits of detectability of temperature and/or velocity signals is now given. Reference will be made to the formulas for the respective signals or background noise given in the last Section.

Temperature Signal

The minimum detectable temperature variation is calculated first. The rms "signal" in this case is

$$VM\beta\delta T \quad ,$$

The "noise" consists either of Johnson noise which is important at low electrode power, or velocity fluctuations which are important at higher electrode power. Boiling noise is of negligible importance over the range of interest for temperature measurements. At low power the temperature measurement is said to be "detector-noise-limited," and in this case

$$\Delta v^2(\text{temperature}) = \lambda\,(v_n)_{rms}$$

or

$$M^2 V^2 M_1 \beta^2 \delta T_{v_1}^2 = 4\lambda M_3 F R R T \Delta f \quad ,$$

where the minimum detectable temperature is denoted by δT_{v_1}, and λ is the minimum signal-to-noise ratio for detectability of the signal. Let the input resistance of the bridge network be M_2R, and P the power dissipated

---

*The noise figure is 10 log F.

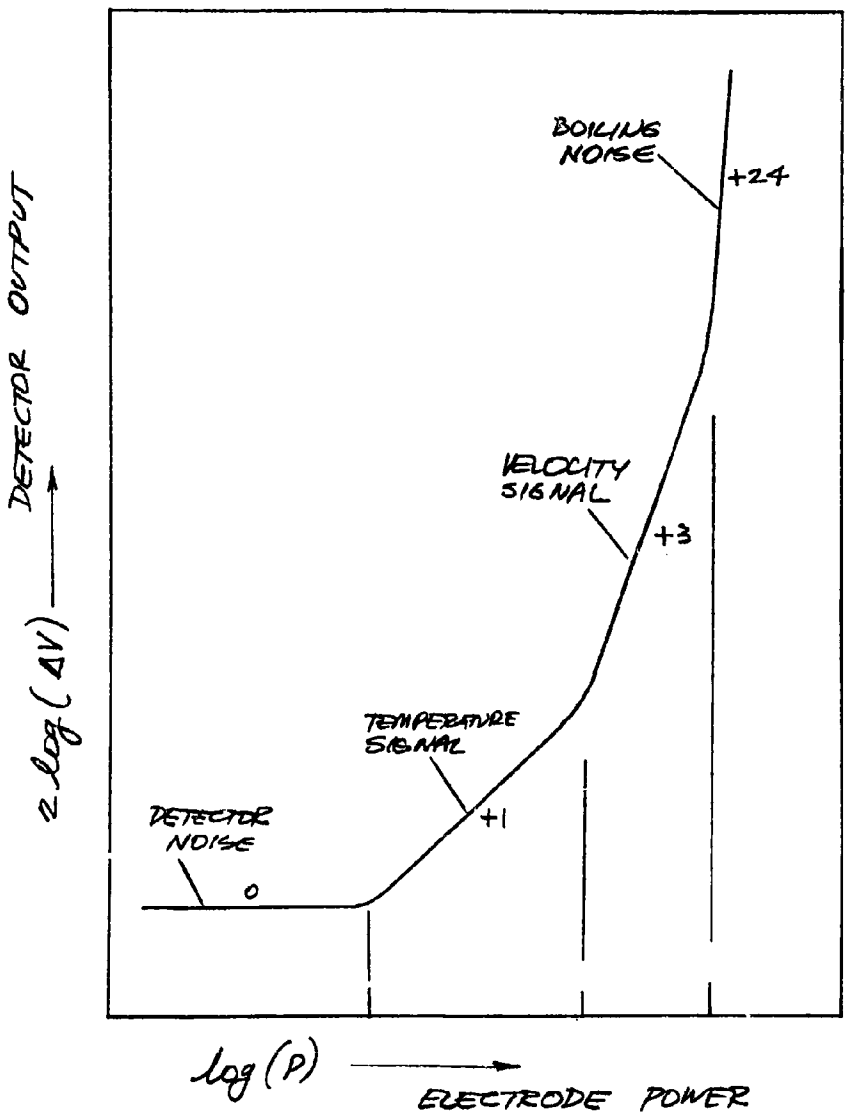

Figure 8.1. Detector Output Signals as a Function of Electrode Power

in the electrode(s) which is a factor M_4 of the total power into the bridge (Sec. 15.2):

$$P = M_4\left(\frac{V^2}{M_2 R}\right) \quad .$$

The bandwidth, Δf, of the detection system corresponds to the cutoff frequency of the electrode of dimension, b, and moving at speed, U, through the water (Sec. 9.1):

$$\Delta f = \frac{U}{m_3 b}$$

where $m_3 b$ is the "cutoff wavelength" of the electrode (Sec. 13.1). The "cutoff wavenumber," k_c is

$$k_c = \frac{2\pi}{m_3 b} \quad .$$

Combining the above relations, we obtain the minimum detectable temperature variations (for a given required signal-to-noise ratio) in the detector-noise-limited case:

$$\delta T_{v_1} = \left[\left(\frac{4\lambda F m_3 m_4}{m_3 M_2 M^2 M_1}\right)\cdot\left(\frac{kTU}{\beta^2 P b}\right)\right]^{1/2} .$$

The sensitivity improves as the electrode power, P, is increased. This situation is illustrated in Figure 8.2 in the low power region of the graph.

At higher electrode power where $\overline{\Delta T}$ is appreciable, the temperature measurements are limited by velocity noise. The temperature measurement is "velocity-noise-limited" in this case

$$\Delta V^2(\text{temperature}) = \lambda \ \Delta V^2(\text{velocity})$$

or

$$M_1 V^2 M^2 \beta^2 \delta T_{v2}^2 = \lambda M_1 V^2 M^2 \beta^2 \overline{\Delta T}^2 \left(\frac{\delta U}{U}\right)^2 ,$$

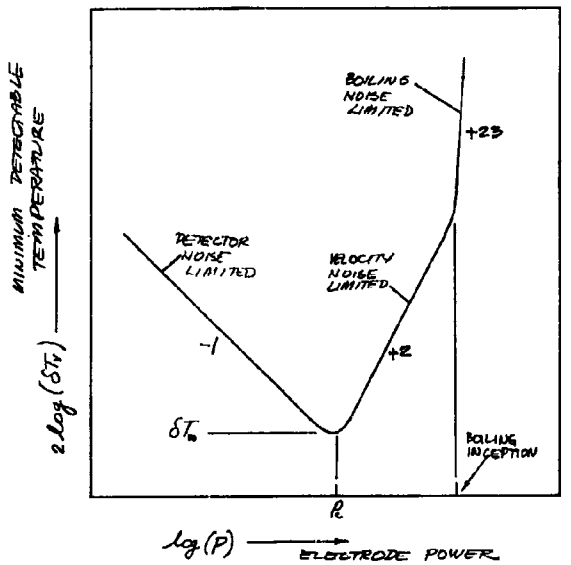

Figure 8.2. Minimum Detectable Temperature as a Function of Electrode Power

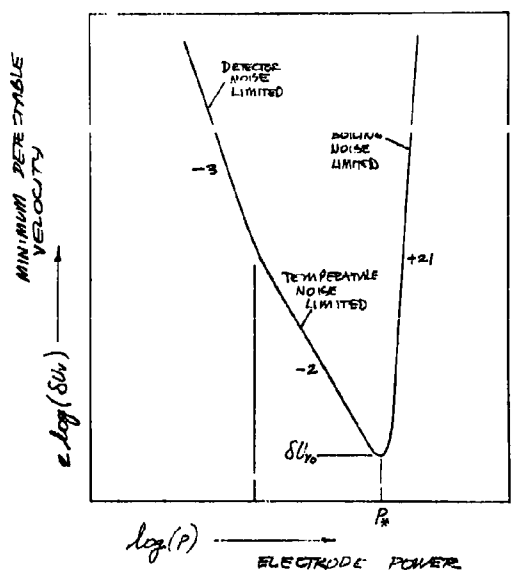

Figure 8.3. Minimum Detectable Velocity as a Function of Electrode Power

or

$$\delta T_{V2} = \lambda^{1/2} \overline{\Delta T} \left(\frac{\delta U}{U}\right) .$$

The temperature rise, $\overline{\Delta T}$, due to electrode heating is (Sec. 12.5):

$$\overline{\Delta T} = \frac{P}{2m_4 c b^2 U} .$$

Thus, in the velocity-noise-limited case

$$\delta T_{V2} = \left(\frac{\lambda^{1/2}}{2m_4}\right) \cdot \left(\frac{P}{c b^2 U}\right) \cdot \left(\frac{\delta U}{U}\right) .$$

The sensitivity decreases as the electrode power is increased. This behavior is shown in Figure 8.2 .

The limiting cases considered above indicate that there is an optimum electrode power, called "critical power," for temperature measurements, $P = P_c$, where the minimum temperature variations are detected. This optimum value applies when

$$2\,\delta T_{V2}^2 = \delta T_{V1}^2 .$$

Combining this relation with previous expressions we find

$$P_c = \left[\left(\frac{8 M_3 M_4 m_4^2 F}{M_1 M_2 M^2 m_3}\right) \cdot \left(\frac{kT c^2 U^3 b^3}{\beta^2}\right) \cdot \left(\frac{\delta U}{U}\right)^{-2} \right]^{1/2} .$$

At this optimum value of electrode power, the minimum detectable temperature variation, δT_{V0}, is

$$\delta T_{V0} = \sqrt{3}\ \delta T_{V2} = \sqrt{\frac{3}{2}}\ \delta T_{V1}$$

or

$$\delta T_{V0} = \left[\left(\frac{3\sqrt{3}\,\lambda^{3/2} F M_3 M_4}{M_2 M^2 M_1 m_3 m_4}\right) \cdot \left(\frac{kT}{c\beta^2 b^3}\right) \cdot \left(\frac{\delta U}{U}\right) \right]^{1/3} .$$

The significant dependence of δT_v on these parameters is

$$\delta T_v \sim b^{-1} \left(\frac{\delta U}{U}\right)^{1/3} ,$$

thus, small temperature variations are best measured at high speed with large electrodes (provided they are not larger than the temperature structure under study) and in waters of low ambient turbulence. The dependence on relative turbulence level is insensitive, however.

The variation of δT_v with P is conveniently expressed in terms of the optimum temperature sensitivity, δT_{vo}, and the critical power, P_c, as follows:

$$\delta T_v = \delta T_{vo} \left[\frac{1}{3} \left(\frac{P}{P_c}\right)^2 + \frac{2}{3} \left(\frac{P_c}{P}\right) \right]^{1/2} ,$$

where δT_v is velocity-noise-limited for $P > P_c$ and detector-noise-limited for $P < P_c$. This function is shown in Figure 8.2 .

As an estimate of the minimum detectable temperature variation, δT_{vo}, and the critical power for temperature measurements, P_c, we assume a unity signal-to-noise ratio and a noise factor (Sec. 16.1) of two:

$$\lambda = 1 \qquad (0 \text{ db})$$
$$F = 2 \qquad (3 \text{ db}) .$$

Also assume the use of a double sensing element bridge using eye-type electrodes (the values of m-and M-numbers are given in Table 8.3). Under these conditions we have

$$\left(\frac{3\sqrt{3}\, \lambda^{3/2} F\, M_3 M_4}{M^2 M_2 M_1 m_3 m_4}\right) = 4.0$$

and

$$\delta T_{vo} = 1.6 \left[\frac{kT}{c\beta^2 b^3} \left(\frac{\delta U}{U}\right)\right]^{1/3} ,$$

$$\left(\frac{8 M_3 M_4 m_4^2 F}{M^2 M_2 M_1 m_3}\right) = 21 ,$$

and

$$P_c = 2.7 \left[\frac{kT\, c^2\, U^3\, b^3}{\beta^2} \left(\frac{\delta U}{U} \right)^{-2} \right]^{1/3} .$$

These values of δT_{v_0} and P_c are tabulated for several situations in Table 8.4 of the next Section.

Velocity Signal

The minimum detectable velocity variation is now calculated. The "signal" in this case is

$$V M \beta \overline{\Delta T} \left(\frac{\delta U}{U} \right) ,$$

and the "noise" is that due to internal noise, temperature variations and boiling noise. In the case of velocity measurements, we must distinguish between the voltage V_1(rms) applied to the bridge for the purpose of the measurement and the (incoherent) voltage V_2(rms) which is utilized solely to heat the water flowing in the electrode volume. The total power dissipated in each electrode, P, consists of the power, P_1, due to the signal source, and the power, P_2, due to the heater source:

$$P = P_1 + P_2 .$$

This matter is discussed in more detail in Section 8.5 .

If the velocity measurements are "detector-noise-limited," then

$$\Delta V^2(\text{velocity}) = \lambda \, (v_n)^2_{rms} ,$$

where λ is, now, the minimum signal-to-noise ratio for velocity measurements. This equation implies

$$M_1 M^2 V_1^2 \beta^2 \overline{\Delta T} \left(\frac{\delta U_{v_1}}{U} \right)^2 = \lambda 4 k T M_3 R F \Delta f$$

where

$$\overline{\Delta T} = \frac{P_1 + P_2}{2 m_4 c b^2 U}$$

$$P_1 = M_4 \left(\frac{V_1^2}{M_2 R} \right)$$

$$P_2 = M_4 \left(\frac{V_2^2}{M_2 R} \right)$$

and

$$\Delta f = \frac{U}{m_3 b} .$$

The minimum detectable rms velocity variation in this case is δU_{v1}. Combining these relations, we find

$$\left(\frac{\delta U_{v1}}{U} \right) = \left[\left(\frac{16 \lambda F M_3 M_4 m_4^2}{M_1 M_2 M^2 m_3} \right) \cdot \left(\frac{kT c^2 b^3 U^3}{P_1 (P_1 + P_2)^2 \beta^2} \right) \right]^{1/2} .$$

As discussed in Section 8.5 , this equation is applicable when the auxiliary heater power is off ($P_2 = 0$). This expression is shown in Figure 8.3 in the low power region of the graph. The velocity detectability improves as the electrode power increases.

At higher electrode power where the velocity measurement is "temperature-noise-limited" we have

$$\Delta V^2(\text{velocity}) = \lambda \, \Delta V^2(\text{temperature})$$

or

$$\left(\frac{\delta U_{v2}}{U} \right) = \lambda^{1/2} \left(\frac{\delta T}{\overline{\Delta T}} \right)$$

$$= \frac{2 \lambda^{1/2} m_4 c b^2 U \delta T}{P_1 + P_2} .$$

The detectability continues to improve as the power increases.

At very high power, where the measurement is "boiling-noise-limited"

$$\Delta v^2(\text{velocity}) = \lambda \quad \Delta v^2(\text{boiling})$$

or

$$M^2 V_1^2 M_1 \beta^2 \overline{\Delta T}^2 \left(\frac{\delta U_{v3}}{U}\right)^2 = \lambda M^2 V_1^2 M_1 K \left(\frac{P}{P_1}\right)^n$$

or

$$\left(\frac{\delta U_{v3}}{U}\right) = \frac{\lambda^{1/2} K^{1/2}}{\beta \overline{\Delta T}} \left(\frac{P}{P_1}\right)^{n/2}$$

where

$$P = P_1 + P_2 \ .$$

In this case, the detectability is worsened by further increasing the power. Thus, an optimum power, P*, exists for the detection of velocity fluctuations.

The net minimum detectable velocity variation, δU_v, is determined by the sum of the background noises, thus, in general

$$\left(\frac{\delta U_v}{U}\right)^2 = \left(\frac{\delta U_{v1}}{U}\right)^2 + \left(\frac{\delta U_{v2}}{U}\right)^2 + \left(\frac{\delta U_{v3}}{U}\right)^2 .$$

A graph of this function is shown in Figure 8.3 as a function of total electrode power, P, for $P_2 = 0$. In actual operation, however, when $P \gg P_c$, the signal power P_1 is held constant and further increase in P is made up by an increase in P_2. When P is comparable with or less than P_c, the heater power is off ($P_2 = 0$). This matter is discussed in Section 8.5 .

The absolute minimum detectable velocity variation, δU_{vo}, occurs, generally, at a power level well above P_c, where Johnson noise is negligible and P_1 is a constant. In this region, only the last two terms of the above equation are appreciable and

$$\delta U_v = \delta U_{vo} \sqrt{\frac{n-2}{n}} \left(\frac{P_*}{P}\right) \left[1 + \left(\frac{2}{n-2}\right)\left(\frac{P}{P_*}\right)^n \right]^{1/2}$$

where P* is the optimum electrode power and

$$\left(\frac{P_*}{P}\right)^n = \left(\frac{2}{n-2}\right)\left(\frac{\beta^2 \delta T^2}{K}\right)$$

and

$$\left(\frac{\delta U_{vo}}{U}\right) = \left(\frac{\lambda n}{n-2}\right)^{1/2} \cdot \left(\frac{P_\Lambda}{P_*}\right) \cdot \left(\frac{\delta T}{\overline{\Delta T}_\Lambda}\right),$$

where $\overline{\Delta T}_\Lambda$ is the electrode temperature rise at $P = P_\Lambda$, i.e.

$$\overline{\Delta T}_\Lambda = \frac{P_\Lambda}{2m_4 c b^2 U} \quad .$$

For large values of n, $P_* \approx P_\Lambda$ and

$$\frac{\delta U_{vo}}{U} \approx \lambda^{1/2} \left(\frac{\delta T}{\overline{\Delta T}_\Lambda}\right) \quad .$$

Thus, velocity measurements are best performed at the highest possible electrode temperature, consistent with the limitations of boiling noise, and at low electrode velocity (for example, in the vicinity of a stagnation point). Numerical examples of the minimum detectable velocity are given at the end of Section 8.4 .

Resistance Signal

The minimum detectable resistance change, ΔR_v(rms), as determined by Johnson noise is

$$\frac{\lambda (v_m)^2_{rms}}{V^2} = M_1 M^2 \left(\frac{\Delta R}{R}\right)_v^2$$

or

$$4\lambda k T M_3 R \Delta f F = M_1 M^2 V^2 \left(\frac{\Delta R}{R}\right)_v^2$$

or

$$\left(\frac{\Delta R}{R}\right)_{\nu} = \left(\frac{M_3 M_4}{M_1 M_2 M^2}\right)^{1/2} \cdot \left(\frac{4\lambda F k T \Delta f}{P}\right)^{1/2}.$$

The ultimate detectability of resistance variations is set by the maximum allowable electrode temperature rise. This follows since, if

$$\Delta f = \frac{U}{m_3 b}$$

and

$$P = 2 m_4 c b^2 U \overline{\Delta T}$$

then

$$\left(\frac{\Delta R}{R}\right)_{V_0} = \left(\frac{2\lambda F m_3 m_4}{m_3 m_4 M_1 M_2 M^2}\right)^{1/2} \cdot \left(\frac{kT}{\overline{\Delta T}\, c b^3}\right)^{1/2}.$$

This expression represents the minimum detectable resistance change due to any effect taking place at the electrode which changes the electrode resistance. For an optimum differential bridge with two resistive eye-type electrodes, we have

$$\left(\frac{M_3 M_4}{m_3 m_4 M_1 M_2 M^2}\right) = 0.39$$

and

$$\left(\frac{\Delta R}{R}\right)_{V_0} = 0.63 \left(\frac{\lambda F k T}{\overline{\Delta T}\, c\, b^3}\right)^{1/2}.$$

As a numerical example, assume

$\lambda = 1$

$F = 2$

$kT = 4 \times 10^{-21}$ joule

$\overline{\Delta T} = 10^{\circ}C$

$c = 4.1$ joule/cm^3/$^{\circ}$C

$b = 0.5$ cm

then

$$\left(\frac{\Delta R}{R}\right)_{N_D} = 2.5 \times 10^{-11}.$$

8.4 Signal-to-Noise Ratio

Consider a fluid medium with velocity fluctuations δU(rms) and temperature fluctuations δT(rms) in the pass band of a detector moving at velocity U through the medium. The signal-to-noise ratios for temperature and velocity measurements are, respectively:

$$\lambda_T = \lambda \left(\frac{\delta T}{\delta T_V}\right)^2$$

$$\lambda_U = \lambda \left(\frac{\delta U}{\delta U_V}\right)^2 ,$$

where λ is the minimum signal-to-noise ratio for the detectability of a signal. These ratios are now investigated as a function of electrode power.

Temperature Signal

The signal-to-noise ratio, λ_T, is a maximum where the minimum detectable temperature is smallest, i.e., at $P = P_c$ where $\delta T_V = \delta T_{V_0}$:

$$(\lambda_T)_{MAX} = \lambda \left(\frac{\delta T}{\delta T_{V_0}}\right)^2 .$$

At other values of electrode power in the vicinity of P_c, we have

$$\lambda_T = \lambda \left(\frac{\delta T}{\delta T_{V_0}}\right)^2 \left[\frac{1}{3}\left(\frac{P}{P_c}\right)^2 + \frac{2}{3}\left(\frac{P_c}{P}\right)\right]^{-1} .$$

This function is illustrated in Figure 8.4 . The useful range of power, P, for temperature measurements is determined by the condition:

$$\lambda_T \geq \lambda \quad .$$

In order to determine the limits of this range of electrode power, assume $\delta T \gg \delta T_{V_0}$. The lower limit is set by the internal detector noise; denote

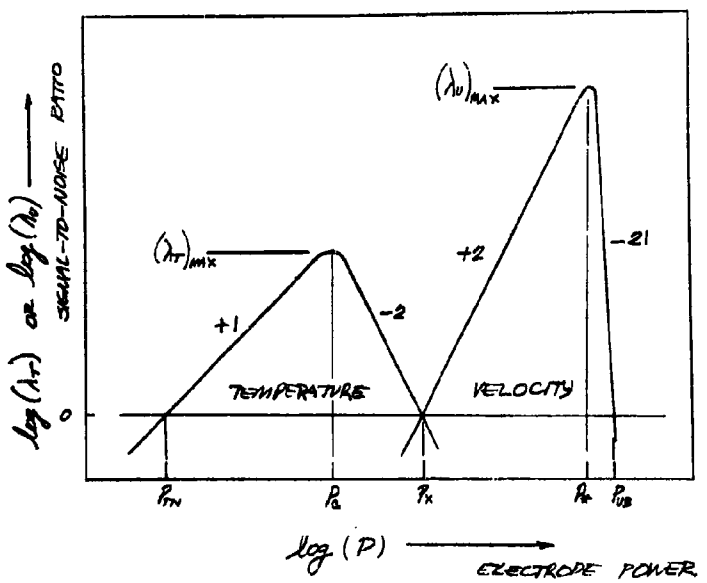

Figure 8.4. Signal-to-Noise Ratio for Temperature and Velocity Measurements as a Function of Electrode Power

this limiting power by P_{TN}:

$$\lambda_T = \lambda \approx \lambda \left(\frac{\delta T}{\delta T_{VO}}\right)^2 \cdot \frac{3}{2} \cdot \left(\frac{P_{TN}}{P_c}\right)$$

or

$$P_{TN} = P_c \quad \frac{2}{3} \left(\frac{\delta T_{VO}}{\delta T}\right)^2$$

or

$$P_{TN} = \left(\frac{4F\lambda m_3 m_4}{M_1 M_2 M^2 m_3}\right) \cdot \left(\frac{kTU}{b\beta^2 \delta T^2}\right).$$

The upper limit is set by velocity noise; denote this limiting power by P_X':

$$\lambda_T = \lambda \approx \lambda \left(\frac{\delta T}{\delta T_{VO}}\right)^2 \cdot 3 \left(\frac{P_c}{P_X'}\right)^2$$

or

$$P_X' = P_c \cdot \sqrt{3} \left(\frac{\delta T}{\delta T_{VO}}\right)$$

or

$$P_X' = \left(\frac{2 m_4}{\lambda^{1/2}}\right) c b^{1/2} U \delta l \left(\frac{\delta U}{U}\right)^{-1}$$

or

$$P_X' = \frac{2CAU^2}{\lambda^{1/2}} \left(\frac{\delta T}{\delta U}\right),$$

where A is the frontal area of the electrode. Thus, the useful range of electrode power for temperature measurements is

$$P_{TN} \leqslant P \leqslant P_X' \quad ,$$

and the following inequality is valid:

$$P_{TN} < P_c < P_X' \quad .$$

In terms of the quantities P'_x, P_{TN} and P_c, we have

$$\lambda_T = \frac{2}{3}\lambda\left(\frac{P_c}{P_{TN}}\right)\left[\frac{1}{3}\left(\frac{P}{P_c}\right)^2 + \frac{2}{3}\left(\frac{P_c}{P}\right)\right]^{-1}$$

and

$$(\lambda_T)_{MAX} = \frac{2}{3}\lambda\left(\frac{P_c}{P_{TN}}\right)$$

and

$$P_{TN}\left(P'_x\right)^2 = 2P_c^3 .$$

Velocity Signal

The signal-to-noise ratio, λ_v, is a maximum where the minimum detectable velocity is the smallest, i.e., at P = P* where $\delta U = \delta U_{Vo}$:

$$(\lambda_v)_{MAX} = \lambda\left(\frac{\delta U}{\delta U_{Vo}}\right)^2 .$$

At other values of electrode power in the vicinity of P*, we have

$$\lambda_v = \lambda\left(\frac{\delta U}{\delta U_{Vo}}\right)^2\cdot\left(\frac{n}{n-2}\right)\cdot\left(\frac{P}{P_*}\right)^2\left[1+\left(\frac{2}{n-2}\right)\left(\frac{P}{P_*}\right)^n\right]^{-1}$$

This function is illustrated in Figure 8.4 . The useful range of power, P, for velocity measurements is determined by the condition:

$$\lambda_v \geq \lambda .$$

In order to determine the limits of this range, assume $\delta U \gg \delta U_{Vo}$. The lower limit is set by temperature background noise and occurs at $P = P''_x$:

$$\lambda_v = \lambda \approx \lambda\left(\frac{\delta U}{\delta U_{Vo}}\right)^2\cdot\left(\frac{n}{n-2}\right)\cdot\left(\frac{P''_x}{P_*}\right)^2$$

or

$$P''_x = P_\lambda\,\lambda^{1/2}\left(\frac{\delta T}{\delta U}\right)\cdot\left(\frac{U}{\Delta T_\lambda}\right) ,$$

or

$$P_x'' = \lambda^{1/2}\, 2cAU\left(\frac{\delta T}{\delta U}\right).$$

For $\lambda = 1$, $P_x'' = P_x' \equiv P_x$, and, in general,

$$P_x = \left(P_x'' P_x'\right)^{1/2} = 2cAU\left(\frac{\delta T}{\delta U}\right).$$

The upper limit is set by boiling noise and occurs at $P = P_{UB}$:

$$\lambda_U = \lambda \approx \lambda \left(\frac{\delta U}{\delta U_{VO}}\right)^2 \cdot \left(\frac{n}{2}\right) \cdot \left(\frac{P_*}{P_{UB}}\right)^{n-2}$$

or

$$P_{UB} = P_\lambda \left[\left(\frac{\delta U}{U}\right) \cdot \frac{\beta \overline{\Delta T_\lambda}}{\sqrt{\lambda K}}\right]^{\frac{2}{n-2}}.$$

Thus, the useful range of electrode power for velocity measurements is

$$P_x'' \leq P \leq P_{UB}$$

and the following inequality is valid:

$$P_x'' < P_* < P_{UB}.$$

In terms of the quantities P_x'', P_* and P_{UB}, we have

$$\lambda_U = \lambda \left(\frac{P}{P_x''}\right)^2 \left[1 + \left(\frac{2}{n-2}\right)\left(\frac{P}{P_*}\right)^n\right]^{-1}$$

and

$$(\lambda_U)_{MAX} = \lambda \left(\frac{n-2}{n}\right)\left(\frac{P_*}{P_x''}\right)^2$$

and

$$(P_{UB})^{n-2}(P_x'')^2 = \left(\frac{n-2}{2}\right) P_*^n.$$

Numerical Examples

The results of the previous Sections are now evaluated under specific assumed conditions as examples of the quantities that have been discussed. Three representative situations in which the detection equipment might be used are: a) experiments in the laboratory, b) oceanographic experiments, and c) water tunnel experiments. The conditions which are assumed to pertain in these experimental situations are described in more detail below. In all cases, the use of an optimum double element wheatstone bridge with eye-type electrodes is assumed.

Laboratory An experimental arrangement similar to that used for the work of this Report is assumed. A tub of artificial sea water is stirred in such a way that the turbulence intensity is high ($\sim$10 %) and the average water speed is low (0.5 knot). By appropriate thermal shielding the thermal microstructure may be reduced to a low level (10 μ°C) for structure of small scale (1 cm).

Ocean An experimental arrangement at sea is assumed in which the detector is moved at low speed (3 knots) through deep ocean water where the turbulence level (.001 knot) and temperature variations (10 μ°C) are small for structure of small size (1 cm).

Water Tunnel Assume the detector is used for hydrodynamic research in a water tunnel filled with NaCl solution (or tap water). A relatively high speed (20 knots) is assumed in water of 1 % turbulence intensity, and high temperature microstructure (.01°C). A small scale probe (.05 cm) is used in the tests.

Numerical examples of the minimum detectable signals, and other parameters, are listed in Table 8.4 under the assumed conditions listed in Table 8.5 .

Table 8.4 . Numerical Examples of Minimum Detectable Signals

Parameter	Laboratory	Ocean	Tunnel
U	0.5 knots	3.0 knots	20 knots
$(\delta U/U)$	0.1	.0003	.01
δT	10 $\mu^{o}C$	10 $\mu^{o}C$	.01 ^{o}C
δU	.05 kts	.001 kts	0.2 kts
δT_{vo}	3.2 $\mu^{o}C$	0.5 $\mu^{o}C$	9.0 $\mu^{o}C$
δU_{vo}	0.8 μkts	4.8 μkts	.018 kts
$(\lambda_T)_{max}$	10 db	26 db	60 db
$(\lambda_U)_{max}$	96 db	46 db	21 db
b	0.3 cm	0.3 cm	.05 cm
A	0.13 cm^2	0.13 cm^2	.0038 cm^2
R	27 ohms	27 ohms	160 ohms
Δf	24 cps	150 cps	5.9 kc
P_{TN}	.035 mw	0.25 mw	.008 μw
P_c	0.52 mw	0.15 watts	16 mw
P_x	2.8 mw	5.0 watts	31 watts
P^*	170 watts	1.0 kw	350 watts
P_{VB}	600 watts	1.9 kw	490 watts
P_Λ	550 watts	3.3 kw	640 watts
k_c	6.0 cm^{-1}	6.0 cm^{-1}	36 cm^{-1}

Table 8.5 . Assumed Values of Numerical Examples

Parameter	Value
M	0.25
M_1	2
M_2	1
M_3	0.5
M_4	0.5
m_3	3.5*
m_4	1.5
K	.002
n	23
λ	1
F	2
$\overline{\Delta T_\Lambda}$	$20^\circ C$
c	4.09 joule/$cm^3/^\circ C$
β	2.1 % per $^\circ C$
kT	4×10^{-21} joule

*A more suitable value is $m_3 \approx 2$. See Section 13.1 and 14.1.

8.5 Mode of Operation

The performance of a velocity detector depends on the mode of operation of the electronics, for example, constant-current or constant-temperature operation. A general description of the mode of operation of a detector is given in this Section. Techniques for determining the temperature and velocity structure in the medium, and for locating the optimum operating power, are also considered.

Velocity Detector Mode

Consider a resistive sensing element, R, utilized to detect the velocity of a flowing medium. It is customary to distinguish four modes of operation of this sensing element in conjunction with the associated electronic equipment:

1. Constant-current-operation (CCO)
2. Constant-resistance-operation (CRO) (Sometimes called constant-temperature operation, CTO)
3. Constant-voltage-operation (CVO)
4. Constant-power-operation (CPO).

This terminology is used in connection with the operation of a hot-wire anemometer, and is, of course, directly applicable to the velocity detector of this Report.

These four modes of operation are never exactly achieved in practice and all gradations between the "pure" modes of operation are possible. It is useful to introduce a single parameter, the "mode angle," φ, which is capable of characterizing any mode of operation.

Suppose a voltage, V, is applied to the resistance, R, causing a current, I, to flow and dissipating a power, P. These four electrical quantities are interrelated and if any two are known, the other two may be calculated. We would prefer to think of I and V as the independent variables and P and R as the dependent variables (orthogonal pairs). Let the steady state or average values of these quantities be denoted by a zero subscript. Ohm's Law is

$$R = \frac{V}{I} ,$$

and the Joule Heating Law is

$$P = VI .$$

For a particular mode of operation, a known relation between the inde-

pendent variables (voltage and current) exists, therefore only one variable suffices to determine the other three. Considering only small increments of the variables about their average values, a simple diagram can be drawn to show the various modes of operation as in Figure 8.5 . The slope of these (linear) relations local to the average operating point is

$$R_o \left(\frac{dI}{dV}\right)_o = - \tan\varphi$$

where φ is the "mode angle." Clearly, by the proper choice of this angle the four modes of operation may be identified as well as all intermediate modes. For a unique characterization, we require that

$$-\pi/2 < \varphi \leqslant \pi/2 \quad .$$

The values of φ for the main modes of operation are listed in Table 8.6 below.

Table 8.6 . Mode Angle for Detector Operation

Mode Angle φ	Mode of Operation
0^o	CCO
45^o	CPO
90^o	CVO
-45^o	CRO

Several relations between the electrical variables are conveniently written down by introducing the following dimensionless variables suitable for small signal analysis:

$$v = \frac{V - V_o}{V_o} \qquad r = \frac{R - R_o}{R_o}$$

$$i = \frac{I - I_o}{I_o} \qquad p = \frac{P - P_o}{P_o} \quad .$$

The current-voltage relation becomes

$$i = -v \tan\varphi$$

and

$$r = v - i$$

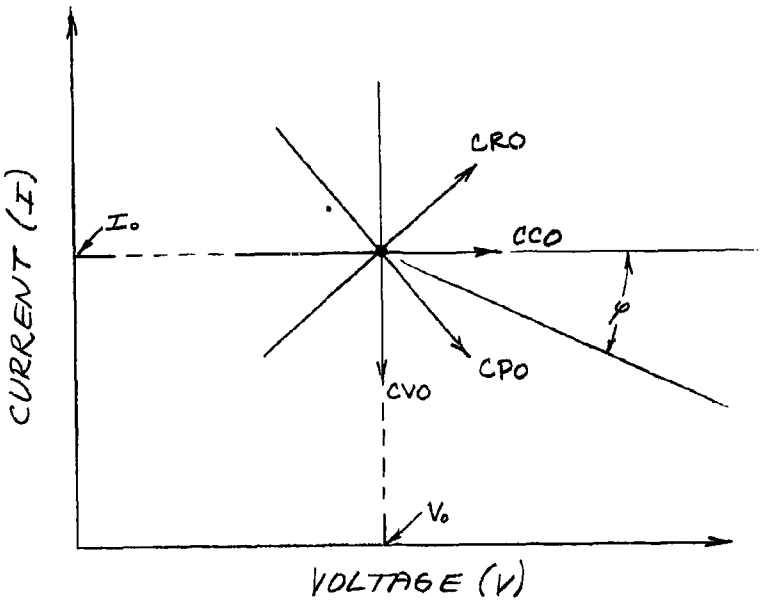

Figure 8.5. Mode Angle

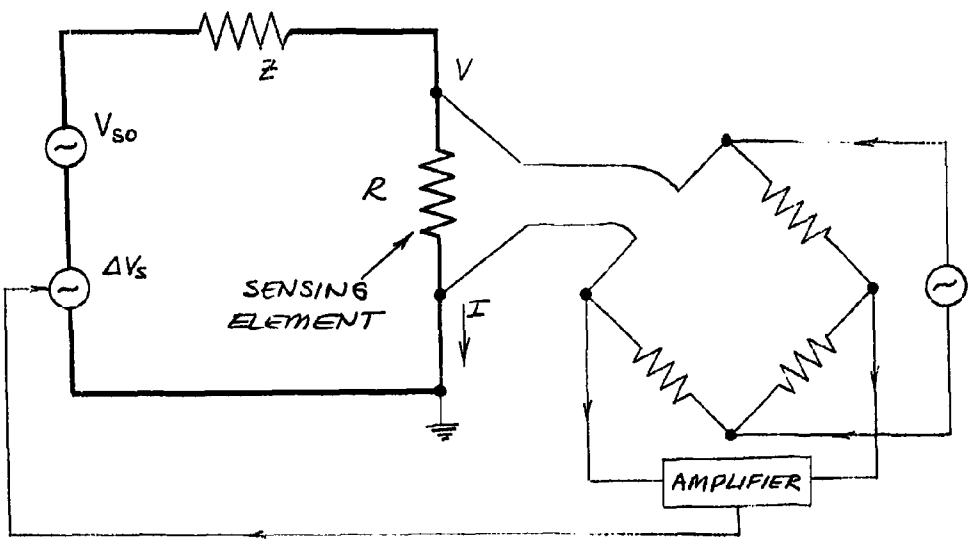

Figure 8.6. Feedback Circuit for the Active Mode of Operation

$$r = v\,(1 + \tan\varphi) = i\left(\frac{1 + \tan\varphi}{-\tan\varphi}\right)$$

and

$$p = v + i$$
$$= v(1 - \tan\varphi) = i\left(\frac{\tan\varphi - 1}{\tan\varphi}\right)$$

and

$$p = r\left(\frac{1 - \tan\varphi}{1 + \tan\varphi}\right) = r\,\tan\left(\frac{\pi}{4} - \varphi\right).$$

It follows from the relation

$$i = -\,v \tan\varphi\,,$$

that the relative current fluctuations are larger than the relative voltage fluctuations (therefore, preferably measured) for those modes for which

$$\pi/4 \leq |\varphi| \leq \pi/2\,,$$

and, conversely when

$$0 \leq |\varphi| \leq \pi/4\,.$$

Active Mode

The negative mode angles $-\pi/2 < \varphi < 0$ apply to instruments utilizing negative feedback to regulate the electrical variables. The most important example of this is the CRO mode in which the resistance is held constant by regulating the power to the sensing element.

Consider the sensing element as a load on a source of voltage V_S which has an internal impedance Z. The resultant voltage, V, and current, I, of the sensing element are

$$V = V_S\left(\frac{R}{R + Z}\right)$$

$$I = \frac{V_S}{R + Z}\,.$$

The voltage source, V_S, consists of a constant voltage, V_{SO}, and a variable voltage, ΔV_S, which originates in a feedback loop based on variations in the resistance of the sensing element:

$$V_S = V_{SO} + \Delta V_S \quad .$$

The main circuit for the sensing element is shown in dark lines in Figure 8.6 ; the light lines of this Figure correspond to a bridge network to measure resistance variations providing the input signal for the feedback loop. Assume the light and dark circuits are independent (for example, by operating the two at different frequencies) except for the signal in the feedback loop which sets ΔV_S.

Small changes in the variables of the equation

$$V = V_S \left(\frac{R}{R + Z} \right) \quad ,$$

yields

$$\left(\frac{\Delta V}{V_o} \right) = \left(\frac{\Delta V_S}{V_o} \right) + \left(\frac{\Delta R}{R_o} \right) - \left(\frac{R_o}{R_o + Z} \right) \cdot \left(\frac{\Delta R}{R_o} \right)$$

or

$$v = v_S + rM \quad ,$$

where

$$v_S = \frac{\Delta V_S}{V_{SO}}$$

and

$$M = \left(\frac{Z}{Z + R_o} \right) \qquad (0 < M < 1)$$

The feedback loop involving the wheatstone bridge makes a measurement of

$$\frac{\Delta R}{R_o}$$

and amplifies it by a factor A and, thus, generates the signal ΔV_S. These quantities are related by

$$\frac{\Delta V_S}{V_{SO}} = A \left(\frac{\Delta R}{R_o} \right) \quad ,$$

or

$$v_s = Ar \quad .$$

This defines the meaning of the gain, A. Combining the above equations we get

$$v = (A + M)\, r \quad ,$$

comparing this equation with that involving the mode angle:

$$r = (1 + \tan\varphi)\, v \quad ,$$

we find

$$\tan\varphi = \left(\frac{1 - A - M}{A + M}\right) \quad .$$

The total circuit is called "passive" if the feedback loop is non-operative (A = 0) and "active" otherwise. The values for the three main passive modes are given in Table 8.7 below.

Table 8.7 . Passive Modes of Operation

Mode	φ	$(\frac{R}{Z})$	M	$\tan\varphi$
CCO	0°	∞	1	0
CPO	45°	1	1/2	1
CVO	90°	0	0	∞

The interesting "active" case is when the feedback is large ($A \rightarrow -\infty$); in this case

$$\tan\varphi = -1 \quad \text{and} \quad \varphi = -45^\circ \quad ,$$

which corresponds to constant-resistance-operation.

The feedback loop can be characterized by its transconductance, g_m, which is defined as

$$g_m = \left(\frac{\Delta I}{I\, \Delta R}\right) = \frac{i}{r R_o}$$

or

$$R_o g_m = \frac{-\tan\varphi}{1+\tan\varphi}$$

or

$$\tan\varphi = \frac{-R_o g_m}{1+R_o g_m} .$$

Dual Operation

Methods are now considered for determining the temperature and velocity fluctuations in a medium with detection equipment capable of dual velocity and temperature measurements.

Consider the output signal from the bridge, with the exclusion of boiling noise;

$$\Delta V^2 = (v_n)^2_{rms} + \Delta V^2(\text{temperature}) + \Delta V^2(\text{velocity}) .$$

Let the intrinsic signal-to-noise ratio of the detector output be

$$\Lambda_o = \frac{\Delta V^2}{(v_n)^2_{rms}} .$$

The above expression for, ΔV, may be written

$$\Lambda_o = 1 + AP_1 + BP_1(P_1 + P_2)^2 ,$$

where the quantities A and B are determined as follows. The temperature signal is equal to the detector noise at $P_1 = P_{TN}$:

$$1 \approx AP_{TN} .$$

The temperature signal is equal to the velocity signal at $P_1 + P_2 = P_X$:

$$A \approx BP_X^2 .$$

It follows that,

$$\Lambda_o = 1 + \left(\frac{P_1}{P_{TN}}\right) + \left(\frac{P_1}{P_{TN}}\right)\cdot\left(\frac{P_1+P_2}{P_x}\right)^2 .$$

The dependence of Λ_o (which is proportional to the detector output) on P_1 and P_2 provides a means for determining P_{TN} and P_x from which the properties of the turbulent medium may be determined.

The power level P_{TN} is determined experimentally by first observing the output for $P_2 = P_1 = 0$ which is due entirely to Johnson noise:

$$\Lambda_o = 1 .$$

Then, with $P_2 = 0$, the signal power is increased until the output is doubled at which point $P_1 = P_{11}$

$$2 = \frac{P_{11}}{P_{TN}} + 1$$

or

$$P_{11} = P_{TN} .$$

The term due to velocity is neglected at this power level. Then, with $P_1 = P_{11} = P_{TN}$, the heater power is increased until the output is again doubled at which point $P_2 = P_{22}$:

$$4 = 2 + \left(\frac{P_{TN} + P_{22}}{P_x}\right)^2$$

or

$$P_{22} = \sqrt{2}\,P_x - P_{TN} \simeq \sqrt{2}\,P_x \quad , \quad (P_{TN} \ll P_x) .$$

Now that P_{TN} and P_x have been determined, the optimum operating power for temperature measurements is calculated as follows:

$$P_c = \left(\frac{P_{TN}\,P_x^2}{2}\right)^{\frac{1}{3}} .$$

A similar technique may be used for determining the optimum operating power, P_*, for velocity measurements, however, a close estimate is

$$P_* \approx 0.5\ P_{vB} \quad ,$$

where P_{vB} is the point where boiling noise is comparable with the velocity signal. The above equation is useful since the boiling noise decreases very rapidly below P_{vB}.

In dual operation, a procedure must be defined for setting the values of the signal power, P_1, and heater power, P_2. The signal-to-noise ratios for temperature and velocity measurements are degraded only slightly, or not at all, if the following "program" is followed. For temperature measurements where $P \leq P_x$, shut off the heater source ($P_2 = 0$) so that $P_1 = P_2$. For velocity measurements where $P \geq P_x$, set the signal source so that $P_1 = P_x$ and make up the additional power with the heater source:

$$P_2 = P - P_x \quad .$$

Following this procedure, the temperature measurements are not at all impaired and, in the case of the velocity measurements, λ_v is reduced below its full value (for $P_1 = P$, $P_2 = 0$) by at most a factor

$$1 - \left(\frac{P_{TN}}{P_x}\right) \quad ,$$

which is nearly equal to unity. In general, it may be shown that it is necessary only that $P_1 >> P_{TN}$ in order that λ_v is not reduced appreciably below its full value.

9. ELECTRODES

The properties of electrodes suitable for measuring the conductivity in a flowing medium are studied in this Section. Surface contact electrodes are covered primarily, although some of the properties of induction-coupled and capacity-coupled probes are also considered. Experimental measurements on electrodes and design techniques are described at the end of this Section.

9.1 General Considerations

The electrodes for detection purposes in water should be designed with two considerations in mind, one relating to the electrical properties and the other to the hydrodynamic properties of the electrode configuration. The combined constraints of these factors on the choice of an electrode are the following. It is required that the fluid flow be laminar and uniform over the sensitive volume of the electrode, and that the field of the electrode be localized and as uniform as possible. The uniformity of the flow and electrode field is important to avoid "hot spots" which occur at a stagnation point or at the edge of an electrode. The only way to avoid the high current density which occurs at an edge is to have the electrode and insulators intersect at 90°. A well localized field is produced by two electrodes in close proximity with an electrode area comparable with the area of the insulators between the electrodes. It has not been possible to design an electrode which meets all these requirements, in particular, one that a) has no stagnation point, b) has a favorable (decreasing) pressure gradient over the sensing volume, c) is of smooth or streamlined shape, and, d) has a finite and fairly uniform current density over the entire electrode volume. The ruggedness of the electrodes is an important practical consideration. One type of electrode which fulfills all of these requirements, except for the "edge effect," is an electrode flush mounted in a plane. The simplest type of flush electrode is the "eye-type" consisting of a central electrode, a concentric insulator and an outer electrode of large extent. For measurements which call for a small sensitive volume, a "probe-type" configuration is used. This consists of a thin streamlined probe with an electrode located at the tip.

The theoretical properties of the electrode studied in this Section are based on the analysis developed in other Sections, in particular, the formulas of Section 10.

Electrode Characteristics

The various properties of an electrode arrangement are described by "characteristic numbers" which, along with some reference dimension, may

be used to calculate the performance of the sensor. These properites have been developed at various points in the Report and are brought together here for a comprehensive understanding of electrodes. The characteristic numbers depend only on the "shape" of the electrode configuration and are referred to some reference dimension, b, which is chosen arbitrarily to characterize the "size" of the electrode. The dimension b is usually comparable with the radius of the configuration.

Resistance Number

The resistance of an electrode is ordinarily described by the "cell constant," $R\sigma$, which has units of inverse length. The "resistance number," m, is defined by the equation

$$R\sigma b = m \quad .$$

Effective Electrode Area

For electrodes with dissimilar positive and negative electrodes, with non-uniform current density, the "effective electrode area," S, is defined by the equation (Sec. 10.5)

$$I = \frac{1}{2} S R^2 \sigma^2 \left\{ \int_+ (\nabla\phi)^2 dA + \int_- (\nabla\phi)^2 dA \right\}$$

$$= \frac{1}{2} R\sigma S \left\{ \int_+ w\, dA + \int_- w\, dA \right\},$$

where the integration is carried out over the surface of both electrodes and

$$w = R\sigma\, (\nabla\phi)^2.$$

The effective separation between the electrodes, might be described by the length

$$R\sigma S \quad .$$

If the field is uniform, the area S is just equal to the actual electrode area. The characteristic number of S is defined by

$$S = m_6 b^2 \quad .$$

Frontal Area

The average temperature rise, $\overline{\Delta T}$, of water passing through the electrode volume is given by

$$\overline{\Delta T} = \frac{P}{2cAU}$$

where P is the power dissipated in the water, c is the heat capacity per unit volume of the water, U is the water velocity and A is the "frontal area" of the electrode (Sec. 12.1). The characteristic number for A is

$$A = m_4 b^2 .$$

Effective Volume

A measure of the volume of the field of an electrode is the "effective volume," v_e defined by (Sec. 12.2)

$$I = v_e \int w^2 dv$$

and

$$v_e = m_2 b^3 .$$

Dipole Moment

The field at great distance from an electrode corresponds to that of a dipole. The number, m_e, which determines the dipole moment of the electrode is defined by the equation (Sec. 10.1)

$$\phi = m_e \left(\frac{b}{r}\right)^2 \sin\psi$$

where r is the radius from the center of the electrode, and $\pi/2 - \psi$ is the polar angle from the axis of symmetry of the electrodes.

Radius

The root-mean-square radius of the electrode configuration is defined by

$$r_{rms}^2 = \int r^2 w \, dv$$

and the corresponding characteristic number is

$$r_{rms} = m_1 b \quad .$$

The average radius is defined simply as

$$\bar{r} = \int r w dv .$$

Cutoff Wavenumber

The finite size of the electrode configuration limits the size of the smallest blobs of water whose properties are measured with full response. The cutoff wavenumber for temperature measurements, k_c, of an electrode due to its finite size is defined to be (Sec. 13.1)

$$k_c = \sqrt{3}\left[\int r^2 w dv\right]^{-1/2} = \frac{2\pi}{m_3 b}$$

which is related to the rms-radius by the equation

$$k_c = \frac{\sqrt{3}}{r_{rms}} \quad .$$

The cutoff wavenumber for velocity measurements is (Sec. 14.1)

$$k_c = \sqrt{3}\left[\int r^2 w dv - \left(\int \vec{r} w dv\right)^2\right]^{-1/2}$$

$$= \sqrt{3}\left[r_{rms}^2 - c^2\right]^{-1/2} = \frac{2\pi}{m_3 b} \quad ,$$

where $c = |\vec{c}|$ is the first moment of the w-distribution:

$$\vec{c} = \int \vec{r} w dv .$$

Temperature Uniformity

The maximum temperature rise, ΔT_{max}, of water passing through an electrode sets the limit of electrode power before boiling sets in. The average electrode temperature rise, $\overline{\Delta T}$, however, determines the sensitivity to the velocity of the medium. The "temperature uniformity" of the electrode is defined as (Sec. 12.2)

$$m_5 = \frac{\overline{\Delta T}}{\Delta T_{max.}} < 1.$$

Uniformity is desirable in order to achieve high sensitivity.

Static Heat Transfer

If the water in the electrode volume is static, the heat transfer to the medium is determined by thermal conduction. The "static heat transfer constant," m_7, is defined by the equation (Sec. 12.3)

$$\overline{\Delta T} = \frac{P}{m_7 K b} ,$$

where K is the thermal conductivity of the medium.

A list of the characteristic numbers discussed above is given in Table 9.1 .

Table 9.1 . Electrode Characteristic Numbers

Parameter	m-Number
Resistance Number	m
rms-Radius	m_1
Effective Electrode Area	m_6
Frontal Area	m_4
Effective Volume	m_2
Dipole Moment	m_o
Cutoff Wavenumber	m_3
Temperature Uniformity	m_5
Static Heat Transfer Constant	m_7

9.2 Eye-Type Electrode

One of the simplest and most practical flush electrodes is the eye-type electrode illustrated in Figure 9.1 . The simplicity of this electrode configuration does not extend to its mathematical analysis. Neither closed form or series expressions have been obtained for its potential field or resistance. The negative or ground electrode lies in a plane in the region $\rho \geqslant b$ where $2b$ is the outer diameter (pupil) of the electrode configuration. The positive electrode also lies in the plane in the region $\rho \leqslant a$ where $2a$ is the inner diameter (iris) of the arrangement. The region $b > \rho > a$ is a coplanar insulator. The "size" of the electrode refers

to the dimension, b, and the "shape" to the ratio $\alpha = a/b$.

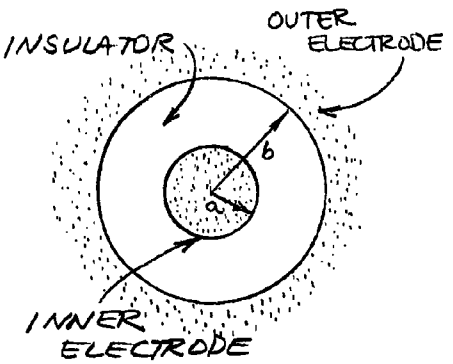

Figure 9.1 . Eye-Type Electrode

Resistance

The resistance of the eye-type electrode is evaluated only in the limiting cases of small ($\alpha \rightarrow 0$) or large ($\alpha \rightarrow 1$) inner electrode. The resistance for intermediate values of α ($0 < \alpha < 1$) is estimated graphically with the aid of the limiting cases.

The limiting case $a \lesssim b$ is considered first. In this case the resistance is low and the field in the gap is similar to that of a slit between semi-infinite planes of opposite polarity as discussed in Section 9.3 . The current density near the center of the electrode is approximately equal to that for the case when a = b, for which the solution is known. The unit potential gradient for the case $\alpha = 1$ is (1,2,3)

$$\frac{\partial \phi}{\partial n} = \frac{1}{b}\int_0^\infty x\, J_1(x)\, J_0(\lambda x)\, dx$$

$$= \frac{2}{\pi b}\,\frac{E(\lambda)}{1-\lambda^2}\,, \qquad (\lambda < 1)$$

where $\rho = \lambda b$, $J_0(x)$ and $J_1(x)$ are Bessel functions of the first and second order, ρ is the radius, and $E(\lambda)$ is the complete elliptic integral of the second kind. The resulting current density in this case becomes infinitely large for $\rho \rightarrow b$ and the electrode resistance is zero. However, if in the region $\rho \approx b$, the gradient is replaced by that of a corresponding slit with a gap $(b - a)$, a finite electrode resistance is obtained which is an approximation for the case $\alpha \rightarrow 1$. The unit potential gradient for the slit is given in Section 9.3 as

$$\frac{\partial \phi}{\partial n} = \frac{1}{\pi\sqrt{x^2 - a_1^2}}$$

where

$$x = \rho - \left(\frac{a+b}{2}\right)$$

and

$$a_1 = \frac{b-a}{2} .$$

Provided $b - a << a$, the above approximations to the potential gradient feather into each other in the vicinity of $\rho \approx a$. Calculating the resistance by the formula (Sec. 10.3)

$$\frac{1}{R\sigma} = \int_0^a \left(\frac{\partial \phi}{\partial n}\right) 2\pi\rho d\rho$$

we find

$$(R\sigma b)^{-1} \approx 2 \ln \left(\frac{32\alpha}{1-\alpha}\right) - 4 .$$

This is the approximation to the resistance number for the eye-type electrode for $\alpha \approx 1$, and is shown in Figure 9.2 as the dotted curve in the region $\alpha \approx 1$.

In the limit $\alpha \rightarrow 0$, the resistance reduces to that of a disc (Sec. 9.3):

$$R\sigma a = \frac{1}{4}$$

or

$$R\sigma b = \frac{1}{4\alpha} .$$

The next higher approximation in terms of small α requires the use of the variational method described in Section 10.3 , however, that has not been done because of the complexity of the method. This approximation has been carried out in the following way: Assume that the gradient over the central electrode is approximately the same as that for a disc, viz.,

$$\nabla\phi = f\left(\frac{\rho}{a}\right) (\nabla\phi)_{DISC},$$

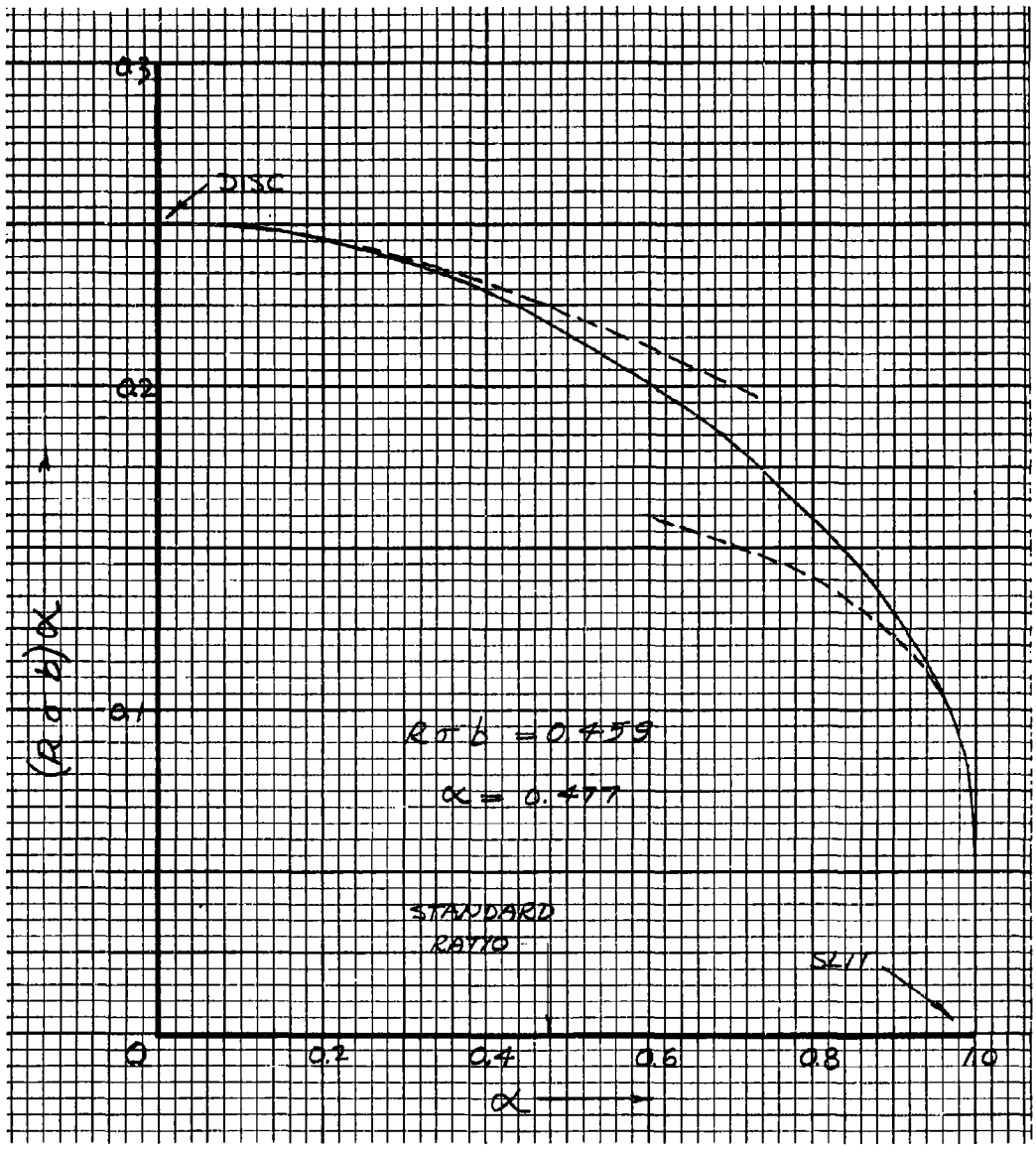

Figure 9.2. Resistance Number of the Eye-Type Electrode

where

$$f\left(\frac{\rho}{a}\right) = A_0(\alpha) + A_1(\alpha)\left(\frac{\rho}{a}\right) + \cdots$$

and

$$(\nabla\phi)_{DISC} = \frac{-2}{\pi a \sqrt{1-\left(\frac{\rho}{a}\right)^2}} .$$

The coefficients A_0 and A_1 are known in the two limiting cases:

$\alpha = 1$:	$A_0 = \pi/2$	$A_1 = \pi/4$
$\alpha = 0$:	$A_0 = 1$	$A_1 = 0$.

The resistance number is

$$R\sigma a = \frac{1}{4\left[A_0 + \frac{2}{3}A_1 + \cdots\right]} .$$

On the basis of the values of A_0 and A_1 in the limiting cases, the following estimation is made for small α:

$$A_0 + \frac{2}{3}A_1 + \cdots = 1 + \frac{1}{2}\alpha^2 + \cdots$$

which corresponds to the values:

$$A_0 = 1 + 0.36\,\alpha^2$$

$$A_1 = 0.49\,\alpha^2 \quad .$$

The approximate resistance number is

$$(R\sigma b)\alpha = \frac{1}{4\left(1 + 0.5\alpha^2\right)} ,$$

OR

$$(R\sigma b)^{-1} = 4(\alpha + \tfrac{1}{2}\alpha^3).$$

This function is shown in Figure 9.2 as the dotted curve in the region of small α values. A smooth curve joining the two limiting approximations is also shown in Figure 9.2 , and the resulting resistance number is listed in Table 9.2 . The "standard" eye-type electrode used in this work is

$$\alpha = 0.477$$

$$(R\sigma b)\alpha = 0.219$$

$$R\sigma b = 0.459 \ .$$

Table 9.2 . Resistance Number for the Eye-Type Electrode

α	$(R\sigma b)\alpha$	$(R\sigma b)$
0.0	0.250	∞
0.1	0.249	2.49
0.2	0.246	1.23
0.3	0.239	0.797
0.4	0.229	0.573
0.5	0.216	0.432
0.6	0.200	0.333
0.7	0.182	0.260
0.8	0.159	0.199
0.9	0.129	0.143
1.0	0.000	0.000

Potential Field

The potential gradient for the region $\rho < a$ is approximately

$$b(\nabla\phi)_\nu = -\left(\frac{2}{\pi\alpha}\right)\frac{f(\nu)}{\sqrt{1-\nu^2}}$$

where $\rho = \nu a$ and $f(\nu) = A_0 + A_1\nu^2$. The gradient for the region $\rho > b$ is found from the above expression by integration over the inner electrode (4):

$$b(\nabla\phi)_\lambda = \left(\frac{4\alpha}{\pi^2}\right)\frac{g(\lambda)}{\lambda^2\sqrt{\lambda^2-1}}$$

where $\rho = \lambda b$ and

$$g(\lambda) = \left(A_0 + \tfrac{2}{3}A_1\right) + \left(\tfrac{2}{3}A_0 + \tfrac{8}{15}A_1\right)\left(\frac{1}{\lambda^2} - \frac{1}{2}\right)\alpha^2.$$

The potential in the gap $a < \rho < b$ is calculated from the above potential gradients by an approximate method since the direct analytical method is too complicated. The approximation is based on the fact that near the

of the electrodes, whether on the electrode proper or in the gap, the magnitudes of the gradients are approximately equal. On this basis we conclude that near the inner electrode

$$b\,(\nabla\phi)_{\nu\ GAP} = -\left(\frac{2}{\pi\alpha}\right)\frac{f(1)}{\nu\sqrt{\nu^2-1}}\ , \qquad (\nu>1)$$

and near the outer electrode the gradient is

$$b\,(\nabla\phi)_{\lambda\ GAP} = \left(\frac{4\alpha}{\pi^2}\right)\frac{g(1)}{\lambda^2\sqrt{1-\lambda^2}}\ , \qquad (\lambda<1).$$

Integrating these expressions in the gap region we obtain the dashed curves of Figure 9.3 for $\alpha = 0.477$. The smooth curve joining these is approximately equal to the potential in the electrode gap. Of course, the potential is zero for $\rho > b$ and unity for $\rho < a$. The axial potential is shown in Figure 9.3 as the dotted curve and represents a smooth curve joining the known values close to, and far from, the surface. The first moment, m_0, of the surface potential found by numerical integration of the curve of Figure 9.3 is

$$m_0 = \int_0^1 \lambda\ \phi(\lambda)\,d\lambda = 0.23\ .$$

The moment m_0 may also be obtained from the surface gradient at large distance from the electrode:

$$\nabla\phi_\lambda \rightarrow \left(\frac{4\alpha}{\pi^2 b}\right)\frac{g(\infty)}{\lambda^3}\ . \qquad (\rho = \lambda b)$$

According to Section 10.1 , the gradient for a dipole field is

$$\nabla\phi \rightarrow \frac{m_0}{b}\,\frac{1}{\lambda^3}$$

and on comparing these expressions we find

$$m_0 = \frac{4\alpha\, g(\infty)}{\pi^2} \approx 0.21$$

which is in fair agreement with the above graphical method of obtaining m_0.

The corresponding potential gradient, given by the expressions above

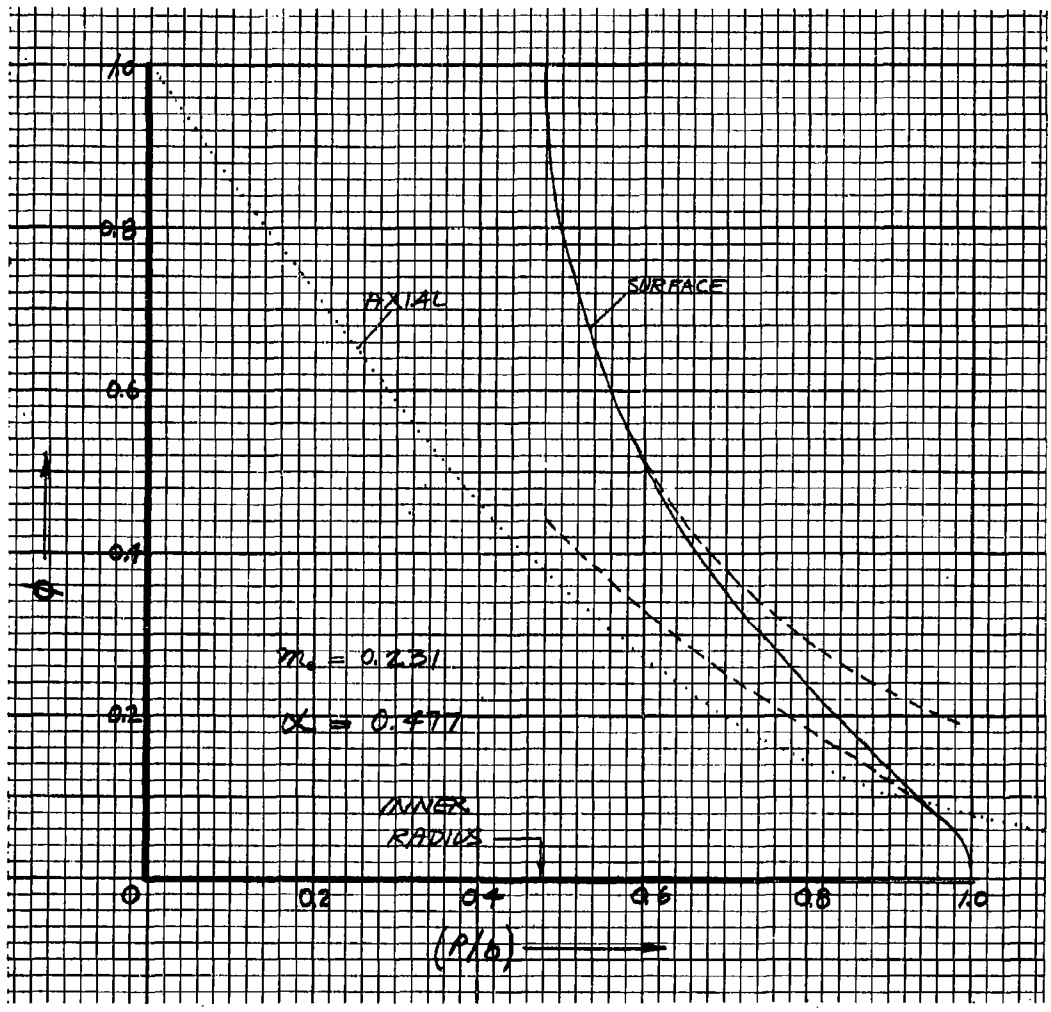

Figure 9.3. Surface and Axial Potential of the Eye-Type Electrode

for $b(\nabla\phi)$, is shown in Figure 9.4 . The divergence of the current density at the edges of the electrodes is apparent in this graph. The axial potential gradient is shown as the dotted curve in Figure 9.4 .

At great distance from the electrode ($\rho >> b$) the potential field corresponds to that of a dipole. The equipotential (solid lines) and current (dotted lines) surfaces in this case are shown in Figure 9.5 , where the two opposite charges, which constitute the virtual dipole, are located at the center of the electrode. The horizontal line corresponds to the plane of the electrode.

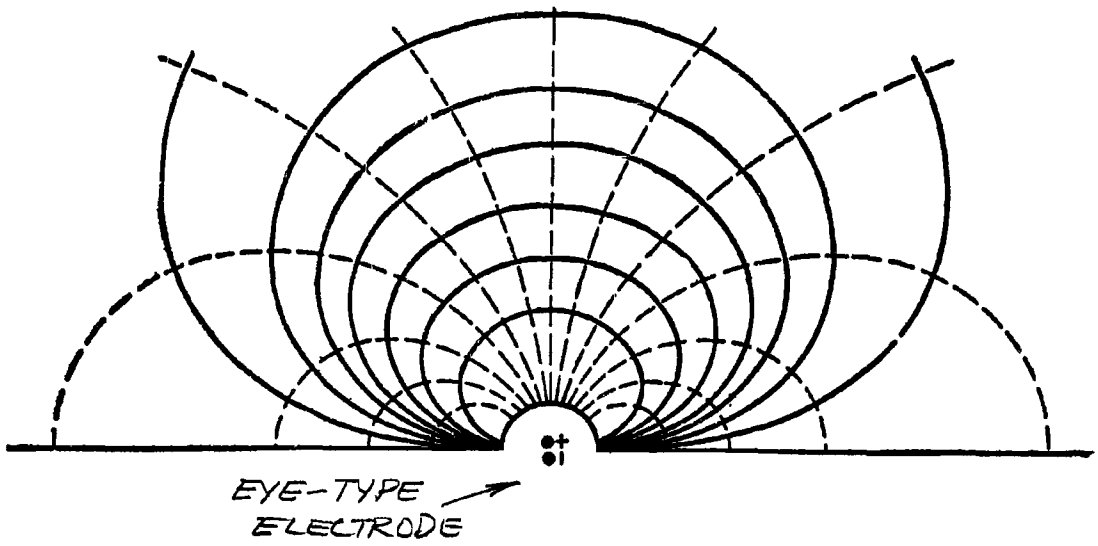

Figure 9.5 . "Potential and Current Surfaces at Great Distance from the Eye-Type Electrode"

The sensing function, w, is

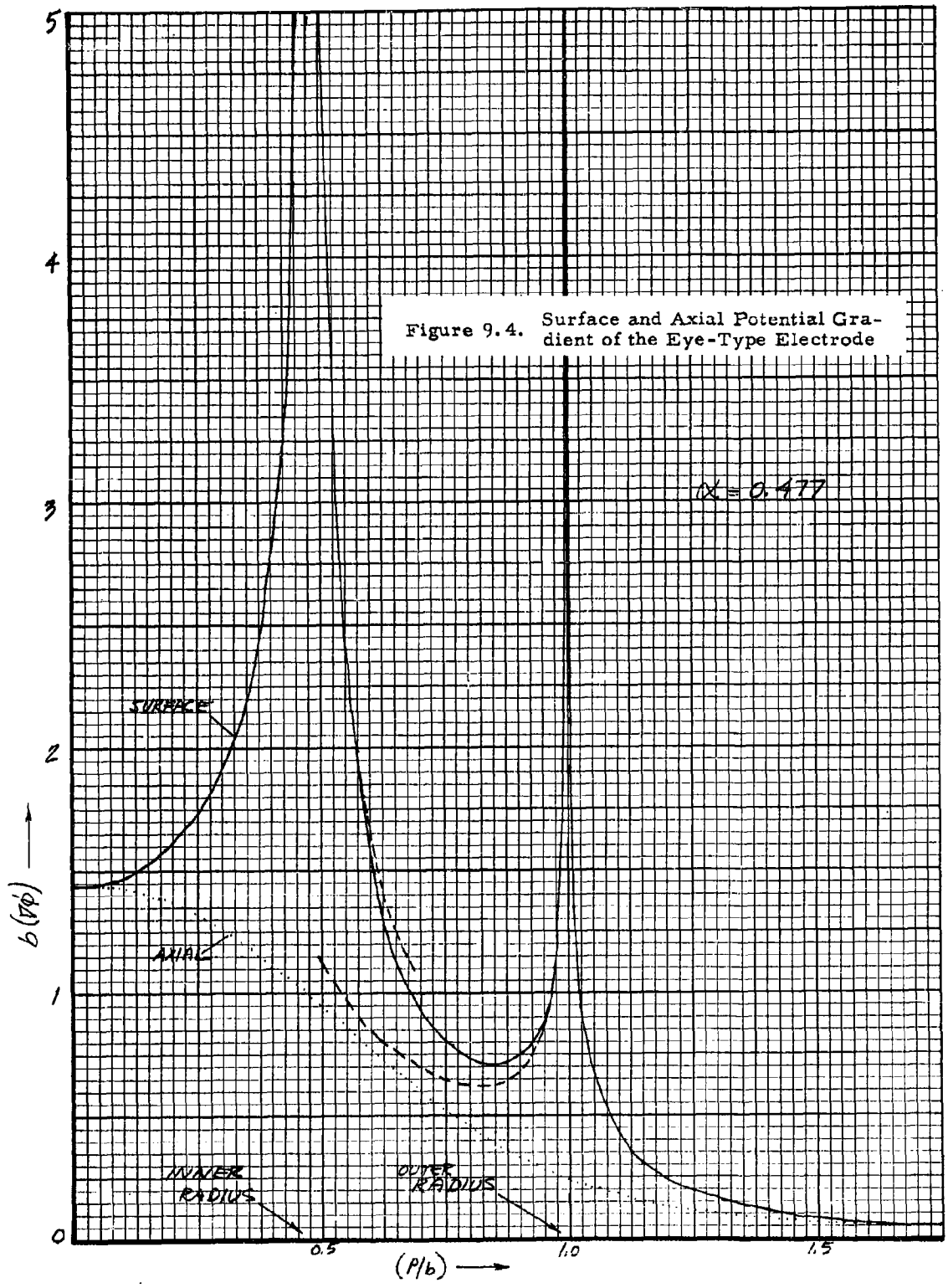

Figure 9.4. Surface and Axial Potential Gradient of the Eye-Type Electrode

$$w = R\sigma\,(\nabla\phi)^2$$
$$= \frac{(R\sigma b)}{b^3}\,(b\nabla\phi)^2 .$$

This function shows even a larger range of variation over the electrode volume than the gradient, $b(\nabla\phi)$, plotted in Figure 9.4 .

Characteristic Numbers

Because of the complexity of the field of an eye-type electrode, it is not possible to calculate the characteristic numbers exactly. In addition, a difficulty arises because of the infinitely large current density at the electrode edges, which causes the "effective volume," v_0, and "effective electrode area," S, to be zero. Both of these quantities are finite if a slight radius of curvature at the edges is assumed; in that case the parameters depend logarithmically on the radius of curvature. The frontal area, A, is estimated to be

$$A = 1.5\ b^2 , \quad \text{or} \quad m_2 = 1.5$$

for $\alpha = 0.48$. As shown earlier the resistance number in this case is

$$R\sigma b = m = 0.459 ,$$

and the dipole number is

$$m_0 = 0.23 .$$

9.3 Other Electrodes

The properties of several other types of electrodes are of use in the theoretical and experimental analysis of the present detection techniques. Most of the ones discussed below have been singled out because of their intrinsic simplicity and ease of mathematical analysis.

Parallel Plates

The simplest electrode arrangement consists of two parallel rectangular plates with a uniform field between the plates. Edge effects are neglected. The simplest parallel plate geometry corresponds to a cubic electrode volume with sides of length 2b. This arrangement is used several times in this Report to illustrate basic principles. The characteristic numbers of this simple electrode arrangement are listed in Table 9.3 .

Table 9.3 . Characteristic Numbers of Spherical, Cubic and Cylindrical Electrodes

Parameter	Sphere	Cube	Square Cylinder
Velocity Cutoff Wavenumber	1.40	-	1.61
Temperature Cutoff Wavenumber	2.81	-	3.45
Average Radius	0.750	-	-
rms-Radius	0.775	-	-
Frontal Area	2.79	4.00	3.71
Effective Volume	4.20	8.00	6.28
Effective Electrode Area	-	4.00	3.14
Temperature Uniformity	0.375	0.500	0.426
Dipole Moment	-	-	-
Resistance Number	-	0.500	0.636
Static Heat Transfer Constant	10.5	-	-

Uniform Spherical Volume

A spherical sensing volume inside of which the potential gradient is uniform and zero outside is an ideal distribution function in that it is of least extent for a given effective volume. Such a distribution function is not realizable in a practical electrode configuration with infinitely conducting electrodes. Let b be the radius of the distribution, and w_o the value of the distribution inside the sphere. By the normalization condition we have

$$1 = \int w\,dv = w_o \int_0^b 4\pi r^2 dr = w_o \left(\frac{4}{3}\pi b^3\right).$$

The rms-radius is

$$r_{rms}^2 = \int r^2 w\,dv = w_o \int_0^b 4\pi r^4 dr = w_o \frac{4\pi}{5} b^5$$

or

$$r_{rms} = \sqrt{\frac{3}{5}}\, b.$$

The average radius $\bar{r}$ is

$$\bar{r} = \int r w dv = \frac{3}{4} b.$$

The frontal area, A , is (Sec. 12.2)

$$I = A 2\pi \int_0^\infty \rho d\rho \left(\int_{-\infty}^{+\infty} w dx \right)^2,$$

where ρ is the transverse distance from a given axis through the center of the sphere, and x is the distance along that axis. The fluid flow is assumed to be uniform throughout the spherical volume. Evaluating the integral we find

$$A = \left(\frac{8\pi}{9}\right) b^2 \quad , \qquad m_4 = \frac{8\pi}{9} \quad .$$

The effective volume, v_o, is simply the volume of the sphere:

$$I = v_o \int w^2 dv = v_o w_o \int w_o dv = v_o w_o .$$

thus,

$$v_o = \frac{4\pi}{3} b^3 \quad , \quad m_2 = \frac{4\pi}{3}$$

The cutoff wavenumber for temperature and velocity are given in Sections 13.1 and 14.1. The resistance and effective electrode area of the spherical volume are undefined. The static heat transfer constant is calculated in Section 12.3 . The maximum temperature rise occurs on the path along a diameter:

$$\Delta T_{max} = \frac{2bP}{v_o c U} \quad \text{and} \quad \overline{\Delta T} = \frac{P}{2cAU} .$$

The temperature uniformity is

$$m_5 = \frac{\overline{\Delta T}}{\Delta T_{max}} = \frac{v_o}{4bA} = 3/8.$$

The above characteristic numbers for the uniform spherical volume are listed in Table 9.3 , where b is the reference dimension.

Uniform Cylindrical Volume

The (square) cylindrical volume with a uniform potential gradient and equal diameter and height is useful in the comparison of the present detector with the resistance wire sensor. It is a type of parallel plate electrode, where the ends of the cylinder represent disc electrodes. Fringe field effects are neglected. The cutoff wavenumber for temperature and velocity for this electrode volume is estimated in Sections 13.1 and 14.1. The maximum temperature rise occurs for a path along a diameter so that the temperature uniformity ratio is

$$\frac{\overline{\Delta T}}{\Delta T_{max}} = \frac{4}{3\pi} = m_5 .$$

The characteristic numbers of the square cylinder are listed in Table 9.3 , where b is the reference dimension (b = cylinder radius).

Dipole Electrodes

The dipole electrode consists of two spheres of radius, a, whose centers are separated by a distance, 2b. The potential field and resistance of such an electrode is treated in References (5,6). An optimum ratio (a/b) exists for a given separation, 2b, at which the current density is a minimum. A single ellipsoidal electrode is considered in Reference (7).

Toroidal Type

The configuration whose electrodes coincide with the surfaces of a toroidal coordinate system is termed a "toroidal electrode." A sketch of such an electrode is shown in Figure 9.6 . The arrangement is similar to the eye-type electrode with the exception of the donut insulator. The current density is not infinitely large at the edges of this electrode. Exact expressions are available for the resistance of the general toroidal electrode (8,9,10).

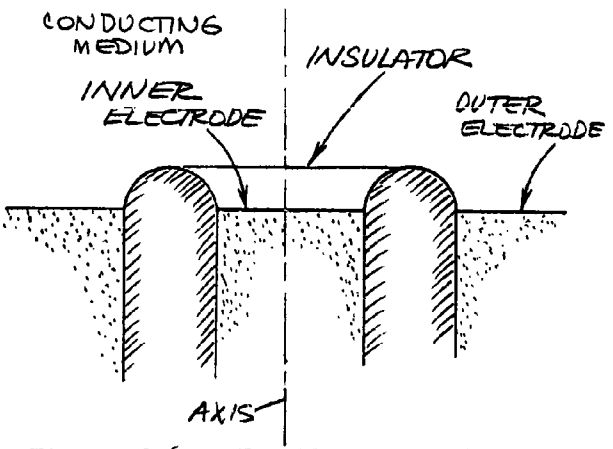

Figure 9.6 . Toroidal Electrode

Slit-Type

Two coplanar semi-infinite plates whose edges are separated by a distance, 2a, form a slit-electrode as illustrated in Figure 9.10 . The resistance between the plates is zero (logarithmically). The

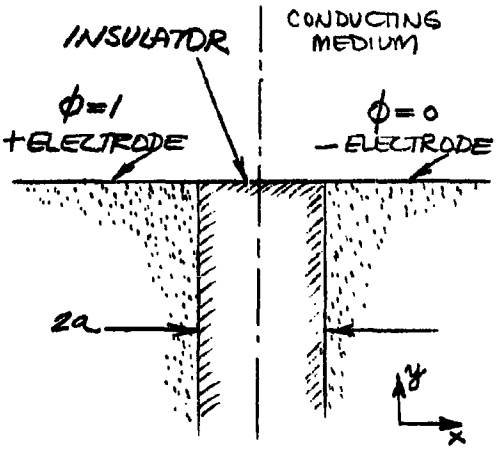

Figure 9.10. Slit-Electrode

A two-dimensional strip-type electrode of finite resistance is discussed in References (12,13).

current density becomes infinitely large at the edges of the slit. The unit potential gradient in this case is (11):

$$\frac{\partial \phi}{\partial y} = \frac{\operatorname{sgn}(x)}{\pi \sqrt{x^2 - a^2}}$$

for $|x| > a$ and $y = 0$. For $|x| < a$ and $y = 0$

$$\frac{\partial \phi}{\partial x} = \frac{-1}{\pi \sqrt{a^2 - x^2}} .$$

The potential in the gap on the surface is

$$\phi = \frac{1}{\pi} \cos^{-1}\left(\frac{x}{a}\right).$$

Disc Electrode

A special case of the eye-type electrode is the disc electrode which occurs in the limit $a \ll b$, where a is the radius of the disc. The resistance number of the disc electrode (one side only) is (14):

$$R_{\square a} = \frac{1}{4} .$$

The unit potential gradient on the surface is ($\rho < a$)

$$\frac{\partial \phi}{\partial n} = \frac{-2}{\pi \sqrt{a^2 - \rho^2}} ,$$

and for $\rho > a$

$$\frac{\partial \phi}{\partial \rho} = \frac{-2a}{\pi \rho \sqrt{\rho^2 - a^2}} ,$$

and the potential in the plane of the disc is ($\rho > a$)

$$\phi = \frac{2}{\pi} \sin^{-1}\left(\frac{a}{\rho}\right).$$

Parallel Wires

Two parallel wires of finite length make a convenient electrode for experimental purposes. The resistance between wires of finite length, ℓ, with guard insulators to reduce the potential problem to that of wires of infinite length is (15,16)

$$R\sigma\ell = \frac{1}{\pi} \cosh^{-1}\left(\frac{c}{d}\right)$$

where d is the wire diameter and c is the separation distance between the wire axes. This function is plotted in Figure 9.11 . An optimum shape factor, c/d, exists for a given separation, c, for which the (peak) current density is a minimum.

Cross-Wires

Two wires which cross at 90° and whose axes are separated by a distance larger than, but comparable to, the wire diameter is a convenient arrangement for producing an electrode with a small sensitive volume. The resistance between such wires of infinite length is finite. This arrangement is discussed in Section 5.5 .

Arc-Type

Two opposed probe shaped electrodes, as usually used to produce an arc, are also a convenient arrangement for producing a small sensitive volume. The resistance of such an arrangement is studied in Reference (17).

9.4 Polarization Impedance

The resistance of an electrode is attributable to the volume conductivity and the impedance at the surfaces of the electrodes. The surface impedance is due to polarization effects which are discussed below.

In the absence of complicating effects, the conduction of electricity in electrolyte solution obeys Ohm's Law. The chief complicating factor is polarization. This effect comes from some inhomogeneity in the electrolyte at the electrode surfaces caused by the ionic motion. For example, in some electrode processes a film of oxide or some other substance forms on the electrode surface and sets up a resistance to the passage of current across it. Other effects which cause a surface impedance are a) a difference in concentration of ions between the electrode solution interface and the bulk solution, b) a reaction occurring on deposition of ions, or c) the evolution of gases at the electrode surfaces. Polarization effects are always traceable to rate phenomena of some sort.

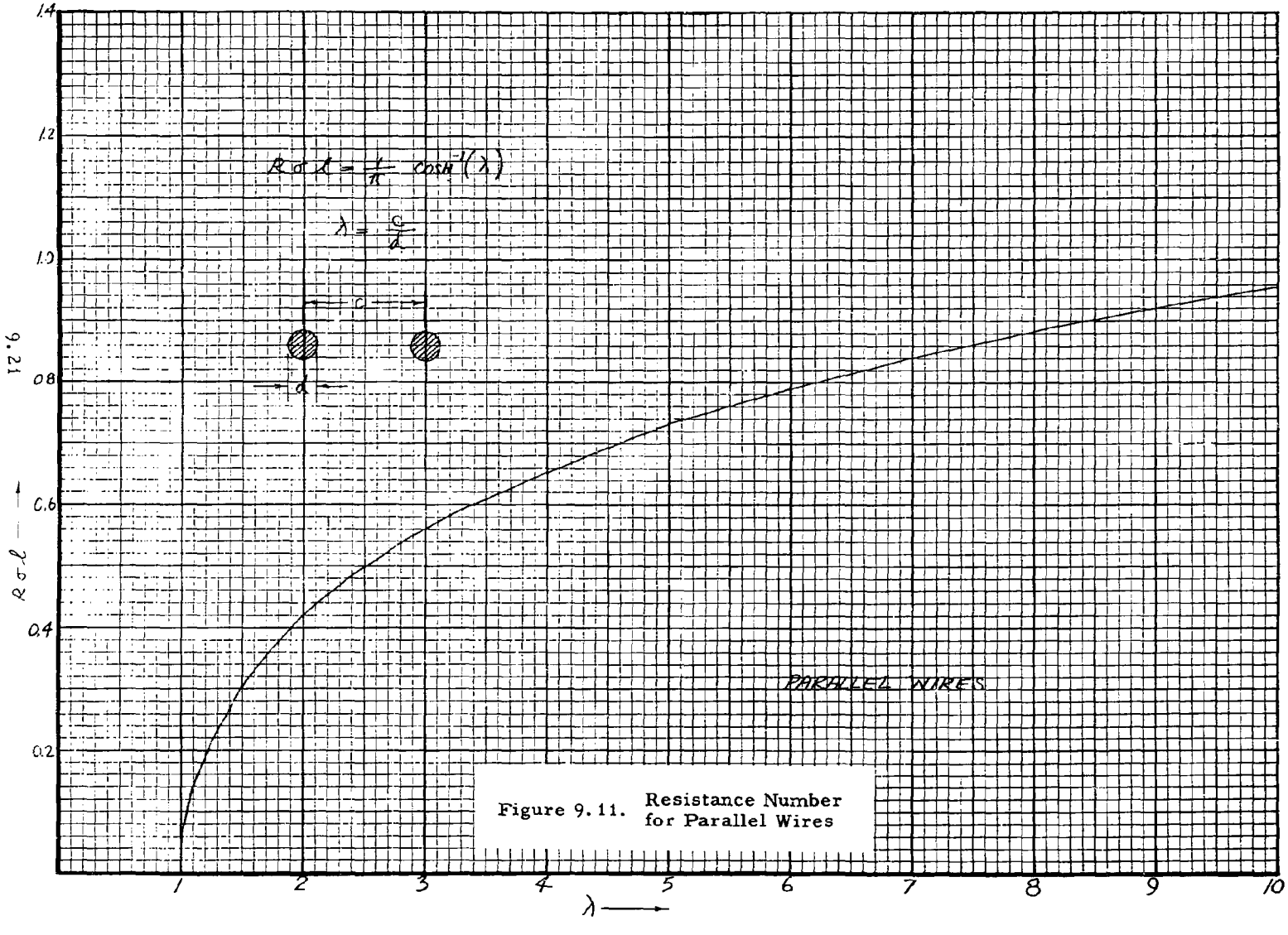

Figure 9.11. Resistance Number for Parallel Wires

These involve the slowness in diffusion of dissolved substances, slowness in establishment of subsidiary chemical equilibria and slowness in the electrochemical reactions themselves. The various contributing factors are not always sharply distinguishable.

For polarization effects which are determined by diffusion of concentration gradients, the thickness of the surface layer is estimated by means of the diffusion constant for the process. For an alternating electrode current of angular frequency, ω, the "skin depth" is of the order of

$$\frac{2D}{\omega} \quad ,$$

where D is the diffusion constant. For an electrode in sea water with a 40 kc applied voltage we have

$$D = 1.47 \times 10^{-5} \text{ cm}^2/\text{sec}$$

$$\omega = 2.5 \times 10^{5}$$

and

$$\frac{2D}{\omega} = 7.7 \times 10^{-6} \text{ cm} ,$$

which is about 200 molecular diameters. This result applies approximately to all solutions at the same frequency.

Electric Double Layer

In addition to the surface effects mentioned above, there is an atomic polarization associated with the distribution of electric charges in the immediate vicinity of the interface between the two phases. As a consequence of this charge distribution, a virtual electric double layer exists with a corresponding effective capacity per unit area.

Probably the simplest concept, of the nature of the charge distribution at an electrode solution interface is that due to Helmholtz who proposed that the site of the potential difference between two phases lay across two layers of charges of opposite sign. This Helmholtz electrical double layer structure is analogous to a parallel-plate condenser with the distance between the plates corresponding to the thickness of the double layer. The capacity, C_o, of an electrode area, A, is by this model

$$\frac{C_o}{A} = \frac{KK_o}{d} \quad ,$$

where K_o is the dielectric constant of free space (8.85×10^{-12} farad/meter),

d is the molecular distance between the plates and K is the effective dielectric constant in the interface region. As an example, in water where $K = 80$ and the molecular size of $d \approx 2 \times 10^{-8}$ cm, we find a capacity of 350 mfd/cm^2. This proves to be about two orders of magnitude larger than found by experimental measurement. Gouy advanced the theory that the solution side of the layer consisted of a diffuse layer of ions in equilibrium with the field of the electrode and thermal kinetic forces of the solution. Gouy and Chapman (18) calculated the capacity per unit area as

$$\frac{C_0}{A} = \left(\frac{F}{R_x T}\right) \cdot \left(\frac{K R_x T c}{2\pi}\right)^{1/2} = \left[\left(\frac{F^2}{R_x T}\right) \cdot \left(\frac{Kc}{2\pi}\right)\right]^{1/2},$$

where F is the Faraday constant, R_x is the gas constant, c is the concentration, and T is the absolute temperature. This expression also yields values which are too high, but because of its fundamental simplicity and because it shows the proper dependence on the concentration, it will be used for reference purposes. A constant of proportionality, λ, will absorb any discrepancies. As an example, consider sea water at 20° C (0.57 mole/liter solution of NaCl) and a dielectric constant $K = 74$, we find by the above formula $C_0/A = 580$ mfd/cm^2. Experimental results will be compared with the Gouy-Chapman formula as follows

$$\frac{C_0}{A} = \lambda \left[\left(\frac{F^2}{R_x T}\right) \cdot \left(\frac{Kc}{2\pi}\right)\right]^{1/2}$$

where λ is of the order of .01.

Electrode Reaction

The electrode polarization, aside from the electric double layer, has its origin in the factors at the surface which operate in controlling the speed of an electrode reaction, viz., the rate of the electrode process itself and the rates of diffusion of the reactant and product. Concerning the mechanism of these processes, Randles (19) has made a theoretical investigation of the current passed by an electrode at which an electrochemical reaction is in equilibrium, when it is subjected to a small alternating potential relative to the solution. Consideration of the electrode process and diffusion shows that the reaction is equivalent, electrically, to a capacity and resistance in series.

Randles' analysis shows that if the reaction at the electrode (e.g., the neutralization of positive ions by electrons at the cathode) takes place at a rate kc moles/sec/unit area, where c is the concentration of the reactants, then the effective electrical resistance and capacity of the reaction are

$$R_p = \frac{RT}{F^2AC}\left(\sqrt{\frac{2}{\omega D}} + \frac{1}{k}\right)$$

$$C_p = \frac{F^2AC}{RT}\sqrt{\frac{D}{2\omega}} \quad ,$$

where F is the Faraday constant, R the gas constant, and D the diffusion constant of the reactants. At high frequency the capacity is small and the resistance depends only on the reaction rate. At low frequency the capacity is large, and the resistance is large and independent of the reaction rate ($k \ll \sqrt{\omega D/2}$).

Electrode Impedance

The equivalent circuit of the overall electrode impedance is shown in Figure 9.12 . The volume resistance due to the conductivity of the electrolytic solution is represented by R; the capacity of the electric double layer is C_o; and we have chosen to separate the impedances calculated by Randles into one which corresponds to the resistance of the reaction rate, R_k (reaction resistance), which is independent of frequency and the other so-called "Warburg impedance," z_w. The Warburg impedance consists of a resistance and capacity of equal impedance, and which are determined by the diffusion constant of the reactants and varies inversely as $\sqrt{\omega}$ (20,21,22). The electrolysis processes are represented by the loop in parallel with the double layer capacity and the current which passes through it is termed the "Faradaic leakage" current. The reaction resistance, Warburg impedance and double layer capacity are all associated with phenomena located at the immediate surface of the electrode. The dotted parallel capacity in Figure 9.12 is the volume capacity of the solution between the electrodes and is ordinarily quite small.

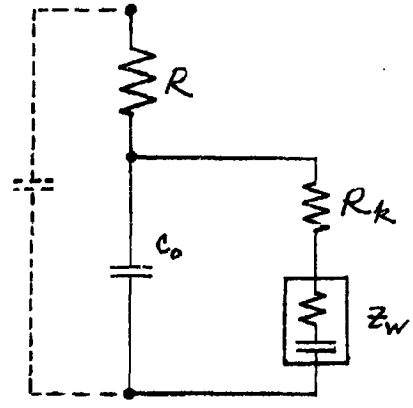

Figure 9.12 . Equivalent Circuit of Electrode Impedance

Combining the previous expressions, the components of the surface impedances are

$$C_0 = A\lambda \left[\left(\frac{K}{2\pi}\right)\left(\frac{F^2C}{RT}\right)\right]^{1/2}$$

$$R_k = \frac{1}{kA}\left(\frac{RT}{CF^2}\right)$$

$$Z_w = \frac{1}{A}\sqrt{\frac{2}{\omega D}}\left(\frac{RT}{CF^2}\right)(1-i).$$

With these formulas, we can illustrate the limiting conditions under which one has either a non-polarizable or completely polarizable electrode. The electrode surface is completely polarized if the reaction rate is zero ($k = 0$), i.e., there is no ion flux across the double layer; or if the diffusion constant is zero ($D = 0$); or if the frequency is very high ($\omega \rightarrow \infty$) where the double layer capacity effectively shunts the Faradaic impedance components. In these cases the electrode surface behaves reversibly. The electrode is non-polarizable if both the reaction rate and diffusion constant are large ($k \rightarrow \infty$, $D \rightarrow \infty$).

Electrochemistry

The electrolytic conductivity of an aqueous solution and the phenomena associated with electrode processes are fundamental topics of electrochemistry. For an understanding of these complex topics it has been found necessary to consult numerous texts to adequately cover the subject. A list of the important works are given in the References (18, 21,23-29).

9.5 Induction Probe

The problems of electrochemical effects with contact electrodes are eliminated by the use of a probe based on magnetic induction. Alternating currents are induced in the medium without making electrical contact with the medium. This "induction probe" produces a well localized sensing field and can be placed in a streamlined housing without producing "hot spots," which is not possible in the case of a contact electrode. This method is accomplished by having the electrolytic solution constitute a conducting link between a current transformer and a voltage transformer. In another arrangement the solution forms the secondary winding of a transformer whose impedance is being measured. The induction probe has been used successfully for precision electrochemical conductivity measurements (30,31,32,33), in physiological conductivity measurements (34), and in salinity measurements of sea water (35-41). The relations between the operating frequency, probe size and electrical properties are ana-

lysed below with special reference to the application of this kind of sensor to the present detection equipment. The toroidal configuration is natural to this type of sensor and will be used throughout the analysis as an example of the method (42). Some of the analysis of the electromagnetic log velocity meter (43) is pertinent to the induction probe.

Analysis

A fundamental requirement for high sensitivity resistance measurements of any electrode system is that most of the electrical energy required for the measurement be dissipated in the resistance being measured. The efficiency, η , of the measurement is defined here as the ratio of the energy dissipated in the water to total energy dissipated in the induction probe coil and water. Assume that the resistance of the water is determined by measuring the reflected impedance of the probe transformer. This situation is illustrated in Figure 9.9a and the equivalent circuit of this arrangement is shown in Figure 9.9b . The conducting path in the electrolyte

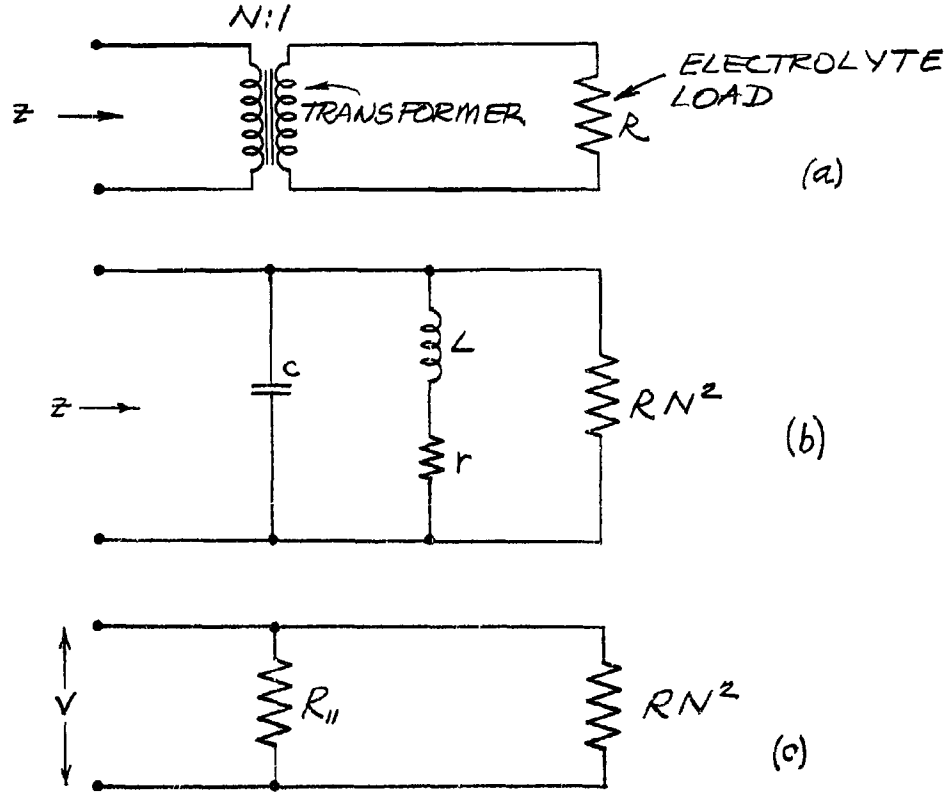

Figure 9.9 . Equivalent Circuit of Induction Probe

solution constitutes a single turn secondary winding of the transformer. The capacity in parallel with the primary is resonantly tuned to the operating frequency in order to neutralize the inductance of the transformer. The core losses and winding resistance are effectively lumped together in the resistance r in Figure 9.9b which determines the Q of the transformer. The resistance of the conducting path in the medium is R and its reflected impedance is N^2R where N is the turns ratio of the transformer. At resonance the equivalent circuit is that of Figure 9.9c where R_{11} is the parallel resonant resistance of the LC-circuit. The impedance of the transformer is a pure resistance in this case given by

$$Z = \frac{R_{11} N^2 R}{R_{11} + N^2 R}$$

where

$$R_{11} = Q\omega L = rQ^2$$

and

$$Q = \frac{\omega L}{r} \quad .$$

The efficiency, η , of the electrode is

$$\eta = \frac{(V^2/RN^2)}{\left(\frac{V^2}{RN^2}\right) + \left(\frac{V^2}{R_{11}}\right)} = \frac{1}{1 + \frac{RN^2}{R_{11}}} = \frac{1}{1+\epsilon}$$

where

$$\epsilon = \frac{RN^2}{R_{11}} \quad ,$$

and V is the input voltage to the transformer. For high efficiency, ϵ should be small ($\epsilon \ll 1$). Let the resistance of the electrolyte, R, and the inductance, L, of the toroidal transformer be given by

$$R = \frac{m}{\sigma b}$$

and

$$L = nN^2 \mu_0 b \quad ,$$

where m and n are numbers characteristic of the toroidal geometry, b is

the outer diameter of the toroid, μ is the permeability of the toroid core material, μ_0 is the permeability of free space and σ is the conductivity of the solution. Combining the above relations we obtain the following condition on the operating frequency:

$$f = \frac{m}{2\pi n \epsilon Q \mu \mu_0 \sigma b^2} .$$

This result is independent of the number of turns N. For a given efficiency and toroid proportions (ϵ,m,n fixed) the operating frequency is low if the Q, permeability (μ), conductivity (σ), and size (b) are large. Thus, a small induction electrode in tap water calls for a relatively high operating frequency. As an example, consider the following numerical example which corresponds to a commercially available toroidal core operating in sea water:

$$m = 2$$
$$n = 0.1$$
$$\epsilon = 0.4$$
$$Q = 100$$
$$\mu = 200$$
$$\mu_0 = 4\pi \times 10^{-7} \text{ henry/meter}$$
$$\sigma = 4.8 \text{ ohm}^{-1} \text{ meter}^{-1}$$
$$b = 1 \text{ cm} = 10^{-2} \text{ meters} .$$

Then

$$f = 660 \text{ kc}$$
$$\eta = 70\% .$$

For N = 100 turns we have

$$L = 2.5 \text{ mh}$$
$$C = 230 \text{ mmfd}$$
$$r = 100 \text{ ohms} .$$

The resistance r also includes core loss. The maximum power that can be transferred to the medium is determined by the saturation limit of the core.

9.6 CP-Electrode

Metal electrodes immersed in an electrolyte introduce an impedance

of their own associated with the electrode surfaces. Conventionally, this effect is minimized by greatly roughening the surface microscopically by the platinum black process, thus, providing a larger electrode area. The exact opposite of this is to make the surface a poor conductor of ionic currents by coating it with a very thin but non-conducting coat of insulating material. In this way the Faradaic currents are eliminated and electrical energy is coupled to the medium through the capacity of the insulating coat. This coating functions as a reaction rate inhibitor ($k = 0$ in Sec. 9.4) by stopping the flux of reaction components across the electrode/solution interface. An electrode with this property is termed "completely polarized," thus, the designation "CP-electrode." Some aspects of this type of electrode are discussed by Reilly (33).

An inductance coil is placed in series with the electrode leads and is tuned

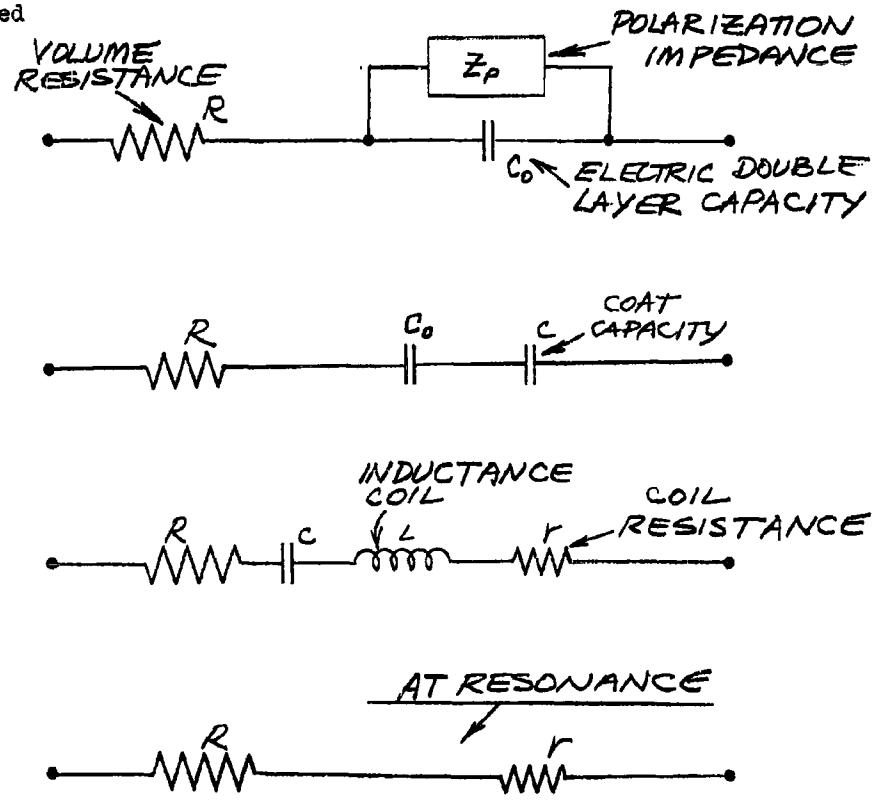

Figure 9.13 . Equivalent Circuit of CP-Electrode

to the series capacity of the coat and double layer. This eliminates the capacitive reactance leaving only the desired resistance of the conductivity cell. This is better understood by considering the sequence of diagrams shown in Figure 9.13 . The upper diagram (a) shows the equivalent circuit of a conventional electrode consisting of the primary volume resistance, R, the electric double layer capacity, C_e; and the polarization impedance, z_p, which provides the path for Faradaic leakage currents. With the addition of the thin insulating coat to the electrode surfaces, the equivalent circuit becomes that of diagram (b) in which the polarization impedance has been eliminated because of the high resistance of the coating. The inductance coil shown in diagram (c) tunes out the electrode capacities at some relatively low frequency. The small resistance, r, shown in diagram (c) is the residual resistance of the inductance coil and only the coat capacity has been drawn since it is found to be much smaller (therefore higher reactance) than the double layer capacity. Diagram (d) shows the overall equivalent circuit at resonance where the reactance of the coil exactly cancels that of the coat capacity. In this case the impedance is purely resistive, consisting of the unknown, R, and the known coil resistance, r.

As an illustration of a CP-electrode, consider an eye-type electrode coated with a thin layer of insulating material of thickness, Δ, as shown in Figure 9.14 . This coating can be made non-conducting, inert, anti-

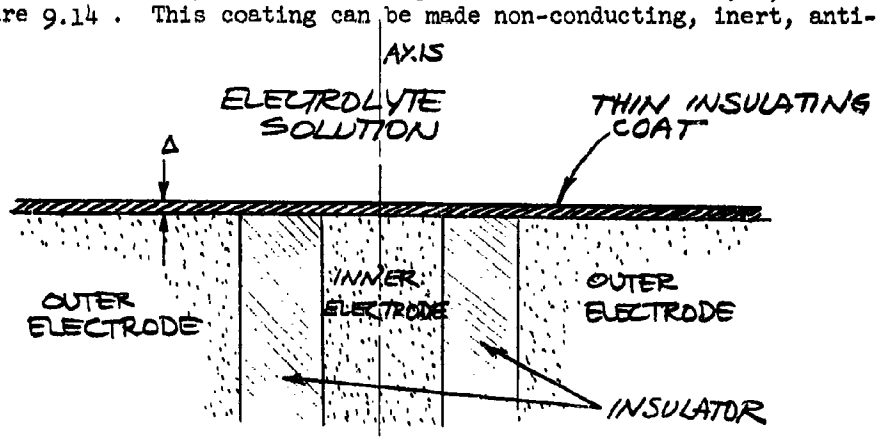

Figure 9.14 . Coated Eye-Type Electrode

corrosive, and impermeable even at thicknesses of the order of .0001 inches. An anodized surface is such an example which has found wide practical use even in hostile marine environments and where rough handling is involved.

Analysis

We now determine the relations between the operating frequency,

conductivity of the medium, electrode size and insulating coat parameters. This analysis is based on the equivalent circuit diagram of Figure 9.13 with the condition that the series inductance, L, and capacity, C, are resonant at the operating frequency, f. The figure-of-merit of the inductance coil is

$$\frac{\omega L}{r} = Q \quad ,$$

where ω is the operating angular frequency and r is the residual resistance of the inductance coil. The maximum attainable value of Q in practice is of the order of 100. The volume resistance, R, of the medium satisfies the relation

$$R\sigma b = m \quad ,$$

where σ is the conductivity of the water, m is a dimensionless number of the order of unity and b is a typical dimension of the probe, say, the outer radius. The condition for resonance of the coil and condenser is

$$\omega^2 LC = 1 \quad .$$

The capacity, C, of the insulating coating between the metal backing and conducting solution is

$$C = \frac{\kappa K_0 n b^2}{\Delta} \quad ,$$

where κ is the dielectric constant of the insulating coat, n is a dimensionless number of the order of unity which is characteristic of the probe geometry, and Δ is the thickness of the coating. Suppose that the resistance r is some factor, ϵ, times the volume resistance, R, of the electrode

$$\epsilon R = r \quad .$$

This parameter should be relatively small so that most of the input electrical power is dissipated in the water whose conductivity is being measured.

Combining the above five relations, we find the operating frequency, f:

$$f = \left(\frac{\sigma}{2\pi \kappa K_0}\right)\left(\frac{\Delta}{b}\right)\frac{1}{m n \epsilon Q} \quad .$$

Thus, once the optimum values of the quantities κ, Δ, ϵ, Q have been

determined, the operating frequency depends primarily on the electrode size, b, and the average conductivity of the water, σ.

The required inductance value, L, for the given conditions is

$$L = \left(\frac{m \epsilon Q}{\sigma}\right)^2 \frac{K K_0 n}{\Delta}$$

which is independent of the size of the electrode. The residual coil resistance is simply

$$r = \frac{\epsilon m}{\sigma b}$$

and the capacity of the insulating coat is

$$C = \frac{K K_0 n h^2}{\Delta} \quad .$$

Both of these components are independent of the frequency.

A measure of the quality of a CP-electrode is the ratio of displacement current across the capacity of the coating to the conduction current through the coating. It is only the conduction current which gives rise to the undesirable effects of the polarization impedance. The leakage conduction current through the insulating coat is through an effective resistance R_c indicated in Figure 9.15 below. The impedance, z, of the

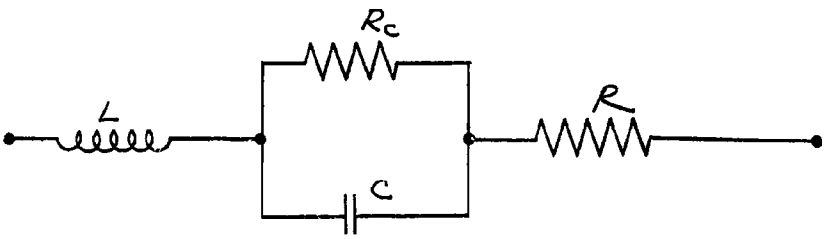

Figure 9.15 . Coat Capacity Leakage Resistance

network of Figure 9.15 is

$$z = i\omega L + R + \frac{R_c \left(\frac{1}{i\omega C}\right)}{R_c + \frac{1}{i\omega C}}$$

or

$$Z = \left(R + \frac{R_c}{1+K^2}\right) + i\left(\omega L - \frac{R_c K}{1+K^2}\right),$$

where $K = \omega C R_c = \left(\frac{R_c}{R}\right)\frac{1}{\epsilon Q}$. The inductance value is chosen so that there is no reactance component which, if $K \gg 1$, implies the resonance condition $\omega^2 LC = 1$. In this case, the impedance is purely resistive

$$Z = R\left(1 + \frac{1}{R R_c \omega^2 C^2}\right) .$$

The figure-of-merit, F_c^*, of the coating is defined as the inverse of the correction term in the above expression

$$F_c^* = R R_c \omega^2 C^2 = \left(\frac{R}{R_c}\right) K^2 .$$

The resistance R_c is given by

$$R_c = \frac{\rho_c \Delta}{nb^2} ,$$

where ρ_c is the dc resistivity of the coating. This formula may be optimistic because of the possibility of pin-holes in the coating. Dielectric loss in the coating is not pertinent in connection with reducing the effects of Faradaic currents. The figure-of-merit of the coating is

$$F_c^* = \left(\frac{\Delta}{b}\right)\frac{\rho_c \sigma}{n m \epsilon^2 Q^2} = \frac{K}{\epsilon Q}$$

and

$$K = \left(\frac{\Delta}{b}\right)\left(\frac{\rho_c \sigma}{n m \epsilon Q}\right).$$

We note the figure-of-merit increases with increasing conductivity in contrast to the figure-of-merit of ordinary conductivity cells.

The peak voltage across the film must not be high enough to cause electrical breakdown, If V is the rms voltage across R and ΔV the rms voltage across the coat, then we have approximately

$$\frac{\Delta V}{V} = \frac{1}{R\omega C} = \epsilon Q = \frac{\omega L}{R} .$$

For the case of interest with $\epsilon Q \gg 1$, the voltage across the insulated coating is much larger than the voltage applied to the volume resistance. The peak voltage across the condenser is $\sqrt{2}\ \Delta V$. If P is the power dissipated in the resistance R then the peak value of ΔV is

$$(\Delta V)_{peak} = \epsilon Q \sqrt{2PR} \quad .$$

This peak voltage should be some safety factor, say five, below the breakdown voltage of the coating determined by the dielectric strength of the insulating material. This represents a condition on the maximum allowable power input to the electrode. For precision measurements this is of no real concern because the power involved is small, but for the high power applications of this Report, this peak voltage limitation is important. If there were no recourse from this limitation (see below), then coated electrodes would, in fact, be unuseable for the high power applications involving heating at the electrode.

The peak voltage calculated above is much larger than the voltage across R because the circuit is resonant. If electrical power is coupled to the medium at a frequency, ω, well above the resonant frequency, ω_o, then

$$\frac{\Delta V}{V} = \frac{1}{R\omega C} = \left(\frac{\omega_o}{\omega}\right) \frac{1}{R\omega_o C} = \epsilon Q \left(\frac{\omega_o}{\omega}\right) \quad ,$$

where

$$\frac{1}{R\omega_o C} = \frac{\omega_o L}{R} = \epsilon Q \quad .$$

In terms of input power, we have

$$(\Delta V)_{peak} = \epsilon Q \left(\frac{\omega_o}{\omega}\right) \sqrt{2PR} \quad .$$

Thus, an effective way of coupling high power to the water without voltage breakdown is to operate at a frequency well above the resonant frequency of the CP-electrode.

The power efficiency, η, is

$$= \frac{R}{R + r} = \frac{1}{1 + \epsilon} \quad .$$

Even for ϵ as large as 0.4 the efficiency is relatively good (70 %).

The dissipation of power (resulting in a temperature rise) in the resistance r is not important if a) the temperature coefficient of r is small, b) an adequate heat sink mounting is used, and c) if the residual effect is corrected by temperature compensation networks.

The requirements of the insulating coat are that it be durable with rough usage; non-corrosive in the chemical environment; non-conducting; of high dielectric constant; easy to apply; low dielectric loss factor; low thermal conductivity; high dielectric strength; low absorption of water or be impermeable to the solution in question; not a catalyst to the chemical components of the solution; and be capable of operating satisfactorily to temperatures of 100°C; and these requirements must be met for coat thickness from 10 microinches to 1 mil. A number of practical coating materials have been developed which largely meet these requirements (44). Two important examples are teflon and the anodized surface (45,46,47,48).

The magnitudes of the quantities calculated above are illustrated for the case of sea water and tap water. The coating material is assumed to be aluminum oxide which is the main constituent of an anodized metal surface*. The assumed values and calculated parameters are listed in Table 9.4 . The electrode volume is a simple cube 1 cm on a side (b = 0.5 cm).

9.7 Electrode Measurements

Experimental measurements of the impedance of an electrode are discussed in this Section. The experimental equipment used for this purpose is described in Section 17.1 . The dependence of the electrode impedance on the following variables is considered: temperature, concentration, size, shape, frequency, age, non-linearity, electrode material, and the evolution of gas at high power.

Size

The resistance of an electrode in a conducting solution is inversely proportional to the size of the electrode configuration for a given shape. For an eye-type electrode, the resistance is given by

$$R_o \sigma b = m \quad ,$$

where R_o is the electrode (volume) resistance, σ the (volume) conductivity of the solution, b the outer radius of the electrode and m is the resistance number which is only a function of the ratio of the inner-to-outer diameters, (a/b). The approximate electrode resistance for the two important cases of sea water and tap water are shown in Figure 9.16 for an eye-type electrode of "standard" proportions: a/b = 0.48 and m = 0.46.

The impedance of a practical electrode is complicated by polarization

*...and teflon.

Table 9.4 . Numerical Values for CP-Electrode in Sea Water and Tap Water

Parameter	Sea Water	Tap Water
Insulating Material	Aluminum Oxide	Teflon
Electrode Resistance (R)	21 ohm	2100 ohm
Conductivity (σ)	.048 $ohm^{-1}cm^{-1}$	.00048 $ohm^{-1}cm^{-1}$
Coat Thickness (Δ)	.0001"	.0003"
Electrode Size (b)	0.5 cm	0.5 cm
Inductance Coil - Q	100	50
ϵ-Parameter	0.1	0.4
Dielectric Constant (κ)	8.8	2.1
Resonance Frequency (f_o)	250 kc	16 kc
Coat Capacity (C)	3100 mmfd	240 mmfd
Inductance (L)	130 μh	0.42 h
ϵQ-Parameter	10	20
n-Parameter	4.0	4.0
m-Parameter	0.5	0.5
Power Efficiency (η)	91 %	71 %
Coat Resistivity (ρ)	3×10^{14} ohm-cm	10^{17} ohm-cm
Coat Resistance (R_c)	7.5×10^{10} ohm	7.5×10^{13} ohm
K	3.7×10^{8}	2.0×10^{10}
Figure-of-Merit (F_c^*)	3.7×10^{7}	10^{9}
Voltage Safety Factor	5	5
Dielectric Strength	200 volts/mil	1000 volts/mil
Maximum Heater Voltage (ΔV_{max})	13 volts	120 volts
Maximum Heater Power (P)	1 kw	1 kw
Heater Power Frequency (f)	40 mc	5.4 mc

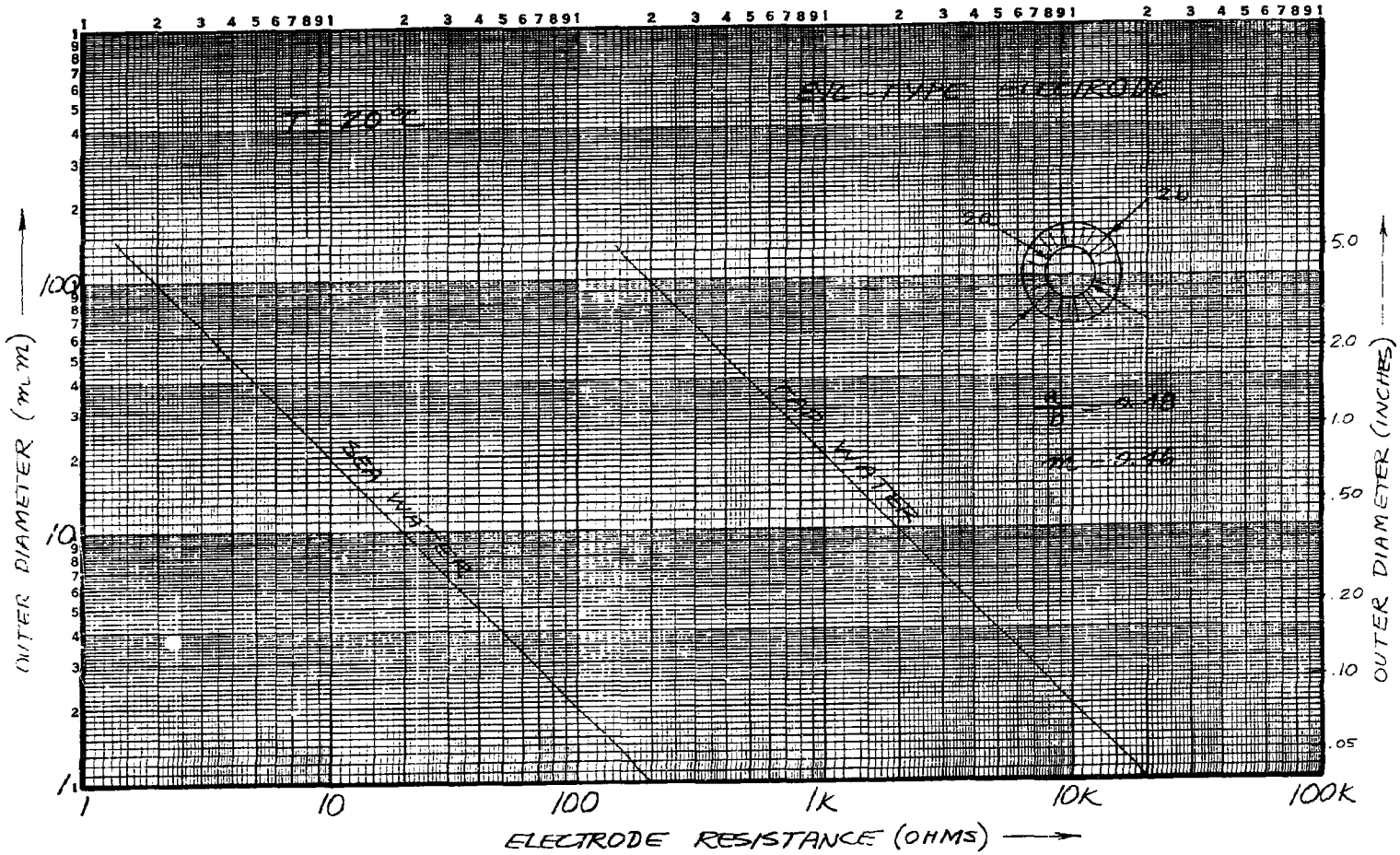

Figure 9.16. Resistance of Eye-Type Electrode

effects at the electrode surfaces. The impedance associated with the surface, which is part resistive and part reactive, varies inversely as the square of the electrode size for a given shape. The fact that the surface impedance and volume resistance depend differently on electrode size suggests a method for measuring the two independently. Jones and Christian (49) used the technique of making measurements with a cylindrical electrode volume (uniform field) of variable length. For a complex electrode field, such as that of the eye-type electrode, it is necessary to keep the relative proportion (shape) of the electrode constant and obtaining the size dependence by constructing two or more similar electrodes of different size. Two such electrodes were used in tests which were about a factor of three different in size as shown in Table 9.5 . The average diameter ratio, (2a/2b), of both electrodes is 0.474; the average size ratio is 3.00. The average values of a number of measurements on these electrodes are shown in Table 9.6 ; R is the series resistance; R_{11} the parallel resistance; C the series capacity and C_{11} the parallel capacity; and $k_{11} = \omega R_{11} C_{11}$. The relation between these quantities is

Table 9.5 . Proportions of Two Eye-Type Electrodes

Electrode	(Inches) 2a	(Inches) 2b	Ratio ↓
1	.399	.848	.471
2	.134	.281	.477
Ratio →	2.98	3.02	

$$R = R_{11}\left(\frac{1}{1+k_{11}^2}\right)$$

$$C = C_{11}\left(\frac{1+k_{11}^2}{k_{11}^2}\right)$$

and

$$kk_{11} = 1$$

$$X = \frac{1}{\omega C}$$

$$k = R\omega C \quad ,$$

The quantities actually measured are R_{11} and C_{11}, and are corrected to 20°C. The salinity of the solution is approximately 38 ‰ and a 40 kc source of low amplitude (~.05 v.) was used.

The reason for performing the measurements is to determine the surface capacity and the resistive contributions of the volume and surface. These quantities are obtained in the following way. Let the subscripts 1 and 2 refer to the two electrodes, ΔR is the resistance of the electrode surface, R_o is the volume resistance, ΔX is the surface reactance, and λ is a pure number independent of electrode size and is defined by

$$\Delta R = \lambda \Delta X \quad .$$

Table 9.6 . Impedance Measurements

Electrode	1	2
R_{11}	7.95 ohm	25.7 ohm
C_{11}	.0365 mfd	.0332 mfd
k_{11}	.0725	0.213
R	7.91 ohm	24.5 ohm
C	6.97 mfd	0.764 mfd
k	13.8	4.71
X	0.574 ohm	5.23 ohm

The quantity $-\lambda^{-1}$ is the phase factor of the surface impedance. The four measured quantities R_1, R_2, X_1, X_2 are related by

$$R_1 = R_{10} + \Delta R_1 \qquad X_1 = \Delta X_1$$

$$R_2 = R_{20} + \Delta R_2 \qquad X_2 = \Delta X_2 \ .$$

Since the volume resistances for the two electrode sizes are known to be related by

$$R_{20} = \left(\frac{b_1}{b_2}\right) R_{10} \ ,$$

we can rewrite the above equations as

$$R_1 = R_{10} + \lambda X_1$$

$$R_2 = R_{10}\left(\frac{b_1}{b_2}\right) + \lambda X_2$$

with the solutions for R_{10} and λ :

$$\lambda = \frac{R_2 - \alpha R_1}{X_2 - \alpha X_1}$$

and

$$R_{10} = \frac{R_{20}}{\alpha} = \left(\frac{X_2 R_1 - X_1 R_2}{X_2 - \alpha X_1}\right) \ ,$$

where $\alpha = (b_1/b_2)$. With the data of Table 9.6 , we obtain the constant λ which is independent of size and only sightly dependent on temperature and salinity for a given electrode shape (a/b = 0.48):

$$\lambda \approx 0.24 \ .$$

The volume resistance for the two electrodes are

$$R_{10} = 7.77 \text{ ohms}$$

$$R_{20} = 23.3 \text{ ohms} \quad .$$

A check of the fact that the surface impedance varies inversely as the square of electrode size is

$$\left(\frac{b_1}{b_2}\right)\sqrt{\frac{X_1}{X_2}} = 1.006 \quad ,$$

that is, the agreement with theory is within 1 % error.

Temperature

The electrode impedance, consisting of the volume resistance and surface resistance and capacity, are functions of temperature. Measurements of the temperature coefficients were performed by two methods, as described in Section 17.1 . Data obtained for the two different experiments are shown in Figure 9.17a and Figure 9.17b . The volume resistance, R_ρ, is calculated from the measured series resistance R and surface reactance, X, (due to the surface capacity) by the expression

$$R_\rho = R - \lambda X \quad ,$$

where $\lambda = 0.24$. The correction term λX is typically about 7 % R. The temperature coefficient of resistance at 25 °C for the data given is

$$\beta_T = -\frac{1}{R_0}\left(\frac{\partial R_\rho}{\partial T}\right) = .019 \pm .002 \text{ per } ^\circ\text{C} \quad ,$$

which agrees with the expected coefficient given in Section 7.2 (β_T = +2.02 % per °C) within the accuracy of the data. The temperature coefficient of the surface capacity as determined from the data of Figure 9.17a and 9.17b, is only a rough value because of the rather serious scatter of the data points due to hysterysis temperature effects at the electrode surface. The temperature coefficient of surface capacity of Figure 9.17b is +0.4 % per °C and for Figure 9.17a +2.0 % per °C. This is only one illustration of the erratic and confusing behavior of the surface capacity which is a sensitive function of the nature of the electrolyte solution and electrode surface condition and well as other variables. The temperature coefficients of the surface impedances found by Jones and Christian (49) is of this same order of magnitude (+1 % per °C) for dif-

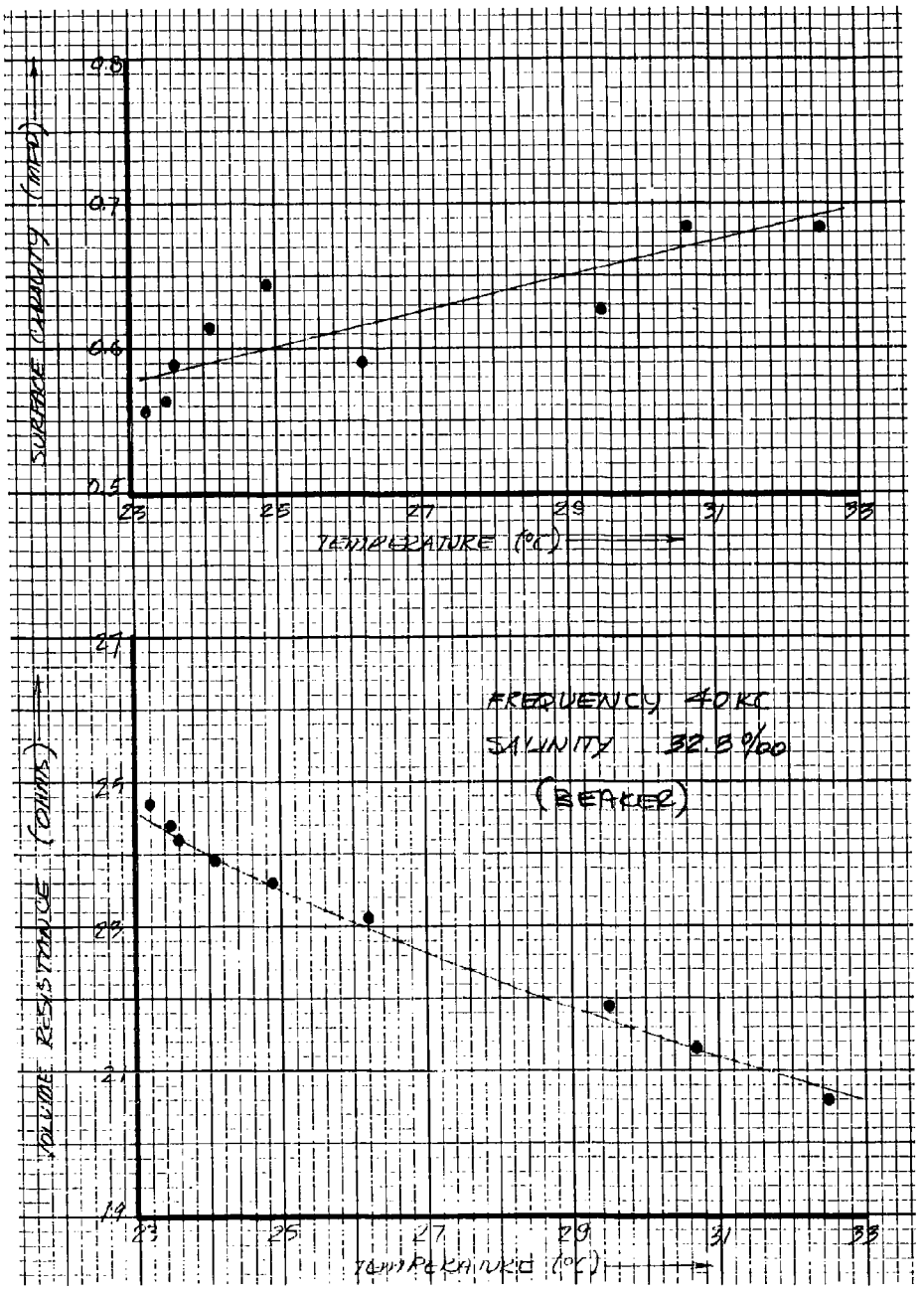

Figure 9.17a. Temperature Dependance of Electrode Resistance and Capacity

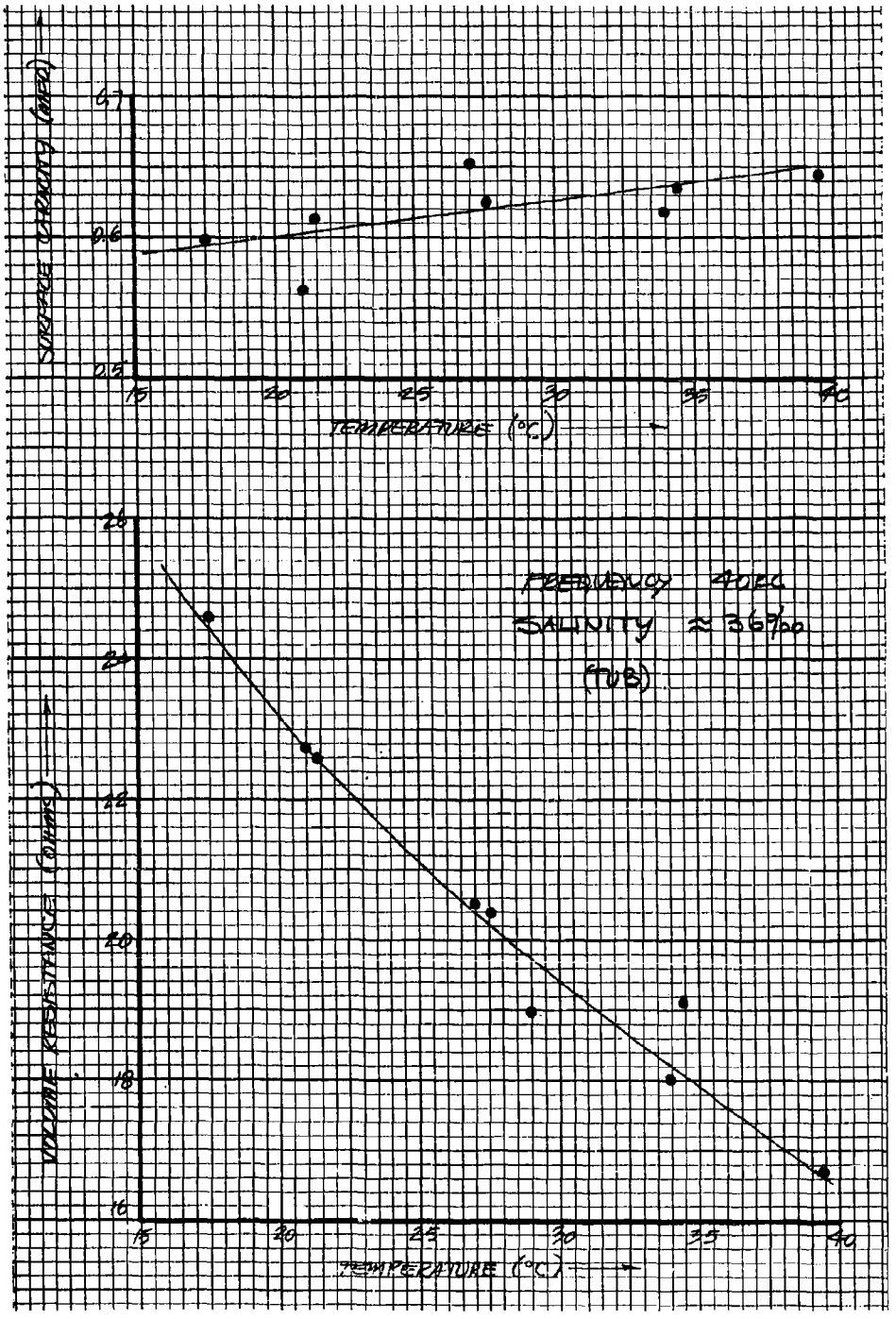

Figure 9.17b. Temperature Dependance of Electrode Resistance and Capacity

ferent solutions and electrode materials.

Concentration

The variation of total series electrode resistance and series capacity with concentration (salinity) of NaCl solution for an eye-type electrode is shown in Figure 9.18 . The series capacity is due to the surface impedance exclusively, but the series resistance includes both the volumes and surface contributions. A stainless steel eye-type electrode was used (a/b = 0.48) and the measurements were performed at 40 kc and 23 °C. The measured salinity coefficients of resistance and capacity at a salinity of 32.8 ‰ (corresponding to standard sea water) are

$$\frac{1}{C}\left(\frac{\partial C}{\partial S}\right) = \frac{+0.49}{32.8\ ‰} = +1.50\ \%\ \text{per}\ ‰ \ .$$

$$\frac{1}{R}\left(\frac{\partial R}{\partial S}\right) = \frac{-0.80}{32.8\ ‰} = -2.45\ \%\ \text{per}\ ‰ \ .$$

The salinity coefficient of resistance agrees with that expected from the known data for NaCl solutions (Sec. 7.2). The variation of resistance over the range from 1 ‰ to 100 ‰ is almost inversely proportional to the salinity; the difference being accounted for by the variation of equivalent conductance with the concentration. The variation of surface capacity with salinity (or concentration, c) agrees with that for the electric double-layer capacity:

$$\frac{C}{\pi a^2} = \lambda\left[\left(\frac{F^2}{RT}\right)\left(\frac{Kc}{2\pi}\right)\right]^{1/2} \sim \sqrt{c} \ ,$$

where the expression on the right is the capacity per unit area expected from the Gouy-Chapman theory of the electric double-layer capacity (Sec. 9.4). The measured exponent of the concentration dependence is +0.49 which agrees with the above expression. At a salinity of 32.8 ‰ (c = 0.57 mole/liter) corresponding to standard sea water:

$$\left[\left(\frac{F^2}{RT}\right)\cdot\left(\frac{Kc}{2\pi}\right)\right]^{1/2} = 580\ \text{mfd/cm}^2 ,$$

and for the electrode area of (a = 0.170 cm)

$$\pi a^2 = .091\ \text{cm}^2 \ ,$$

the measured value of C = 0.35 mfd yields

$$C/\pi a^2 = 3.8\ \text{mfd/cm}^2$$

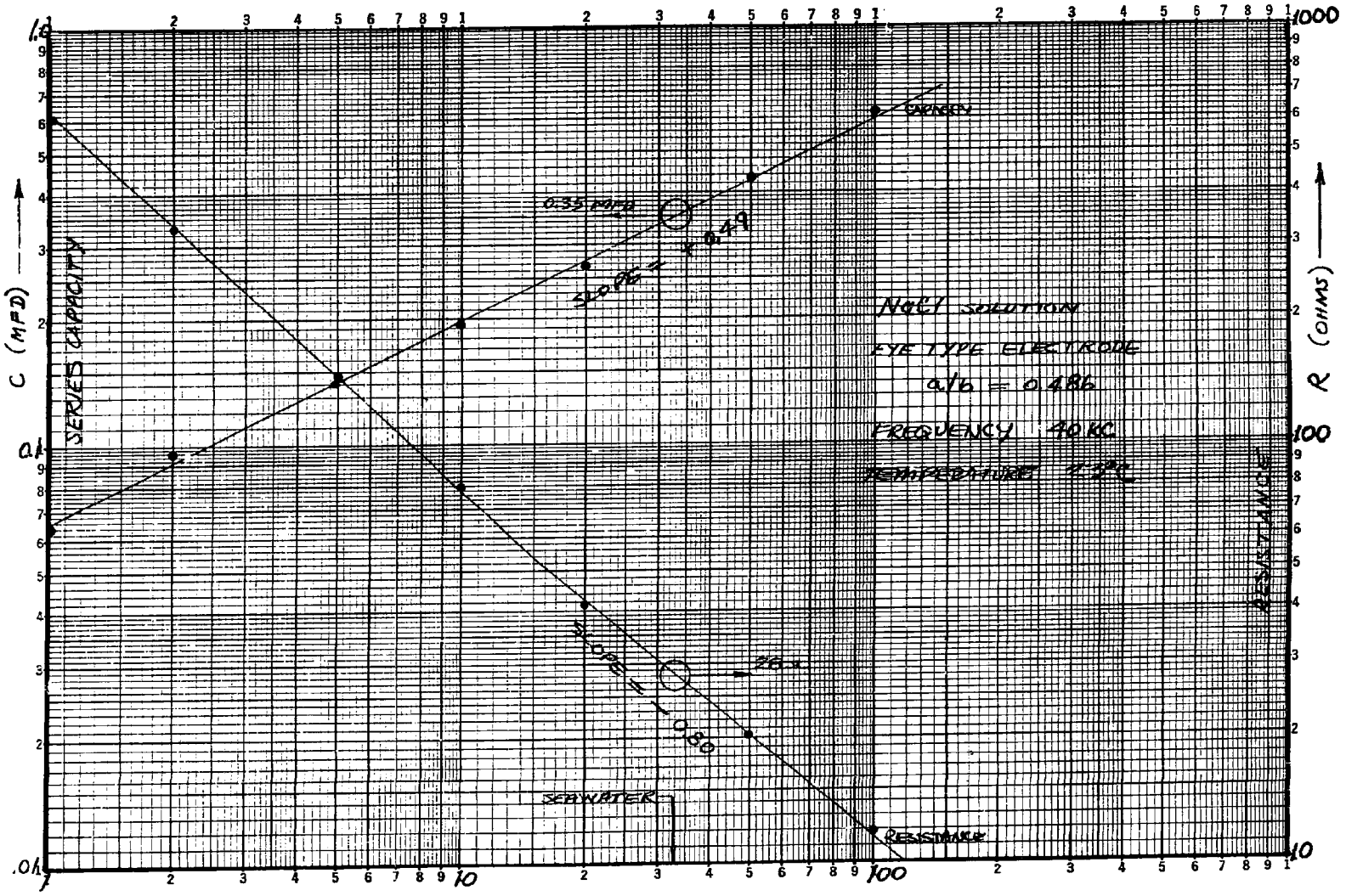

Figure 9.18. Concentration Dependance of Electrode Resistance and Capacity

or

$$\lambda = .0066 \quad .$$

Shape

The variation of electrical properties with the relative proportions (shape) of the eye-type electrode is measured with the equipment described in Section 17.1 which consists of ten eye-type electrodes with the same outer radius b but different inner radius (a). Table 9.7 lists the dimensions of each electrode. The outer diameter of all electrodes is 1.27 cm (0.500"). The impedance measurements were performed at 40 kc in NaCl solution of 32.8 ‰ salinity, and a conductivity $\sigma = .0479$ ohm^{-1}cm^{-1}. The electrodes were made of stainless steel and the data was taken at 20.8 °C and corrected to 20 °C. Table 9.8 lists the measured quantities (R_{11} and C_{11}) and derived electrical properties for each electrode. The volume resistance, R_o, is calculated from the formula

$$R_o = R - \frac{\lambda}{\omega C} \quad ,$$

where it is assumed that $\lambda = 0.24$ approximately for all (a/b). The volume resistance, R_o, and surface capacity are also shown in Figure 9.19 . In order to compare the observed properties with theory, the capacity per unit area, $C/\pi a^2$, is plotted in Figure 9.20 and the resistance number, $R_o\sigma a$, in Figure 9.21. The theoretical curve of $R_o\sigma a = (a/b)m$ from Section 9.2 is also plotted in Figure 9.21 and agrees with the observed data within experimental error. For a "standard" eye-type electrode with $(a/b) \approx 0.48$, we find

Table 9.7 . Proportions of Eye-Type Electrodes

Electrode No.	(a/b)	a (cm)	πa^2 (cm^2)
1	0.105	.067	0.014
2	0.198	.126	0.050
3	0.299	.190	0.113
4	0.399	.254	0.203
5	0.500	.318	0.318
6	0.599	.380	0.453
7	0.700	.444	0.620
8	0.800	.508	0.810
9	0.900	.634	1.261

$$m(0.48) = R_o\sigma b \approx 0.215 \times (0.48)^{-1} = 0.45 \quad .$$

A theoretical expression for the capacity per unit area for the eye-type electrode has not been developed. For the particular electrodes of this experiment the following figure is approximately valid

$$C/\pi a^2 \approx 8 \text{ mfd/cm}^2 \quad .$$

This parameter is sensitive to the properties of the solution and condition of the electrode surfaces.

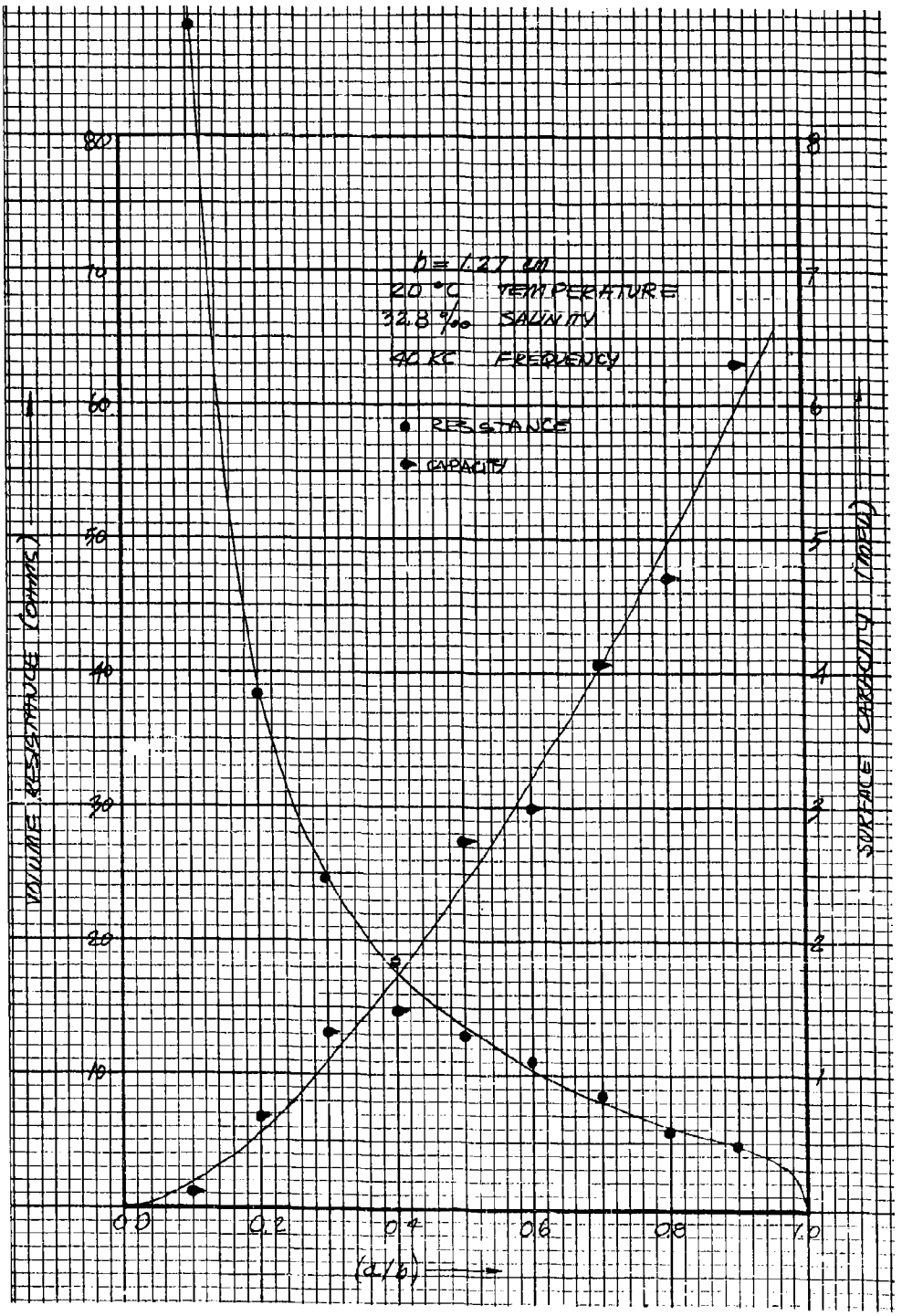

Figure 9.19. Volume Resistance and Surface Capacity as a Function of Shape Factor

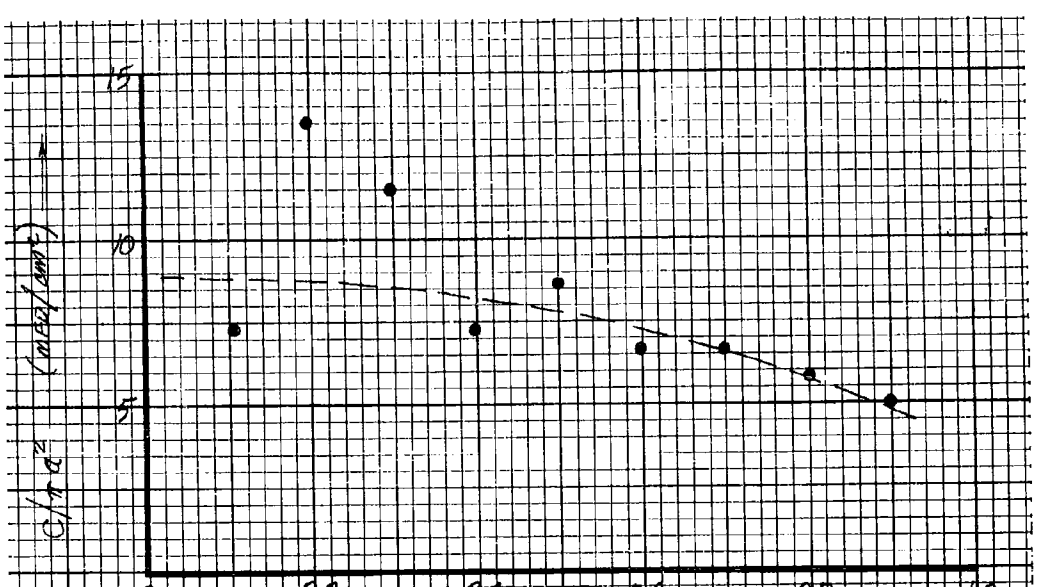

Figure 9.20. Capacity Per Unit Area Versus Shape Factor

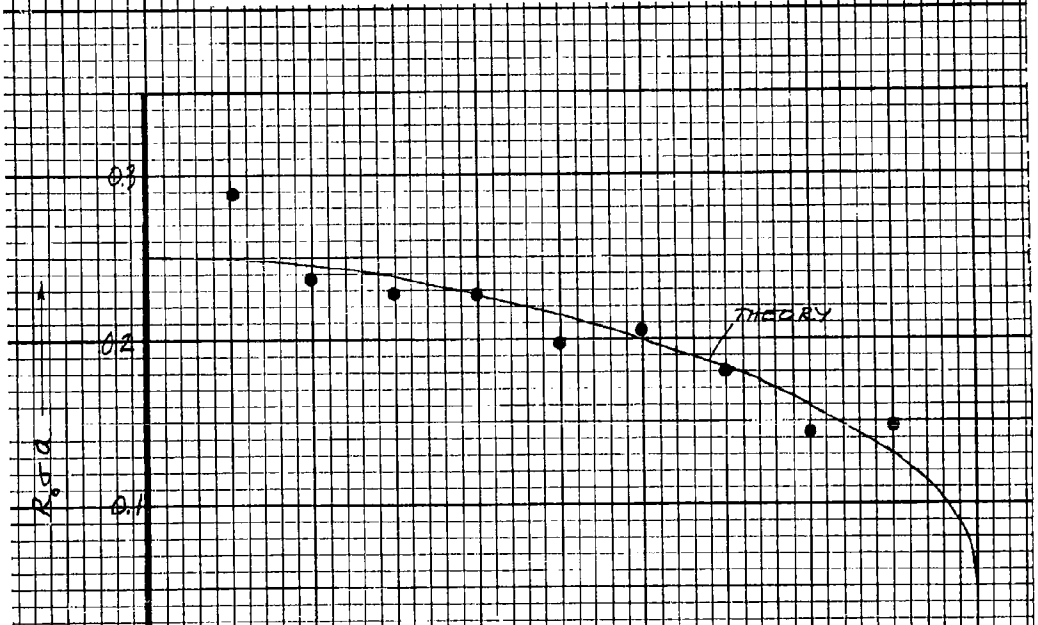

Figure 9.21. Resistance Number Versus Shape Factor

Table 9.8 . Impedance Measurements vs. Shape Factor

Electrode No.	R_{11}(ohm)	C_{11}(mfd)	k_{11}	R(ohm)	C(mfd)	R_p(ohm)	$C/\pi a^2$ (mfd/cm^2)
1	113	.0140	0.398	97.6	0.102	89.6	7.28
2	40.6	.0146	0.149	39.8	0.673	39.0	13.5
3	25.7	.0188	0.121	25.3	1.30	25.0	11.5
4	19.4	.0296	0.144	19.0	1.46	18.6	7.22
5	13.3	.0330	0.111	13.2	2.73	13.0	8.60
6	11.4	.0415	0.119	11.3	2.99	11.2	6.61
7	8.65	.053	0.115	8.55	4.06	8.46	6.56
8	6.7	.077	0.129	6.60	4.70	5.85	5.80
9	5.0	.103	0.129	4.93	6.30	4.86	5.00

Frequency

The resistance of an electrode due to the volume conductivity of sea water is known to be independent of frequency over a very wide range of frequency extending from dc to radar frequencies. This is not the case for the surface impedance, however, since the Warburg impedance (Sec. 9.4) is a function of frequency. The electric double-layer capacity and reaction resistance are supposedly independent of frequency. The surface impedance is in series with the volume resistance; at very high frequencies the volume dielectric constant gives rise to a capacity in parallel with the volume resistance. As a result of these effects the total electrode series resistance, R, and capacity, C, or parallel resistance, R_{11}, and capacity, C_{11}, are functions of frequency. Ordinarily the frequency dependence of electrolytic cells for electrochemical measurements is determined by several point measurements in the region from 1 kc to 10 kc. The frequency dependence in such cells can be kept quite small by proper cell design which makes the volume resistance large in comparison to surface impedance. This is not possible with the present electrodes since the size of the electrode is fixed by other considerations. Thus, at high concentrations (e.g., sea water) the volume resistance is not large in comparison with the surface impedance. This is particularly true if smooth stainless steel or brass surfaces are used instead of the more desirable platinum black surfaces. For this reason the frequency dependence of the eye-type electrodes is relatively large and is measurable over a wide range of frequency.

The total series resistance, R, and reactance, X, of the brass eye-type electrode of Figure 9.36 is shown in Figure 9.22 as a function of frequency

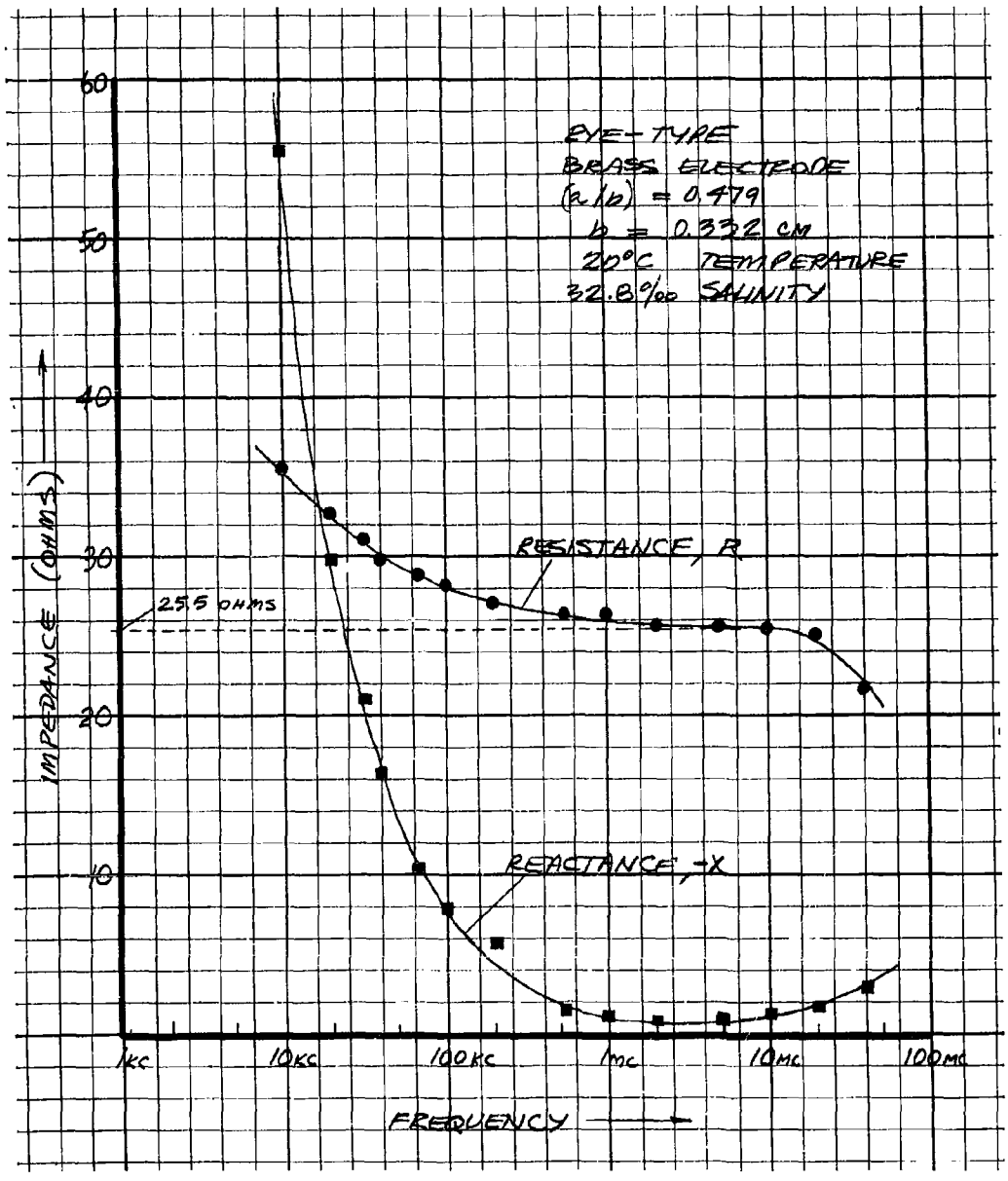

Figure 9.22. Electrode Impedance as a Function of Frequency

from 10 kc to 40 mc. The temperature and salinity of the NaCl solution is 20 °C and 32.8 ‰. The resistance does not become independent of frequency until the range from 1 mc - 10 mc are reached where, presumably, the resistance is due almost exclusively to the volume conductivity of the solution. This limiting resistance is 25.5 ohms from which the resistance number, m, of the electrode can be calculated:

$$R_o \sigma b = m = 25.5 \times .0479 \times 0.332 = 0.41 \quad ,$$

where $\sigma = .0479$ ohm^{-1}cm^{-1} is the conductivity of the 32.8 ‰ NaCl solution and $b = 0.332$ cm is the outer radius of the eye-type electrode. This value of resistance number for $(a/b) \approx 0.48$ is lower than the theoretical value (0.459) and the value measured previously by another method. This may be partly due to the drop in resistance which is noticeable in Figure 9.22 for frequency greater than 10 mc. This effect can be formally explained by a capacity in parallel with the volume resistance. Such a capacity is constituted by the volume dielectric constant of the water, however, it is too small to explain the observed effect. If C_o is the volume capacity, it is related to R_o by

$$R_o C_o = \frac{K K_o}{\sigma} \quad ,$$

where K (=74) is the dielectric constant of the sea water; and K_o (=8.85 x 10^{-12} farad/meter) is the permittivity of free space. Combining this with the previous relation, we obtain

$$C_o = \frac{K K_o b}{m} = 4.7 \text{ mmfd} \quad .$$

The parallel capacity necessary to explain the effect of Figure 9.22 above 10 mc is found to be about 120 mmfd which is considerably larger than the volume capacity expected. The explanation of this effect is not known. Other measurements to higher frequencies from 50 mc to 400 mc were made to confirm the observed effect. A further reduction in series resistance and an increase in series reactance was found, though at a somewhat slower rate than indicated in Figure 9.22 . The origin of the observed effect may be in an electrochemical effect at the electrode surface, or in the capacity and inductance of the leads to the electrode proper.

For frequencies below about 3 mc, the observed reactance is due exclusively to the series capacity associated with the electrode surface. Other measurements indicate that this capacity is largely that of the electric double-layer and as such should be independent of frequency. The series capacity of the electrode is shown in Figure 9.23 and is found to be only somewhat frequency dependent below 3 mc. It is again concluded, therefore, that the series capacity is mostly due to the electric double-layer. The contribution of the Warburg and reaction resistance is, however, not negligible

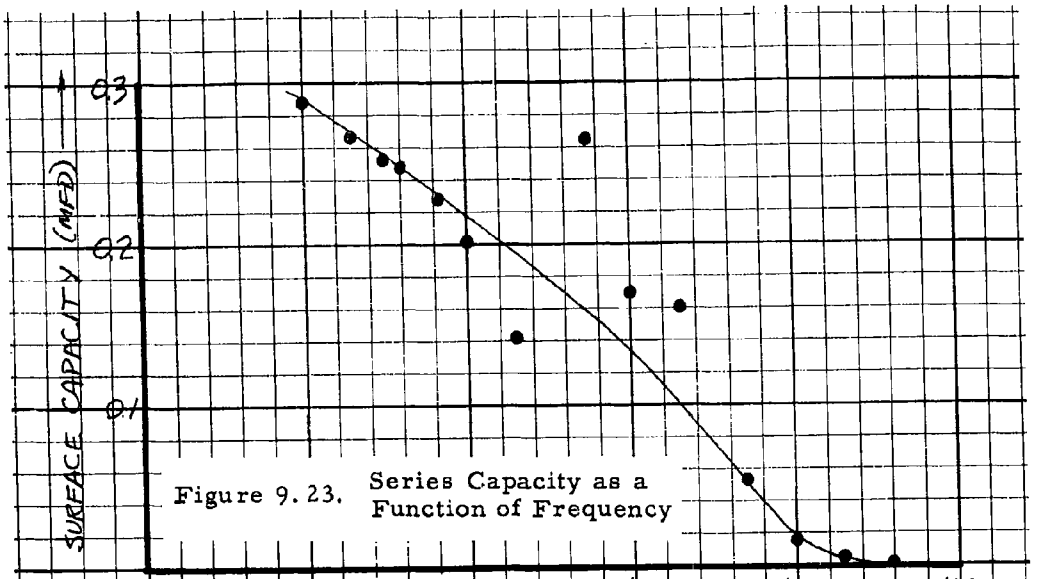

Figure 9.23. Series Capacity as a Function of Frequency

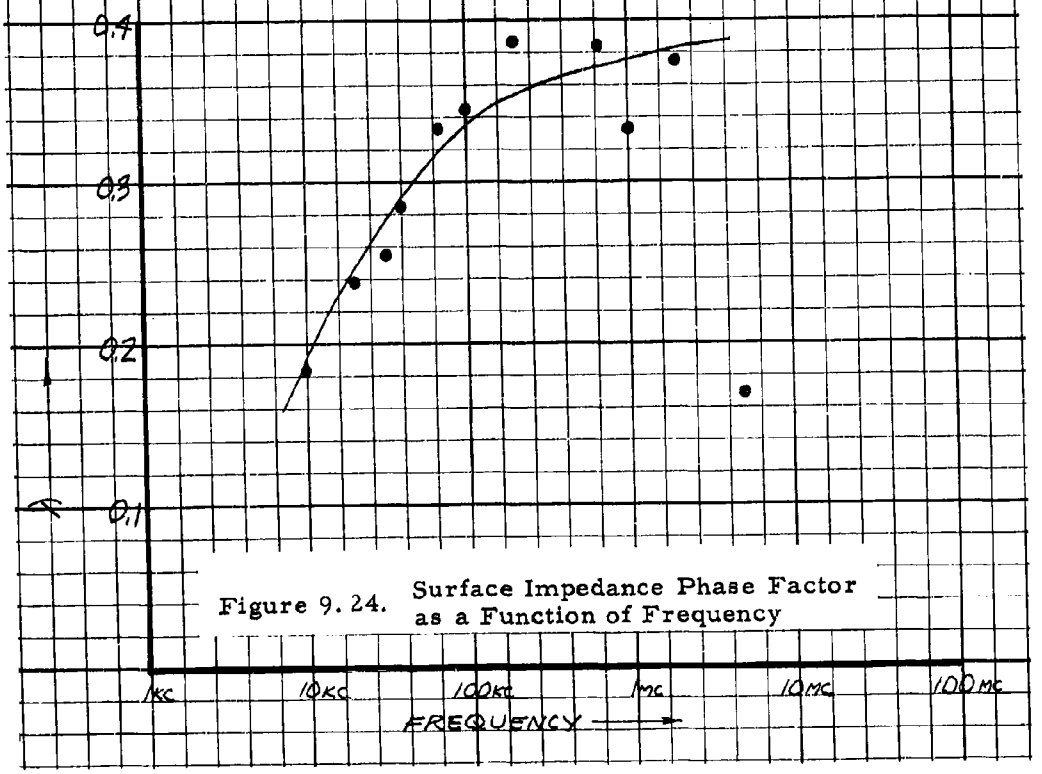

Figure 9.24. Surface Impedance Phase Factor as a Function of Frequency

in its effect on the total series resistance as shown in Figure 9.22 where at frequency below 3 mc, the resistance R increases with decreasing frequency. Measurements on a stainless steel eye-type electrode have been performed down to 1 kc. Both the resistance and reactance continue to rise sharply as indicated in Figure 9.22 , although the series capacity is found to be larger (lower reactance) for stainless steel than for the brass electrode. If ΔR is the series resistance due to the surface

$$R = R_0 + \Delta R \quad ,$$

and $\Delta X \equiv X$ is the surface reactance, the ratio

$$\lambda = \frac{\Delta R}{\Delta X}$$

can be calculated from the observed data as shown in Figure 9.24 . The variation of λ with frequency is not large and at 40 kc the value is approximately

$$\lambda \approx 0.28 \quad ,$$

which compares fairly well with the value $\lambda = 0.24$ obtained for a stainless steel electrode at 40 kc by the method of measuring the size dependence.

The data of Figure 9.22 is pertinent to the choice of the operating frequency of detection equipment using such electrodes. Ideally, one would want to measure only the volume resistance without any contribution from the surface impedance. It is clear that even at 40 kc, which was used in the detection equipment, the contribution of the surface impedance is by no means negligible. At 40 kc, the following data applies:

$$\lambda = 0.28$$
$$-X = 16.3 \text{ ohm}$$
$$R = 30.0 \text{ ohm}$$
$$\Delta R = 4.6 \text{ ohm}$$

and

$$\tan \phi = \frac{-X}{R} = -0.54$$
$$\phi = -28^\circ$$

and

$$Z = (R^2 + X^2)^{1/2} = R(1.29) = 38.8 \text{ ohms} \quad .$$

In this case, about 15 % of the power to the electrode is dissipated in the surface resistance:

$$\left(\frac{\Delta R}{R}\right) = \frac{4.6}{30.0} = 0.153 \quad .$$

The optimum frequency for operation appears to be at about 3 mc where the electrode reactance is a minimum. This fact was decisive in the choice of the high power heater source used to heat the water in the detection equipment for velocity measurements; a frequency of 3.7 mc was finally decided upon.

Age

If all experimental variables are held constant and measurements of electrode resistance and capacity are made as a function of time, it is found that the measured quantities vary with time. This is termed the "aging effect." The variation is largest immediately after cleaning the surface of the electrode or immediately after immersing it in a solution. The capacity variations are largest, amounting to about 100 % change within a day; the resistance variation amounts to about 2 % change over the same time interval. All things being equal, the variation of impedance shows a regular behavior with time; both capacity and resistance vary logarithmically with time.

This effect was determined experimentally by thoroughly cleaning six standard eye-type stainless steel electrodes with No. 600A Wet-O-Dry emery paper. The resulting surface was bright and smooth with the exception of the very fine mesh of random scratches caused by sanding. The appearance of the surface was unchanged under visual inspection at the end of the experiment when removed from the solution. Care was taken to see that while immersed no bubles or other contaminants formed on the electrode surface. The resulting data is shown in Figure 9.25 . The measurements began a few minutes after cleaning and were continued almost two days at which time the rate of change had become small and difficult to measure with reliability. Only the curve of best fit to the many data points is included in this Figure in the interest of clarity. The six straight lines of negative slope correspond to the measured capacity of the six electrodes and the lines of positive slope to the corresponding resistances. These lines show similar behavior for resistance and capacity, respectively, but differences in slope between electrodes is observed.

The observed changes with time can be expressed by the following formulas which take the time t = 100 minutes as a convenient reference value:

$$C(t) - C(100) = A \log\left(\frac{t}{100}\right) C(100)$$

$$R(t) - R(100) = B \log\left(\frac{t}{100}\right) R(100)$$

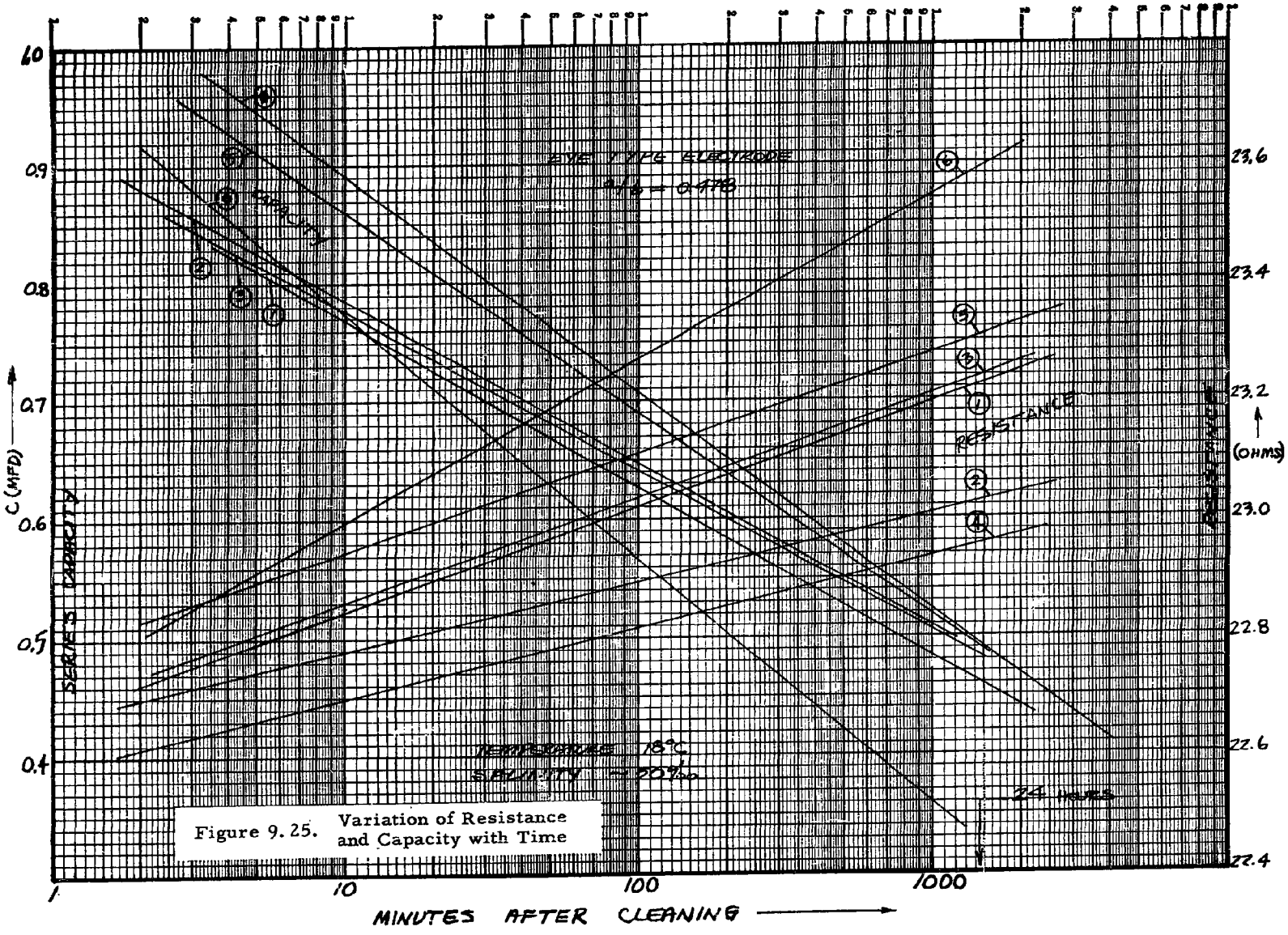

Figure 9.25. Variation of Resistance and Capacity with Time

where C is the series capacity and R the series resistance, and the average values of the constants for the six electrodes are

$$A = -0.26$$
$$B = +.0078$$
$$C(100) = 0.65 \text{ mfd}$$
$$R(100) = 23.0 \text{ ohms} \quad .$$

These formulas indicate rapid changes in the impedance values as $t \rightarrow 0$, which is precisely what is observed; the changes take place so fast in the first minute after cleaning that it is somewhat difficult to make the measurements fast enough to track the changes due to the aging effect. These tests were performed at 18 °C and 50 ‰NaCl salinity, however, similar behavior has been observed with these and other electrodes at other temperatures and salinities.

Non-Linearity

The impedance of an electrode is dependent on the applied voltage, i.e. it is a non-linear element. This effect is measurable even below the point where the current density is high enough to cause gas evolution, where, of course, a marked change in resistance and capacity is experienced. Two methods are used to measure the non-linearity, a) the direct measurement of the impedance as a function of applied voltage or, b) an indirect method based on the deviation from balance conditions of a non-linear bridge as the input voltage is varied. The theory of this method is developed briefly below.

Assume a wheatstone bridge measurement in which all arms are approximately equal to the resistance being measured, R(0). For simplicity we assume a purely resistive measurement. This arrangement is shown in Figure 9.26 , where the error voltage output from the bridge is ΔV, V is the voltage across the load being measured, and 2V is the voltage applied to the bridge. The wheatstone bridge resistances are

$$R_3 = R_4 = R(0) \quad \text{and} \quad R_2 \approx R(V) \approx R(0) \quad ,$$

where R(0) is the resistance of the load at zero voltage. The load resistance, R(V), is assumed to be only slightly non-linear. For an equilateral bridge we have the approximate relation

$$\left(\frac{\Delta V}{2V}\right) = \frac{1}{4}\left[\frac{R(V) - R(V_0)}{R(0)}\right] \quad ,$$

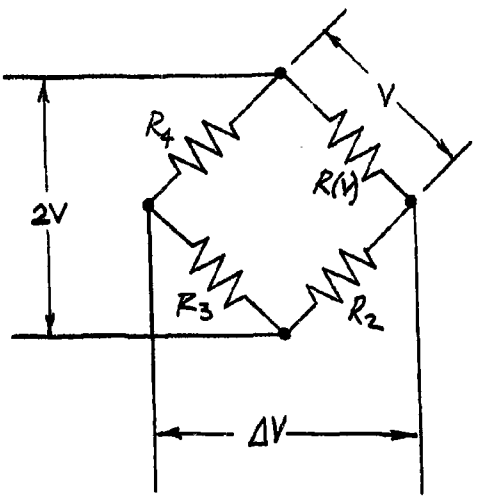

Figure 9.26 . Non-Linear Wheatstone Bridge

where the bridge is adjusted to balance ($\Delta V = 0$) at $V_o = V$. The load resistance is assumed to be a linear function of voltage:

$$R(V) = R(0) + k\,R(0)\,V$$

where

$$k = \frac{1}{R(0)}\left(\frac{\partial R}{\partial V}\right)$$

is the voltage coefficient of resistance. Combining these relations we find

$$\Delta V = \frac{k}{2} V (V_o - V)$$

or

$$\left(\frac{\Delta V}{V_o}\right) = \frac{k V_o}{2} \left(\frac{V}{V_o}\right)\left(1 - \frac{V}{V_o}\right).$$

The curve is shown in dimensionless form in Figure 9.27 . In measurements of rms voltages, only the magnitude of the output voltage is measured, so that the sign of k must be determined independently. The bridge output is maximum at $V = V_o/2$ where

$$8\left(\frac{\Delta V_\Lambda}{V_o}\right) = kV_o \quad ,$$

which provides a convenient way to measure voltage coefficients. The main virtue of this technique is that the accurate measurement of the actual impedance values is not necessary. The measurement of ΔV depends on the gain, G, of the bridge detection equipment.

In actual measurements the bridge is never brought to precise balance at $V = V_o$ because of noise voltages in the detection system or, because of imperfect settings of both the resistive and reactive components necessary to balance the bridge. As a consequence, added to the above parabolic curve, is a linear term as shown by the dotted line of Figure 9.28 .

Measurements of this type were performed on the standard eye-type electrode in 33.2 ‰NaCl water at 40 kc. The data is plotted in Figure 9.28 . Similar data was obtained at V_o = 0.1, 0.2, 0.5 and 2.0 volts, from which the voltage coefficient was calculated as shown in Figure 9.29 . At low voltages (less than 1 volt) a coefficient of about 0.75 % per volt is found.

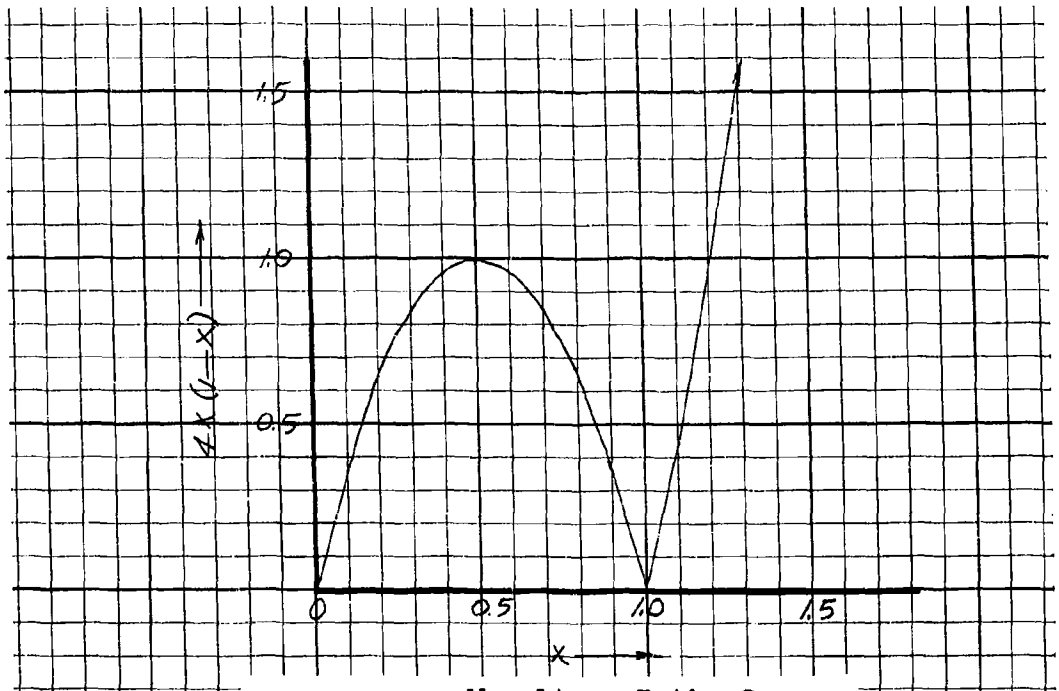

Figure 9. 27. Non-Linear Bridge Output Versus Input Function

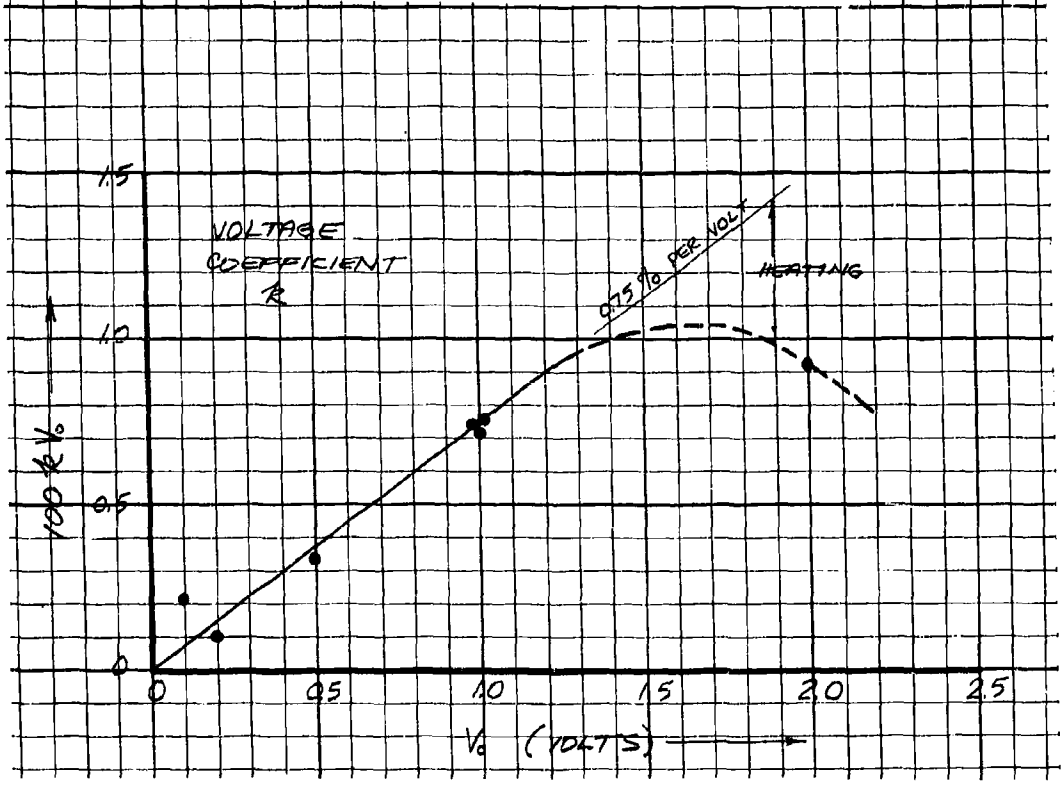

Figure 9.29. Voltage Coefficient of Electrode Resistance

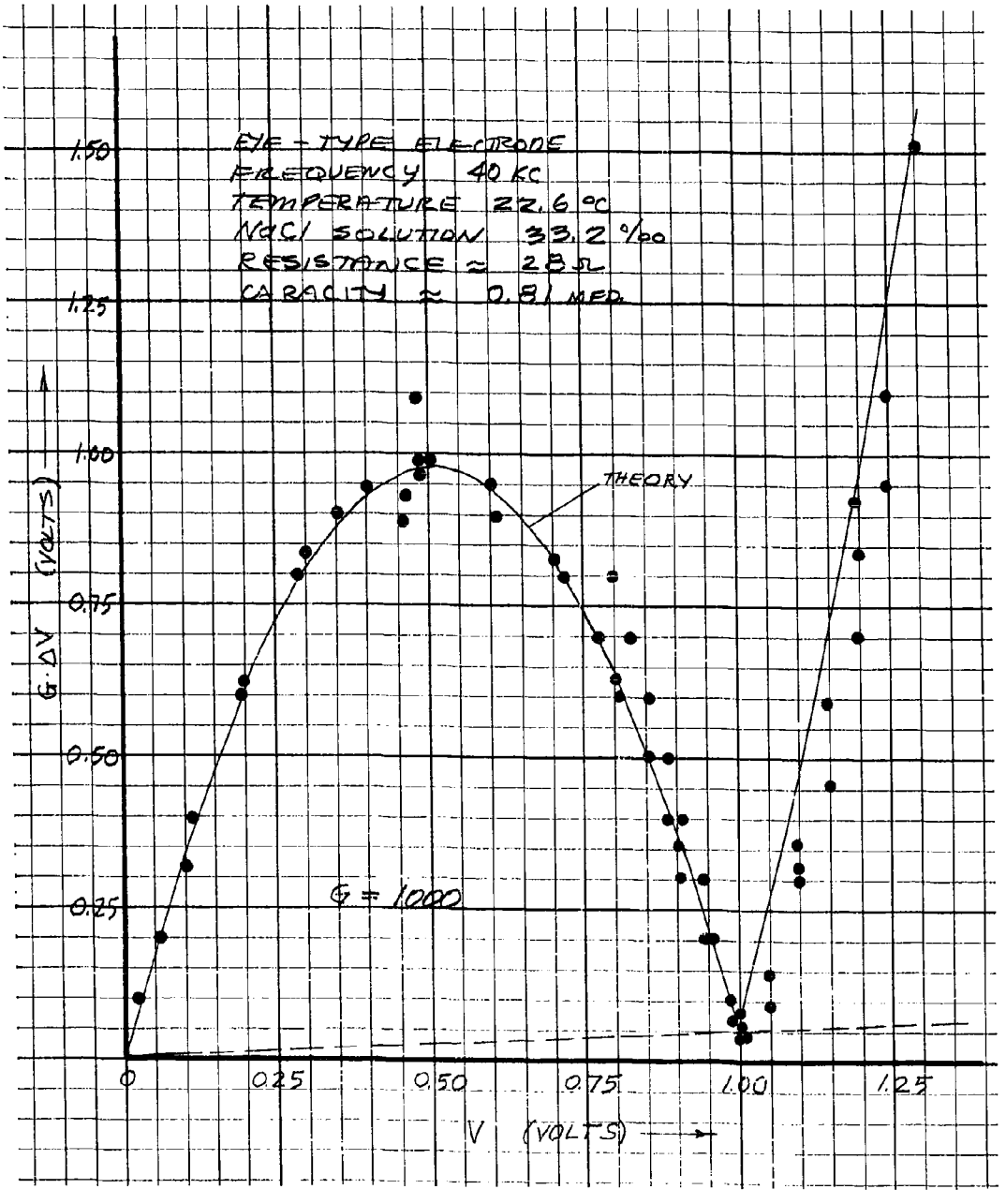

Figure 9.28. Non-Linear Bridge Output Versus Input Measurements

This is about 25 times as large as that of usual composition type resistors. Above 1 volt a marked deviation is observed which it is believed is due to heating in the electrode volume, or a higher order non-linear contribution.

Direct measurements of resistance and capacity of the electrode shows that the series capacity increases markedly with increasing voltage. The voltage coefficient of capacity amounts to +30 % per volt at 5 kc and falls to +3 % per volt at 40 kc. Above a certain critical voltage, which varies from 0.6 volt at 1 kc to 3 volts at 40 kc, where electrolysis effects become important, the capacity makes a large and erratic jump. The resistance of the electrode is found to decrease with increasing voltage. The coefficient, k, is about-1 % per volt which is in accord with the above measurement technique. Above the voltage where electrolysis effects are important, the resistance also shows an erratic change as found with the series capacity.

Gas Evolution

The evolution of gases at an electrode due to electrolysis effects for dc currents is a well known phenomenon. For alternating currents the electrolysis process is limited by reaction rate effects and the effect of ionic diffusion. Generally, one would expect the evolution of gas products to decrease as the frequency increases because of the tendency of the reactions to more closely approximate a reversible process (52).

The evolution of gas at the electrode surfaces is due to electrolysis and boiling or out-gassing of the water if the electrical heating of the water is sufficient. The observation of these processes is complicated by the fact that part of the gas may be reabsorbed in the water making the bubbling less profound. Visual observation is, of course, the simplest method and for this reason was used in spite of the limitations it holds for the interpretation of the data. Another more sensitive method of observing the inception of electrolysis effects or other non-linear processes is to measure the rectified dc current produced for a given applied ac current. This technique proves more sensitive than the visual technique, although the observed rectified voltages are relatively small (.01 % of applied voltage). The rectified current behaves the following way: no rectified current is measured until a certain critical applied voltage is reached (of the order of 1 volt depending on frequency) when the rectified current suddenly jumps to a definite but small value which was more or less independent of further increases in applied voltage. The "jump" was used as an indication of the inception of appreciable electrolysis effect.

The critical potential (rms) at which gas evolution is detected is shown in Figure 9.30 as a function of frequency. The data for the eye-type electrode (30 ohm at 40 kc) as measured by the two techniques shows a similar behavior, but the visual method is less sensitive than the rectifier method. We will rely more on the rectifier method since it is the first to

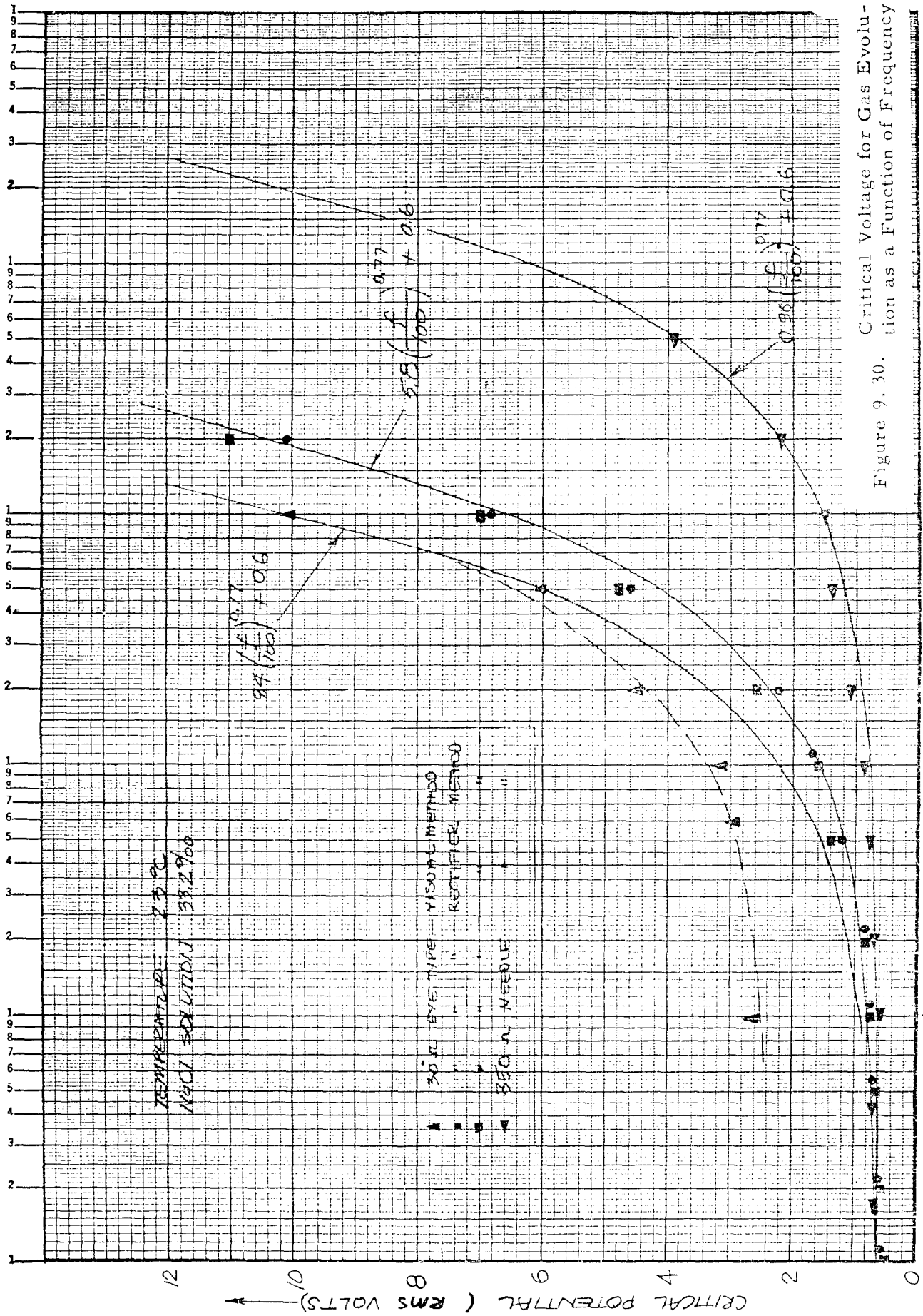

Figure 9.30. Critical Voltage for Gas Evolution as a Function of Frequency

indicate the presence of gas evolution effects. As expected, a higher applied voltage is required to cause electrolysis at higher frequency. The curve to the far right is for a needle type electrode (350 ohm at 40 kc) of much smaller dimensions than the eye-type electrode. It requires less voltage to cause electrolysis on this electrode at a given frequency due to the higher current density. The data points of Figure 9.30 can be expressed in the form

$$V_c - V_o = A V_o \left(\frac{f}{100}\right)^{0.77} \cdot \left(\frac{d}{1}\right)^{0.77} ,$$

where V_c is the critical applied potential at the inception of gas evolution, V_o is the critical voltage at low frequency, the frequency f is expressed in kilocycle (kc) units, A is a dimensionless constant, and d is the effective diameter of the electrode in centimeters. The values of the constants obtained from the data of Figure 9.30 are

$$V_o = 0.6 \text{ volts}$$

$$A = 13.2 ,$$

where the diameter ratio between the 30 ohm eye-type electrode and the 350 ohm needle electrode is 10.5.

The above empirical relation sets an upper limit to the power that can be usefully dissipated at an electrode in a static solution without adverse effects of gas evolution. This relation must be taken into consideration in the design of a high power electrode. The critical electrode power, P_c, at which gas evolution is detectable in static water is

$$P_c = \frac{V_c^2}{R} = \sigma h V_c^2$$

where R is the electrode resistance, and h the typical dimension of the electrode (actually, the inverse cell constant). We wish to plot specific data based on this expression, but must first determine whether this critical value depends on the conductivity of the water solution.

The measurement of the critical voltage as a function of salinity was determined by the simpler visual method. The resulting data is shown in Figure 9.31 . These measurements were performed only on the 30 ohm eye-type stainless steel electrode at 40 kc. The current density is plotted as a function of salinity and is a slowly varying function of salinity. The critical current density, J_c, in amps/cm^2, fits the formula

$$J_c = 3.2 \left(\frac{S}{10}\right)^{0.22} ,$$

where S is the salinity in ‰. The critical current density for sea water

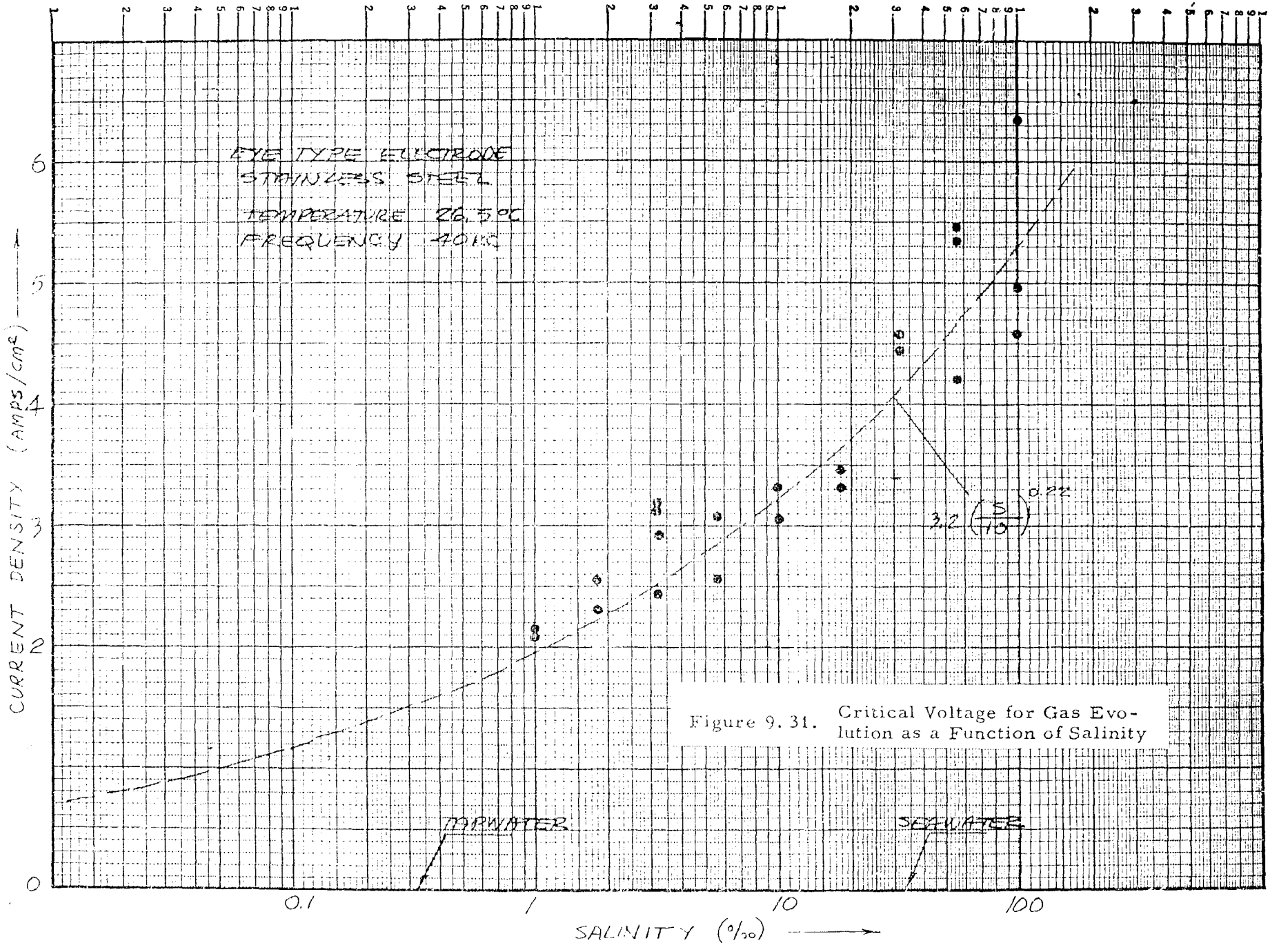

Figure 9.31. Critical Voltage for Gas Evolution as a Function of Salinity

and tap water are

$$\text{Sea water:} \quad J_c = 4.2 \text{ amp/cm}^2 \quad \text{at } S = 33 \text{ ‰}$$

$$\text{Tap water:} \quad J_c = 1.5 \text{ amp/cm}^2 \quad \text{at } S = 0.33 \text{ ‰} .$$

The above experimental data is combined to give the maximum applied electrode power which can usefully be used as a function of frequency for the cases of the 30 ohm eye-type electrode (6.6 mm diameter) and 350 ohm needle electrode (0.63 mm diameter) in static tap water and sea water. The resulting curves are shown in Figure 9.32 .

Electrode Material

Certain electrode materials are more suitable for use in a given solution than others (50,51). Experiments have been performed with electrodes of the following materials: platinum, stainless steel, gold plate, brass and copper. Quantitative measures of the relative merits of these materials have not been made, but it was found that the platinum electrodes are superior to all others. This is particularly true at high electrode power. Stainless steel electrodes are satisfactory at lower voltages. Brass and copper electrodes proved to be subject to corrosion or tarnishing. Combinations of electrode materials such as copper and stainless steel are not satisfactory because of their instability.

9.8 Design and Construction

The details of the design and construction of electrodes used in experimental work are discussed in this Section. The conductivity cells of the present work have been made, not only with the conventional considerations in mind, but also the requirement of compatibility with the hydrodynamic flow conditions at the electrodes. Two classes of electrode types are considered: the flush type and probe type. The metal of the electrodes is an important factor in its behavior in a given electrolyte solution. Platinum is the preferred material but, because of the expense and lack of availability, only wire stock has been used to form electrode arrangements. Stainless steel has been used mostly for electrodes because of its availability and resistance to corrosion. Epoxy resin is the most used insulating material although hysol, teflon, and formvar have also been exploited.

The design and construction of conventional conductivity cells is reviewed briefly below.

Conventional Cells

Electrolytic conductivity cells of conventional design are made either

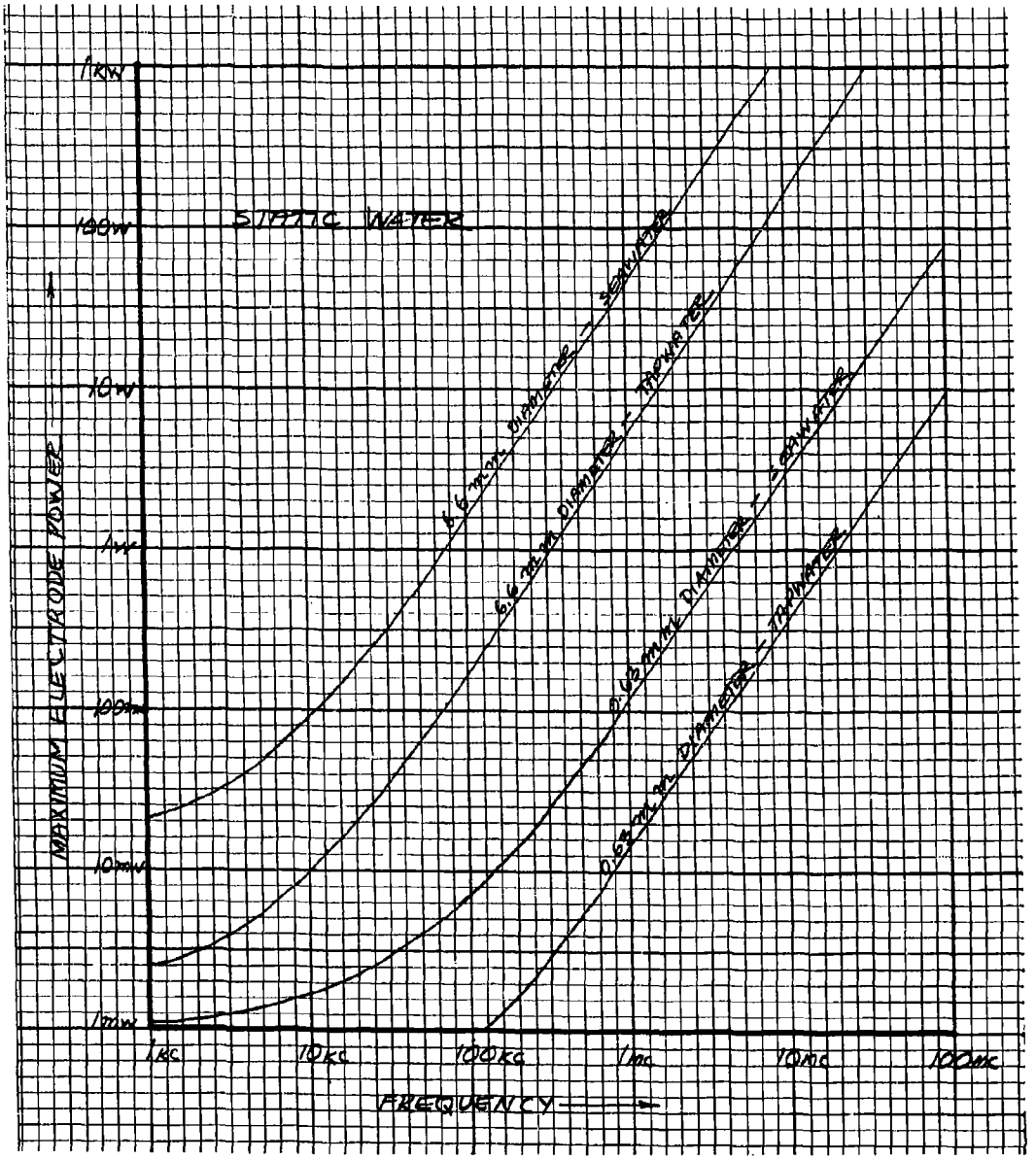

Figure 9.32. Maximum Electrode Power Without Gas Evolution in Static Water as a Function

for precision measurements in which a fixed sample volume is measured or for measurements to monitor chemical processes.

For precision measurements of resistance with alternating current the cell resistance should not be too high because of errors due to stray capacities, nor too low because of residual lead resistance. A convenient resistance is about 1000 ohms. An example of a convenient cell design is given in Reference (59). Conductivity cell proportions are chosen so that for a given solution conductivity the cell resistance is of this order. This is not possible for the present detection equipment since both the size and conductivity are specified. The impedance of the solution due to the volume conductivity is a pure resistance at frequencies less than the radio frequency range. In practice several other effects give rise to reactive components which introduce errors in the resistance measurements. The simplest example of this is the capacity between the cell leads and the small capacity in parallel with the cell, with the solution as the dielectric. Another of these is the "Parker effect" associated with capacitive coupling between the cell leads and the solution (53). Surface impedance effects can be minimized by a method due to Kohlrausch in which the electrodes are coated with platinum black. The platinizing solution recommended by Jones and Bollinger (54) is 0.025N hydrochloric acid containing 0.3 percent of platinic chloride and 0.025 percent of lead acetate; the lead acetate improves the adherence of the deposit. The platinizing current should be 10 ma/cm^2, the polarity being reversed every ten seconds. Even a barely visible deposit greatly reduces the frequency dependence (due to the reactance of the effects at the electrode surface) and a deposit corresponding to a few $coulombs/cm^2$ is ample. The electrode effects are largest at high concentration, and is strongly dependent on the nature of the surface material and electrolyte solution. Double cell compensation techniques are effective in minimizing the errors due to both temperature and surface effects (55,56). Also, two independent leads to each electrode may be used so that lead resistances can be completely eliminated by the "four leads" method used in resistance-wire thermometry. A modification of the four leads method also makes possible accurate dc measurements without serious surface impedance problems (57,58).

Flush Type Electrodes

The flush type electrode presents a locally flat surface for the fluid flow. In addition it should be rugged, electrically well shielded, possess a localized field, and not be exposed to impact, as it would be if placed on a leading edge of the detector head. Several examples of this type of electrode have been constructed and are described below.

Hydrofoil Electrode - the first electrode constructed with hydrodynamic considerations in mind is shown in Figure 9.33 . Four No. 14 gauge platinum wires are placed in the leading edge of a hydrofoil shaped head made of Epocast epoxy resin. The arrangement consists of two conductivity cells placed in close proximity for differential spacial measurements. The

(b)

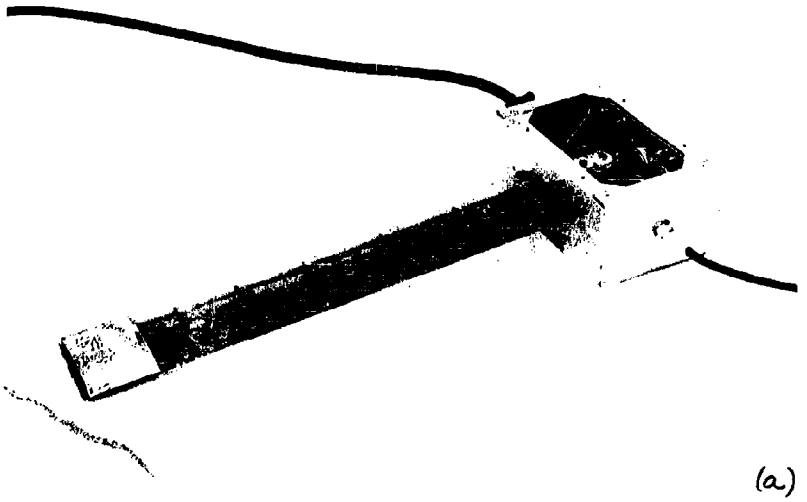

(a)

Figure 9.33 . Hydrofoil Electrode

spacing between centers of a pair of wires is 1/8 inch and between the centers of each pair is 3/8 inch. The full angle of the leading edge is about 80°.

The lessons learned from this construction are the following. It is undesirable to place the electrodes at a sharp leading edge since they are particularly subject to damage in ordinary handling. The electrodes are not in a well shielded arrangement and it was necessary to add a large area copper plate below the electrodes to provide an adequate localized ground connection. Also the construction technique for this type is unsatisfactory, particularly because the whole detection head is cast of epoxy resin. It is obvious that the tolerances of construction were poor so that the electrode pairs are geometrically dissimilar.

10 Ohm Wedge Electrode - the second flush type electrode constructed embodies the lessons learned from the hydrofoil electrode. This stainless steel electrode is shown in Figure 2.5 . The resistance of this electrode in sea water at 40 kc is about 10 ohms. The wedge angle is 36°, the length in the direction of flow of the wedge face is 3.2 inches, the height of the leading edge is 5.0 inches, the outer and inner electrode diameters are 0.86 inches and 0.41 inches, respectively, and the corresponding inner/outer diameter ratio is 0.476. Identical electrodes are placed in the same position on each of the wedge faces. The currents flow from the central electrode to the main stock which is a common ground for both electrodes. The central electrodes are mounted in position by an epoxy resin cast. This is found to be poor practice; the electrode should be mounted mechanically by some means before the insulating epoxy resin is cast.

30 Ohm Wedge Electrode - a larger stainless steel detector head is shown in Figure 9.34 with six electrodes, three on each side of the wedge faces. These electrodes are used in pairs for differential measurements; variations in spacing are obtained by choosing various combinations of electrodes. The wedge angle is 36°, the length of the wedge face is 6.37 inches, the height of the leading edge is 12.0 inches, the outer and inner electrode diameters are .279 inches (.709 cm) and .123 inches (.340 cm), respectively, and the inner/outer diameter ratio is 0.480. The main stock is a common ground for all six electrodes. In construction, the central electrodes were positioned by a press fit insert and then cast into position by Epocast epoxy resin. The flush electrode surface was obtained by grinding. The leads to the electrodes are brought through drill holes in the back of the wedge block.

30 Ohm Dipping Electrodes - a convenient dipping electrode for laboratory work is shown in Figure 9.35 . The length and diameter of the stainless steel cylindrical body are 6.0 inches and 1.25 inches, the outer and inner electrode diameters are .281 inches (.714 cm) and .136 inches (.317 cm), and the inner/outer diameter ratio is 0.484. The diameter of the cylinder is sufficiently large to insure that the electrode closely approximates

Figure 9.34 . 30 Ohm Wedge Electrode

Figure 9.35 . Dipping Electrode

the eye-type electrode in an infinite plane. The electrical connection to the BNC connector is made through the hole at the end of the cylinder.

Brass Electrode - a brass electrode constructed for laboratory use at radio frequencies is shown in Figure 9.36 . The electrode proper is located in close proximity to the type-N RF connector which facilitated the measurements at very high frequency. The attached glass container, which is attached with beeswax, holds the electrolyte solution in the vertical position. The sensitive volume of the electrode is well contained within the solution volume. The diameter of the brass ground plate is 4.0 inches, the outer and inner diameter of the electrodes are .261 inches (.663 cm) and .125 inches (.317 cm), respectively, and the diameter ratio is 0.478. The brass center electrode is cast in epoxy resin.

Probe Type

The small size and streamlined shape is of primary concern in the design of the probe-type electrodes described below.

No. 21 Hypodermic Needle - a convenient design for a probe-type electrode consists of a hypodermic needle with an insulated coaxial center wire, the sensitive volume is located at the tip. This design is relatively rugged, the center wire is electrically shielded by the needle tube, and the tip is readily streamlined. Such a probe was constructed with a No. 21 gauge (.0318 inch diameter) stainless steel hypodermic needle with .016 inch diameter stainless steel center wire. This probe is shown in Figure 9.37 . One of the problems of construction was application of the insulating coat to the center wire. If a wire is simply dipped in a lacquer solution and brought out, beads of lacquer form on the wire instead of a uniform coat. It is found that by removing the wire very slowly from the coating solution, this beading phenomenon does not take place. taper on a coated wire is obtained by light sanding, in this condition it may be firmly pulled into the needle tube in order to fix into position. The streamlined tip is easily shaped by means of a slowly revolving sanding table with fine wet sandpaper. The tip is shaped by varying the angle of contact of the needle with the sandpaper while simultaneously spinning the needle between thumb and forefinger. The center wire should be tested electrically for self-continuity and isolation from the needle tube. If the tip is damaged in use it is easily reshaped by the above sanding process. The probe impedance in sea water at 40 kc is about 350 ohms.

Platinum Wire Probe - a probe well suited to high power operation was constructed using two parallel 0.0126 inch diameter platinum wires (No. 28) of 1.7 mm length and separated by 0.7 mm. A close-up of the end of this probe is shown in Figure 17.21 . A problem developed with this electrode because of small cavities in the front of the stem where stagnant water was easily heated to boiling temperature, thus, producing noise. The stem of this probe is not strong enough for relatively long lengths (say, 30 diameters) to withstand vibration when exposed to turbulent flow. The probe impedance

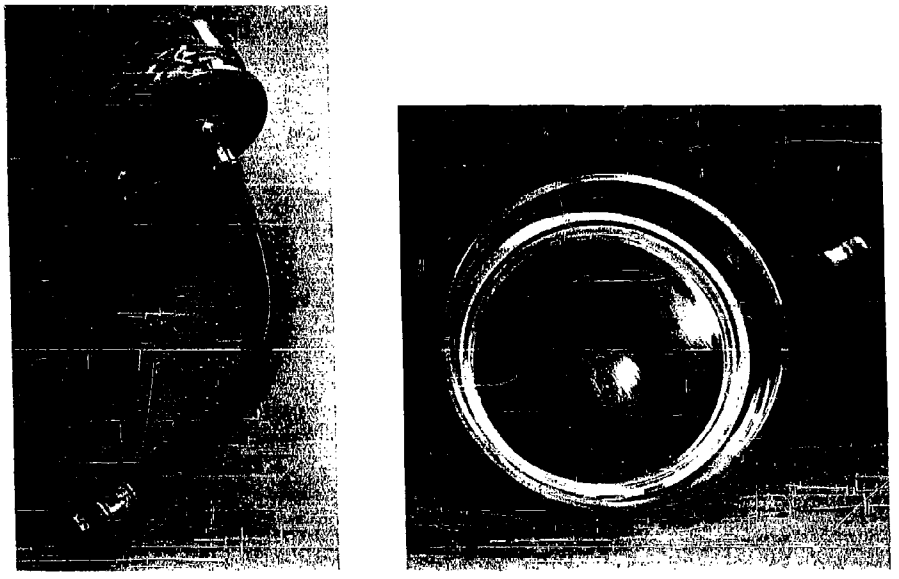

Figure 9.36 . Brass Electrode

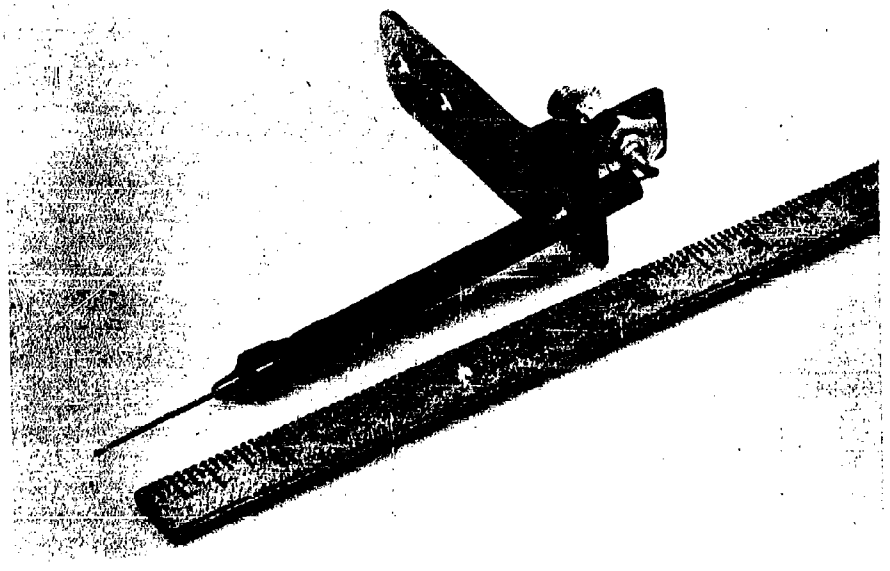

Figure 9.37 . No. 21 Hypodermic Needle Probe

in sea water at 40 kc is about 40 ohms.

No. 27 Hypodermic Needle - in the interest of making probes as small as possible, an electrode was made using the smallest available hypodermic needle size which is No. 27 gauge or .016 inches (0.4 mm) diameter and 1/2" in length. This is about half the diameter of the No. 21 gauge needle. A photograph of this unit is shown in Figure 9.38 . The construction procedure was similar to that of the No. 21 gauge needle above but a No. 34 formvar coated copper center wire was used. The wire was secured in the tube with Epocast. The gap between the center wire and tube at the tip is approximately .001" (.03 mm) which is an indication of the smallest scale of microstructure that can be detected with this probe. The probe resistance in sea water at 3.5 mc is about 400 ohms. No problems of construction were encountered with this small probe and, if smaller tubes were available, it would be reasonable to attempt construction of a smaller probe.

A convenient electrode configuration whose resistance is approximately calculable from the geometry is the parallel wire electrode as shown in Figure 9.39 . This consists of two No. 28 platinum wires 0.4 inches in length and spaced 0.13 inches apart. The electrode resistance of this unit is about 30 ohms in sea water. One important thermal advantage of this parallel wire arrangement is the low thermal time constant of the electrode surfaces due to the high thermal conductivity and low heat capacity of the metal wires.

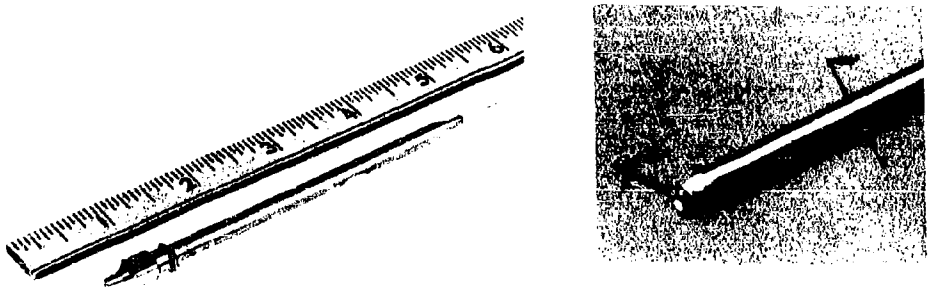

Figure 9.38 . No. 27 Hypodermic Needle Probe

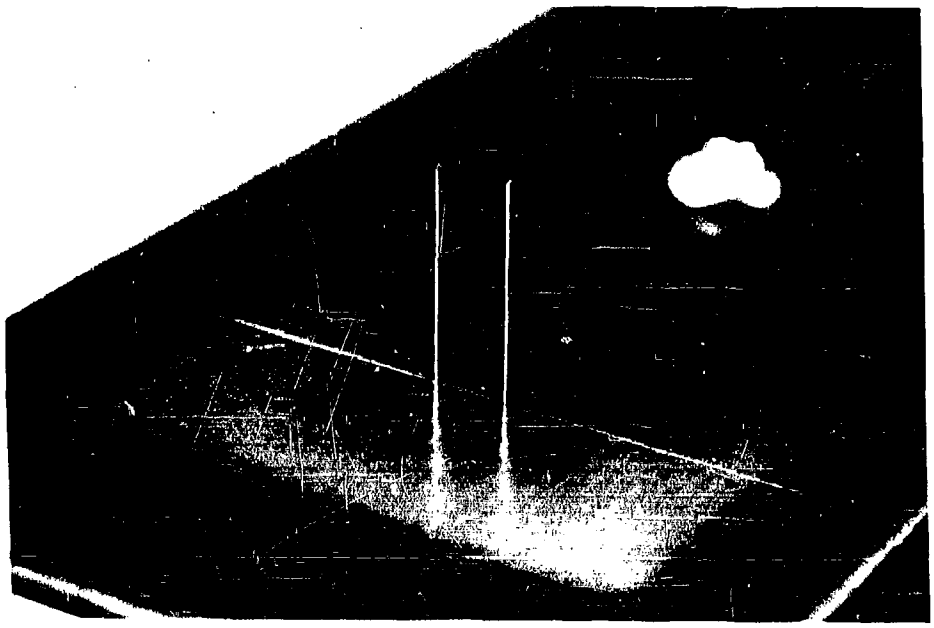

Figure 9.39 . Parallel Wire Electrode

10. RESISTANCE CALCULATION

The analytical machinery necessary for calculating the resistance of a given electrode configuration is developed in this Section. Consideration is given to the case of the potential field and associated functions in both a homogeneous and inhomogeneous conducting medium. It will be apparent that the analysis of the potential problem for even the simplest electrode configurations is complicated and approximate methods must be resorted to.

10.1 Potential Theory

The fundamental definitions and certain properties of the potential field of an electrode configuration are discussed below.

Fundamentals

We are interested in obtaining the electric potential as a function of position for a given electrode configuration. With a knowledge of this function all properties of the electrode arrangement may be calculated. Static potentials will be considered since the resulting fields are applicable, for the electrodes of interest, to alternating fields up to radio frequencies.

The general double electrode configuration is one which consists of two surfaces of infinite conductivity (electrodes) immersed in a conducting medium of conductivity, σ, which is confined in a volume of given shape by surfaces of zero conductivity (insulators) which are terminated on the electrode surfaces and/or at infinity. The conducting medium is contained in the surface consisting only of electrodes and insulators. A potential is maintained between the electrodes by a source of electromotive force.

Denote the potential at a point in the medium by V. Assume that the potential on the "negative" electrode is zero, and that on the "positive" electrode is V_o. It is convenient to introduce the "unit potential," ϕ, which satisfies

$$V = \phi V_o \quad ,$$

thus, $\phi = 1$ on the positive electrode and $\phi = 0$ on the negative electrode. The electric field at a point in the medium is

$$-\vec{\nabla} V = -V_o \vec{\nabla} \phi .$$

The current density, $\vec{j}$, is given by

$$\vec{J} = -\sigma \vec{\nabla} V = -\sigma V_0 \vec{\nabla} \phi .$$

The rate at which energy is dissipated in the medium by Joule heating at a point, i.e., the power density, P_v, is

$$P_v = \vec{J} \cdot (-\vec{\nabla} V) = \sigma V_0^2 (\vec{\nabla} \phi)^2 .$$

If P is the total power dissipated in the electrode volume and R is the electrode resistance, then

$$P = \frac{V_0^2}{R} .$$

The power density may be written,

$$P_v = P R \sigma (\vec{\nabla} \phi)^2 = P w$$

where

$$w = R \sigma (\vec{\nabla} \phi)^2 .$$

This function satisfies the relation

$$\int w \, dv = 1$$

where the integration extends over the entire volume of the conducting medium. It follows from the fact that

$$\int P_v \, dv = P .$$

The function w plays a fundamental roll in the theory of electrode sensors and is termed the "sensitivity distribution function." The equation of continuity is (1):

$$\vec{\nabla} \cdot \vec{J} = 0$$

or

$$\vec{\nabla} \cdot (\sigma \vec{\nabla} \phi) = 0 .$$

For a homogeneous conducting medium the potential problem reduces to the

solution of Laplace's equation

$$\vec{\nabla} \cdot \vec{\nabla} \phi = \nabla^2 \phi = 0 \ ,$$

for the boundary conditions:

$$\phi = 1 \quad \text{on positive electrode}$$

$$\phi = 0 \quad \text{on negative electrode}$$

$$\frac{\partial \phi}{\partial n} = 0 \quad \text{on insulator surfaces} \ .$$

The latter boundary condition implies no current flow through the insulator surfaces.

Except for those fortunate cases where the electrodes and insulators coincide with some natural coordinate system, the solution of the above Laplace equation is difficult, at best, and usually requires integral equation methods. This arises because of the mixed boundary conditions on the enclosing surface which consists partly of electrodes ($\sigma = \infty$) and partly of insulators ($\sigma = 0$). In many cases, approximate methods must be used to obtain the potential field.

Validity of Electrostatic Theory

The periodic potential at a point in the electrode volume may be calculated by electrostatic theory provided the frequency is not too high. The relaxation time of the medium sets the upper frequency limit. This same limit also occurs when the electrode resistance, R, due to the conductivity of the medium is comparable with the electrode capacity, C, which depends on the dielectric constant, K, of the medium. If f_x is this maximum frequency, then

$$2\pi f_x RC = 1 \ ,$$

where

$$RC = \frac{K K_0}{\sigma} \ ,$$

hence,

$$f_x = \frac{\sigma}{2\pi K K_0} \ ,$$

and $K_0 = 8.85 \times 10^{-12}$ farad/meter is the permittivity of free space. Another limitation at high frequency which modifies the potential field

at some distance from the electrode is the skin effect. The skin depth, δ, is given by (2)

$$\delta = \left[\pi f \mu_0 \mu \sigma\right]^{-1/2},$$

where $\mu_0 = 4\pi \times 10^{-7}$ henry/meter is the permeability of free space. Since the distribution function, w, ordinarily falls off rapidly with distance from the electrode, we arbitrarily set as an upper limit to the frequency due to the skin effect as

$$\delta = b \quad ,$$

where b is the mean radius of the electrode configuration. Denoting this frequency by f_δ, we have

$$f_\delta = \left[\pi b^2 \mu_0 \mu \sigma\right]^{-1}.$$

Numerical examples of these limiting frequencies are listed in Table 10.1 for sea water and tap water. The smaller of the two frequencies f_x or f_δ sets the upper limit for the validity of electrostatic theory in the given medium and for the given electrode.

Table 10.1 . Maximum Frequency for Validity of Electrostatic Theory

	Sea Water	Tap Water
f_x	1.2 kmc	11 mc *
f_δ	530 mc *	53 kmc
K	74	81
σ	4.8 $ohm^{-1}m^{-1}$	.048 $ohm^{-1}m^{-1}$
b	1 cm	1 cm
μ	1.0	1.0

*Maximum Frequency

Inhomogeneous Medium

If the conductivity of the medium is inhomogeneous, the potential does not satisfy Laplace's equation; but satisfies the equation

$$\vec{\nabla} \cdot (\sigma \vec{\nabla} \phi) = 0,$$

where σ is a (known) function of position. Expanding this equation we find

$$\nabla^2 \phi = -\frac{1}{\sigma} \vec{\nabla}\sigma \cdot \vec{\nabla}\phi.$$

If the conductivity gradients are everywhere perpendicular to the currents which flow in the homogeneous case, the solution to the inhomogeneous potential problem is identical with the homogeneous case. A first order equation for the potential is obtained by defining

$$\phi = \phi_0 + \varphi$$
$$\sigma = \sigma_0 (1 + \varepsilon) \quad ,$$

where σ_o is the average conductivity of the medium and ϕ_o is the unit potential for the homogeneous case. Neglecting second order terms, we find

$$\nabla^2\varphi = -\vec{\nabla}\varepsilon \cdot \vec{\nabla}\phi_o ,$$

which is Poisson's equation since the quantity on the right side is known everywhere. The boundary conditions on the first order potential correction are

$$\varphi = 0 \quad \text{on both electrodes}$$
$$\frac{\partial \varphi}{\partial n} = 0 \quad \text{on insulators} \quad .$$

Impedance Boundary Condition

Electrode surfaces are not always perfect conductors. Extremely thin deposits of partially conducting material may form on the metalic electrodes. As a consequence, the potential problem is modified in that the boundary conditions for the problem are changed. Suppose that the surface admittance per unit area of the electrodes is $\gamma + i\omega\beta$ which is due to an (assumed) infinitely thin contaminating film. Within the conducting medium the potential, ϕ, still satisfies Laplace's equation:

$$\nabla^2\phi = 0 ,$$

however, the boundary conditions are now mixed

$$\phi + \left(\frac{\sigma}{\gamma + i\omega\beta}\right)\frac{\partial \phi}{\partial n} = 1 \quad \text{on positive electrode}$$

$$\text{"} = 0 \quad \text{on negative electrode}$$

$$\frac{\partial \phi}{\partial n} = 0 \quad \text{on insulators} \quad .$$

The additional terms are due to the (complex) impedance of the boundary. If the surface impedance is low

$$|\gamma + i\omega\beta| \gg \sigma ,$$

the first order solution, φ, to the potential problem satisfies the approximate boundary conditions

$$\varphi = -\left(\frac{\sigma}{\gamma + i\omega\beta}\right)\cdot\left(\frac{\partial \phi_0}{\partial n}\right) \qquad \text{on both electrodes}$$

$$\frac{\partial \varphi}{\partial n} = \frac{\partial \phi_0}{\partial n} = 0 \qquad \text{on insulators ,}$$

where ϕ_0 is the solution for zero surface impedance and $\Phi = \phi_0 + \varphi$. If the surface impedance is small, the following relation is approximately valid

$$\vec{\nabla}\Phi = \vec{\nabla}\phi_0 \left[\phi_2 - \phi_1\right],$$

where ϕ_2 is the potential in the medium at a point on the positive electrode and ϕ_1 the potential in the medium at a point on the negative electrode ($\phi_2 \leq 1$, $\phi_1 \geq 0$).

Dipole Field

The potential field of a simple electric dipole is of interest because of its close similarity to the field at great distance from certain double electrode configurations.

The potential field, V, of a dipole is (3)

$$V = \frac{\vec{p}\cdot\vec{r}}{4\pi K K_0 r^3} = \frac{p \sin\psi}{4\pi K K_0 r^2}$$

where $\vec{p}$ is the electric dipole moment, ψ is the angle between the radius vector $\vec{r}$ and the plane of symmetry of the dipole. A dipole field is obtained for a positive and negative charge of magnitude q separated by a distance ℓ, provided $r \gg \ell$. The magnitude of the dipole moment is

$$p = q\ell .$$

The "equivalent dipole moment" of a double electrode configuration may be defined in the following way. Let b be a reference dimension of the electrode, and suppose that the unit potential field at large distance ($r \gg b$) from the electrodes is

$$\phi = m_0 \left(\frac{b}{r}\right)^2 \sin\psi ,$$

where m_0 is a dimensionless number which depends on the details of the

electrode geometry. Equating the potential of a dipole to that of the electrode system:

$$V_0 m_0 \left(\frac{b}{r}\right)^2 \sin\psi = \frac{p \sin\psi}{4\pi K K_0 r^2} ,$$

we obtain the equivalent dipole moment

$$p = V_0 (4\pi K K_0 m_0 b^2) .$$

The quantity in brackets is termed the "unit dipole moment." If C is the capacity of the electrode configuration, the induced charge, q, on the electrodes is

$$q = CV_0 .$$

This provides a means of defining the "effective length," ℓ , of the equivalent electric dipole of the electrode:

$$p = q\ell$$

or

$$\ell = \left(\frac{p}{V_0}\right)\frac{1}{C} = \frac{4\pi K K_0 m_0 b^2}{C} .$$

The capacity, C, of the electrodes is related to the resistance between the electrodes by (Sec. 10.3):

$$R\sigma = \frac{KK_0}{C} .$$

Consequently, the effective size of the equivalent dipole is

$$\ell = 4\pi(R\sigma b)\, m_0 b .$$

The function $(\vec{\nabla}\phi)^2$ for a dipole field is found by differentiation:

$$(\vec{\nabla}\phi)^2 = \left(\frac{\partial\phi}{\partial r}\right)^2 + \frac{1}{r^2}\left(\frac{\partial\phi}{\partial\psi}\right)^2$$

$$= \left(\frac{m_0}{b}\right)^2 \left(\frac{b}{r}\right)^6 (3\sin^2\psi + 1).$$

10.2 Axisymmetric Potential

The potential field of an axially symmetric electrode configuration is a useful special case to consider. The electrodes of primary interest are of this type. The flush type electrode has the added simplification that the potential defined on the electrodes and insulators lies in a plane. Formulas for obtaining the axisymmetric potential field are discussed below. These formulas are later used to calculate the resistance of a given electrode.

Green's Function

The electrostatic potential of a given surface potential distribution may be obtained by Green's function method (4):

$$\phi = \int \phi_0 \left(\frac{\partial G}{\partial n}\right) dA$$

where ϕ_0 is, the surface distribution, G is the Green's function (which is zero on the boundary in this case), and the integration is carried over the surface which contains the field distribution. For a plane boundary (e.g., z = 0) with a radially symmetric potential distribution, $\phi_0(\rho)$, a particularly simple Green's function is obtained by the image method (5)

$$\phi = \frac{z}{2\pi}\int_0^\infty \rho\,\phi_0(\rho)\,d\rho \int_0^{2\pi} \frac{d\theta}{r_1^3} \quad ,$$

where r_1 is the distance between the source point and the field point as shown in Figure 10.1 and

$$r_1^2 = \rho^2 + r^2 - 2\rho r \cos\psi \cdot \cos\theta$$

$$\sin\psi = \frac{z}{r} \, .$$

The potential on the axis ($\psi = 90^\circ$) is

$$\phi = z\int_0^\infty \frac{\rho\,\phi_0(\rho)\,d\rho}{\left[\rho^2 + z^2\right]^{3/2}} = \phi(z).$$

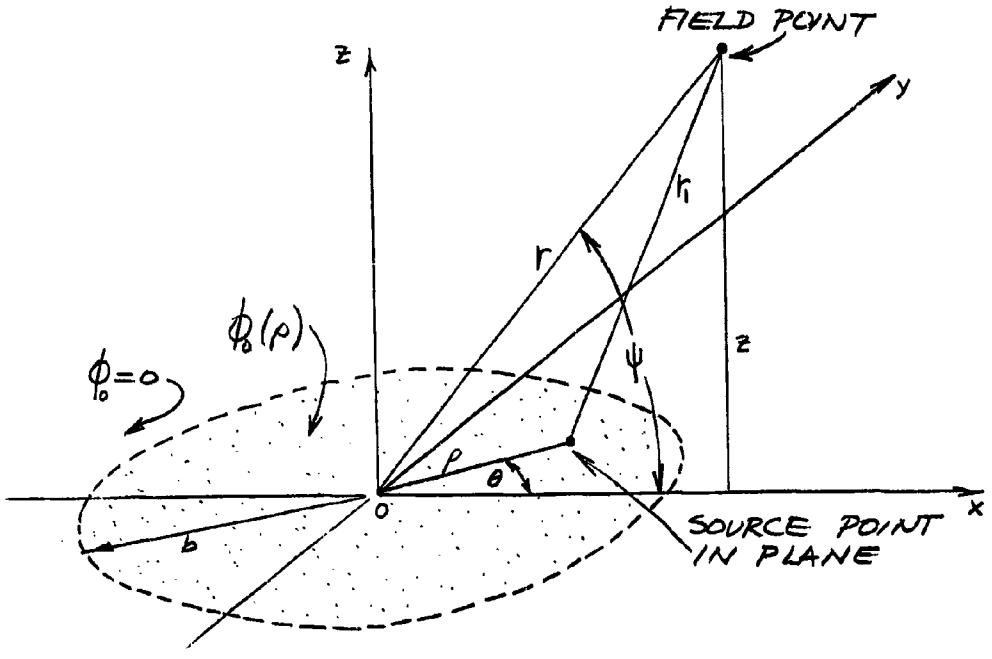

Figure 10.1 . Plane Axisymmetric Potential Distribution

Legendre Polynomial Expansion

Consider the axisymmetric potential field corresponding to the surface distribution which is zero for $\rho > b$. The inverse distance r_1^{-1} may be developed in a series of Legendre polynomials (6)

$$\frac{1}{r_1} = \frac{1}{r} \sum_{n=0}^{\infty} \left(\frac{\rho}{r}\right)^n P_n (\cos\theta \cdot \cos\psi),$$

where it is assumed that

$$0 \leq \rho \leq b < r \quad .$$

Differentiating with respect to the argument of P_n, we get the expansion for r_1^{-3} (7):

$$\frac{1}{r_1^3} = \frac{1}{r^3} \sum_{n=0}^{\infty} \left(\frac{\rho}{r}\right)^n P'_{n+1} (\cos\theta \cdot \cos\psi),$$

where the prime denotes differentiation. Substituting this expansion in

the integral

$$\phi = \frac{z}{2\pi} \int_0^b \phi_0(\rho)\, \rho\, d\rho \int_0^{2\pi} \frac{d\theta}{r_1^3}$$

we find

$$\phi = \left(\frac{b}{r}\right)^2 \sin\psi \sum_{n=0}^{\infty} m_n \left(\frac{b}{r}\right)^n F_n(\cos\psi)$$

where

$$m_n = \int_0^1 \xi^{n+1}\, \phi_0(\xi)\, d\xi$$

and

$$F_n(\cos\psi) = \frac{1}{2\pi} \int_0^{2\pi} P'_{n+1}(\cos\theta \cdot \cos\psi)\, d\theta .$$

The numbers m_n are the moment coefficients of the potential distribution ϕ_0 over the plane $0 \leq \rho \leq b$. The functions $F_n(\cos\psi)$ are obtained from the known expressions for P_n; the first few of which are:

$$F_0 = 1$$
$$F_1 = 0$$
$$F_2 = \frac{15}{4}\cos^2\psi - \frac{3}{2}$$
$$F_3 = 0$$
$$F_4 = \frac{945}{64}\cos^4\psi - \frac{105}{8}\cos^2\psi + \frac{15}{8}$$
$$F_5 = 0 \quad \ldots \quad \text{etc.}$$

In general $F_{ODD}(\cos\psi) = 0$.

At a great distance from the potential distribution ($r \gg b$) only the leading term is important:

$$\phi \approx m_0 \left(\frac{b}{r}\right)^2 \sin\psi ,$$

which is just the field of a dipole. The constant m_o is

$$m_o = \int_0^{\prime} \xi \, \phi_o(\xi) \, d\xi .$$

Laplace's Formula

An expression due to Laplace for an axisymmetric potential distribution is (8):

$$\phi = \frac{1}{2\pi} \int_0^{2\pi} \Phi(z + i\rho \sin\psi) \, d\psi ,$$

where

$$z^2 + \rho^2 = r^2$$

$$\cos\psi = \frac{z}{r} \quad .$$

The function $\Phi(z)$ is just the axial value of the potential $\phi(\rho, z)$

$$\Phi(z) = \phi(0,z) \quad .$$

If no axial charges exist, the above expression gives the potential, ϕ, at all points accessible from the axis without crossing a charged surface (9).

Bessel Integral

Solutions of Laplace's equation in cylindrical coordinates for axisymmetric boundary conditions in the plane may be represented by the integral (10,11)

$$\phi = \int_0^{\infty} e^{-k|z|} F(k) \, J_o(k\rho) \, dk ,$$

where F(k) is a weight function determined by the boundary conditions. On the plane boundary

$$\phi = \phi_o(\rho) = \int_0^{\infty} F(k) \, J_o(k\rho) \, dk .$$

Inverting this expression by the Fourier-Bessel integral (12) the function F(k) is found to be

$$F(k) = k \int_0^\infty \phi_0(w)\, J_0(wk)\, w\, dw.$$

10.3 Homogeneous Volume

The calculation of resistance of a given electrode in a homogeneous medium is, at best, difficult. Certain methods of calculation are more suited to a given configuration than others. In the interest of a wider choice, several methods of resistance calculation are considered below.

Surface Integral

Frequently the simplest direct way of calculating the electrode resistance is the following. The current, I, from the positive electrode is

$$I = \int_+ \vec{J} \cdot d\vec{A},$$

where $\vec{J}$ is the current density and the integral is carried out over the surface of the positive electrode. By convention, $\vec{J}$ points into the medium on the positive electrode and is parallel to $d\vec{A}$. The current density is

$$\vec{J} = -\sigma \vec{\nabla} V = -\sigma V_0 \vec{\nabla} \phi,$$

where V_0 is the potential between the electrodes. By Ohm's Law $V_0 = IR$. Combining the above relations we have

$$\frac{1}{R\sigma} = -\int_+ \vec{\nabla}\phi \cdot d\vec{A} = -\int_+ \left(\frac{\partial \phi}{\partial n}\right) dA.$$

Similarly on the negative electrode

$$I = -\int_- \vec{J} \cdot d\vec{A}$$

and

$$\frac{1}{R\sigma} = \int_- \vec{\nabla}\phi \cdot d\vec{A} = \int_- \left(\frac{\partial \phi}{\partial n}\right) dA.$$

Volume Integral

Another formula for electrode resistance is obtained by considering the total power dissipated in the electrode medium. The power density is

$$P_v = \vec{J} \cdot (-\vec{\nabla} V) = \sigma V_o^2 (\vec{\nabla}\phi)^2 .$$

The volume integral of the power density is equal to the total electrode power

$$P = V_o \int \sigma (\vec{\nabla}\phi)^2 \, dv \quad .$$

By the Joule heating relation:

$$V_o^2 = PR$$

or

$$\frac{1}{R} = \int \sigma (\vec{\nabla}\phi)^2 \, dv .$$

For a homogeneous medium

$$I = R\sigma \int (\vec{\nabla}\phi)^2 \, dv .$$

Defining $w = R\sigma(\vec{\nabla}\phi)^2$, we have as before:

$$1 = \int w \, dv \quad .$$

Green's Function Surface Integral

An expression for the resistance may be derived from the Green's function representation of the potential field. The potential by Green's function method is (4)

$$\phi = \int \left(\phi_o \frac{\partial G}{\partial n} - G \frac{\partial \phi}{\partial n} \right) dA ,$$

where the integration is carried out over the surface enclosing the conducting medium, and G is a Green's function suitable to the problem.

First, let G_1 be a Green's function which is unity on one electrode (say, the positive one) and zero on the rest of the surface, then

$$\phi = \int \phi_0 \frac{\partial G_1}{\partial n} dA - \int_+ \frac{\partial \phi}{\partial n} dA .$$

Now, let G_2 be a Green's function which is unity on the negative electrode and zero over the rest of the enclosing surface, then

$$\phi = \int \phi_0 \frac{\partial G_2}{\partial n} dA - \int \frac{\partial \phi}{\partial n} dA .$$

It will be recalled that

$$\frac{1}{R\sigma} = - \int_+ \frac{\partial \phi}{\partial n} dA$$

and

$$\frac{1}{R\sigma} = \int \frac{\partial \phi}{\partial n} dA ,$$

hence, it follows that

$$\int \phi_0 \frac{\partial G_1}{\partial n} dA + \frac{1}{R\sigma} = \phi = \int \phi_0 \frac{\partial G_2}{\partial n} dA - \frac{1}{R\sigma}$$

or

$$\frac{1}{R\sigma} = \int \phi_0 \frac{\partial}{\partial n} \left\{ \frac{G_2 - G_1}{2} \right\} dA .$$

Define another Green's function G^*, such that

$$G^* = \left\{ \frac{G_2 - G_1}{2} \right\} ,$$

thus,

$$\frac{1}{R\sigma} = \int \phi_0 \left(\frac{\partial G^*}{\partial n} \right) dA .$$

This formula gives the desired result of the electrode resistance as a surface integral involving only the boundary value potential.

It remains to get the functions G_1 and G_2 which can be done in a direct manner from the solution of a particular potential problem. This will not be done, however, since a simpler means of obtaining the function $(\partial\sigma^*/\partial n)$ is found later in the next paragraphs.

For a radially symmetric plane potential distribution which is zero for $\rho > b$ (i.e., on the negative electrode) the above integral becomes (with $\rho = \lambda b$, $n = \nu b$)

$$\frac{1}{R\sigma b} = 2\pi \int_0^1 \phi_0(\lambda) \left(\frac{\partial \sigma^*}{\partial \nu}\right) \lambda \, d\lambda .$$

Bessel Surface Integral

Consider an axisymmetric potential distribution in the plane $z = 0$ which is zero for $\rho > b$. The Bessel integral representation for such a potential given in Section 10.2 is

$$\phi = \int_0^\infty e^{-k\zeta} F(k) \, J_0(k\lambda) \, dk ,$$

where

$$\rho = \lambda b$$

and

$$z = \zeta b \quad .$$

The normal gradient of ϕ on the surface is

$$\left.\frac{\partial \phi}{\partial z}\right|_{z=0} = \frac{1}{b} \left.\frac{\partial \phi}{\partial \zeta}\right|_{\zeta=0} = \frac{-1}{b} \int_0^\infty k \, F(k) \, J_0(k\lambda) \, dk .$$

The integral of this expression over the surface of one electrode or the other is $(R\sigma)^{-1}$. Assume, for example, that one electrode is the region $\lambda > 1$ (over which $\phi = 0$) and the other is the region $0 < \lambda < \alpha$ (over which $\phi = 1$). This is the "eye-type" electrode (Sec. 9.2). In this case

$$\frac{1}{R\sigma} = -b \int_0^\infty 2\pi\lambda \left(\frac{\partial\phi}{\partial z}\right)_{z=0} d\lambda$$

or

$$\frac{1}{R\sigma b} = \int_0^\infty 2\pi\rho\, d\rho \int_0^\infty k\, F(k)\, J_0(k\rho)\, dk$$

$$= 2\pi \int_0^\infty k\, F(k)\, dk \int_0^\infty \rho\, J_0(k\rho)\, d\rho$$

$$= 2\pi\alpha \int_0^\infty F(k)\, J_1(k\alpha)\, dk.$$

The expression for F(k) is (Sec. 10.2)

$$F(k) = k \int_0^\infty \phi_0(w)\, J_0(wk)\, w\, dw.$$

Substituting this expression and inverting the order of integration we get

$$\frac{1}{R\sigma b} = 2\pi\alpha \int_0^\infty \phi_0(w)\, w\, dw \int_0^\infty k\, J_0(wk)\, J_1(k\alpha)\, dk.$$

Let $w = \alpha x$ and $k\alpha = u$, then

$$\frac{1}{R\sigma b} = 2\pi\alpha \int_0^\infty \phi_0(x\alpha)\, x\, dx \left[\int_0^\infty u\, J_0(xu)\, J_1(u)\, du\right].$$

The integral in square brackets is (13,14,26)

$$\int_0^\infty u\, J_0(ux)\, J_1(u)\, du = \begin{cases} \left(\frac{2}{\pi}\right)\frac{E(x)}{1-x^2}, & x<1 \\ -\left(\frac{2}{\pi}\right)\frac{K'\left(\frac{1}{x}\right)}{x^2}, & x>1, \end{cases}$$

where K(x) and E(x) are complete elliptic integrals of the first and second kind, respectively. Call this integral $\Lambda(x)/x$. Finally, with the assumed limitations on boundary potential:

$$\frac{1}{R\sigma b} = 2\pi\alpha \int_0^{\infty} \phi_0(\alpha x)\,\Lambda(x)\,dx$$

$$= 2\pi \int_0^{\infty} \phi_0(\lambda)\,\Lambda\left(\frac{\lambda}{\alpha}\right) d\lambda \,,$$

where $\alpha\beta = 1$. Thus, an integral over the surface potential distribution ϕ_0 may be made to obtain the electrode resistance. This is just what was accomplished previously by a Green's function method. Comparing the two results, it follows that

$$\frac{\partial \varphi^*}{\partial \nu} = \frac{1}{\lambda}\Lambda\left(\frac{\lambda}{\alpha}\right) = \frac{1}{\alpha}\int_0^{\infty} u\, J_0\left(\frac{\lambda u}{\alpha}\right) J_1(u)\, du.$$

Approximate Methods

Upper and lower limits to the electrode resistance can be obtained by the following technique (15). If a non-conducting surface is introduced into the electrode volume the electrode resistance is greater than without it. Frequently, by the introduction of an appropriate surface, the current lines can be distorted into those corresponding to a simpler potential problem in which the resistance is more readily calculated. The resistance calculated in this way is an upper limit to the actual electrode resistance. Similarly by the appropriate introduction of conducting surfaces, a lower limit to the resistance can be obtained.

A variational principle may be used to obtain a least upper limit of the electrode resistance when an approximate expression for the resistance is known (15). The principle is based on the fact that the power dissipated in the electrode is least if the expression for the resistance is precisely equal to the actual value. Thus, any expression for the resistance with an adjustable parameter can be optimized to obtain a least upper limit to the actual resistance. Several examples of this technique are given in References (16,17,18,27).

10.4 Inhomogeneous Volume

Formulas are developed below for several cases where the conductivity of the medium is inhomogeneous over the sensitive volume of the electrode.

These expressions are used to study the response of an electrode to random fields with microstructure smaller than the size of the electrode, and the response to small bubbles and boundary layer effects.

Gradual Inhomogeneity

Conductivity variations in the field of the electrode introduce small perterbations in the unit potential function, ϕ, obtained for the case of homogeneous conductivity. If ϕ_1 is the new solution, introduce the small error potential u so that

$$\phi_1 = \phi + u \quad .$$

Since the boundary conditions for ϕ_1 and ϕ are the same, the error potential, u, has the boundary condition that it is zero on both the electrodes and $\vec{\nabla} u$ is parallel to the insulator surfaces. Let the conductivity at a given position be σ_1 and it is assumed that it differs only slightly from the average conductivity σ. Define a dimensionless function of position, ξ, which accounts for the variations in conductivity:

$$\xi = \frac{\sigma_1 - \sigma}{\sigma} \quad ,$$

where $|\xi| << 1$. The expression for the resistance variations is best obtained by considering the power dissipated at the electrode. The electrode power, P, is

$$P = \frac{V_0^2}{R_1} = V_0^2 \int \sigma_1 (\vec{\nabla}\phi_1)^2 dv \quad ,$$

where R_1 is the electrode resistance. Combining the above relations and neglecting second order terms:

$$\frac{1}{\sigma R_1} = \int (1+\xi)(\vec{\nabla}\phi + \vec{\nabla}u)^2 dv$$

$$= \int (\vec{\nabla}\phi)^2 dv + \int \xi (\vec{\nabla}\phi)^2 dv + 2\int \vec{\nabla}\phi \cdot \vec{\nabla}u \, dv.$$

The second order terms are small if the conductivity variations are small and vary gradually with position. Since

$$\frac{1}{\sigma R} = \int (\vec{\nabla}\phi)^2 dv$$

we have

$$\frac{1}{\sigma R}\left(\frac{\Delta R}{R}\right) = -\int \xi (\vec{\nabla}\phi)^2 dv - 2\int \vec{\nabla}\phi \cdot \vec{\nabla}u \, dv,$$

where $\Delta R = R_1 - R$. The last term is zero, as shown below. From the identity

$$\vec{\nabla} \cdot [u \vec{\nabla} \phi] = \vec{\nabla} u \cdot \vec{\nabla} \phi + u \nabla^2 \phi^{0},$$

integrating and applying Gauss' theorem

$$\int u \vec{\nabla} \phi \cdot d\vec{S} = \int \vec{\nabla} u \cdot \vec{\nabla} \phi \, dv.$$

The surface integral extends over the electrodes and the non-conducting (insulator) boundaries. Since the u is zero on both positive and negative electrodes and $\vec{\nabla}\phi$ is parallel to the non-conducting boundaries, the surface integral is zero.

Finally, we have

$$\left(\frac{\Delta R}{R}\right) = - R\sigma \int \xi \, (\vec{\nabla}\phi)^2 \, dv = - \int \xi \, w \, dv.$$

The factor $R\sigma$ is the cell constant of the electrode. The minus sign indicates that an increase in conductivity ($\xi > 0$) causes a decrease in electrode resistance. If ξ is uniform over the electrode volume then

$$\frac{\Delta R}{R} = - \xi.$$

Spherical Inhomogeneity

Consider a small spherical volume of radius a in the electrode field of conductivity σ_1 which is a factor K times the conductivity, σ, of the rest of the medium:

$$K = \frac{\sigma_1}{\sigma} .$$

The diameter of the sphere is much smaller than the typical dimensions of the electrode so that the (undistorted) potential gradient is essentially constant in the vicinity of the sphere. The potential field distortion in the vicinity of the sphere is a well-known problem in potential theory. The problem corresponds to the electric field in the vicinity of a spherical dielectric inhomogeneity (19). The potential is given by

$$\phi_1 = \phi_0 + \left(\frac{K-1}{K+2}\right) \frac{a^3}{r^2} \cos\theta \, (\nabla \phi_0)$$

for $r > a$ and

$$\phi_i = -\left(\frac{3}{K+2}\right)\phi_o \quad ,$$

for $r < a$ where

$$\phi_o = \nabla\phi_o \cdot r\cos\theta \quad ,$$

is the undisturbed potential field in the vicinity of the sphere. The field inside the sphere is uniform but a factor $(3/K+2)$ smaller than the undisturbed field. The induced field outside the sphere is that of a dipole.

The electrode resistance, R_o, before the insertion of the sphere is

$$\frac{1}{R_o} = \sigma \int_{v_o} (\nabla\phi)_o^2 \, dv$$

where σ is uniform over the total electrode volume v_o. The electrode resistance with the spherical inhomogeneity is

$$\frac{1}{R} = \int_{v_o} \sigma(\vec{r}) (\nabla\phi)^2 \, dv$$

$$= \sigma \int_{v_o - \Delta v} (\nabla\phi_i)^2 \, dv + \sigma_i \int_{\Delta v} (\nabla\phi_i)^2 \, dv,$$

where Δv is the volume of the sphere. Substituting the above values for the distorted potentials and integrating over the respective volumes, we obtain

$$\frac{1}{R\sigma} = \frac{1}{R_o\sigma} + \left\{ K\left(\frac{3}{K+2}\right)^2 + 2\left(\frac{K-1}{K+2}\right)^2 - 1 \right\} \cdot (\nabla\phi_o)^2 \cdot \Delta v$$

or, if $\Delta R = R - R_o \ll R_o$, then

$$\left(\frac{\Delta R}{R_o}\right) = -\left(\frac{K-1}{K+2}\right)(\nabla\phi_o)^2 \cdot \Delta v \cdot R_o\sigma \, .$$

Thus, the change of resistance depends on the local value of the function, $(\nabla\phi)^2$, and the volume of the sphere. This is basically a result of Weiss' sphere theorem (20). This result is valid for a small shpere which is not close to the boundaries of the electrode volume. It will be noticed that this expression does not reduce to the expression previously obtained for the case of a small gradual inhomogeneity ($K \rightarrow 1$). This, presumably, is because the change in conductivity is <u>not</u> gradual everywhere; in partic-

ular, at the spherical boundary where an abrupt change is experienced. For the case of a non-conducting spherical volume (K = 0) we get the "resistance of a bubble"

$$\frac{\Delta R}{R_0} = \frac{1}{2} R_0 \sigma (\nabla \phi_0)^2 \cdot \Delta v = \frac{1}{2} w \cdot \Delta v \quad .$$

This fact will be used in Section 13.4 to analyze the response of the detector to bubbles.

Similar analysis has been applied to the change of conductivity of conducting solutions due to a suspension of small non-conducting volumes, i.e., the so-called "obstruction-effect" in electrolytes (21). Other shapes such as oblate and prolate ellipsoids of given orientation have been analyzed with respect to this effect (22,23,24,25).

Surface Layer Inhomogeneity

Consider a conducting medium which is otherwise homogeneous except for a very thin volume of material at the surfaces of electrodes. The thickness of this surface layer inhomogeneity is assumed to be small in comparison with the typical dimensions of the electrodes so that the current density is essentially uniform over the surface layer. If the magnitude of the boundary layer inhomogeneity is small, the following expression is valid

$$\left(\frac{\Delta R}{R}\right) = - R\sigma \int \xi \ (\nabla \phi)^2 \, dv \ ,$$

where ξ is the fractional change in conductivity:

$$\xi = \frac{\sigma - \sigma_0}{\sigma_0}$$

and σ is the boundary value of conductivity and σ_0 the average value. If y denotes the local coordinate perpendicular to the electrode surfaces, the above integral can be broken into two parts consisting of integrals over the positive and negative electrodes:

$$-\left(\frac{\Delta R}{R}\right) = R\sigma \left\{ \int_+ dA \, (\nabla \phi)^2 \int_0^\infty \xi \, dy + \int_- dA \, (\nabla \phi)^2 \int_0^\infty \xi \, dy \right\} ,$$

where $(\nabla \phi)^2$ is essentially constant over the layer region, and the upper limit to the integral of ξ with respect to y indicates integration over the complete depth of the boundary layer where ξ is finite. Define the boundary layer thickness, δ^*, by

$$\xi_\infty \delta^* = \int_0^\infty \xi(y) \, dy \ ,$$

where ξ_Λ is the maximum value of ξ in the vicinity of the electrode surface as shown in Figure 10.2 , and

$$-\left(\frac{\Delta R}{R}\right) = R\sigma\left\{\int_+ dA\,(\nabla\phi)^2\,\xi_\Lambda\,\delta^* + \int_- dA\,(\nabla\phi)^2\,\xi_\Lambda\,\delta^*\right\}.$$

If the fractional change ξ is independent of position on the electrodes the expression simplifies to

$$-\left(\frac{\Delta R}{R}\right) = \xi_\Lambda\,\delta^* R\sigma\left\{\int_+ dA\,(\nabla\phi)^2 + \int_- dA\,(\nabla\phi)^2\right\}.$$

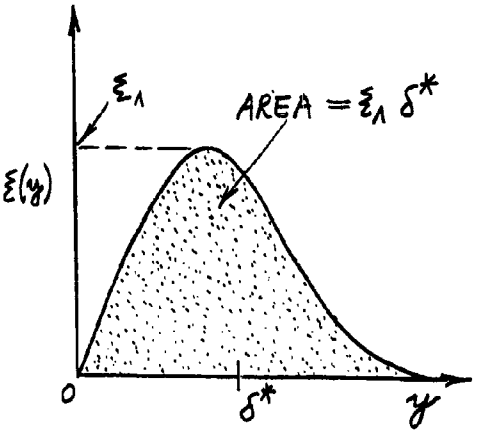

Figure 10.2 . Boundary Layer Inhomogeneity

A useful definition for the effective electrode area (of each) follows from this expression by comparison with the result for parallel electrodes of area S which are separated by a distance ℓ. In this case of a uniform field

$$-\left(\frac{\Delta R}{R}\right) = \frac{2\,\xi_\Lambda\,\delta^*}{R\sigma S}\,.$$

The area S for a general electrode is defined by equating the above expression for a uniform field with that for the actual field:

$$I = \frac{1}{2} S R^2\sigma^2\left\{\int_+ dA\,(\nabla\phi)^2 + \int_- dA\,(\nabla\phi)^2\right\}.$$

S is called the "effective electrode area" and represents an average area for each electrode. In this notation the fractional change of electrode resistance for a uniform boundary layer is

$$\left(\frac{\Delta R}{R}\right) = -\,\frac{2\,\xi_\Lambda\,\delta^*}{R\sigma S}\,.$$

If the electrode field, $(\nabla\phi)^2$, is uniform but $\xi(y)$ varies with position, the expression is

$$\left(\frac{\Delta R}{R}\right) = -\,\frac{1}{v_0}\left\{\int_+ \xi_\Lambda\,\delta^*\,dA + \int_- \xi_\Lambda\,\delta^*\,dA\right\}.$$

where v_o is the "electrode volume" (Sec. 12.2). This expression is used in Section 14.4 to calculate the boundary layer resistance of an electrode.

10.5 Homogeneous Surface

The theory of developed in this Section for the surface impedance of an electrode. Only the simplest case is considered of a surface of uniform properties but the existence of a non-uniform current density is included.

Surface Impedance

Consider a double electrode configuration with a uniform surface admittance per unit area $\gamma + i\omega\beta$ immersed in a homogeneous conducting medium. The surface conductance per unit area is γ, and the surface capacitance per unit area is β. The surface layer is assumed infinitely thin. Consider the tube of current shown in Figure 10.3 in which the element of area dA_2 on electrode No. 2 is the projection along the current lines of the element of area dA_1 on electrode No. 1. The conductance of the tube of current due to its volume conductivity is

$$\frac{\sigma\, dA_1\, \nabla\phi_1}{\phi_2 - \phi_1} = \frac{\sigma\, dA_2\, \nabla\phi_2}{\phi_2 - \phi_1} \quad ,$$

where ϕ_2 and ϕ_1 are the unit potentials on each of the electrodes which depend on the point on the electrode. Define the function f such that

$$f(\phi_2 - \phi_1) = \nabla\phi .$$

The surface admittance of electrodes No. 1 and No. 2 are, respectively

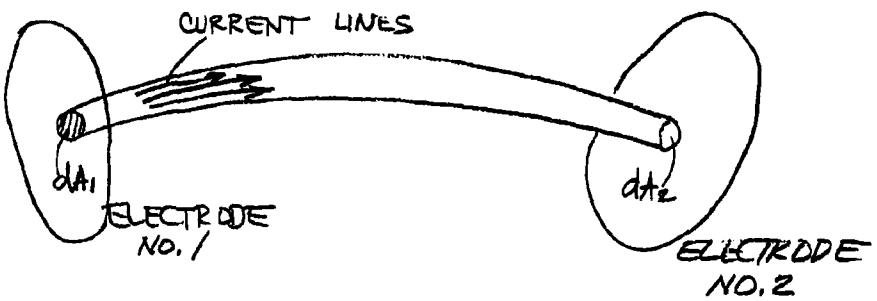

Figure 10.3 . Elementary Tube of Current

$$(\gamma + i\omega\beta)\, dA_1 \quad \text{and} \quad (\gamma + i\omega\beta)\, dA_2 .$$

The net differential electrode admittance due to the currents flowing through these elements of area is

$$d\left(\frac{1}{z}\right) = \left\{ \frac{1}{\sigma\, dA_1\, f_1} + \frac{1}{(\gamma + i\omega)\, dA_1} + \frac{1}{(\gamma + i\omega\beta)\, dA_2} \right\}^{-1}$$

Define the quantity, λ , such that

$$\frac{dA_2}{dA_1} = \lambda = \frac{(\nabla\phi)_1}{(\nabla\phi)_2}$$

or

$$dA_2 = \lambda\, dA_1 .$$

This quantity depends only on the electrode configuration, and is unity for identical electrodes in a symmetrical arrangement. Substituting in the above equation, we find

$$d\left(\frac{1}{z}\right) = \frac{\sigma f_1\, dA_1}{1 + \left(\frac{\sigma}{\gamma + i\omega\beta}\right)\left(\frac{\lambda + 1}{\lambda}\right) f_1} .$$

Define the ratio, F, of the volume conductivity of the electrolyte to surface admittance as (28,29)

$$F = \frac{\sigma}{\gamma + i\omega\beta} .$$

The dimensions of this complex quantity are inverse length, and depend only on the physical properties of the electrolyte and electrode material. With these definitions, we have

$$\frac{R}{z} = \int \frac{R\sigma f\, dA}{1 + F\left(\frac{\lambda + 1}{\lambda}\right) f} ,$$

where R is the electrode resistance for zero surface impedance. The integration may be taken over the surface of either electrode (if λ is properly defined), hence, the subscript has been dropped.

The important case of practical interest is when the surface imped-

ance is small compared with the volume resistance, i.e.,

$$\frac{2}{(\gamma + i\omega\beta)S} \ll R$$

or

$$2F \ll R\sigma S \sim f^{-1}$$

or

$$2Ff \ll 1 \quad ,$$

where S is the effective electrode area and $R\sigma$ is the cell constant of the electrode. We saw in Section 10.1 that if the surface impedance is small $f \approx \nabla\phi_0$, where ϕ_0 is the potential for zero surface impedance. In this case, to first approximation:

$$\frac{R}{Z} = \int R\sigma (\nabla\phi_0)\, dA - R\sigma F \int (\nabla\phi_0)^2 \left(\frac{\lambda+1}{\lambda}\right) dA.$$

The first integral is unity. The effective electrode area, S, defined earlier is given by

$$1 = \frac{1}{2} S R^2\sigma^2 \left\{ \int_+ (\nabla\phi_0)_1^2\, dA_1 + \int_- (\nabla\phi_0)_2^2\, dA_2 \right\}.$$

By the definition of λ, this may also be written

$$1 = \frac{1}{2} S R^2\sigma^2 \left\{ \int_+ (\nabla\phi_0)_1^2 \left(\frac{\lambda+1}{\lambda}\right) dA \right\}.$$

Utilizing this fact, we find

$$\frac{Z}{R} \approx 1 + \frac{2F}{R\sigma S} \quad .$$

The "figure-of-merit," F^*, with respect to surface effects of a given electrode/electrolyte interface is defined as

$$F^* = \frac{2|F|}{R\sigma S} \quad .$$

It is usually desirable in practice, that this number be small. The figure-of-merit improves (smaller) if the electrode configuration is of large dimensions; the volume conductivity is small and the surface admittance is large.

A difficulty is sometimes encountered with the above definition of S, since at the "edges" of certain electrodes the current density becomes infinitely large in such a way that S is zero. The quantity, F, may be written

$$F = \frac{\sigma}{\gamma + i\omega\beta} = \frac{\sigma}{\gamma(1+ik)} = \left(\frac{\sigma}{\gamma}\right)\cdot\left(\frac{1-ik}{1+k^2}\right)$$

where

$$k = \frac{\omega\beta}{\gamma}$$

is the phase factor of the surface admittance. The figure-of-merit is

$$F^* = \frac{2}{R\gamma S\sqrt{1+k^2}} .$$

Applications of this theory of the effects of the surface impedance of electrodes is found in References (30,31,32).

11. DETECTOR HEAD

The sensing electrodes described in an earlier Section must be mounted in such a way that they are exposed to the fluid flow in order to measure the properties of the medium. The mounting configuration for the electrodes is termed the "detector head." It is necessary to study the hydrodynamic flow about this solid on which the elements are mounted. This flow may be laminar or turbulent and may involve either potential or boundary layer flow. The detector head distorts, in one way or another, the previously existing velocity field at the point of measurement because of the presence of the probe. This Section deals with these hydrodynamic considerations as they relate to the properties and performance of the detector for measuring velocity and scalar turbulence fields in water.

Two main types of electrodes can be distinguished: the "probe type" consisting of a small electrode occupying the end region of a long, thin probe-shaped body and the "flush type" which is an electrode configuration which can be imbedded in a surface allowing locally rectilinear flow. Numerous detector head shapes can be mentioned which fall into these two classes. Each of these has various advantages and disadvantages. The sensing elements may be mounted singly or as double (differential) or multiple sensors on the same or different detector heads. The basis for determining the relative merits of a given shape are discussed in this Section. Also, three specific types are discussed in detail: 1) Rankine probe, 2) cylindrical head, and 3) wedge head. A description of the optimum position for the electrodes on the detector head is based on the above analysis.

11.1 General Considerations

The velocity field about the detector head is of importance to the present instrumentation both as a velocity detector and a temperature or concentration detector. The hydrodynamic properties of the axisymmetrical probe type head and two dimensional flush type detector heads involve the determination of the velocity field for potential flow, the velocity boundary layer thickness and the point where the flow becomes turbulent on the surface of the probe. The velocity field about the sensing electrode is fundamental to the determination of the effective frontal area of the electrode for the heating equation (Sec. 12.2). The boundary layer thickness, which should be as small as possible relative to the electrode dimensions, is of importance in connection with the dynamic response of the detector (Sec. 14.4), and determines the extent of the undesirable temperature rise at the surface due to electrical heating (Sec. 12.4). The turbulence transition point on the surface of the detector head dictates the limiting position of the electrode on the head, since, for proper performance, the sensing element must be located in the undisturbed laminar flow region usually found on the forward surface of the body. If the electrode is operated in the turbulent region of the flow, it is measuring fluctuating signals due to the probe itself. The velocity field for potential flow

yields information on the directional response of the detector as a velocity sensor and information on the point where cavitation may result and confuse the measurements.

There are two main classes of electrodes; the "probe type" and the "flush type." The probe type is characterized as follows: an electrode is mounted on the end of an axially symmetric probe-shaped body. The stem of the probe is cylindrical a short distance from the nose and the electrode dimensions are comparable to the stem diameter. The dimensions of the probe are usually small, say, of the order of 1 mm. The velocity field in the region of the electrode at the nose of the probe is not uniform over the sensing volume of the electrode and a stagnation point exists within the electrode volume. The boundary layer thickness is not constant on the surface of the electrode. The analytical study of probe type detector heads is complicated because of the general nature of the flow over the region of importance at the nose.

The flush type is characterized by an electrode which can be imbedded in a surface over which the fluid can be locally uniform. The simplest case of this is a plane surface with a flush mounted electrode in it; the surface may be cylindrical, as for example on the inside of a pipe or outside of a rod with the electrode flush with the surface; or lastly, the surface can be doubly convex or concave if the radii of curvature are much larger than the typical dimension of the electrode. Ordinarily no stagnation point exists in the electrode region. The flow in the region of the electrode is two-dimensional and the velocity boundary layer thickness there can be considered constant over the surface of the electrode. The analysis of the flow in this case is generally simpler than that for the probe type because of the simpler velocity distribution.

Examples of the flush type detector heads for two-dimensional flow are cylinders of circular, parabolic, elliptic and wedge shaped or airfoil cross section. Some of these types are illustrated in Figure 11.1 ; the small rectangles indicate the possible location of pairs of flush type electrodes. The two simple types, the circular cylinder and the wedge, are studied in detail later in this chapter.

Examples of the probe type detector head are the Rankine semi-infinite solid, cone, hemisphere and ogive. Some of these types are illustrated in Figure 11.2 ; the shading at the nose represents the location of the insulator between the center and outer electrode. The flow properties of the Rankine half-body are considered in detail below.

11.2 Rankine Probe

The only probe shape which fulfills the requirements for a practical detector probe and which has a velocity field for potential flow which can be put in relatively simple analytical form is the semi-infinite Rankine solid. Its surface corresponds to the interface between a fluid

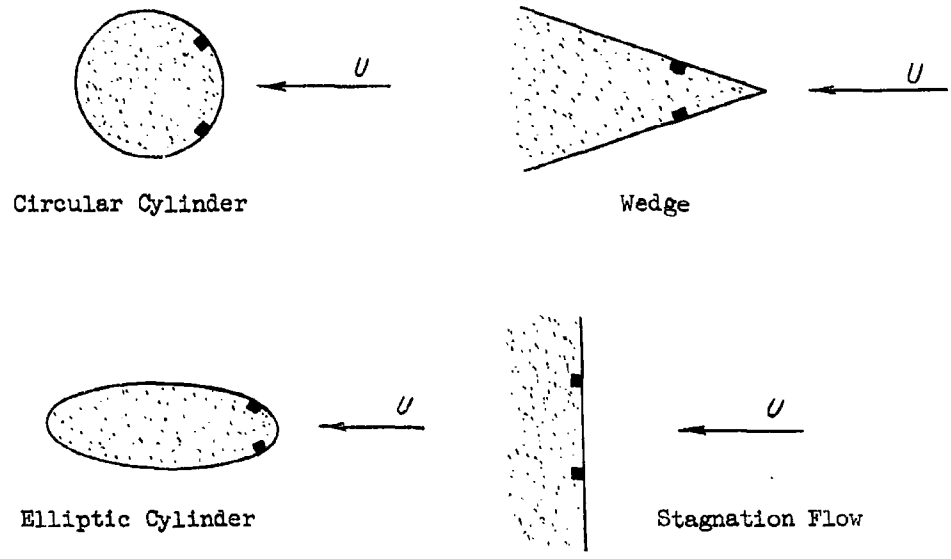

Figure 11.1 . Two-Dimensional Detector Heads for Flush-Type Electrodes

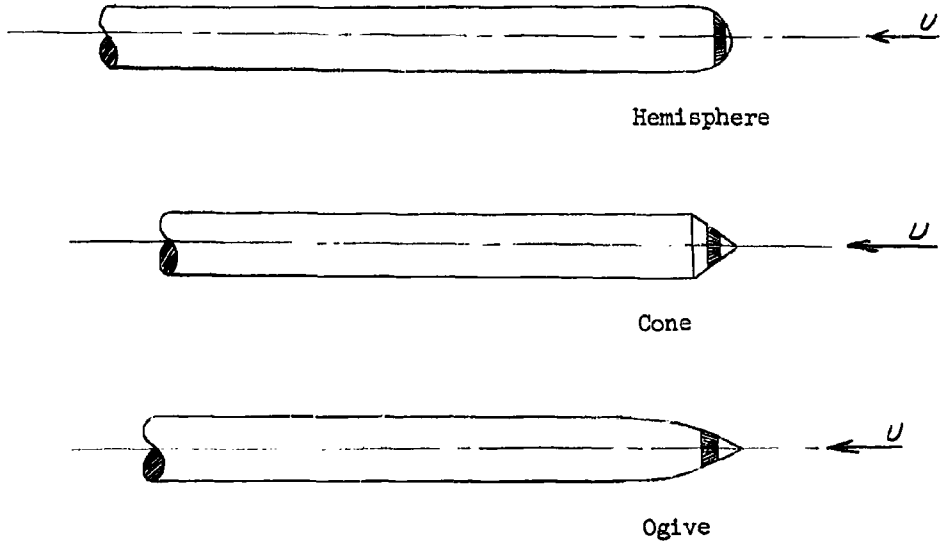

Figure 11.2 . Axisymmetric Probe Type Detector Heads

in uniform flow in which is placed a point source of another fluid. The resulting streamlined shape is rounded at the nose and assumes an almost constant stem diameter a short distance from the nose. Although the analysis given below is strictly true for a Rankine half-body, it is approximately valid for a rod terminated by a particular ellipsoid of revolution, in particular, a hemispherical tip. Since the Rankine probe shape is defined in an intrinsic way, only a single parameter (e.g. diameter) is necessary to specify its geometry fully. In spite of the fact that the velocity field can be expressed analytically in closed form, we will see that the details of this probe are somewhat complicated. This is in marked contrast with the simple shapes of the circular cylinder and wedge considered in the next Sections.

Potential Flow

The velocity field for axisymmetric flow about a rankine semi-infinite body is obtained by superimposing the fields of a point fluid source and a uniform stream (1,2). For flow from right to left as shown in Figure 11.3 , the velocity potential function, ϕ, and Stokes Stream Function, ψ, are

$$\phi = +Ur\cos\theta + \frac{Ua^2}{r}$$

$$\psi = +\frac{1}{2}Ur^2\sin^2\theta - Ua^2(1-\cos\theta),$$

where r is the radius from the point source, and a is the distance from the source to the stagnation point.

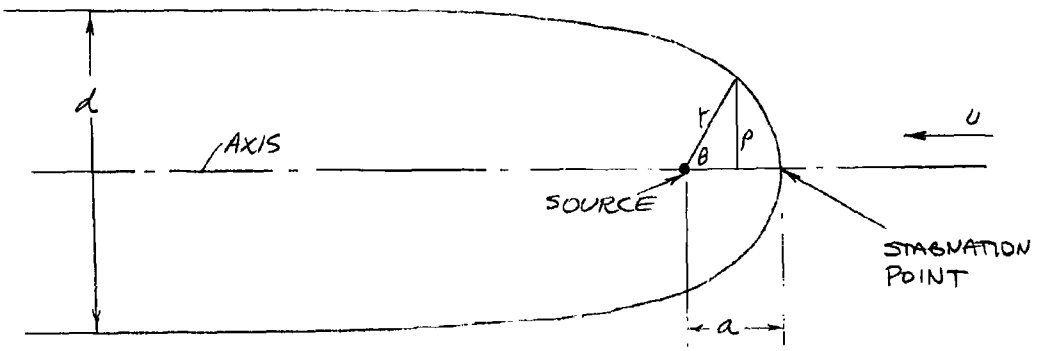

Figure 11.3 . Flow About a Rankine Semi-Infinite Solid

The radial and angular components of velocity are

$$u_r = -\frac{1}{r^2 \sin\theta}\left(\frac{\partial \psi}{\partial \theta}\right) = -\frac{\partial \phi}{\partial r} = -U\cos\theta + \frac{Ua^2}{r}$$

$$u_\theta = \frac{1}{r\sin\theta}\left(\frac{\partial \psi}{\partial \theta}\right) = -\frac{1}{r}\left(\frac{\partial \phi}{\partial \theta}\right) = +U\sin\theta .$$

The stagnation point where $u_r = u_\theta = 0$ obviously occurs where $\theta = 0$ and $r = a$. The streamline surface (ψ = const.) which passes through the stagnation point also corresponds to the shape of the probe body:

$$\psi = 0 = \frac{1}{2} U r^2 \sin^2\theta - Ua^2(1 - \cos\theta),$$

therefore the surface of the Rankine probe is described by

$$r = a \sec(\theta/2) .$$

On this surface the stream function is zero ($\psi_0 = 0$). The potential function at the stagnation point assumes the value $\phi_0 = 2Ua$. This surface can be traced by Rankine's method (3) or direct calculation from this equation. If $\rho = r\sin\theta$ is the distance from the axis, the equation of the surface is given by

$$\rho^2 = 2a^2(1 - \cos\theta) .$$

If $x = r\cos\theta$ is the distance along the axis, the surface is described in parametric form by

$$x = a\cos\theta \cdot \sec(\theta/2)$$

$$\rho = a\sin\theta \cdot \sec(\theta/2) .$$

These variables have been calculated for a range of values and are listed in Table 11.1 . At great distance from the stagnation point on the surface of the body, ($\theta \rightarrow \pi$) we see that the radius approaches $\rho = 2a$ and the constant a is related to the stem diameter by

$$a = \frac{d}{4} .$$

A curve of the Rankine surface is plotted in Figure 11.4 where it may be seen that the probe shape assumes the diameter d only a short distance from the nose. At a distance along the axis from the stagnation point

Table 11.1 . Rankine Body Functions

Degrees θ	$\left(\frac{x}{a}\right)$	(ρ/a)	$s^*(\theta)$	u/U	(ℓ/a)	$\left(\frac{s}{a}\right)$
0	1.000	0.0000	1.0000	0.0000	0.0000	0.0000
10	0.9886	0.1743	0.9973	0.1738	0.0114	0.1746
20	0.9542	0.3473	0.9960	0.3432	0.0458	0.3512
30	0.8966	0.5177	0.9914	0.5045	0.1034	0.5312
40	0.8152	0.6841	0.9845	0.6533	0.1848	0.7168
50	0.7093	0.8452	0.9754	0.7865	0.2907	0.9096
60	0.5774	1.0000	0.9639	0.9014	0.4226	1.113
70	0.4175	1.1472	0.9502	0.9955	0.5825	1.331
80	0.2267	1.2856	0.9333	1.068	0.7733	1.566
90	0.0000	1.4142	0.9136	1.118	1.0000	1.827
100	- 0.2701	1.5321	0.8904	1.146	1.270	2.122
110	- 0.5963	1.6383	0.8631	1.154	1.5963	2.466
120	- 1.000	1.7321	0.8313	1.146	2.000	2.880
130	- 1.521	1.8126	0.7943	1.124	2.521	3.408
140	- 2.240	1.8794	0.7550	1.095	3.240	4.148
150	- 3.346	1.9319	0.7016	1.059	4.346	5.236
160	- 5.412	1.9696	0.6438	1.029	6.412	7.302
170	-11.300	1.9925	0.5770	1.007	12.300	13.190
180	$-\infty$	2.0000	0.5000	1.000	∞	∞

(Continued) Table 11.1 . Rankine Body Functions

Degrees θ	(ℓ/d)	(ρ/d)	(s/d)	u/U
0	0.0000	.0000	0.0000	0.0000
10	0.0029	.0436	0.0437	0.1738
20	0.0115	.0868	0.0878	0.3432
30	0.0259	.1294	0.1328	0.5045
40	0.0462	.1710	0.1792	0.6533
50	0.0727	.2113	0.2274	0.7865
60	0.1057	.2500	0.2783	0.9014
70	0.1456	.2868	0.3328	0.9955
80	0.1933	.3214	0.3915	1.068
90	0.2500	.3536	0.4568	1.118
100	0.3175	.3830	0.5305	1.146
110	0.3991	.4096	0.6165	1.154
120	0.5000	.4330	0.7200	1.146
130	0.6303	.4532	0.8520	1.124
140	0.8100	.4699	1.037	1.095
150	1.087	.4830	1.309	1.059
160	1.603	.4924	1.826	1.029
170	3.075	.4981	3.298	1.007
180	∞	.5000	∞	1.000

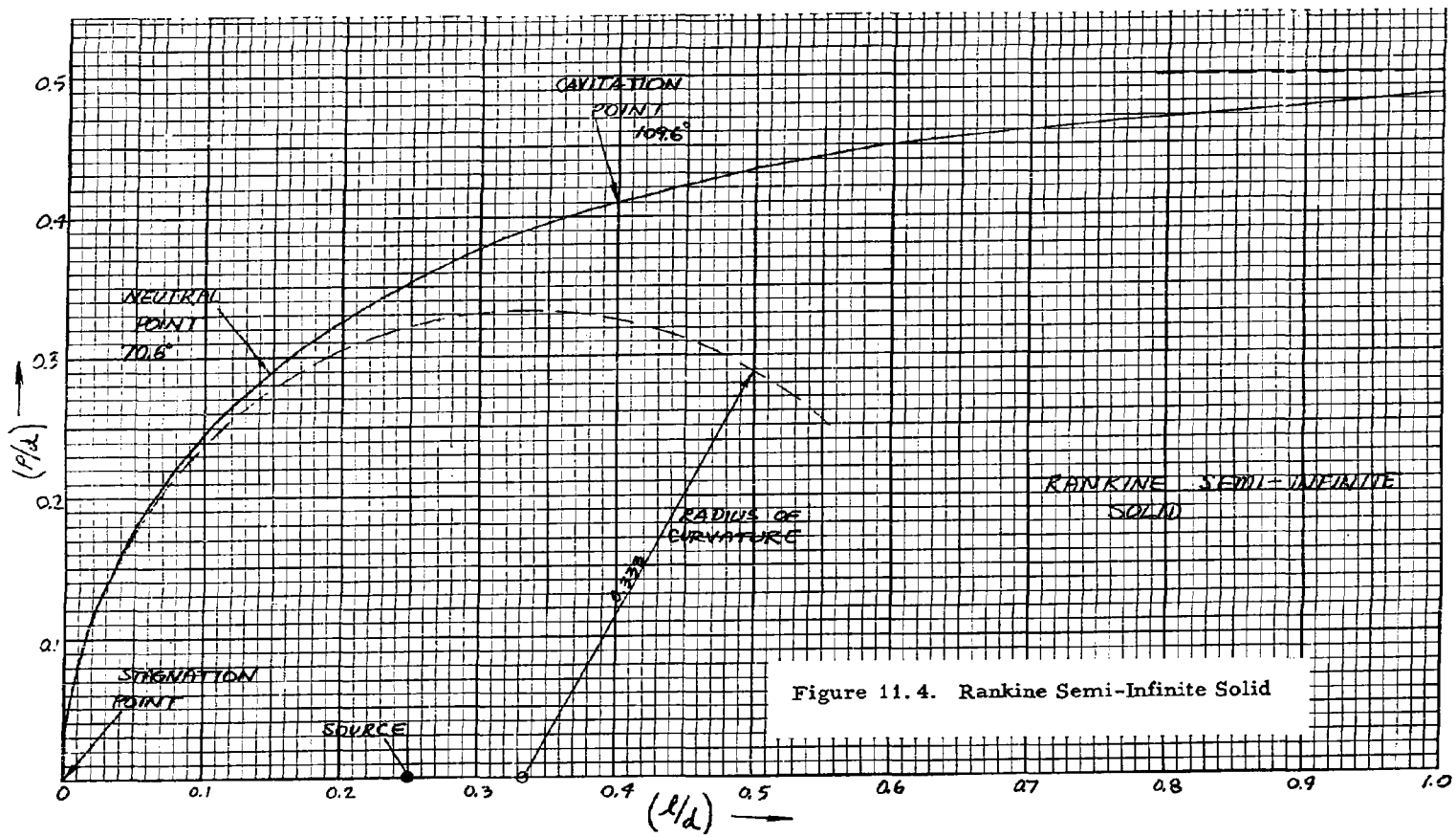

Figure 11.4. Rankine Semi-Infinite Solid

equal to the stock diameter (where $\theta = 147^{\circ}$) the probe diameter is already 96 % of the asymptotic value. The radius of curvature at the stagnation point is found by differentiation (4) to be $(4/3)a = \frac{1}{3} d$. The distance from the nose in the direction of flow (i.e. toward the stem of the probe) is denoted by ℓ:

$$\ell = a - x .$$

The theory of potential flow about a Rankine solid is most simply expressed in parametric form with θ as the parameter. It is sometimes more descriptive if the flow properties can be plotted as a function of arc length, s, along the surface from the stagnation point. The arc length for negative values is understood to be the distance along the axis up stream. Beginning with the expressions

$$r = a \sec(\theta/2)$$

and

$$\frac{ds}{d\theta} = r\left\{\frac{1}{r^2}\left(\frac{dr}{d\theta}\right)^2 + 1\right\}^{1/2}$$

and with some algebraic manipulation, the arc length is given in integral form by either

$$\frac{s}{a} = \int_0^{\tan(\theta/2)} \left(\frac{\mu^2+4}{\mu^2+1}\right)^{1/2} d\mu$$

or

$$\frac{s}{a} = 2\int_0^{\theta/2} \frac{\sqrt{1-k^2\sin^2\varphi}}{\cos^2\varphi}\, d\varphi \quad , \qquad k = \sqrt{\frac{3}{4}} ,$$

which can be reduced to integrals of elliptic form. For small θ the arc length is approximated by

$$s = 2a\tan(\theta/2)\left[1 - \frac{1}{8}\tan^2\left(\frac{\theta}{2}\right)\right],$$

which is a good approximation up to $\theta = \pi/2$. The integral expressed in terms of elliptic functions is (5)

$$\frac{s}{a} = 2\tan\left(\frac{\theta}{2}\right)\sqrt{1-\frac{3}{4}\sin^2\left(\frac{\theta}{2}\right)} + 2F\left(\frac{\theta}{2}, \sqrt{\frac{3}{4}}\right) - 2E\left(\frac{\theta}{2}, \sqrt{\frac{3}{4}}\right),$$

where $F(\varphi,k)$ and $E(\varphi,k)$ are elliptic integrals of the first and second kind of modulus k and amplitude φ. This function is tabulated in Table 11.1 ; also tabulated there is the function $s^*(\theta)$:

$$s = 2a \tan(\theta/2)\, s^*(\theta)$$

where

$$s^*(\theta) = \sqrt{1 - \tfrac{3}{4}\sin^2(\tfrac{\theta}{2})} + (F - E)\cot(\theta/2).$$

The arc length, s, is always greater than the distance along the axis from the nose but

$$\lim_{\theta \to \pi} (s - \ell) \approx 0.89\, a$$

The velocity on the axis ($\theta = 0$) is

$$\left(\frac{u}{U}\right) = 1 - \left(\frac{a}{r}\right)^2 \qquad (r \geq a)$$

and the velocity on the surface is

$$\left(\frac{u}{U}\right)^2 = \sin^2(\theta) + \sin^4\left(\frac{\theta}{2}\right)$$

or

$$\left(\frac{u}{U}\right) = 2 \sin(\theta/2) \sqrt{1 - 3/4 \sin^2(\theta/2)} \ .$$

This latter velocity distribution is tabulated in Table 11.1 and plotted in Figure 11.5 as a function of arc length. For comparison the surface and axial velocity for a sphere are:

$$\frac{u_{AXIAL}}{U} = 1 - (a/r)^3 \ , \quad (r \geq a)$$

$$\frac{u_{SURFACE}}{U} = 3/2 \sin\theta$$

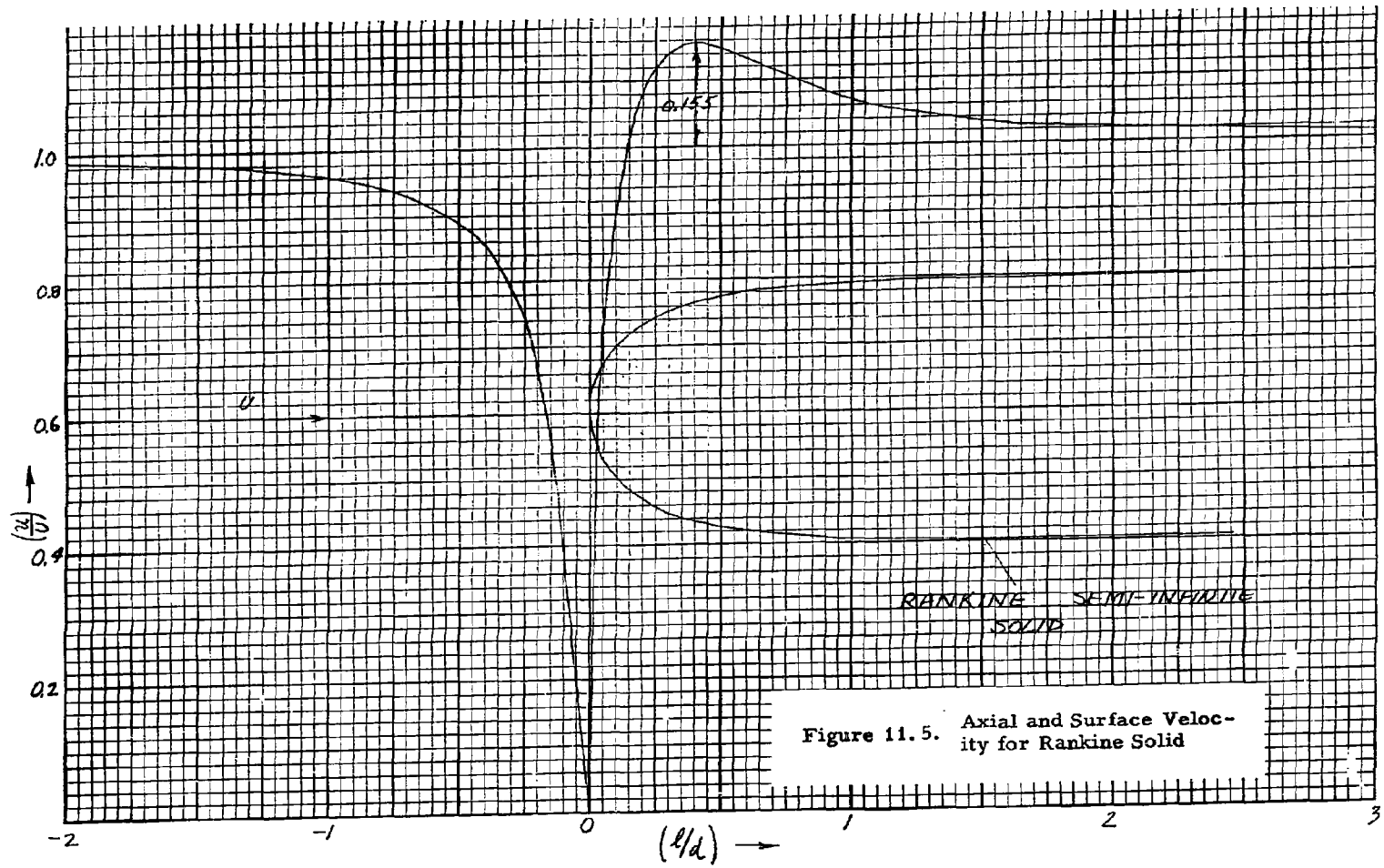

Figure 11.5. Axial and Surface Velocity for Rankine Solid

In order to relate some of the results of stagnation flow to the flow at the nose of a probe, we will be interested in the rate of change of the axial velocity with distance from the stagnation point. For a Rankine body it is (at r = a)

$$-\frac{du}{dr} = 2\left(\frac{U}{a}\right) = 8\left(\frac{U}{d}\right) .$$

For a sphere it is

$$-\frac{du}{dr} = 3\left(\frac{U}{a_s}\right) = 6\left(\frac{U}{d_s}\right) ,$$

where, here, a_s and d_s are the radius and diameter of the sphere, respectively. The sphere with the same velocity in the stagnation flow region as a Rankine half-body is that one for which

$$8\left(\frac{U}{d}\right) = 6\left(\frac{U}{d_s}\right)$$

or

$$d_s = \left(\frac{3}{4}\right) d .$$

There are four points of interest on the surface of the Rankine body. 1) The stagnation point where the velocity is zero and the pressure equal to the ambient plus dynamic pressure $1/2\ \rho U^2$, 2) The "neutral point" where the velocity and pressure assume the ambient or free stream values, 3) The "cavitation point" where the velocity is a maximum and the pressure a minimum, and 4) The transition point where the flow becomes turbulent. The stagnation point, of course, occurs at the nose. The neutral point occurs where

$$2\sin^2(\theta/2)\left\{1 - \frac{3}{4}\sin^2(\theta/2)\right\} = 1$$

or

$$3\sin^4(\theta/2) - 4\sin^2(\theta/2) + 1 = 0$$

which has two solutions

$$\sin(\theta/2) = 1 , \quad \theta = \pi$$

and

$$\sin(\theta/2) = 1/\sqrt{3} \quad , \qquad \theta = 70.6^{\circ} \; .$$

The latter value is the one of interest and occurs at $s \approx a(1.34)$. The cavitation point occurs where u is a maximum or where

$$\frac{du}{d\theta} = 0 \; .$$

This applies when

$$\sin(\theta/2) = \sqrt{2/3}$$

or

$$\theta = 109.3^{\circ} \; , \qquad s = a(2.43) \; .$$

At this point the velocity assumes the value

$$u_{max} = \frac{2}{\sqrt{3}} \; U \; ,$$

so that the theoretical cavitation number, σ, of the Rankine body is (6) (local underpressure coefficient).

$$\sigma = \frac{4}{3} = 1.33 = \left(\frac{u_{max}}{U}\right)^2 .$$

The transition point is considered later as a special topic related to turbulent flow.

In connection with the directional response, it is of interest to study the yaw flow about a Rankine body. This problem is complicated but can be analysed by the distributed dipole source method of Von Kármán (7).

Boundary Layer

The thickness of the velocity boundary layer on a Rankine solid has not been calculated, however, methods are available for carrying out this calculation (8,9). The lengthwise boundary layer for a thin cylinder has been treated by Glauert and Lighthill (10).

Transition Point

Because of the favorable pressure gradient at the nose of the Rankine probe, the transition point from laminar to turbulent flow occurs beyond

the neutral point ($\theta = 71^\circ$). The location of this point has not been calculated but methods for this purpose are available (11).

11.3 Cylinder

A cylinder constitutes one of the simplest shapes as a detector head for one or several individual electrodes. The cylinder has the practical advantage of being a convenient shape for construction purposes. The pertinent hydrodynamic properties of a cylinder for flow perpendicular to its axis are now considered.

Potential Flow

The incompressible flow about the cylinder of diameter d illustrated in Figure 11.6 is described by the potential function, ϕ, and stream function, ψ, as follows (12)

$$\phi = U\left(r + \frac{a^2}{r}\right)\cos\theta$$

$$\psi = U\left(r - \frac{a^2}{r}\right)\sin\theta$$

where $a = d/2$ is the radius of the cylinder. The free-stream flow is perpendicular to the axis of the cylinder. The radial and angular velocity components are

$$u_r = -\frac{\partial\phi}{\partial r} = -U\left[1 - \left(\frac{a}{r}\right)^2\right]\cos\theta$$

$$u_\theta = -\frac{1}{r}\left(\frac{\partial\phi}{\partial\theta}\right) = +U\left[1 + \left(\frac{a}{r}\right)^2\right]\sin\theta .$$

At the stagnation point $\phi_0 = 2Ua$, and $\psi_0 = 0$. The velocity on the plane $\theta = 0$ is

$$\left(\frac{u}{U}\right) = 1 - \left(\frac{a}{r}\right)^2$$

and on the surface $r = a$

$$\left(\frac{u}{U}\right) = 2\sin\theta .$$

At the stagnation point
$(r = a, \theta = 0)$

$$\frac{du}{dr} = -2\left(\frac{U}{a}\right) = -4\left(\frac{U}{d}\right) .$$

The neutral point, where the velocity and pressure assume the free stream value, occurs at

$$\sin\theta = 1/2 \quad \text{or} \quad \theta = 30^{\circ} .$$

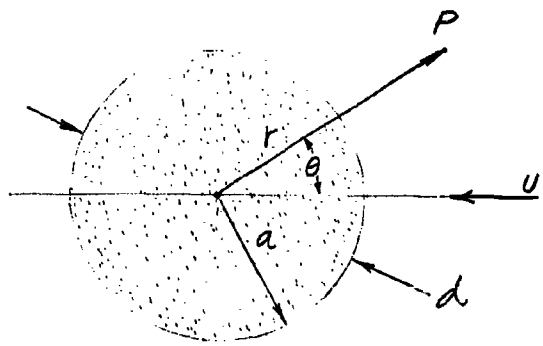

Figure 11.6 . Flow About a Cylinder

The cavitation point where the velocity is a maximum and the pressure a minimum occurs at $\theta = 90^{\circ}$ where $u_{max} = 2U$ and the theoretical cavitation number (underpressure coefficient is (6)

$$\sigma = \left(\frac{u_{max}}{U}\right)^2 = 4 .$$

If two sensing elements are located at $\theta = \pm \theta_1$ and the cylinder is rotated at an angle α from its steady state position, the difference in velocity Δu, at the two sensors is

$$\frac{\Delta u}{U} = 2\left\{\sin(\theta_1 - \alpha) - \sin(\theta_1 + \alpha)\right\}$$

or

$$\frac{\Delta u}{U} = 4\cos\theta_1 \cdot \sin\alpha \approx 4\alpha\cos\theta_1 . \quad (\alpha < 1)$$

If both sensors are on the same side, no difference in velocity is experienced between the elements for variations in α.

Boundary Layer

The thickness of the boundary layer on a cylinder is given in Table 11.2 in dimensionless form as a function of angular distance along the surface (13). The velocity profiles cannot be expressed in similarity form, but change shape with distance from the stagnation point. The quantity η is refined by

$$\eta = \frac{y}{a}\sqrt{\frac{Ua}{\nu}} ,$$

where y is the distance normal to the surface. The rate of change of velocity with distance from the surface is characterized by the value η_s which satisfies

$$\frac{du}{d\eta} = \frac{U}{\eta_s} \quad ;$$

the displacement thickness is denoted by η^*

$$\eta^* = \int_0^\infty \left(1 - \frac{u}{U}\right) d\eta \quad ;$$

and η_{99} denotes the thickness where the velocity differs by only 1 % of the potential flow value.

Table 11.2 . Boundary Layer Thickness for Flow Past a Cylinder

(Degrees) θ	η^*	η_s	η_{99}	$\left(\frac{Ua}{\nu}\right)_{min}$
0	0.43	0.62	1.46	1850
10	0.45	0.66	1.53	2030
20	0.47	0.70	1.60	2210
30	0.49	0.75	1.67	2400
40	0.51	0.81	1.75	2600
50	0.53	0.87	1.83	2810
60	0.55	0.94	1.93	3020
70	0.60	1.03	2.04	3600
80	0.68	1.16	2.17	4620
90	0.84	1.41	2.34	7050

The relative thickness of the boundary layer with respect to the electrode size, and the relative size of the electrode with respect to the size of cylinder are the pertinent factors which must be considered in the design of cylindrical head with flush type electrodes. If b is the radius of the sensing electrode, define a ratio m such that

$$m = \frac{a}{b} \quad ,$$

where a is the radius of the cylinder. This ratio should be as large as conveniently possible, and in practice should be of the order of 10 if the

electrode is operated so that it can be considered a flush type. If y^* is the displacement thickness of the boundary layer, define the ratio n such that

$$n = \frac{b}{y^*} \quad .$$

This quantity should be large to avoid the limitations associated with boundary layer flow (Sec. 14.4); it should be of the order of ten or greater. Combining these expressions we obtain a constraint which depends only on the flow about the cylinder, viz.,

$$mn = \frac{a}{y^*} \quad ,$$

which should be comparable or greater than 100. This condition implies

$$mn = \frac{1}{\eta^*} \sqrt{\frac{aU}{\nu}}$$

where

$$y^* = a\eta^* \sqrt{\frac{\nu}{aU}} \quad .$$

A condition is thus established on the minimum value of the Reynolds number (Ua/ν) as a function of position on the surface of the cylinder; for mn = 100 this condition is

$$R_{min} = \left(\frac{Ua}{\nu}\right)_{min} = 10^4(\eta^*)^2 \quad ,$$

which is listed in Table 11.2 . As an example, suppose a cylinder of 4" diameter (10 cm) is being considered for a detector head for research at speeds less than 100 knots. The value of mn as a function of Θ and U is shown in Figure 11.7 , where it is seen that the head becomes unsuitable for measurements ($mn < 100$) at speeds of the order of 0.1 knots if the electrodes are mounted at an angle of 30°.

Transition Point

Because of the favorable pressure gradient on the forward side of the cylinder, the turbulence transition point does not occur on the forward side and occurs at approximately $\Theta = 90^\circ$ over a wide range of Reynolds

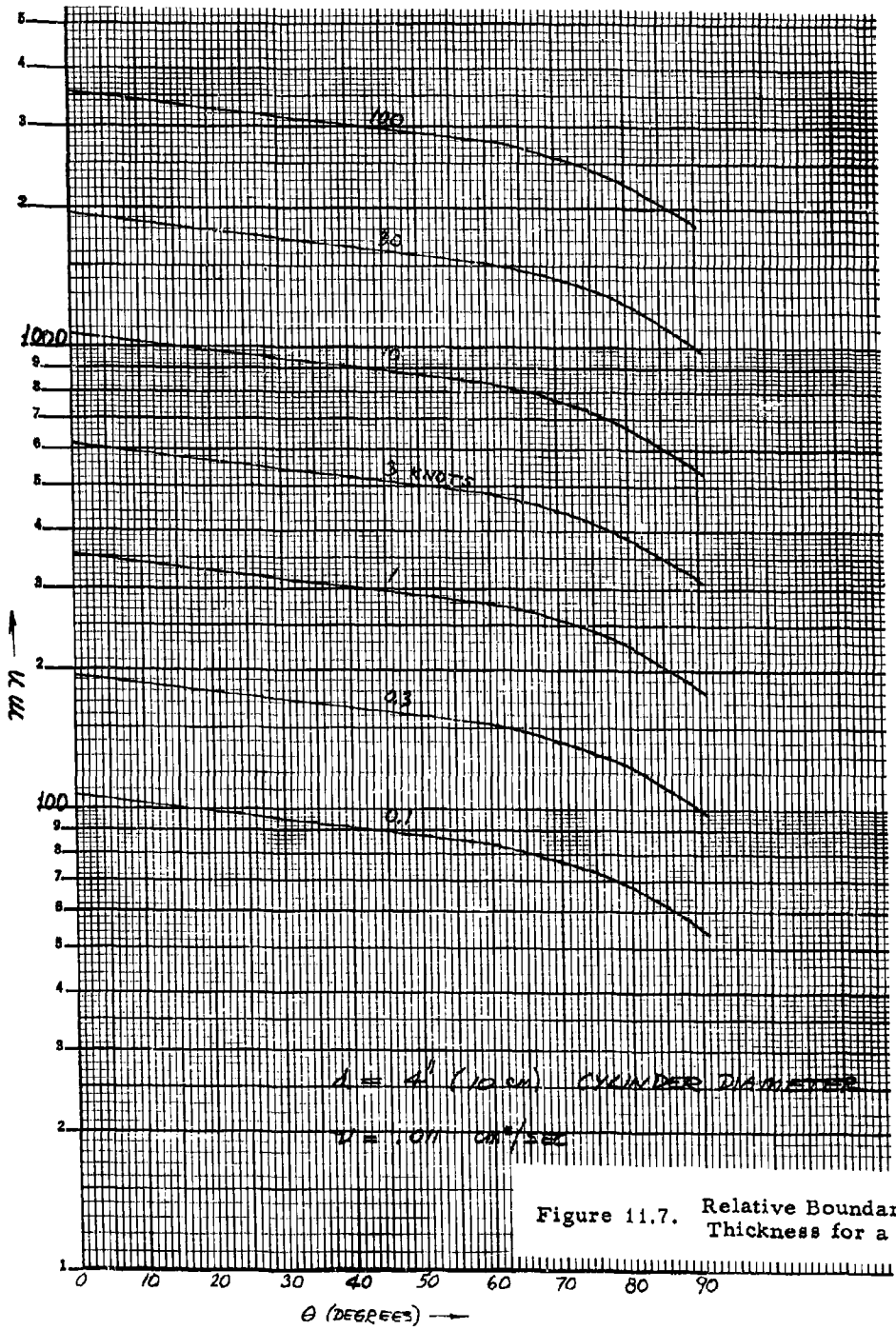

Figure 11.7. Relative Boundary Layer Thickness for a Cylinder

numbers (14). This situation is illustrated in Figure 11.8 where the angle θ_x, at which transition occurs, is plotted against the Reynolds number based on the cylinder radius. Also plotted there are the curves mn = 100, 1000. The allowed region for the location of an electrode is to the right of the curve mn = 100 which sets the minimum Reynolds number based on boundary layer thickness; and at angles less than θ_x where the flow is laminar. As an example, the dotted curve of Figure 11.8 refers to a 4" cylinder with an electrode at 30° for speeds from 0.1 knot to 100 knots. Such an electrode is well removed from the turbulent region of the cylinder over the entire velocity range.

11.4 Wedge

The flow about a wedge is similar in several respects to that of a flat plate, and the angular region between the faces provides space required for connections and placement of flush type electrodes. A notable difference between flat plate and wedge flow is the delay of the turbulence transition point in the case of the wedge due to a favorable pressure gradient. The properties of flow about a wedge are considered below.

Potential Flow

The flow about a wedge at zero angle of attack is described by Laplace's equation for the wedge shaped boundary (15). By complex variable techniques it may be shown that the radial and angular components of the velocity field are

$$u_r = - Uk\left(\frac{r}{\ell}\right)^m \cos (m + 1)\,\theta$$

$$u_\theta = + Uk\left(\frac{r}{\ell}\right)^m \sin (m + 1)\,\theta$$

where kU is the velocity on the plane of symmetry ($\theta = 0$) at a distance ℓ upstream from the leading edge, and m is a parameter given by

$$\beta = \frac{2m}{m + 1} ,$$

and $\beta\pi$ is the wedge angle as shown in Figure 11.9 . The constant k is a pure number of the order of unity to be described later. Stagnation flow corresponds to $\beta = 1$ ($m = 1$) and flow along a flat plate to $\beta = 0$ ($m = 0$). The magnitude of the velocity at the radius r is independent of θ:

$$u = \left(u_r^2 + u_\theta^2\right)^{1/2} = Uk\left(\frac{r}{\ell}\right)^m .$$

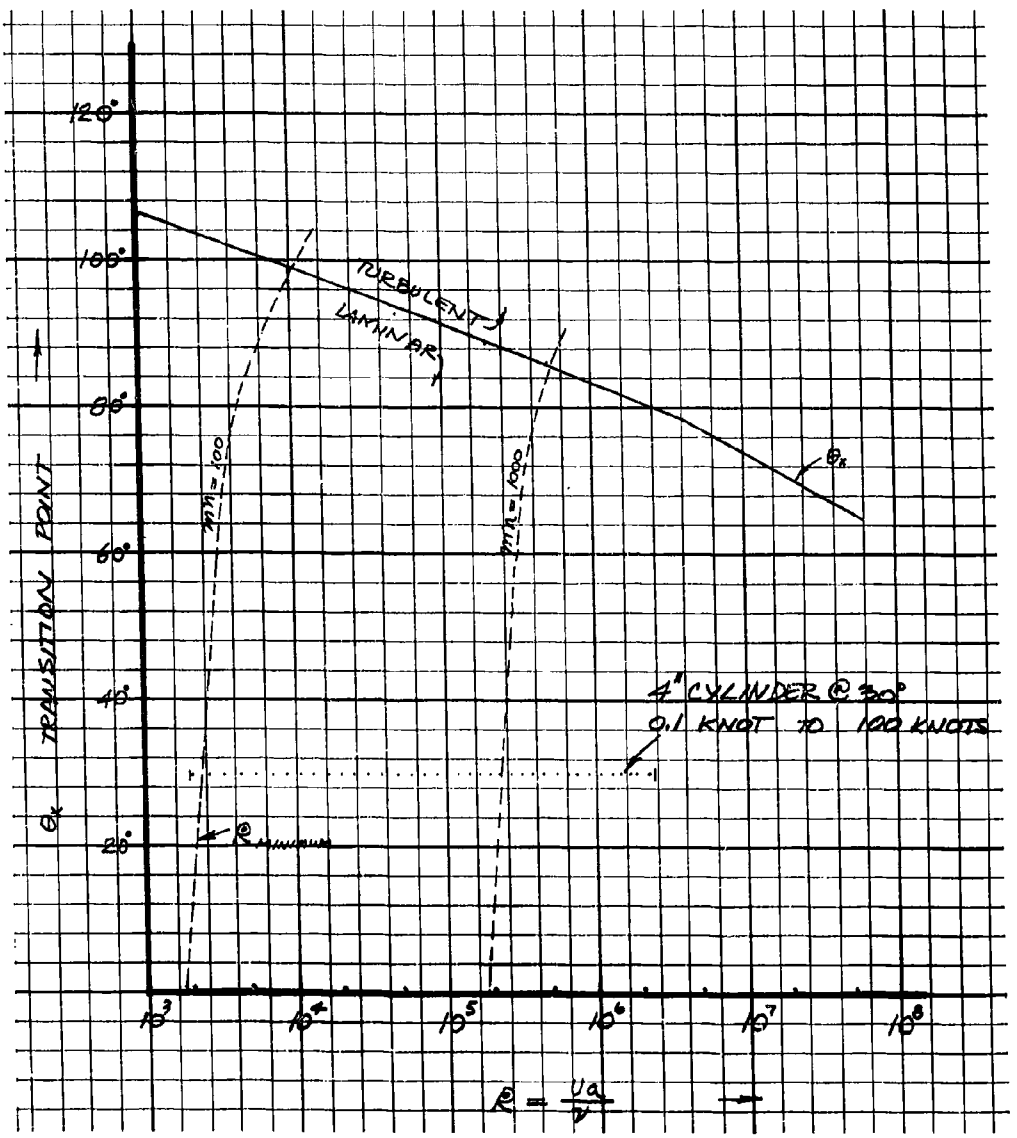

Figure 11.8. Turbulence Transition Point for a Cylinder

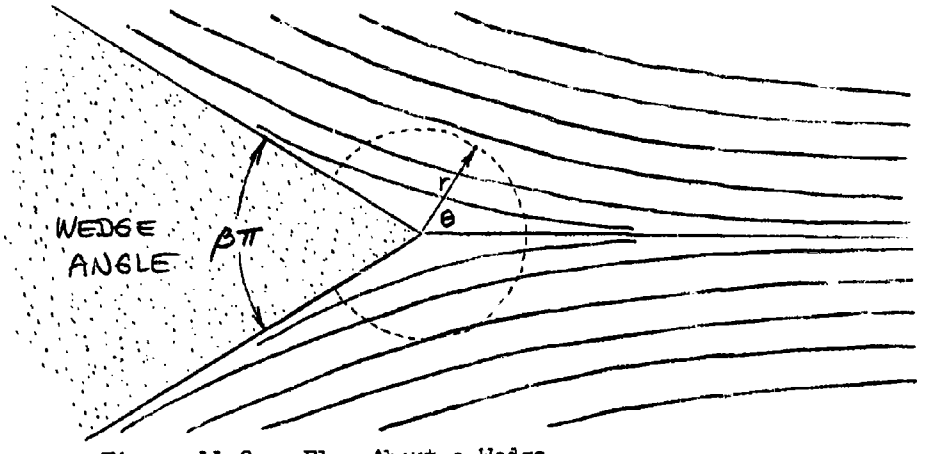

Figure 11.9 . Flow About a Wedge

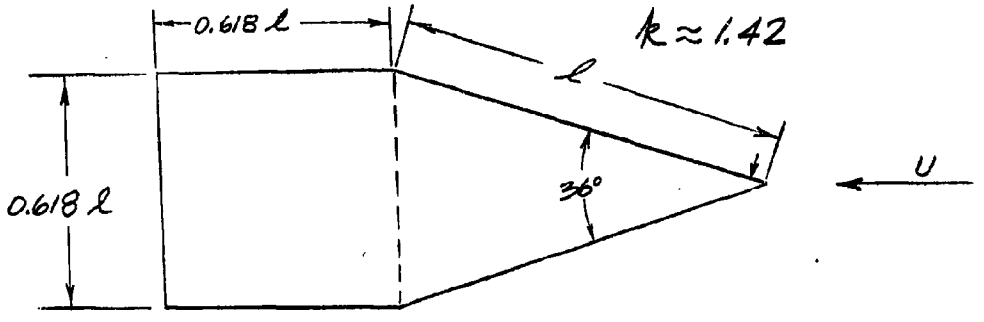

Figure 11.10. Finite Wedge with Square Base

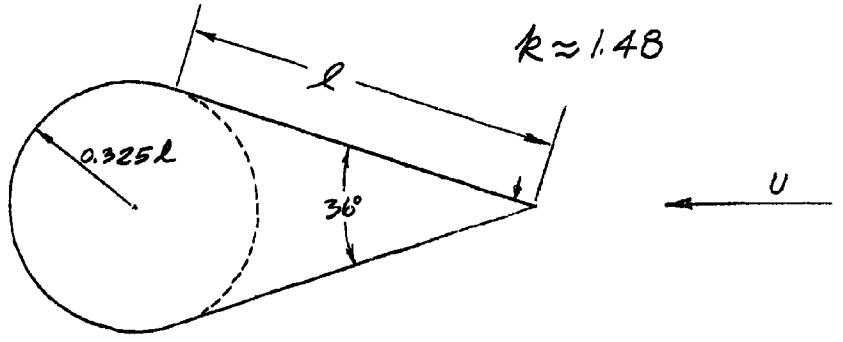

Figure 11.11. Finite Wedge with Circular Base

This represents, therefore, the velocity on the wedge surface and plane of symmetry.

The above expressions assume a wedge of infinite extent. As a result, the velocity becomes indefinitely large (for $m > 0$) at great distance from the edge. For a detector head of finite size with a wedge shaped leading edge this is of course, not so. The above velocity field does apply in the vicinity of the edge, and the constant k can be selected so that U corresponds to the free stream velocity at great distance from the detector head. If we consider the two finite wedge shapes of 36° wedge angle shown in Figure 11.10 and Figure 11.11, and let the length ℓ represent the length of the wedge face, then the constant k is about 1.42 for the square base and 1.48 for the round base. These constants are most readily obtained by the resistance-paper plotting method for solving two dimensional potential problems (16). In the case of the finite wedge with the square base, the side of the square was chosen equal to the base of the isosceles triangle of angle $\beta\pi$,

$$\text{side} = 2\ell \sin\left(\beta \frac{\pi}{2}\right) .$$

In the case of the finite wedge with a circular base, the circle was chosen to be tangent to the faces of the wedge so that its radius is

$$\text{radius} = \ell \tan\left(\beta \frac{\pi}{2}\right) .$$

The stagnation point on the wedge at the leading edge is degenerate for an infinitely sharp wedge and usual stagnation flow results cannot be used there unless a finite rounded edge is assumed. The neutral point where the velocity and pressure assume free stream values has meaning only for a finite wedge and occurs at about $(.035)\ell$ from the leading edge of the finite wedges of Figure 11.10 and Figure 11.11 as indicated by the small arrows in these Figures. The cavitation point on the wedges occurs soon after the transition from the wedge face to the base shape.

The flow about other types of finite wedges are given in References (17,18).

Table 11.3 . Wedge Functions

Wedge Angle	β	m	ξ^*	ξ_s	ξ_{99}	$R_x(\beta)$
0	0	0	1.72	3.02	5.14	660
36°	0.2	.111	1.33	2.08	4.16	3200
90°	0.5	.333	0.99	1.44	3.59	6600
180°	1	1	0.65	0.80	2.45	12600

Boundary Layer

The boundary layer velocity profiles for (infinite) wedge flow can be expressed in similarity form with the parameter

$$\eta = y \sqrt{\frac{m+1}{2}} \cdot \sqrt{\frac{u(r)}{\nu r}} \quad ,$$

where y is the distance normal to the wedge surface, and u(r) is the velocity on the surface corresponding to potential flow at a distance r from the leading edge. Define another parameter, ξ, such that

$$\eta \sqrt{\frac{2}{1+m}} = \xi = y \sqrt{\frac{u(r)}{\nu r}} \quad .$$

The rate of change of the boundary profile velocity with distance from the wall is characterized by the value ξ_s:

$$\frac{du(r)}{d\xi} = \frac{u(r)}{\xi_s} \quad .$$

The displacement thickness, ξ^*, of the boundary layer is

$$\xi^* = \int_0^\infty \left(1 - \frac{u}{u(r)}\right) d\xi .$$

The distance from the wedge face where the velocity differs by only 1 % from the potential theory value is denoted by ξ_{99}. The three measures of the boundary layer thickness are listed in Table 11.3 for several values of wedge angle (19).

The thickness of the boundary layer based on the displacement thickness y^* relative to the typical radius of the sensing electrode, b, mounted on the face of the wedge is denoted by n:

$$n = \frac{b}{y^*} \quad ,$$

and should be of the order of 10 or greater to minimize the undesirable effects associated with boundary layer flow (Sec. 14.4). The extent of the wedge face, ℓ, with respect to the diameter of the electrode, 2b,

is denoted by m:

$$m = \frac{\ell}{2b} \quad ,$$

and should be large, say, of the order of 10. Combining these factors, we arrive at a constraint which depends only on the flow properties

$$mn = \frac{\ell}{2y^*} = \frac{\ell}{2\xi^*} \sqrt{\frac{u(r)}{\nu r}} \quad .$$

This can be rewritten as

$$mn = \frac{\sqrt{k}}{2\xi^*} \left(\frac{\ell}{r}\right)^{\frac{1-m}{2}} \sqrt{\frac{U\ell}{\nu}} \quad ,$$

where use has been made of the relation

$$u(r) = kU \left(\frac{r}{\ell}\right)^m \quad .$$

A minimum value for mn is about 100 to insure satisfactory performance. The corresponding minimum value of Reynolds number is

$$R_{min} = \left(\frac{U\ell}{\nu}\right)_{min} = 4 \times 10^4 \left(\frac{\xi^{*2}}{k}\right)\left(\frac{r}{\ell}\right)^{1-m} \quad .$$

These minimum values are listed in Table 11.4 as a function of position (r/ℓ) of the electrode on the wedge face for a 36° wedge with k = 1.5, m = 0.111 and $\xi^* = 1.33$. The above relation of mn vs. (r/ℓ) is plotted in Figure 11.12 for a 36° finite wedge for which the value of k = 1.5 is assumed. The length of the wedge face (ℓ) is taken to be 4" (10 cm) and the velocity covers the range from 0.1 knot to 100 knots. It is seen that the wedge shaped detector head is not suitable ($mn < 100$) for velocities below 0.3 knots for an electrode placed at $r/\ell = 0.3$.

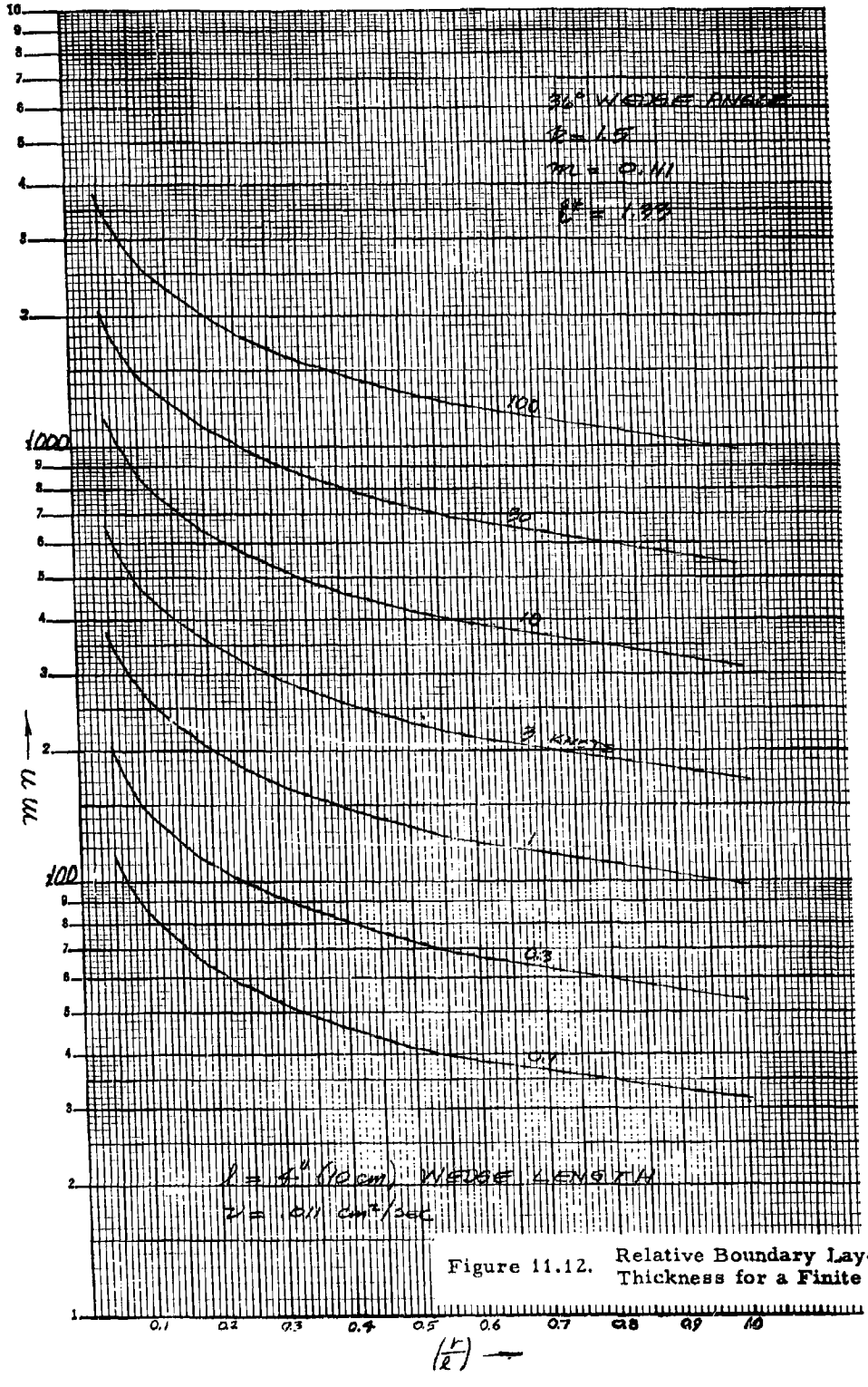

Figure 11.12. Relative Boundary Layer Thickness for a Finite Wedge

Table 11.4 . Minimum Reynolds Number for mn = 100 and 36° Wedge Angle with k = 1.5

(r/ℓ)	$\left(\frac{U\ell}{\nu}\right)_{\text{minimum}}$
0.1	6,150
0.2	11,400
0.3	16,300
0.4	21,100
0.5	25,600
0.6	30,200
0.7	34,600
0.8	38,900
0.9	43,200

Transition Point

The point on the surface of a wedge where the flow becomes turbulent is farther removed from the leading edge the greater the wedge angle because of the more favorable pressure gradient. In particular the transition point on a wedge ($\beta \neq 0$) occurs later than that on a flat plate. Flow stability calculations by Pretch (20) yield the result

$$\frac{u(r)\, y^*}{\nu} = R_x(\beta) \quad ,$$

where $R_x(\beta)$ is a critical Reynolds number based on the displacement boundary layer thickness which is a function of the wedge angle and determines the point at which the flow becomes turbulent. The number $R_x(\beta)$ is listed in Table 11.3 for several wedge angles. Substituting the relations

$$y^* = \xi^* \sqrt{\frac{\nu r}{u(r)}}$$

and

$$u(r) = kU\left(\frac{r}{\ell}\right)^m \quad ,$$

we obtain the critical Reynolds number based on the length ℓ and the position of the transition (r/ℓ):

$$\left(\frac{r}{\ell}\right)_x^{m+1}\left(\frac{\ell U}{\nu}\right)_x = \frac{1}{k}\left(\frac{R_x}{\xi^*}\right)^2$$

This proves to be of no practical importance as a constraint on the head design. For 36° wedge angle and $k = 1.5$ and $r = \ell$ we have

$$\left(\frac{\ell U}{\nu}\right)_x = \frac{1}{k}\left(\frac{R_x}{\xi^*}\right)^2 = 3.9 \times 10^6 \quad .$$

At 100 knots, the length ℓ is 7.5 cm (3"); thus, even in this extreme case the length of the wedge face is not small.

11.5 Electrode Position

The optimum position of an electrode on a detector head depends on whether the sensor is used for conductivity (temperature, or salinity) or velocity measurements. These two cases are considered separately.

A conductivity detector is least subject to noise associated with turbulence (by the heating effect) if the average velocity over the electrode volume is high. Therefore, for a given free stream velocity, U, the electrode should be placed where the surface velocity on the detector head is highest, i.e., at the cavitation point. Opposing this consideration is the requirement that the electrode be removed as far as possible from the region on the head where the flow becomes turbulent (transition point). This is accomplished by moving the electrode forward towards the stagnation point where a favorable pressure gradient exists for maintaining the stability of the flow. Another consideration is the thickness of the boundary layer which should be thin in comparison with the size of the electrode. This, again, is accomplished if the electrode is moved forward where the boundary layer is thinnest. The variation of boundary layer thickness, over the surface is, however, not large. A compromise of the above considerations suggests positioning the electrode about half-way between the stagnation point and the transition point. Usually this is in the vicinity of the neutral point where the surface velocity equals the free stream velocity.

A velocity detector is least subject to conductivity fluctuations (due to temperature or salinity fluctuations) if the electrode is operated at high average temperature rise ($\overline{\Delta T}$ large). If the power to the electrode is limited by other considerations and the electrode boiling point has not been reached, a large temperature rise is obtained by moving the electrode to a position on the detector head where the velocity is lowest. This calls for placing the electrode in the vicinity of the stagnation point. This position is also favorable from the standpoint of boundary layer thickness and distance from the turbulent flow region. A difficulty with placing the electrode right at the stagnation point is the large variation

in velocity over the sensitive volume of the electrode so that a hot spot within this volume occurs which causes a lower limiting average electrode temperature and, consequently, a lower velocity sensitivity. Thus, the optimum electrode position for the velocity detector is close to the stagnation point (comparable with the electrode dimensions) but not centered on the stagnation point.

12. HEATING EFFECT

The operation of the probe to detect the velocity of the medium (U-meter) depends on the electrical heating of the fluid as it passes through the electrode volume. This heating effect is investigated in greater detail in this Section and involves the process of internal heat generation and heat transfer in the electrode volume. Relatively simple special cases are analysed to study these complicated processes independently.

12.1 Elementary Heating

We consider now the simplest case of the heating effect, illustrative of the process in a general electrode.

The simplest electrode geometry is that of parallel plates with a uniform field between the plates. We assume fringe field effects are zero. The geometry is shown in Figure 12.1 , the velocity is assumed to be constant in time and uniform over the field of the electrode and parallel to the length side (ℓ) which is the x-axis. Boundary layer effects are neglected. The volume, $\mathcal{V}_o$, of the electrode is

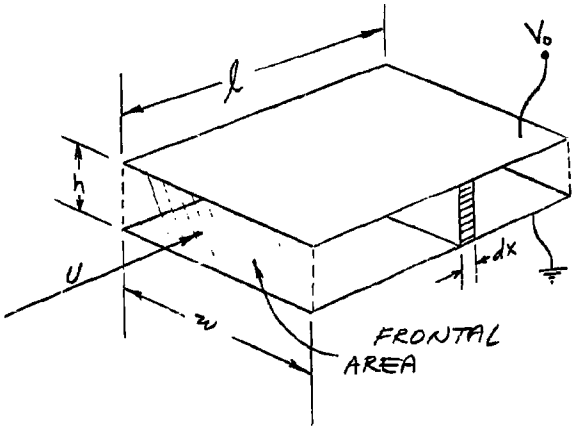

Figure 12.1 . Parallel Plate Electrode

$$\mathcal{V}_o = \ell w h \quad ,$$

and the area of the electrode is

$$S = \ell w \quad .$$

The "frontal area," A, of this geometry is the projected area of the field volume on a plane perpendicular to the x-axis:

$$A = hw \quad .$$

The resistance of the electrode, R, is

$$R = \frac{h}{\sigma \ell w} \quad .$$

The power, P, dissipated in the water is

$$P = \frac{V_o^2}{R} \quad ,$$

where V_o is the applied rms voltage. The resultant Joule heating causes an increase in temperature of the water as it moves through the electrode volume. The power per unit volume, P_v, (i.e., the power density) is

uniform throughout the sensing volume:

$$P_v = \frac{P}{\ell wh} \quad .$$

Consider a small incremental volume, dv, of thickness dx and area A = hw moving at speed U through the electrode:

$$dv = A dx \quad ,$$

the rate at which heat energy is dissipated in this volume is

$$P_v dv = \frac{P}{\ell} dx = c\left(\frac{dT}{dt}\right) dv \quad ,$$

where c is the heat capacity per unit volume of the water and (dT/dt) is the rate of temperature rise of the water. Since dx/dt = U, we have

$$\frac{dT}{dx} = \frac{P}{\ell cAU} \quad ,$$

or integrating with respect to x

$$T(x) = \left(\frac{P}{cAU}\right)\left(\frac{x}{\ell}\right) \quad .$$

Thus, the temperature (relative to ambient) increases linearly from zero to its maximum value (at $x = \ell$) called the "exit temperature rise," ΔT, given by

$$\Delta T = \frac{P}{cAU} \quad .$$

This situation is illustrated in Figure 12.2 . This is the fundamental

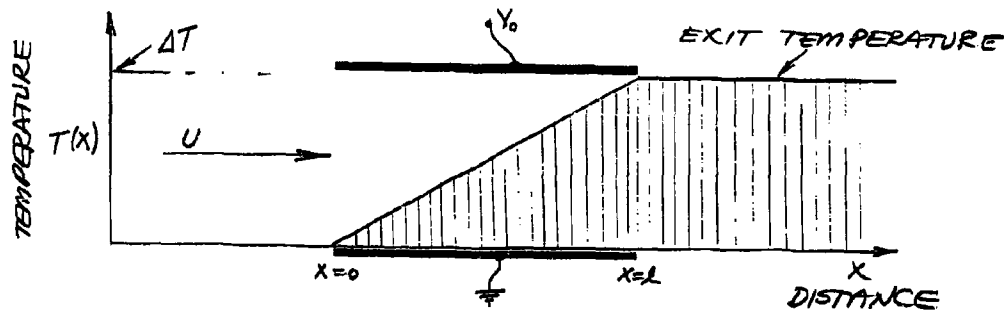

Figure 12.2 . Temperature Rise in Electrode Field

equation for the heating effect. The average temperature, $\overline{\Delta T}$, in the field of the electrode is half this value:

$$\overline{\Delta T} = \frac{1}{2} \Delta T \quad .$$

As a numerical example, consider sea water flowing at 3 knots through electrodes with a 1 mm x 1 mm frontal area into which 10 watts of electrical power is being dissipated:

$$U = 3 \text{ knots} = 154 \text{ cm/sec}$$
$$c = 4.09 \text{ joule/cm}^3/^\circ\text{C}$$
$$A = (1 \text{ mm})^2 = 0.01 \text{ cm}^2$$
$$P = 10 \text{ watts}$$

then
$$\Delta T = 1.6 \ ^\circ\text{C}$$

and
$$\overline{\Delta T} = 0.8 \ ^\circ\text{C} \quad .$$

It is clear that a great deal of power is necessary to heat water even a small amount and this only at relatively low velocities and in small electrodes.

Curves of the heating equation

$$\Delta T = \frac{P}{cAU} = 2\overline{\Delta T}$$

are plotted in Figures 12.3a and 12.3b . Two graphs are necessary because of the number of variables involved and the power per unit area, (P/A), is used as a parameter to couple the two graphs. The graphs apply to pure water ($c = 4.18$ joule/cm^3/$^\circ$C) but may be used only with slight error for sea water ($c = 4.09$ joule/cm^3/$^\circ$C). For example, if 1 watt is dissipated in an electrode of 3 mm frontal dimension ($\sqrt{A}$), Figure 12.3a indicates the power per unit area is 12 watts/mm^2. Figure 12.3b indicates that if it is moving through the water at 10 knots, the exit temperature rise is 0.54 $^\circ$C. The average electrode temperature rise is half this value: 0.27 $^\circ$C.

12.2 General Electrode

The heating equation for a general electrode configuration is now considered. The analysis of such an electrode is reduced to the specification of several parameters of the electrode geometry which serve to characterize its properties with respect to the heating effect. An illustration of the temperature distributions due to electrical heating

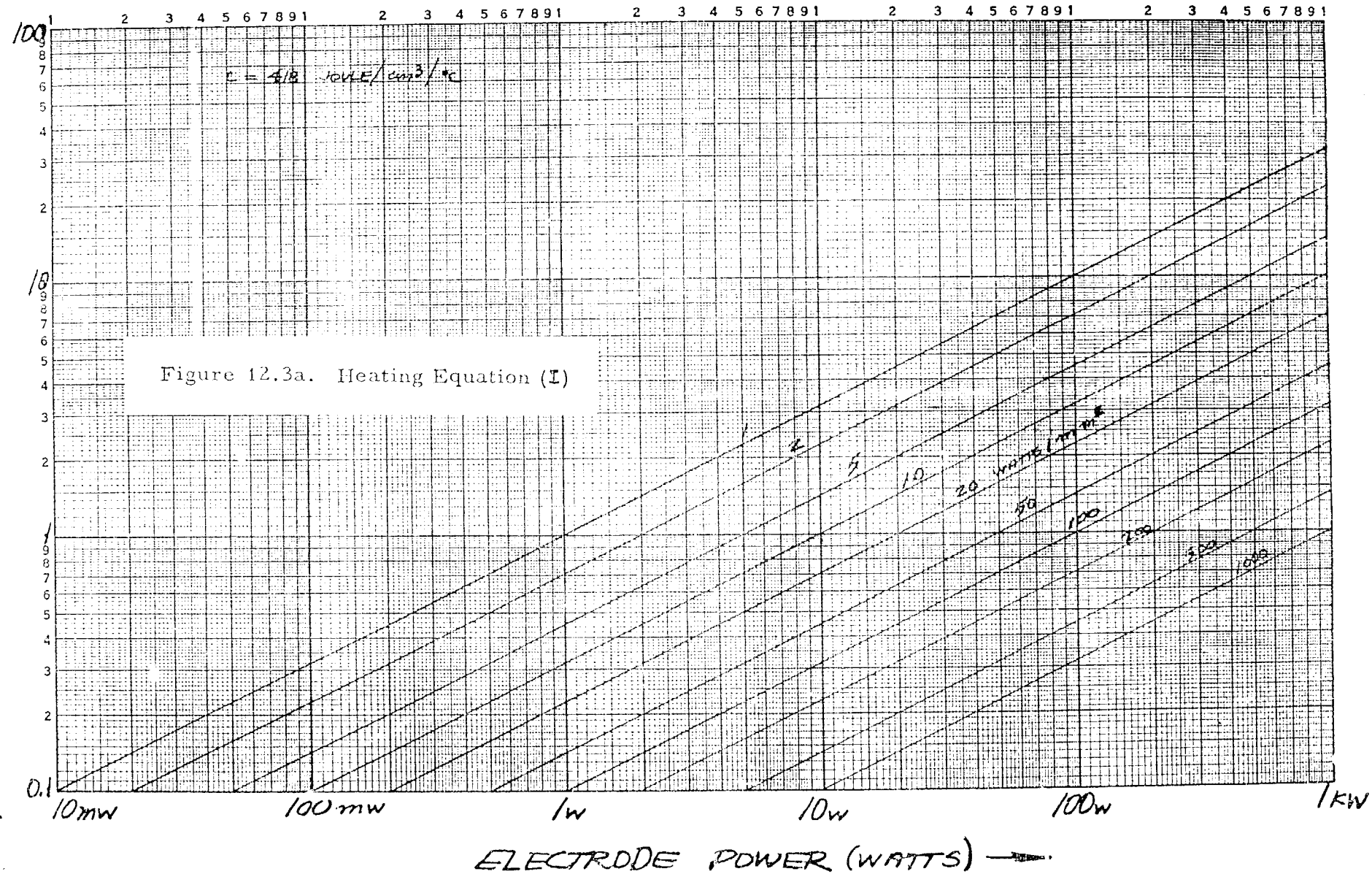

Figure 12.3a. Heating Equation (I)

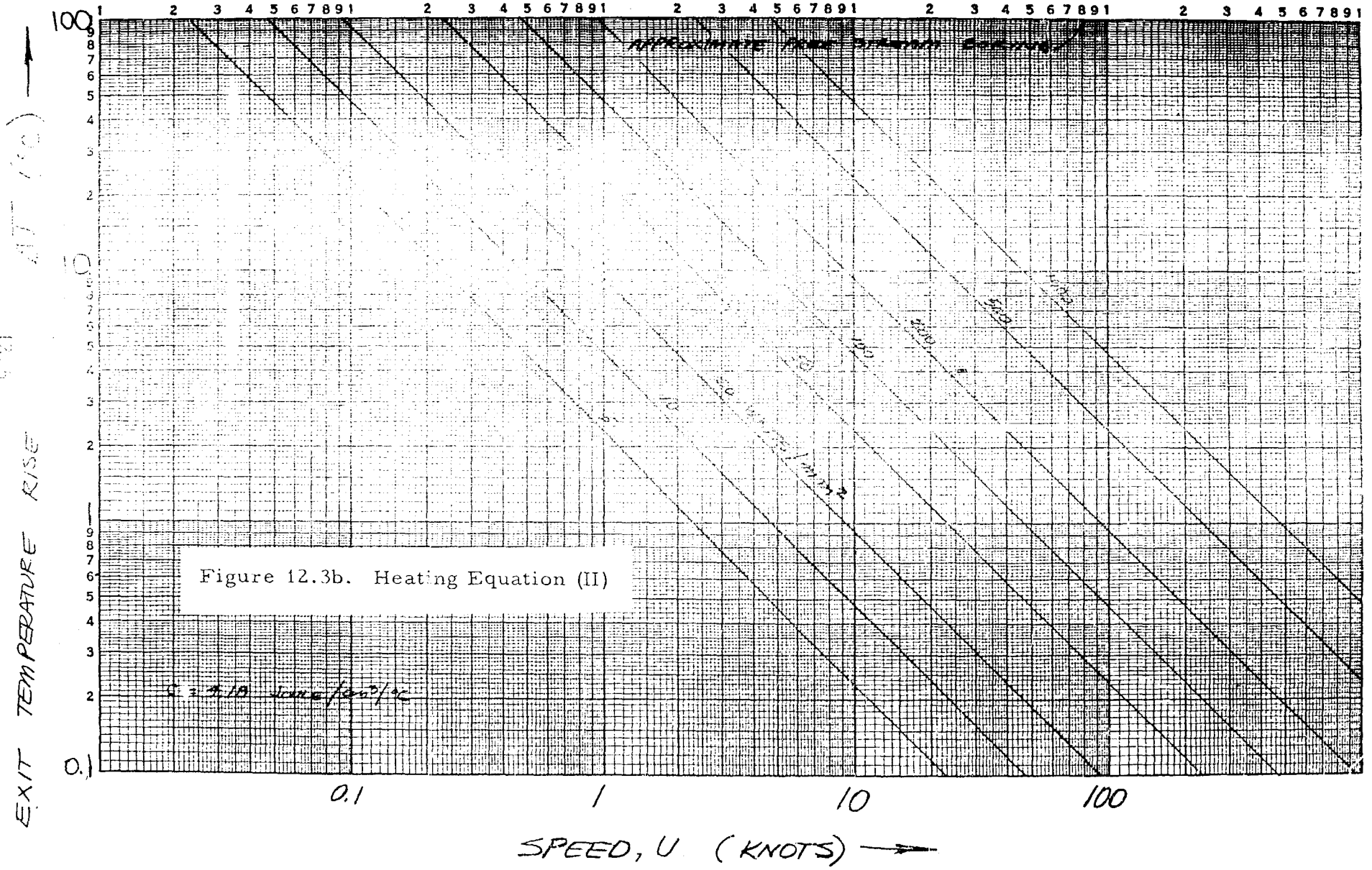

Figure 12.3b. Heating Equation (II)

Best Available Copy

which might be expected for probe and flush type electrodes are shown in Figure 12.4 .

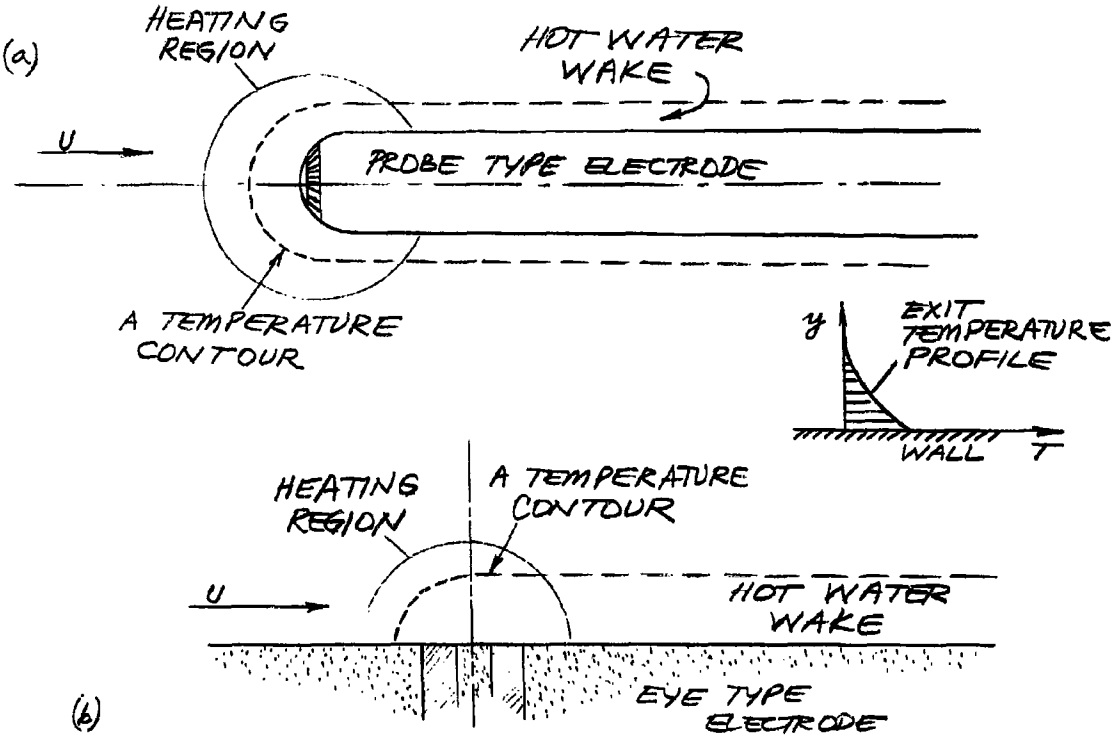

Figure 12.4. Electrical Heating in Electrode Volume

Joule Heating

Consider an electrically conducting medium of conductivity σ. The power density at a point is

$$P_v = \vec{j} \cdot \vec{E} \quad ,$$

where $\vec{j}$ and $\vec{E}$ are the current density and electric field, respectively. By Ohm's Law we have

$$\vec{j} = \sigma \vec{E} \quad ,$$

and

$$\vec{E} = -V_o \vec{\nabla} \phi \quad ,$$

where V_o is the electrode potential (rms) and ϕ is the unit potential. Substituting the above relations we get

$$P_v = \sigma V_o^2 \left(\vec{\nabla}\phi\right)^2 \quad .$$

If P is the electrode power, and R its resistance then

$$P = \frac{V_o^2}{R}$$

and

$$P_v = R\sigma P \left(\vec{\nabla}\phi\right)^2 \quad ,$$

where $R\sigma$ is the cell constant (Sec. 9.1) of the electrode. Integrating over the volume of the electrode field we get the identity

$$\int R_v \, dv = P\left[R\sigma \int (\vec{\nabla}\phi)^2 dv\right] = P$$

In terms of the function

$$w = R\sigma \left(\vec{\nabla}\phi\right)^2,$$

the power density at a point is

$$P_v = Pw \quad ,$$

and the "average power density," $\overline{P_v}$, over the sensitive volume of the electrode is

$$\overline{R_v} = \int w P_v \, dv = P \int w^2 dv = \frac{P}{v_o} ,$$

where the "effective volume," v_o, of the electrode is

$$1 = v_o \int w^2 dv \quad .$$

Thermal Energy Equation

The temperature at a point in a medium satisfies an equation which

accounts for the transfer of heat by convection and thermal conduction and internal heat generation. We assume an incompressible medium with properties, such as density, thermal conductivity, heat capacity, which are independent of temperature. The dynamic relation between these quantities is (1,2)

$$c\frac{\partial T}{\partial t} + c\,\vec{u}\cdot\vec{\nabla}T = \kappa\nabla^2 T + P_v$$

where $\vec{u}$ is the fluid velocity, κ is the thermal conductivity, and c is the heat capacity per unit volume of the medium. The temperature, T, is understood to be the temperature relative to the average ambient temperature. The terms in the above thermal energy equation due to friction heating and bouyant (natural) convection have been omitted. Since the medium is incompressible

$$\vec{\nabla}\cdot\vec{u} = 0 ,$$

and by a vector identity we have

$$\vec{\nabla}\cdot(T\vec{u}) = T\,\cancel{\vec{\nabla}\cdot\vec{u}}^{\,0} + \vec{u}\cdot\vec{\nabla}T .$$

Thus, the energy equation may be written in the form

$$\frac{\partial T}{\partial t} + \vec{\nabla}\cdot(T\vec{u}) = \alpha\nabla^2 T + \frac{P_v}{c}$$

where $\alpha = \kappa/c$ is the thermal diffusivity. Thermal conduction is important only where temperature gradients change rapidly with position, that is, in the thermal boundary layer. Outside this boundary layer region the conduction term may be neglected and

$$\frac{\partial T}{\partial t} + \vec{\nabla}\cdot(T\vec{u}) = \frac{P_v}{c} = \left(\frac{P}{c}\right)w ,$$

which applies for the case of heat transfer by forced convection only. For steady-state forced convection

$$\vec{u}\cdot\vec{\nabla}T = \left(\frac{P}{c}\right)w .$$

Frontal Area

The heating equation for forced convection described in Section 12.1 is

$$\overline{\Delta T} = \frac{P}{2cAU} ,$$

where $\overline{\Delta T}$ is the average electrode temperature rise, P is the electrode power, c is the heat capacity per unit volume, U is the free stream, and A is an area termed the "frontal area" of the electrode. A formula for the frontal area for a general axisymmetric electrode in non-uniform steady flow is described below. The special case of uniform flow is considered at the end of this Section.

Let φ be the velocity potential function and ψ be the (Stokes) stream function for fluid flow over a streamlined axisymmetric probe. Fluid flow is from left to right. The streamlines $\psi(y)$ pass a radial distance y from the axis of symmetry at infinity to the left. The arc length along a stream line is s and is zero on the potential surface which goes through the stagnation point at the nose of the probe. The potential function φ is a function of y and s: $\varphi(y,s)$,

and

$$\varphi(y,0) = 0 \qquad \text{for all } y .$$

The thermal energy equation for forced convection only, is

$$\vec{u} \cdot \vec{\nabla} T = \frac{P}{c} w = u \left(\frac{\partial T}{\partial s}\right),$$

since $\vec{u}$ is parallel with the streamlines. If U is the velocity of the medium relative to the electrode, define the parameter η such that

$$u = \eta U \quad ,$$

at great distance up-stream from the electrode $\eta = 1$. In this notation

$$\frac{\partial T}{\partial s} = \frac{w}{\eta} \left(\frac{P}{cU}\right) \quad ,$$

which is the rate of temperature rise of a water particle following a given streamline. Integrating this, we obtain the temperature at the point T(s, y):

$$T(s,y) = \left(\frac{P}{cU}\right) \int_{-\infty}^{s} \frac{w(\xi,y)\, d\xi}{\eta(\xi,y)} \quad .$$

The "exit temperature profile" is defined to be

$$T(\infty,y) = \left(\frac{P}{cU}\right) \int_{-\infty}^{+\infty} \frac{w\, ds}{\eta} \quad .$$

The "average electrode temperature rise," $\overline{\Delta T}$, due to electrical heating is defined to be*

$$\overline{\Delta T} = \int wT dv \quad ,$$

where the integration extends over the entire volume of the conducting medium.

The element of volume, dv, is (See Fig. 12.5)

$$dv = (2\pi\rho dh)ds \quad ,$$

but by the continuity equation we have

$$(2\pi y dy)U = (2\pi\rho dh)u$$

and

$$dv = 2\pi y dy \left(\frac{ds}{\eta}\right) \quad .$$

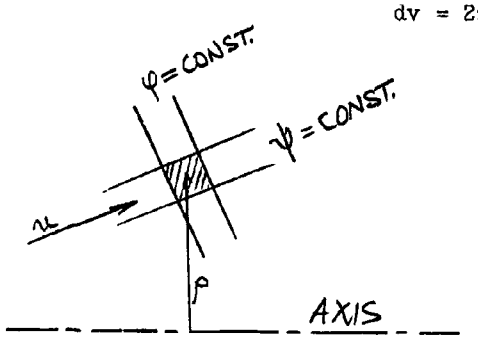

Figure 12.5. Axisymmetric Flow

The exit temperature profile, when integrated over the plane perpendicular to the axis of symmetry, is

$$\int_0^\infty 2\pi y dy\, T(\infty, y) = \left(\frac{P}{cU}\right) \int_0^\infty 2\pi y dy \int_{-\infty}^{+\infty} \frac{w\, ds}{\eta}$$

$$= \left(\frac{P}{cU}\right) \int w dv = \frac{P}{cU} .$$

This quantity is equal to a temperature, ΔT, times an area, A:

$$\Delta T \cdot A = \frac{P}{cU} \quad .$$

The temperature, ΔT, is termed the "exit temperature," and A the "frontal area." By definition, we require that the exit temperature is twice the average electrode temperature rise, or

$$\overline{\Delta T} = \frac{\Delta T}{2} \quad .$$

With these definitions, it is now possible to derive a formula for the frontal area, A, of the electrode which is a function only of the electrode geometry. The expression for $\overline{\Delta T}$ may be rearranged as follows

$$\overline{\Delta T} = \int wT dv = \int_0^\infty 2\pi y dy \int_{-\infty}^{+\infty} \frac{wT}{\eta} ds$$

*Remember $\int w dv = 1$

$$= \left(\frac{cU}{P}\right) \int_{-\infty}^{+\infty} 2\pi y\, dy \int_{-\infty}^{+\infty} \left(\frac{\partial T}{\partial s}\right) T\, ds$$

$$= \left(\frac{cU}{P}\right) \int_{-\infty}^{+\infty} 2\pi y\, dy \cdot \frac{1}{2} T^2(\infty, y) \,,$$

or

$$\overline{\Delta T} = \frac{1}{2} \frac{\int_0^{\infty} 2\pi y\, dy\, T^2(\infty, y)}{\int_0^{\infty} 2\pi y\, dy\, T(\infty, y)} \,.$$

By the definition of the frontal area, A, we find

$$A = \frac{\left\{\int_0^{\infty} 2\pi y\, dy\, T(\infty, y)\right\}^2}{\int_0^{\infty} 2\pi y\, dy\, T^2(\infty, y)}$$

Substituting the expression for the exit temperature profile, T(∞, y), we find

$$I = A \int_0^{\infty} 2\pi y\, dy \left(\int_{-\infty}^{+\infty} \frac{w\, ds}{\eta}\right)^2 .$$

This integral depends only on the electrode geometry.

In the case of uniform flow ($\eta = 1$) over a flush-type electrode, the above formulas become

$$T(x, y, z) = \left(\frac{P}{cU}\right) \int_{-\infty}^{x} w\, d\xi$$

$$T(y, z) = \left(\frac{P}{cU}\right) \int_{-\infty}^{+\infty} w\, d\xi$$

$$A = \frac{\left\{\int_0^{\infty} dz \int_{-\infty}^{+\infty} dy\; T(y, z)\right\}^2}{\int_0^{\infty} dz \int_{-\infty}^{+\infty} dy\; T^2(y, z)}$$

and

$$I = \int_0^{\infty} dz \int_{-\infty}^{+\infty} dy \left\{\int_{-\infty}^{+\infty} w\, dx\right\}^2 ,$$

where the x-axis is the direction of flow, the y-axis is perpendicular to the plane of the electrode, and the z-axis lies in the plane perpendicular to the direction of flow. This relatively complicated definition of electrode frontal area reduces, in the case of the uniform field of Figure 12.1 , to the frontal area described there.

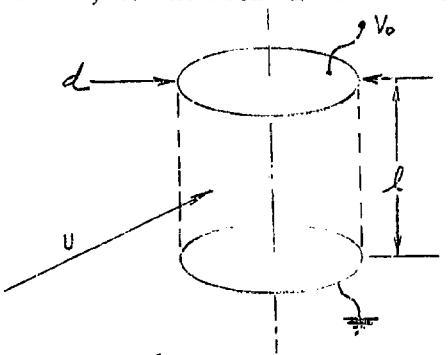

Figure 12.6 . Cylindrical Electrode

As an example of the concept of frontal area, consider the cylindrical electrode volume of Figure 12.6 . The flow is assumed uniform and perpendicular to the axis of the cylinder and parallel to the disc electrodes at the ends of the cylinder. The current density is assumed uniform within the cylinder and zero outside. Performing the integration, we find

$$A = \left(\frac{3\pi^2}{32}\right) l\, d \quad ,$$

where

$$W = \frac{4}{\pi l d^2}$$

inside the cylinder and zero outside.

Temperature Uniformity

We saw in the case of a simple rectangular electrode that the temperature increases linearly with distance in the electrode field to the maximum temperature equal to the exit temperature. This temperature rise is uniform over the surface of the electrode volume perpendicular to the direction of flow. In a general electrode configuration this is not the case; the exit temperature rise varies with position over the down-stream region of the electrode volume. Let ΔT_{max} denote the maximum temperature at some point in electrode volume (down-stream), the "temperature uniformity" is defined as the ratio (denoted by m_5).

$$m_5 = \frac{\overline{\Delta T}}{\Delta T_{max}} < 1 \quad .$$

In the case of the uniform parallel plate electrode, of Figure 12.1 , the uniformity is 50 %; in the case of the cylindrical electrode of Figure 12.6 , the uniformity is 42 %. High uniformity is desirable since more power may be dissipated in the water (with resultant higher velocity sensitivity) before boiling sets in at a "hot spot." When the effects of boundary layer heating (Sec. 12.4) are taken into consideration, the uniformity is

much less than that calculated from the geometry of the electrode. In practice the uniformity seldom exceeds 10 %.

12.3 Internal Heat Generation

The temperature distribution produced by internal heat generation in several problems is studied in this Section. Heat generation is by Joule heating associated with the electrical power dissipated in the electrode volume. The results of this Section are used to develop the general heat transfer equation described in Section 12.5 . Although boundary layer heating should appropriately be included in this Section, it is treated as a separate topic in Section 12.4 because of the extent of the subject.

Thermal Conduction

Consider the case of internal heat generation in a static fluid (like a solid) and the resultant steady-state temperature distribution. The thermal energy equation is

$$k \nabla^2 T = - P_N$$

and assume the boundary condition T = 0 at infinity and $(\partial T/\partial n) = 0$ at the surface of the electrodes. The latter condition assumes the thermal conductivity of the wall is much less than that of the medium ($K_w << K$). The exact solution of this equation for a given electrode configuration is, in general, not possible to obtain. As an illustration of a soluble problem, consider the case of a uniform spherical electrode volume of radius b. Since the thermal conductivity of the wall is small, this problem also corresponds to a uniform hemispherical volume at a plane boundary as shown in Figure 12.7 . The general time dependent solution, after the electrode power is switched on, is given in References (3,4). The steady-state solution of this radially symmetric problem is obtained in the following way. The sensing function is

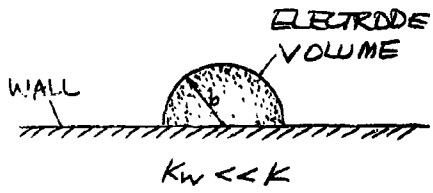

Figure 12.7 . Hemispherical Electrode Volume

$$w = \begin{cases} \frac{1}{v_0} & , \text{ FOR } 0 \le r \le b \\ 0 & , \quad \text{for } r > b \end{cases} ,$$

where $v_0 = 4\pi b^3/3$ is the effective volume of the spherical electrode.

Define the quantity θ such that

$$\nabla^2 \theta = \begin{cases} -\frac{1}{b^2} & , \quad 0 \le r \le b \\ 0 & , \quad r > b \end{cases} ,$$

that is

$$T = \frac{3P\Theta}{4\pi bK} \quad .$$

The solution for the condition $\Theta(\infty) = 0$, is

$$\Theta = \begin{cases} \frac{1}{2} - \frac{1}{6}\left(\frac{r}{b}\right)^2 , & \text{FOR } 0 \leq r \leq b \\ \frac{1}{3}\left(\frac{b}{r}\right) , & \text{FOR } r \geq b \end{cases} .$$

This distribution is shown in Figure 12.8 . The average electrode temperature rise, $\overline{\Delta T}$, is defined to be

$$\overline{\Delta T} = \int_w T \, dw = \frac{3P}{10\pi bK} .$$

For a general electrode, we introduce the dimensionless number, m_7, such that

$$\overline{\Delta T} = \frac{P}{m_7 bK} ,$$

where, in this case, b is the reference dimension for the electrode. In the case of a hemispherical volume

$$m_7 = \frac{5\pi}{3} = 5.24 .$$

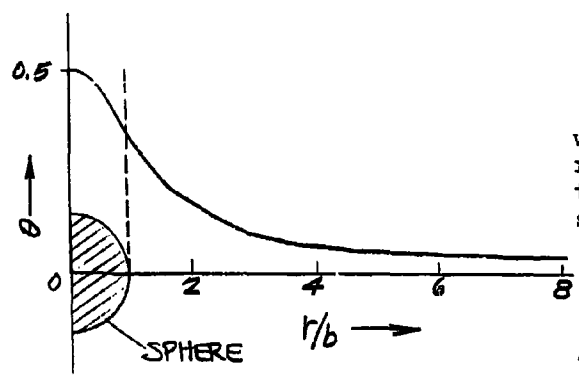

Figure 12.8 . Radial Temperature Distribution of the Heated Spherical Volume

As a numerical example for a sphere in water

$$m_7 = \frac{10\pi}{3} = 10.5$$

$$K = .006 \text{ watt/cm/}^{\circ}\text{C}$$

$$b = 0.5 \text{ cm}$$

$$P = 1 \text{ watt}$$

and

$$\overline{\Delta T} = 32 \ ^{\circ}\text{C}$$

$$T_{max} = 40 \ ^{\circ}\text{C} .$$

If the ambient temperature is 20 $^{\circ}$C, the peak temperature at the center of

the sphere is 60 °C.

Pulse Heating

Consider the case of the dissipation of a very short pulse of electrical energy in the electrode volume. The duration of the pulse is short in comparison with the transit time for flow through the electrode volume, b/U, and short in comparison with the time for heat transfer by conduction or convection to be appreciable. The thermal energy equation is, in this case,

$$c\left(\frac{\partial T}{\partial t}\right) = Pw \quad ,$$

where P is the pulse power and c is the heat capacity per unit volume of the water. The resulting temperature field is

$$T = \left(\frac{Pw}{c}\right) t \quad ,$$

where t is the pulse duration. The average electrode temperature is

$$\overline{\Delta T} = \int w T \, dv = \left(\frac{Pt}{c}\right) \int w^2 dv .$$

If w is uniform over a volume v_o, then

$$\overline{\Delta T} = \frac{Pt}{v_o c} \quad ,$$

since

$$\int w dv = 1 \quad \text{and} \quad w v_o = 1 \quad .$$

The "effective volume," v_o of a general field distribution is defined by analogy with this expression:

$$1 = v_o \int w^2 dv$$

or

$$1 = v_o R^2 \sigma^2 \int (\vec{\nabla}\phi)^4 dv \quad ,$$

and, as before

$$1 = \int w dv \quad .$$

The average electrode temperature satisfies the relation

$$\overline{\Delta T} = \frac{1}{v_o} \int T dv \quad .$$

As a numerical example, suppose the pulse is comparable with those used in radar applications:

$$t = 1\ \mu\text{sec}$$
$$P = 200\ \text{kw}$$
$$v_0 = (1\ \text{mm})^3 = .001\ \text{cm}^3$$
$$c = 4.1\ \text{joule/cm}^3/^\circ\text{C}$$

and

$$\overline{\Delta T} = 50\ ^\circ\text{C}\ .$$

Surface Heating

A certain fraction of power dissipated in an electrode is lost in the surface resistance. If $\gamma + i\omega\beta$ is the (uniform) admittance per unit area of the electrodes (Sec. 10.5), the power dissipated per unit area is

$$\frac{dP}{dS} = V_s^2\,\gamma$$

where V_s is the root-means-square of the voltage drop, v_s, across the surface impedance at the point under consideration, and $v_s v_s^* = V_s^2$. If the surface impedance is small in comparison with volume resistance, we have

$$v_s = \frac{j_n}{\gamma + i\omega\beta}$$

where j_n is the current density perpendicular to the electrode surface. Substituting the relation

$$j_n = \sigma v_0 \left(\frac{\partial\phi}{\partial n}\right)$$

where v_0 is the electrode voltage, we find

$$V_s = V_0\,\frac{\sigma\left(\frac{\partial\phi}{\partial n}\right)}{\gamma\sqrt{1+k^2}}$$

where $k = \omega\beta/\gamma$. The power dissipated per unit area is

$$\frac{dP}{dS} = \frac{V_0^2\sigma^2\left(\frac{\partial\phi}{\partial n}\right)^2}{\gamma(1+k^2)}$$
$$= \frac{PR\sigma^2\left(\frac{\partial\phi}{\partial n}\right)^2}{\gamma(1+k^2)}\ .$$

where P is the power dissipated in the medium (which is approximately the total dissipated power). The total power dissipated in the surfaces,

P_s, is

$$P_s = \int \left(\frac{dP}{dS}\right) dS = \frac{P R^2 \sigma^2}{R\gamma(1+k^2)} \int_{\pm} \left(\frac{\partial \phi}{\partial n}\right)^2 dS$$

where the surface integration extends over both electrode surfaces. By means of the definition of "effective electrode area," S (Sec. 10.5):

$$1 - \frac{1}{2} \leq R^2 \sigma^2 \int_{\pm} \left(\frac{\partial \phi}{\partial n}\right)^2 dS$$

we have

$$\frac{P_s}{P} = \frac{2}{R\gamma(1+k^2)S} .$$

As a numerical example, consider the case of a surface impedance which is predominantly capacitive (Sec. 9.7):

$$k = 4$$
$$R = 30 \text{ ohms}$$
$$\gamma = .026 \text{ ohm}^{-1}\text{cm}^{-2}$$
$$S = 1 \text{ cm}^2$$

and

$$P_s = (0.15)\, P ,$$

or 15 % of the electrode power is lost in the surfaces. The power dissipated in this manner is ultimately transferred to the flowing medium by conduction and thence by forced convection from the electrode volume. The theory of this process is similar to that of the hot-film anemometer (5).

12.4 Boundary Layer Heating

In this Section, the consequences of uniform internal heat generation in the boundary layer region of the electrodes are considered. Several simple cases are analyzed first in order to estimate the temperature distribution in an actual velocity boundary layer.

Uniform Velocity

Consider the case of a fluid flowing with uniform velocity parallel to a flat wall of thermal conductivity which is either zero or infinite.

There is no velocity boundary layer. The fluid is heated internally and uniformly throughout the region $0 < x < \ell$ at a power density, P_v, as shown in Figure 12.9 . The steady-state temperature equation is

$$c\,U\,\frac{\partial T}{\partial x} = K\left(\frac{\partial^2 T}{\partial x^2} + \frac{\partial^2 T}{\partial y^2}\right) + P_v$$

where U is the fluid velocity, K the thermal conductivity of the fluid and c is its heat capacity per unit volume. In order to solve the boundary layer equation we assume $(\partial^2 T/\partial x^2)$ is small compared with $(\partial^2 T/\partial y^2)$. At great distance from the wall, outside the thermal boundary layer, the temperature is determined by forced convection only

$$cU\left(\frac{\partial T}{\partial x}\right) = P_v \quad ,$$

with the solution

$$T_0(x) = \left(\frac{x}{\ell}\right)\frac{\ell P_v}{cU} \quad .$$

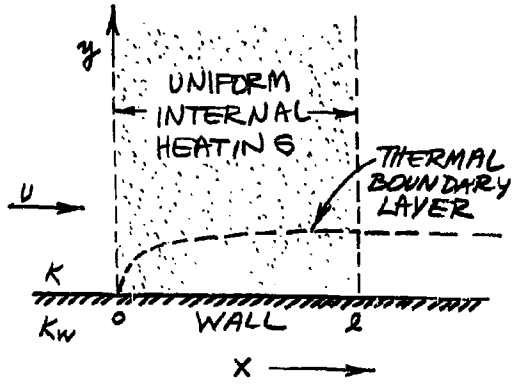

Figure 12.9 . Thermal Boundary Layer for Uniform Velocity

Assume a temperature distribution of the similarity form

$$T(x,y) = v(\eta)\, f(x)$$

where $y = \eta\, y_0(x)$. It may be shown by substitution that such a solution is possible if

$$y_0 = \sqrt{\frac{Kx}{cU}}$$

$$f(x) = T_0(x) = \left(\frac{x}{\ell}\right)\left(\frac{\ell P_v}{cU}\right)$$

and the function, v, satisfies the equation

$$v'' + \tfrac{1}{2}\eta v' - v + 1 = 0 \quad ,$$

with the boundary conditions

$$v(0) = 0 \quad , \qquad \text{for } K_w \gg K$$

$$v'(0) = 0 \quad , \qquad \text{for } K_w \ll K \, .$$

The solution for v in the case of zero wall conductivity is trivial,

it is as if no wall were there at all: $v = 1$ for $y > 0$. The solution for the case of infinite wall thermal conductivity may be found exactly by ordinary methods (6), however, this solution has not been carried out. A sketch of the expected solution is shown in Figure 12.10. The slope at the wall, $v'(0)$, is of the order of unity for $K_w \gg K$. The thermal boundary layer thickness at $x = \ell$ and $\eta = 1$ is

$$\delta_T = \sqrt{\frac{\ell k}{cU}} = \ell \sqrt{\frac{\alpha}{\ell U}}$$

or

$$\delta_T = \frac{\ell}{\sqrt{PR}}$$

where

$$P = \frac{\nu}{\alpha} \qquad \alpha = \frac{k}{c}$$

$$R = \frac{\ell U}{\nu} \qquad (\nu = \text{kinematic viscosity}).$$

Linear Velocity Profile

Consider, now, a velocity profile which varies linearly with the distance from the wall.

$$U(y) = U\left(\frac{y}{\delta}\right) ,$$

where U is the velocity at a distance δ from the wall. The boundary layer temperature equation in this case is

$$cU\left(\frac{y}{\delta}\right)\frac{\partial T}{\partial x} = k\frac{\partial^2 T}{\partial y^2} + P_v .$$

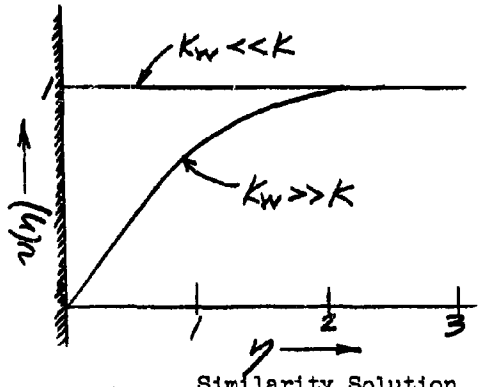

Figure 12.10. Similarity Solution for Uniform Velocity

At great distance from the wall, outside the boundary layer, this equation becomes

$$U\left(\frac{y}{\delta}\right)\cdot\left(\frac{\partial T}{\partial x}\right) = P_v ,$$

which has the solution

$$T_0(x,y) = \left(\frac{x}{\ell}\right)\cdot\left(\frac{\delta}{y}\right)\cdot\left(\frac{\ell P_v}{cU}\right).$$

Again, we seek a similarity solution in the form

$$\tau(x,y) = v(\eta) f(x),$$

with $y = \eta\, y_0(x)$. This solution requires that

$$y_0 = \left(\frac{K\delta x}{cU}\right)^{1/3}$$

$$f(x) = \left(\frac{x}{\ell}\right)\left(\frac{\delta}{y_0}\right)\left(\frac{\ell R_\ell}{cU}\right) \sim x^{2/3},$$

and $v(\eta)$ satisfies

$$\ddot{v} + \tfrac{1}{3}\eta^2 \dot{v} - \tfrac{2}{3}\eta v + 1 = 0,$$

with the boundary conditions

$$v(\infty) = 0$$

and

$$v(0) = 0 \quad \text{for } K_w \gg K$$

$$\dot{v}(0) = 0 \quad \text{FOR } K_w \gg K .$$

The solution to this equation has not been obtained and probably is not expressible in closed form. A sketch of the expected solution is shown in Figure 12.11. The thermal boundary layer thickness at $x = \ell$ for $\eta = 1$

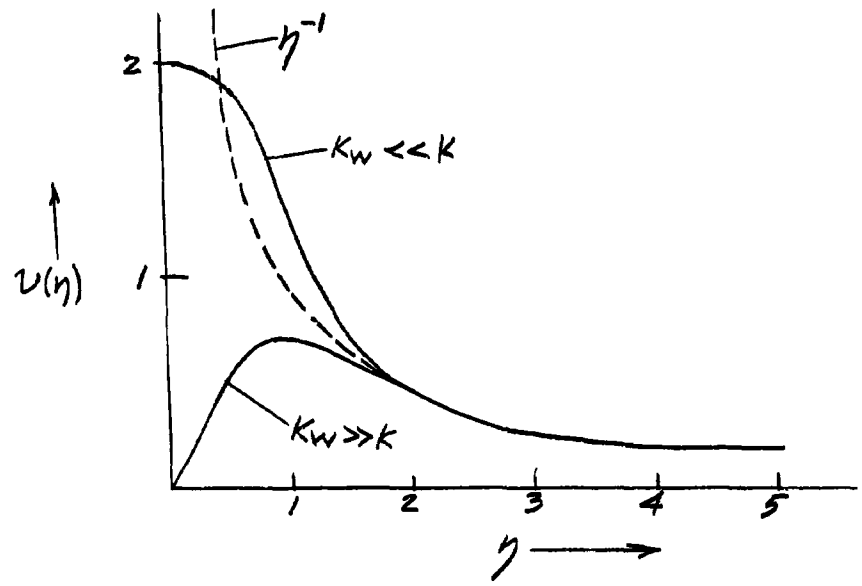

Figure 12.11. Similarity Solution for Linear Velocity Profile

is

$$\delta_T = \left(\frac{K\delta\ell}{cU}\right)^{1/3} = \ell\left[\frac{(\delta/\ell)}{PR}\right]^{1/3}.$$

For the case of zero wall conductivity the temperature distribution along the wall, T(x,0), is

$$T(x,0) = v(0)\,f(x) = v(0)\cdot\left(\frac{x}{\ell}\right)^{2/3}\cdot\left(\frac{\delta}{\ell}\right)^{2/3}\cdot(PR)^{1/3}\cdot\left(\frac{\ell R_\ell}{cU}\right).$$

Boundary Layer Profile

The above cases are now applied to the analysis of the thermal boundary layer for a boundary layer velocity profile.

The velocity distribution in the boundary layer of a flat plate at a distance L from the leading edge has a thickness comparable with

$$\delta_U = \sqrt{\frac{\nu L}{U}}$$

The rate of change of velocity at the boundary is (7)

$$\frac{du}{dy} = 0.332\ \frac{U}{\delta_U}$$

If the region of uniform heating of length ℓ is located relatively far ($\ell \ll L$) from the leading edge, the boundary layer flow may be considered approximately parallel to the wall.

It is readily shown that in water the thermal boundary layer is thinner than the velocity boundary layer. Assuming this to be the case, the thermal boundary layer forms in the linear velocity profile of the velocity boundary layer. Thus, the result of the previous case is approximately valid for boundary layer flow. In that case, we found

$$\delta_T = \left(\frac{\alpha\delta\ell}{U}\right)^{1/3},$$

where for a flat plate δ satisfies

$$0.332\,U\sqrt{\frac{U}{\nu L}} = \frac{U}{\delta}$$

or

$$\delta = 3.02\sqrt{\frac{\nu L}{U}}.$$

The ratio of thermal and velocity boundary layer thicknesses is

$$\left(\frac{\delta_T}{\delta_U}\right) = \left(\frac{\alpha \delta \ell}{U}\right)^{1/3} \cdot \left(\frac{U}{\nu L}\right)^{1/2} = \left[\frac{3.02}{P}\left(\frac{\ell}{L}\right)\right]^{1/3}.$$

For example, if $L = 10\ell$ and $P = 5$, then $\delta_U = 2.6\ \delta_T$. The following References are cited in connection with the theory of the thermal boundary layers with internal heat generation (8-12).

Maximum Boundary Temperature

The temperature in an electrode volume reaches its maximum value in the velocity boundary layer as a consequence of the lower velocity there. The "temperature uniformity" described in Section 12.2 is the ratio

$$m_5 = \frac{\overline{\Delta T}}{\Delta T_{max}} \quad ,$$

where $\overline{\Delta T}$ is the average electrode temperature rise and ΔT_{max} is the peak temperature in the electrode volume. This uniformity ratio is determined by the sensing function distribution, w, which is primarily a geometrical consideration, and, more importantly, by the temperature distribution in the boundary layer region. The uniformity is calculated below for the approximate formulas for boundary layer heating developed in this Section.

The maximum temperature in the boundary layer for $k_w << k$ and $x = \ell$ was found to be

$$\Delta T_{max} = v(0)\left(\frac{\delta}{\ell}\right)^{2/3} \cdot (PR)^{1/3} \cdot \left(\frac{\ell P_V}{cU}\right)$$

where

$$\delta = 3.02\sqrt{\frac{\nu L}{U}}.$$

The temperature distribution over most of the electrode volume is assumed to be that corresponding to uniform velocity:

$$T_0(x) = \frac{x}{\ell}\left(\frac{\ell P_V}{cU}\right)$$

Thus, the average electrode temperature is

$$\overline{\Delta T} = \frac{1}{2}\left(\frac{\ell P_V}{cU}\right).$$

The temperature uniformity is

$$m_5 = \frac{\overline{\Delta T}}{\Delta T_{max}} = \left[2\, v(0) \left(\frac{\delta}{\ell}\right)^{2/3} \cdot (PR)^{1/3} \right]^{-1}$$

$$\approx \frac{0.24}{v(0)} \left(\frac{\ell}{PL}\right)^{1/3}$$

$$\approx \frac{0.17}{v(0)} \left(\frac{\delta T}{\delta U}\right).$$

Unfortunately, the value v(0) has not been computed, but is expected to be approximately two. As a numerical example of the temperature uniformity as determined by boundary layer heating, assume the values

$$v(0) = 2$$

$$P = 4$$

$$L = 3\ell$$

then $$m_5 = 5\ \%\ \text{uniformity}\ .$$

Thus, boiling inception in the downstream boundary layer takes place ($\Delta T_{max} = 80^{\circ}$, ambient temperature = $20^{\circ}C$, and absolute temperature = $100^{\circ}C$) when the average electrode temperature is

$$\overline{\Delta T} = .05 \times 80\ ^{\circ}C = 4\ ^{\circ}C\ .$$

This illustrates the relatively severe limitation on the highest operating temperature of the electrode set by boundary layer heating. If this effect could be removed by some artifice, a uniformity of the order of 35 % would be expected, or

$$\overline{\Delta T} = 0.35 \times 80\ ^{\circ}C \approx 30\ ^{\circ}C\ .$$

The uniformity in the boundary layer is somewhat improved over that calculated above since the Prandtl number, P, decreases rapidly with increasing temperature.

Boundary Layer Flux

We wish now to evaluate the heat transfer by convection in the boundary layer region. In particular, we want to evaluate the boundary layer flux thickness, δ^*:

$$\delta^* = \int_{\delta}^{\infty} (1 - u\theta)\, dy,$$

where the integral is evaluated at $x = \ell$ and

$$u = \frac{U(y)}{U} \quad , \quad \theta = \frac{T(\ell, y)}{\Delta T}$$

and

$$\Delta T = \frac{\ell P_v}{cU} \quad .$$

The case of zero wall thermal conductivity is simple for any velocity distribution near the wall:

$$\delta^* = 0 \quad .$$

This is a result of the continuity equation for thermal energy:

$$c \vec{\nabla} \cdot (T \vec{u}) = K \nabla^2 T + R$$

Integrating this equation over the volume enclosed by a surface just outside the region where P_v is finite (e.g., in the wall $K = 0$) the conduction term is zero:

$$\int_0^h U(y)\, T(y)\, dy = \left(\frac{\ell P_v}{cU}\right) Uh.$$

Thus, by the definition of u and θ we have

$$\int_0^h (1 - u\theta)\, dy = 0,$$

and the quantity δ^* is zero. As a corollary to this result, we find that wherever the conduction term is small compared with the convection term, the contribution to δ^* is small. This is true even where u is a function of y since in the region where conduction is small we have $u\theta \approx 1$. Thus, the contribution to δ^* occurs only in the region where thermal conductivity is important, i.e., in the thermal boundary layer. It follows that

$$\delta^* \approx \delta_T \quad .$$

For the case of infinite wall conductivity we consider first the case of uniform velocity. The temperature distribution is

$$T(\ell, y) = v(\eta)\, f(\ell) = v(\eta) \left(\frac{\ell P_v}{cU}\right)$$

and

$$\theta = v(\eta) \quad .$$

Since the velocity is uniform, u = 1, and

$$\delta^* = \int_0^\infty (1 - u\theta)\, dy = y_0(\ell) \int_0^\infty (1-\theta)\, d\eta$$

$$= \delta_T \int_0^\infty (1-\theta)\, d\eta$$

i.e., δ^* is euqal to the "displacement thickness" of the thermal boundary layer.

For a linear velocity profile at the wall we have

$$T(\ell, y) = v(\eta)\, f(x) = v(\eta) \left(\frac{\delta}{y_0}\right)\left(\frac{\ell R_v}{cv}\right)$$

and

$$\theta = v(\eta) \left(\frac{\delta}{y_0}\right).$$

The velocity, u, is given by

$$u = \frac{U(y)}{U} = \left(\frac{y}{\delta}\right) .$$

The boundary layer flux thickness is

$$\delta^* = \int_0^\infty \left[1 - \theta \left(\frac{y}{y_0}\right)\right] dy = \delta_T \int_0^\infty [1 - \eta\theta]\, d\eta.$$

Where conduction is negligible, $\eta\theta \approx 1$.

Stagnation Flow

In the region of a stagnation point the velocity is low and, consequently, the temperature rise is large. A thermal boundary layer forms in this region with a peak value which exceeds the average electrode temperature. The analysis of this problem may be carried out as above for boundary layer flow and the temperature rise depends primarily on the value of the distribution w along the streamline which passes through the stagnation point.

12.5 Heat Transfer Equation

The electrical power dissipated in the flowing conducting medium is transferred away from the electrode region by a number of physical mechanisms. The heat transfer equation is the relation between the electrical

input power and the rate of heat loss by all the mechanisms of importance for steady-state equilibrium conditions. The derivation of this equation is extremely difficult for a given electrode configuration. As a consequence, it will be necessary to make a dimensional analysis of the transfer mechanisms instead of solving the problem for a specific electrode configuration. The results of this simplified analysis will allow us to decide which mechanisms are of importance and under what conditions. To estimate the magnitude of each heat loss mechanism a ratio (denoted by the subscript λ) will be taken with respect to the primary mechanism of heat transfer, forced convection without conduction.

The typical dimension of the electrode volume is ℓ, and the velocity of the electrode relative to the medium is U. Only the case of low wall conductivity ($K_w \ll K$) is considered. The following mechanisms of heat transfer are considered:

Forced Convection

Conduction

Free Convection

Radiation .

Forced Convection

Forced convection is the primary mechanism of heat transfer from the electrode volume. This process consists of the mechanical displacement of the internally heated water from the electrode volume by the transport of the fluid flow. Conduction is not necessary for this process to take place. The rate of heat transfer, $\dot{Q}$, is

$$\dot{Q}(\text{forced convection}) = 2cAU\overline{\Delta T} = 2c m_4 b^2 U \overline{\Delta T}$$
$$\approx 2c\ell^2 U\overline{\Delta T} = c\ell^2 U \Delta T,$$

where $\overline{\Delta T}$ is the average temperature rise due to heating, and c is the heat capacity per unit volume. The other mechanisms of heat transfer are compared with this expression.

Since we have assumed that the wall conductivity is low ($K_w \ll K$), the heat transfer in the boundary layer region does not require special consideration as it would if heat were transferred to the wall.

Conduction

Heat transfer by conduction to the medium outside the electrode volume is important only at very low velocity. We saw in Section 12.3 that

$$\dot{Q}(\text{conduction}) = m_7 bK\Delta T \approx 3\ell K \overline{\Delta T},$$

where the numerical coefficient is a rough estimate for a typical electrode. Comparison with forced convection yields

$$\dot{Q}_{\lambda}\,(\text{conduction}) = \frac{\dot{Q}(\text{conduction})}{\dot{Q}(\text{forced convection})} = \frac{1}{2}\left(\frac{m_7}{m_4}\right)\left(\frac{K}{cbU}\right)$$

$$\approx \frac{3K}{2cLU} = \frac{3}{2}\,\frac{1}{PR}\,.$$

In terms of the Prandtl and Reynolds numbers

$$P = \frac{\nu}{\alpha} = \frac{\nu c}{K}$$

$$R_b = \frac{Ub}{\nu}\,,$$

we have

$$\dot{Q}_1(\text{CONDUCTION}) = \frac{1}{2}\left(\frac{m_7}{m_4}\right)\frac{1}{PR_b}\,.$$

This relation is valid for very low velocity or more exactly, for small Péclet number:

$$PR_b = \frac{Ub}{\alpha} << 1.$$

For the case of large Péclet number, PR $\gg$ 1, a thermal boundary layer forms at the surfaces of the electrode volume. Neglecting heat transfer to the non-conducting wall, we have approximately

$$\dot{Q}(\text{CONDUCTION}) \approx 6\,K\ell\,\Delta T\,\sqrt{PR}$$

where the boundary layer temperature gradient is assumed to be approximately

$$\sqrt{\frac{L}{x}}\;\sqrt{PR}\left(\frac{\Delta T}{\ell}\right).$$

The ratio of heat flux relative to forced convection is

$$\dot{Q}(\text{CONDUCTION}) \approx \frac{6}{\sqrt{PR}}\,.$$

The expressions for the flux due to conduction at high and low Péclet number are equal at the value

$$PR \approx .06\,.$$

If the "edges" of the electrode distribution are not sharp, the transition Péclet number is more nearly equal to unity.

Free Convection

As a consequence of the slight decrease in density of water as it is heated, a bouyant force acts on the water passing through the electrode volume. The coefficient of expansion is defined as

$$-\frac{1}{d}\left(\frac{\partial d}{\partial T}\right)=\gamma,$$

where d is the density of water. This bouyant force gives rise to heat transfer by natural convection out the top of the electrode volume. A simplified analysis of this effect is given below for a cubical volume of dimension ℓ.

First, consider the case when the inertial forces on the water accelerated by the bouyant force is larger than the viscous forces, i.e., the Reynolds number is large compared to unity:

$$R=\frac{U\ell}{\nu}>>1.$$

The bouyant force, δF, on an incremental slab of water of thickness δx and area ℓ^2 is

$$\delta F=(\ell^2\delta x)\,\Delta d\,g$$

where Δd is the change in density due to the temperature rise $\Delta T(x)$ at station x

$$\Delta d=d\gamma T_0(x),$$

and the temperature rise is assumed to be

$$T_0(x)=\left(\frac{x}{\ell}\right)\Delta T$$

where

$$\Delta T=\frac{\ell P_v}{cU}.$$

Thus, we have

$$\delta F\,(\text{BOUYANT})=(\ell^3 g\gamma d\,\Delta T)\left(\frac{x}{\ell}\right)\delta\left(\frac{x}{\ell}\right).$$

The inertial force on this incremental volume due to its vertical acceleration is

$$\delta F\,(\text{INERTIA})=(\ell^2\delta x)\,d\left(\frac{d^2y}{dt^2}\right).$$

where (d^2y/dt^2) is the vertical acceleration of the slab. Assume that the vertical velocity is some power, n, of the distance x:

$$\left(\frac{dy}{dt}\right) = \left(\frac{x}{\ell}\right)^n \Delta U$$

where ΔU is some velocity factor to be determined. Differentiating this expression we find

$$\frac{d^2y}{dt^2} = \frac{d}{dx}\left(\frac{dy}{dt}\right)\frac{dx}{dt} = Un\left(\frac{x}{\ell}\right)^{n-1}\frac{\Delta U}{\ell}$$

and

$$\delta F(\text{INERTIA}) = \left(\ell^2 d U n \Delta U\right)\left(\frac{x}{\ell}\right)^{n-1}\delta\left(\frac{x}{\ell}\right).$$

Equating this to the bouyant force

$$\delta F(\text{inertia}) = \delta F(\text{bouyant}),$$

we find that n = 2 and

$$2\ell^2 d U \Delta U = \ell^3 g \gamma d \Delta T$$

or

$$\Delta U = \frac{\ell g \gamma \Delta T}{2U}$$

or

$$\left(\frac{\Delta U}{U}\right) = \frac{1}{2}\frac{G}{R^2}$$

where G is the Grashoff number

$$G = \frac{\ell^3 g \gamma \Delta T}{\nu^2}$$

and the Reynolds number is

$$R = \frac{U\ell}{\nu}.$$

The heat flux through the top of the cube is (for $R \gg 1$)

$$\dot{Q}(\text{FREE CONVECTION}) = c\ell\int_0^\ell \left(\frac{dy}{dt}\right)\Delta T(x)\, dx$$

$$= c\ell^2\left(\frac{1}{2}\frac{G}{R^2}\right)\Delta T\, U\left[\int_0^\ell \left(\frac{x}{\ell}\right)^3 d\left(\frac{x}{\ell}\right)\right]$$

OR

$$\dot{Q}(\text{FREE CONVECTION}) = \frac{c\ell^2 U \Delta T}{\mathcal{B}} \left(\frac{\mathcal{G}}{R^2}\right).$$

The ratio of this flux to that due to forced convection is ($R \gg 1$).

$$\dot{Q}_\lambda(\text{free convection}) = \frac{1}{\mathcal{B}}\left(\frac{\mathcal{G}}{R^2}\right)$$

where

$$\dot{Q}(\text{forced convection}) = c\,\ell^2 U \Delta T \ .$$

For the case where the viscous forces on the incremental slab dominate over the inertial forces ($R \ll 1$) we have

$$\delta F(\text{VISCOUS}) = \ell^2 \mu \frac{d^2}{dx^2}\left(\frac{dy}{dt}\right) \delta x$$

where μ is the viscosity and the derivative represents the vertical shear velocity. Again, assuming the form (with a new n and ΔU)

$$\frac{dy}{dt} = \left(\frac{x}{\ell}\right)^n \Delta U,$$

we have

$$\frac{d^2}{dx^2}\left(\frac{dy}{dt}\right) = n(n-1)\left(\frac{x}{\ell}\right)^{n-2} \frac{\Delta U}{\ell^2} \ .$$

Equating the viscous and bouyant forces

$$\delta F(\text{viscous}) = \delta F(\text{bouyant})$$

we find that n = 3 and

$$6\mu \Delta U = \ell^2 g \gamma d \Delta T$$

or

$$\Delta V = \frac{\ell^2 g \gamma d \Delta T}{6\mu}$$

or

$$\left(\frac{\Delta U}{V}\right) = \frac{1}{6}\left(\frac{\mathcal{G}}{R}\right).$$

The heat flux in this case is ($R \ll 1$)

$$\dot{Q}(\text{FREE CONVECTION}) = c\ell \int_0^\ell \left(\frac{dy}{dt}\right) \Delta T(x)\, dx \ ,$$

$$= \frac{c\ell^2 \nu \Delta T}{30}\left(\frac{G}{R}\right).$$

The ratio of heat flux by free convection to forced convection is

$$\dot{Q}_\lambda(\text{FREE CONVECTION}) = \frac{1}{30}\left(\frac{G}{R}\right).$$

The expressions for free convection heat flux at high and low Reynolds number become equal at a Reynolds number of

$$R = \frac{30}{8} \approx 4 \quad .$$

Radiation

Since the heated water in the electrode volume is at a higher temperature than the environmental temperature, it looses heat energy by thermal radiation. The heat flux per unit area lost by a body at absolute temperature T in an environment at absolute temperature T_o is

$$e\,\sigma_{SB}\,(T^4 - T_o^4)$$

where e is the emissivity of the surface and σ_{SB} is the Stefan-Boltzmann constant:

$$\sigma_{SB} = 5.68 \times 10^{-12} \text{ watts/cm}^2 \quad .$$

If $(T - T_o) << T_o$ the radiation law is approximately

$$3\,e\,\sigma_{SB}\,(\bar{T})^3 \Delta T(x)$$

where $\bar{T}$ is the average absolute temperature and $\Delta T(x)$ is the temperature rise at a point on the surface of the body. Averaging this expression over the surface of the cubical electrode volume, we obtain approximately $(\Delta T << T_o)$

$$\dot{Q}(\text{radiation}) = \frac{15}{2} T_o^3 \ell^2 \Delta T\, e\, \sigma_{SB} .$$

The ratio of radiation to forced convection heat flux for unity emissivity is approximately

$$\dot{Q}_\lambda(\text{radiation}) \approx 7\left(\frac{\sigma_{SB} T_o^3}{cU}\right).$$

Summary

In order to estimate the importance of the above contributions to the net heat transfer from the electrode volume, let us determine when each contribution is comparable to the primary mechanism of forced convection. This implies the condition $\dot{Q}_\lambda$ (mechanism) = 1.

The conduction term is comparable to forced convection when

$$\dot{Q}_\lambda \text{ (conduction)} = \frac{6}{\sqrt{PR}} = 1. \qquad (PR \gg .06)$$

or

$$PR = 36 .$$

This condition is plotted in Figure 12.12 for water and P = 4. For R < 9 the conduction term is larger than the forced convection term and conversely for R > 9.

The free convection term is comparable to forced convection when

$$\dot{Q}_\lambda \text{ (free convection)} = 1 = \frac{1}{8}\left(\frac{G}{R^2}\right) \qquad \text{for } R \gg 4$$

and

$$\dot{Q}_\lambda \text{(free convection)} = 1 = \frac{1}{30}\left(\frac{G}{R}\right) \qquad \text{for } R \ll 4$$

where the Grashoff number, G, is

$$G = \frac{\ell^3 g \gamma \Delta T}{\nu^2} .$$

The above conditions are plotted in Figure 12.12 for the case

$$\gamma = 2.5 \times 10^{-5} \ ^\circ C^{-1}$$
$$\nu = .01 \text{ cm}^2/\text{sec}$$
$$g = 980 \text{ cm/sec}^2$$

and

$$\Delta T = 20 \ ^\circ C .$$

The latter temperature is approximately the maximum allowable exit temperature without boiling in the boundary layer. Free convection is more important than forced convection in the region below the curve denoted by "free convection" in Figure 12.12.

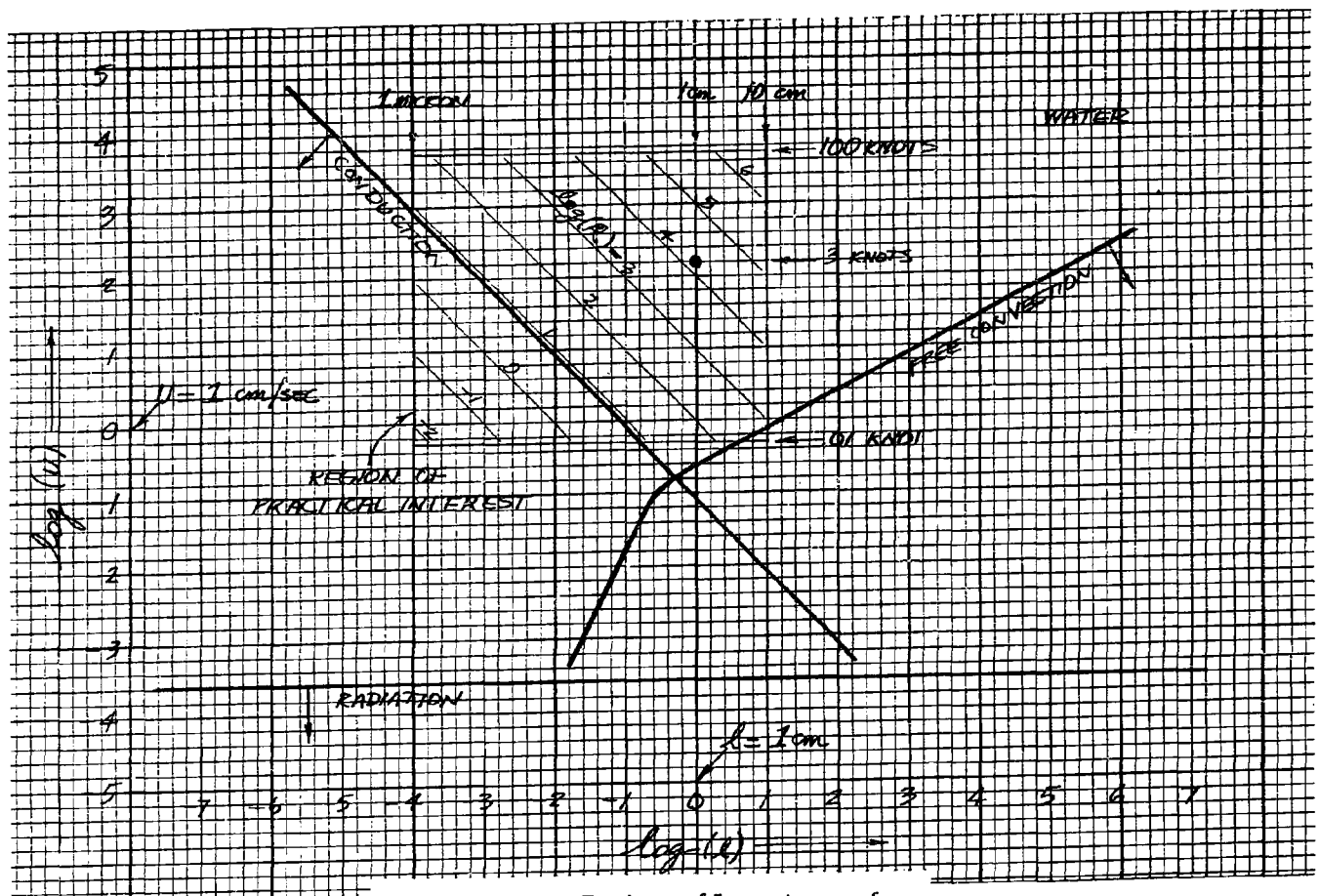

Figure 12.12. Regions of Importance of Heat Transfer Mechanisms

The radiation term is comparable to the forced convection term when

$$\dot{Q}_\lambda\,(\text{RADIATION}) = 1 = 7\left(\frac{\sigma_{SB}\,T_o^3}{cU}\right)$$

or

$$U = \frac{7\sigma_{SB}\,T_o^3}{c} \quad .$$

This condition, which is independent of electrode size, is plotted in Figure 12.12 for the values

$$\sigma_{SB} = 5.7 \times 10^{-12} \text{ watt/cm}^2$$
$$T_o = 293\ ^\circ\text{K}$$
$$c = 4.1 \text{ joule/cm}^3/^\circ\text{C} \quad .$$

Radiation dominates forced convection for a velocity less than

$$U = 2.5 \times 10^{-4} \text{ cm/sec} \quad .$$

The heat transfer by radiation is much less than that by free convection and conduction in all circumstances and may, consequently, be neglected.

The region of practical interest for the values of velocity, U, and electrode size, ℓ, as shown in Figure 12.12 is taken to be

$$.01 \text{ kts} < U < 100 \text{ kts}$$

and

$$10^{-4}\text{cm} < \ell < 10 \text{ cm} \quad .$$

The spot in this Figure corresponds to the values of U = 3 kts and ℓ = 1 cm which are typical values for oceanographic experiments. This point is well within the region where heat transfer is almost completely due to forced convection.

The heat transfer equation is based on steady-state or equilibrium conditions when the input electrical power, P, is equal to the total heat flux, $\dot{Q}$, from the electrode volume. In this case,

$$P = \dot{Q}$$

and

$$\dot{Q} = \dot{Q}(\text{forced convection}) + \dot{Q}(\text{free convection}) + \dot{Q}(\text{conduction}) + \dot{Q}(\text{radiation}) \quad ,$$

or

$$P = \dot{Q}(\text{forced convection})\left\{1 + \dot{Q}_\lambda\,(\text{conduction}) + \dot{Q}_\lambda\,(\text{free convection})\right\},$$

where, in the last equation, the contribution of radiation flux is neglected. The terms in wiggly brackets are denoted by $\dot{Q}_\lambda$. The following expression is suggested as one which is applicable for a wide range of conditions

$$\dot{Q}_\lambda = 1 + \frac{3\sqrt{1+16\,\mathcal{P}\mathcal{R}}}{2\,\mathcal{P}\mathcal{R}} + \frac{\mathcal{G}}{8\mathcal{R}[4+\mathcal{R}]},$$

where the second term is due to conduction and the last term to free convection. This form is chosen since it reduces, in limiting cases, to the expressions previously obtained. For most practical cases, this expression is approximately

$$\dot{Q}_\lambda = 1 + \frac{6}{\sqrt{\mathcal{P}\mathcal{R}}},$$

which contains only the term due to conduction. This function is plotted in Figure 12.13 for $\mathcal{P} = 4$.

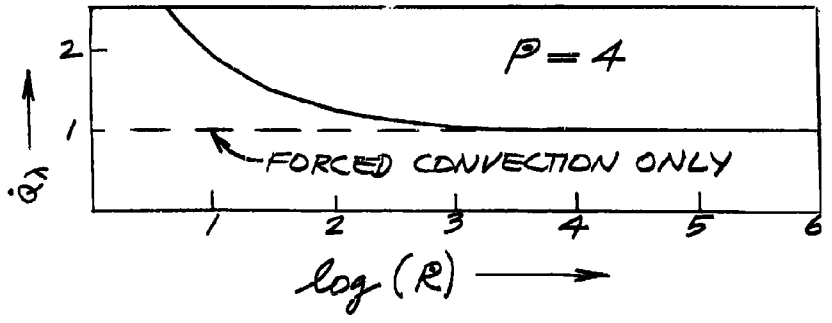

Figure 12.13. Heat Transfer Equation Correction Term

Finally, the heat transfer equation is

$$P = 2cAU\sqrt{\Delta T}\cdot\dot{Q}_\lambda$$

$$\approx 2cAU\sqrt{\Delta T}\left\{1 + \frac{6}{\sqrt{\mathcal{P}\mathcal{R}}}\right\}.$$

This expression is considered only an approximation to the actual heat transfer equation, which must be determined experimentally for <u>each</u> given electrode configuration.

12.6 Non-Linear Heating

The theory developed in previous Sections assumed that the conductivity of the medium is a linear function of temperature. This assumption is valid for relatively small temperature changes (say, less than 10 ^{o}C). We now consider the general case where the conductivity is an arbitrary function of temperature and wide temperature variations will be considered. Since the resulting inhomogeneity in the electrode volume is extremely difficult to analyze in general, only two special cases of uniform flow in a parallel plate electrode are considered. The analysis of this one-dimensional flow provides information to estimate the sensitivity of the electrode to velocity changes in the case of heating to the boiling point of water.

One-Dimensional Flow

The two special cases of non-linear heating in one-dimensional flow are: a) parallel plate electrodes with uniform fluid flow parallel to the plates. This case will be denoted by ($\perp$) because the fluid flow is perpendicular to the electrical current lines. This situation is illustrated in Figure 12.14 . Fringe field effects are neglected, and the separation between the plates is small enough so that the current lines are perpendicular to the electrodes in spite of non-uniformity in the conductivity, b) parallel plate electrodes (porous screens) with uniform fluid flow perpendicular to the plates (from one to the other). This case will be denoted by (11) because the flow is parallel to the electrical currents. This situation is illustrated in Figure 12.15 . Fringe field effects are neglected. These examples serve to illustrate the extremes of non-linear heating corresponding to electrical current flow ($\vec{\nabla}\phi$) perpendicular and parallel, respectively, to the fluid velocity ($\vec{v}$) and electrical conductivity gradient ($\vec{\nabla}\sigma$). An actual electrode presumably demonstrates a non-linear heating behavior intermediate to the above extreme cases.

($\perp$) Case - The temperature rise due to electrical heating increases in the direction of fluid flow, therefore, the electrical conductivity of the medium also increases in this direction. Since the current density is perpendicular to the flow velocity and conductivity gradient, we have

$$\vec{\nabla}\phi \cdot \vec{\nabla}\sigma = 0 ,$$

which implies there is no potential field distortion (since $\nabla^2\phi = 0$) due to the inhomogeneity of the medium (Sec. 10.1).

The temperature distribution satisfies the equation

$$\frac{dT}{dx} = \frac{PR}{cV}\,\sigma(\vec{\nabla}\phi)^2 ,$$

where P is the electrode power, R the resistance, c the heat capacity per

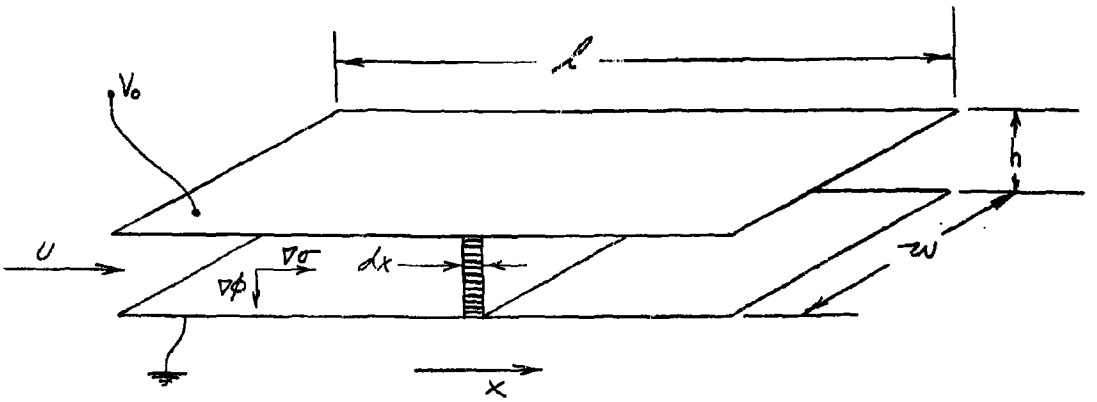

Figure 12.14. Perpendicular ($\perp$) Double Plate Electrode Heating Arrangement

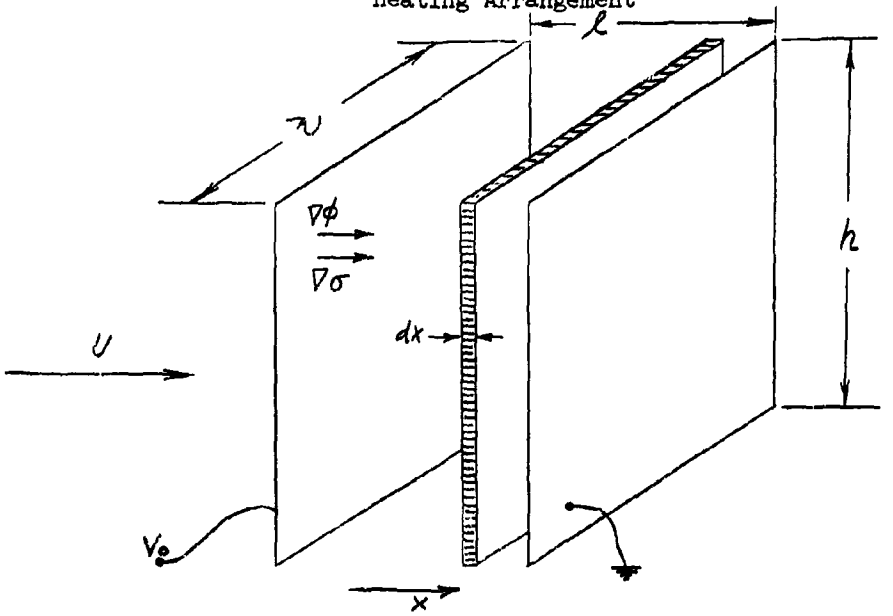

Figure 12.15. Parallel (11) Double Plate Electrode Heating Arrangement

unit volume of the water, U the flow velocity, T the temperature and σ the conductivity of the water which is a function of temperature. The uniform unit potential gradient is

$$|\vec{\nabla}\phi| = \frac{1}{h}$$

and rewriting the above equation:

$$\frac{\sigma(T_0)}{\sigma(T)}\,dT = \frac{PR\,\sigma(T_0)}{cU\,h^2}\,dx,$$

where $\sigma(T_0)$ is the conductivity at the ambient temperature T_0. Integrating over the length, ℓ, of the electrode

$$\int_{T_0}^{T_\Lambda} \frac{\sigma(T_0)}{\sigma(T)}\,dT = \frac{PR\,\sigma(T_0)\ell}{cU\,h^2} \equiv F_\perp(T_0, T_\Lambda),$$

where T_Λ is the exit temperature, and the function $F_\perp$ (units of temperature) is defined by the above integral of the conductivity. If we denote the "cold resistance" by R_0 then

$$R_0 = \frac{h}{\sigma(T_0)\ell w},$$

and the frontal area of the electrode is

$$A = wh .$$

The parameter $\eta_\perp$ (which gives the reduction of resistance due to the heating) is defined by

$$R = \eta_\perp R_0 \qquad (\eta_\perp < 1)$$

and

$$F_\perp = \left(\frac{P}{cUA}\right)\eta_\perp .$$

Integrating the heating equation again with the conductivity as a function of position, $\sigma[T(x)]$, we get

$$T_\Lambda - T_0 = \frac{P}{cUA}\left\{\frac{Rw}{h}\int_0^\ell \sigma\,dx\right\}$$

but the term in brackets is unity (Sec. 10.3), thus

$$T_\Lambda - T_0 = \frac{P}{cUA}$$

and

$$\eta_\perp = \frac{\int_{T_0}^{T_\Lambda} \frac{\sigma(T_0)}{\sigma(T)}\, dT}{T_\Lambda - T_0} \equiv \eta_\perp (T_0, T_\Lambda),$$

and

$$(T_\Lambda - T_0)\, \eta_\perp = F_\perp .$$

This parameter may be evaluated if the variation of the conductivity, $\sigma(T)$, of the medium is known over the temperature range of interest T_0 to T_Λ.

(11) Case - In this case the full effects of potential field distortion are present since the conductivity gradient is everywhere parallel to the potential gradient (current lines). Although the field intensity is distorted because of the inhomogeneity of the conducting medium, in this simple case the direction of the current lines is unchanged and is everywhere parallel to the flow velocity ($\vec{U}$). The total electrode current, I, is independent of x, thus

$$I = (wh)\, V_0\, \sigma\, \nabla\phi = \text{CONSTANT}$$

where V_0 is the electrode voltage, and A = wh. The electrode resistance, R, satisfies

$$\frac{1}{R} = \frac{I}{V} = A\sigma\, \nabla\phi \quad ,$$

and the temperature distribution satisfies

$$\frac{dT}{dx} = \frac{PR}{cU}\, \sigma\, (\nabla\phi)^2$$

Combining these relations, we have

$$\frac{dT}{dx} = \left(\frac{P}{cUA}\right) \frac{1}{RA\sigma} .$$

Integrate this equation with σ a function of temperature, $\sigma(T)$:

$$\int_{T_0}^{T_\Lambda} \frac{\sigma(T)}{\sigma(T_0)}\, dT = \left(\frac{P}{cUA}\right) \frac{l}{RA\sigma(T_0)} \equiv F_{11}(T_0, T_\Lambda),$$

which defines the function F_{11}. The "cold resistance," R_0, in this case is

$$R_0 = \frac{l}{\gamma(T_0) A} \quad ,$$

and define the parameter η_{11} (which gives the reduction of resistance due to heating) such that

$$R = \eta_{11} R_0 \qquad (\eta_{11} < 1)$$

then

$$\eta_{11} F_{11} = \left(\frac{P}{CUA}\right).$$

Now, integrating the temperature equation with σ a function of x, $\sigma[T(x)]$, we obtain

$$T_\Lambda - T_0 = \frac{P}{CUA}\left\{\frac{1}{RA}\int_0^\ell \frac{dx}{\sigma}\right\}.$$

The term in brackets is unity (since $RA\sigma \nabla\phi = 1$), thus

$$T_\Lambda - T_0 = \frac{P}{CUA},$$

and

$$\eta_{11} = \frac{T_\Lambda - T_0}{\int_{T_0}^{T_\Lambda} \frac{\sigma(T)}{\sigma(T_0)}\, dT} \equiv \eta_{11}(T_0, T_\Lambda),$$

and

$$\eta_{11} F_{11} = T_\Lambda - T_0.$$

This parameter may be evaluated by means of data on the temperature dependence of the conductivity.

If the conductivity is independent of temperature

$$\sigma(T) = \sigma(T_0)$$

$$F_{11} = F_\perp = T_\Lambda - T_0 \quad .$$

and

$$\eta_{11} = \eta_\perp = 1 \quad .$$

The conductivity of 32.8 ‰NaCl solution (Sec. 7.2) has been used

to calculate the parameters $\eta_\perp$ and η_{11}. An initial temperature of 20 °C = T_o is used for the situation in laboratory work where the maximum exit temperature before boiling at 1 atmosphere is 100 °C = T_Λ. An initial temperature of 0 °C = T_o is used for the situation deep in the ocean where the temperature is near freezing and the pressure is high enough that temperatures as high as 360 °C = T_Λ (critical point) may be reached before boiling sets in. These curves are shown in Figure 12.16. Unfortunately the small temperature dependence of the heat capacity was not included in this data. The resulting error is, however, only about 2 %, at worst. The curve of $\eta(T_o, T_\Lambda)$ for a general electrode will presumably lie between the respective η_{11} and $\eta_\perp$ curves. The velocity dependence of the electrode resistance for non-linear heating is now considered.

Velocity Dependence

The variation of electrode resistance with velocity follows from the relations

$$R = \eta(T_o, T_\Lambda) R_o$$

and

$$T_\Lambda - T_o = \frac{P}{cAU} \quad .$$

For a given power, P, and cold resistance, R_o, the resistance, R, depends on the velocity, U, through the temperature dependence of η. In order to plot this dependence it is convenient to define a reference velocity, U_{100}, which represents the velocity at which the exit temperature is 100 °C or

$$U_{100} = \frac{P}{cA(100 - T_o)} \quad .$$

The method of measuring the electrode resistance depends on the mode of operation of the associated electronic equipment. Three modes of operation may be distinguished: a) constant-current-operation, b) constant-power-operation, and c) constant-voltage-operation. The constant-temperature mode is not pertinent to the present analysis.

For constant-power-operation (CPO) the velocity U relative to U_{100} is found to be

$$\frac{U}{U_{100}} = \left(\frac{100 - T_o}{T_\Lambda - T_o}\right).$$

For constant-current-operation (CCO) the power is

$$P = I^2 R \quad ,$$

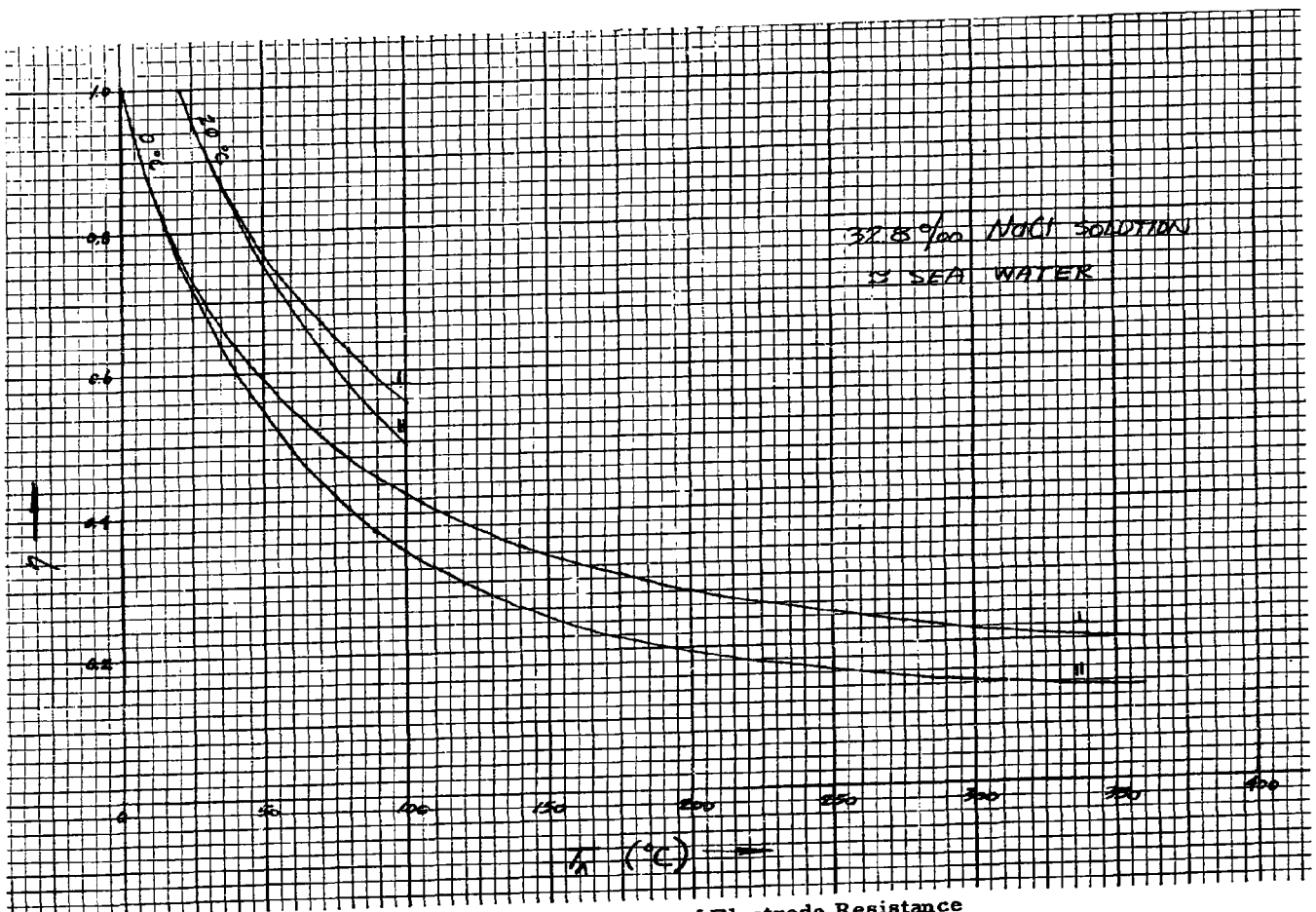

Figure 12.16. Reduction of Electrode Resistance as a Function of Exit Temperature

where the electrode current I is held constant. Then

$$T_\Delta - T_0 = \frac{P}{cAU} = \frac{I^2 R}{cAU}$$

$$= \left(\frac{P_0}{cAU}\right)\eta$$

where $P_0 = I^2 R_0$. The relative velocity is

$$\frac{U}{U_{100}} = \left\{\frac{\eta(T_0, T_\Delta)}{\eta(T_0, 100)}\right\} \cdot \left(\frac{100 - T_0}{T_\Delta - T_0}\right)$$

and

$$U_{100} = \frac{P_0\, \eta(T_0, 100)}{cA(100 - T_0)} \quad .$$

For constant voltage operation (CVO) the power is

$$P = \frac{V_0^2}{R} \quad ,$$

where the electrode voltage, V_0, is held constant. Then

$$T_\Delta - T_0 = \left(\frac{V_0^2}{R}\right)\frac{1}{cAU}$$

$$= \left(\frac{P_0}{cAU}\right)\frac{1}{\eta}$$

where $P_0 = V_0^2/R_0$. It follows that the relative velocity is

$$\frac{U}{U_{100}} = \left\{\frac{\eta(T_0, 100)}{\eta(T_0, T_\Delta)}\right\} \cdot \left(\frac{100 - T_0}{T_\Delta - T_0}\right)$$

and

$$U_{100} = \frac{P_0}{cA(100 - T_0)\,\eta(T_0, 100)} \quad .$$

Curves of η_Δ and η_{11} vs. (U/U_{100}) for these three modes of operation are shown in Figure 12.17 for CPO, Figure 12.18 for CCO, and Figure 12.19 for CVO. These curves are calculated directly from the data of Figure 12.20, which shows the relation between U/U_{100} and T_Δ and T_0 for the three modes of operation. The data of Figure 12.20 follows from that of Figure 12.16.

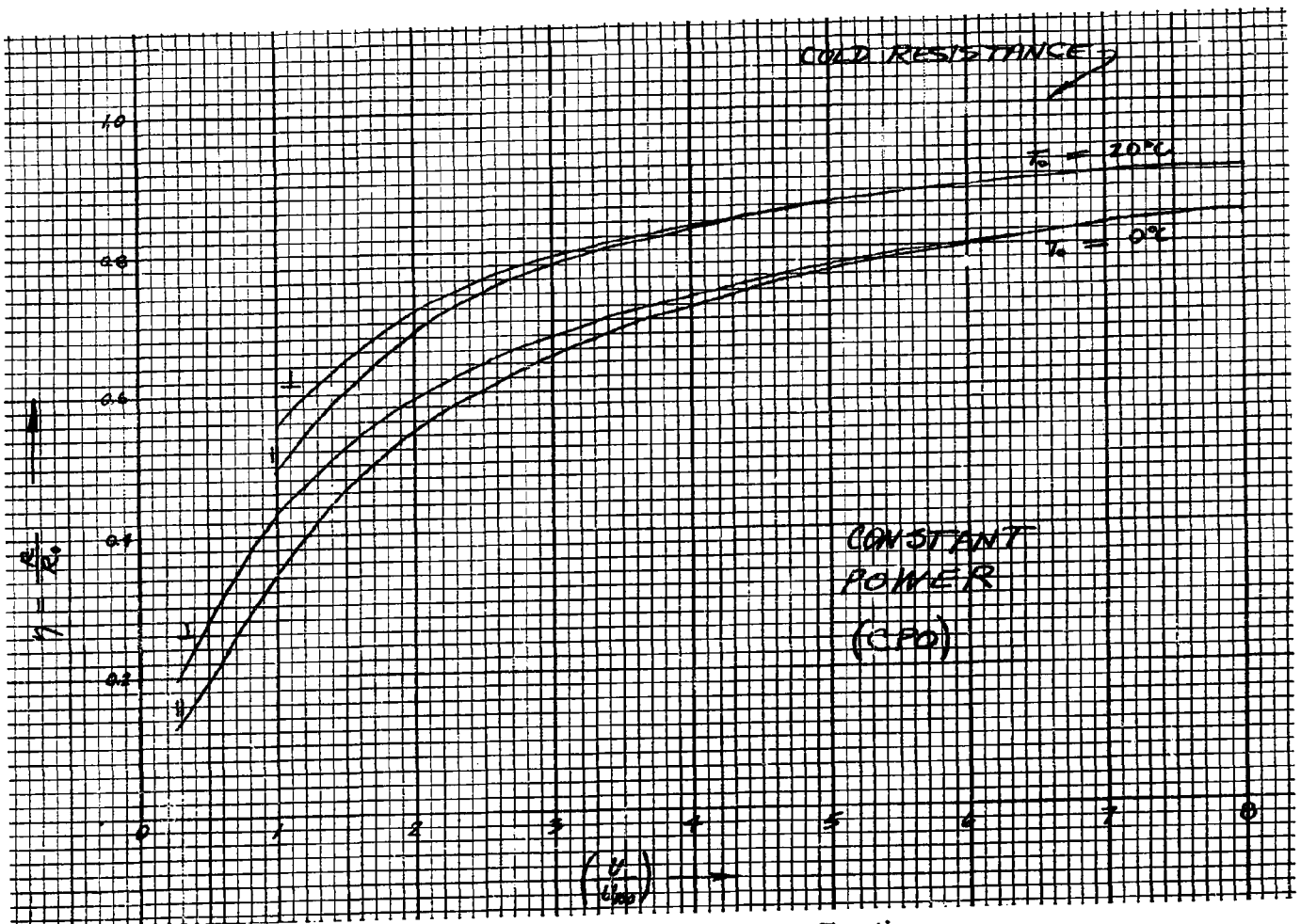

Figure 12.17. Electrode Resistance as a Function of Velocity for Constant-Power-Operation

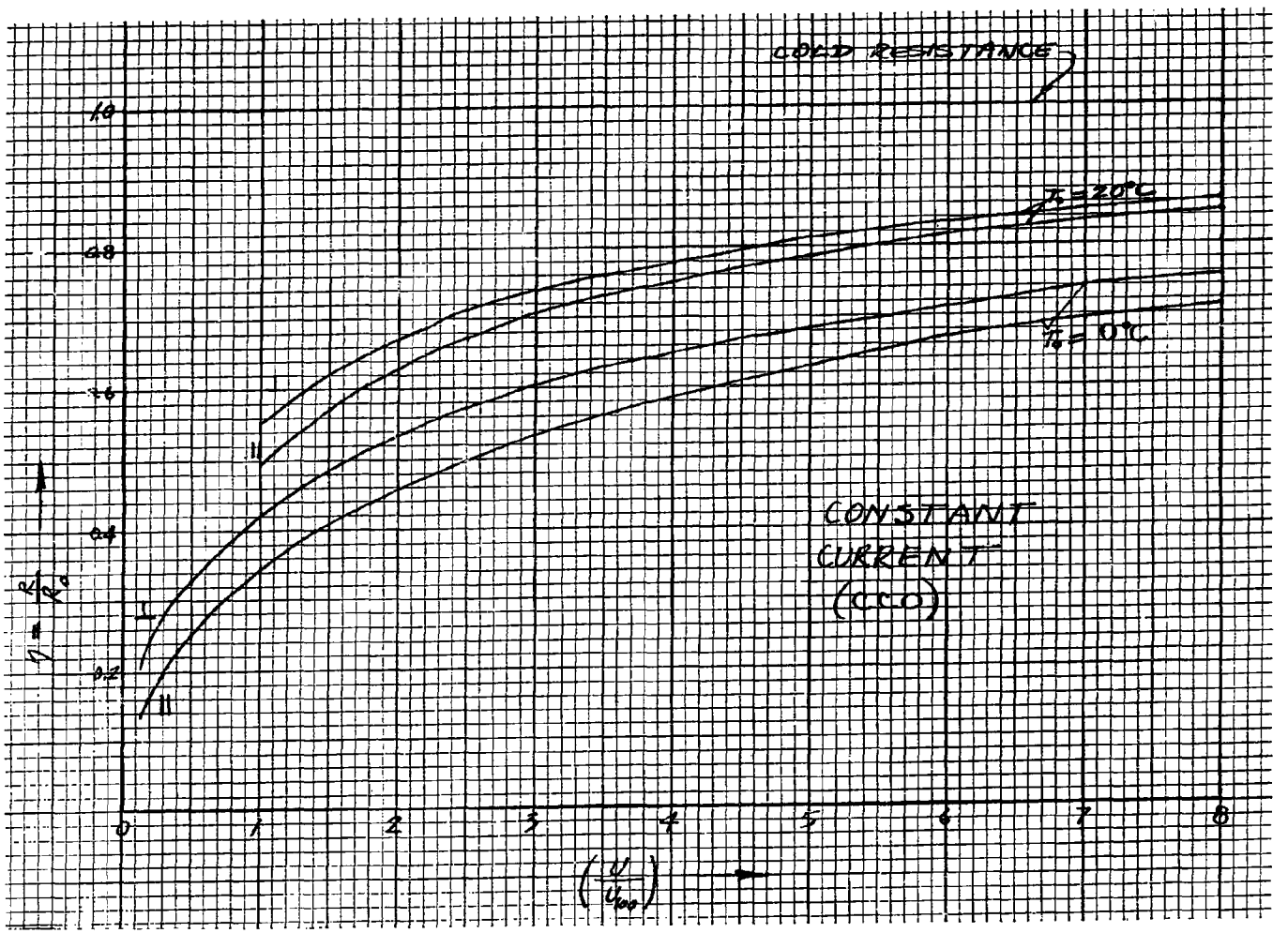

Figure 12.18. Electrode Resistance as a Function of Velocity for Constant-Current-Operation

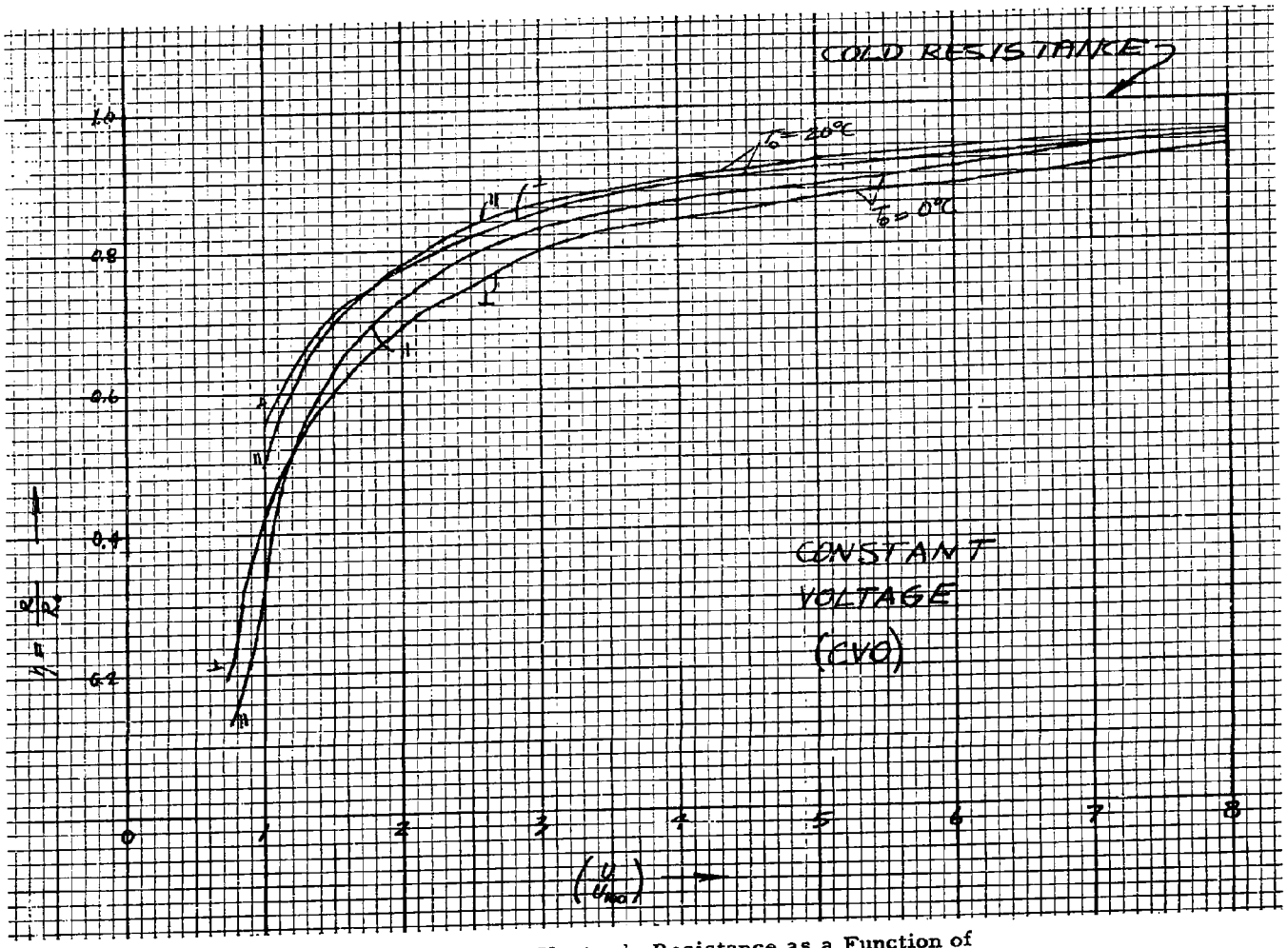

Figure 12.19. Electrode Resistance as a Function of Velocity for Constant-Voltage-Operation

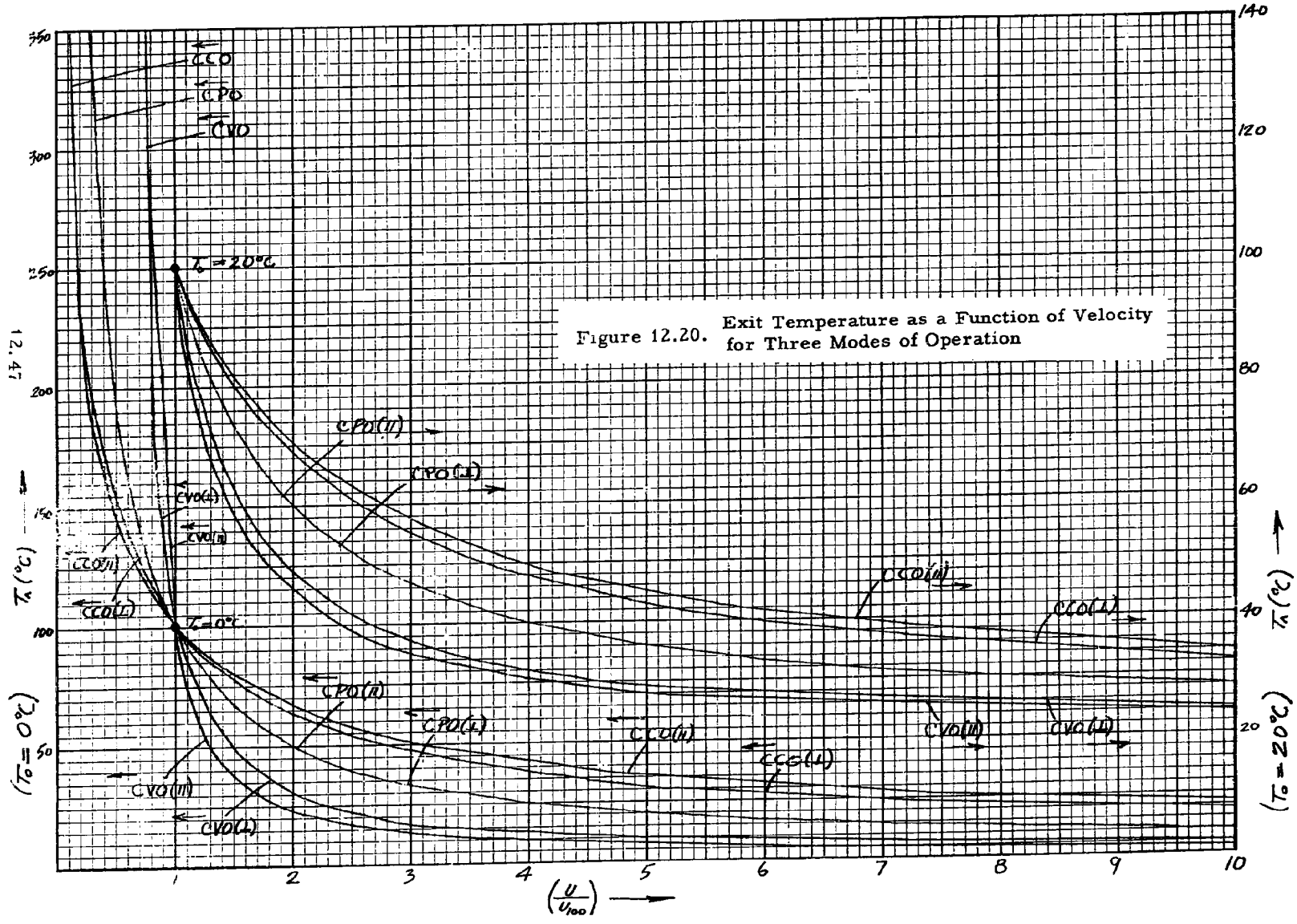

Figure 12.20. Exit Temperature as a Function of Velocity for Three Modes of Operation

It will be noticed that changes in resistance due to changes in velocity become larger in all cases at low speeds of the order of U_{100} where the temperature rise due to heating is large. If we assume that the characteristic curves for a general electrode lie at some intermediate value between the ($\perp$) and (11) cases, the average (45°) of these two cases is approximately applicable to most electrodes. These curves are shown in Figure 12.21 for $T_o = 20^{\circ}C$, and Figure 12.22 for $T_o = 0^{\circ}C$.

The differential sensitivity of resistance to small changes in velocity is calculated in the following way. Define the "velocity sensitivity exponent," α_u, as (Sec. 6.2)

$$\frac{\delta R}{R} = \alpha_u \left(\frac{\delta U}{U}\right) \quad ,$$

where δR and δU are small increments in resistance and velocity, respectively, at the steady-state operating point. Now

$$\delta R = \left(\frac{\partial R}{\partial U}\right) \delta U$$

and

$$R = \eta \; R_o$$

thus,

$$\frac{\partial R}{\partial U} = R_o \left(\frac{\partial \eta}{\partial T_\Lambda}\right)\left(\frac{\partial T_\Lambda}{\partial U}\right).$$

Since

$$T_\Lambda - T_o = \frac{P}{cAU} = \Delta T \quad ,$$

it follows that

$$\frac{\partial T_\Lambda}{\partial U} = \left(\frac{P}{cAU}\right)\left\{\frac{1}{P}\left(\frac{\partial P}{\partial U}\right) - \frac{1}{U}\right\}$$

$$= \left(\frac{P}{cAU}\right)\left\{\frac{1}{P}\left(\frac{\partial P}{\partial R}\right)\left(\frac{\partial R}{\partial U}\right) - \frac{1}{U}\right\}.$$

The derivative $(\partial P/\partial R)$ depends on the mode of operation of the electronics. Collecting the above expressions we obtain

$$\frac{\partial R}{\partial U} = R_o \left(\frac{\partial \eta}{\partial T_\Lambda}\right)\left(\frac{P}{cAU}\right)\left\{\frac{1}{P}\left(\frac{\partial P}{\partial R}\right)\left(\frac{\partial R}{\partial U}\right) - \frac{1}{U}\right\}$$

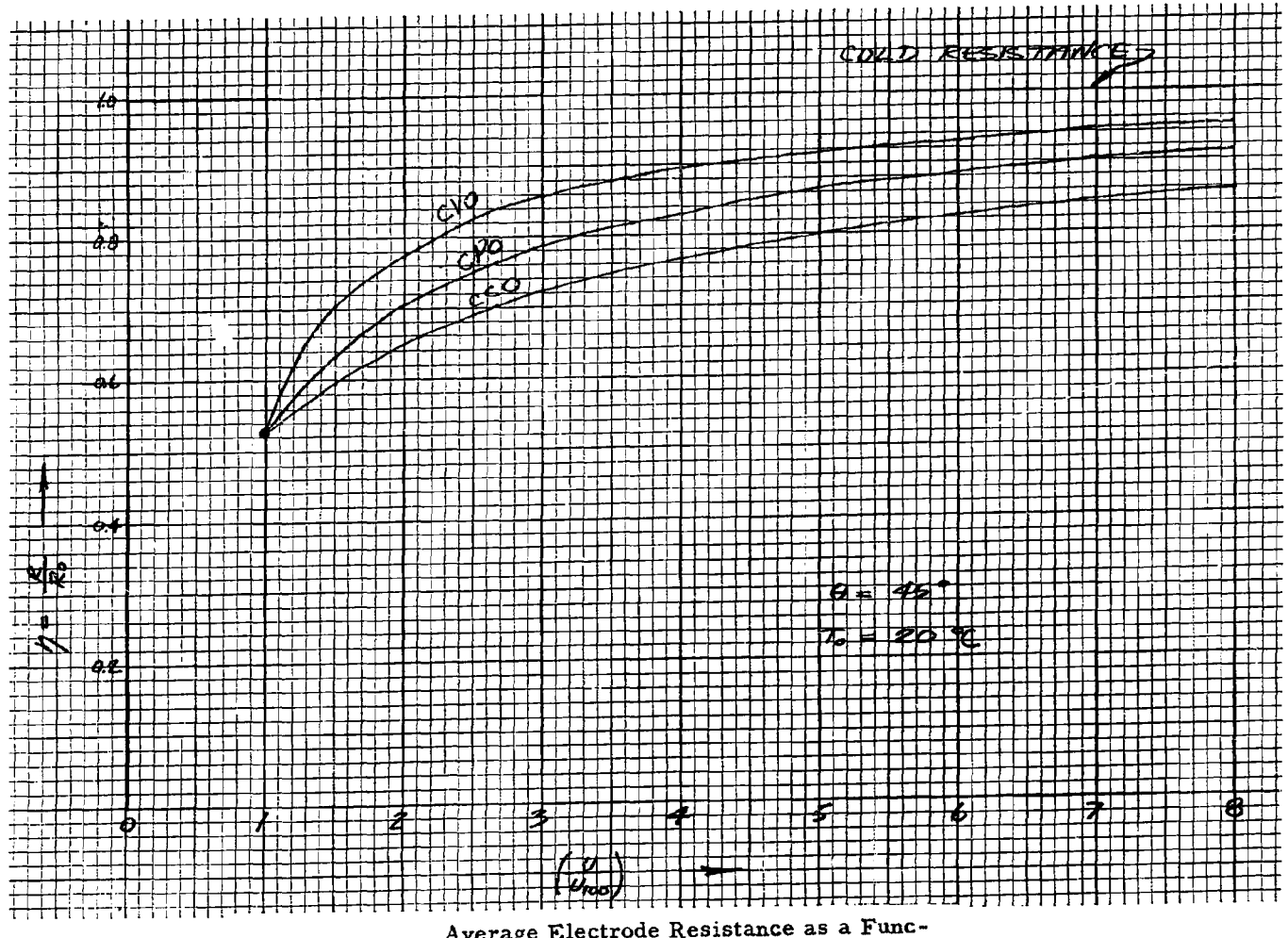

Figure 12.21. Average Electrode Resistance as a Function of Velocity for Three Modes of Operation and 20 °C Ambient Temperature

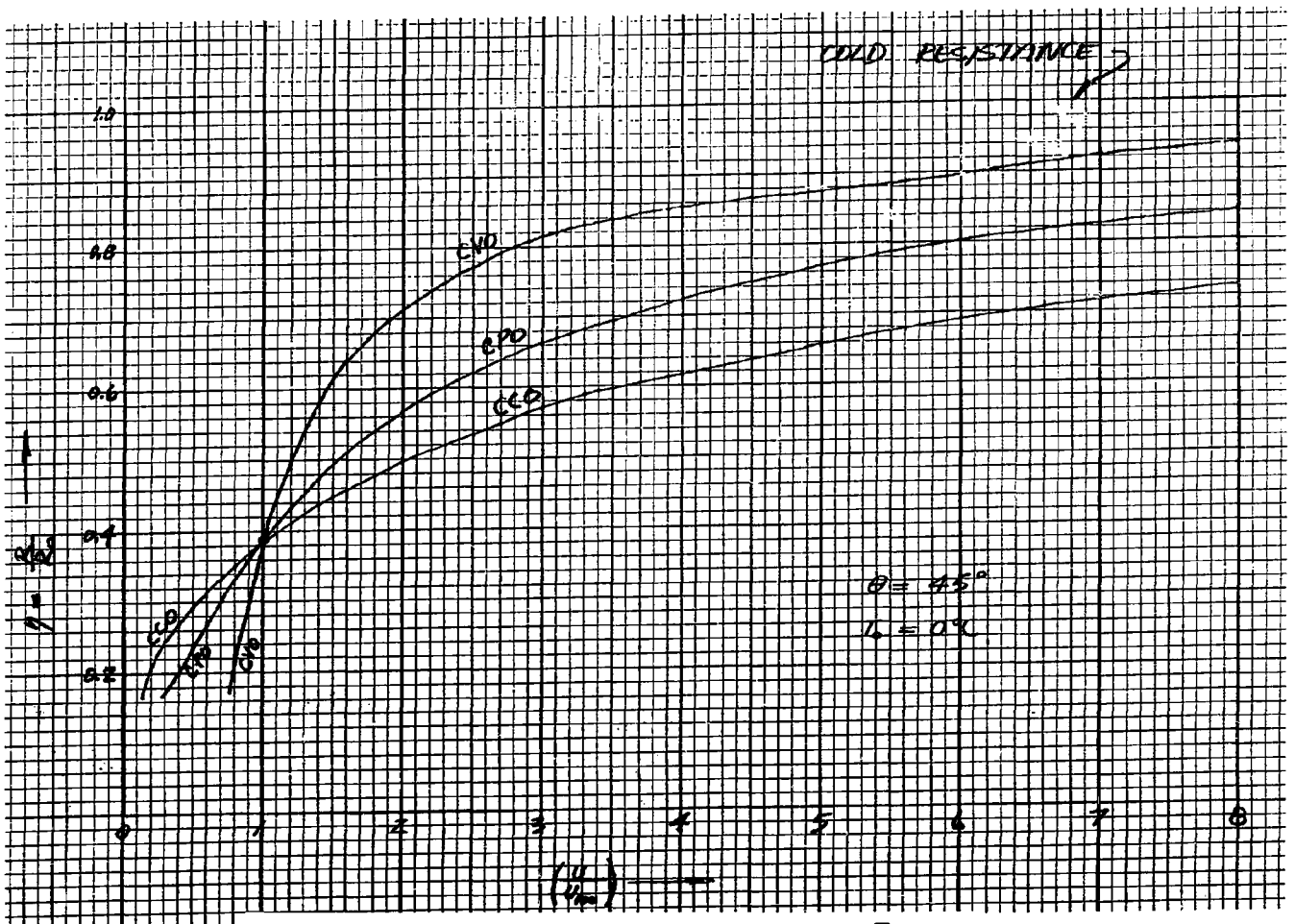

Figure 12.22. Average Electrode Resistance as a Function of Velocity for Three Modes of Operation and 0 °C Ambient Temperature

OR
$$\frac{\partial R}{\partial U} = R\left(\frac{\Delta T}{\eta}\right)\left(\frac{\partial \eta}{\partial T_\Delta}\right)\left\{\frac{1}{P}\left(\frac{\partial P}{\partial R}\right)\left(\frac{\partial R}{\partial U}\right) - \frac{1}{U}\right\}.$$

It is convenient to define a factor M as follows:

$$M = \frac{\Delta T}{\eta}\left(\frac{\partial \eta}{\partial T_\Delta}\right) \qquad (M < 0)$$

Solving the above equation for $(\partial R/\partial U)$ we find

$$\left\{1 - M\ \frac{R}{P}\left(\frac{\partial P}{\partial R}\right)\right\}\left(\frac{\partial R}{\partial U}\right) = -\frac{R}{U}M \ .$$

Furthermore, define the quantity Φ such that

$$\Phi = 1 - M \cdot \frac{R}{P}\left(\frac{\partial P}{\partial R}\right) \ .$$

Thus, we can write

$$\frac{\partial R}{\partial U} = -\left(\frac{R}{U}\right)\frac{M}{\Phi}$$

and

$$\frac{\delta R}{R} = -\left(\frac{M}{\Phi}\right)\left(\frac{\delta U}{U}\right)$$

or

$$\alpha_U = -\frac{M}{\Phi} \ .$$

To evaluate Φ, consider the circuit of Figure 12.23 which shows the sensing element of resistance R as a load on a power source of internal impedance Z and voltage V_s (which is a constant). The voltage on the electrode is

$$V_e = V_s\left(\frac{R}{R + Z}\right) \ ,$$

and the power dissipated in the electrode is

$$P = V_s^2\ \frac{R}{(R + Z)^2} \ .$$

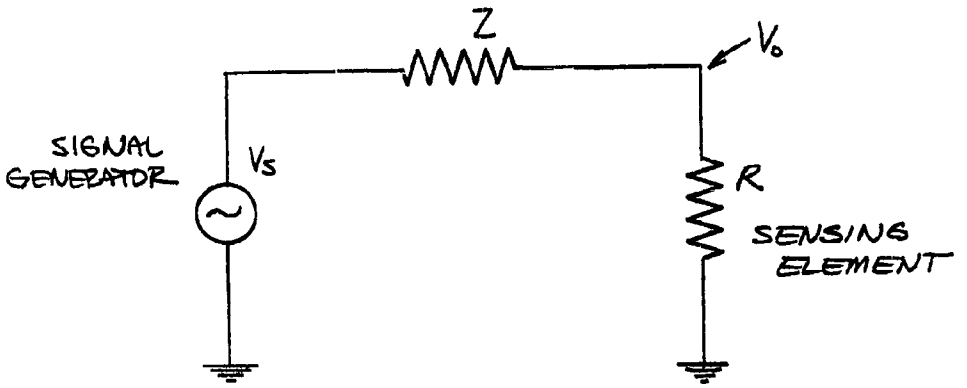

Figure 12.23. Signal Generator and Sensing Element

It is easily shown that

$$\frac{R}{P}\left(\frac{\partial P}{\partial R}\right) = \left(\frac{Z - R}{Z + R}\right) \quad ,$$

therefore

$$\Phi = 1 - M\left(\frac{Z - R}{Z + R}\right).$$

The values of this function for three modes of operation are shown in Table 12.1 .

Table 12.1 . The Function Φ for Three Modes of Operation $(M < 0)$

Mode of Operation	Source Impedance	Φ
CPO	$Z = R$	1
CCO	$Z \gg R$	1 - M
CVO	$Z \ll R$	1 + M

The CPO mode is of particular interest:

$$\Phi = 1$$

and

$$\alpha_u = -M \quad .$$

This sensitivity coefficient is evaluated for the simple cases (⊥) and (11) considered previously, which take into account the non-linear heating. It should be remembered that if the exit temperature rise, ΔT, is relatively small (say, less than $10^{\circ}C$) the sensitivity coef-

ficient reduces to that obtained previously for linear heating, viz.,

$$\alpha_v = + \beta_T(T_0)\ \frac{\Delta T}{2} = \beta_T\ (T_0)\ \overline{\Delta T}$$

$$\approx 0.15 \quad \text{at} \quad T_0 = 0\ ^\circ C, \quad \Delta T = 10\ ^\circ C$$

$$\approx 0.10 \quad \text{at} \quad T_0 = 20\ ^\circ C, \quad \Delta T = 10\ ^\circ C \ .$$

For the ($\perp$) case we have

$$M_\perp = \frac{\Delta T}{\eta_\perp}\left(\frac{\partial \eta_\perp}{\partial T_\Lambda}\right)$$

and

$$\eta_\perp = \frac{\int_{T_0}^{T_\Lambda} \frac{\sigma(T_0)}{\sigma(T)}\, dT}{\Delta T} \ .$$

It follows that

$$\frac{\partial \eta_\perp}{\partial T_\Lambda} = \frac{1}{\Delta T}\left\{ \frac{\sigma(T_0)}{\sigma(T_\Lambda)} - \eta \right\}$$

and

$$- M_\perp = \alpha_{v\perp} = 1 - \frac{\sigma(T_0)}{\eta_\perp(T_i, T_\Lambda)\,\sigma(T_\Lambda)} \ .$$

In a similar manner, it may be shown in the (11) case that

$$- M_{11} = \alpha_{v\,11} = \frac{\eta_{11}(T_0, T_\Lambda)\,\sigma(T_\Lambda)}{\sigma(T_0)} - 1.$$

These two limiting sensitivity exponents, are shown in Figure 12.24 as a function of exit temperature for ambient temperatures of 0 $^\circ$C and 20 $^\circ$C. The velocity sensitivity exponent, α_v, for an actual electrode will assume a value intermediate between $\alpha_{v\perp}$ and α_{v11} shown in this Figure (45°).

For operation at atmospheric pressure, high velocity sensitivity calls for the highest possible electrode power without boiling (T_Λ = 100°C). For operation at greater pressure, for example deep in the ocean, an optimum power level exists which corresponds to an exit temperature of about 150°C.

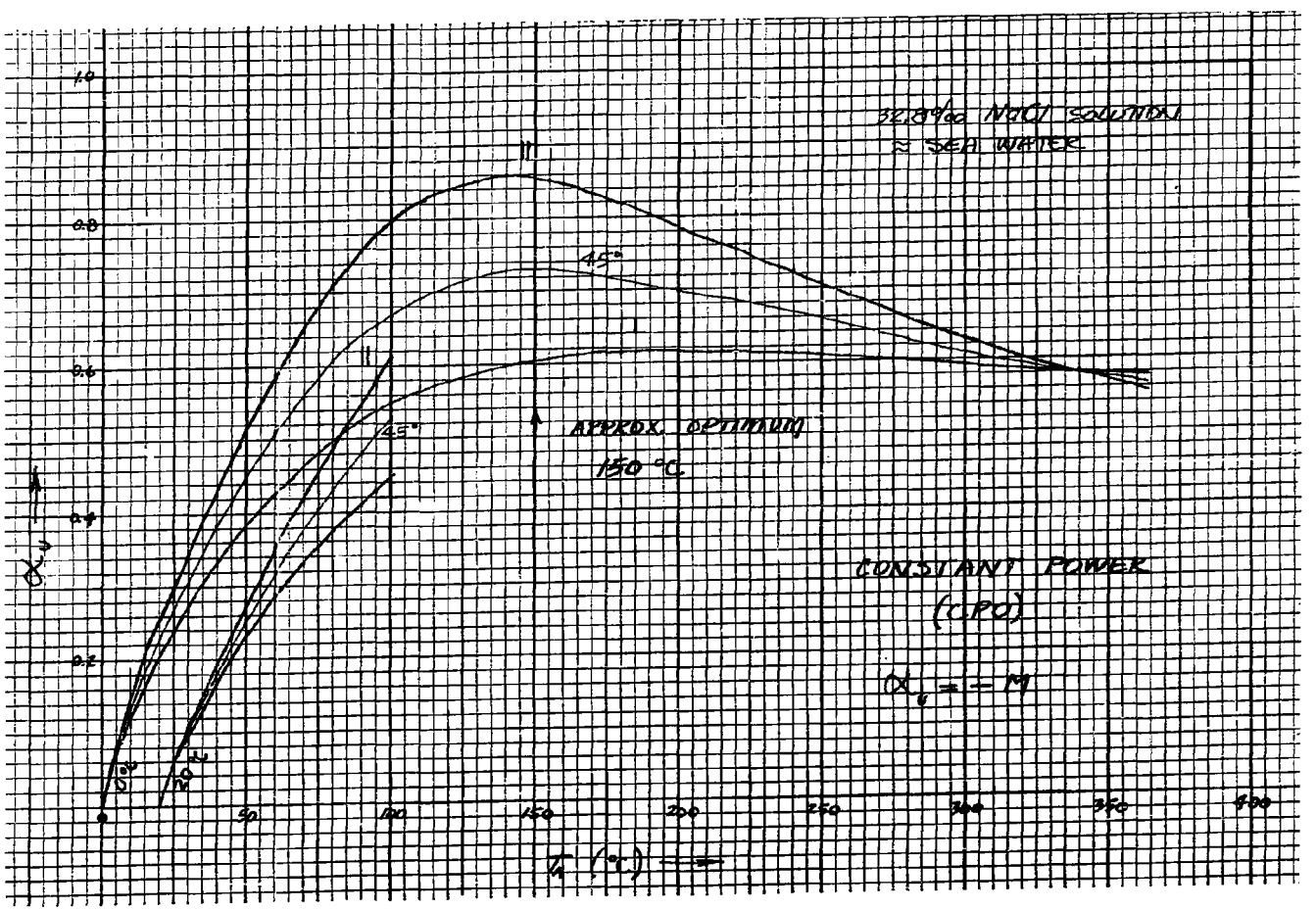

Figure 12.24. Velocity Sensitivity Exponent as a Function of Exit Temperature

13. CONDUCTIVITY RESPONSE

The factors which set the limits on the frequency response of a measurement of the electrolytic conductivity with an electrode probe are considered in this Section. The analysis covers those variables which effect the conductivity directly, as temperature and salinity, or indirectly, such as bubbles. The self-heating at the electrode is assumed small enough so that velocity effects may be neglected. The primary factors which determine the conductivity response are the size and configuration of the electrode structure, the velocity boundary layer flow, and thermal and ionic diffusion processes.

The frequency response of a probe is related to its physical size and velocity through the medium. The relations between physical dimensions, frequency, and probe velocity are summarized below. If a component of the conductivity structure in the medium has a physical wavelength, λ , the frequency, f, of the resultant electrode resistance variations is related to the speed, U, of the probe through the medium by

$$\lambda f = U \quad \text{or} \quad f = \frac{U}{\lambda} \quad .$$

The wavenumber, k, of this component is

$$k = \frac{2\pi}{\lambda} \quad \text{or} \quad \lambda = 2\pi\, k^{-1}$$

and

$$f = \frac{kU}{2\pi} \quad \text{or} \quad \omega = kU$$

where

$$\omega = 2\pi f \quad .$$

The inverse wavenumber, k^{-1}, is a measure of the "blob size" of the structure under consideration in the medium. The relation between frequency, wavelength and velocity is plotted in Figure 13.1 for the range of these variables which are of interest in most fluid measurements. As an example,

U = 3 knots = 154 cm/sec
k^{-1} = 3 mm
k = 3.3 cm^{-1}
λ = 1.8 cm

and

f = 85 cps .

Reference must be made to the temperature and salinity structure of

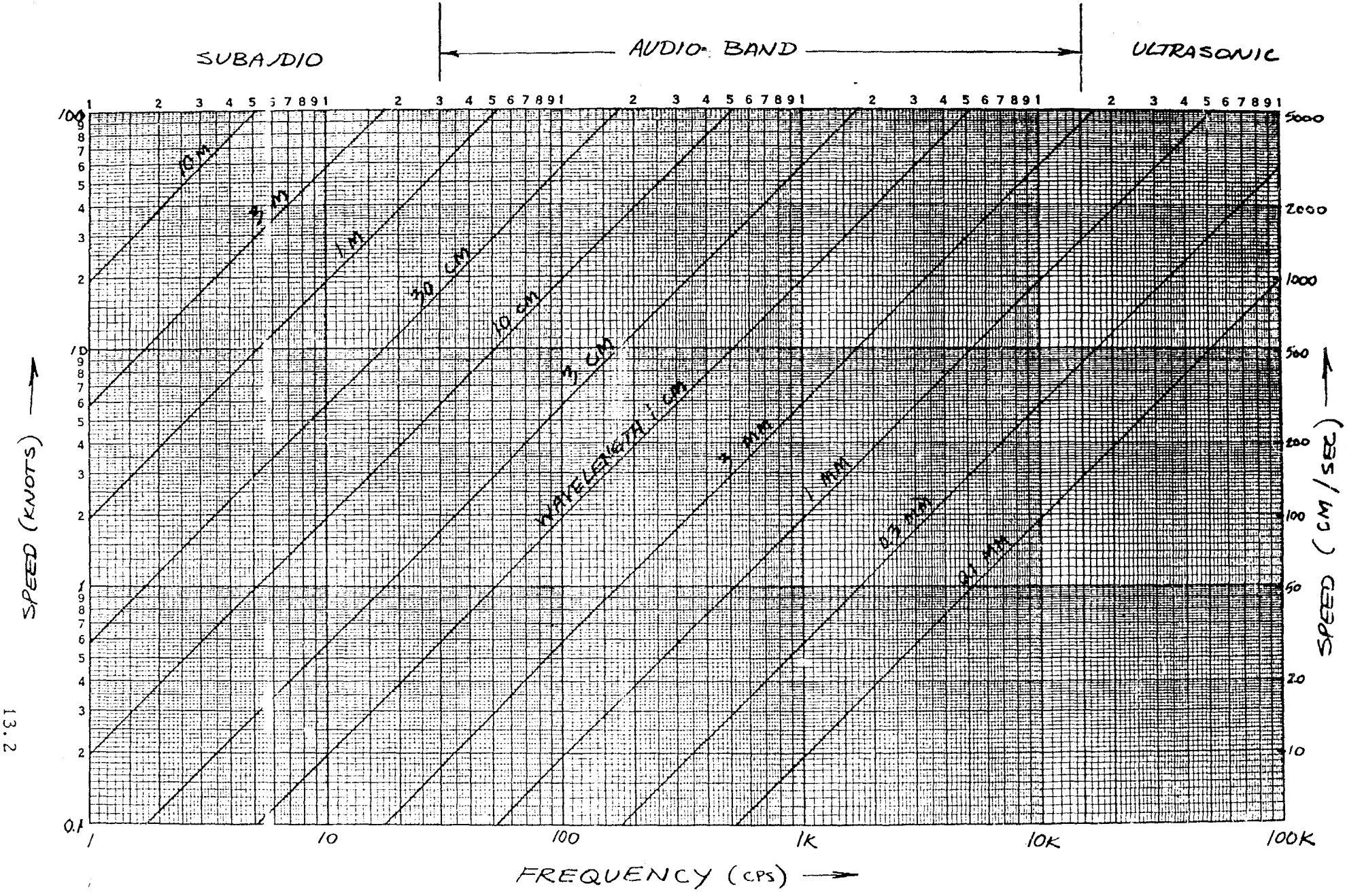

Figure 13.1. Relation Between Physical Wavelength, Frequency and Velocity

the medium when the response to conductivity structure involves diffusion processes. This is necessary since the conductivity at a point is a function only of the temperature and salinity, and thermal diffusion is not the same as (more rapid) ionic diffusion. Thus, the diffusion of the conductivity structure involves the combined effects of thermal and ionic diffusion. If σ, T, S, represent small variations of the conductivity, temperature, and salinity about their respective average values then

$$\sigma = \beta_T T + \beta_S S \quad ,$$

where β_T and β_S are the temperature and salinity coefficients of the conductivity. The equations which govern the temperature and salinity structure at a point in the medium where the velocity is $\vec{u}$, are

$$\frac{\partial T}{\partial t} + \vec{u} \cdot \vec{\nabla} T = \alpha \nabla^2 T$$

$$\frac{\partial S}{\partial t} + \vec{u} \cdot \vec{\nabla} S = D \nabla^2 S \, ,$$

where α and D are the thermal and ionic diffusivity constants of the medium. These equations relate to the redistribution of the respective scalar variables by forced convection and diffusion. It is clear that, unless the diffusion terms are small, the conductivity structure depends on the individual temperature and salinity structure. If the structure is determined by convection only, then

$$\frac{\partial \sigma}{\partial t} + \vec{u} \cdot \vec{\nabla} \sigma = 0$$

In this case the response of the probe to conductivity, temperature and salinity are identical. In an isotropic homogeneous turbulent field with random temperature and salinity structure, the size of structure where viscous forces are important is (1,2)

$$\left(\frac{\nu^3}{\epsilon}\right)^{\frac{1}{4}}$$

where ν is the kinematic viscosity, and ϵ is the dissipation per unit mass. This dissipation length in the ocean is of the order of 3 mm which is the approximate size of the smallest turbulent blobs of sea water. The corresponding size which determines the smallest blob size for temperature and salinity structure is smaller than this dimension since the Prandtl number, P, and Schmidt number, S, are greater than unity in water:

$$\nu = \alpha P \qquad \text{and} \qquad P \approx 7$$

$$\nu = D S \qquad \text{and} \qquad S \approx 800 \quad .$$

Since $S \gg P$, the salinity structure extends to smaller scales than the temperature structure.

The determination of the response in the general case for a given electrode configuration involves the description of the random conductivity field in a turbulent medium, consideration of the effects of thermal and ionic diffusion in the region of the boundaries of the probe, and the distortion of the random field by the non-uniform flow velocity in the immediate region of the probe. This general case is exremely difficult to analyze and certain simplifying assumptions and special cases will be studied to understand the main factors which limit the response of the probe. The theory of the flow of the random scalar field through the sensitive volume of the electrode involves the motion of points in the medium, thus the Lagrangian description (instead of the Eulerian) is appropriate (3). In the case of non-uniform flow in the electrode region the analysis of the identity transport is cumbersome and involves the concept of "drift". For uniform flow (U = constant) the problem is relatively simple. The analysis is greatly simplified by assuming a "frozen" random scalar field which is static and not decaying by diffusion (i.e., $\alpha \rightarrow 0$, $D \rightarrow 0$). Special cases of the above considerations are the subject matter of the following paragraphs. The response of the probe to small bubbles in motion through the electrode volume is also considered.

13.1 Temperature Fluctuations

The response in the case of uniform flow without diffusion is now considered. Since the response in this case is the same for conductivity as well as temperature and salinity structure, we will talk in terms of temperature response because of the numerous cases in which the conductivity signal may be assigned almost exclusively to a temperature signal. Since the velocity is uniform, no account is made of the effect of the distortion of the random temperature field by the probe itself. Two special cases are considered: a) the simple case of a one-dimensional temperature field and one-dimensional electrode field distribution, and b) the more general case of a three-dimensional temperature field and electrode distribution.

One-Dimensional Case

We assume:

a) One-dimensional electrode along x-axis.

b) Constant velocity, U, parallel to x-axis.

c) No boundary layer effects.

d) Small temperature fluctuations.

e) One-dimensional temperature variations along the x-axis.

The dynamic temperature equation for the temperature field is

$$\frac{\partial T}{\partial t} + \vec{u} \cdot \vec{\nabla} T = 0.$$

Making the substitutions:

$$S = \frac{T - T_o}{T}$$

$$\vec{u} = U\hat{x} \quad ,$$

where T_o is the average ambient temperature, and $\hat{x}$ is a unit vector in the direction of the x-axis, the dynamic equation becomes simply

$$\frac{\partial s}{\partial t} + U \frac{\partial s}{\partial x} = 0.$$

This has the general solution

$$s = s(x - Ut) \quad ,$$

which represents the "frozen" temperature structure of the medium as it flows through the field of the electrode. The temperature field $s(x)$ is assumed to be known, at least with respect to its average statistical properties. The average relative temperature over the electrode, θ, is defined as

$$\theta = \int_{-\infty}^{+\infty} s\, w(x)\, dx$$

and

$$\int_{-\infty}^{+\infty} w(x)\, dx = 1,$$

where w, here, is the electrode distribution function for unit frontal area. Therefore, the average temperature as a function of time is

$$\theta(t) = \int_{-\infty}^{+\infty} s(x - Ut)\, w(x)\, dx \quad ,$$

or as a function of distance

$$\theta(x) = \int_{-\infty}^{+\infty} s(\xi - x)\, w(\xi)\, d\xi \, .$$

We proceed in the conventional way to analyze the stochastic properties of the average temperature over the electrode by means of correlation functions and power spectra.

The correlation function, $R_\theta(\tau)$, of θ is defined as (4)

$$R_\theta(\tau) = \underset{L \to \infty}{\text{LIMIT}} \frac{1}{2L} \int_{-L}^{+L} \theta(x)\, \theta(x+\tau)\, dx \, ,$$

and is an even function of τ. Carrying out this operation we find

$$R_\theta(\tau) = \int_{-\infty}^{+\infty} dx \int_{-\infty}^{+\infty} dx' \; w(x)\, w(x') \left\{ \underset{L\to\infty}{\text{LIMIT}} \frac{1}{2L} \int_{-L}^{+L} s(x-\xi)\, s(x'-\xi-\tau)\, d\xi \right\},$$

however the quantity in wiggly brackets is just the correlation function of the temperature at points in the medium:

$$R_s(x'-x-\tau) = \underset{L\to\infty}{\text{LIMIT}} \frac{1}{2L} \int_{-L}^{+L} s(x-\xi)\, s(x'-\xi-\tau)\, d\xi.$$

With further manipulation, we find

$$\begin{aligned} R_\theta(\tau) &= \int_{-\infty}^{+\infty} dx \int_{-\infty}^{+\infty} dx' \; w(x)\, w(x')\, R_s(x'-x-\tau) \\ &= \int_{-\infty}^{+\infty} dx \int_{-\infty}^{+\infty} d\xi \; w(x)\, w(x+\xi)\, R_s(\xi-\tau), \qquad (\xi = x'-x) \\ &= \int_{-\infty}^{+\infty} d\xi \; R_s(\xi-\tau) \int_{-\infty}^{+\infty} w(x)\, w(x+\xi)\, dx \\ &= \int_{-\infty}^{+\infty} R_s(\xi-\tau)\, R_w(\xi)\, d\xi, \end{aligned}$$

where the correlation function of the electrode sensing function, w, is

$$R_w(\xi) = \int_{-\infty}^{+\infty} w(x)\, w(x+\xi)\, dx.$$

The expression

$$R_\theta(\tau) = \int_{-\infty}^{+\infty} R_s(\xi-\tau)\, R_w(\xi)\, d\xi,$$

gives the correlation function of θ in terms of the known or given correlation functions of the probe and the temperature fluctuations of the medium. By the convolution theorem, the relation between the corresponding power spectra may be obtained as follows. The power spectrum of θ is

$$\Phi_\theta(\omega) = \frac{1}{\pi} \int_{-\infty}^{+\infty} R_\theta(\tau)\, \cos(\omega\tau)\, d\tau,$$

$$\Phi_\theta(\omega) = \frac{1}{\pi}\int_{-\infty}^{+\infty} d\tau \cos(\omega\tau) \int_{-\infty}^{+\infty} R_s(\xi-\tau)\, R_w(\xi)\, d\xi$$

$$= \int_{-\infty}^{+\infty} d\xi\, R_w(\xi) \left\{ \frac{1}{\pi}\int_{-\infty}^{+\infty} R_s(\xi-\tau)\cos(\omega\tau)\, d\tau \right\}$$

$$= \int_{-\infty}^{+\infty} d\xi\, R_w(\xi)\, \Phi_s(\omega)\cos(\omega\xi)$$

$$= \pi\, \Phi_w(\omega)\cdot\Phi_s(\omega).$$

Thus, a very simple result is obtained for the power spectrum of the average electrode temperature fluctuations. The quantity $\pi\,\Phi_w(\omega)$ is the power spectral density response of the temperature probe. At low frequency (or long physical wavelength) we have ($\omega \to 0$)

$$\Phi_w(0) = \int_{-\infty}^{+\infty} R_w(\xi)\, d\xi$$

$$= \frac{1}{\pi}\int_{-\infty}^{+\infty} dx\, w(x) \int_{-\infty}^{+\infty} w(x+\xi)\, d\xi = \frac{1}{\pi}.$$

Thus, for the large scale temperature structure

$$\pi\,\Phi_w(0) = 1$$

and

$$\Phi_\theta(0) = \Phi_s(0).$$

Three-Dimensional Case

We now consider the detector response in an isotropic homogeneous random temperature fluctuation field under the assumption that the probe does not disturb this turbulent field. The temperature field is frozen and three-dimensional, and the electrode field distribution is also three-dimensional. This assumption is valid for temperature structure considerably larger than the sensing volume of the probe but is unrealistic for the smaller scale of structure. As shown in Section 10.4 the fractional change in electrode resistance, ΔR, is given by

$$\left(\frac{\Delta R}{R}\right) = -R\sigma \int \left(\frac{\Delta\sigma}{\sigma}\right)\cdot(\nabla\phi)^2\, dv,$$

where R is the electrode resistance, σ the mean conductivity of the water,

and $\Delta\sigma$ the change of conductivity relative to the mean value. The volume integration extends over the entire electrode volume. If the conductivity is uniform over this volume, the above formula reduces simply to

$$\frac{\Delta R}{R} = - \frac{\Delta\sigma}{\sigma}$$

since

$$R\sigma \int (\nabla\phi)^2 dv = 1.$$

In terms of the distribution function $w = R\sigma(\nabla\phi)^2$, the fractional change of resistance formula is

$$\frac{\Delta R}{R} = - \int w \left(\frac{\Delta\sigma}{\sigma}\right) dv.$$

In the analysis below, we follow the theory developed by Uberoi and Kovasznay (5) for the measurement of random fields. Following their notation for the case of mapping a scalar field we have

$$\Omega = \frac{\Delta R}{R} \qquad K = w = R\sigma(\nabla\phi)^2 \qquad \xi = -\frac{\Delta\sigma}{\sigma}$$

and

$$\Omega(\vec{x}) = \int \xi(\vec{s})\, K(\vec{s}-\vec{x})\, dV(\vec{s}),$$

or

$$\Omega(\vec{x}) = \int K(\vec{s})\, \xi(\vec{s}+\vec{x})\, dV(\vec{s}),$$

where integration extends over all field points $\vec{s}$ in the electrode volume. The kernel $K(\vec{s})$ is normalized so that

$$\int K(\vec{s})\, dV(\vec{s}) = 1.$$

The correlation functions of the conductivity structure (due to temperature structure), $\rho(\Delta)$, and measured field, $\beta(\Delta)$, are

$$\rho(\Delta) = \langle \xi(\vec{x}+\vec{\Delta})\, \xi(\vec{x}) \rangle_{AVE.}$$

$$\beta(\Delta) = \langle \Omega(\vec{x})\, \Omega(\vec{x}+\vec{\Delta}) \rangle_{AVE.},$$

where we assume an isotropic homogeneous field so that these functions depend only on the magnitude of, $\vec{\Delta}$, the distance between the two points in question. The above averages represent averages of the quantities over a large volume of the fluid with homogeneous statistical properties. The corresponding spectra of $\xi(\vec{x})$ and $\Omega(\vec{x})$ are

$$E(k) = \frac{1}{8\pi^3} \int \rho(\Delta) \left(\frac{\sin k\Delta}{k\Delta}\right) dV(\Delta)$$

$$\Gamma(k) = \frac{1}{8\pi^3} \int \beta(\Delta) \left(\frac{\sin k\Delta}{k\Delta}\right) dV(\Delta),$$

and the inverse relations are

$$\rho(\Delta) = \int E(k) \left(\frac{\sin k\Delta}{k\Delta}\right) dV(k)$$

$$\beta(\Delta) = \int \Gamma(k) \left(\frac{\sin k\Delta}{k\Delta}\right) dV(k).$$

The correlation function of the sensitivity distribution function, $\psi(\tau)$, is

$$\psi(\tau) = \int K(\vec{s})\, K(\vec{s}+\vec{\tau})\, dV(\vec{s}),$$

and the corresponding power sensitivity spectrum

$$S(k) = \int \psi(\tau) \left(\frac{\sin k\tau}{k\tau}\right) dV(\tau),$$

where, again, we have assumed the simplest case of a sensing function which is radially symmetric ($K(\vec{s}) = K(s)$, $s = |\vec{s}|$). The measured correlation function, $\beta(\Delta)$, is related to the actual correlation function, $\rho(\Delta)$, by

$$\beta(\Delta) = \int \psi(\vec{\tau})\, \rho(\vec{\Delta}-\vec{\tau})\, dV(\vec{\tau}),$$

and the power spectra are related by

$$\Gamma(k) = S(k) \cdot E(k) \quad .$$

The correlation function $\psi(\tau)$ is normalized such that

$$\int \psi(\tau)\, dV(\tau) = 1.$$

This follows since

$$\int \psi(\tau)\, dV(\tau) = \int K(\vec{s})\, dV(\vec{s}) \cdot \int K(\vec{s}+\vec{\tau})\, dV(\vec{\tau})$$
$$= \left[\int K(\vec{s})\, dV(\vec{s})\right]^2 = 1.$$

The sensitivity power spectrum, S(k), also satisfies the condition

$$S(0) = 1 \quad ,$$

since

$$S(0) = \int \psi(\tau)\, dV(\tau) = 1.$$

Even in the case of radial symmetry the expressions for the correlation function and spectrum of the electrode sensing function are

complicated. Two cases of interest can be analyzed and are of use in estimating the response of the electrode to random fields.

The first of these is the first order correction to the mean-square output of the detector, i.e., $\beta(0)$, when the extent of the correlation function $\rho(\Delta)$ becomes comparable to the extent of the electrode configuration, i.e., comparable with the extent of the correlation function $\psi(\tau)$. The mean-square output, $\beta(0)$, is given by

$$\beta(0) = \int \psi(\tau)\, \rho(\tau)\, dV(\tau) \cdot$$

If the correlation function $\psi(\tau)$ is of small extent in comparison with $\rho(\tau)$ then

$$\beta(0) = \rho(0) \int \psi(\tau) dV(\tau) = \rho(0),$$

and the actual and measured mean-square values are equal. The first order correction is obtained by assuming for small τ

$$\rho(\tau) = \rho(0)\{1 - a\tau^2\}.$$

The "micro-scale" (1) of the temperature (scalar) fluctuations is $a^{-1/2}$. Substituting this in the expression for $\beta(0)$, we get

$$\beta(0) = \rho(0) - a\,\rho(0) \int \tau^2 \psi(\tau)\, dV(\tau).$$

The latter integral can be expressed in terms of the root-mean-square extent of the kernel function K as follows

$$\int \tau^2 \psi(\tau) dV(\tau) = \int K(s) dV(s) \left\{ \int \tau^2 K(\vec{s}+\vec{\tau})\, dV(\tau) \right\}.$$

Let $\vec{\tau} = \vec{x} - \vec{s}$, then on integration over the angle between $\vec{x}$ and $\vec{s}$ we obtain

$$\int \tau^2 K(\vec{s}+\vec{\tau})\, dV(\tau) = \int x^2 K(x)\, dV(x) + s^2 \int K(x)\, dV(x)$$

and

$$\int \tau^2 \psi(\tau) dV(\tau) = 2 \int x^2 K(x)\, dV(x)$$

$$= 2\, X_{rms}^2,$$

where

$$X_{rms}^2 = \int x^2 K(x)\, dV(x).$$

The correction to the measured correlation function becomes

$$\frac{\beta(0)}{\rho(0)} = 1 - 2\, a\, X_{rms}^2,$$

For an electrode with a uniform spherical sensing distribution of radius c, we have

$$x_{rms} = \sqrt{\frac{3}{5}}\, c \quad .$$

In order to get an idea of the response of the electrode in the case where the scale of the microstructure is small in comparison with the size of the electrode, we consider the second simple case of an ideal spherical distribution function. If the radius of the sphere is c, the value, K_o, of the sensitivity kernel within the sphere is

$$K_o\left(\frac{4}{3}\right)\pi c^3 = 1 \quad ,$$

that is, K_o is just the inverse of the effective volume, v_o, of the sphere. The correlation function $\psi(\tau)$ is proportional to the volume of intersection of two spheres of radius c with centers a distance τ apart. With this geometric interpretation the integral which gives ψ is found to be

$$v_o\psi(\tau) = \left(1 - \frac{\tau}{2c}\right)^2\left(1 + \frac{\tau}{4c}\right).$$

This correlation function is shown in Figure 13.2 . The corresponding power sensitivity spectrum is

$$S(k) = \frac{9}{(kc)^6}\left[(kc)\cos(kc) - \sin(kc)\right]^2.$$

This function also is shown in Figure 13.2 . For large wavenumber ($kc \gg 1$) the spectrum varies as the inverse 4th power of k.

The "cutoff wavenumber," k_c, of a given electrode in a random scalar field is defined in the following way. The power sensitivity spectrum of a typical electrode is shown in Figure 13.3 . For small wavenumbers, the spectrum is given approximately by

$$S(k) = 1 - \left(\frac{k}{k_c}\right)^2,$$

which defines the meaning of the cutoff wavenumber, k_c, in analogy with the micro-scale of the fluctuation field. Expanding the expression

$$S(k) = \int \psi(\tau)\left(\frac{\sin k\tau}{k\tau}\right) dV(\vec{\tau}),$$

for small $k\tau$, we find

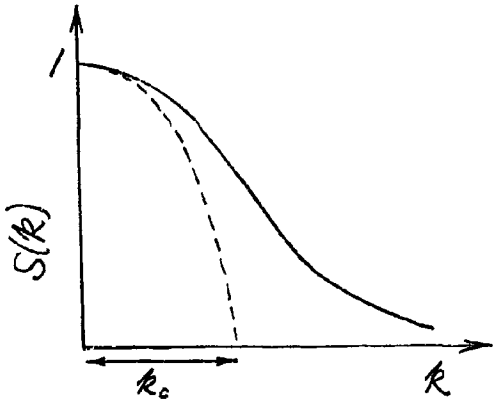

Figure 13.3 . Cutoff Wavenumber for Electrode in a Random Scalar Fluctuation Field

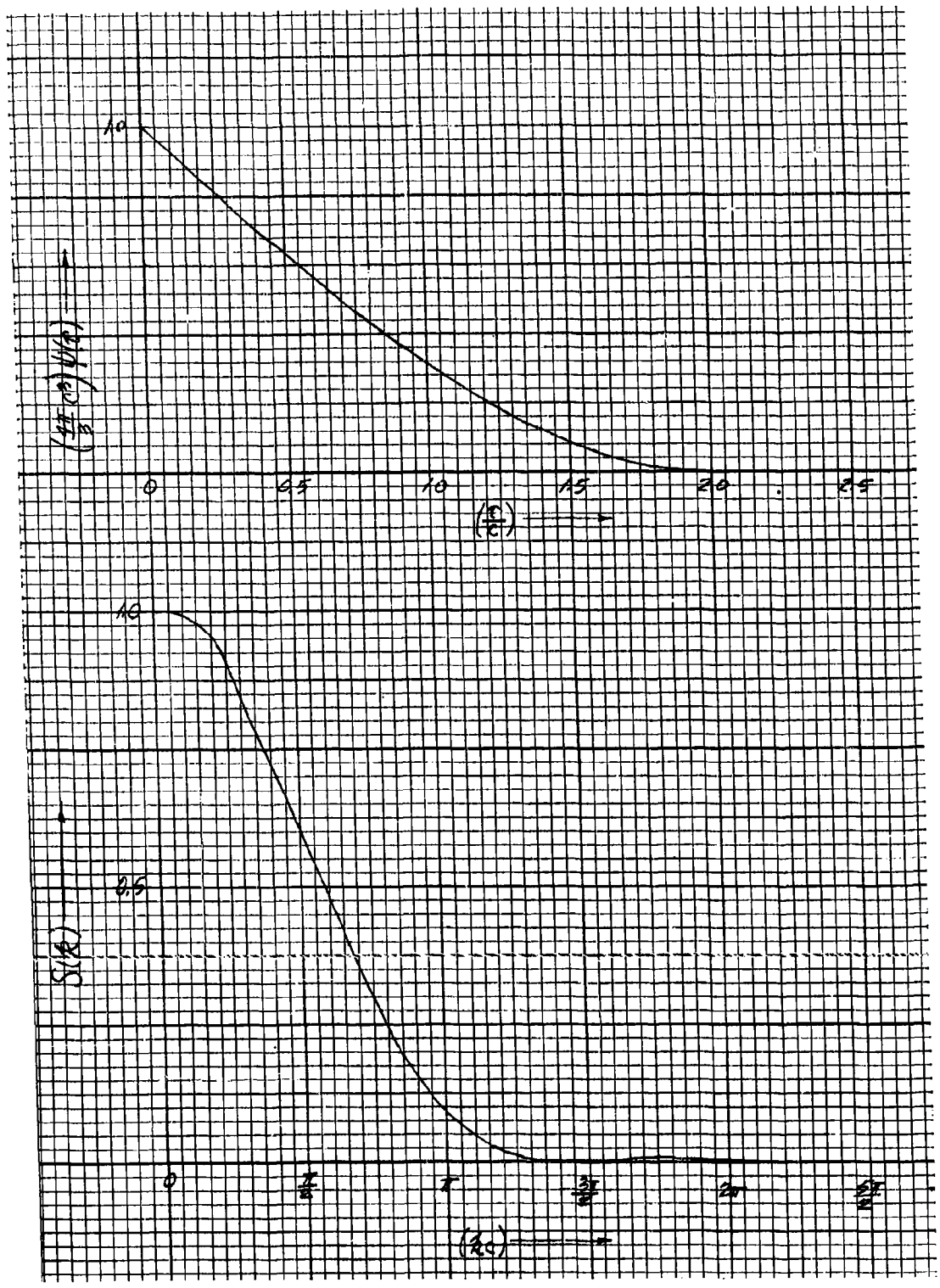

Figure 13.2. Correlation Function and Power Sensitivity Spectrum for a Spherical Electrode Volume

$$S(k) = \int \psi(\tau)\, dV(\tau) - \frac{k^2}{3!} \int \tau^2 \psi(\tau)\, dV(\tau)$$

or

$$= 1 - \frac{k^2}{3} \int x^2 K(x)\, dx$$

or

$$k_c = \frac{\sqrt{3}}{x_{rms}} \quad .$$

This is the relation between the cutoff wavenumber of the electrode and its rms radius. For a uniform spherical distribution of radius c, we have

$$k_c = \frac{\sqrt{5}}{c} = \frac{2.23}{c} \quad .$$

The power sensitivity spectrum, S(k), obtained for the sphere serves to illustrate the general response of an electrode configuration with a localized field with sharp edges. In the three-dimensional case for a sphere the spectrum varies as the inverse 4th power of a wavenumber; in the two-dimensional case for a cylinder the spectrum varies as the inverse 3rd power of the wavenumber; and for the one-dimensional case of a "box" the spectrum varies as the inverse 2nd power of k. As is well known, the spectra fall off more rapidly if the distribution function, w = K, varies smoothly with position without sharp discontinuities. The sharp discontinuities or edges give rise to a higher content in the spectra at the higher frequencies. The rapid fall off of the spectra in the one-, two- and three-dimensional cases for a smooth distribution function is most markedly illustrated when the kernel K is a Gaussian function of position in which case the corresponding spectra are also Gaussian at large wavenumbers. In the case of a practical electrode distribution, the distribution function varies as the inverse 6th power of the distance from the electrode and in the immediate vicinity of the electrode the sensitivity varies smoothly as a function of position, except in the case where "edges" (Sec. 9.1) exist between the metal electrode and insulators. Therefore, we would expect the power sensitivity spectrum of a three-dimensional electrode configuration to fall off more rapidly than the inverse 4th power of the wavenumber at large values, except for the contribution of the "edges" which probably, again, give rise to the k^{-4} behavior at large k. The problems of obtaining, analytically, the precise form of S(k) for a given eye-type or probe-type electrode are formidable and will not be attempted.

The correction function, $\psi(\tau)$, and power sensitivity spectrum, S(k), are needed in Section 5.5 for the square cylinder (diameter = height) for the analysis there. Since this electrode volume does not have spherical

symmetry, its analysis is considerably more complicated than that of the sphere and is somewhat similar to that obtained for a resistance-wire detector of finite length and zero diameter. As a first approximation to the desired functions, it is asserted that it is very similar to that of a spherical distribution function of the same volume. If d is the cylinder height and diameter, the corresponding sphere has a radius, c, given by

$$d = 2c\sqrt{\frac{2}{3}} = (0.818)\ 2c \quad .$$

The sketch below (Fig. 13.4) shows how similar these two geometric volumes are. Both have sharp edges and should both vary as k^{-4} at large wavenumber. The cutoff wavenumber, based on the value for a sphere, is

$$k_c = \frac{\sqrt{10/3}}{(d/2)} = \frac{1.82}{(d/2)} \quad .$$

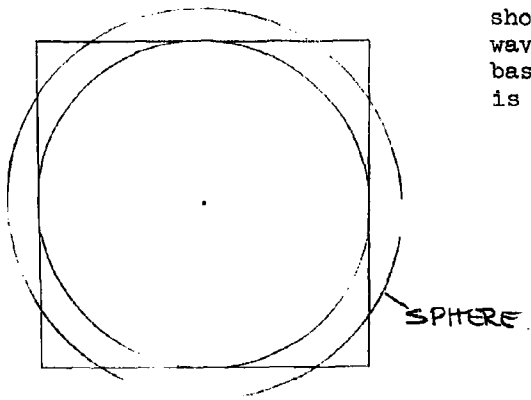

Figure 13.4 . Spherical and Square Cylinder Electrodes

13.2 Boundary Layer Response

The response of a probe when velocity boundary layer effects and diffusion are appreciable is studied in several relatively simple special cases. The response of the electrode resistance to a step-change in the conductivity of the medium for stagnation flow and flow parallel to a flat plate is considered.

Stagnation Flow

Three special cases of stagnation flow of increasing complexity are given below.

Case I - We first consider the simple case of an idealized sensing electrode mounted at the stagnation point in axisymmetrical flow against a wall.

Assume the sensing function of the electrode is uniform over a cylinder of height h and diameter h and is coaxial with the axis of symmetry as shown in Figure 13.9 . Assume the conductivity, σ_1, of the medium has a step-change in it as a function of position:

$$\sigma_1 = \begin{cases} \sigma_0 \ , & h > y > 0 \\ \sigma_0 + \sigma_0 \epsilon \ , & y > h \ , \end{cases}$$

at t = 0, where σ_0 is the ambient or average value of the conductivity. This situation is illustrated in Figure 13.5 ; where

$$\sigma = \frac{\sigma_1 - \sigma_0}{\sigma_0}$$

is the relative conductivity of the medium. As shown in Section 13.3 the material surfaces remain parallel to the wall. Assume, first, that the diffusion constant for the temperature and salinity is zero so that the distribution of σ in space is not subject to a smoothing action due to diffusion processes. In this case, the edge which is at y = h at t = 0 moves toward the wall such that its distance, y_e , from the wall satisfies

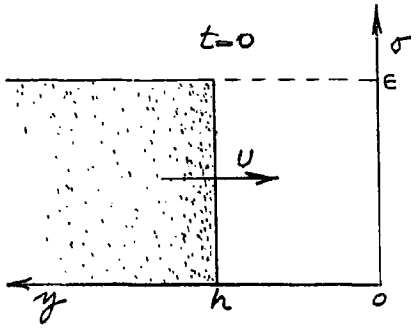

Figure 13.5 . Step-Change in Conductivity

$$y_e = h\, e^{-\frac{Ut}{h}} \ ,$$

and by the continuity equation for the conducting fluid medium, we know that for all time (t > 0) that

$$\sigma = \begin{cases} 0 & \text{FOR} \quad 0 < y < y_e \\ \epsilon & \text{FOR} \quad y_e \leq y \end{cases} \qquad (\epsilon \ll 1).$$

The resistance change, ΔR, of the electrode is

$$\frac{\Delta R}{R_0} = -\frac{1}{v_0} \int \sigma \, dv \ , \qquad v_0 = \frac{\pi}{4} h^3$$

where R_0 is the steady-state value of electrode resistance, v_0 is the electrode volume. Evaluating the integral:

$$-\left(\frac{\Delta R}{R_0}\right) = \epsilon \left(1 - \frac{y_e}{h}\right) = \epsilon \left(1 - e^{-\frac{Ut}{h}}\right).$$

Thus, the step-change in conductivity causes an exponential response in the electrode resistance. This is precisely the same response of an RC electrical network to a step-change in voltage. Following this analogy, the power sensitivity spectrum of the probe in this case is (6)

$$\Phi_w(\omega) = \frac{1}{1+\left(\frac{h\omega}{U}\right)^2} \quad .$$

Case (II) - Next consider the same case of stagnation flow without a velocity boundary layer but include the effect of finite diffusivity of the conductivity of the water through the diffusion of temperature and salinity in the water. We are not interested in the detailed conductivity distribution in the electrode volume but only the average conductivity over the sensing field of the electrode. The dynamic equation for the relative conductivity (assuming only thermal diffusion) is

$$\frac{\partial \sigma}{\partial t} + \vec{u} \cdot \vec{\nabla}\sigma = \alpha \nabla^2 \sigma = \alpha \vec{\nabla} \cdot \vec{\nabla}\sigma .$$

The average electrode resistance is

$$-\left(\frac{\Delta R}{R_o}\right) = \frac{1}{\mathcal{V}_o} \int \sigma \, d\mathcal{V} ,$$

where the volume integration extends over the cylinder of height and diameter h. Since σ is only a function of y we can write

$$-\left(\frac{\Delta R}{R_o}\right) = \frac{1}{h} \int_0^h \sigma(y) \, dy \quad .$$

The axial and radial velocities for potential flow are

$$u = -U\left(\frac{y}{h}\right)$$

$$v = \frac{1}{2} U \left(\frac{\rho}{h}\right) \quad .$$

Integrating the dynamic equation we have

$$\frac{\partial}{\partial t} \int \sigma \, d\mathcal{V} + \int \vec{\nabla} \cdot (\sigma \vec{u}) \, d\mathcal{V} = \alpha \int \vec{\nabla} \cdot \vec{\nabla}\sigma \, d\mathcal{V}$$

or

$$\frac{\partial}{\partial t} \int \sigma \, d\mathcal{V} + \int \sigma \vec{u} \cdot d\vec{S} = \alpha \int \vec{\nabla}\sigma \cdot d\vec{S} ,$$

where the surface integrals extend over the surface of the cylindrical electrode volume. The term on the right is zero since there is no conductivity gradient in the direction perpendicular to the cylindrical surface (i.e., parallel to the wall) nor is there a gradient allowed at the wall itself and the contribution to the integral due to the end of the cylinder at y = h is negligibly small if h is much larger than the diffusion layer. The other surface integral is

$$\int \sigma \vec{n} \cdot d\vec{s} = -\epsilon U\left(\frac{\pi}{4}\right)h^2 + \frac{\pi}{4} hU \int_0^h \sigma(y)\,dy ,$$

where use has been made of the fact that the conductivity is only a function of y and the radial velocity (v) is only a function of the radius. The volume integral is

$$\int \sigma\, dv = \frac{\pi}{4} h^2 \int_0^h \sigma(y)\,dy .$$

Combining the above expressions we have

$$\frac{h}{U}\frac{\partial}{\partial t}\left(\frac{1}{h}\int_0^h \sigma\, dy\right) - \epsilon + \left(\frac{1}{h}\int_0^h \sigma\, dy\right) = 0$$

or

$$\frac{h}{U}\frac{\partial}{\partial t}\left(\frac{\Delta R}{R_0}\right) + \left(\frac{\Delta R}{R_0}\right) = -\epsilon .$$

The solution to this equation is

$$-\left(\frac{\Delta R}{R_0}\right) = \epsilon\left(1 - e^{-\frac{Ut}{h}}\right).$$

It is important to note that the same response is obtained in the case of finite diffusivity as in the case of zero diffusivity and that no recourse has been made to the details of the conductivity distribution in the electrode volume. The basic assumption that made this possible was that y = h was well outside the region where diffusion is appreciable i.e.,

$$h \gg \frac{\alpha}{U} \qquad \text{(heat diffusion)}$$

or

$$h \gg \frac{D}{U} \qquad \text{(salinity diffusion),}$$

which are very small distances in practice ($\sim 10^{-5}$cm). These conditions can be restated as

$$RP \gg 1 \qquad \text{(heat diffusion)}$$

$$RS \gg 1 \qquad \text{(salinity diffusion),}$$

where R is the Reynolds number based on the typical electrode dimension h and

$$P = \frac{\nu}{\alpha} \qquad \text{(Prandtl number)}$$

$$S = \frac{\nu}{D} \qquad \text{(Schmidt number)} .$$

Case III - In the case of flow with a velocity boundary layer, we shall see in Section 13.3 that the leading edge of a step-change in conductivity proceeds toward the wall in such a way that the distance from the wall falls off exponentially with time outside the velocity boundary layer, but within the boundary layer this distance varies inversely with time. This has the result that the overall electrode resistance rises exponentially at first, but later it rises more slowly to the peak value. This situation is illustrated in Figure 13.6 . The long tail which lingers on due to the boundary layer effect can be considered undesirable in that it implies a poor response characteristic to variations in conductivity flowing into the detector volume. In the actual situation, however, this tail does not continue on indefinitely, since thermal and ionic diffusion processes come into play when the conductivity gradients near the wall become large. This effect occurs when the edge of the step-change in conductivity has moved well into the velocity boundary layer (since the Prandtl and Schmidt numbers are considerably greater than unity in water). When these diffusion processes become operative the "tail" again proceeds to fall off exponentially but with a different time constant than (h/U) and also at a rate which depends on the diffusion constant. In the following paragraphs we attempt to express this situation analytically.

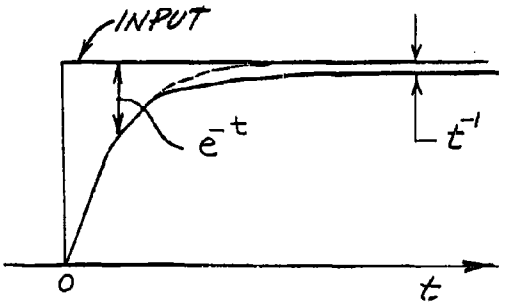

Figure 13.6 . Response to Step-Change in Conductivity in Stagnation Flow

The equation for the conductivity distribution is (thermal diffusion only)

$$\frac{\partial \sigma}{\partial t} + \vec{u} \cdot \vec{\nabla} \sigma = \alpha \nabla^2 \sigma$$

or in cylindrical coordinates

$$\frac{\partial \sigma}{\partial t} + u \frac{\partial \sigma}{\partial y} + v \frac{\partial \sigma}{\partial \rho} = \alpha \left\{ \frac{1}{\rho} \frac{\partial}{\partial \rho} \left(\rho \frac{\partial \sigma}{\partial \rho} \right) + \frac{\partial^2 \sigma}{\partial y^2} \right\},$$

where u and v are the axial and radial velocities, respectively. For potential flow these velocities are

$$u = -U\left(\frac{y}{h}\right)$$

$$v = \frac{1}{2} U\left(\frac{\rho}{h}\right) \quad ,$$

and for flow in which a boundary layer is present we have (7)

$$u = -U\sqrt{\frac{2\nu}{hU}}\,\phi(\zeta)$$

$$v = \frac{1}{2} U\left(\frac{\rho}{h}\right)\phi'(\zeta)$$

where $\phi(\zeta)$ is a tabulated boundary layer function and

$$\zeta = y\sqrt{\frac{U}{2h\nu}} .$$

Only the case of a conductivity distribution which is a function of y is considered so that the radial terms in the above equation are zero since σ is independent of ρ:

$$\frac{\partial\sigma}{\partial t} - U\sqrt{\frac{2\nu}{hU}}\,\phi(\zeta)\frac{\partial\sigma}{\partial y} = \alpha\frac{\partial^2\sigma}{\partial y^2} \quad ,$$

or by a change of variable ($y \rightarrow \zeta$):

$$\frac{h}{U}\left(\frac{\partial\sigma}{\partial t}\right) - \phi(\zeta)\frac{\partial\sigma}{\partial\zeta} = \left(\frac{\alpha}{2U}\right)\frac{\partial^2\sigma}{\partial\zeta^2} .$$

To solve this equation for the given boundary conditions, which are

$$y = h , \qquad \sigma = \epsilon(t)$$

$$y = 0 , \qquad \frac{\partial\sigma}{\partial y} = 0 \quad ,$$

we begin with separable solutions

$$\sigma = T(t)\,Z(\zeta) .$$

Substituting this form, the two equations for T and ζ are obtained

$$\dot{T} = -\lambda\left(\frac{UT}{h}\right)$$

and

$$\frac{1}{2P} Z'' + \phi(\zeta) Z' + \lambda Z = 0,$$

where λ is a parameter (eigenvalue). The corresponding equation for ionic diffusion is obtained by replacing the Prandtl number, P, by the Schmidt number, S. The solutions to these equations (eigenfunctions) are

$$T = T_\lambda(0)\, e^{-\frac{Ut\lambda}{h}}$$

$$Z = Z_\lambda(\zeta)$$

where $Z_\lambda(\zeta)$ is some function which is not readily obtainable for the general form for $\phi(\zeta)$ and satisfies the boundary conditions

$$Z'_\lambda(0) = 0$$

$$Z_\lambda(\infty) = 0 \quad .$$

The time dependent boundary condition at y = h is satisfied by developing the function $\epsilon(t)$ in the above eigenfunctions as follows:

$$\epsilon(t) = \int_0^\infty T_\lambda(0)\, Z_\lambda(\zeta_0)\, e^{-\frac{\lambda U t}{h}}\, d\lambda$$

where

$$\zeta_0 = h\sqrt{\frac{U}{2h\nu}} = \sqrt{\frac{hU}{2\nu}}.$$

The eigenvalues (and associated eigenfunctions) may consist of a discrete set of values in which case this integral becomes a summation over these discrete values. We will not attempt to solve the equation for $Z_\lambda(\zeta)$ in the general case but will consider one limiting case of that set of functions. Suppose $\epsilon(t)$ is some function of time of finite duration, i.e., a pulse. At times which are great in comparison with the pulse length or (h/U), we see that because of the decay of the exponential factor in the above integral that only the contribution for the least value of λ remains. This means that the input pulse finally attains a limiting shape near the wall, the amplitude of which delays exponentially with time.

If the flowing is without a boundary layer, i.e., potential flow, the velocity function is

$$\phi(\zeta) = \zeta,$$

in which case the least eigenvalue and corresponding eigenfunction are readily found to be

$$\lambda = 1$$

and

$$z_1(\zeta) = z_1(0)\, e^{-p\zeta^2},$$

and the limiting conductivity distribution is

$$\sigma = T_1(0)\, z_1(0)\, e^{-\frac{Ut}{h}}\, e^{-p\zeta^2}.$$

The decay of the overall electrode resistance in this case has already been considered irrespective of the existence, or not, of a diffusion process and agrees with the above value of time constant ($\lambda = 1$). In the velocity boundary layer ($\zeta < 1$) where ϕ is approximately

$$\phi(\zeta) \approx \frac{m}{2}\zeta^2 \qquad (m = 1.3120),$$

the solution in this case is more difficult (8). A rough estimate of the least eigenvalue can be obtained in the following way. Beginning with the equation

$$\frac{1}{2p} z'' + \frac{m}{2}\zeta^2 z' + \lambda z = 0,$$

we approximate the derivatives by

$$z'' \approx -\frac{z}{\delta^2} \quad \text{and} \quad z' \approx -\frac{z}{\delta},$$

where δ is a distance comparable with the distance over which z is appreciable. To this approximation, the minimum eigenvalue is the minimum with respect to δ of the expression

$$\lambda \approx \frac{1}{2p\delta^2} + \frac{m}{2}\delta^2 \frac{1}{\delta}$$

or

$$\lambda \approx \frac{3}{2}\left(\frac{m}{2}\right)^{2/3} p^{-1/3} = 1.15\, p^{-1/3}$$

at

$$\delta \approx \left(\frac{2}{mp}\right)^{1/3} = 1.15\, p^{-1/3}.$$

The final state distribution is appreciable over distances of the order of

$$\zeta \approx \frac{1}{\sqrt[3]{p}},$$

and decays in time approximately as

$$e^{-\left(\frac{Ut}{h}\right)\frac{1}{\sqrt[3]{p}}}.$$

For water $\mathbb{P}^{1/3} \approx 2$ and $\mathbb{S}^{1/3} \approx 10$, so that this distribution is within the velocity boundary layer but not much thinner in the case of thermal diffusion.

To summarize the above analysis of the response of the detector to a step-change in conductivity at a stagnation point, we can identify four stages of the rise of the overall electrode resistance to the final value:

1. Exponential region with a time constant (h/U) corresponding to potential flow with no diffusion.
2. Hyperbolic region in which boundary layer flow is operative but not diffusion.
3. Exponential region with time constant $(h/U)\mathbb{P}^{-1/3}$ for boundary layer flow with thermal diffusion causing that part of the conductivity change associated with a temperature change to diffuse into the medium, and
4. Exponential region with time constant $(h/U)\mathbb{S}^{-1/3}$ for boundary layer flow with ionic diffusion causing that part of the conductivity change associated with a salinity change to diffuse into the medium.

Since the thermal diffusion layer is comparable with the velocity boundary layer thickness, the hyperbolic region is not of long duration when the step-change in conductivity is due primarily to a temperature change. One observes simply a smooth transition from one exponential curve to the other.

Flat Plate Flow

The response of a uniform electrode imbedded some distance from the leading edge of a flat plate, as shown in Figure 13.7 , is now considered with respect to the effects of the potential and boundary layer flow and diffusion processes.

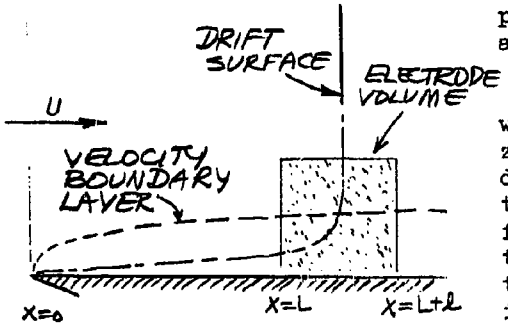

Figure 13.7 . Electrode Volume in Flat Plate Flow

In the case of uniform flow without a boundary layer and with zero diffusion, the response of the detector to a step-change in conductivity shows a fundamental difference from that of stagnation flow, viz., there is no "lingering." The position of the edge of the step-change in conductivity is

$$x_e = Ut$$

where it is assumed to be at the leading edge of the plate at zero time. The resulting electrode resistance as a function of time is

$$-\left(\frac{\Delta R}{R_o}\right) = \begin{cases} 0 , & t < \frac{L}{U} \\ \epsilon\left(\frac{Ut-L}{\ell}\right) , & \frac{L}{U} < t < \frac{L+\ell}{U} \\ \epsilon , & t > \frac{L+\ell}{U} , \end{cases}$$

where ϵ is the step fractional change in conductivity and the electrode of length ℓ is located a distance L from the leading edge. This response curve is shown as the solid line in Figure 13.8 . The rise of the elec-

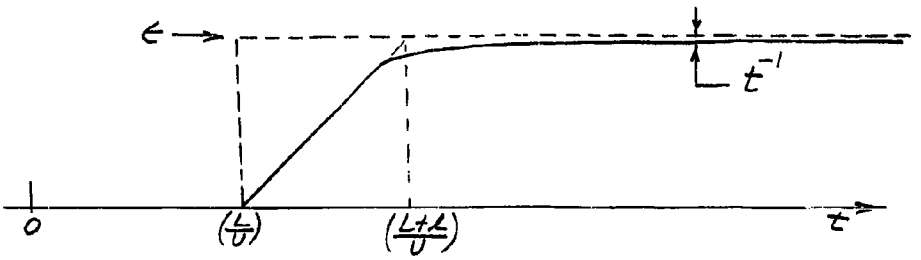

Figure 13.8 . Response to Step-Change in Conductivity in Flat Plate Flow

trode resistance is linear with time and complete after a time (ℓ/U); this was not the case for stagnation flow which gave an exponential response.

If diffusion is allowed but no velocity boundary layer the above situation is changed only in that the edge of the step-change becomes "fuzzy" when it reaches the electrode and causes rounding of the sharp changes in slope in the above Figure at the front and back edges of the electrode. The extent of this fuzzy edge is of the order of (L = 1 cm, U = 3 kts = 154 cm/sec)

$$2\sqrt{\frac{\alpha L}{U}} \approx 3 \times 10^{-3} \text{ cm}$$

for thermal diffusion and

$$2\sqrt{\frac{DL}{U}} \approx 3 \times 10^{-4} \text{ cm}$$

for ionic diffusion, both of which are quite small.

For the case of finite boundary layer flow but no diffusion, we need the results for flow on a flat plate discussed in Section 13.3 . There we find that in the boundary layer, the surface of the step-change in conduc-

tivity becomes distorted as shown in Figure 13.7 and Figure 13.13. Well after the step has passed the back side of the electrode volume in the uniform flow ($tU \gg L + \ell$), the thickness of the boundary layer, y, is (Sec. 13.3)

$$\left(\frac{y}{L}\right) \approx \left(\frac{4}{5m}\right)\left(\frac{L}{Ut}\right)\sqrt{\frac{\nu}{UL}} \qquad (m = 0.332),$$

If the height of the uniform electrode is ℓ , then, in this case, a "tail" varying inversely with time is obtained on the response of the overall electrode resistance change:

$$-\left(\frac{\Delta R}{R_o}\right) = \epsilon\left[1 - 2.4\left(\frac{L}{\ell}\right)\sqrt{\frac{\nu}{UL}}\left(\frac{L}{Ut}\right)\right],$$

as shown in Figure 13.8 . This situation is analogous to the behavior in stagnation flow under the corresponding conditions. The magnitude of this effect when it first sets in ($Ut \simeq L$) is about 20 % of the final value for U = 3 kts, L = 1 cm, ν = .01 cm^2/sec, and ℓ = 1 mm. The effect is, thus, appreciable. As with stagnation flow this undesirable effect does not persist indefinitely because thermal and ionic diffusion processes set in which give rise to the exponential tail.

The diffusion process becomes important at a distance δ from the wall when the conductivity gradient (σ/δ) causes diffusion transport comparable to the convection transport:

$$\propto \left(\frac{\sigma}{\delta}\right) \approx \sigma U m \sqrt{\frac{U}{\nu L}} \qquad (m = .332)$$

or

$$\delta \approx \frac{L}{m}\left(\frac{\nu}{UL}\right)^{3/4} \mathcal{P}^{-1/2}.$$

The velocity boundary layer thickness, δ_v , is of the order of

$$\delta_v \approx \frac{L}{m}\left(\frac{\nu}{UL}\right)^{1/2}$$

so the diffusion process takes place well within the velocity boundary layer since

$$\frac{\delta}{\delta_v} \approx \left(\frac{\nu}{UL}\right)^{\frac{1}{4}} \mathcal{P}^{-\frac{1}{2}} \approx 0.04$$

for thermal diffusion, and

$$\frac{\delta}{\delta_v} \approx \left(\frac{\nu}{UL}\right)^{\frac{1}{4}} \bar{S}^{-1/2} \approx 0.003 ,$$

for ionic diffusion with U = 3 kts, L = 1 cm and $\nu = .01$ cm^2/sec.

When the above diffusion processes set in, the tail on the overall electrode resistance response curve changes from the inverse time characteristic to an exponential one with a time constant related to the rate at which conductivity (via temperature or salinity) leave the boundary region by diffusion, i.e., a time constant of the order of

$$\frac{\ell\delta}{\alpha} \approx \left(\frac{\ell}{U}\right)\frac{P^{1/4}}{m}\left(\frac{UL}{\nu}\right)^{1/4} \approx 80\left(\frac{\ell}{U}\right),$$

for thermal diffusion and

$$\frac{\ell\delta}{D} \approx \left(\frac{\ell}{U}\right)\frac{S^{1/4}}{m}\left(\frac{UL}{\nu}\right)^{1/4} \approx 1000\left(\frac{\ell}{U}\right),$$

for ionic diffusion and the conditions assumed above. This analysis shows that the effects of boundary layer response are definitely appreciable and lead to response times considerably longer than the time to transit the electrode volume, (ℓ/U).

In summary, four distinct phases in the overall response of the detector to a step-change in conductivity for flow along a flat plate can be identified:

1. A linear region where diffusion and velocity boundary layer flow are not important.
2. A hyperbolic region associated with the slower velocities in the velocity boundary layer but where diffusion is not yet operative.
3. An exponential region with a time constant much larger than the electrode transit time caused by the diffusion of temperature (heat) to the boundary layer and finally,
4. An exponential region with a still larger time constant caused by diffusion of salt concentration to the region near the wall.

On comparison with stagnation flow we also find the same four corresponding regions, with the exception that the initial period in flat plate flow is linear instead of exponential. Concerning the magnitude of these effects limiting the electrode response, we find that they are much larger and distinct for flat plate flow. An obvious conclusion to be drawn from these facts is that to avoid the limitations of boundary layer response, the sensing electrode should be used in a probe-like configuration with the sensing volume occupying primarily the stagnation flow region.

13.3 Drift

Sir Charles Darwin (9) introduced to concept of "drift" which refers

to the deformation in fluid flow of material surfaces, i.e., the motion of individual fluid particles. Classical hydrodynamics usually involves the velocity field streamlines as a function of position relative to the moving body, as specified in the Eulerian manner. The study of hydrodynamic drift involves knowledge concerning the history of individual particles which is described by the time at which a fluid particle reaches any given point. In addition to the customary streamline surfaces, then, there exists surfaces of constant "drift" i.e., surfaces on which the time relative to the initial reference configuration is constant. Darwin (9) studied the drift surfaces for the cylinder in uniform flow perpendicular to its axis and Lighthill (10) obtained the corresponding information for a sphere. In the paragraphs below we consider drift surfaces when laminar boundary layers are involved in stagnation and flat plate flow.

Stagnation Flow

Consider the axisymmetrical flow of a fluid impinging on a wall at right angles to it and flowing away radially in all directions. Such a case occurs in the neighborhood of a stagnation point of a body of revolution in a flow parallel to its axis. This situation is illustrated in Figure 13.9 where y is the distance from the wall, ρ is the radial distance from the axis and the velocity on the axis is U towards the wall at the reference distance y = h. First consider the case of potential flow in which no velocity boundary layer exists at the wall. The radial and axial velocity components in this case are:

$$v = \frac{1}{2} U \left(\frac{\rho}{h}\right)$$

$$u = -U \left(\frac{y}{h}\right) \quad .$$

Since the axial velocity is independent of radius, fluid particles which lie in the plane y=const initially, do so for all time. The distance of the material surface from the wall is determined by the equation

$$\frac{dy}{dt} = -U\left(\frac{y}{h}\right)$$

which has the solution

$$y = h\, e^{-\frac{Ut}{h}} .$$

The "drift surfaces" are t = constant, and refers to planes parallel to the wall.

The velocity field in the case of axisymmetric stagnation flow with finite viscosity in which a boundary layer is formed (axisymmetrical Hiemenz flow) is known (7). The velocity field is given by

$$v = \rho f'(y) \qquad u = -2 f(y)$$

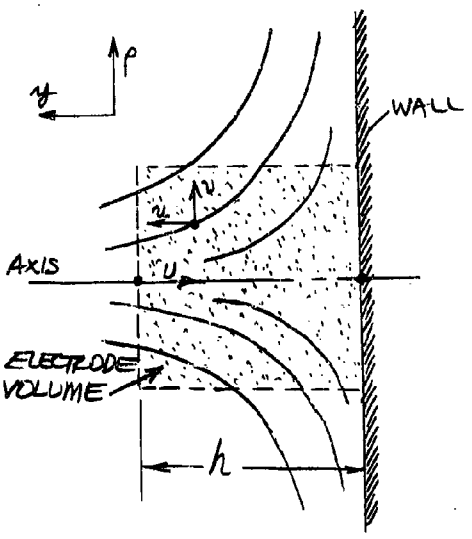

Figure 13.9 . Axisymmetric Stagnation Flow

where

$$f(y) = \sqrt{\frac{\nu U}{2h}}\ \phi(\zeta)$$

and

$$\zeta = \sqrt{\frac{U}{2h\nu}}\ y,$$

and the function ϕ satisfies the equation

$$\phi''' + 2\phi\phi'' - \phi'^2 + 1 = 0$$

with $\zeta = 0$: $\phi = \phi' = 0$; $\zeta = \infty$: $\phi' = 1$. Since the axial velocity is independent of radius, the material surfaces parallel to the wall initially remain so for all time. The distance from the wall satisfies the equation

$$\frac{dy}{dt} = -2 f(y)$$

or

$$\frac{d\zeta}{dt} = -\left(\frac{U}{h}\right)\phi(\zeta).$$

Integrating this equation we get

$$\int_{\zeta_0}^{\zeta} \frac{d\xi}{\phi(\xi)} = -\frac{Ut}{h}, \qquad \zeta_0 = \sqrt{\frac{Uh}{2\nu}}.$$

For $\zeta \gg 1$ this equation yields the same result as the potential flow given previously, but for $\zeta \ll 1$ the material surfaces move slower than in the case of potential flow and linger much longer in the boundary layer before approaching the wall closely. The function $\phi(\xi)$ can be approximated by

$$\phi = \xi - \xi_0, \qquad \text{with} \quad \xi_0 = 0.5690$$

for $\xi \geq 1$ and by

$$\phi = \frac{m}{2}\xi^2, \qquad \text{with } m = 1.3120$$

for $\xi \leq 1$. The integral above is, for the case $\zeta > 1$, approximately equal to

$$\int_{\zeta_0}^{\zeta} \frac{d\xi}{\xi-\xi_0} = \ln\left(\frac{\zeta-\xi_0}{\zeta_0-\xi_0}\right)$$

or

$$\zeta-\xi_0 = (\zeta_0-\xi_0)\, e^{-\frac{Ut}{h}},$$

which approximates potential flow if both ζ and ζ_0 are much greater than unity. For the case $\zeta < 1$, the integral is approximately

$$\int_{\zeta_0}^{1} \frac{d\xi}{\xi-\xi_0} + \int_{1}^{\zeta} \frac{d\xi}{\frac{m}{2}\xi^2} = \ln\left(\frac{1-\xi_0}{\zeta_0-\xi_0}\right) - \frac{2}{m}\left(\frac{1}{\zeta}-1\right).$$

Thus, well within the boundary layer the distance from the wall varies approximately inversely with time:

$$\zeta \approx \frac{2}{m}\left(\frac{h}{Ut}\right).$$

Flat Plate Flow

Consider a fluid flowing parallel to a flat plate at velocity U in the undisturbed stream as shown in Figure 13.10. In the absence of a velocity boundary layer, the drift surfaces are simply

$$x = Ut$$

for $0 \leq y$, which are planes perpendicular to the surface of the flat plate. The existence of a velocity boundary layer modifies the drift surfaces near the plate in the following way. At a distance x downstream from the leading edge, the fluid that passes between the wall and the height y_2 is equal to the amount of fluid that passes between the wall and y_1 if y_2 lies on the trajectory of a particle which passes through y_1:

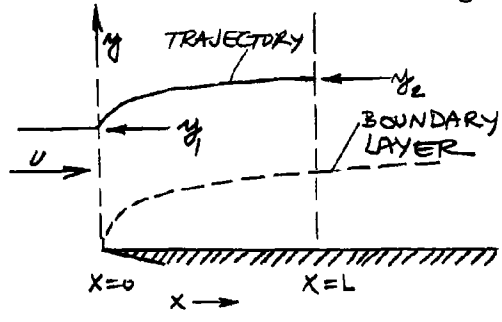

Figure 13.10. Flat Plate Flow

$$\int_0^{y_1} u_x(0,y)\,dy = \int_0^{y_2} u_x(L,y)\,dy,$$

where $U_x(x,y)$ is the velocity at the point (x,y) parallel to the plate. This provides a means for obtaining the equation of the particle trajectories. The velocity field in the boundary layer of a flat plate is given by (11)

$$u_x = U f'(\eta)$$

where

$$\eta = y\sqrt{\frac{U}{\nu x}} ,$$

and $f(\eta)$ is a function which satisfies the equation

$$f f'' + 2 f''' = 0$$

with $\eta = 0$: $f = f' = 0$; $\eta = \infty$: $f' = 1$. Values of this function are recorded in Table 13.1 and plotted in Figure 13.11. Evaluating the above integral we find

$$y_1\sqrt{\frac{U}{\nu x}} = f\left(y_2\sqrt{\frac{U}{\nu x}}\right) .$$

This is the equation of particle trajectories or streamlines. The time required for a particle beginning at y_1 at $t = 0$ to reach the point (L, y_2) downstream is found by integrating the equation

$$dt = \frac{dx}{U_x} = \left(\frac{dx}{d\eta}\right)\frac{d\eta}{U_x}$$

where the integration is carried out over the trajectory so that

$$y_1 = \sqrt{\frac{\nu x}{U}}\, f(\eta) = \text{CONSTANT}$$

and

$$\frac{dx}{d\eta} = -\left(\frac{2U y_1^2}{\nu}\right)\frac{f'}{f^3} .$$

Performing the integration we get

$$Ut = \frac{2U y_1^2}{\nu}\int_{\eta_2}^{\infty}\frac{d\eta}{f^3}$$

with

$$\eta_2 = y_2\sqrt{\frac{U}{\nu L}} .$$

If we let $\xi = \eta_2$ the drift integral becomes

$$\frac{Ut}{L} = 2 f^2(\xi)\int_{\xi}^{\infty}\frac{d\eta}{f^3} .$$

This simple closed form for the drift in the boundary layer of a flat plate has been evaluated with the known values of the function f and is recorded in Table 13.1 and plotted in Figure 13.12. If $\xi > 3$ the function $f(\eta)$

Table 13.1 . Functions for Boundary Layer Drift for a Flat Plate

ξ	$\left(\frac{L}{Ut}\right)$ or X	$f(\xi)$	Y
0.0	.0000	.0000	0.0000
0.2	.0830	.0066	0.0576
0.4	.1660	.0266	0.1630
0.6	.249	.0597	0.2994
0.8	.332	0.1061	0.4610
1.0	.415	0.1656	0.6442
1.2	.488	0.2380	0.8383
1.4	.566	0.3230	1.0533
1.6	.637	0.4203	1.2770
1.8	.696	0.5295	1.5017
2.0	.7500	0.6500	1.7320
2.2	.7939	0.7812	1.9591
2.4	.8446	0.9223	2.2049
2.6	.8793	1.0725	2.4376
2.8	.9079	1.2310	2.6660
3.0	.9309	1.3968	2.8931
3.2	.9491	1.5691	3.1173
3.4	.9633	1.7470	3.3365
3.6	.9740	1.9295	3.5529
3.8	.9819	2.1161	3.7637
4.0	.9877	2.3058	3.9740
4.2	.9919	2.4981	4.1810
4.4	.9947	2.6924	4.3868
4.6	.9968	2.8883	4.5907
4.8	.9980	3.0853	4.7952
5.0	.9990	3.2833	4.9975
5.2	.9993	3.4819	5.1973
5.4	.9998	3.6809	5.3972
5.6	.9999	3.8803	5.5971
5.8	.9999	4.0799	5.7970
6.0	1.0000	4.2796	6.0000

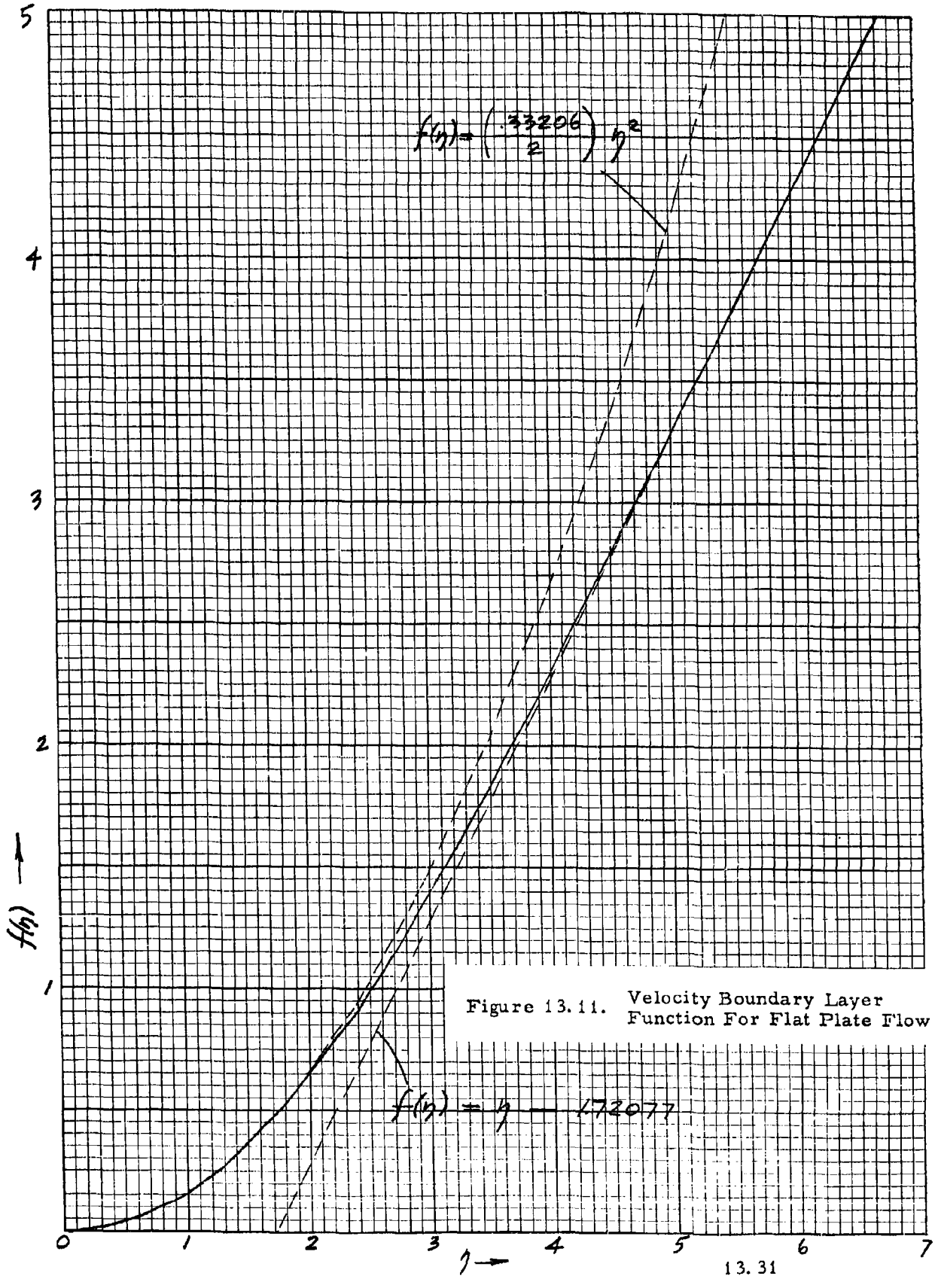

Figure 13.11. Velocity Boundary Layer Function For Flat Plate Flow

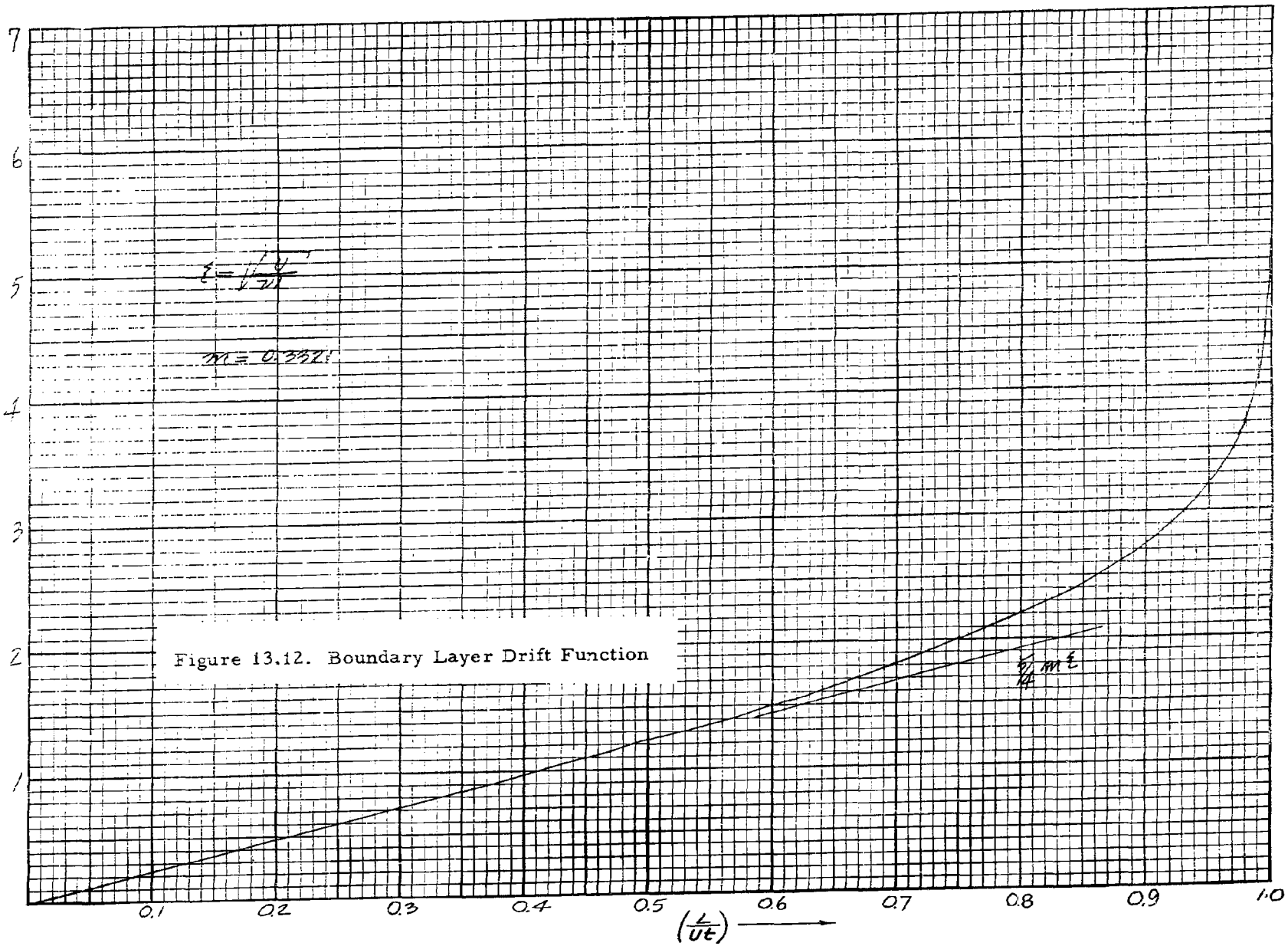

Figure 13.12. Boundary Layer Drift Function

is approximated closely by

$$f(\eta) = \eta - \eta_0 \quad , \qquad \text{with} \quad \eta_0 = 1.72077.$$

The drift integral in this case is easily evaluated to be

$$\left(\frac{Ut}{L}\right) = 1 \quad ,$$

as expected outside the boundary layer. For $\frac{\eta}{2} < 3$ (inside the boundary layer) the function $f(\eta)$ is approximated by

$$f(\eta) = \frac{m}{2}\eta^2 \quad , \qquad \text{with } m = 0.33206.$$

In this case, the drift integral becomes

$$\left(\frac{Ut}{L}\right) = \frac{4}{5}\left(\frac{1}{m\frac{\eta}{2}}\right) \quad .$$

To find the equation of the drift surfaces (t = constant), introduce the dimensionless similarity variables

$$X = \left(\frac{x}{Ut}\right)$$

$$Y = \frac{y}{\sqrt{\nu t}} \quad ,$$

then for t = constant, a functional relation exists between (X,Y) which is just the shape of the material surfaces. Substituting these variables:

$$\frac{1}{X} = 2 f^2\left(\frac{Y}{\sqrt{X}}\right) \int_{\frac{Y}{\sqrt{X}}}^{\infty} \frac{d\eta}{f^3(\eta)} \quad .$$

These similar drift surfaces are drawn in Figure 13.13 and tabulated in Table 13.1. For small X:

$$Y = \left(\frac{4}{5m}\right) X^{3/2} .$$

The trajectories or streamlines of the fluid have the equation

$$\frac{Y_1}{\sqrt{X}} = f\left(\frac{Y}{\sqrt{X}}\right) .$$

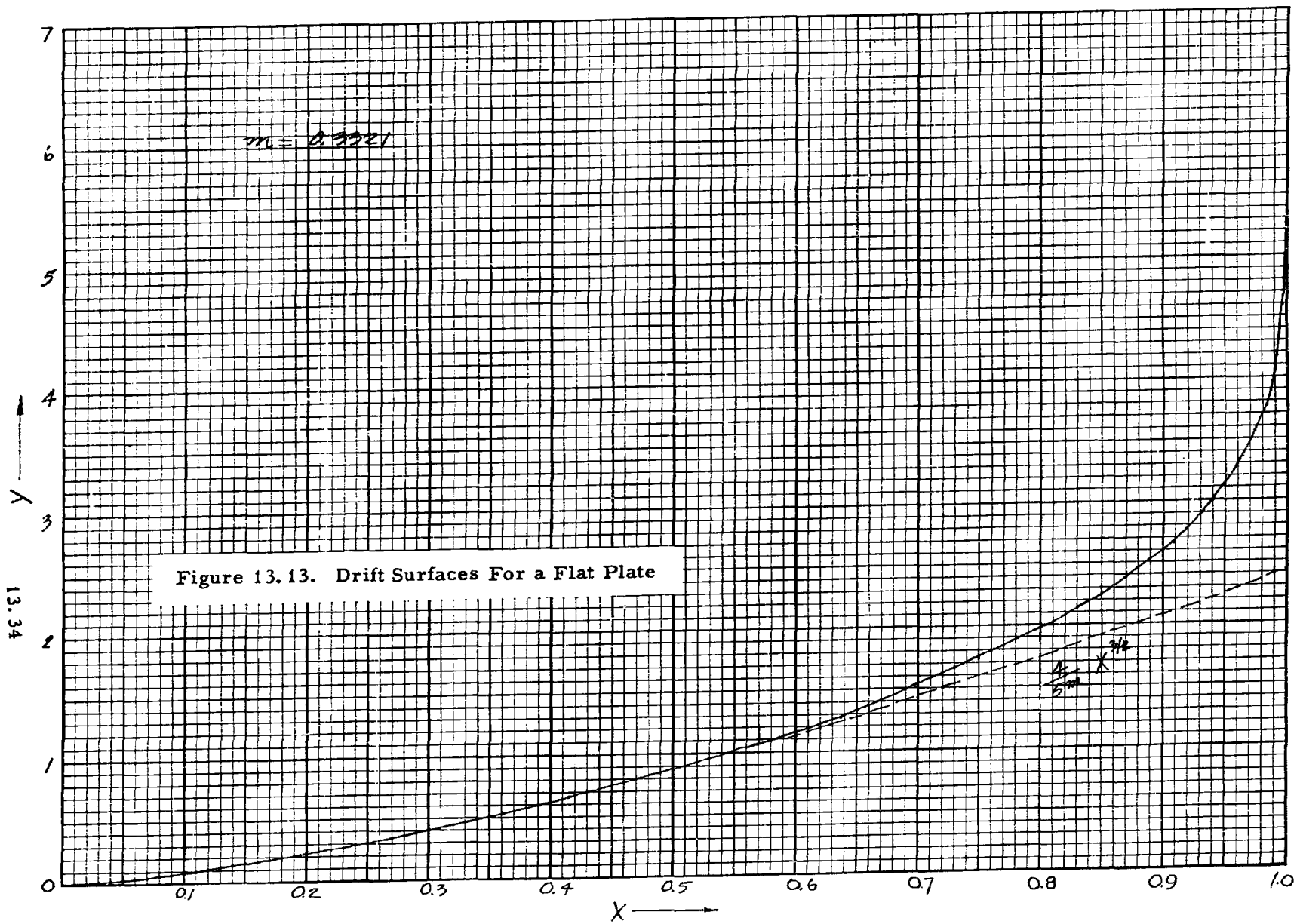

Figure 13.13. Drift Surfaces For a Flat Plate

13.4 Response to Bubbles

The effective change in electrode resistance, ($\Delta R/R$), due to the presence of a small spherical cavity of different conductivity in the field of the electrode was found in Section 10.4 to be

$$\frac{\Delta R}{R} = -\left(\frac{K-1}{K+2}\right)(\vec{\nabla}\phi)^2 \cdot \Delta v \cdot R\sigma$$

where Δv is the volume of the spherical cavity, $R\sigma$ is the cell constant, K is the ratio of the conductivity σ_1 of the cavity to the conductivity σ of the medium:

$$K = \frac{\sigma_1}{\sigma}$$

and the field gradient $\vec{\nabla}\phi$ is that which would be obtained at the location of the cavity if it were not present. For a non-conducting bubble, K = 0. The pulse shape of the resistance variation is described by the trajectory of the bubble as it passes through the electrode field, w.

The average resistance change due to a cavity is defined as

$$\left(\frac{\Delta R}{R}\right)_{AVE} = \int w\left(\frac{\Delta R}{R}\right) dv \,, \qquad w = R\sigma(\vec{\nabla}\phi)^2$$

$$= -\left(\frac{K-1}{K+2}\right)\Delta v \int w^2 dv$$

$$= -\left(\frac{K-1}{K+2}\right)\left(\frac{\Delta v}{v_0}\right) \,,$$

where v_0 is the effective electrode volume. For a bubble (K = 0)

$$\left(\frac{\Delta R}{R}\right)_{AVE} = \frac{1}{2}\left(\frac{\Delta v}{v_0}\right).$$

A simple case for which a pulse height distribution can be calculated is when the sensing function of the probe is a function only of the radial distance, r, from the center of the electrode and the velocity is uniform. Consider a flush electrode with the uniform flow velocity parallel to the wall and along the z-axis. The sensing function, w, is only a function of the radius, r, from the center of the electrode. The trajectory of the bubble is along the z-axis and through the point (x,y). The radial distance is $r^2 = x^2 + y^2 + z^2$ and $z = Ut$. If w is a decreasing function of radius, the pulse height occurs at the least value of r, i.e., at z = 0, and at

that point equals the "distance of closest approach," ρ, where $\rho^2 = x^2 + y^2$. The pulse height is then (for a given bubble volume Δv)

$$\frac{\Delta R}{R} = \frac{1}{2} w(\rho) \cdot \Delta v \qquad (K = 0)$$

and the maximum pulse height occurs at $\rho = 0$:

$$\left(\frac{\Delta R}{R}\right)_{MAX} = \frac{1}{2} w(0) \cdot \Delta v$$

Define the relative pulse height, h:

$$w(\rho) = h\, w(0),$$

where $0 \leq h \leq 1$. The number of pulses, dN, of pulse height h is proportional to the element of frontal area $\pi\rho d\rho$ at the radius corresponding to the pulse height h:

$$dN = c\,(\pi \rho\, d\rho)\, U t,$$

where c is the concentration of bubbles of volume Δv, U is the speed of the detector and t is the time. The number of pulses per unit pulse height is

$$\frac{dN}{dh} \sim \pi \rho \left(\frac{d\rho}{dh}\right),$$

and can not be normalized in the usual way because there are infinitely many (non-integrable) very small pulses. It is necessary to define the "pulse height distribution," $\psi(h)$, as follows

$$\frac{1}{N_v}\left(\frac{dN}{dh}\right) = \psi(h),$$

where N_v is some reference number of pulses which is equal to the number that would pass through a (frontal) area A_v :

$$N_v = cA_vUt \quad .$$

Therefore, we have

$$\psi(h) = \frac{\pi}{A_v} \rho \left(\frac{d\rho}{dh}\right) .$$

The integral distribution function of this function is defined as

$$\psi_\Sigma = \int_h^1 \psi(x)\, dx = \frac{\pi}{2A_v}\, \rho^2(h).$$

The average pulse height and higher moments are all zero because the distribution is not integrable:

$$\int_0^\infty \psi(h)\,dh = \frac{\pi\rho^2}{2A_v} \to \infty \quad , \quad \text{AS} \quad \rho \to \infty .$$

As an example of the pulse height distribution function, assume a radial sensing function which approximates that of a dipole electrode (Sec. 10.1)

$$w(\rho) = \frac{w(0)}{1 + \left(\frac{\rho}{b}\right)^6} \quad ,$$

where b determines the size of the electrode. In terms of h we have

$$h = \frac{1}{1 + \left(\frac{\rho}{b}\right)^6}$$

or

$$\rho = b \cdot \left(\frac{1-h}{h}\right)^{\frac{1}{6}} .$$

Carrying through the differentiation of this expression, we get the distribution function

$$\psi(h) = \frac{\pi}{A_v}\left(\frac{b^2}{6}\right)(1-h)^{-2/3}\,h^{-4/3} .$$

It is easily shown that this distribution has a minimum at

$$h = h_v = 2/3 \quad .$$

This provides a convenient standard for reference. Define A_v as the frontal area corresponding to pulses of height $1 \geqslant h \geqslant 2/3$:

$$A_v = \pi b^2\, 2^{-4/3}$$

and

$$\psi(h) = \frac{2^{1/3}}{3}(1-h)^{-2/3}\,h^{-4/3} .$$

This function as well as its integral distribution is shown in Figure 13.14 . The following relations hold for this distribution:

$$\psi\left(\frac{2}{3}\right) = \frac{3}{2}$$

$$\psi_\Sigma(1) = 0$$

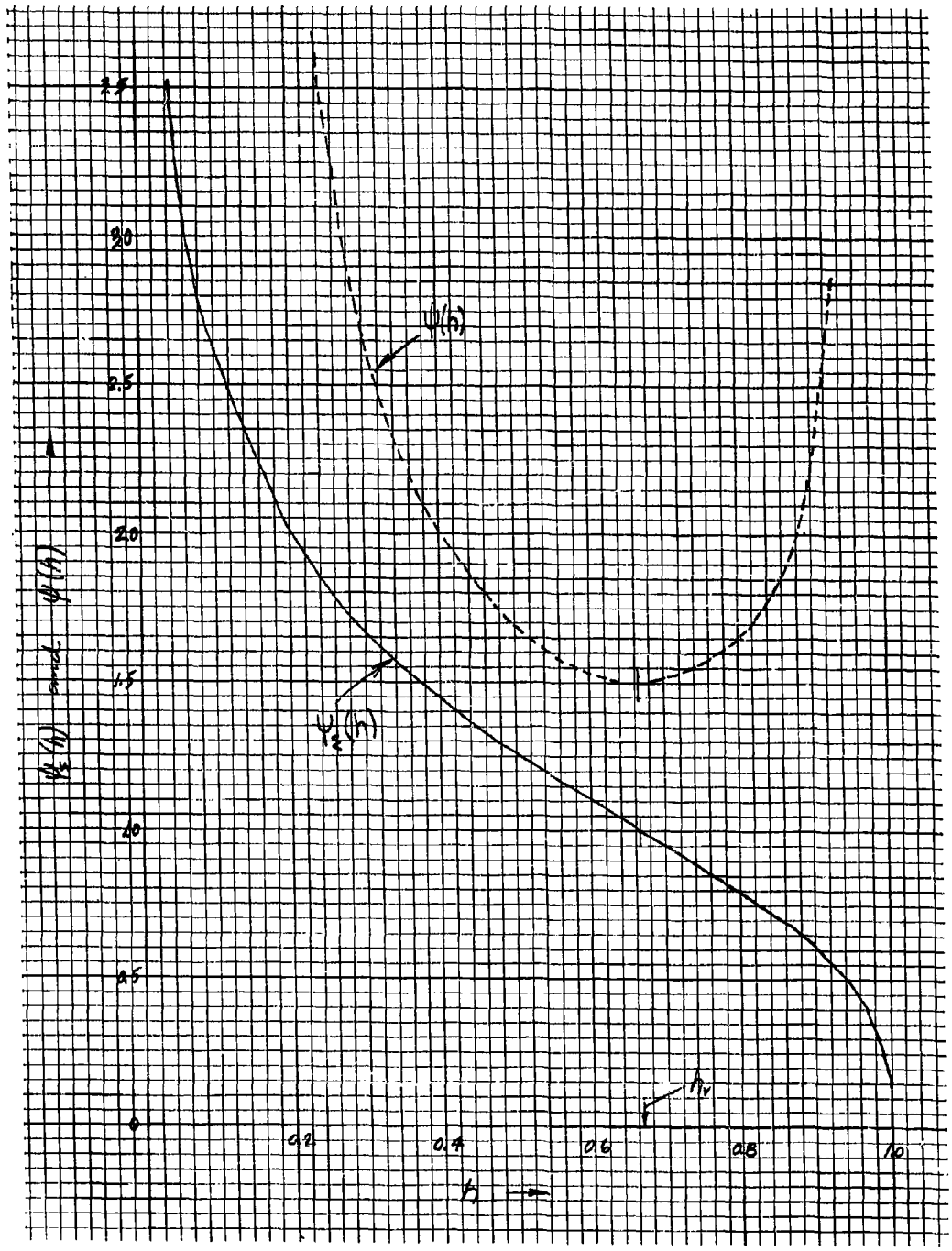

Figure 13.14. Bubble Pulse Height Distribution

$$\psi_\Sigma\left(\frac{2}{3}\right) = 1$$

$$\psi_\Sigma(0) = \infty \quad ,$$

and

$$\psi_\Sigma(h) = 2^{1/3}\left(\frac{1-h}{h}\right)^{1/3}.$$

The above analysis assumed a uniform bubble size. If there is also a distribution in the size of bubbles, the overall pulse height spectrum consists of a weighted average of the above pulse height distribution function.

13.5 Differential Probe

The overall response of a differential double element probe is different than that for each probe, since large scale conductivity structure measured by each probe tends to cancel out. We consider the overall detector response of such a double probe for measurements in an isotropic-homogeneous fluctuation field. The analysis applies equally well to the measurement of velocity (turbulence) and scalar variables such as temperature and salinity. The probe elements are assumed to be very small in comparison with the separation distance, 2ℓ, between the probes.

The analysis follows the lines of the three dimensional case in Section 13.1. Let $K_1(\vec{s})$ and $K_2(\vec{s})$ be the sensing distribution functions of each probe normalized so that

$$\int K_1(\vec{s})\, dV(\vec{s}) = \int K_2(\vec{s})\, dV(\vec{s}) = 1.$$

The outputs $\Omega_1(\vec{x})$ and $\Omega_2(\vec{x})$ from each probe are combined in the wheatstone bridge network such that the net output $\Omega(\vec{x})$ is the difference of the outputs of each probe:

$$\Omega(\vec{x}) = \Omega_2(\vec{x}+\vec{\ell}) - \Omega_1(\vec{x}-\vec{\ell}) \quad ,$$

where $\vec{\ell}$ and $-\vec{\ell}$ are the position vectors of the two (point) probes relative to the mid-point between the two. The differential probe geometry is shown in Figure 13.15. Since we are concerned here only with isotropic turbulence fields, the orientation of the vector $\vec{\ell}$ is unimportant. The individual outputs are given by

$$\Omega_1(\vec{x}-\vec{\ell}) = \int K_1(\vec{s}-\vec{x}+\vec{\ell})\, \xi(\vec{s})\, dV(\vec{s})$$

and

$$\Omega_2(\vec{x}+\vec{\ell}) = \int K_2(\vec{s}-\vec{x}-\vec{\ell})\,\xi(\vec{s})\,dV(\vec{s}),$$

where $\xi(\vec{s})$ is the measured quantity at the field point $\vec{s}$. The overall output is

$$\Omega(\vec{x}) = \Omega_2(\vec{x}+\vec{\ell}) - \Omega_1(\vec{x}-\vec{\ell})$$

$$= \int \left\{ K_2(\vec{s}-\vec{x}-\vec{\ell}) - K_1(\vec{s}-\vec{x}+\vec{\ell}) \right\} \xi(\vec{s})\,dV(\vec{s}).$$

It is convenient to define the overall kernel as

$$K(\vec{s}) = K_2(\vec{s}-\vec{\ell}) - K_1(\vec{s}+\vec{\ell}).$$

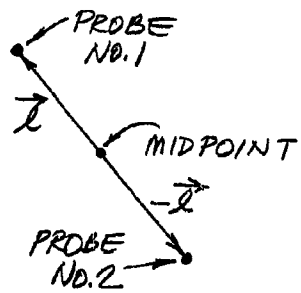

Figure 13.15. Differential Probe

If we assume the probes to be ideal point probes (K_1 and K_2 are delta-functions) the overall output is the difference of the values of ξ at the two probe points:

$$\Omega(\vec{x}) = \xi(\vec{x}+\vec{\ell}) - \xi(\vec{x}-\vec{\ell}).$$

We seek the correlation function $\psi(\vec{\tau})$ and spectrum $S(\vec{k})$ of the distribution function $K(\vec{s})$ under the assumption that the two probes experience no relative motion (no variation of separation and no rotation) as the double probe is translated through the random medium (i.e., $\vec{\ell}$ is a constant). The correlation function is

$$\psi(\vec{\tau}) = \int K(\vec{s})\,K(\vec{s}+\vec{\tau})\,dV(\vec{s})$$

$$= \int \{ K_2(\vec{s}-\vec{\ell})K_2(\vec{s}+\vec{\tau}-\vec{\ell}) + K_1(\vec{s}+\vec{\ell})K_1(\vec{s}+\vec{\tau}+\vec{\ell})$$

$$- K_2(\vec{s}-\vec{\ell})K_1(\vec{s}+\vec{\tau}+\vec{\ell}) - K_2(\vec{s}+\vec{\tau}-\vec{\ell})K_1(\vec{s}+\vec{\ell}) \}\,dV(\vec{s}).$$

In addition, assume that the distribution functions of each individual probe is identical (but located at different positions) so

$$K_1(\vec{s}) = K_2(\vec{s}) = K_0(\vec{s}) \quad ,$$

and that this distribution is spherically symmetric. In this case the correlation function is

$$\psi(\vec{\tau}) = \psi_0(\vec{\tau}) + \psi_0(\vec{\tau}) - \psi_0(\vec{\tau}+2\vec{\ell}) - \psi_0(\vec{\tau}-2\vec{\ell}),$$

where

$$\psi_0(\vec{\tau}) = \psi_0(0) = \int K_0(\vec{\xi})\, K_0(\vec{\xi}+\vec{\tau})\, dV(\vec{\xi}).$$

In the limit of a point probe these correlation functions become δ-functions. The overall correlation function $\psi(\vec{\tau})$ is <u>not</u> spherically symmetric. The spectrum, $S(\vec{k})$, of the double probe is given by (5)

$$S(\vec{k}) = \int \psi(\vec{\tau})\, e^{-i\vec{k}\cdot\vec{\tau}}\, dV(\vec{\tau}).$$

Evaluating this integral under the assumption that the probes are ideal points, we get

$$S(\vec{k}) = 2\left[1 - \cos(\vec{k}\cdot\vec{\ell})\right],$$

and the spectral response depends on the relative orientation of the double probe and the wavenumber. In an isotropic random field we are concerned only with the angular average of $S(\vec{k})$

$$\overline{S}(k) = \frac{1}{2}\int_0^{\pi} \sin\theta\, S(\vec{k})\, d\theta,$$

where θ is the angle between $\vec{k}$ and $\vec{\ell}$. Carrying out this integral we find

$$\overline{S}(k) = 2\left[1 - \frac{\sin k\ell}{k\ell}\right].$$

This is the power sensitivity spectrum for a double (differential) detector with point probes. For small scale structure, which is not correlated over the distance between the two probes ($k\ell \gg 1$), the response is just that of two independent probes as expected. For turbulent structure which is large with respect to the separation distance ($k\ell \ll 1$) the response spectrum is given approximately by

$$\overline{S}(k) \approx \frac{1}{3}(k\ell)^2,$$

which approaches zero for $k\ell \to 0$, which illustrates the cancellation of the large structure by the differential probe.

For probes of finite size the behavior of $\bar{S}(k)$ approximates that of the individual probes provided the separation distance 2ℓ is relatively large in comparison with the typical dimensions of the probe electrodes. If the finite size of these electrodes is included, the overall spectrum is given approximately by

$$\bar{S}(k) = 2 S_o(k) \left[1 - \frac{\sin k\ell}{k\ell} \right] ,$$

where $S_o(k)$ is the power sensitivity spectrum of each probe. As an example of this, the overall response for a differential probe is sketched in Figure 13.16 for electrodes with a k^{-4} behavior at large wavenumber. The cutoff wavenumber, k_c, is

$$k_c = \frac{\sqrt{3}}{x_{rms}} ,$$

where x_{rms} is the rms radius of the electrode distribution. The lower cutoff wavenumber, k_v, for the differential probe is defined by

$$\frac{1}{3} (k_v \ell)^2 = 2$$

or

$$k_v = \frac{\sqrt{6}}{\ell} .$$

The ratio of upper and lower cutoff wavenumbers is

$$\left(\frac{k_c}{k_v} \right) = \frac{1}{\sqrt{2}} \left(\frac{\ell}{x_{rms}} \right) .$$

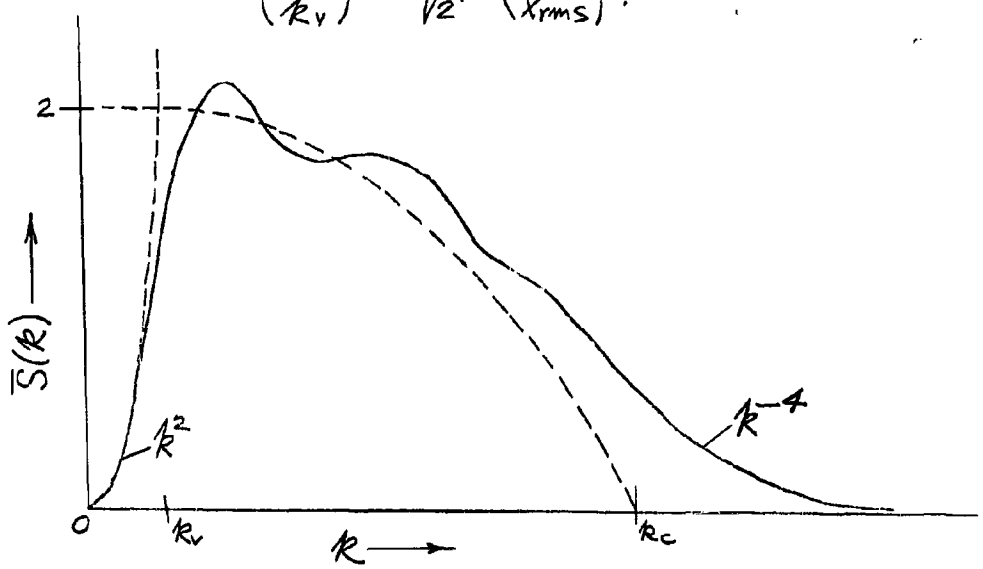

Figure 13.16. Overall Differential Probe Response

14. VELOCITY RESPONSE

The factors which determine the frequency response of the U-meter are considered in this Section. The primary factors are the size and configuration of the probe electrode, the velocity and thermal boundary layers at the electrode surfaces, and the thermal properties of the probe materials. Simplified special cases are analyzed to understand these effects individually. These simplifications are similar to the ones which were first used in connection with the analysis of the response of the hot-wire anemometer (1). The temperature(and salinity) of the medium is assumed to be uniform throughout the medium except for changes caused by electrode heating. The velocity response in a given mode of operation (e.g., CTO) is considered at the end of this Section.

14.1 Isotropic Turbulence

What is the response of the velocity detector to an isotropic homogeneous turbulence field? We can attempt to solve this case only under the assumption that the probe itself does not disturb the flow. While this assumption is valid for turbulent structure, large in comparison with the sensing electrode, it is not so for turbulent structure comparable to or smaller than the probe. The turbulence is actually quenched to some degree where the shear flow is high near the surface of the probe. This effect will be neglected in what follows.

The analysis of the turbulent response for the velocity sensor is analogous to that of Section 13.1 for the response of a temperature detector to a random temperature field. First it is necessary to establish how a turbulent velocity field in the vicinity of the electrode determines the change in electrode resistance. The assumption that the turbulent field is not disturbed by the probe is satisfied if the average velocity is uniform over the electrode volume; we assume this to be the case. Let T_1 be the temperature at a point in the fluid medium which has an average value T_o and a fluctuating value T:

$$T_1 = T_o + T$$

with

$$T_{AVE.} = 0 \quad .$$

The average temperature T_o , which is a function of position with respect to the electrode, is assumed to be zero at great distance upstream from the heating field of the electrode (zero ambient temperature). If we consider only heating due to Joule heating by the electrical power dissipated in the electrode, and neglect thermal diffusion and friction heating,

it is shown in Section 12.2 that the temperature T_1 satisfies the equation

$$\frac{\partial T_1}{\partial t} + \vec{u}_1 \cdot \vec{\nabla} T_1 = \left(\frac{P}{C}\right) w$$

where P is the average total electrode power, c is the heat capacity per unit volume of the fluid, w is the electrode sensing distribution function, and $\vec{u}_1$ is the velocity of the medium at a point which consists of an average component $\vec{U}$ and a turbulent component $\vec{u}$:

$$\vec{u}_1 = \vec{U} + \vec{u} \quad .$$

We assume the velocity field $\vec{U}$ is independent of time and we are attempting to measure the turbulent velocity field, $\vec{u}$, with the sensing electrode.

The velocity detector responds to the temperature of the medium averaged over the electrode volume

$$\left(\frac{\Delta R_1}{R}\right) = -\beta_T \int T_1(\vec{s})\, w(\vec{s})\, dV(\vec{s}),$$

where the integration extends over the entire volume of the fluid about the electrode. Dividing the electrode resistance into static and fluctuating components we have

$$\frac{\Delta R_0}{R} = -\beta_T \int T_0(\vec{s})\, w(\vec{s})\, dV(\vec{s})$$

$$\frac{\Delta R}{R} = -\beta_T \int T(\vec{s},t)\, w(\vec{s})\, dV(\vec{s}) \quad .$$

The term $(\Delta R/R)$ is a time dependent quantity which is a measure of the fluctuating time dependent temperature $T(\vec{s},t)$ which, in turn, is a function of the turbulent velocity field.

We obtain the first order equation for T under the assumption that the velocity fluctuations are small in comparison with the average velocity:

$$\frac{|\vec{u}|}{U} \ll 1 \quad .$$

Also we assume constant-power-operation (CPO), although the move general case of the other modes of operation may easily be obtained. The dynamic temperature equation when expanded in static and fluctuating terms is

$$\cancel{\frac{\partial T_0}{\partial t}}^{\,0} + \vec{U}\cdot\vec{\nabla}T_0 + \frac{\partial T}{\partial t} + \vec{U}\cdot\vec{\nabla}T + \vec{u}\cdot\vec{\nabla}T_0 +$$

$$+ \cancel{\vec{u}\cdot\vec{\nabla}T}_{\text{SMALL}} = \left(\frac{\rho}{c}\right) w .$$

Neglecting the second order term and separating static and fluctuating terms:

$$\vec{U}\cdot\vec{\nabla}T_0 = \frac{\rho w}{c}$$

and

$$\frac{\partial T}{\partial t} + \vec{U}\cdot\vec{\nabla}T = -\vec{u}\cdot\vec{\nabla}T_0 .$$

The first of these determines the temperature field in the vicinity of the electrode and the latter is the relation between the fluctuating temperature field, T, and the turbulent velocity field, $\vec{u}$.

The fundamental problem in the response of the velocity detector is to find the statistical properties of $(\Delta R/R)$ in terms of the statistical properties of $\vec{u}$ (correlation function and power spectrum) from the equations

$$\frac{\partial T}{\partial t} + \vec{U}\cdot\vec{\nabla}T = -\vec{u}\cdot\vec{\nabla}T_0$$

and

$$\frac{\Delta R}{R} = -\beta_T \int T w \, dv$$

and

$$\vec{U}\cdot\vec{\nabla}T_0 = \frac{\rho w}{c} \quad ,$$

under the boundary condition that T_0 is zero at great distance from the electrode except downstream in the wake of the electrode volume. It should be mentioned that, while $\vec{u}$ is assumed to be a homogeneous turbulent field, T is <u>not</u> a homogeneous fluctuation field, being most intense in the immediate vicinity of the electrode volume and in the electrode wake, and small elsewhere. As a matter of fact it can be shown that the rms value of T is proportional to the static temperature field T_0. The inhomogeneity of the T-field is not, however, of a nature which precludes the direct analysis of the problem since the above relations are linear and the $\vec{u}$-field <u>is</u> homogeneous.

The simplest method to obtain the statistical properties of $(\Delta R/R)$ is to decompose the velocity field into individual wavenumber components

and obtain the periodic amplitude of detector output. Let the velocity at a point in the medium be

$$\vec{u} = \vec{a}(\vec{k})\, e^{-i\vec{k}\cdot\vec{r}}$$

where $\vec{r}$ is the position vector relative to a frame fixed in the medium. The position of the probe in the medium is

$$\vec{r} = \vec{s} - \vec{U}t \quad ,$$

where $\vec{s}$ is the position of the point in the medium relative to the probe. The velocity field relative to the probe is, thus,

$$\vec{u}_1 = \vec{U} + \vec{a}(\vec{k})\, e^{-i\vec{k}\cdot(\vec{s}-\vec{U}t)} .$$

We seek a solution of the form

$$T = \theta(\vec{s})\, e^{-i\vec{k}\cdot(\vec{s}-\vec{U}t)} .$$

Substituting this in the differential equation for T, we find

$$U\left(\frac{\partial\theta}{\partial x}\right) = -a_x\left(\frac{\partial T_0}{\partial x}\right)$$

which has the solution

$$\theta(\vec{s}) = -\left(\frac{a_x}{U}\right) T_0(\vec{s}) .$$

The T_0-distribution generated by heating in the electrode field satisfies the equation

$$\vec{U}\cdot\vec{\nabla}T_0 = \frac{Pw}{c}$$

or

$$\frac{\partial T_0}{\partial x} = \left(\frac{P}{cU}\right) w ,$$

with the boundary condition $T_0(x,y,z) = 0$ at $x = -\infty$. The solution of this equation is

$$T_0 = \left(\frac{P}{cU}\right)\int_{-\infty}^{x} w(\xi, y, z)\, d\xi .$$

The temperature at a point in the medium is, thus,

$$T = -\left(\frac{a_x}{U}\right)\left(\frac{P}{cU}\right) e^{-i\vec{k}\cdot\vec{s}} \int_{-\infty}^{x} w\, d\xi \cdot e^{-i\vec{k}\cdot\vec{U}t} .$$

The electrode resistance as a function of time is

$$\frac{\Delta R}{R} = -\beta_T \int T w \, dV(\vec{\xi})$$

$$= \beta_T \left(\frac{a_x}{U}\right)\left(\frac{P}{cU}\right) e^{i\vec{k}\cdot\vec{U}t} \int e^{-i\vec{k}\cdot\vec{\xi}} w \int_{-\infty}^{x} w \, d\xi \; dV(\vec{\xi}).$$

If the turbulent structure is large in comparison with the probe size ($k \to 0$), this reduces to

$$\frac{\Delta R}{R} = \beta_T \left(\frac{a_x}{U}\right)\left(\frac{P}{cU}\right) e^{i\vec{k}\cdot\vec{U}t} \int w \int_{-\infty}^{x} w \, d\xi \; dV(\vec{\xi})$$

$$= \beta_T \, \overline{\Delta T} \left(\frac{a_x}{U}\right) e^{i\vec{k}\cdot\vec{U}t} \quad ,$$

since, as we saw in Section 12.2,

$$\left(\frac{P}{cU}\right) \int dV(\vec{\xi}) \, w \int_{-\infty}^{x} w \, d\xi = \int_{-\infty}^{+\infty} dy \int_{-\infty}^{+\infty} dz \left(\frac{Uc}{P}\right) \frac{1}{2} \int_{-\infty}^{+\infty} \frac{\partial}{\partial x} (T_o)^2 \, dx$$

$$= \left(\frac{cU}{P}\right) \frac{1}{2} \int_{-\infty}^{+\infty} dy \int_{-\infty}^{+\infty} dz \; T_o^2(+\infty, y, z)$$

$$= \left(\frac{cU}{P}\right) 2 \left(\overline{\Delta T}\right)^2 A$$

$$= \overline{\Delta T}$$

where

$$\overline{\Delta T} = \frac{P}{2cAU} \quad ,$$

and $T_o(+\infty, y, z)$ is the exit temperature distribution. If $\vec{\ell}$ is the position of the probe in the medium,

$$\vec{\ell} = -\vec{U}t$$

then, the electrode resistance measured at the position $\vec{\ell}$ is

$$\frac{\Delta R(\vec{\ell})}{R} = -\beta_T \frac{a_x e^{-i\vec{k}\cdot\vec{\ell}}}{U} \left(\frac{P}{cU}\right) \int e^{-i\vec{k}\cdot\vec{\xi}} w \int_{-\infty}^{x} w \, d\xi \; dV(\vec{\xi}) \quad ,$$

$$\frac{\Delta R(\vec{\ell})}{R} = \beta_T \overline{\Delta T} \left(\frac{a_x e^{-i\vec{k}\cdot\vec{\ell}}}{U}\right) \int e^{-i\vec{k}\cdot\vec{s}} \left\{2A w \int_{-\infty}^{x} w\, d\xi\right\} dV(\vec{s}).$$

Define the quantity $\Omega(\vec{\ell})$ so that

$$\Omega(\vec{\ell}) = \frac{\Delta R(\vec{\ell})}{R}\left(\frac{U}{\beta_T \overline{\Delta T}}\right) ,$$

which has the units of a velocity:

$$\Omega(\vec{\ell}) = a_x e^{-i\vec{k}\cdot\vec{\ell}} \int e^{-i\vec{k}\cdot\vec{s}} \left\{2A w \int_{-\infty}^{x} w\, d\xi\right\} dV(\vec{s}) .$$

Now turn to the formulation used in Section 13.1due to Kovasznay and Uberoi (2)

$$\Omega(\vec{\ell}) = \int \vec{u}(\vec{\ell}+\vec{s})\cdot\vec{K}(\vec{s})\, dV(\vec{s}),$$

where the kernel $\vec{K}(\vec{s})$ is a function of the sensing distribution of the probe. Assuming a periodic velocity field, as before, we find

$$\vec{u}(\vec{r}) = \vec{a}(\vec{k})\, e^{-i\vec{k}\cdot\vec{r}}$$

and

$$\Omega(\vec{\ell}) = e^{-i\vec{k}\cdot\vec{\ell}} \int (\vec{a}\cdot\vec{K})\, e^{-i\vec{k}\cdot\vec{s}}\, dV(\vec{s}).$$

If this is compared with the expression obtained previously

$$\Omega(\vec{\ell}) = e^{-i\vec{k}\cdot\vec{\ell}} \int a_x \left\{2A w \int_{-\infty}^{x} w\, d\xi\right\} e^{-i\vec{k}\cdot\vec{s}}\, dV(\vec{s}) ,$$

we find

$$K_y(\vec{s}) = K_z(\vec{s}) = 0$$

and

$$K_x(\vec{s}) = K(\vec{s}) = 2A w \int_{-\infty}^{x} w\, d\xi .$$

The power sensitivity spectrum, $S(\vec{k})$ of the probe is

$$S(\vec{k}) = \int \psi(\vec{\tau})\, e^{-i\vec{k}\cdot\vec{\tau}}\, dV(\vec{\tau}) \quad ,$$

where $\psi(\vec{\tau})$ is the correlation function of the kernel:

$$\psi(\vec{\tau}) = \int K(\vec{s})\, K(\vec{s}+\vec{\tau})\, dV(\vec{s}).$$

In an isotropic turbulent field we are interested only in

$$\bar{S}(k) = \frac{1}{2} \int S(\vec{k}) \sin\theta \, d\theta$$

where θ is the angle between $\vec{k}$ and $\vec{\tau}$. Carrying out this integration

$$\bar{S}(k) = \int \psi(\vec{\tau}) \left(\frac{\sin k\tau}{k\tau}\right) dV(\vec{\tau}).$$

The calculation of the power sensitivity spectrum, $\bar{S}(k)$, with the kernel

$$K(\vec{s}) = 2A\, w(\vec{s}) \int_{-\infty}^{x} w(\xi, y, z)\, d\xi$$

where

$$\vec{s} = x\hat{i} + y\hat{j} + z\hat{k}$$

is not simple even in the case of a radially symmetric and uniform (spherical) electrode distribution function w. Relatively simple expressions may be obtained, however, for a one-dimensional distribution function and a one-dimensional turbulent field.

The cutoff wavenumber, k_c, for the velocity probe is defined by the value such that

$$\bar{S}(k) = 1 - \left(\frac{k}{k_c}\right)^2 \quad ,$$

for small wavenumbers ($k << k_c$). From the expansion

$$\frac{\sin(k\tau)}{k\tau} \approx 1 - \frac{1}{6}(k\tau)^2 \, ,$$

we have

$$\frac{k_c}{6} \int \psi(\vec{\tau})\, \tau^2\, dV(\vec{\tau}) = 1.$$

Substituting the expression for $\psi(\vec{\tau})$:

$$\int \psi(\vec{\tau})\, \tau^2\, dV(\vec{\tau}) = \int K(\vec{s})\, dV(\vec{s}) \int K(\vec{s}+\vec{\tau})\, \tau^2\, dV(\vec{\tau})$$

$$= 2\int s^2 K(\vec{s})\, dV(\vec{s}) - 2\left|\int \vec{s}\, K(\vec{s})\, dV(\vec{s})\right|^2_1$$

where the latter expression follows from a change of variable and order of integration and the fact that

$$\int K(\vec{s})\, dV(\vec{s}) = 1 \quad .$$

The above integrals may be evaluated in a straight forward, though somewhat tedious, manner to obtain the cutoff wavenumber of a probe with a uniform distribution function over a spherical volume. If b is the radius of the sphere, we find

$$\int s^2 K(\vec{s})\, dV(\vec{s}) = \left(\frac{5}{9}\right) b^2$$

$$\left|\int \vec{s}\, K(\vec{s})\, dV(\vec{s})\right| = \left(\frac{1}{4} + \frac{\pi}{8}\right) b$$

and

$$k_c(\text{sphere}) = \frac{4.5}{b} \quad .$$

An approximate expression for the cutoff wavenumber for a square-cylinder (height = diameter = d) is obtained from the above result by requiring that the sphere have the same frontal area as the square-cylinder, viz.,

$$\left(\frac{8\pi}{9}\right) b^2 = \frac{3\pi^2}{8}\left(\frac{d}{2}\right)^2$$

or

$$b = 1.15\left(\frac{d}{2}\right)$$

and

$$k_c(\text{square-cylinder}) = \frac{7.8}{d} = \frac{3.9}{(d/2)}$$

In Section 5.5 the sensitivity of a hot-wire anemometer is compared with that of the U-meter under the assumption that their respective cutoff

wavenumbers are equal, and that the U-meter probe is a square-cylinder. The cutoff wavenumber of a hot-wire of length ℓ follows from the analysis of References (2,3):

$$k_c(\text{hot-wire}) = \frac{6.00}{\ell} \quad .$$

Thus, the U-meter and HWA have the same cutoff wavenumber if

$$\frac{d}{\ell} = 1.29 \quad .$$

14.2 One-Dimensional Case

The formulas of the last Section are now evaluated for the case of a uniform one-dimensional electrode distribution and a one-dimensional turbulent field. We have (for unit frontal area, A = 1)

$$S(k) = \int_{-\infty}^{+\infty} \psi(\tau) \cos(k\tau)\, d\tau$$

$$\psi(\tau) = \int_{-\infty}^{+\infty} K(s)\, K(s+\tau)\, ds$$

$$K(x) = 2\, w(x) \int_{-\infty}^{x} w(\xi)\, d\xi$$

and

$$\int_{-\infty}^{+\infty} w(x)\, dx = 1$$

$$\int_{-\infty}^{+\infty} K(x)\, dx = 1.$$

Assume a uniform electrode distribution function:

$$w(x) = \begin{cases} \frac{1}{\ell} & 0 < x < \ell \\ 0 & \text{otherwise} \end{cases} ,$$

then

$$K(x) = \begin{cases} \frac{2}{\ell}\left(\frac{x}{\ell}\right) & 0 < x < \ell \\ 0 & \text{otherwise} \end{cases} .$$

The corresponding correlation function is

$$\psi(\tau) = \frac{1}{\ell}\left\{ \frac{4}{3} - 2\left|\frac{\tau}{\ell}\right| + \frac{2}{3}\left|\frac{\tau}{\ell}\right|^3 \right\}$$

and the power sensitivity spectrum is

$$S(k) = \frac{4}{\alpha^2}\left\{ 1 + \left[\frac{\sin(\alpha/2)}{(\alpha/2)}\right]^2 - 2\,\frac{\sin\alpha}{\alpha} \right\}$$

where $\alpha = k\ell$. These four functions as sketched in Figure 14.1.

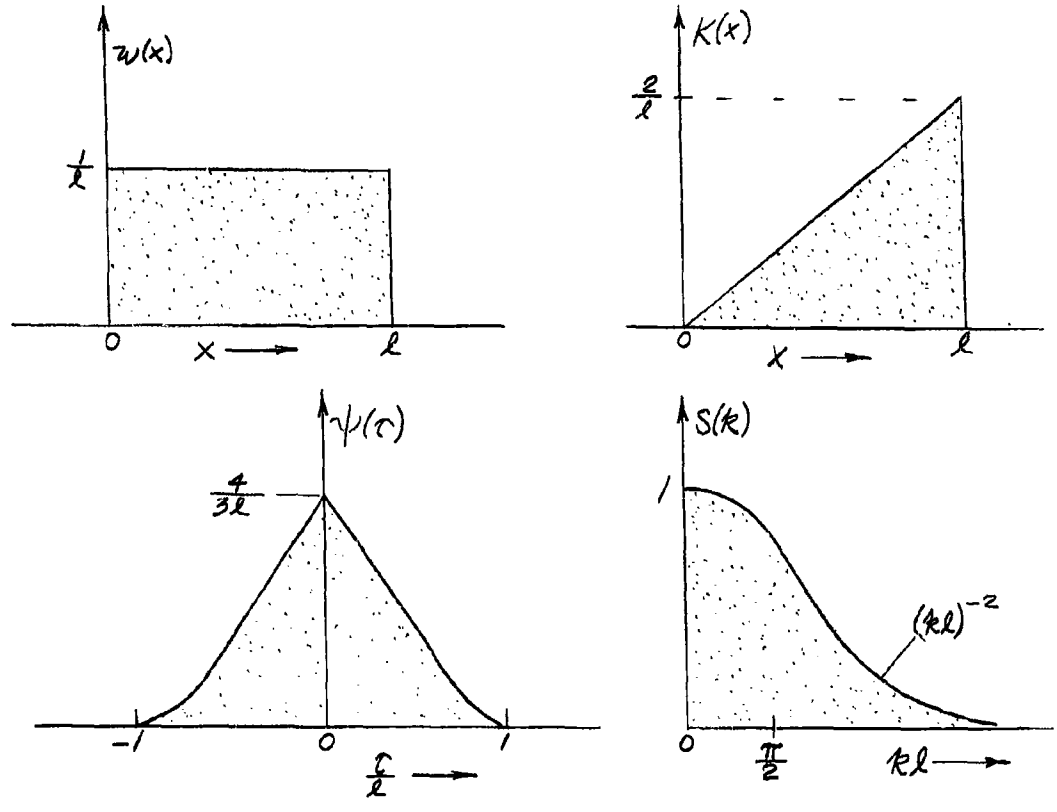

Figure 14.1. Velocity Response Functions for One-Dimensional Case

14.3 Proportional Fluctuating Flow

An important and realistic simplification is the assumption that the

fluctuations in the velocity at a point, $\vec{U}$, is proportional to the steady-state velocity at the point, $\vec{U}_o$ and the constant of proportionality, u, is independent of position:

$$\vec{U} - \vec{U}_o = u\,\vec{U}_o \quad , \qquad (|u| << 1)$$

where u is small and only a function of time. This is termed "proportional fluctuating flow." The analysis for this case is now set up for flow about a probe which distorts the otherwise uniform flow in the vicinity of the probe. A solution is not carried through because of the great analytical complexity, however, a simple experimental method for measuring the power sensitivity spectrum in this case is developed.

The temperature equation in three-dimensions is

$$\frac{\partial T_1}{\partial t} + \vec{U} \cdot \vec{\nabla} T_1 = \frac{P w}{C} \quad ,$$

where P is the electrode power, w is the electrode distribution function, and $\vec{U}$ is not necessarily uniform. Let

$$\vec{U} = \vec{U}_o + u\vec{U}_o \quad ,$$

$$T_1 = T_o + T \quad ,$$

and

$$P = P_o + pP_o \quad ,$$

where, here, we allow for variations in the total electrode power. Substituting these expressions, neglecting second order terms, and separating static and varying quantities, we find

$$\vec{U}_o \cdot \vec{\nabla} T_o = \frac{P_o w}{C}$$

and

$$\frac{\partial T}{\partial t} + \vec{U}_o \cdot \vec{\nabla} T = (p - u) \frac{P_o w}{C}$$

where $T_o(\vec{r})$ is the steady-state temperature distribution due to the electrode heating. The electrode resistance depends on the average electrode temperature

$$\overline{\Delta T_1} = \overline{\Delta T_o} + \overline{\Delta T}$$

where

$$\overline{\Delta T_o} = \int T_o \, w \, dv$$

and

$$\overline{\Delta T} = \int T w \, dv .$$

The power spectrum of $\overline{\Delta T}$ is not easily calculated from the electrode geometry. A very convenient experimental method exists, however, which was first used by Ziegler to measure the response of a hot-wire anemometer by a power modulation technique (4). We notice in the differential equation for T that power fluctuations, p, enter in the same way as velocity fluctuations, u. For this reason, the variation of $\overline{\Delta T}$ with u for constant power (p = 0) is identical with the variation of $\overline{\Delta T}$ with -p for constant velocity (u = 0). Thus, since it is experimentally easier to make arbitrary variations in p electronically than to vary the fluid flow velocity u, the $\overline{\Delta T}$-response is best measured by making appropriate modulation of the electrode power at constant fluid velocity. This experimental method of determining the velocity response is so simple and direct that it is not worthwhile to carry out a laborious analytical computation of the response.

14.4 Boundary Layer Response

The temperature rise at the surfaces of the electrodes experiences a more or less abrupt increase near the surface due to the existence of the velocity boundary layer (Sec. 12.4). The resulting temperature boundary layer makes an additional contribution to the overall electrode resistance, called the "boundary layer resistance." We study in this Section how this resistance contribution responds to fluctuations in the velocity of the conducting medium. In general, for a given electrode geometry, this is a very complicated problem and is necessarily analyzed here under simplified limiting cases of very low and very high frequency periodic velocity fluctuations.

The electrode geometry considered is shown in Figure 13.7 and consists of a uniform electrode field of length ℓ imbedded in a flat plate at a distance L from the leading edge. The free stream flow is parallel to the plate and the velocity boundary layer in the vicinity of the electrode is essentially constant if $L \gg \ell$. Since we are dealing with water as the flowing medium with a Prandtl number of about 5, the thermal boundary layer is thinner than the velocity boundary layer and their relative thickness is some fractional power (e.g., 1/2 or 1/3) of the ratio

$$P\left(\frac{L}{\ell}\right) .$$

For this analysis we assume this ratio to be very large so that the velocity profile in the vicinity of the thermal boundary layer varies in proportion with the distance from the wall (Sec. 12.4). The free stream velocity is assumed to vary periodically:

$$U(1 + \epsilon e^{i\omega t}) \quad . \qquad (\epsilon \ll 1)$$

The temperature and velocity boundary layers are calculated in the two extreme cases of very low ($\omega \to 0$) and very high ($\omega \to \infty$) frequencies. The intermediate frequency between these extremes occurs when all the differential terms of the dynamic equation for temperature

$$c\frac{\partial T}{\partial t} + c\,U(y)\frac{\partial T}{\partial x} = K\frac{\partial^2 T}{\partial y^2} + R$$

are comparable. This occurs when the following approximate relations hold:

$$cT\omega \approx cU\left(\frac{\delta_T}{\delta}\right)\frac{T}{\ell} \approx K\frac{T}{\delta_T^2} \quad ,$$

where δ_T is the thermal boundary layer thickness and δ is the velocity boundary layer thickness. Solving these equations

$$\delta_T \approx \left(\frac{\delta \ell \alpha}{U}\right)^{1/3} = \left(\frac{L}{\ell}\right)^{1/6}\left(\frac{\ell\nu}{U}\right)^{1/2}\left(\frac{\alpha}{\nu}\right)^{1/3} ,$$

$$\omega \approx \left(\frac{U}{\ell}\right)\left[\frac{\alpha \ell}{\nu L}\right]^{1/3} = \frac{U}{\ell}\left(\frac{\ell}{PL}\right)^{1/3} ,$$

where we have used the fact that the thickness of the velocity boundary layer is

$$\delta = \sqrt{\frac{\nu L}{U}} \quad ,$$

and the Prandtl number is

$$P = \frac{\nu}{\alpha} \qquad \text{and} \qquad \alpha = \frac{K}{c} \quad .$$

For example, assume the values

$$L = 10\ell \qquad P = 5 \qquad \nu = .01 \text{ cm}^2/\text{sec}$$

$$U = 3 \text{ knots } (154 \text{ cm/sec}) \qquad \ell = 1 \text{ mm} \quad ,$$

then

$$\delta_T = 2 \times 10^{-3} \text{ cm} = \frac{1}{50}\ell$$

$$\frac{\omega}{2\pi} = f = 60 \text{ cps} \quad .$$

Thus, the cases considered below are for velocity fluctuations much lower and much higher than a frequency of the order of 100 cps. The periodic temperature associated with the velocity fluctuations is expressed in the form

$$T(x,y) = T_0(x,y) + \epsilon\, T_1(x,y)\, e^{i\omega t} \quad .$$

Low Frequency Limit

First we calculate the temperature boundary layer in the limiting case of low frequency velocity fluctuations. Assume the thermal conductivity of the wall, K_w, is much less than that of the water, K. The solution to this problem is obtained in four steps:

1) Obtain quasi-static temperature variation in water for the case $K_w = 0$.
2) This quasi-stationary temperature variation at the boundary implies a heat flux between the wall and the water for K_w finite but $K_w \ll K$.
3) Solve the temperature boundary layer equation for given boundary flux.
4) Integrate resultant boundary layer temperature over surface to get boundary layer resistance as a function of frequency.

This procedure will give the first order approximation to the fluctuating temperature field in the low frequency limit.

The dynamic temperature equation in the boundary layer approximation is

$$c\,\frac{\partial T}{\partial t} + c\,U(y)\,\frac{\partial T}{\partial x} = K\,\frac{\partial^2 T}{\partial y^2} + P_v$$

where U(y) is the velocity as a function of distance from the wall (independent of x), and P_v is the uniform power density in the field of the electrode. Near the wall the velocity U(y) is expressible in the form

$$U(y) = U\left(\frac{y}{\delta}\right) \quad ,$$

where U is the free stream velocity and δ is a distance determined by the slope of the velocity boundary layer at the wall at a distance L from the leading edge. The steady-state solution of this equation is discussed

in Section 12.4 in similarity form and will be denoted by T_o:

$$T_o(x,y) = v(\eta) f(x) \quad , \qquad \eta = \frac{y}{y_o}$$

where

$$y_o = \left(\frac{k x \delta}{cU}\right)^{1/3} = \left(\frac{\alpha x \delta}{U}\right)^{1/3} \quad , \qquad \left(\alpha = \frac{k}{c}\right)$$

and

$$f(x) = \left(\frac{x}{\ell}\right)\left(\frac{\delta}{y_o}\right)\left(\frac{\ell R_v}{cU}\right) = \left(\frac{x}{\ell}\right)^{2/3}\cdot\left(\frac{\delta}{\ell}\right)^{2/3}\cdot\left(\frac{U\ell}{\alpha}\right)^{1/3}\cdot\left(\frac{\ell R_v}{cU}\right) ,$$

and v satisfies the following second order linear differential equation with boundary conditions appropriate to a wall of zero thermal conductivity ($K_w = 0$)

$$v'' + \frac{1}{3}\eta^2 v' - \frac{2}{3}\eta v + 1 = 0$$

with

$$v'(0) = 0 \ , \quad v(\infty) = 0 \ .$$

The quasi-static solution of the dynamic temperature equation which applies in the limit $\omega \to 0$ is simply the secular solution in which the temperature change is that obtained from the static solution by a direct variation of the velocity U i.e.,

$$T_{10} = U \frac{\partial T_o}{\partial U} = U f v' \frac{\partial \eta}{\partial U} + U v \frac{\partial f}{\partial U}$$

$$= -\frac{2}{3} T_o + \frac{1}{3} y \left(\frac{\partial T_o}{\partial y}\right) ,$$

which follows from the velocity dependence given above for the static solution T_o. At the wall the quasi-stationary solution is

$$T_{10}(x,0) = -\frac{2}{3} T_o(x,0) = -\frac{2}{3} v(0) f(x) \ .$$

This temperature variation at the wall corresponds to the case of zero wall conductivity ($K_w = 0$). In the next paragraph we use this temperature variation to find the temperature field in the solid wall for k_w finite but very much smaller than that of the water ($k_w \ll K$). This finite but small conductivity would only slightly change the wall temperature $T_{10}(x,0)$ obtained for the case $K_w = 0$.

The solution for the temperature field in a solid with a periodic wall temperature is given in Carslaw and Jaeger (5). If $T_w(x,y,t)$ is the temperature at the point (x,y) in the solid at time t, and if the harmonic boundary temperature is the real part of

$$T_w(x,0,t) = A(x)\, e^{i\omega t} ,$$

then the temperature in the solid wall is the real part of

$$T_w = A\, e^{-y\sqrt{\frac{i\omega}{\alpha_w}}}\, e^{i\omega t} = A\, e^{-y(1+i)\sqrt{\frac{\omega}{2\alpha_w}}}\, e^{i\omega t}$$

where $\alpha_w = K_w/c_w$ is the thermal diffusivity of the wall material and y is the distance into the wall. We assume here that the variation of the wall temperature, A(x) along the wall is much less than the variation of temperature into the wall so that conduction along the direction parallel to the wall can be neglected. The resulting heat flux <u>from</u> the wall to the medium of thermal conductivity K at its surface satisfies

$$-K\left(\frac{dT}{dy}\right)_0 = K_w\left(\frac{dT_w}{dy}\right)_0$$

where T is the temperature in the medium bounding the wall (water) and the temperature gradients are evaluated <u>at</u> the interface (y = 0). We assume that $K_w << K$ so that

$$-\left(\frac{dT}{dy}\right)_0 = \frac{K_w}{K}\left(\frac{dT_w}{dy}\right)_0 << \left(\frac{dT_w}{dy}\right)_0 .$$

The temperature gradient in the water is much less than that in the solid wall. The expression for the temperature gradient in the wall is

$$\left(\frac{dT_w}{dy}\right)_0 = A(x)\sqrt{\frac{i\omega}{\alpha_w}} ,$$

which is 45° out of phase (lag) with the periodic surface temperature fluctuations. With the knowledge of (dT/dy) we seek in the next paragraph the resulting temperature field in the water which would result from such a boundary flux.

We seek a similarity solution of the form

$$T_F = w(\eta)\, g(x) \qquad \text{WITH} \qquad \eta y_0 = y$$

and

$$y_0 = \left(\frac{\kappa \delta x}{cU}\right)^{1/3} = \left(\frac{\alpha \delta x}{U}\right)^{1/3} ,$$

where these quantities are the same as those in Section 12.4 . We consider the steady-state solution to this problem since it corresponds to the quasi-stationary solution which is appropriate to the first order approximation in the low frequency limit. The steady-state temperature equation in the boundary layer approximation without internal heating and with a linear velocity profile is

$$cU\left(\frac{y}{\delta}\right)\left(\frac{\partial T_F}{\partial x}\right) = \kappa\left(\frac{\partial^2 T_F}{\partial y^2}\right)$$

which, with the substitution of the above similarity solution, becomes

$$w'' = \left(\frac{cU y_0^3}{\kappa \delta x}\right)\eta\left\{-w'\eta\left(-\frac{x}{y_0}\frac{y_0'}{y_0}\right) + w\left(\frac{x g'}{g}\right)\right\} .$$

This equation must satisfy the boundary condition that the temperature gradient at the wall is proportional to some power, n, of the distance, x, along the wall

$$\left(\frac{dT_F}{dy}\right)_0 = \frac{w'(0)\, g(x)}{y_0(x)} = B\left(\frac{x}{\ell}\right)^n ,$$

or g(x) satisfies the equation

$$g(x) = \frac{B}{w'(0)}\, y_0(x)\left(\frac{x}{\ell}\right)^n .$$

Without loss of generality, we may set

$$w'(0) = 1$$

in order to make the value of g(x) definite. It follows that

$$\frac{x g'(x)}{g(x)} = n + \frac{1}{3}$$

and the similarity function, w, satisfies the ordinary linear differential equation of second order

$$w'' + \tfrac{1}{3}\eta^2 w' - \eta\left(n + \tfrac{1}{3}\right) w = 0$$

with $w(\infty) = 0$ and $\dot{w}(0) = 1$. The solution of this equation is difficult and has not been obtained. The temperature in the flowing medium is

$$T_F(x,y) = w(\eta)\, B\, y_0(x) \left(\frac{x}{\ell}\right)^n$$

where B and n are specified by the boundary heat flux. We show later that $n = 2/3$ for the problem of interest.

The results of the previous four paragraphs are now combined to obtain the expression for the quasi-stationary boundary layer temperature profile. The quasi-stationary temperature fluctuation at the wall for zero wall conductivity ($K_w = 0$) is

$$\epsilon\, e^{i\omega t}\, T_{10}(x,0) = -\frac{2}{3} v(0) f(x) \epsilon\, e^{i\omega t}$$

$$= -\frac{2}{3} v(0) \left(\frac{x}{\ell}\right)^{2/3} \left(\frac{\delta}{\ell}\right)^{2/3} \left(\frac{U\ell}{\alpha}\right)^{1/3} \left(\frac{\ell R_v}{cU}\right) \epsilon\, e^{i\omega t}.$$

This temperature is equated to the wall temperature of the solid boundary

$$A(x) = \epsilon\, T_{10}(x,0).$$

The resulting boundary heat flux from the wall to the water for K_w small, but finite, produces a boundary layer temperature profile in the water which is the first order correction to the quasi-stationary solution in the low frequency limit and will be denoted by ϵT_{11}. The gradient of ϵT_{11} is specified by the known flux from the wall. The gradient at the wall in the water is

$$-\epsilon \left(\frac{dT_{11}}{dy_0}\right)_0 = \left(\frac{K_w}{K}\right)\left(\frac{dT_w}{dy}\right)_0 = \epsilon \left(\frac{K_w}{K}\right) T_{10}(x,0) \sqrt{\frac{i\omega}{\alpha_w}}.$$

This temperature gradient represents the given boundary condition for the boundary layer problem of cooling a wall in a linear velocity profile:

$$\epsilon \left(\frac{dT_{11}}{dy_0}\right)_0 = B \left(\frac{x}{\ell}\right)^n$$

Substituting previous expressions we get

$$B\left(\frac{x}{\ell}\right)^n = -\epsilon \left(\frac{K_w}{K}\right) \sqrt{\frac{i\omega}{\alpha}} \left(-\frac{2}{3}\right) \left(\frac{x}{\ell}\right)^{\frac{2}{3}} \left(\frac{\delta}{\ell}\right)^{2/3} v(0) \left(\frac{U\ell}{\alpha}\right)^{1/3} \left(\frac{\ell R_v}{cU}\right)$$

Thus

$$n = 2/3$$

and

$$B = + \frac{2}{3} v(0) \epsilon \left(\frac{K_w}{K}\right) \sqrt{\frac{i\omega}{\alpha}} \left(\frac{\delta}{\ell}\right)^{2/3} \left(\frac{U\ell}{\alpha}\right)^{1/3} \cdot \left(\frac{\ell P_r}{cU}\right) .$$

With these values we obtain the expression for T_{11}:

$$T_{11} = + \frac{2}{3} v(0) \left(\frac{K_w}{K}\right) w(\eta) \left(\frac{\ell P_r}{cU}\right) \left(\frac{x}{\ell}\right) \sqrt{\frac{i\omega\delta^2}{\alpha}} .$$

The fluctuating boundary temperature is

$$\epsilon \left(T_{10} + T_{11}\right) e^{i\omega t} .$$

By definition, the quasi-stationary solution, T_{10}, follows the velocity fluctuations in phase and without attenuation. The first order correction term does not. The ratio (T_{11}/T_{10}) can be obtained from the expressions for each:

$$\left(\frac{T_{11}}{T_{10}}\right) = - \left(\frac{x}{\ell}\right)^{1/3} \cdot \left(\frac{K_w}{K}\right) \cdot \left[\frac{v(0)\, w(\eta)}{v(\eta) - \frac{1}{2}\eta v'(\eta)}\right] \cdot \left(\frac{i\omega L}{U}\right)^{1/2} \cdot \left(\frac{PL}{\ell}\right)^{1/6} \cdot k^{1/3}$$

where the velocity boundary layer has a slope at the wall of (U/δ) where

$$\delta = k \sqrt{\frac{\nu L}{U}} \qquad . \qquad (k \approx 3)$$

We notice that

$$\frac{T_{11}}{T_{10}} \sim - \sqrt{i} = - e^{i\frac{\pi}{4}} = e^{-\frac{3}{4}\pi i} ,$$

so that the first order correction term lags the quasi-stationary solution (therefore the velocity) by 135°, thus, tending to cancel it out to some degree.

The frequency response of the boundary resistance at low frequency is obtained by integrating the temperature field over the volume of the electrode field. The change in electrode resistance ($\Delta R/R$) with the change in velocity $\epsilon = \Delta U/U$ is (Sec. 5.3)

$$\frac{\Delta R}{R} = R\sigma \int \beta (T_{10} + T_{11}) (\nabla\phi)^2 dv \cdot \left(\frac{\Delta U}{U}\right)$$

where β is the temperature coefficient of electrical conductivity of the water. For a uniform sensing function $(\vec{\nabla}\phi)^2$ this expression becomes

$$\frac{\Delta R}{R} = \left(\frac{\Delta U}{U}\right) \frac{\beta}{v_0} \int (T_{10} + T_{11}) dv$$

where v_0 is the effective electrode volume. At zero frequency ($\omega \longrightarrow 0$) and $T_{11} \longrightarrow 0$, we have

$$\left(\frac{\Delta R}{R}\right)_0 = \left(\frac{\Delta U}{U}\right) \frac{\beta}{v_0} \int T_{10}\, dv \quad .$$

The boundary layer amplitude and phase response of the electrodes to velocity changes is the ratio

$$\left(\frac{\Delta R}{\Delta R_0}\right) = \frac{\int (T_{10} + T_{11})\, dv}{\int T_{10}\, dv} = 1 + \frac{\int T_{11}\, dv}{\int T_{10}\, dv} ,$$

where the integration is carried out over the entire electrode volume. It is shown in Section 12.4 that the temperature profile T_{10} consists of two parts, one corresponding to heating in the region near the wall where the velocity boundary layer plays an important role (T_{101}) and the other corresponding to simple heating in the free stream (T_{100}). If the velocity boundary layer is thin in comparison with the typical electrode dimensions, then the integral for the quasi-stationary term is (Sec. 12.2)

$$\int T_{10}\, dv \approx \int T_{100}\, dv = - \left(\frac{v_0 \ell P_v}{cU}\right).$$

To this approximation and by referring to the expression for T_{11} we have

$$\frac{\int T_{11}\, dv}{\int T_{10}\, dv} = - \frac{1}{v_0} \int dv \, \frac{2}{3} v(0) \left(\frac{Kw}{K}\right) \sqrt{\frac{i\omega\delta^2}{\alpha}} \left(\frac{x}{\ell}\right) w(\eta)$$

$$= - \frac{2}{3} v(0) \left(\frac{Kw}{K}\right) \left(\frac{i\omega\delta^2}{\alpha}\right)^{1/2} \frac{\ell}{v_0} \int_0^{\ell} \left(\frac{x}{\ell}\right) y_0(x)\, dx \cdot 2 \int_0^{\infty} w(\eta) d\eta ,$$

where the electrode volume is assumed cubical for simplicity, $v_0 = \ell^3$, and the integral over $w(\eta)$ has been doubled because of a contribution at both electrodes. Performing the integrations we get

$$\frac{\int \tau_{11}\, dv}{\int \tau_{10}\, dv} = -\frac{4}{7} v(0) \int_0^\infty w(\eta)\, d\eta \left(\frac{Kw}{k}\right) k^{\frac{4}{3}} \left(\frac{L}{\ell}\right)^{2/3} \frac{\sqrt{\omega\nu}}{U} P^{1/6} \sqrt{i}$$

$$= -\frac{\sqrt{i\omega\nu}}{U} m_o$$

where

$$m_o = \frac{4}{7} v(0) \int_0^\infty w(\eta)\, d\eta \left(\frac{Kw}{k}\right) k^{\frac{4}{3}} \left(\frac{L}{\ell}\right)^{2/3} P^{1/6} .$$

For the following conditions:

$P = 5$ (water at 40 °C)

$L = 10\ell$

$k = 3$ (flat plate)

$K = 20\, Kw$ (water and celluloid)

and estimated values for the boundary layer functions, the value of m_o is about

$$m_o \approx 3 .$$

Finally, the response amplitude is

$$\left(\frac{\Delta R}{\Delta R_o}\right) = 1 - m_o \frac{\sqrt{i\omega\nu}}{U} ,$$

which, if the correction term is small, can be written approximately as

$$\left(\frac{\Delta R}{\Delta R_o}\right) = \left[1 - \frac{m_o}{U}\sqrt{\frac{\omega\nu}{2}}\right] e^{-i \frac{m_o}{U}\sqrt{\frac{\omega\nu}{2}}} .$$

This is the desired expression for the electrode response to velocity fluctuations in the low frequency limit when boundary layer effects are taken into account.

The next order correction term at low frequencies can be developed from the work of Lighthill (6). The term makes a contribution even for zero wall

conductivity ($K_w = 0$) and varies as the first power of frequency, consequently it becomes smaller than the above correction term in the limit of low frequency velocity fluctuations.

High Frequency Limit

In the limit of very high frequency velocity fluctuations, the velocity boundary layer and temperature boundary layer become very thin. This has the desirable result that for a velocity detector which senses a volume of the fluid, instead of the surface conditions (such as a hot-film anemometer), the response improves at higher frequency. This situation applies only to the boundary layer effects. The analysis for this problem follows the work of Lighthill (6) and others (7,8).

If the impressed velocity is

$$U\left(1 + \epsilon\, e^{i\omega t}\right) \quad ,$$

where U is the uniform free stream velocity parallel to the plate. Lighthill shown that in the limit of high frequencies, the periodic velocity profile at the boundary is

$$U_0(y) = U\left[1 - e^{-y\sqrt{\frac{i\omega}{\nu}}}\right] e^{i\omega t} \quad .$$

In this case the velocity boundary layer thickness is of the order of

$$\sqrt{\frac{\nu}{\omega}} \quad .$$

In this analysis we assume the velocity boundary layer to be of constant thickness with respect to x (parallel flow) so that the boundary layer velocity component perpendicular to the wall is zero.

The dynamic temperature equation for the thermal boundary layer is

$$c\,\frac{\partial T}{\partial t} + c\,U(y)\,\frac{\partial T}{\partial x} = K\,\frac{\partial^2 T}{\partial x^2} + P_v$$

where

$$T = T_0 + \epsilon T_1 e^{i\omega t}$$

$$U(y) = U_0(y) + \epsilon U_0(y) e^{i\omega t} \quad , \qquad (\epsilon << 1)$$

Substituting these expressions we get the equation for the static temperature profile

$$c\,U_0(y)\left(\frac{\partial T_0}{\partial x}\right) = K\left(\frac{\partial^2 T_0}{\partial y^2}\right) + P_v$$

which has been solved before (Sec. 12.4), and the equation for the periodic temperature profile is

$$c\,i\omega\,T_1 + c\,U_0\left(\frac{\partial T_0}{\partial x}\right) + c\,U_0\left(\frac{\partial T_1}{\partial x}\right) = K\left(\frac{\partial^2 T_1}{\partial y^2}\right).$$

The approximation to the limiting case of high frequency ($\omega \to 0$) is obtained by retaining only the terms involving ω and the highest derivative order of the dependent variable T_1:

$$c\,i\omega\,T_1 + c\,U_0\left(\frac{\partial T_0}{\partial x}\right) = K\left(\frac{\partial^2 T_1}{\partial y^2}\right).$$

The solution at great distance from the wall where the diffusion term is small is simply

$$T_1 = i\,\frac{U}{\omega}\left[1 - e^{-y\sqrt{\frac{i\omega}{\nu}}}\right]\left(\frac{\partial T_0}{\partial x}\right)$$

which, if the exponential term is small, is just the temperature fluctuation obtained in Section 14.3 where boundary effects are not considered. For the solution near the boundary we assume a wall of zero conductivity ($K_w = 0$) so that

$$\left(\frac{\partial T_0}{\partial y}\right)_0 = 0$$

and T_0 is essentially independent of y over the high frequency boundary layer since it is thinner than the static one. In his case the solution valid near the wall (as well as elsewhere) is

$$T_1 = i\left(\frac{U}{\omega}\right)\left(\frac{\partial T_0}{\partial x}\right)\left\{1 - \left(\frac{\nu}{\nu-\alpha}\right)e^{-y\sqrt{\frac{i\omega}{\nu}}} + \sqrt{\frac{\alpha}{\nu}}\left(\frac{\nu}{\nu-\alpha}\right)e^{-y\sqrt{\frac{i\omega}{\alpha}}}\right\}.$$

This result supersedes the previous approximate solution at great distance from the wall and agrees with it (for $P \gg 1$) except for the factor

$$\frac{\nu}{\nu-\alpha} = \frac{P}{P-1} \approx 1.3 \quad \text{in water.}$$

Lighthill (6) gives the solution for constant wall temperature and a finite temperature gradient at the wall.

The electrode resistance is

$$\frac{\Delta R}{R} = + R\sigma \int \beta T_1 (\nabla\phi)^2 dv \left(\frac{\Delta U}{U}\right)$$

$$= \frac{\beta}{v_o}\left(\frac{\Delta U}{U}\right) \int T_1 dv ,$$

where $(\nabla\phi)^2$ is uniform over the electrode volume. Assume the exponential boundary layer is much thinner than the static boundary layer, T_o, and the typical dimension of the electrode (ℓ) is much larger than the thickness of the boundary layers. In this case,

$$\frac{1}{v_o}\int i\left(\frac{U}{\omega}\right)\frac{\partial T_o}{\partial x} dv \approx \frac{i}{\ell}\left(\frac{U}{\omega}\right)\left(\frac{\ell R_v}{cU}\right)$$

since throughout most of the electrode volume

$$T = \left(\frac{x}{\ell}\right)\left(\frac{\ell P_v}{cU}\right) .$$

Thus, we have,

$$\frac{1}{v_o}\int T_1 dv = \frac{i}{\ell}\left(\frac{U}{\omega}\right)\left(\frac{\ell R_v}{cU}\right) + 2$$

$$+ i\left(\frac{U}{\omega}\right)\left(\frac{\nu}{\nu-\alpha}\right)\frac{2}{\ell}\left\{\int_0^\ell \left(\frac{\partial T_o}{\partial x}\right)_{y=0} d\left(\frac{x}{\ell}\right)\right\}\int_0^\infty\left\{\sqrt{\frac{\alpha}{\nu}}\, e^{-y\sqrt{\frac{i\omega}{\alpha}}} - e^{-y\sqrt{\frac{i\omega}{\nu}}}\right\} dy$$

where a factor of two has been included in the boundary layer integral to account for integration at both electrodes and the limit of the integral has been extended to infinity because $(\partial T_o/\partial x)$ is constant over the region where the boundary layer functions are appreciable. From Section 12.4 we know that

$$\int_0^\ell \left(\frac{\partial T_o}{\partial x}\right)_{y=0} d\left(\frac{x}{\ell}\right) = \frac{v(0)}{\ell}\left(\frac{\delta}{\ell}\right)\cdot^{2/3}\left(\frac{U\ell}{\alpha}\right)^{1/3}\left(\frac{\ell R_v}{cU}\right)$$

and the exponential integral is

$$\int_0^\infty \{\cdots\}\, dy = -\frac{\nu-\alpha}{\sqrt{i\omega\nu}} .$$

Combining these results we get

$$\frac{1}{v_0}\int \tau_1 \, dv = i\left(\frac{U}{\omega l}\right)\left(\frac{lR}{CU}\right)\left[1 - \frac{m_\infty}{l}\sqrt{\frac{\nu}{i\omega}}\right]$$

where

$$m_\infty = 2\,v(0)\left(\frac{\delta}{l}\right)^{2/3}\cdot\left(\frac{Ul}{\alpha}\right)^{1/3}$$

$$= 2\,k^{2/3}\,v(0)\,P^{1/3}\left(\frac{L}{l}\right)^{1/3} .$$

For water and $L = 10\,l$, this is estimated to be approximately

$$m_\infty \approx 30 \quad .$$

The reduction in response due to the boundary layer effects is expressed as the ratio of the change in resistance, ΔR, with the boundary layer term to that without the boundary layer term, denoted by, ΔR_∞. The resulting amplitude response is:

$$\left(\frac{\Delta R}{\Delta R_\infty}\right) = 1 - \frac{m_\infty}{l}\sqrt{\frac{\nu}{i\omega}} .$$

If the correction term is small this may be expressed as

$$\left(\frac{\Delta R}{\Delta R_\infty}\right) = \left[1 - \frac{m_\infty}{l}\sqrt{\frac{\nu}{2\omega}}\right] e^{-i\frac{m_\infty}{l}\sqrt{\frac{\nu}{2\omega}}} .$$

This expression is similar to the low frequency approximation. It should be mentioned that ΔR_∞ goes over into ΔR_0 as the frequency goes from a very high value to a very low value where the response is not limited by the physical size of the detector probe.

The reduction of the velocity detector response due to boundary layer effects is shown in Figure 14.2 , in the limits of very low and very high frequency. This curve of this Figure gives both the amplitude and phase response as a function of frequency $f = \omega/2\pi$. In the low frequency limit the response is determined by the term

$$\frac{m_0}{U}\sqrt{\frac{\omega\nu}{2}}$$

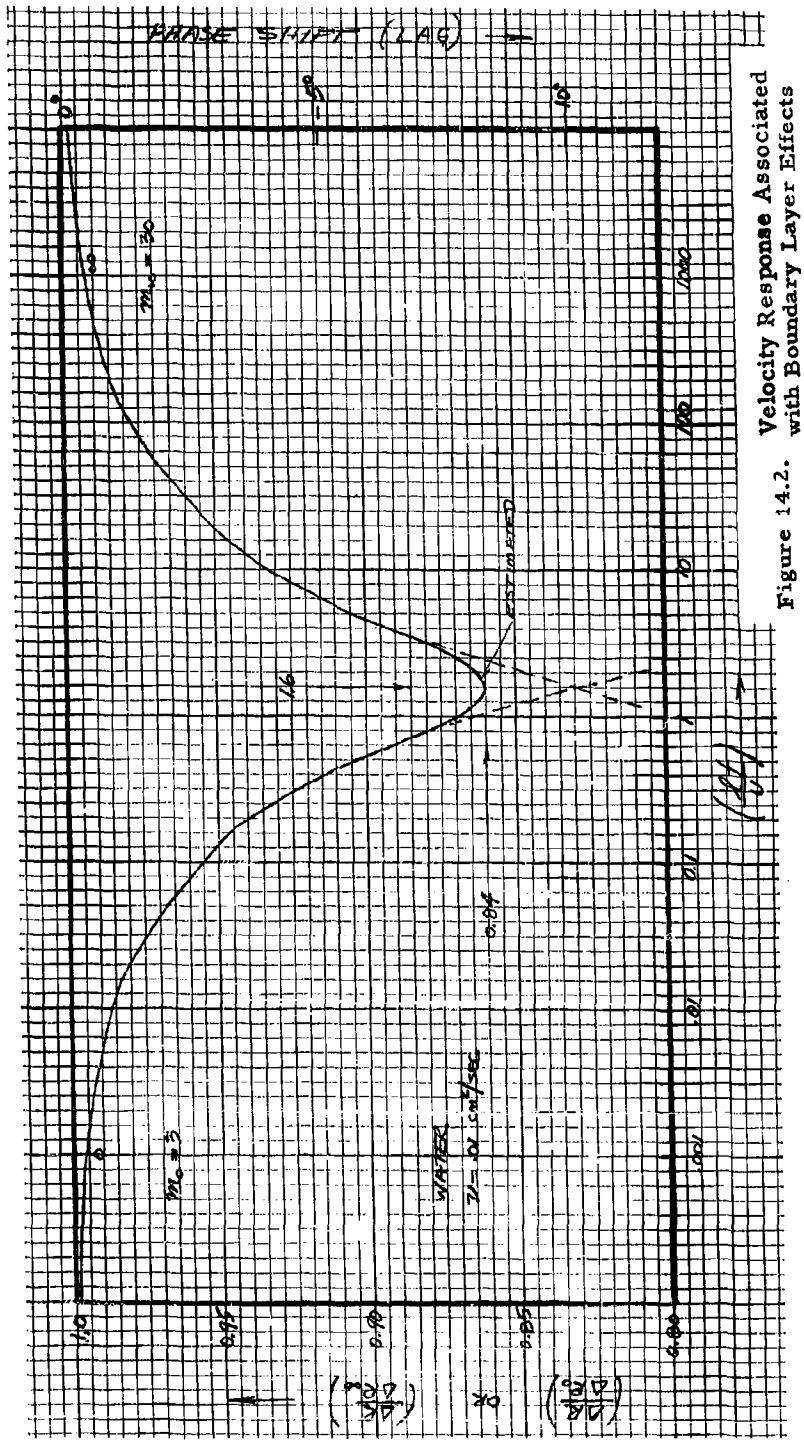

Figure 14.2. Velocity Response Associated with Boundary Layer Effects

and in the high frequency limit by

$$\frac{m_\infty}{\ell}\sqrt{\frac{\nu}{2\omega}} \quad .$$

These two factors are of equal importance at the frequency

$$f = \left(\frac{m_\infty}{2\pi m_o}\right)\frac{U}{\ell}$$

and at this frequency both terms equal

$$\left(\frac{m_o m_\infty}{2}\right)^{1/2}\cdot\left(\frac{\nu}{U\ell}\right)^{1/2} = \sqrt{\frac{m_o m_\infty}{2R}}$$

where R is the Reynolds number based on the length ℓ. For water (ν = .01 cm^2/sec) and

$$\begin{aligned} m_o &= 3 & U &= 154 \text{ cm/sec} \\ m_\infty &= 30 \ , & \ell &= 0.1 \text{ cm} \end{aligned} \ ,$$

the frequency and response factors are

$$f = 2.5 \text{ kc} \qquad \frac{\ell f}{U} = 1.6$$

$$\left(\frac{m_o m_\infty}{2R}\right)^{1/2} = 0.17 \quad .$$

It is important, and fortunate, that the detector response is little affected by boundary layer phenomena, and the small effect that there is, is quite small at all frequencies except in the region corresponding to the time to transit the electrode volume.

14.5 Mode of Operation

The velocity response in a given mode of operation is now considered. Assume a proportional fluctuating velocity field. The relative change in electrode resistance, $r = (\Delta R/R_o)$, is related to the relative change in average electrode temperature, $\theta = (T/\overline{\Delta T})$, by

$$r = -\alpha\theta \ ,$$

where $\alpha = \beta_T \overline{\Delta T}$. The relative change in velocity, u, for periodic fluctuations is given by (for constant electrode power)

$$\theta = -h(\omega)u \quad ,$$

where ω is the angular frequency and $h(\omega)$ is the complex transfer function of the probe. We saw in Section 14.3 that if the electrode power also experiences a fractional change, p, that

$$\theta = -h(\omega)(u - p) \quad .$$

Combining the above relations, we find

$$r = \alpha h(u - p) \quad .$$

In a given mode of operation, the power and resistance fluctuations are related by (Sec. 8.5)

$$p = r \tan\left(\frac{\pi}{4} - \varphi\right) ,$$

where φ is the "mode angle." If the resistance, r, is measured in order to determine the velocity fluctuations then

$$r = u\left[\frac{\alpha h}{1 + \alpha h \tan\left(\frac{\pi}{4} - \varphi\right)}\right] .$$

In the constant-power-mode of operation ($\varphi = \pi/4$)

$$r = \alpha h(\omega)u \quad .$$

At higher frequencies, $\omega \rightarrow \infty$, the response $h(\omega)$ falls off due to the finite size of the probe and the electrode resistance does not respond fully to the velocity fluctuations. This difficulty is alleviated by operation in the constant-resistance mode (CTO). To show this, assume that the power, p, is now measured in order to determine the velocity fluctuations, then

$$p = u\left[\frac{\alpha h \tan\left(\frac{\pi}{4} - \varphi\right)}{1 + \alpha h \tan\left(\frac{\pi}{4} - \varphi\right)}\right] .$$

It is clear that the quantity in brackets becomes independent of $h(\omega)$ if we choose $\varphi = -45^{\circ}$, which corresponds to constant-resistance operation, and

$$p = u \quad .$$

Thus, in this case the velocity fluctuations are fully measured even

though the transfer function $h(\omega)$ may be falling off due to the response limitations of the probe. This shows that the advantage of the CTO mode applies equally well to the U-meter as it is known to apply to the hot-wire anemometer. The applicability is valid only, however, if the velocity fluctuations are proportional to the steady-state velocity field. Thus, in this case, the frequency response of the U-meter probe may be improved over the limits set by its finite size.

The degree to which this is possible is set by the feedback loop in the electronics which makes the constant-resistance-operation possible. As shown in Section 8.5 , if R_o is the electrode resistance, and g_m the transconductance of the feedback loop, then

$$\tan\left(\frac{\pi}{4} - \varphi\right) = 1 + 2 R_o g_m .$$

The amplitude response in this mode of operation falls to half-value (-6 db) when

$$\alpha h(\omega)\left[1 + 2 R_o g_m\right] = 1 = h(0),$$

or when the probe response has fallen to

$$\frac{h(\omega)}{h(0)} = \frac{1}{\alpha\left[1 + 2 R_o g_m\right]}$$

As an example, assume the probe response varies as (power spectrum varies as inverse fourth power):

$$h(\omega) = h(0)\left(\frac{\omega_c}{\omega}\right)^2 ,$$

where ω_c is the cutoff frequency without constant-resistance-operation. Also assume,

$$\beta = .02 \text{ per } {}^{o}C$$
$$\overline{\Delta T} = 20 \, {}^{o}C$$
$$\alpha = 0.40$$
$$R_o = 30 \text{ ohms}$$
$$g_m = 10 \text{ ohm}^{-1}$$

then, the new cutoff frequency is

$$\omega_c' = 1.5 \, \omega_c \quad .$$

Thus, the bandwidth of the U-meter is increased by a factor of 15 in the CTO mode.

If the velocity field is turbulent in three dimensions, instead of a proportional fluctuation field, the advantage of the CTO mode is nullified for the U-meter. Only a "statistical" compensation is possible in this case to account for the fall off of the power sensitivity spectrum at high wavenumber.

15. ELECTRONICS ANALYSIS

The performance of the detection equipment depends primarily on its ability to detect minute changes in the sensing elements. The optimization of the electronic instruments for measuring such changes is studied in this Section. In particular, the best type of wheatstone bridge, the reduction of internal noise, and practical problems of operating with balanced bridges are considered. More advanced techniques for further improving the detection equipment are discussed briefly at the end of this Section.

15.1 Wheatstone Bridge

Some of the fundamental properties of wheatstone bridge networks are established below. It is necessary in the theory of alternating current networks to introduce complex quantities for the variables under consideration - we adopt the convention that small letters represent complex quantities (e.g. voltage v) and capital letters the magnitude of these quantities (e.g. voltage V). The conjugate of a variable v is denoted by v^* (thus, $v\,v^* = V^2$). First, the relation between input and output for a general bridge is developed and then the optimum sensitivity for a special bridge of practical importance is obtained. The input impedance of a bridge is also derived.

The measurement of small changes in the impedance of an electrical element is best made with the aid of a bridge network. This is due to the fact that in such a network an output which is proportional to the variations can be obtained rather than an output which also includes the large contribution due to the average value of the electrical component. Examples of such networks are shown in Figure 15.1 and Figure 15.4 .

A number of advantages of the use of bridge networks can be pointed out in connection with performing differential measurements in which two elements of identical properties are used to measure a variable to which the elements are responsive. These sensing elements constitute two arms of a bridge network and are physically located at different points where the values of the variable being measured may not be equal at all times, but are on the average. Thus, the average bridge output can be adjusted to zero, and, then, if a finite output is observed, it indicates differences in the magnitude of the physical variable being measured at the two points separated in space. Such an arrangement is well suited to measure slight differences in properties of microstructure in a medium. Large changes in the measured variable which are uniform over distances of the order of the separation between the sensing elements are not detected. Since the output of the bridge circuit is small in magnitude in comparison with the input voltage required to make the measurement, a large amplification of the output signal can be used before the signal becomes inconveniently large. Such large amplifi-

cation would not be possible without a bridge network unless a filter was used to pass only these frequencies of interest. The use of such a filter is not possible if the bridge is operated at high frequency and the fluctuations of interest extend to low frequencies because of practical limitations in the construction of very narrow band filters. The differential-spacial bridge arrangement is also well suited for canceling out spurious electrical noise signals which are homogeneous over the separation distance of the electrodes but which have large time-varying components in the frequency band of interest. Finally the measurements become essentially independent in amplitude and phase fluctuations in the electrical power source for the measurement.

As is well known the output of a bridge is proportional (for small increments) to the combination (1)

$$z_1 z_3 - z_2 z_4$$

where the four quantities are the impedances of the arms of the bridge; the balance condition for null output is

$$z_1 z_3 = z_2 z_4 \quad .$$

A symmetrical bridge is defined as one in which, on the average, we have

$$z_1 = z_2 \qquad \text{and} \qquad z_3 = z_4 \quad .$$

In a symmetrical bridge if z_1 and z_2 are the sensing elements, the output is proportional to

$$\left(\frac{\Delta z_1}{z}\right) - \left(\frac{\Delta z_2}{z}\right)$$

where z is the average value of z_1 and z_2 and Δz_1 and Δz_2 are the respective variations of these two impedances. The rms average output in this case is $\sqrt{2}$ larger than the individual component variations if the two are uncorrelated, i.e., the output of a double element bridge is $\sqrt{2}$ times larger than that of a single element bridge; if three elements are used the improvement factor is $\sqrt{3}$; and if all arms of the bridge are sensing elements, the improvement is $\sqrt{4} = 2$.

In the following paragraphs some of the detailed properties of bridge networks are considered.

Bridge Equation

Consider the four-arm wheatstone bridge network of Figure 15.1 in which $z_1 = z + \Delta z$ is the sensing element consisting of an average value z and a small variation Δz; z_2, z_3 and z_4 are the complex impedances in

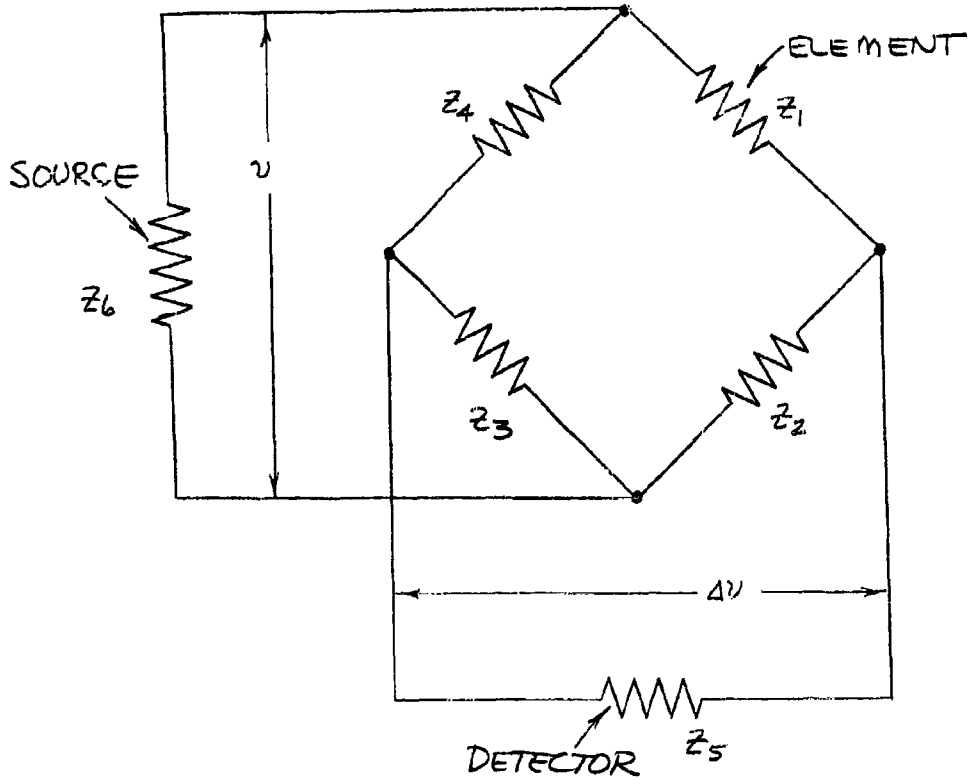

Figure 15.1. Wheatstone Bridge Network

the other arms; and z_5 and z_6 are the input and output impedances of the detector and source, respectively. The complex voltage applied to the bridge network is v, and the bridge output voltage is Δv. As is well known, the bridge is balanced so that there is no output ($\Delta v = 0$) when

$$z_1 z_3 = z_2 z_4 .$$

We will assume this condition to hold precisely only for average values, consequently

$$z z_3 = z_2 z_4 ,$$

which holds only when $\Delta z = 0$. In the analysis of the bridge we will assume only slight deviations from balance and only first order terms will be retained. The voltage v appearing across the input impedance to the bridge, z_s, is given by

$$v = \left(\frac{z_s}{z_6 + z_s}\right) v_6$$

where v_6 is the source voltage in series with z_6. For a detector of infinite impedance ($z_5 = \infty$), the voltage Δv_∞ which appears across the detector is given by the well known expression (2)

$$\Delta v_\infty = \frac{(z_1 z_3 - z_2 z_4)}{(z_1 + z_2)(z_3 + z_4)} v = bv$$

where

$$b = \frac{z_1 z_3 - z_2 z_4}{(z_1 + z_2)(z_3 + z_4)}$$

is the "complex balance factor" or "bridge transfer function." Small increments in the bridge elements are proportional to b. By Thévenin's theorem, the voltage Δv which appears across a detector of finite impedance, z_5, is

$$\Delta v = \left(\frac{z_5}{z_5 + z_d}\right) \Delta v_\infty$$

where z_d is the impedance of the bridge looking back from the detector. Combining the above relations (and temporarily writing $\Delta v = v_5$ for symmetry of notation), we have the general bridge equation:

$$\frac{v_5}{v_6} = \frac{(z_1 z_3 - z_2 z_4)}{(z_1 + z_2)(z_3 + z_4)} \left(\frac{z_3}{z_3 + z_6}\right)\left(\frac{z_5}{z_d + z_5}\right).$$

For first order theory the source impedance, z_6, and detector impedance, z_5, appear only as shown in the last two factors since to first order z_5 is independent of z_5, and z_4 is independent of z_6. This fact is discussed in a later paragraph.

An important special case of the above bridge equation is when the source is matched to the bridge ($z_6 = z_s^*$) and when the detector input impedance is infinite ($z_5 = \infty$):

$$\frac{\Delta v}{v} = \frac{z z_3}{(z+z_2)(z_3+z_4)} \left(\frac{\Delta z}{z}\right) = b$$

where we have used the fact that $z_1 = z + \Delta z$. Define the (complex) bridge factor, m, as

$$m = \frac{z z_3}{(z+z_2)(z_3+z_4)}$$

or since $z\, z_3 = z_2 z_4$, m can be expressed in the more symmetrical form (involving only two instead of four impedances) as

$$m = \frac{z z_2}{(z+z_2)^2} \quad .$$

The bridge equation now takes the simple form

$$\frac{\Delta v}{v} = m\left(\frac{\Delta z}{z}\right) \quad .$$

The bridge equation can always be written in this form even without the special assumptions used here. If we consider the magnitudes of the above equation it becomes

$$\frac{\Delta V}{V} = M\left(\frac{\Delta Z}{Z}\right) ,$$

where M is called simply "bridge factor." If we consider the rms value of the above equation, the voltage ratio of output to input is called the (steady state) "balance factor," B,

$$\left(\frac{\Delta V}{V}\right)_{rms} = B = |b| \quad .$$

Sensitivity

The sensitivity of a bridge (or any device) is defined as the change in output, ΔV, per unit change in the measured quantity, ΔZ:

$$\left(\frac{\Delta V}{\Delta Z}\right),$$

and the "sensitivity exponent" or "fractional sensitivity" as

$$\left(\frac{Z}{V}\right)\left(\frac{\Delta V}{\Delta Z}\right) = M = |m|$$

which is identical with the bridge factor.

Let us find the optimum sensitivity (i.e. maximum M) for a given impedance z (3,4). Let the ratio of z_2 to z be

$$\frac{z_2}{z} = n\, e^{i\varphi} \qquad (n \geq 0)$$

where

$$n = \frac{z_2}{z} \qquad \varphi = \theta_2 - \theta$$

and

$$z_2 = Z_2 e^{i\theta_2} \qquad z = Z e^{i\theta}$$

It follows that

$$M = \frac{n}{|1 + 2n\cos\varphi + n^2|}$$

The optimum (maximum) value of M is found first with respect to n by the condition

$$\frac{\partial M}{\partial n} = 0,$$

with the result n = 1, or $z_2 = z$. The value of M, now, is

$$M = \frac{1}{2(1+\cos\varphi)}.$$

It would seem that for $\varphi = \pi$ the sensitivity is infinite (a resonance condition) but because of the finite resistance of z, the value of φ must be less than π. We find this optimum φ-value by observing that the real (resistive) parts of z and z_2 must be positive (for passive linear

elements) so

$$\cos \theta_2 \geq 0 \qquad \text{or} \qquad -\frac{\pi}{2} \leq \varphi - \theta \leq +\frac{\pi}{2}$$

also

$$\cos \theta \geq 0 \qquad \text{or} \qquad -\frac{\pi}{2} \leq \theta \leq \frac{\pi}{2} \quad .$$

With a little consideration it is easily shown that the optimum value of φ which is consistent with these constraints is

$$\cos \varphi = -\sin \theta \ ,$$

so that the optimum M-value is

$$M_{max} = \frac{1}{2(1-\sin \theta)} \quad .$$

If z is a pure reactance ($\theta = \pi/2$), the sensitivity is infinite. If z is approximately a pure resistance as is the case for electrodes, we have $\theta \approx 0$ and

$$M_{max} \approx \frac{1}{2} \quad .$$

In this case $X_2 = X \approx 0$ and $z_2 = z \approx R = R_2$. The values for z_3 and z_4 can be any finite value provided

$$\frac{z_3}{z_4} = \frac{z_2}{z} = n e^{i\varphi} \approx 1 \quad .$$

We will see later that different optimum values are obtained if we are concerned with the signal-to-noise ratio rather than the less fundamental sensitivity of the bridge. The sensitivity of the wheatstone bridge is considered under other conditions in References (5,6,7,8).

Input and Output Impedance

The input impedance, z, to the wheatstone bridge network shown in Figure 15.2 is required. The source voltage and current are v and s,

respectively. The quantities A,B,C,D and X are complex impedances and

$$v = sz \ .$$

Following Maxwell's theory of networks, we write

$$v = s(A+B) + t(A) + w(B)$$

$$0 = s(A) + t(A+X+D) + w(-X)$$

$$0 = s(B) + t(-X) + w(B+C+X) \ .$$

The solution to these three linear equations by determinants is

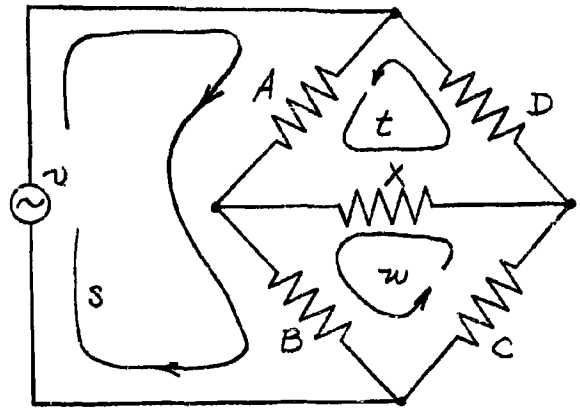

Figure 15.2 . Bridge Impedance

$$s = \frac{\begin{vmatrix} v & A & B \\ 0 & A+D+X & -X \\ 0 & -X & B+C+X \end{vmatrix}}{\begin{vmatrix} A+B & A & B \\ A & A+D+X & -X \\ B & -X & B+C+X \end{vmatrix}}$$

Expanding and simplifying, we obtain

$$\frac{v}{s} = z = \frac{DC(A+B) + AB(D+C) + X(A+B)(C+D)}{(A+D)(B+C) + X(A+B+C+D)} \ .$$

It is convenient to define three quantities:

$$z_o = \frac{(A+B)(C+D)}{(A+B+C+D)}$$

$$z_x = \left|\frac{AB}{A+B}\right| + \left|\frac{CD}{C+D}\right| + X$$

$$b = \frac{(AC-BD)}{(A+B)(C+D)}$$

The first of these, z_o, has the form of the input impedance when the bridge is balanced; i.e., when AC = BD, and is independent of X. The quantity, b, is the balance factor for the wheatstone bridge; at balance b = 0. These quantities are related to z by

$$\frac{1}{z} = \frac{1}{z_o} + \frac{b^2}{z_x}$$

which may be shown by direct substitution, and some amount of algebraic manipulation. This is an exact expression - not one developed as an approximation which retains leading terms in powers of b. A similar result is obtained for the impedance of the wheatstone bridge looking back from the detector (impedance X is then the source internal impedance).

It will be noticed that near balance where

$$B = |b| \ll 1 ,$$

that $$z \approx z_o .$$

Therefore, to first order in the balance factor, b, we can write

$$z = z_o ,$$

which is the familiar result for an exactly balanced bridge.

15.2 Optimum Bridge Networks

The wheatstone bridge of optimum sensitivity is not necessarily optimum with respect to signal-to-noise ratio if noise is generated internally in the arms of the bridge. This topic is studied in some detail in this Section for single and double sensing element bridges. The basic concept on which the optimization of these bridges is based is considered first.

Detectability Concept

The relative merit of a bridge is frequently expressed in terms of the "sensitivity" of the network. The sensitivity is defined as the magnitude of output signal for a given (small) change in one arm of the bridge which is due to changes in the particular physical variable being detected. A more important basis for judging the merit of a bridge

network in a detection system is the "minimum detectable signal" (9). This is defined as the smallest change in the physical variable under consideration which is just detectable by the instrument. The term "just detectable" requires a statement of the signal-to-noise ratio which is assumed for the signal to be considered "detected." In optimizing a given detection instrument, it is preferable to optimize the "detectability" rather than the "sensitivity." The former concept is intrinsically involved with background noise whereas the latter is involved essentially with the "gain" of the instrument. Thus, "maximum sensitivity" is not considered as important as the "minimum detectable signal."

The noise which limits a certain instrument is of two distinct types: that which originates in the instrument itself (internal noise) and that which is in the medium (external noise). In the case of an internal noise limited instrument, the concept of detectability is of prime importance and will not necessarily have optimum conditions which are the same as those based on maximum sensitivity. For an external noise limited instrument the minimum detectable signal is set already by the environment, and it is proper in this case to optimize the detector by maximizing the sensitivity.

Optimization Criterion

The criterion for optimizing the wheatstone bridge network for the detection of small changes in impedance will be based on the "detectability" concept. This assumes that the noise which limits the measurements is internal to the bridge network. The criterion is the following: given the total power, P, developed in the bridge network; the impedance z which is subject to variations which one is trying to detect; the source of noise is due to Johnson thermal noise only; and the signal-to-noise ratio, λ, which just permits the detection of a signal (over the passband of the equipment); then choose the impedances of the source, detector and bridge network such that the detectable impedance variation is a minimum. If the noise limiting the measurement is due to an external source, the "sensitivity concept" applies and the bridge is optimized in the conventional way for maximum bridge output signal power. Lord Rayleigh (6) shows that this is achieved by matching the source impedance to the bridge input impedance (conjugates of each other); the detector impedance is matched to the output impedance of the bridge (conjugates of each other); and all arms of the bridge are of equal impedance, i.e., equal to the impedance, z, of the measured element. The optimization of the bridge which follows, refers properly to the operation of the detector with impedances which are independent of applied power, that is, for the measurement of temperature and salinity, but not for velocity. As is known, the sensitivity to velocity fluctuations depends on the mode of operation, i.e., CCO, CVO, CPO (Sec. 5.3), but for impedances which are independent of applied power (linear elements) the mode of operation is not of importance.

Single Element Bridge

In Section 15.1 we saw that the output signal, Δv, from a bridge is given by (see Figure 15.1)

$$\Delta v = v\, b \left(\frac{z_5}{z_5 + z_d}\right)$$

where

$$b = \frac{z_1 z_3 - z_2 z_4}{(z_1 + z_2)(z_3 + z_4)} .$$

Added to the output, Δv, is a noise voltage, v_n, due to thermal noise voltage fluctuations. The root-mean-square of the thermal noise is (10,25):

$$(v_n)^2_{rms} = \tfrac{1}{2}|v_n|^2 = 4kT\,\Delta f\, Re\left\{\frac{z_5 z_d}{z_5 + z_d}\right\}$$

where k is Boltzman's Constant, T the absolute temperature, Δf the bandwidth and Re $\{x\}$ denotes the real part of x. This thermal noise is due to the resistive part of the impedance in parallel with the detector input, i.e., z_5 and z_d.

The total signal, Δv_T, at the detector input is

$$\Delta v_T = \Delta v + v_n ,$$

where the signal, Δv, and noise, v_n, are assumed to be uncorrelated. The signal-to-noise ratio (power), λ, is defined as

$$\lambda = \frac{(\Delta v)^2_{rms}}{(v_n)^2_{rms}} ,$$

and is assumed to be given and fixed. Combining relations

$$4\lambda kT\,\Delta f\, Re\left\{\frac{z_5 z_d}{z_5 + z_d}\right\} = |b|^2 \left|\frac{z_5}{z_5 + z_d}\right| P \frac{|z_5|^2}{Re\{z_5\}} ,$$

where P is the given total power dissipated in the bridge,

$$P = \tfrac{1}{2}|v|^2 Re\left\{\frac{1}{z_5}\right\} = \tfrac{1}{2}|v|^2 \frac{Re\{z_5\}}{|z_5|^2} .$$

Rewriting the above equation we get

$$|b|^2 = \left(\frac{4\lambda kT\Delta f}{P}\right)\left|\frac{z_5+z_d}{z_5}\right|^2 \frac{Re\{z_s\}}{|z_s|^2}\, Re\left\{\frac{z_5 z_d}{z_5+z_d}\right\}$$

which is the square of the balance factor averaged over the band of frequencies, Δf.

The optimum source and detector impedance are determined by minimizing the above expression. Since the source impedance does not appear in this equation (except for a second order term in z_d) it is not pertinent to the persent optimization criterion. In practice it is matched to the bridge network ($z_s^* = z_6$) for maximum power transfer. The detector impedance is determined by minimizing

$$\left|\frac{z_5+z_d}{z_5 z_d}\right|^2 Re\left\{\frac{z_5 z_d}{z_5+z_d}\right\} = Re\left\{\frac{1}{z_d}\right\} + Re\left\{\frac{1}{z_5}\right\}$$

which requires (since Re $\{z_5\}$ is positive)

$$Re\left\{\frac{1}{z_5}\right\} = \frac{Re\{z_5\}}{|z_5|^2} = 0.$$

Thus, the detector impedance is a pure reactance (preferably large). Using this result we have

$$|b|^2 = \left(\frac{4\lambda kT\Delta f}{P}\right) Re\{z_d\}\, Re\left\{\frac{1}{z_s}\right\},$$

which is applicable for either single or double sensing element bridges.

For a single element bridge we have

$$z\, z_3 = z_2 z_4$$

$$z_6 = z_4\left(\frac{z+z_2}{z+z_4}\right)$$

$$z_d = z_2\left(\frac{z+z_4}{z+z_2}\right)$$

and

$$b = \left(\frac{\Delta z}{z}\right)\frac{z\, z_2}{(z+z_2)^2}.$$

Define the magnitude of the fractional impedance imcrement, ξ , as

$$\xi = \left|\frac{\Delta z}{z_0}\right|$$

combining these relations we obtain a relatively complicated relation which is a function only of the impedances z_2 and z_4 and the given impedance z. This expression is, however, symmetrical in z_2 and z_4. It may be shown that the process for optimizing with respect to one is the same as for the other because of the interchangeability of the two variables. This greatly simplifies the analysis because we may set

$$z_2 = z_4 ,$$

and optimize with respect to z_2 (or z_4). Assuming this, we have

$$\xi^2 = \left(\frac{4\lambda kT\Delta f}{P}\right) \frac{|z_2+z|^4}{|z|^2} R_e^2\left\{\frac{1}{z_2}\right\}$$

If we write

$$\frac{z_2}{z} = n\, e^{i\varphi}$$

where

$$n = \frac{Z_2}{Z} \qquad , \qquad \varphi = \theta_2 - \theta$$

and

$$z_2 = Z_2\, e^{i\theta_2} \qquad , \qquad z = Z\, e^{i\theta}$$

then

$$\xi = \left(\frac{4\lambda kT\Delta f}{P}\right)^{1/2} \cdot \left(\frac{1+2n\cos\varphi+n^2}{n}\right) \cdot \cos(\varphi+\theta).$$

The minimization of ξ with respect to n yields the result n = 1, which is the solution of the equation $(\partial\xi/\partial n) = 0$. Thus, the magnitute of z, z_2, z_3 and z_4 are all identical. For this value

$$\xi = \left(\frac{4\lambda kT\Delta f}{P}\right)^{1/2} 4\cos^2\left(\frac{\varphi}{2}\right)\cos(\varphi+\theta).$$

It would appear that ξ could be reduced to zero by an appropriate choice of φ in this equation, however, this is not possible for linear circuit elements (fixed values). This follows because the resistive component of all impedances must be positive or zero:

$$Re\{z\} \geq 0$$

$$Re\{z_2\} = Re\{z_4\} = Re\{z\, n e^{i\varphi}\} \geq 0$$

$$Re\{z_3\} = Re\{z\, n^2\, e^{i2\varphi}\} \geq 0$$

or

$$\cos\theta \geq 0$$

$$\cos(\varphi+\theta) \geq 0$$

$$\cos(2\varphi+\theta) \geq 0 .$$

The optimum value of φ is found by inspection of the "allowed" region of φ for a given θ. The first and last of the above equations set the bounds on this allowed region:

$$-\frac{\pi}{2} \leq \theta \leq \frac{\pi}{2}$$

$$-\frac{\pi}{4} - \frac{\theta}{2} \leq \varphi \leq \frac{\pi}{4} - \frac{\theta}{2} .$$

With some consideration, it may be shown that the optimum value of φ lies on part of the boundary of this region, viz. :

$$\varphi = \frac{\pi}{4}\, sgn(\theta) - \frac{\theta}{2} \quad , \quad |\theta| \leq \pi/2 .$$

At this value, we have

$$\xi = \left(\frac{4\lambda kT\Delta f}{P}\right)^{1/2} M_0(\theta) ,$$

where

$$M_0(\theta) = 4\cos^2\left(\frac{\pi}{8} - \frac{|\theta|}{4}\right)\cos\left(\frac{\pi}{4} + \frac{|\theta|}{2}\right) .$$

This is the minimum detectable signal obtained by the optimization criterion for the single element bridge. For this optimum arrangement, we have

$$z_s = z_1 = z_2 = z_4 = z\,e^{i\varphi}.$$

The voltage, v_1, which appears across $z_1 = z + \Delta z$ is related to the input voltage, v, by

$$\frac{v_1}{v} = \left(\frac{z}{z + z_2}\right).$$

The "efficiency," η, of the bridge is defined as the ratio of power dissipated in the electrode to the total power, P, that is:

$$\eta = \frac{\frac{1}{2}|v_1|^2 \,\mathrm{Re}\left\{\frac{1}{z}\right\}}{\frac{1}{2}|v|^2 \,\mathrm{Re}\left\{\frac{1}{z_s}\right\}} = \frac{\cos\theta}{M_0(\theta)}.$$

The bridge equation is

$$\frac{\Delta v}{v} = b = m\left(\frac{\Delta z}{z}\right) = \frac{z z_2}{(z+z_2)^2}\left(\frac{\Delta z}{z}\right)$$

or

$$\frac{\Delta V}{V} = M\left(\frac{\Delta Z}{Z}\right) \qquad \text{(magnitudes)}$$

where

$$M = \frac{1}{4\cos^2\left(\frac{\varphi}{2}\right)} = \frac{1}{4\cos^2\left(\frac{\pi}{8} - \frac{|\theta|}{4}\right)}.$$

For pure resistance sensing elements, as is approximately the case for the electrodes of this Report, we have $\theta = 0$, $z = R = Z$. In this case $\varphi = \pm \pi/4$, $\theta_2 = \theta_4 = \pm \pi/4$ and

$$M_0 = M_0(0) = 4\cos^2\left(\frac{\pi}{8}\right)\cos\left(\frac{\pi}{4}\right) = \sqrt{3+2\sqrt{2}} = 2.41$$

$$\eta = \frac{1}{2.41} = 0.415,$$

and

$$M = \frac{1}{4\cos^2\left(\frac{\pi}{8}\right)} = 0.294$$

The arms of the bridge are:

$$z = R$$

$$z_2 = R\, e^{\pm i\frac{\pi}{4}} = \frac{R}{\sqrt{2}} \pm i\,\frac{R}{\sqrt{2}} = z_3 = z_4$$

$$z_3 = R\, e^{\pm i\,\pi/2} = \pm i\, R.$$

Such a bridge is shown in Figure 15.3 with inductances as the positive reactive components.

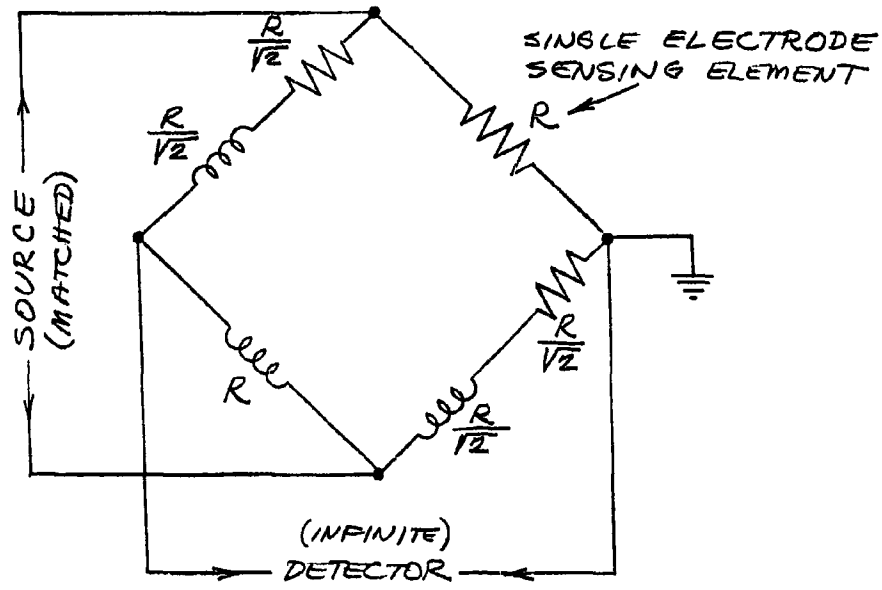

Figure 15.3. Optimum Single Resistive Element Bridge

Double Element Bridge

Consider now the problem of optimizing a wheatstone bridge network with two equal, but independent, sensing elements. The network for this case is that of Figure 15.1 where

$$z_1 = z + \Delta z_1$$

$$z_2 = z + \Delta z_2 \ ,$$

and we must also include an impedance z_x which appears as a load across the bridge input and is due to a possible conducting path between the individual elements. Variations in z_x do not cause variations in bridge output

(to first order). This "cross impedance," z_x, will be written

$$z_x = Kz ,$$

where K is some complex number. The requirement of steady state balance is satisfied if

$$z_3 = z_4 ,$$

which will be assumed. As in the case of a single sensing element the detector impedance is a large pure reactance and the source impedance is the conjugate of the bridge input impedance (matched). The bridge equation in this case is

$$\frac{\Delta v}{v} = b = \frac{z_1 z_3 - z_2 z_4}{(z_1+z_2)(z_3+z_4)} = \frac{1}{4}\left(\frac{\Delta z}{z}\right) ,$$

where $\Delta z = \Delta z_1 - \Delta z_2$ and the bridge factor is

$$M = \frac{1}{4} = 0.250 .$$

The input impedance to the bridge is given by

$$\frac{1}{z_s} = \frac{1}{z_x} + \frac{1}{2z} + \frac{1}{2z_3} = \frac{1}{2K'z} + \frac{1}{2z_3} ,$$

where

$$K' = \frac{K}{K+2} = K' e^{i\varphi'} .$$

The bridge output impedance is

$$z_d = \frac{1}{2}(z + z_3) .$$

The equation for the minimum detectable variation developed previously is

$$\xi^2 = 16\left(\frac{4\lambda kT\Delta f}{P}\right) Re\{z_d\} Re\left\{\frac{1}{z_s}\right\}$$

or

$$M_0^2 = 16\, Re\{z_d\}\, Re\left\{\frac{1}{z_s}\right\}.$$

If we write

$$\frac{z_3}{z} = n\, e^{j\varphi}$$

where

$$n = \frac{Z_3}{Z} \quad , \quad \varphi = \theta_3 - \theta$$

and

$$z_3 = Z_3 e^{j\theta_3} \quad , \quad z = Z e^{j\theta} ,$$

then

$$M_0^2 = 4\left[\cos\theta + n\cos(\varphi+\theta)\right]\left[\frac{\cos(\varphi'+\theta)}{K'} + \frac{\cos(\varphi+\theta)}{n}\right].$$

Minimizing M_0 with respect to n $\left(\partial M_0^2/\partial n = 0\right)$ yields the condition

$$n^2 = K' \frac{\cos\theta}{\cos(\varphi'+\theta)} ,$$

and on substitution of this result we have

$$M_0 = 2\left[\frac{\cos\theta}{n} + \cos(\varphi+\theta)\right].$$

The number n is independent of φ. The optimum value of φ is found by inspection under the constraints

$$Re\{z\} \geq 0 \qquad Re\{n\, e^{j\varphi} z\} \geq 0$$

or

$$\cos\theta \geq 0 \qquad \cos(\varphi+\theta) \geq 0$$

or

$$-\frac{\pi}{2} \leq \theta \leq \frac{\pi}{2} \qquad -\frac{\pi}{2} \leq \theta+\varphi \leq \frac{\pi}{2} .$$

The minimum value of M_0 is clearly at the minimum allowed value of $\cos(\varphi+\theta)$ since all terms are positive, therefore

$$\varphi + \theta = \pm\frac{\pi}{2} .$$

Thus, z and $z_3 = z_4$ are in quadrature independent of the value of K' (or K). Substituting this result, the optimum value of M_o is found to be

$$M_o = \frac{2\cos\theta}{n}$$

where

$$n^2 = \frac{K'\cos\theta}{\cos(\varphi'+\theta)} \quad .$$

For the important case of purely resistive elements and cross resistance ($\theta = 0$, $\varphi' = 0$, $z = R$) we have

$$\varphi = \pm \pi/2$$

$$n = \sqrt{\frac{K}{K+2}}$$

$$M_o = 2\sqrt{\frac{K+2}{K}}$$

$$z_3 = z_4 = \pm i R \sqrt{\frac{K}{K+2}}$$

$$z_d = \frac{R}{2} \pm i \frac{R}{2}\sqrt{\frac{K}{K+2}}$$

and

$$\frac{R}{z_s} = \frac{1}{2}\left(\frac{K+2}{K}\right) \mp \frac{i}{2}\sqrt{\frac{K+2}{K}} \quad .$$

The efficiency (per electrode), η, is

$$\eta = \frac{1}{2}\left(\frac{K}{K+2}\right),$$

and the efficiency for both electrodes together is just 2η. The bridge network corresponding to this case is shown in Figure 15.4 for inductive reactive components.

The simplest case for $K = \infty$ for large cross resistance we have

$$n = 1$$

$$M_o = 2$$

$$z_3 = z_4 = \pm i\, R$$

$$z_d = \frac{R}{2} \pm i\, \frac{R}{2}$$

$$z_s = R \pm i\, R$$

and

$$2\eta = 1 .$$

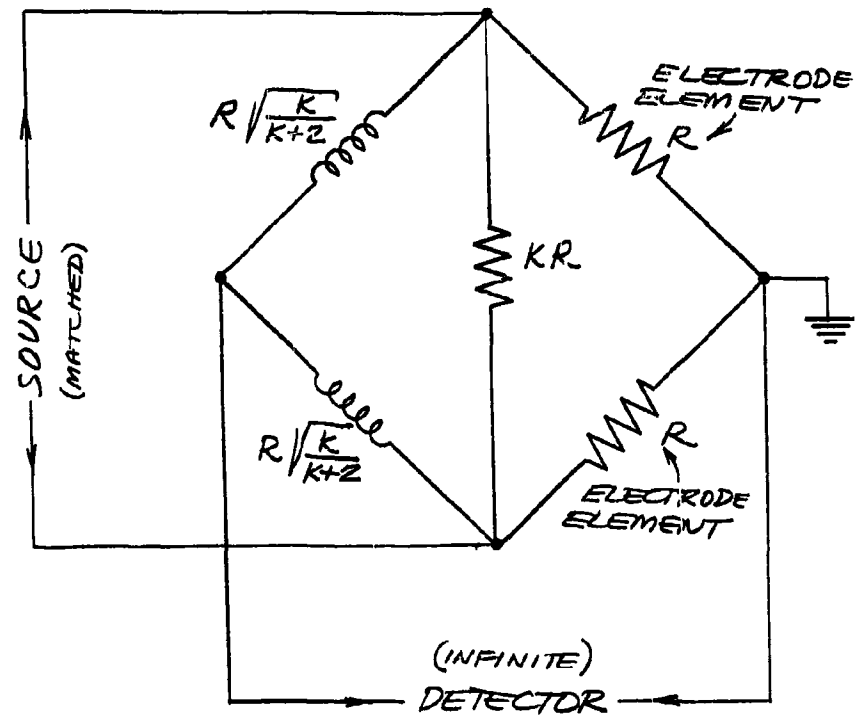

Figure 15.4 . Optimum Double Resistive Element Bridge

Results and Comparison

The results of the analysis above are now given for the case of infinitely large cross resistance ($K = \infty$) in the case of the double sensor. A comparison is made between the single and double sensing elements to show that for differential measurements of microstructure which is not correlated over the separation distance between the double sensing elements, that the double sensor is more suitable, i.e., its minimum detectable signal is smaller than that for a single sensing element. In the case of the single element the smallest detectable impedance difference, ξ_1, was shown to be (assuming a resistive sensing element)

$$\xi_1 = \left(\frac{4\lambda kT\Delta f}{P}\right)^{1/2} 2.41 \quad , \qquad \left(M_o = 2.41\right)$$

and that for a double sensing element is

$$\xi_2 = \left(\frac{4\lambda kT\Delta f}{P}\right)^{1/2} 2.00 \quad , \qquad \left(M_o = 2.00\right)$$

the ratio of these quantities is

$$\frac{\xi_2}{\xi_1} = \left(\frac{4}{3+2\sqrt{2}}\right)^{1/2} = 0.829 .$$

If ΔT is the rms effective temperature fluctuation in the medium which produces signals in the passband of the equipment, and β_T is the temperature coefficient, and if furthermore, the temperature fluctuations at each of the double sensors are uncorrelated (because they are separated sufficiently), it was shown in Section 15.1 that

$$\xi_1 = \beta_T \Delta T_1$$

but

$$\xi_2 = \beta_T \sqrt{2}\, \Delta T_2 \quad ,$$

where the subscripts on ΔT refer to the minimum detectable temperature fluctuations in each arrangement. Finally, combining the above relations we find

$$\left(\frac{\Delta T_2}{\Delta T_1}\right) = \left(\frac{2}{3+2\sqrt{2}}\right)^{1/2} = 0.586 .$$

Thus, the minimum detectable temperature of the double sensor is about 60 % that of the single sensor, i.e., the detectability is about 4.7 db better. It is for this reason, among others, that the high sensitivity detection equipment developed and described in Section 16.1 is based on the double sensing element arrangement.

To summarize, we list in Table 15.1 below some numerical factors which characterize the bridge networks. It is useful to introduce some dimensionless numbers which describe the properties of the bridge; they will be denoted by M_i where i is a subscript which identifies the property of the bridge; M is the bridge factor which has already been introduced (no subscript); M_o is the number already introduced to account for the S/N theory; M_1 is the number of electrodes; M_2 is the resistance of the input impedance to the bridge relative to the resistance R of the sensing element ($\mathrm{Re}\{z_s\} = M_2 R$); M_3 is the resistance of the output impedance of the bridge relative to the resistance R of the sensing element ($\mathrm{Re}\{z_d\} = M_3 R$); $M_4 (= \eta)$ is the fraction of power absorbed by each sensing element; and M_5 is the total power efficiency of the electrodes ($M_5 = M_1 M_4$).

Table 15.1 . Table of M-Numbers for Optimum Wheatstone Bridge Networks

Number	Single Element	Double Elements	Four Elements
M	0.294	0.250	0.250
M_o	2.41	2.00	4.00
M_1	1.00	2.00	4.00
M_2	0.707	1.00	1.00
M_3	0.707	0.500	1.00
M_4	0.415	0.500	0.250
M_5	0.415	1.00	1.00

Also included in the last column are the results for an equilateral bridge with four equal (on the average) resistances, R; the source is matched to the bridge ($z_s = R$); the detector impedance is assumed infinite ($z_5 = \infty$). These are the optimum conditions for the equilateral bridge for maximum detectability.

15.3 Balance Problem

The operation of the detection equipment is improved in several respects if the bridge is adjusted to a high degree of steady state balance. This improvement is associated with the reduction of noise originating in the signal source, linear detector, and spurious noise in the amplifying system. For a system which is manually balanced, there is a practical limit to the degree of balance which is set by the natural instability in the electrode elements. A higher degree of balance is possible when the balance is set by automatic means (Sec. 15.4). The variations in balance conditions can present a very troublesome practical problem if a wide range of gain control is not available and if suitable adjustments of the bridge are not available. This situation sometimes arises if it is necessary to adjust the bridge to balance by an inadequate remote adjusting arrangement and is due to the fact that, if the bridge deviates too far from balance, the output signal is so large that the sensitive input amplifiers saturate. There is no means of determining whether the bridge adjustments are improving or worsening the balance condition in this situation. Proper balancing of the bridge is accomplished most readily by two independent controls which are "orthogonal." The above aspects and others concerning the problem of balancing a bridge network are considered in more detail below.

Balance Convergence

A four arm wheatstone bridge is brought to balance, i.e., a null output, by the adjustment of the components of the bridge. This can be done, in general, only if two adjustments are available which are at least somewhat independent. For a highly refined balance one must make quite a few adjustments, alternating between the two, to achieve the desired balance. Unless care is exercised in choosing the adjustable components it may prove very difficult or impossible to obtain a null condition. This difficulty lies in the degree of dependence or independence of the two controls. This problem of balance convergence has been studied in References (11,12,13,14). The results of these works are briefly summarized here with some minor modifications.

Consider a bridge initially near balance. With reference to Figure 15.5, it may be shown that the bridge output can be represented as the radial distance from the origin to a point in the complex plane. The bridge output lies on a line as any one of the bridge elements is adjusted; the family of lines for any two adjustable elements cross each other at an angle γ. The bridge output follows the zig-zag path of Figure 15.5 as adjustments are alternately made between the two elements. The angle ϵ in this Figure indicates the error in any one adjustment. If the corssing angle between the families of lines, γ, is 90° the bridge balances rapidly, whereas if γ is a small angle the convergence is poor. The two adjustable elements are said to be "orthogonal" if their relative crossing angle is 90°.

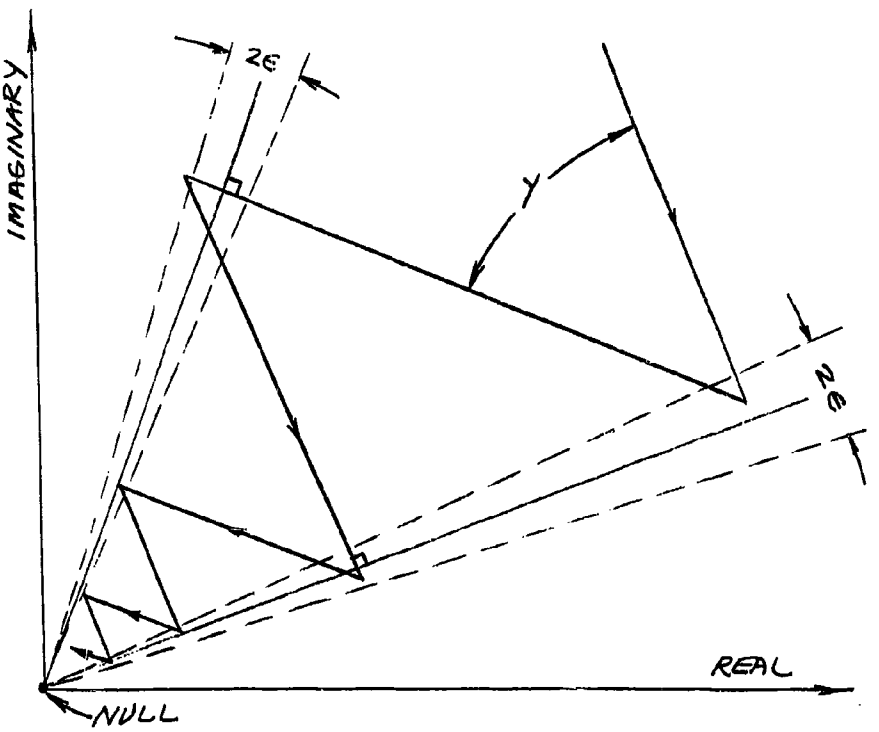

Figure 15.5 . Bridge Balance Convergence

If the bridge output is reduced on the average by a factor k, called the "convergence coefficient," with each adjustment, it may be shown that

$$k^2 = \cos^2\gamma + \sin^2\gamma \cdot \tan^2\epsilon ,$$

where rms values are assumed. In practice the angle ϵ is about 10°. The convergence is rapid and convenient if k is less than about 0.5, in which case the angle γ satisfies, approximately, the condition (for $\tan^2\epsilon = .03$)

$$60^\circ < \gamma < 90^\circ .$$

It remains to find out how to choose the adjustable elements so that the above condition holds. Hague (15) shows that if

$$D = z_1 z_3 - z_2 z_4 ,$$

where the impedances z_1, z_2, z_3 and z_4 are those of the arms of the wheatstone bridge (D = 0 at balance), if x and y are any two adjustable impedance elements of the bridge which are parts of the above impedances, then

$$\tan \gamma = \frac{Im\left\{\frac{\partial D}{\partial x} \cdot \frac{\partial D^*}{\partial y}\right\}}{Re\left\{\frac{\partial D}{\partial x} \cdot \frac{\partial D^*}{\partial y}\right\}} .$$

For the symmetrical differential bridge illustrated in Figure 16.3 used in the high sensitivity detection equipment in which the reactance of the electrodes is relatively small we have

$$z_3 = z_4 = i\omega L$$

$$z_1 \approx r_1 - i r_1^2 c_1 \omega$$

$$z_2 \approx r_2 - i r_2^2 c_2 \omega ,$$

where L is the inductance in two of the arms of the bridge and the electrode resistances and capacities are r_1, r_2 and c_1, c_2, respectively. Assume r_1 and c_1 are the adjustable elements (or r_2 and c_2, see Figure 16.3) then $x = r_1$ and $y = -1/\omega c_1$ and by the above formula

$$\tan \gamma = \frac{1}{2 r_1 c_1 \omega} .$$

For the bridge network of Figure 16.3

$$r_1 = 27\,\Omega \qquad c_1 = .04\ \text{MFD},$$

thus

$$\tan \gamma = 1.85 \qquad \text{and} \qquad \gamma = 62^\circ ,$$

therefore, the convergence of the bridge should be satisfactory.

Degree of Balance

A convenient measure of how well a bridge is balanced is the ratio of the voltage, ΔV, at the output of the bridge to the voltage, V, at the input. This ratio is called the "balance factor" and designated by B:

$$B = \left(\frac{\Delta V}{V}\right) .$$

The degree to which a bridge can be balanced under quasi-steady state conditions depends on the over all stability of the fixed and variable elements of the bridge. If the bridge is of a symmetrical (e.g. Figure 15.4

type the balance factor, will be inherently superior (i.e. smaller) to that of an asymmetrical or single element type bridge (e.g. Fig. 15.3). The balance factor for a symmetrical bridge of the type shown in Figure 15.4 is expressible in terms of the difference, ΔR, in the resistances of the electrodes as

$$B = \frac{\Delta V}{V} = \frac{1}{4}\left(\frac{\Delta R}{R}\right).$$

It is of interest to quote the results of experience with bridge balance adjustments performed in laboratory experiments: if two electrodes are constructed with care so that they are mechanically similar to tolerances readily attainable in shop work, (e.g. the 30Ω electrodes of Fig. 9.34) a balance factor of the order of 3×10^{-3} is obtained straight away based on the similarity of the electrode construction, that is, their resistances are equal to about 1 %; if balance adjustments are made manually and continuously while the electrodes are immersed in flowing water, the balance factor can be improved about a factor of 100, or $B = 3 \times 10^{-5}$; this state of balance is not stable, however, and if adjustments are made about every 15 minutes the average balance factor is about 3×10^{-4}; if good quality resistors are used as bridge elements instead of electrodes in water, a much higher degree of balance is possible, amounting to about $B = 10^{-7}$ in the best cases, for short periods of time.

Methods of Adjustment

In laboratory experiments it is usually a simple matter to provide sufficient adjustable elements (more than two) in a bridge network so that the convergence to a null is virtually guaranteed, even if the convergence coefficient of one pair of controls is not good. In experiments where one does not have easy access to the bridge network because it is remotely located close to the external sensing electrodes, as for example in some oceanographical experiments, greater case must be exercised in choosing the proper adjustable elements. Several methods of making the two independent adjustments may be mentioned which have applicability to the balance of a bridge by remote means.

The first and most direct means is through the use of small reversible motors that adjust suitable bridge elements. The operator controls these motors by means of electrical wires from the detection equipment through cables to the bridge network and electrode elements. For a fine adjustment, the elements must have high resolution and many turns (e.g. ten turn potentiometer). Two such elements are required. Several other indirect means of balancing depend on the non-linearity of some element of the frequency dependence of the bridge network. If the bridge is slightly non-linear the balance may be refined by adjusting the power to the bridge; if it is frequency dependent the balance can be controlled by varying the frequency of the power source slightly. The above have the advantage that no auxiliary wires other than those necessary to drive the bridge are required. Whether these two adjustments are orthogonal or not must be

determined by experiment. Another method involves the use of a heating element attached to a temperature sensitive component, although this requires an additional wire to supply the adjustable electric power to the heating element.

Phase Detector

When a bridge is adjusted to balance, the residual output signal from the bridge has a phase which bears no known relation to that of the input, i.e., the output signal phase relative to the input phase is randomly distributed (but fixed). As a result, if the output signal is envelope detected it may or may not respond fully to the resistance variations of the electrode as desired. A special arrangement, thus, must be used to accomplish this, which involves the use of a phase detector. The theory of this technique is presented below. The output signal* (complex), Δv, from a bridge circuit to which a signal v is applied is given by the form

$$\frac{\Delta v}{v} = m\left(\frac{\Delta z}{z}\right),$$

where m is the "bridge factor," z is the impedance of the sensing element, and Δz is a small change in the sensing element(s). The variables are, in general, complex. If the bridge is balanced ($\Delta z = 0$), the signal Δv is zero; if not, the signal Δv is finite and may be termed the "unbalance signal." If the applied signal is

$$v = \sqrt{2}\, V e^{i\omega t},$$

where V is the rms value of the applied voltage, and

$$m = M e^{i\beta}$$

and

$$z = Z e^{i\theta}$$

$$\frac{\Delta z}{z} = \frac{\Delta Z}{Z} + i\,\Delta\theta,$$

then the output signal is given by

$$Re\{\Delta v\} = \sqrt{2}\, VM\left\{\cos(\omega t+\beta)\left(\frac{\Delta Z}{Z}\right) + \cos(\omega t+\beta+\pi/2)\,\Delta\theta\right\}.$$

It will be noticed that small changes in the magnitude, $(\Delta Z/Z)$, of the sensing element impedance are 90° out of phase with small changes in the impedance phase angle, $\Delta\theta$. The changes ΔZ are due primarily to variations in volume resistance and the changes $\Delta\theta$ are due to variations in surface reactance. The rms value, ΔV, of the output signal is

*The signal is actually the real part of Δv i.e., Re $\{\Delta v\}$.

$$\frac{\Delta V}{V} = M\left\{\left(\frac{\Delta Z}{Z}\right)^2 + \Delta\theta^2\right\}^{1/2}.$$

The actual method of obtaining this signal requires closer consideration. The modulation of the signal Re $\{\Delta v\}$, caused by variations in Z and θ, is obtained by an envelope detector which is operating essentially as a linear detector. As such, the output of the linear detector closely approximates the signal value ΔV. The detection process is subject to several limitations which are discussed below.

The unbalance signal consists of a steady state component and a varying component caused by the constant and variable parts of the impedance changes ΔZ and $\Delta\theta$. Denote the constant parts of ΔZ and $\Delta\theta$ by ΔZ_o and $\Delta\theta_o$ and the variable components by $\Delta Z'$ and $\Delta\theta'$, then

$$\left(\frac{\Delta Z}{Z}\right) = \left(\frac{\Delta Z_o}{Z}\right) + \left(\frac{\Delta Z'}{Z}\right)$$

and

$$\Delta\theta = \Delta\theta_o + \Delta\theta'$$

A faithful reproduction of the signals $\Delta Z'$ and $\Delta\theta'$ is desired from the detection equipment. The limitations encountered may be seen by expanding the output signal, ΔV, as follows:

$$\frac{1}{M}\left(\frac{\Delta V}{V}\right) = \left\{\left(\frac{\Delta Z_o}{Z}\right)^2 + \Delta\theta_o^2 + 2\left(\frac{\Delta Z_o}{Z}\right)\left(\frac{\Delta Z'}{Z}\right) + 2\,\Delta\theta_o\,\Delta\theta' + \left(\frac{\Delta Z'}{Z}\right)^2 + (\Delta\theta')^2\right\}^{1/2}.$$

Unless the variations are small compared with the constant values, nonlinear distortion and harmonic distortion of the signals $\Delta Z'$ and $\Delta\theta'$ will occur. If these variations are small (i.e. the bridge is not critically balanced in the steady state) then the above linear detector output signal is approximated by

$$\frac{1}{M}\left(\frac{\Delta V}{V}\right) = \left(\frac{\Delta Z_o}{\epsilon_o Z}\right)\left(\frac{\Delta Z'}{Z}\right) + \left(\frac{\Delta\theta_o}{\epsilon_o}\right)\Delta\theta' + \epsilon_o$$

where

$$\epsilon_o = \left[\left(\frac{\Delta Z_o}{Z}\right)^2 + \Delta\theta_o^2\right]^{1/2} = \frac{1}{M}\left(\frac{\Delta V_o}{V}\right).$$

The linear detector is followed by a filter which rejects the dc and slowly varying components. The resulting signal is

$$\frac{1}{M}\left(\frac{\Delta V'}{V}\right) = \left(\frac{\Delta Z'}{Z}\right)\left(\frac{\Delta Z}{\epsilon_o Z}\right) + \Delta\theta'\left(\frac{\Delta\theta_o}{\epsilon_o}\right)$$

where

$$\Delta V = \Delta V_0 + \Delta V'.$$

The output signal is, thus, a linear combination of the desired signals. The last, and possibly most important, limitation is that for a given steady state unbalance, ϵ_0, the coefficients

$$-1 \leq \left(\frac{\Delta Z_0}{\epsilon_0 Z}\right) \leq 1 \quad \text{and} \quad -1 \leq \left(\frac{\Delta\theta_0}{\epsilon_0}\right) \leq 1,$$

are, in practice, completely unknown and uncontrollable. Since the variations $\Delta Z'$ are generally considerably larger than $\Delta\theta'$ variations, the output signal can be greatly altered by slight variations in the steady state balance conditions (for a given ϵ_0). Furthermore, it is desirable to make independent measurements of the $\Delta Z'$ and $\Delta\theta'$ variations by some means.

Because of the above limitations of non-linear distortion, harmonic distortion, dependence of the output signal on the details of the bridge balance and the mixing of the impedance magnitude and phase variations, it is not advisable to make a direct linear detection of the bridge output signal. These problems are avoided by a suitable method of phase detection.

Suppose a signal of known amplitude (rms), A, and phase, ϕ, is added to the bridge output signal:

$$\sqrt{2}\,A\cos(\omega t+\phi) + \sqrt{2}\,VM\left\{\left(\frac{\Delta Z}{2}\right)\cos(\omega t+\beta) + \Delta\theta\cos(\omega t+\beta+\pi/2)\right\}$$

and this signal is applied, as above, to the linear detector. In order to avoid non-linear distortion and harmonic distortion, assume that A is much greater than the signal variations. In this case the rms value (averaged over one cycle of the carrier frequency ω) of the signal from the filter which follows the linear detector is

$$\Delta V' = \left(\frac{\Delta Z'}{2}\right) VM\cos(\beta-\phi) + \Delta\theta'\,VM\cos\left(\beta-\phi+\frac{\pi}{2}\right).$$

Since the phase angles β and ϕ are now constant and controllable, the independent variations $\Delta Z'$ and $\Delta\theta'$ may be measured by adjusting the relative phase angle $(\beta-\phi)$ between 0° and 90°, respectively. Thus, the variations of surface impedance ($\Delta\theta'$) may be measured independently of the variations $\Delta Z'$ due primarily to volume resistance variations. Such an arrangement is used in the detection equipment as shown in Figure 16.10.

A measurement of the correlation between $\Delta Z'$ and $\Delta\Theta'$ variations may be made by measuring the rms value of $\Delta V'$ for various relative phase angles $(\beta - \phi)$.

15.4 Low Noise Techniques

Internal noise sets the limits of detectability of the temperature, salinity and velocity sensors in certain experiments, for example, in the ocean. For this reason measures should be taken to reduce internal noise to as low a level as possible. Techniques for noise reduction are now considered.

Amplifier Noise

The output signal from the bridge must be amplified to a suitable level for its proper measurement. As shown in Section 15.2 , the detector input impedance should be a large pure reactance. A vacuum tube amplifier largely fills this requirement and will be used as the basic preamplifier unit. Optimization of detectability is a requirement on the noise figure rather than a requirement on gain. The noise figure, F, is defined as the ratio of signal-to-noise ratios in the input and output circuits:

$$F = \frac{\lambda\,(\text{INPUT})}{\lambda\,(\text{OUTPUT})} \geq 1$$

where λ denotes signal-to-noise ratio. When a number of successive stages are involved with noise figures F_1, F_2, F_3 ..., and power gains G_1, G_2, G_3 ..., then the composite noise figure is given by a formula due to Friis (16)

$$F = F_1 + \frac{F_2 - 1}{G_1} + \frac{F_3 - 1}{G_2} + \cdots$$

When all stages are identical with the first

$$F = \frac{F_1 - \frac{1}{G_1}}{1 - \frac{1}{G_1}} \approx F_1$$

if $G_1 \gg 1$.

The simplest and most effective vacuum tube amplifier at moderately high frequencies is the grounded-cathode triode. This arrangement has the advantages of the highest available power gain (hence maximum possible reduction of second stage noise) and a good noise figure (17). The disadvantage of instability (oscillation) at high gain due to interelectrode capacity may be neutralized by appropriately tuned inductances when the

required bandwidth is sufficiently narrow. The disadvantage of shunting the signal and resultant loss of gain is not important at frequencies of the order of 40 kc. If a wide bandwidth is required, other types of amplifier are more suitable e.g., the double triode cascade amplifier. At moderate frequencies where parasitic capacitances can be neglected, the noise figure of the grounded cathode triode amplifier is (17)

$$F = 1 + \frac{2.5}{g_m R_1} ,$$

where g_m is the transconductance of the triode, R_1, is the effective internal resistance of the signal source at the triode input, and the equivalent noise resistance (due primarily to the shot effect from random emission of electrons from the cathode) is given approximately by (18)

$$R_{eq} = \frac{2.5}{g_m} .$$

A good noise figure may, therefore, be obtained with a triode of large transconductance (and may be further improved by paralleling tubes).

Input Transformer

The degradation in the noise figure of a detection system due to the equivalent noise of the input amplifier tube is reduced by having the signal which is being detected generated in an impedance which is large in comparison with the noise resistance of the amplifier. If the impedance in which the signal is generated is fixed by other considerations, the improvement can be achieved by a transformer which effectively changes the signal impedance level. Consider the idealized input circuit of Figure 15.6 where a signal ΔV is generated in a resistance R_1, and passes through

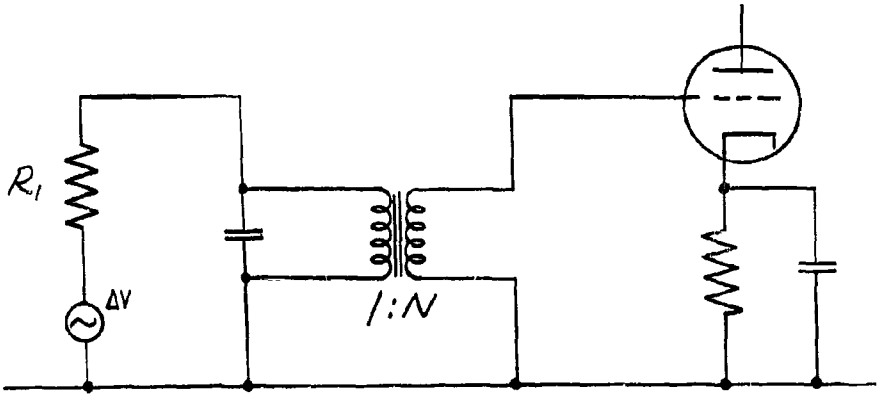

Figure 15.6 . Input Transformer

a transformer of turns ratio N to the grid of the input tube of the amplifier. We assume the inductance of the transformer is tuned out by the capacity shown in the primary over the bandwidth of the signal centered on the carrier frequency; also that the quality of the transformer is high (high Q) so that the input impedance to the transformer is much larger than that of the source impedance R_1. These assumptions are not always valid for very high carrier frequencies (above radio frequencies) but are valid to a high degree in the present detection equipment at 40 kc. The requirement of a good noise figure is that the impedance of the transformer as viewed from the grid of the tube is very much higher than the effective noise resistance of the amplifier tube, that is

$$N^2 R_1 = M \frac{2.5}{g_m}$$

where M is a number much greater than unity. This condition is better achieved by a higher turns ratio; however, for a very high turns ratio the quality of the transformer suffers. The improvement in noise figure for a turns ratio greater than that corresponding to M = 10 is slight, although the signal ΔV does experience a higher gain (equal to N). For the case at hand we have R_1 = 15 ohms, g_m = 9,300 micromhos, N = 30 and M = 50. The corresponding noise figure of this input stage is only 0.1 db. The voltage gain of the input transformer is 30.

Linear Detector Noise

The very slight amplitude modulation on the steady state unbalance carrier wave from the bridge output contains the information concerning the minute variations of the electrode impedance. This low frequency modulation is picked off the carrier wave by a linear detector and further amplified. The linear detector consists of a diode which is a source of ordinary thermal noise at higher frequencies but at lower frequencies an additional noise signal is present, called "excess noise." The noise power density of excess noise is roughly inversely proportional to the frequency (19,20). This additional source of noise can be reduced by proper selection of diodes and operating conditions, and by greatly amplifying the carrier wave plus modulation before envelope detection. A good diode is generally one which has a large contact area, i.e., a junction diode rather than a point contact diode. Operating a number of these diodes in parallel is also helpful in reducing diode excess noise. The diode excess noise power varies roughly as the square of the average diode current, therefore the average rectified diode current should be as small as possible. If this rectified current is zero, the excess noise is zero. If it is possible to amplify the carrier wave plus modulation considerably, before envelope detection, the excess noise of the diode will be relatively small compared with the desired signal and the fundamental thermal noise of the input stages.

This latter method places constraints on the steady state unbalance signal of the bridge network, the peak voltage on the linear detector and

the gain of the preamplifier stages. The conditions imposed on the detection equipment apply at the low end of the band of frequencies of interest in the amplitude modulation signal where the excess noise is largest. The noise ratio due to excess noise may be as large as 40 db at an average current or 1 ma.

Source Noise

Amplitude modulation of the signal source which drives the bridge appears at the output of the bridge and is indistinguishable from the desired modulation if they occur over the same band of frequencies. This source noise is greatly reduced if the bridge can be balanced to a high degree; it is also reduced, of course, by having the source as free as possible of amplitude modulation noise. The requirement imposed on the degree of balance of the bridge and the source noise, in order that it not be a problem, is now calculated under the assumption that the source noise should be equal to the Johnson noise at the output of the optimum differential bridge illustrated in Figure 15.4 . The mean square Johnson noise, $(v_n)_{rms}$, at the bridge output is

$$(v_n)^2_{rms} = 4kT\left(\frac{R}{2}\right)\Delta f \ ,$$

where R is the electrode resistance and Δf is the bandwidth of the modulation signals which one is attempting to detect. This assumes a detector of high input impedance. Let the rms noise modulation, over the band of frequencies of interest, on the source signal, ΔV_n, be a small fraction, ϵ , of the rms voltage, V, applied to the bridge

$$\Delta V_n = \epsilon V \ .$$

The rms noise output voltage, $\delta\Delta V$, from the bridge is

$$\delta\Delta V = \Delta V_n \frac{1}{4}\left(\frac{\Delta R}{R}\right)$$

where ΔR is the steady state difference in the two electrode resistances of the differential bridge and is a measure of the degree of balance of the bridge. We require that the noise at the bridge output due to source noise be so small that

$$\delta\Delta V = (v_n)_{rms} \ .$$

Combining the above relations we find

$$4kT\left(\frac{R}{2}\right)\Delta f = \epsilon^2 V^2 \frac{1}{16}\left(\frac{\Delta R}{R}\right)^2 ,$$

or

$$\epsilon\left(\frac{\Delta R}{R}\right) = 2\sqrt{2}\left(\frac{kT\Delta f}{P}\right)^{1/2}$$

where $P = (V^2/4R)$ is the electrical power dissipated in one electrode. As discussed in Section 15.3, it is reasonable to expect, in practice, a bridge balance (with occasional manual adjustment) of the order of

$$\left(\frac{\Delta R}{R}\right) \approx 10^{-3} .$$

For an electrode power of 100 mw (P = 0.1 watt), and a bandwidth of Δf = 100 cps, this corresponds to a source noise level of

$$\epsilon \approx 6 \times 10^{-6}$$

This is a fairly low level of source noise. Improvements in the amount of source noise can be obtained by regulation as discussed in Section 15.5. Our original requirement in the above calculation was that the noise associated with the source be equal to Johnson noise; in detection systems with very good noise figures (1 db) this requirement should be somewhat more strict.

Other Noise

A very distrubing source of signals is hum associated with the available 60 cps power and its first several harmonics. A large step towards eliminating this problem is to use dc on the filaments. If transformers are used in low signal level circuits they should be wound to cancel ac pick-up and should be adequately shielded from ac fields. Ground loops should be avoided by using a single ground connection and by small resistors approximately placed in the input networks. The contribution of hum is also reduced directly by the use of feedback in the input amplifiers. As a last resort, a hum compensation network can be constructed with variable phase and amplitude to cancel out the residual hum due to power frequencies (although this is usually quite difficult because the first several harmonics must be adjusted to cancellation independently). Notch filters at 60, 120, and 180 cps can also be used. Problems with power frequency hum can sometimes be reduced by the use of 400 cps bulk power, particularly if the signal modulation frequencies of interest cover a bandwidth less than 400 cps.

It is very difficult to construct a detection system of very high sensitivity in the audio band which is not subject to microphonic problems. In spite of the fact that the detection equipment may be microphonic, this source of noise can be largely eliminated by proper shock mounting of sensitive components and by locating or mounting the overall detection electronics in a vibration free environment.

The use of large negative feedback in the amplifier stages is effective in reducing noise due to gain variations associated with component instability, hum, and spurious signal injection caused by variations in the temperature of components in an irregular air cooling stream.

15.5 Advanced Systems

The detection equipment described in Section 16. is capable of very high sensitivity with a relatively narrow bandwidth. Modifications of this equipment to make the operation more convienent: less subject to certain sources of noise; capable of a wider frequency band; and subject to different modes of operation, are more or less direct improvements which would constitute the next stages of development of the equipment. Because of limitations of time the refinements have not been attempted at this time, but will be described briefly below.

Heterodyne Detection System

Detection equipment operating at high frequencies in the radio frequency range or higher, is called for as a possible solution of some problems in the detection technique (e.g. polarization impedance problems) or as a means to make specific measurements of salinity (Sec. 4.3). In such a situation it is not always convenient or even desirable to amplify the bridge output signal directly at the carrier frequency before linear detection. The procedure followed is to change the carrier frequency by a mixing process to a lower frequency (the heterodyne process) for amplification. The intermediate frequency for this amplification is usually of the order of 1 mc (e.g. 455 kc). Mixers for changing the carrier frequency can usually be obtained with a noise figure which does not greatly reduce the sensitivity of the measurements. After amplification at the intermediate frequency, the modulation signal is detected in the usual way. The development of a heterodyne system was not necessary in the present equipment because operation at very high power from the signal source, which calls for high operating frequency, was not necessary at the low operating speeds used in the water tub experiments in the laboratory (Sec. 17.3).

Automatic Source Regulator

If the balance of the bridge is imperfect for one reason or another, the amplitude modulation noise of the source tends to mask the desired signals. Signal sources of good design which have well regulated power supplies and include measures to reduce the effects of hum modulation, have a relatively low level of noise about the carrier frequency of the source (22). Noise of this type can be reduced by a regulating system on the output of the source oscillator which is so designed to insure the reduction of amplitude modulation noise to a low level. Such a system involves a linear detector on the source output followed by high amplifi-

cation to detect the amplitude modulation noise; and then a feedback system using the detected signal as input, to automatically regulate the noise modulation. A feedback system of this type is not easily constructed if it is to operate effectively; no estimate of the amount of improvement of such a system can be reliably given now without experience with it in actual operation.

Automatic Balance Regulator

A high degree of steady state bridge balance has a number of advantages in a practical detection system. Because of inherent spurious instability in electrode systems of identical construction as used in a differential detection system, the degree of bridge balance cannot be maintained better than a certain value; a balance factor of the order of 3×10^{-4} is a practical minimum. A steady state balance to a much higher degree is possible if an automatic fast acting system is used which regulates the bridge to zero average output. The term steady state refers to fluctuations at frequencies from dc to the lowest frequency of interest in the detector system (e.g. 1 cps). The automatic balancing regulator should not work to higher frequencies otherwise it would regulate out the desired signals. Such an automatic system requires two separate and independent channels of regulation, one to regulate amplitude and the other to regulate phase. This is due to the fact, in ac bridges, that it requires two separated adjustments to bring the bridge to balance. A feedback system of this type is complicated and would require considerable development for a practical system, particularly because of its tendency to instability caused by large transient signals. An extension of this balance regulator system is to increase its bandwidth to cover the entire band of frequencies, even those over which the signal is to occur, so that the bridge always has zero output. The signal is obtained, not from the bridge output but, by appropriately filtering the regulating voltages which are replicas of the variations in electrode impedance. Such a technique is similar in some respects to that used in hot-wire anemometers in the constant-temperature-mode of operation.

Wide Band System

The detection equipment of the present Report has been designed for a relatively narrow bandwidth (about 100 cps) but this bandwidth is sufficiently large to cope with the fluctuations measured in laboratory tests and those of interest in many oceanographic measurements. If measurements of very fine microstructure at high speeds are desired, the bandwidth must be much wider. For example, 50 kc bandwidth is required for 0.1 mm structure at 30 knots. In a narrow band system the problem associated with instability in bridge balance is at its worst because it happens at frequencies not far removed from the band of interest. In a wide band system the problems of balance instability can be almost completely eliminated if it is not necessary, also, to measure slowly varying components. This is

accomplished by having a sharp notch filter on the output of the bridge which rejects the carrier and closely neighboring frequencies and passes frequencies well removed from the carrier. This has the consequence that steady state unbalance signals from the bridge network do not reach the input amplifier of the detection system. Consequently, very high gain before linear detection can be used since the amplified wave consists only of the desired signal with no carrier. The practical limitation to this system is the notch filter which sets a lower limit to the signal modulation frequencies detected. In the present narrow band equipment it is not possible because a filter of very high attenuation at the center frequency (40 kc) and also very narrow bandwidth (~1 cps) is not possible. For special applications the wide band system with the notch filter would be quite useful and probably simpler than the present detection equipment. No attempt has been made to develop the methods and techniques of such a wide band system.

Constant Resistance Operation

The technique of constant-temperature-operation, familiar in hot-wire anemometer instrumentation, can be applied directly, without modification, to the present technique for measuring water velocities. Fundamentally, this involves a feedback circuit which regulates the power dissipated in the water so that the electrode temperature, and resistance, is held constant. This system is more complicated than the passive arrangements such as constant-current or constant-power operation. Considerable development work on this mode of operation has been carried out in connection with the hot-wire anemometer and this experience may be used in application to the electrode systems of this Report (23,24).

Impulse Noise Limiter

The passage of localized impurities in the water through the electrode volume, such as bubbles, bits of matter and plankton, causes very large and sharp pulses in the detection system. Unless one is specifically interested in detecting these impurities, they present a troublesome problem to the detection system when set for operation at very high sensitivity. The problem arises in the difficulty for practical amplifying systems to recuperate back to normal operating conditions after a very large transient signal. This is to say nothing of the possible resulting impact damage to paper recording devices and disturbingly loud popping sound produced in audio speaker system for monitoring the detection sounds. This problem can be met by an impulse noise limiting device which functions by not allowing very large transient signals, which occur very rapidly (pulses), from passing through the overall detection equipment (21). Such a device is used in amplitude modulation receivers. This technique is only possible in a situation where

the desired signal does not itself experience changes over a very wide dynamic range in time comparable with the transit time through the sensing volume of the electrode.

16. DETECTION EQUIPMENT

Electronic equipment is described in this Section which embodies the principles and techniques analyzed in the preceding Sections of this Report. This instrumentation distinguishes itself by its ability to detect extremely small changes in the properties of flowing water.

16.1 General Description

Instrumentation for measuring temperature, salinity and velocity fluctuations in sea water by means of electrolytic conductivity is shown in Figure 16.1a and 16.1b. This detection equipment is dual purpose in the sense that the velocity fluctuations and conductivity fluctuations (which are a measure of the temperature and/or salinity fluctuations) can be measured independently by a selection of the operating power level. The sensing elements consist of two identical eye-type electrodes suitably mounted for differential microstructure measurements. The constant-power mode of operation (CPO) is used when detecting velocity fluctuations. In the arrangement for detecting conductivity fluctuations (C-meter) no attempt has been made to separate and identify the contributions due to temperature and salinity. Although, as used in the laboratory tests, the conductivity fluctuations are due almost exclusively to temperature variations since the salinity microstructure is removed by continuous mixing.

Design Considerations

The design philosophy of this equipment has been oriented to the utility of the equipment for laboratory research. As a consequence the design is, in almost all respects, straightforward and simple, in order to insure its easy understanding, checkout, repair and, if necessary, modification. All functional units are built as separate and convenient chassis units. Several of the components are commercially available units which have been integrated into the overall detection equipment. No attempt has been made to miniaturize the equipment or to make the equipment portable.

The choice of the carrier frequency is based on a number of factors. The fundamental consideration is that the carrier frequency be at least an order of magnitude larger than the highest modulation frequency to be detected. The carrier wave frequency should be inaudible (greater than 16 kc) because of the disturbing effects of the high pitched carrier signal in the audio system. The constraints of the electrical components with respect to size, quality, availability, stray capacities, simplicity of design, etc. requires that the carrier frequency be not too high or too low; the LF range (30 kc - 300 kc) is a convenient range in this respect. If a sharp bandpass filter, of the order of a few hundred cycles width at the carrier frequency, is required and inductances of moderately high Q (about 100) are used, instead of crystal filters, a carrier frequency of about 40 kc is arrived at. Because of polarization effects (Sec. 9.4) at the electrodes

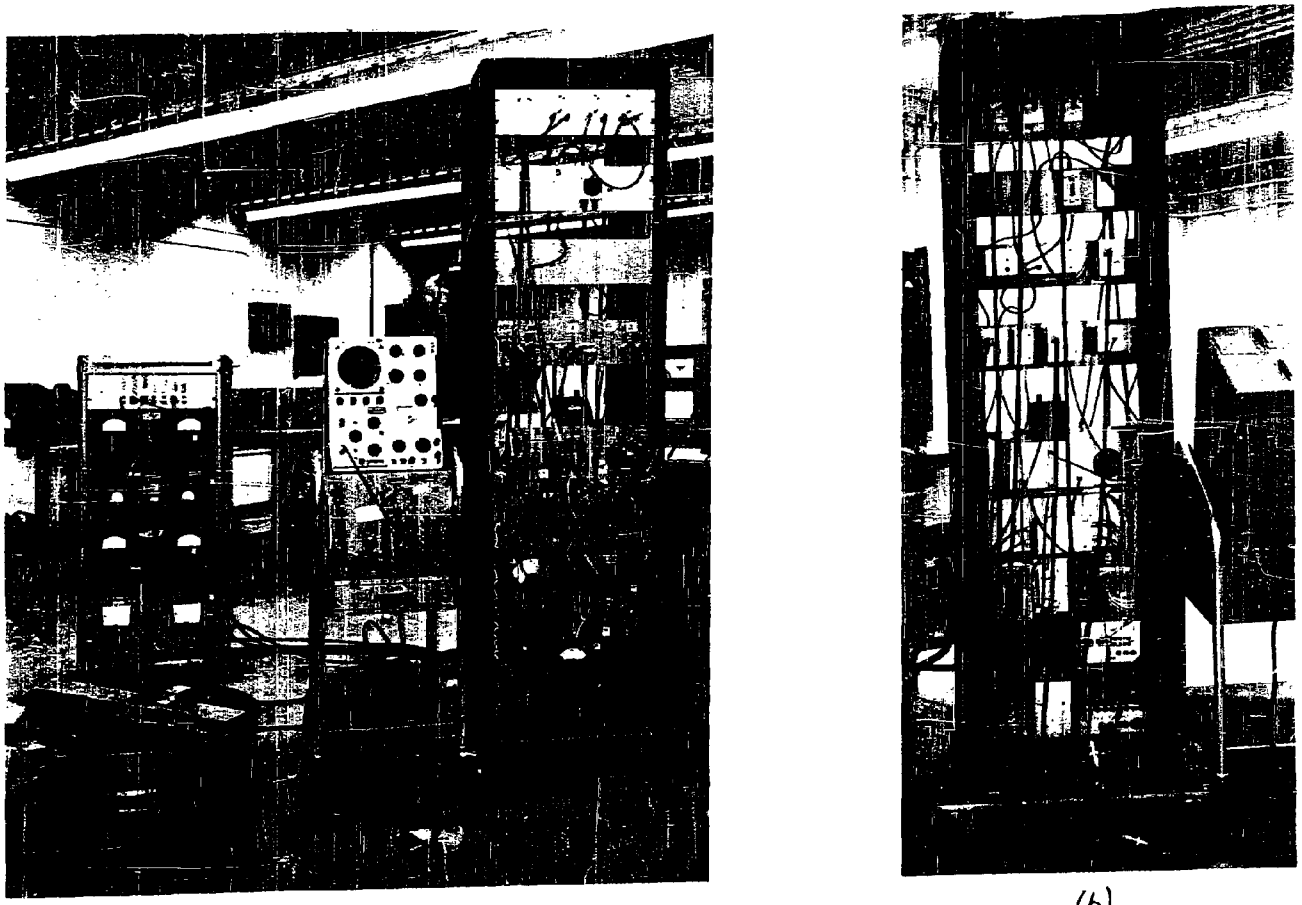

(a) (b)

Figure 16.1. High Sensitivity Detection Equipment

a high operating frequency is called for. A frequency of 40 kc is effective in reducing polarization effects with stainless steel electrodes in sea water (compared with a frequency of 1000 cps which is ordinarily used in electrolytic conductivity measurements). Operation in the radio frequency range is required to completely eliminate electrode polarization effects.

The use of an ordinary radio receiver as a detector of the bridge output has been considered but found unsatisfactory for the present application for the following reasons. The relatively large steady-state output from the bridge saturates an ordinary receiver; the bandwidth before linear detection is too wide; there is no phase detection capability; the output bandwidth does not extend down to 1 cps; the audio system is subject to hum noise; and the linear detector usually does not have the capability of large amplitude input before detection. The modifications of such a receiver would be so extensive that the advantage of its availability would be nullified.

Functional Diagram

The overall functional diagram of the detection equipment is shown in Figure 16.2 ; it consists of the following blocks:

a) Signal source
b) Heater source
c) Bridge network
d) Electrode elements
e) Detection electronics
f) Display units
g) DC power supplies .

These blocks are discussed in detail in Section 16.2 . The equipment functions as follows: The signal source provides the 40 kc power to drive the bridge network and electrodes; the heater source provides the power to the electrodes when velocity measurements are being made; variations in the electrode impedances cause the bridge to unbalance and the bridge network output signal is amplified, detected and filtered in the detection electronics; a suitably large signal consisting of the desired modulation is monitored and analyzed in the display equipment. The dc power supplies provide plate and filament voltages to the most sensitive components of the equipment, viz., the heater source, signal source and detection electronics. The detected signal is sufficiently amplified when it reaches the display equipment so that these units need not be on dc power. The details of each block are indicated by Figure numbers in the overall block diagram of Figure 16.2 .

The basic network of the electronics consists of the symmetrical wheatstone bridge network shown in Figure 16.3 . This is the optimum arrangement for a double sensing element bridge for obtaining the minimum detectable

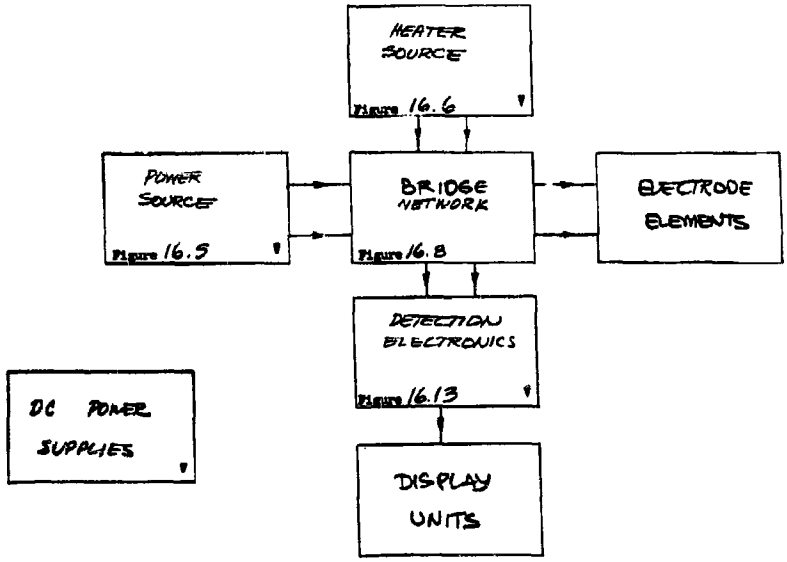

Figure 16.2 . Overall Block Diagram of Detection Equipment

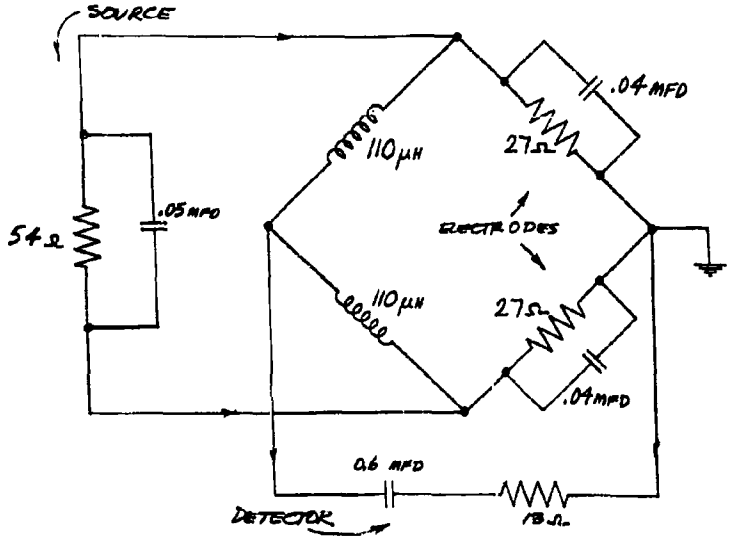

Figure 16.3 . Basic Bridge Circuit Diagram

signal. The capacity in parallel with the source impedance and in series with the detector impedance are for matching purposes (the detector impedance is shown matched to the bridge, however, optimum detectability is obtained if the detector impedance is large). The resistance of the electrodes (27 ohms) is due mainly to the volume conductivity of the sea water; the capacity in parallel with the electrode resistance is due to polarization effects at the electrode surfaces. The other two arms of the symmetrical bridge are equal inductances of reactance equal to the resistance of the electrodes at the operating frequency. The ground on the bridge at the point indicated is required by the constraints of electrode design.

Equipment Design

The typical operating characteristics of the detection equipment are shown in Table 16.1 . The frequency response of the pre-amplifier stages and overall system is shown in Figure 16.4a and 16.4b.

Table 16.1 . Performance Characteristics of Detection Equipment

Carrier Frequency	40 kc
Heater Frequency	3.7 mc
Electrode Impedance	27 ohms
Bandwidth	150 cps
Noise Figure	0.3 db
Overall Gain	160 db
Signal Source	160 mw
Heater Source	15 watts

16.2 Equipment Design

The design details of the electronics of the detection equipment are covered in this Section.

Signal Source

The bridge of the detection equipment is driven by a signal source operating at 40 kc. The block diagram of this source is shown in Figure 16.5 ; it consists of the following units:

a) 40 kc oscillator

b) Attenuator

c) Bandpass filter.

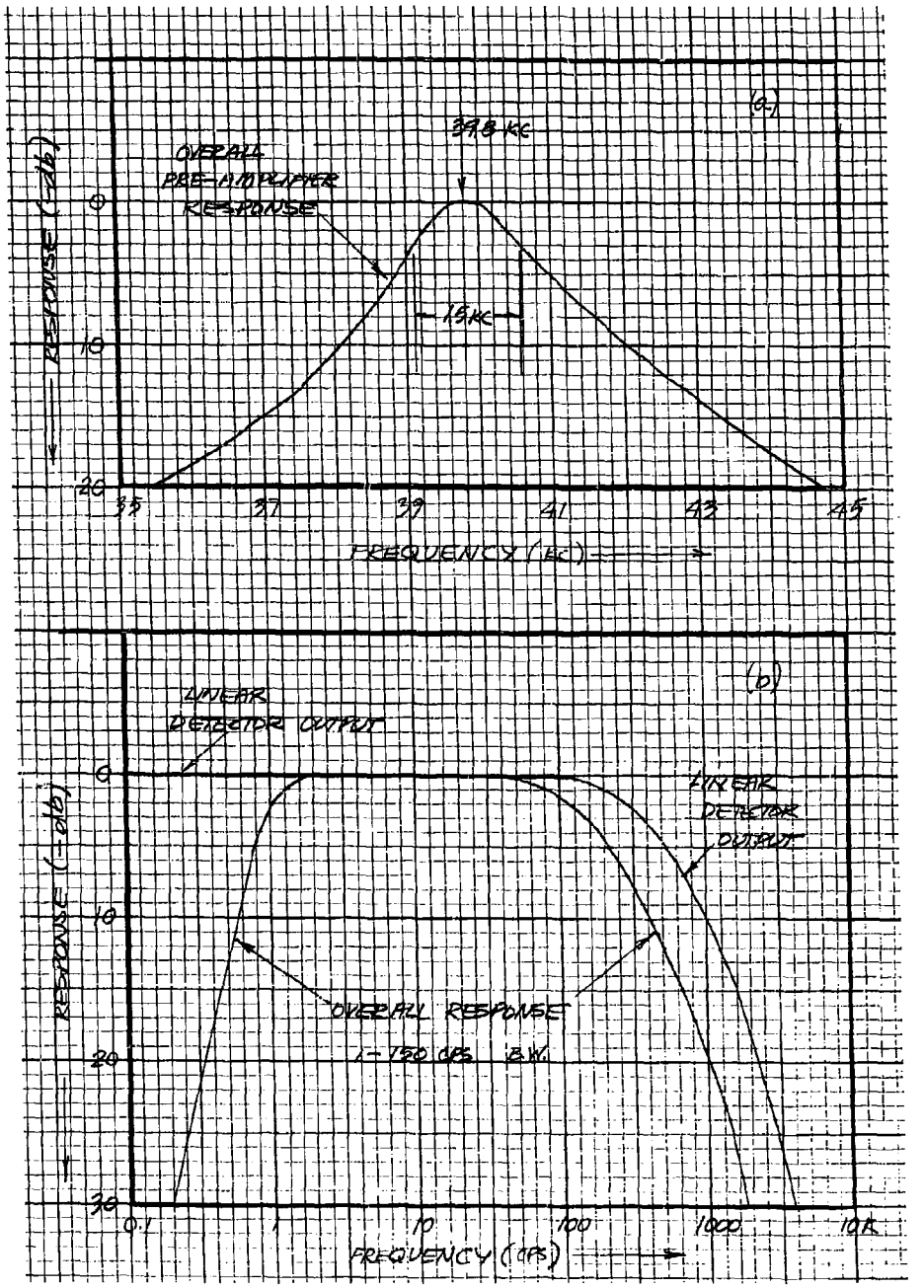

Figure 16.4. Frequency Response

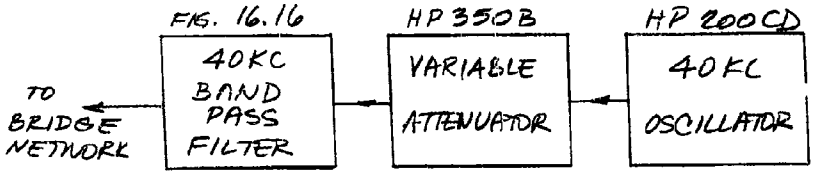

Figure 16.5 . Signal Source Block Diagram

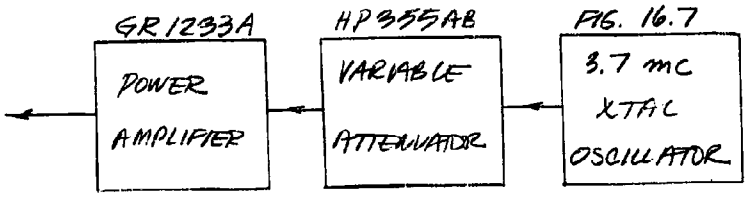

Figure 16.6 . Heater Source Block Diagram

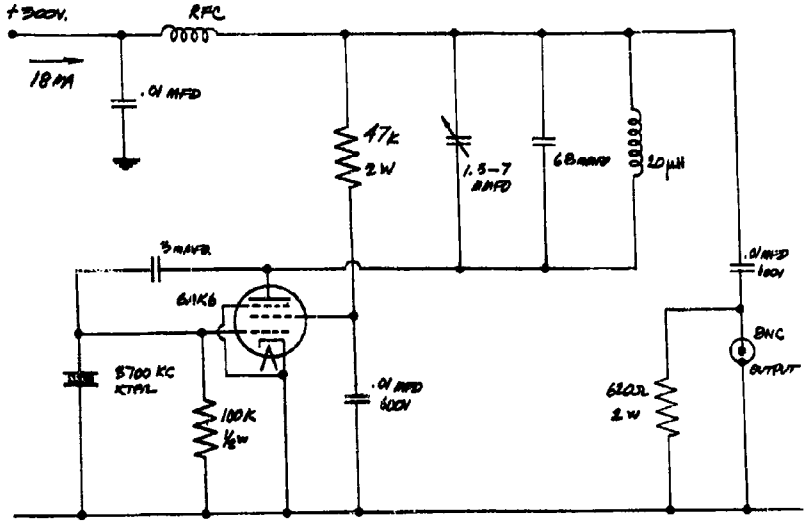

Figure 16.7 . 3.7 mc Crystal Oscillator Schematic

The 40 kc oscillator is a Hewlett-Packard Model 200CD oscillator with 160 mw maximum output into 600 ohms; the attenuator is a Hewlett-Packard Model 350B attenuator of 600 ohm impedance. The 40 kc bandpass filter circuit is shown in Figure 16.16 .

Heater Source

For the detection of velocity fluctuations at the electrode, it is necessary to heat the water flowing through the electrode volume. As discussed in Section 9.4 , this is best done with high frequency power to avoid electrode polarization effects. A frequency much higher than 40 kc is also desirable in order to operate the heating source separately and independent of the signal source without affecting the critical balance conditions of the bridge. The heater source for this purpose operates at 3.7 mc and is capable of about 16 watt output (8 watts per electrode). The block diagram of the heater source is shown in Figure 16.6 ; it consists of the following units

a) Crystal oscillator

b) Variable attenuator

c) Power amplifier.

The variable attenuator is a Hewlett-Packard Model 355B attenuator of 50 ohm impedance. The power amplifier is a General Radio Model 1233A with the output modification described in its manual for operation at the higher than ordinary frequency of 3.7 mc.

a) Crystal Oscillator - The input signal for the power amplifier of the heater source is generated by a stable cyrstal oscillator at 3.7 mc. The crystal oscillator employs the Miller circuit which is equivalent to a tuned-grid-tuned plate arrangement. The schematic for this circuit is shown in Figure 16.7 . Spurious amplitude modulation is avoided by the use of DC filament and plate voltages. The output is 3.1 volts in a 50 ohm load (200 mw).

Bridge Network

The bridge network of the detection equipment consists of the circuits for the adding and distribution of the input signals and output signals. It contains the fixed and adjustable components of the wheatstone bridge, with the exception of the electrodes themselves, and a network for the phase detection of the desired signal. The overall block diagram of the bridge network is shown in Figure 16.8 , and is sub-divided into the following blocks:

a) Balance adjustment unit

b) Variable amplitude and phase unit

c) Input/output unit

d) Coupling unit.

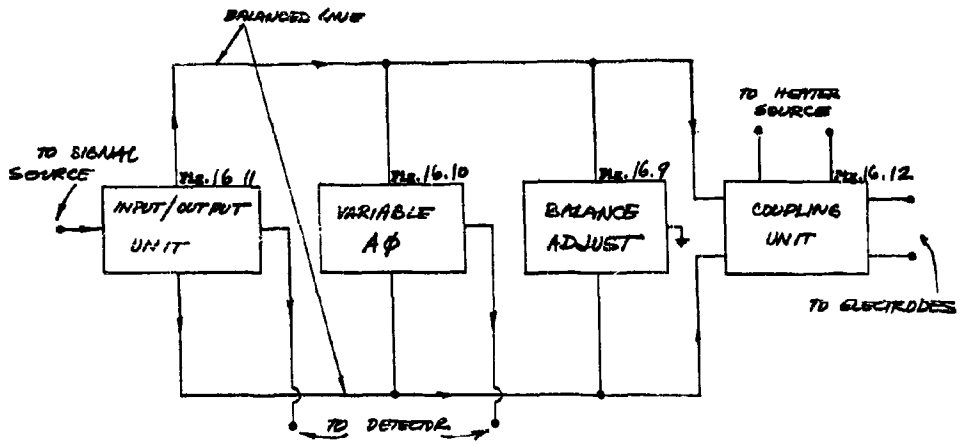

Figure 16.8 . Bridge Network Block Diagram

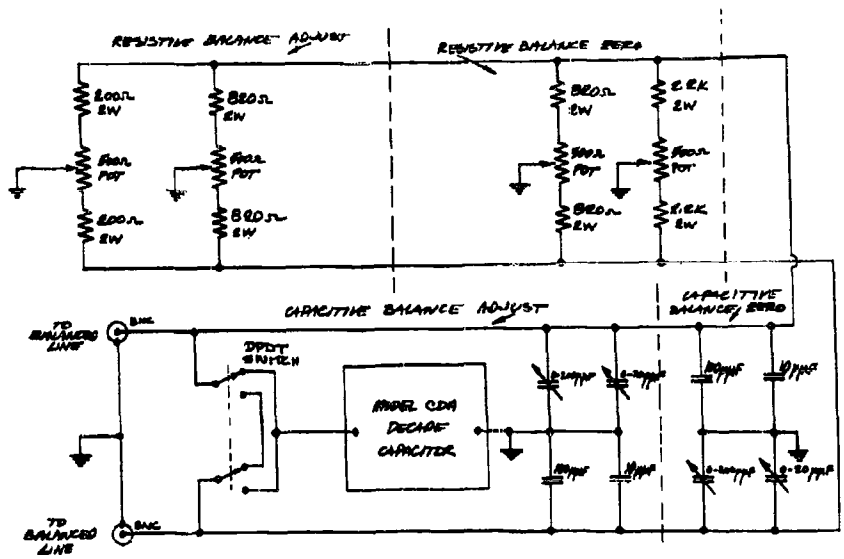

Figure 16.9 . Balance Adjustment Unit Schematic

These are discussed in detail below.

a) Balance Adjustment Unit - The wheatstone bridge is initially unbalanced due to tolerances in electrical components and electrode construction. These errors are compensated for to reduce the average output from the bridge by means of the balance adjustment unit shown in Figure 16.9 . This unit consists of coarse and fine adjustments of both the resistive and reactive bridge components. As shown in Section 15.3 , the components have been chosen so that the controls approach those of the ideal orthogonal controls in order to facilitate the convergence to balance.

b) Variable Aϕ Unit - The amplitude modulation of the small steady-state carrier wave from the bridge is detected after amplification by an envelope detector. As shown in Section 15.3 , the phase angle of the impedance fluctuations at the electrode determines how well the fluctuations are detected by the envelope detector. As a matter of fact, if the phase angle is set at one certain value, the impedance fluctuations would not be detected at all! To rectify this situation an elementary phase detection technique has been used. It consists of mixing (adding) a wave of adjustable amplitude (A) and phase (ϕ) to the bridge output wave. Adjustments of the amplitude and phase of this added signal are accomplished by the network shown in Figure 16.10 . This circuit receives its signal from the balanced line, but is decoupled from this line so that adjustments of its components do not unbalance the bridge. The amplitude is adjusted by means of a Hewlett-Packard Model 350B attenuator. The variable phase shifting network covers the range from -45° to $+135^{\circ}$ by means of a continuous knob adjustment which covers the range $\pm 45^{\circ}$ and a switch selected phase shift of either 0° or $+90^{\circ}$. The continuously adjustable phase network is of somewhat novel design and provides for the above stated range of phase shift with an output amplitude which is essentially independent of phase setting (constant output within ± 0.7 db).

c) Input/Output Unit - The signal applied to the wheatstone bridge is coupled to it through a transformer to the balanced line. The output from the bridge is with respect to ground (single ended) and is taken from the midpoint of two identical inductances, of reactance equal to the resistance of the electrodes, which are across the balanced line and constitute the other two symmetrical arms of the bridge besides the electrodes. This network is shown in Figure 16.11 . Also provided in this circuit are the capacitors in parallel with the input and in series with the output to match the source and detector to the resistance of the bridge.

d) Coupling Unit - Two separate signals are applied to the electrodes: a 40 kc wave from the signal generator source and a 3.7 mc wave from the heater source. In order that these two signals are coupled only to the electrode load and not also into each other's output impedance, a special coupling unit is required. This is accomplished by the network shown in Figure 16.12 . Tank circuits are placed in the lines which pass the appropriate signals and stop the others. The tank circuits in the balance line from the signal source pass the 40 kc signal through the inductances but

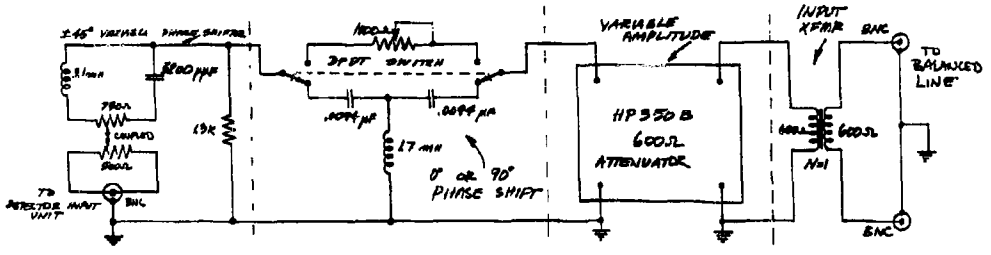

Figure 16.10. Variable Aϕ Unit Schematic

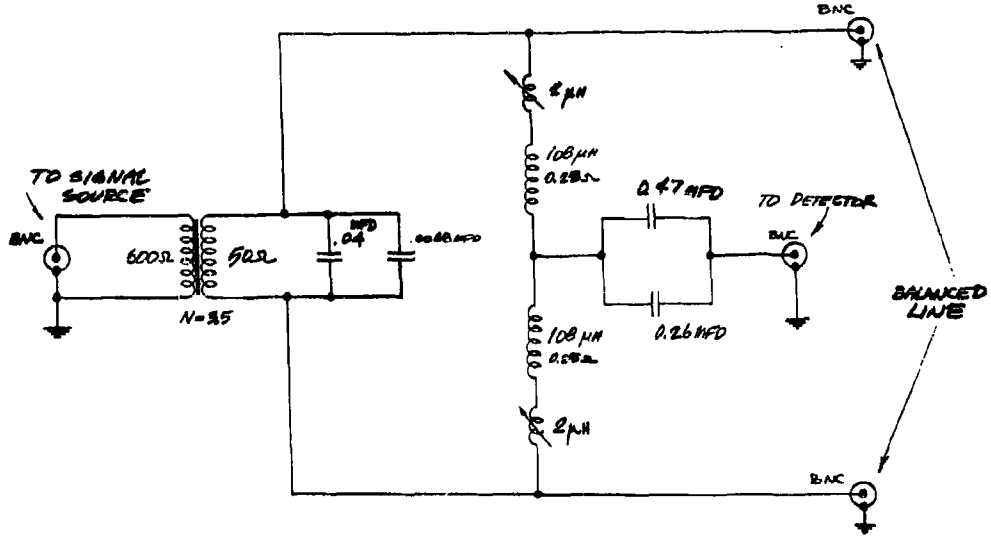

Figure 16.11. Input/Output Unit Schematic

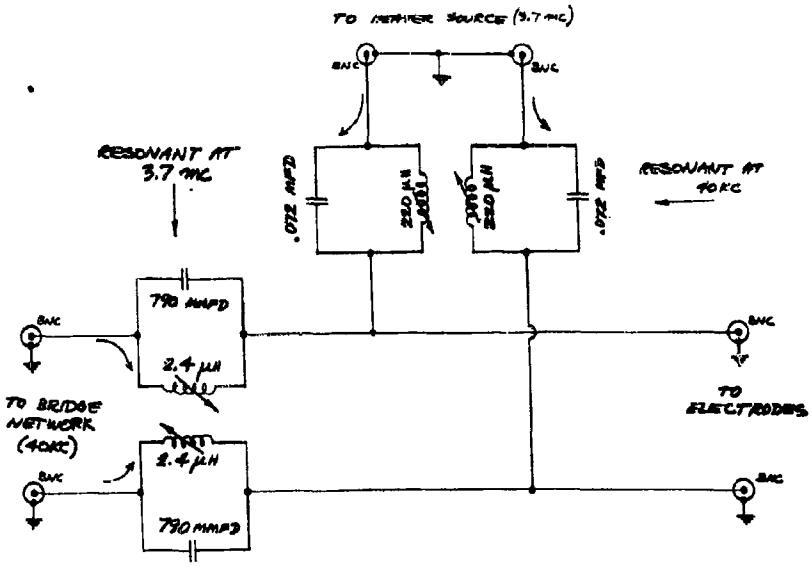

Figure 16.12. Coupling Unit Schematic

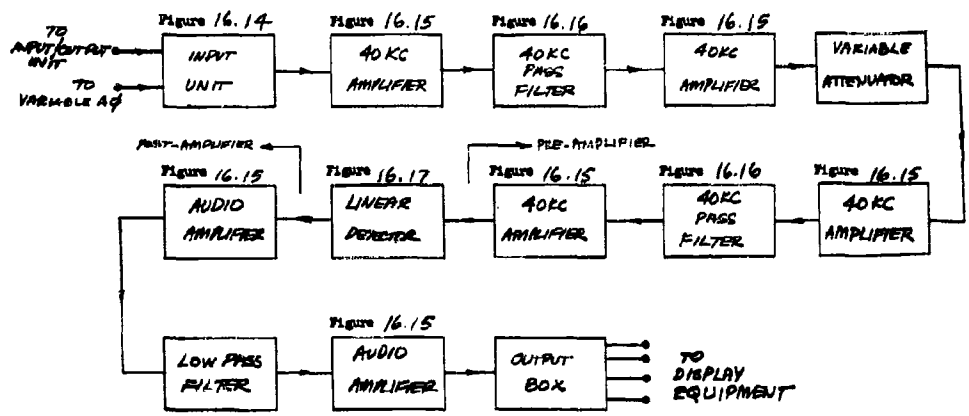

Figure 16.13. Block Diagram of Detection Electronics

stop the heater signal coming from the other direction since they are tuned to 3.7 mc. The tank circuits in the balanced lines from the heater source pass the 3.7 mc power through the capacities but stop the 40 kc signal power coming from the other direction since they are tuned to 40 kc. Since the two signals were separated by almost a factor of 100, it was not necessary to use a more sophisticated balanced bandpass/band-stop filter for each power source. The component values were calculated by requiring the impedance of the units when "passing" to be 1/50 of the electrode resistance and to be resonant at the appropriate frequency. The resulting impedances at resonance are about 50 times that of the electrodes (if $Q > 30$).

Detection Electronics

The function of the detection electronics is to amplify and detect the feeble modulation of the carrier wave and present an adequately large and noiseless signal for input to the monitoring and display instruments. The overall block diagram of the detection electronics is shown in Figure 16.13. The components of this equipment consist of the following:

a) Input unit
b) 40 kc amplifiers
c) 40 kc bandpass filters
d) Variable attenuator
e) Linear detector
f) Audio amplifiers
g) Low pass filter
h) Output box

Basically, the detection electronics serves to transform the impedance level of the signal in the input unit; amplifies and filters the carrier plus modulation in the pre-amplifiers; linearly detects and filters the carrier modulation; further amplifies the low frequency modulation in the post-amplifiers. A number of switching arrangements facilitate all phases of the measurements with the detection electronics.

a) Input Unit - This unit, which is detailed in Figure 16.14 , receives a 40 kc signal from the bridge network output and/or a 40 kc signal from the variable Aϕ unit. The two signals are mixed with a passive adder and transformed from the low 15 ohm impedance level to the relatively high level of 13.5 K to improve the overall noise figure of the detection equipment as discussed in Section 15.4 . The 40 kc signal experiences a gain of 30 in amplitude through the transformer. The high turns ratio of the transformer is made possible by operating the transformer at resonance. The switching arrangement of the input unit allows the independent adjustment and detection of either or both the carrier plus signal and the phase

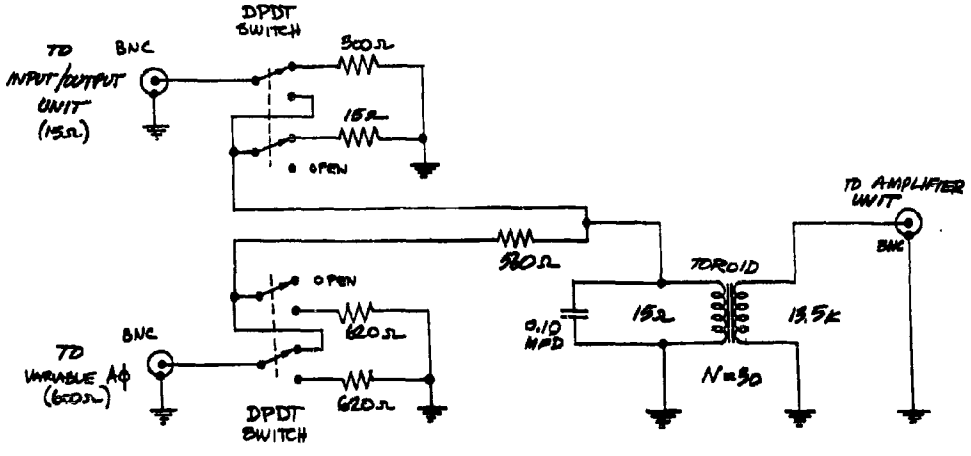

Figure 16.14 . Detector Input Unit Schematic

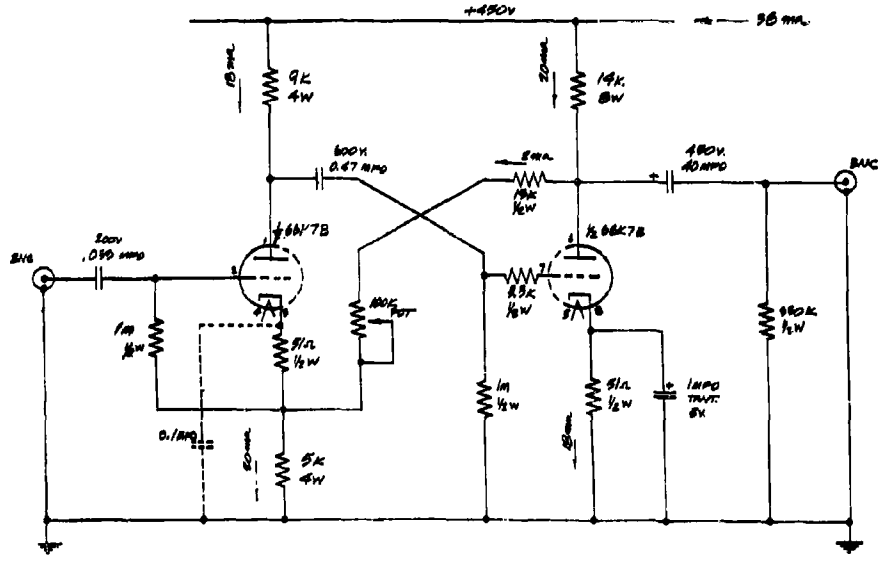

Figure 16.15 . Amplifier Unit Schematic

shifted carrier. The signals are matched for all switching positions.

b) 40 kc Amplifiers - The carrier plus signal modulation is amplified considerably before linear detection by several stages of amplification. The amplifiers for this purpose are operated as individual units. The schematic for these units is shown in Figure 16.15 . The amplifier is designed for low noise operation over a wide frequency range, and consists of an RC coupled amplifier of two stages with negative feedback to reduce distortion and stabilize the gain.

The gain with a 600 ohm load is about 15 db and into a high impedance is about 22 db. A switch to by-pass the amplifier (0 db) is also provided. Approximately 20 db negative feedback is used. The input impedance is of the order of several megohms and the output impedance is about 800 ohms. The frequency response at the -3 db points extends from 3 cps to 1 mc with a 600 ohm load, and from 0.6 cps to 500 kc with a 10 K ohm load. Care was taken in the construction to provide adequate heat sinks for the high power resistors and to protect the other elements from thermal variations due to air currents.

To obtain the lowest noise figure in the first stage of amplification of the detection equipment, it was found necessary to by-pass the feedback network with the 0.1 mfd capacitor which is dotted in Figure 16.15 . With this arrangement the equivalent input noise is 0.12 microvolts for a 1 kc bandwidth. This noise level is about 5 db above the minimum noise expected from the amplifier based on a transconductance of 9,300 micromhos. When the amplifier is used in combination with the input transformer the combined noise figure is about 0.3 db. The amplifier gain in this arrangement with a tuned filter as a load is about 38 db.

c) 40 kc Bandpass Filter - Two of these filters are used as interstage band bandpass filters for the carrier plus modulation between the 40 kc amplifiers. The filters are of the constant-k type with π-section input and output and 600 ohm impedance at the center frequency. The insertion loss is 2.0 db and the 3 db passband is 40 ± 5 kc. Outside the passband, the skirts of the filter characteristic fall off at 18 db per octave. The schematic for this filter is shown in Figure 16.16 .

d) Variable Attenuator - This unit consists simply of a 100 K potentiometer and is used to adjust the signal level to the optimum value for the linear detector.

e) Linear Detector - The signal modulation is removed from the carrier wave by the linear detector and filtering networks shown in Figure 16.17 . The main design consideration in this unit is the provision for the detection of a large amplitude carrier wave. The peak voltage applied to the diode for maximum output of the amplifiers is 36 volts. The filtering networks following the diode have a passband from 0.5 cps (or DC) to 400 cps. The amplitude of the rectified carrier wave is monitored by an external meter.

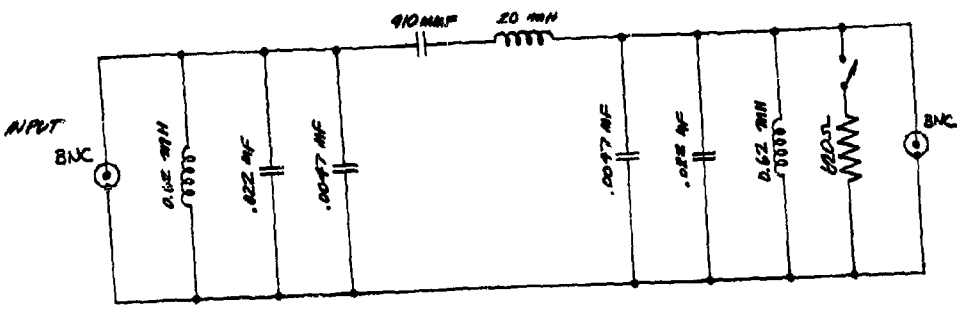

Figure 16.16. 40 kc Bandpass Filter Schematic

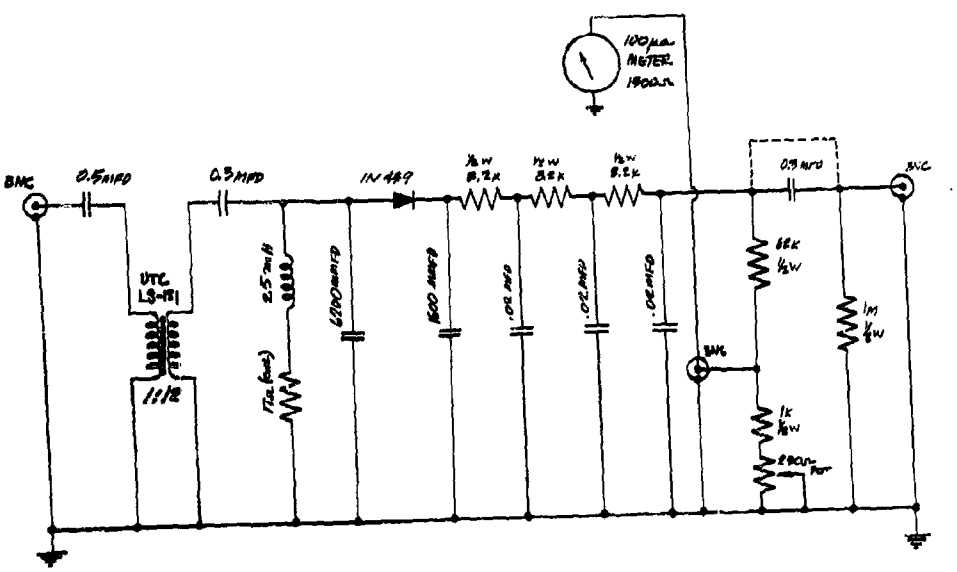

Figure 16.17. Linear Detector Schematic

f) Audio Amplifiers - The signal modulation from the linear detector is further amplified by units which are identical with the 40 kc amplifiers of Figure 16.15 . The load impedance, however, is 10 K ohms instead of 600 ohms. The passband extends from 0.6 cps to 500 kc.

g) Low Pass Filter - This unit consists of a simple RC filter with a time constant suitable for the particular measurements under consideration. The passband used in the present equipment is 150 cps.

h) Output Box - This unit consists simply of four output connectors for the detector signal and a switch for grounding this signal for calibration tests.

Display Equipment

The output signal from the detection equipment is analyzed with the following equipment: voltmeter, paper recorder, speaker system, spectrum analyzer and oscilloscope.

Power Supplies

Direct current power supplies are used to supply plate, bias, and filament power. The supplies are mounted in a separate rack, with a distribution panel, in order to remove all ac power from the detection electronics rack and, consequently, reduce hum levels. Four separate power supplies are required:

a) Lambda Model 50 set at 450 V at 350 ma supplies power to all unit amplifiers, crystal oscillator and HP 200 CD oscillator. A series resistor in the distribution panel lowers the voltage to the HP 200CD oscillator to 190 volts at 90 ma.

b) Lambda Model 50 set at 400 V at 250 ma supplies power to the General Radio Model 1233A RF power amplifier.

c) Lambda Model C-881M set at -300 V at 120 ma supplies bias power to the HP 200CD oscillator and GR 1233A RF power amplifier. Series resistors in the distribution panel lower the voltage to the HP 200CD oscillator to -135 V at 90 ma and to the GR 1233A to -100 V at 30 ma.

d) American Avionics Model 1032A set at 6.3 V at 9.5 amps supplies filament current for all the detection electronics.

The display equipment is operated on ac power since the signal levels are high at the inputs.

17. LABORATORY EXPERIMENTS

Experiments with the probes and associated electronic equipment to measure the temperature, salinity and velocity of water, which have been performed in the laboratory, are described in this Section. This description covers a) the experimental methods for measuring the properties of electrodes, b) water velocity measurements in a special water tunnel capable of laminar and turbulent flow, and c) the measurement of conductivity and velocity structure in a steady-state turbulent medium with high sensitivity detection equipment.

17.1 Electrode Experiments

The apparatus and methods for measuring the characteristics of electrodes in water, the results of which have already been discussed in Sec. 9.7 , are now considered. The experiments have been designed to determine the dependence of the resistive and reactive components of the electrode impedance on frequency, salinity, temperature, and the size, shape and material of the electrodes. Non-linear effects associated with gas evolution and corrosion, and time dependent (aging) effects have also been measured. The special methods for each of these measurements are considered below. The most important of these is the measurement of the electrode impedance under conditions which approximate those of the detection equipment, i.e., under "standard conditions." In most of the work these conditions refer to a temperature of 20 ^{o}C, an NaCl solution of 32.8 ‰ salinity, a frequency of 40 kc, and the eye-type electrode (a/b = .48) of about 30 ohms resistance to which a voltage of about 0.1 volt is applied (3 ma, 0.3 mw). The outside diameter of the standard eye-type electrode is about 0.28 in.

Substitution Bridge

A wheatstone bridge for electrode measurements was assembled to satisfy the requirement for measurements of relatively high precision over a wide variety of experimental conditions. The equipment is of straightforward design and consists of an approximately equal arm resistive bridge network. The substitution method is used as the most reliable method for nullifying bridge defects such as non-linearities, spurious capacities, and unbalance in the input transformer to the bridge. As a back-up provision, a version of Wagner ground arrangement is used to obtain relatively accurate measurements even without the substitution method. This equipment is shown in Figure 17.1a . A commercial unit was not available which covered the range of resistance, reactance, frequency and input power which are of interest in these experiments. General Radio decade resistances and capacities are used as references. A Hewlett-Packard Model 233 oscillator is used as a source to cover the desired amplitude and frequency range. The detector consists of a Hewlett-Packard 450A amplifier

and 400D vacuum tube voltmeter, with either the variable type Kronhite filters, or with fixed bandpass filters at 40 kc for operation under standard conditions. The filters are required to remove the higher harmonics of the carrier frequency in the bridge output in order to obtain a null output. The substitution box for switching between the unknown electrode impedance and the reference impedance is corrected for capacity differences in the cabling in the two switch positions. Measurements to 1 in 10^3 were readily made, and beyond this accuracy, the absolute values of the reference impedances used are in question.

Frequency

In order to investigate the properties of the polarization impedance, which is relatively large for smooth stainless steel electrodes in salt water, it is necessary to cover a very wide frequency range extending from the kilocycle range to the radio frequency range. The measurements from 1 kc to 500 kc were performed with the substitution bridge described above. The range from 0.5 mc to 40 mc was covered with the General Radio RF bridge Model 1606A and a General Radio Model 1330A oscillator as a source. The detector for this range was a Hammarlund SP300 radio receiver. It was found that care must be exercised in the cabling to the electrode for measurements in the radio frequency range. For reliable measurements a special electrode (Fig. 9.36) was constructed which made possible connecting the electrode to the RF bridge with a short low capacity connector. Reliable measurements were made with this arrangement except possibly at the highest frequencies around 50 mc. As a matter of interest, measurements were also made in the region from 50 mc to 400 mc by means of a Hewlett-Packard Model HP830A bridge with an HP608D source, HP417A detector, and HP415B indicator. At these frequencies the polarization impedance of the electrode is negligibly small, however, capacity (and inductance) effects of the electrode volume and lead in wires become measurable.

Temperature

The measurement of the temperature coefficient of electrode resistance and capacity involves some difficulties because of the polarization effects associated with the surface of the electrode. The technique for these measurements involves either the use of the water tub described in Section 17.2 whose temperature can be adjusted from 17 °C to 40 °C, or several beakers of identical solution but at different temperature. If an electrode of high heat capacity is used, the temperature of the electrode proper does not track that of the solution. This has the disadvantage that the surface of the electrode is at a different temperature than that of the bulk solution. As a result, the temperature which affects the surface impedance is different (and unknown) from the measured temperature of the solution. This effect causes erratic measurements of the temperature coefficient. The obvious solution to this problem of allowing time for the temperature of the electrode and solution to stabilize is also complicated by the fact that the polarization impedance is time dependent (aging).

This technique is effective if use is made of electrodes of very low heat capacity and high thermal conductivity. Such an electrode is the parallel wire type shown in Figure 9.39 which has a short thermal time constant. An eye-type electrode made by printed circuit techniques on a material of low thermal conductivity would also be suitable for such measurements.

The measurement of the salinity coefficient of the electrode is not subject to the above difficulties since the electrode has no capacity for salinity. The salinity coefficient is simply measured by varying the concentration of the solution by dilution with distilled water at the same temperature as the original solution.

High-Power

The measurement of electrode impedance at relatively high power is of interest in connection with effects which depend on the electrode current-density and gas evolution. These non-linear effects can be measured by three methods.

The first of these, which is covered in Section 9.7 , is most suitable for small non-linearity effects and is based on the amplitude dependence of bridge balance. This method is not suitable for operation at very high power because of the power consumed by the arms of the bridge other than that being measured.

A second method involves the direct transfer of electrical power from the source to the electrode. A McIntosh MC-30 power amplifier has been used for tests at the highest power levels (30 watts at 40 kc). The impedance is determined by measuring the voltage across the unknown load and across a small resistance in series with this load. If the load has a relatively small reactance, X, and a resistance R, and the small series resistance is r (see Fig. 17.1) the voltage V_1 across the total load is related to the voltage V_2 across the known series resistance by ($r \ll R$, $X \ll R$)

$$R = r\left(\frac{V_1 - V_2}{V_2}\right) \quad .$$

A measurement of V_1 and V_2 gives the (integral) R in terms of the known (small) resistance, r. The phase angle of the unknown load $z = R + iX$ may be measured by means of an oscilloscope. The voltage V_1 is applied to the horizontal plates, V_2 to the vertical plates and the resulting elliptical trace indicates the phase angle $\tan^{-1}(X/R)$ by the usual method. This method is well suited for impedance measurements at high power since essentially all the power generated is dissipated in the unknown load.

Another technique for the observation of gas evolution at high power uses the circuit of Figure 17.1 but the resistance r is paralleled by a

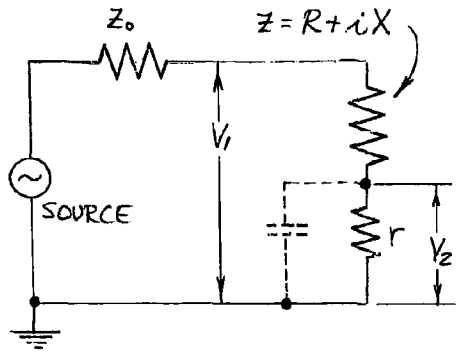

Figure 17.1. Impedance Measurement at High Power

large condenser (dotted) which shunts the high frequency signal to ground. The voltage V_2 is then measured with a dc voltmeter and indicates the rectifier action of the electrode impedance due to its non-linearity. The resistance r need not be small in comparison with R. This technique has been used for qualitative measurements of the inception of gas evolution and proves to be more sensitive for this purpose than the visual method (Sec. 9.7). The method has not been developed to the point where reliable quantitative measurements can be made because of some erratic effects in the variation of V_2 with applied voltage V_1.

Size and Shape

The volume resistance and surface impedance of the eye-type electrode is, in spite of its apparent geometrical simplicity, difficult to calculate on the basis of potential theory. These quantities must be determined by direct measurement. The dependence on size was measured on two eye-type electrodes of (inner/outer) diameter ratio of 0.478 and a factor of three difference in size (resistance of about 10 ohms and 30 ohms in sea water). The shape dependence was determined using the equipment of Figure 17.2 . This arrangement provided for ten insertable eye-type electrodes of various inner diameters and constant outer diameter. The electrode material is stainless steel. The size dependence was also crudely measured to very small size by the use of the hypodermic needle probes (Sec. 9.8) which are roughly similar to the eye-type configuration but about ten times smaller than the 30 ohm eye-type electrode discussed above.

Conducting Solutions

Electrode measurements have almost exclusively been performed in NaCl solutions and tap water. The standard NaCl solution is that one which has the same conductivity as 35 ‰ sea water at 20 °C, viz., a 32.8 ‰ salinity solution (Sec. 7.2). The salt solutions were made up using distilled water and were based on weight rather than volume proportions. For measurements which were not critically dependent on salinity, tap water was mixed with a calculated amount of salt to make up, approximately, the desired salinity. Such a solution was used in the recirculating water tub for water tunnel and other measurements. The salinity of such a solution can be determined after mixing by a hydrometer density measurement.

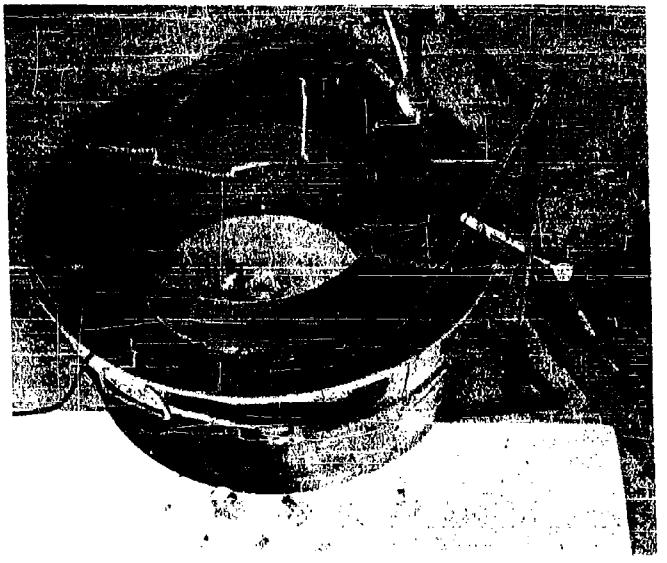

Figure 17.2 Electrode Diameter Ratio Experiment

For this purpose a U.S. C.and G.S. salinity hydrometer was used, with appropriate corrections, for solutions approximating 35 ‰ sea water. Solution temperatures were measured by ordinary glass thermometers to an accuracy of about 0.1 ^{o}C. The conductivity of a given solution, such as that in the water tub, was monitored over long periods by a standard electrode. Loss of water by evaporation or salt by leaks and spilling can be corrected for either by the addition of salt or water, as the case may be.

17.2 Water Tunnel Experiments

Measurements of the velocity of water with the U-meter have been performed in a small water tunnel specially constructed for this purpose. In the paragraphs that follow, the properties of the water tunnel are described and experimental results of velocity measurements in the tunnel are analyzed.

Experimental Equipment

The water tunnel experimental equipment is described below in terms

of the mechanical equipment, electronic instrumentation and hydrodynamic performance characteristics. A functional diagram of the water tunnel experimental arrangement is shown in Figure 17.3 and photographs of the equipment are shown in Figure 17.4 . The equipment consists, basically, of a recirculating reservoir of artificial sea water, a small diameter glass tube test section which is long enough to establish fully developed laminar or turbulent flow, a small electrode probe coaxially mounted at the end of the glass tube, and the associated electronic equipment to provide high power to the electrode and to measure the variations in electrode resistance.

Mechanical Equipment - The water pump filter used is a Sears and Roebuck Model No. C56G2B8 centrifugal pump with a 1/3 HP electric motor capable of a maximum throughput (with filtering) of 1.9 cfm at zero pressure or 20 psi at zero throughput as shown in Figure 17.5 . The maximum fluid power is 1.1 cfm at 12 psi. The filtering system holds about 0.5 cu. ft. water. This system has operated satisfactorily for about one year on artificial sea water. The water tunnel system may also be operated directly from the tap water supply which provides a higher pressure (85 psi) but which is poorly regulated. This arrangement is only suitable for velocity measurements in tap water which has a much lower conductivity (x 100) than sea water. The recirculation tank is an ordinary galvanized wash tub size no. 1 filled to about 8" depth and with a mean diameter of 18" and 1.2 cu. ft. water volume. The mean recirculation time with the pump and filtering system is about 1 minute. The heating and cooling of the water is achieved by a 5 turn copper coil around the tank which is supplied with either hot ($\sim$ 58 ^{o}C) or cold ($\sim$ 18 ^{o}C) tap water. The salt water temperature can be changed fairly rapidly (2.8 ^{o}C/minute) in order to make temperature coefficient measurements. The heating and cooling cycle is shown in Figure 17.6 . The heat power transferred to the water at the maximum rate is 6.5 kw. No temperature regulation system is used. The salt solution is ordinarily a mixture of 99.9 % pure Mortons salt with tap water to a concentration of 32.8 ‰ corresponding to 3.6 lbs. of salt in 110 lbs. of solution (1.7 cu. ft.). This solution has the same electrical conductivity as 35 ‰ sea water at 20 ^{o}C. The water temperature is measured by a glass thermometer in the tub. The concentration of the solution is monitored by means of a calibrated conductivity cell immersed in the tank. The solution is easily adjusted by slight additions of either salt or tap water. The flow to the water tunnel is controlled by a number of gate valves, the first two of which are used to adjust the amout of recirculation to the tank and the driving pressure. The actual flow to the tunnel is controlled by a needle valve with a low pitch thread which is capable of fine adjustment. The rate of flow through the tunnel is monitored by a mercury manometer which measures essentially the pressure drop across the test section glass tube. The water throughput is measured by direct volumetric means and correlated with the manometer readings. The test section consists of a 3.5 mm inside diameter glass tube 28" in length. The probe is mounted at the end of the glass tube where the fluid flow is fully developed for both laminar and turbulent flow. The diameter of the electrode probes is small

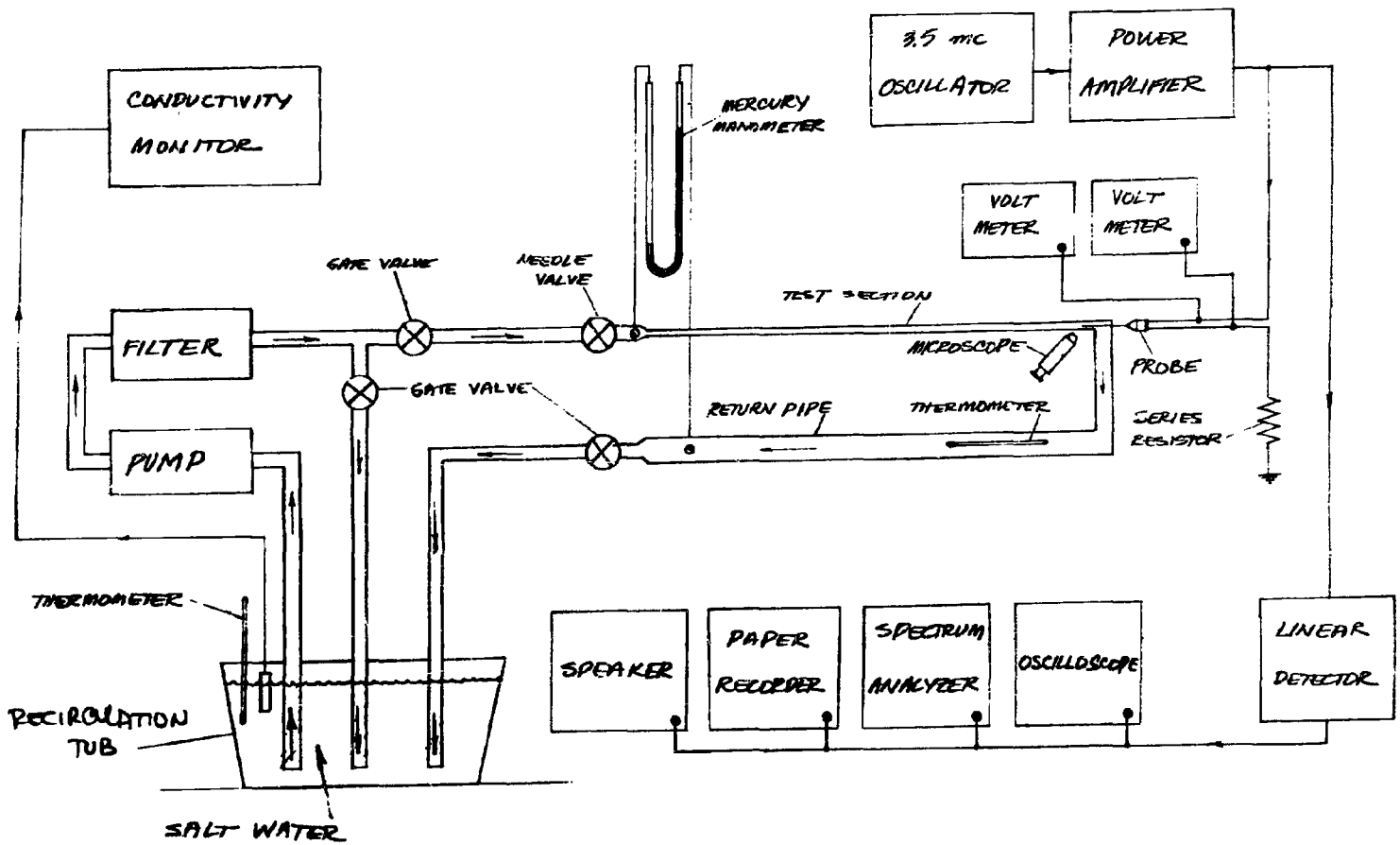

Figure 17.3 . Water Tunnel Experimental Arrangement

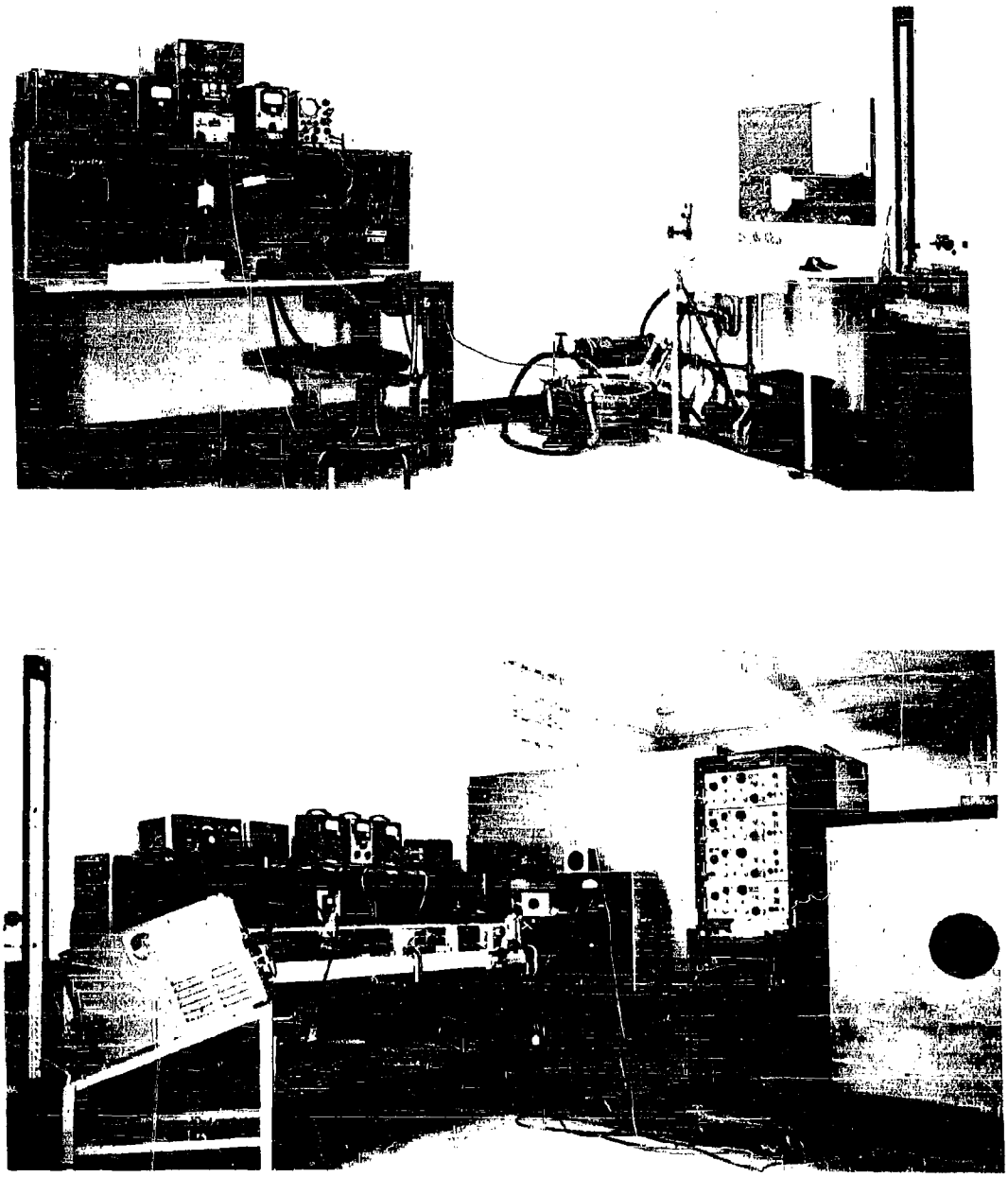

Figure 17.4 . Water Tunnel Experimental Equipment

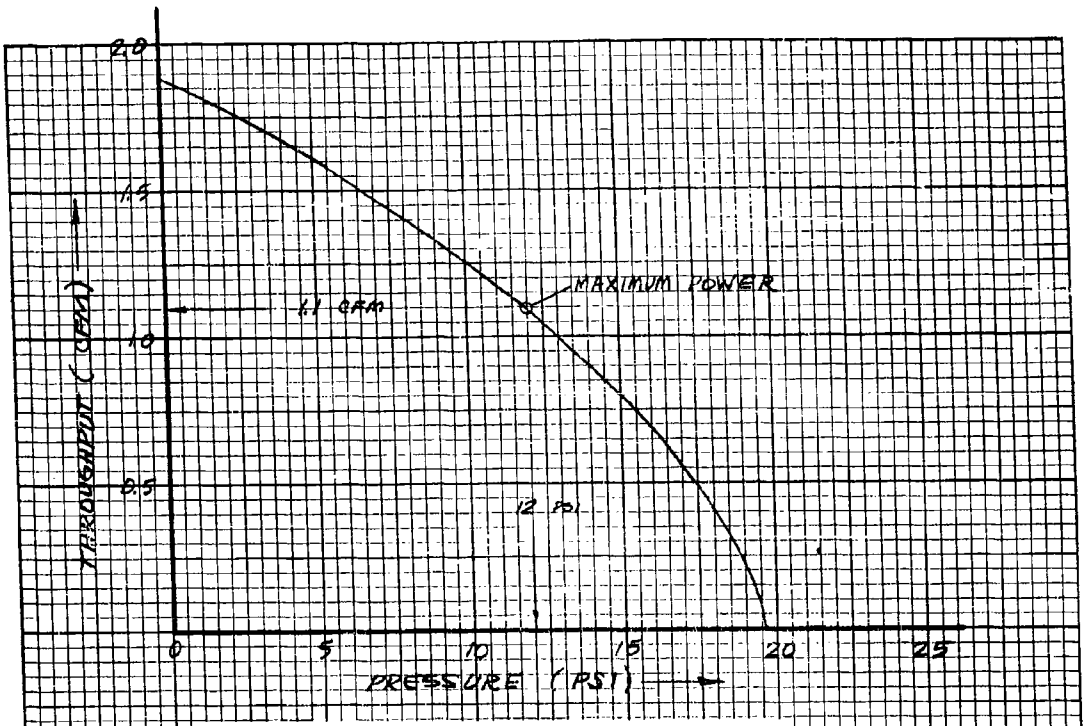

Figure 17.5. Water Pump Performance

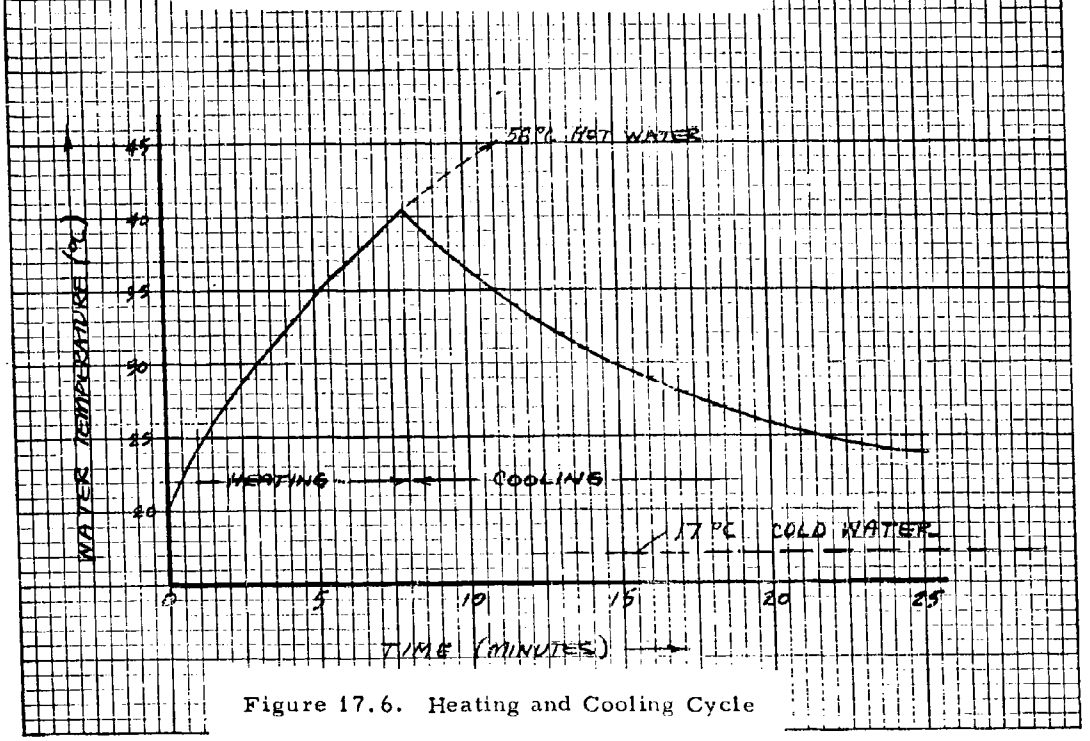

Figure 17.6. Heating and Cooling Cycle

in comparison with the tube diameter so that the axial velocity is approximately equal to the expected theoretical value. The tube is connected to a flexible hose so that the glass tube can be easily backed off from the water seal at the probe to facilitate the changing and maintenance of the detector probes. The flow in the vicinity of the probe is viewed through the glass tube with an X15 power microscope. Because of distortion caused by the glass, a higher magnification was not possible nor desirable. The probe is mounted on an end block which is used to position the probe centrally in the tube and also to provide a low resistance (large area) return path for the water. The return pipe is of large diameter for low resistance and contains a thermometer which shows the increase in water temperature due to the power input at the electrode. The test section, end-block, return pipe and associated valves are mounted on a common wooden frame which protects the glass tubing and provides a rigid alignment.

Electronic Equipment - The electronic equipment necessary for these experiments consists of a high power and high frequency source of electrical energy, and metering equipment to measure the electrical properties of the probe. This equipment is illustrated in Figure 17.3. The source of electrical energy to heat the water is supplied by a Central Electronics Model 600L RF power amplifier driven by a Model 190 Textronix signal source. The RF power is dissipated directly in the resistive load of the probe. The resistance of the probe, while operating at high power, is determined by a measurement of the voltage across the probe and the voltage across a small known resistance in series with the probe resistance. The latter measurement indicated the current in the load, which, together with the total voltage, provided the necessary data to calculate the probe resistance. For refined measurements of changes of resistance with velocity, the probe is operated in a bridge network which is capable of dissipating high power. The variations in probe resistance due to fluctuations in water velocity were observed by means of a linear detector which responds to the envelope of the voltage fluctuations across the load. The detected voltage fluctuations are then recorded and analyzed by the display equipment consisting of an oscilloscope, speaker, paper recorder and spectrum analyzer.

Flow Characteristics - The range of controllable average velocity, $\bar{u}$, and flow, Q, in the water tunnel is

$$1.0 \text{ cm/sec} \leq \bar{u} \leq 570 \text{ cm/sec}$$

$$1.0 \text{ cm}^3/\text{sec} \leq Q \leq 55 \text{ cm}^3/\text{sec} \quad ,$$

which corresponds to the Reynolds number range

$$30 \leq R \leq 19{,}000$$

where, in terms of the tube diameter, d, we have

$$Q = A\bar{u} \qquad A = \left(\frac{\pi}{4}\right)d^2 \qquad R = \frac{\bar{u}d}{\nu}$$

The tube diameter was chosen so that both laminar and turbulent flow could be obtained. The transition between these two flow regimes occurs at a Reynolds number of about 2300 where

$$\bar{u}_x = 76 \text{ cm/sec} = 1.5 \text{ knots}$$

$$Q_x = 7.3 \text{ cm}^3/\text{sec}$$

$$R_x = 2300 \quad .$$

The velocity on the axis, u_Λ, is related to the average velocity, $\bar{u}$, by

$$u_\Lambda = 2.00\ \bar{u} \quad \text{for laminar flow (1)}$$

and

$$u_\Lambda = 1.25\ \bar{u} \quad \text{for turbulent flow (2)}$$

therefore, the full range of axial velocities is

$$2.1 \text{ cm/sec}(.04 \text{ knots}) \leq u_\Lambda \leq 720 \text{ cm/sec}(14 \text{ knots}) \quad .$$

It is this velocity which is measured in the tunnel since the small electrode probes are located on the axis of the tube. The hypodermic needle probes which have been used are small enough that they do not appreciably change the velocity distribution across the tube: the frontal area of a No. 21 gauge needle is 5% A, and that of a No. 27 gauge needle is 1% A, where A is the cross-sectional area of the tube. The turbulence intensity on the axis, just above the critical Reynolds number, is approximately 5%. The length of the tube is long enough that the flow is fully developed in both laminar and turbulent flow (3). For laminar flow it is necessary that $(\ell/d) > 100$ for R = 2300, and for turbulent flow that $(\ell/d) > 50$. A summary of the water tunnel characteristics is given in Table 17.1 . The flow characteristics depend, of course, on the temperature of the water which can be varied from about 15 °C to 50 °C. The velocity profile in laminar and turbulent flow is shown in Figure 17.7 and indicates the size of a No. 21 gauge hypodermic needle probe relative to the tube diameter.

Experimental fluid velocity measurements in the water tunnel described above, are covered in the remaining paragraphs of this Section.

Resistance-Power-Velocity Relation

The relation between the fluid velocity and the electrode resistance and power has been measured in the water tunnel under a wide range of conditions with the No. 21 hypodermic needle probe. The electrode resistance, R, was measured with a bridge network to accurately measure the relatively small changes in resistance with the velocity, U, and power, P.

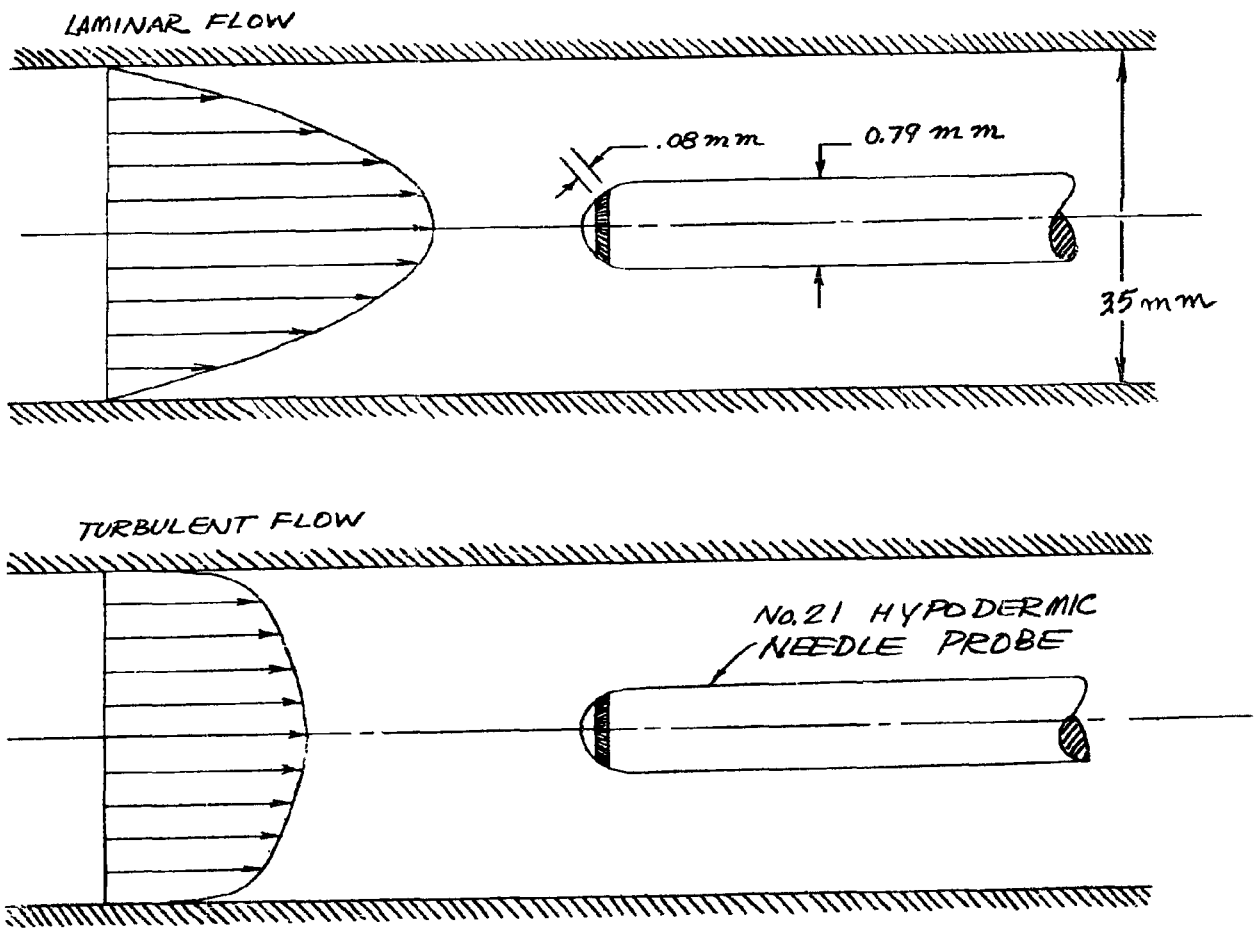

Figure 17.7. Water Tunnel Velocity Profile and U-Meter Probe

Table 17.1 . Water Tunnel Characteristics

Tube Diameter	0.35 cm
Tube Length	70 cm
Length/Diameter	200
Tube Area	.096 cm^2
Maximum Velocity (Turbulent)	720 cm/sec (14 knots)
Maximum Velocity (Laminar)	154 cm/sec (3 knots)
Maximum Flow (Turbulent)	55 cm^3/sec
Maximum Flow (Laminar)	7.3 cm^3/sec

The applied voltage, V, was actually measured and the power computed from the measured resistance ($PR = V^2$). Measurements were carried out only for laminar flow. The resistance measurements were performed at many points in the velocity range 20 cm/sec $< U <$ 100 cm/sec and in the power range 0.5 watt $< P <$ 4 watt. The upper limit to the power was set by the inception of boiling at the electrode due to the electrical heating of the water. Examples of the observed data are shown in Figure 17.8 . The resistance decreases linearly with increasing electrode power (U = constant) for low power and decreases less rapidly at higher electrode power.

The resistance-power-velocity relation follows from the heat transfer equation (Sec. 12.5)

$$P = 2c\Lambda U \, \bar{\Delta T} \, \dot{Q}_\lambda \quad ,$$

and the resistance-temperature equation (Sec. 5.3)

$$R = R_o \left\{ 1 - \beta \, \bar{\Delta T} + k\beta^2 \, \bar{\Delta T}^2 \right\} \quad ,$$

where $\bar{\Delta T}$ is the average electrode temperature rise, k accounts for the nonlinearity of the variation of resistance with temperature, and $\dot{Q}_\lambda$ is a dimensionless factor which accounts for heat transfer from the electrode volume by means other than forced convection. The data of Figure 17.8 may be used to determine the frontal area, A, of the electrode as follows. The measured slope of these curves, $(dR/dP)_o < 0$, at zero power is compared with the above formulas by differentiation:

$$A \dot{Q}_\lambda = - \frac{\beta}{\frac{2cU}{\kappa_o} \left(\frac{\partial R}{\partial P} \right)_o} \quad ,$$

where this expression is evaluated at zero power ($\bar{\Delta T} = 0$). Assuming the values appropriate for sea water at 20 °C

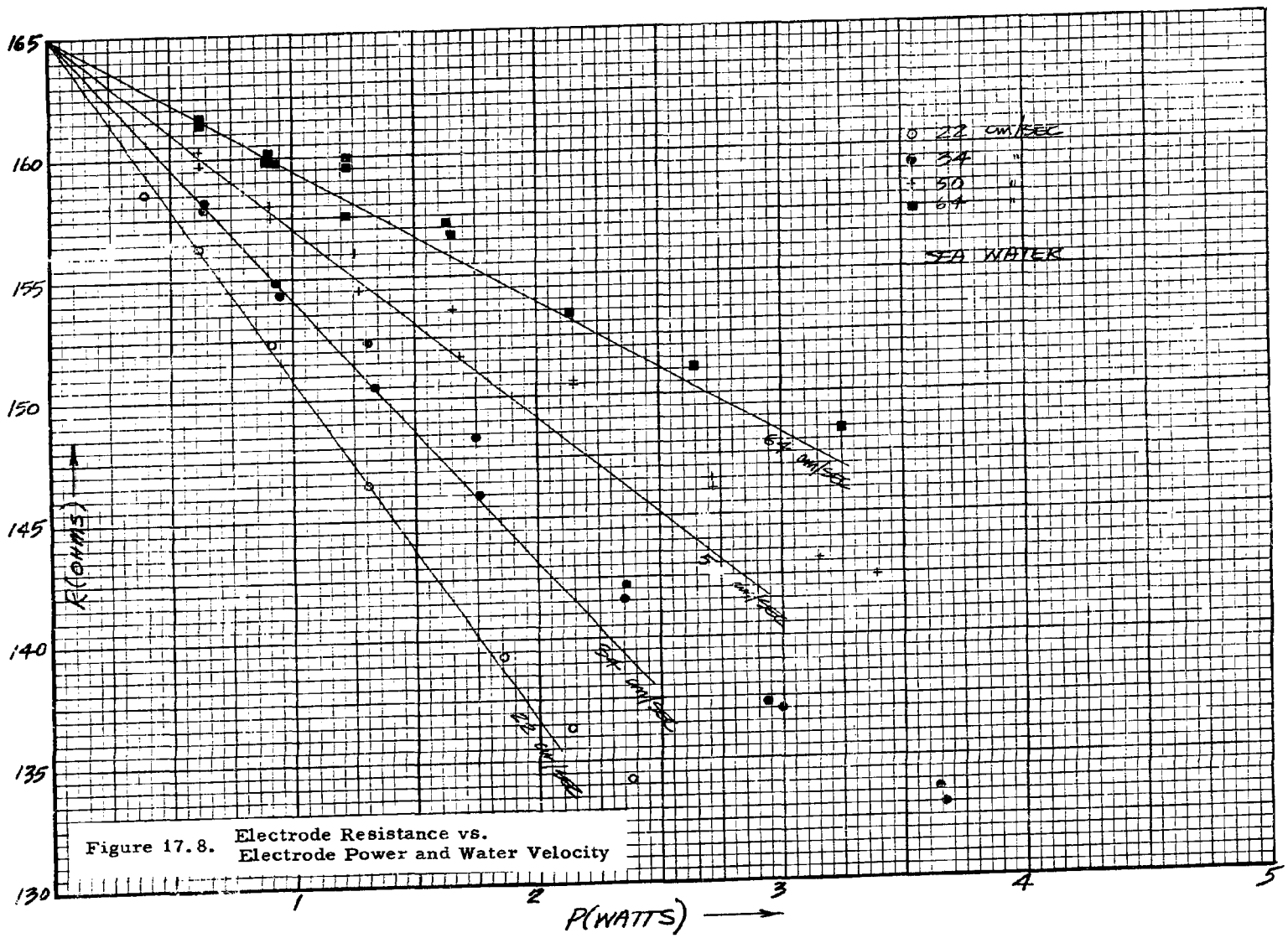

Figure 17.8. Electrode Resistance vs. Electrode Power and Water Velocity

$$\beta = .0213 \text{ per } ^\circ C \qquad c = 4.09 \text{ joule/cm}^3/^\circ C \quad ,$$

and using the measured values of U, R_o, and slope, the value of $A\dot{Q}_\lambda$ is computed and is shown in Figure 17.9 . The slow variation of these quantities with velocity is due to the variation of $\dot{Q}_\lambda$ due to thermal conduction in the boundary layer region (A = constant). The expression developed in Section 12.5 for $\dot{Q}_\lambda$ fits the observed data when

$$\dot{Q}_\lambda = 1 + \frac{30}{\sqrt{PR}}$$

where $P = 7$ and $R = U\ell/\nu$, and $\ell = .008$ cm is the typical dimension of the gap in the hypodermic needle electrode. The factor 30 is considerably larger than the one found from dimensional analysis (30 instead of 6). This could easily be accounted for by the scatter in the data points since the factor is quite sensitive to the (small) slope of the curve. The frontal area, A, is found by considering the asymptotic value of $\dot{Q}_\lambda$ at large velocity ($\dot{Q}_\lambda \to 1$ as $U \to \infty$); the value obtained is

$$A = 4.0 \times 10^{-4} \text{ cm}^2 \quad ,$$

which is what might be expected from the actual dimensions of the electrode gap.

The validity of the two equations relating R, P, $\overline{\Delta T}$ and U over the wide range of velocity and power used in this experiment may be established by expressing the data in the form

$$r = -\alpha\left[1 - k\alpha\right] \quad ,$$

where

$$r = \frac{R - R_o}{R_o} \qquad (r < 0)$$

and

$$\alpha = \beta\overline{\Delta T} = \frac{\beta P}{2cAU\,\dot{Q}_\lambda} \quad . \qquad (\alpha > 0)$$

The value of α is obtained from the observed data by noting that

$$\alpha = -\frac{P}{R_o}\left(\frac{dR}{dP}\right)_o \quad ,$$

where all the quantities on the right are measured. All the data points of this experiment have been reduced in this way and are shown in Figure 17.10.

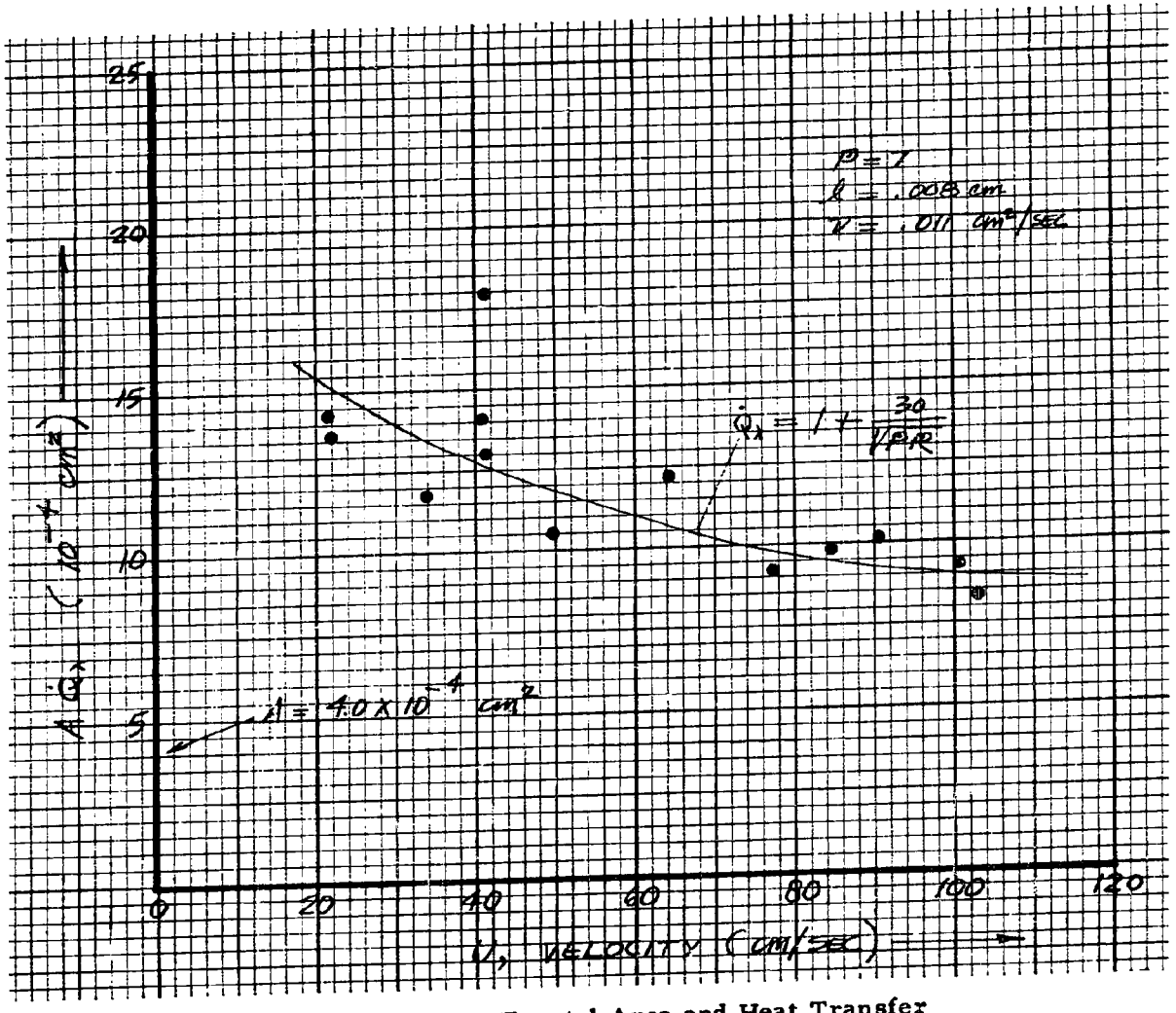

Figure 17.9. Frontal Area and Heat Transfer Factor vs. Water Velocity

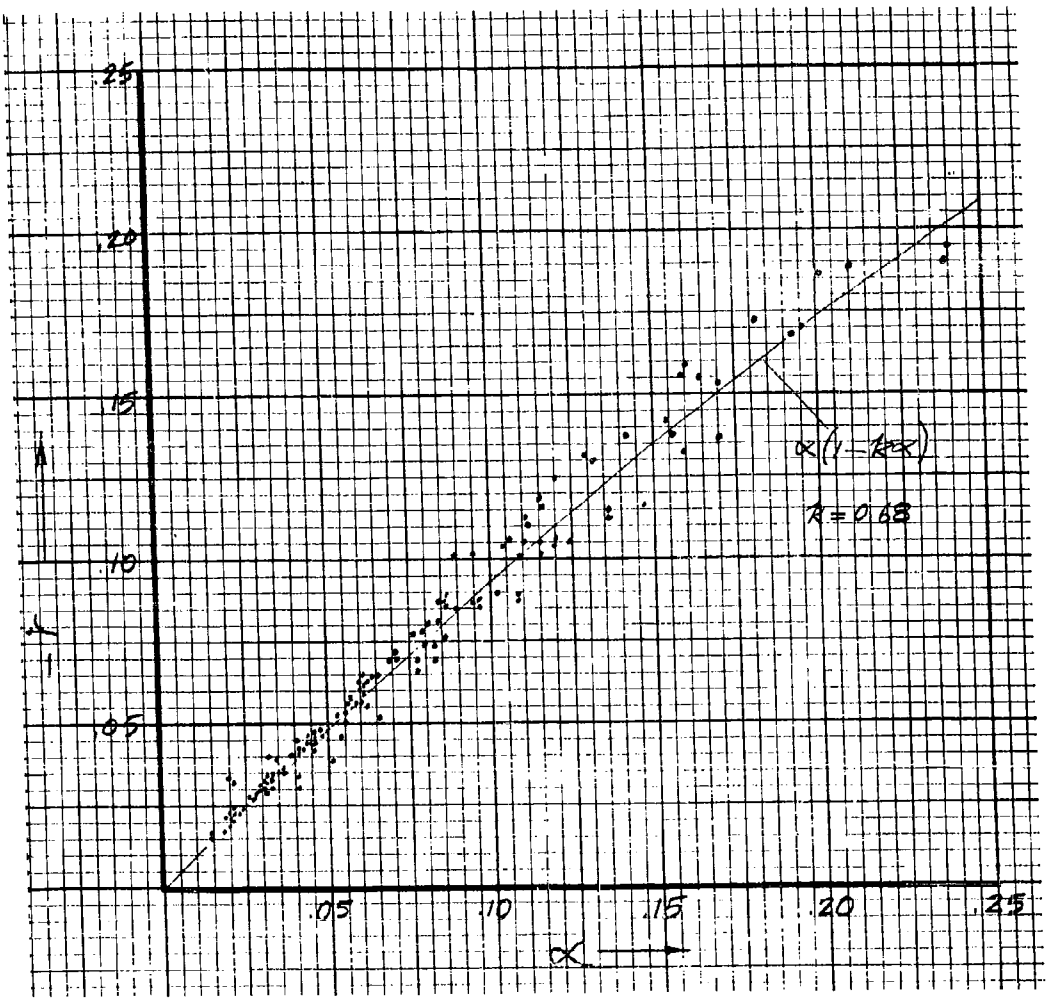

Figure 17.10. Relative Resistance Change vs. Temperature Parameter

The theoretical curve fits the data best if we choose the non-linearity constant to be k = 0.68 (see Addendum No. 1).

A more direct relation which gives the water velocity as a function of the measured resistance and power is obtained in dimensionless form as follows. Solving the equation

$$r = r(\alpha) = -\alpha\left[1 - k\alpha\right]$$

for α, we obtain

$$\alpha = \alpha(r) = \frac{1 - \sqrt{1 + 4kr}}{2k}$$

OR

$$\alpha \approx -r + kr^2 - 2k^2r^3 \qquad (r < 0) .$$

By means of this equation, a measurement of the relative resistance change, r, determines α. The velocity U, is then given by

$$U = \frac{\beta P}{2cA\,\mathcal{Q}_\lambda\,\alpha(r)} .$$

Since $\mathcal{Q}_\lambda$ also depends on velocity (only through the Reynolds number R), it is desirable to rewrite this equation in dimensionless form as follows

$$\mathcal{Q}_\lambda R = \frac{\mathbb{D}}{\alpha(r)} \approx \frac{\mathbb{D}}{-r + kr^2}$$

where the dimensionless number $\mathbb{D}$ is*

$$\mathbb{D} = \frac{\beta P \ell}{2cA\nu} .$$

For the No. 21 hypodermic needle in sea water, we have

$$\frac{2cA\nu}{\beta\ell} = 211 \text{ milliwatt},$$

---

*For a cubic electrode volume of dimension ℓ, we have

$$\mathbb{D} = \frac{\beta P}{2c\ell\nu} .$$

for

$$c = 4.09 \text{ joule/cm}^3\text{sec}$$
$$A = 4.0 \times 10^{-4} \text{ cm}^2$$
$$\nu = .011 \text{ cm}^2/\text{sec}$$
$$\beta = .0213 \text{ per } ^\circ\text{C}$$
$$\ell = .008 \text{ cm}$$

For a given electrode and medium, this dimensionless group depends only on the electrode power. The relation

$$\dot{Q}_\lambda \mathcal{R} = \frac{\mathcal{D}}{-r + kr^2}$$

is plotted in Figure 17.11a for the observed data and is quantitatively expressed by the relation

$$\text{velocity} \sim \frac{\text{power}}{\text{resistance}}$$

The auxiliary graph of $\dot{Q}_\lambda \mathcal{R}$ vs. U, shown in Figure 17.11b, may be used to obtain directly the connection between velocity and $\mathcal{D}/\alpha(r) \sim$ power/resistance.

Laminar-Turbulent Transition

An effective illustration of the performance of the U-meter probe is obtained by observing the U-meter output as the throughput (cm^3/sec) of the water tunnel is slowly increased through the transition region at critical Reynolds number, $R_x \approx 2300$. Below this value, the flow is laminar, and above, the flow is turbulent. The observed velocity fluctuation signal is shown in Figure 17.12.

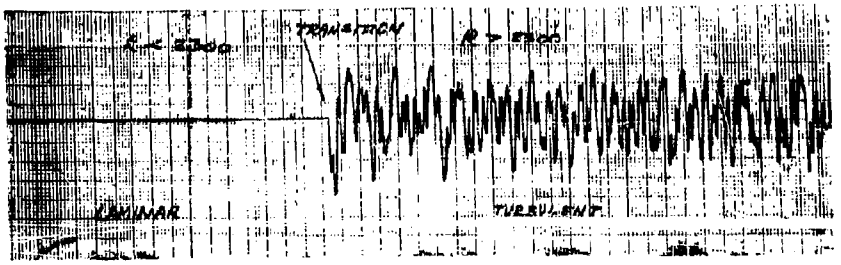

Figure 17.12. U-meter Output in the Laminar–Turbulent Transition Region

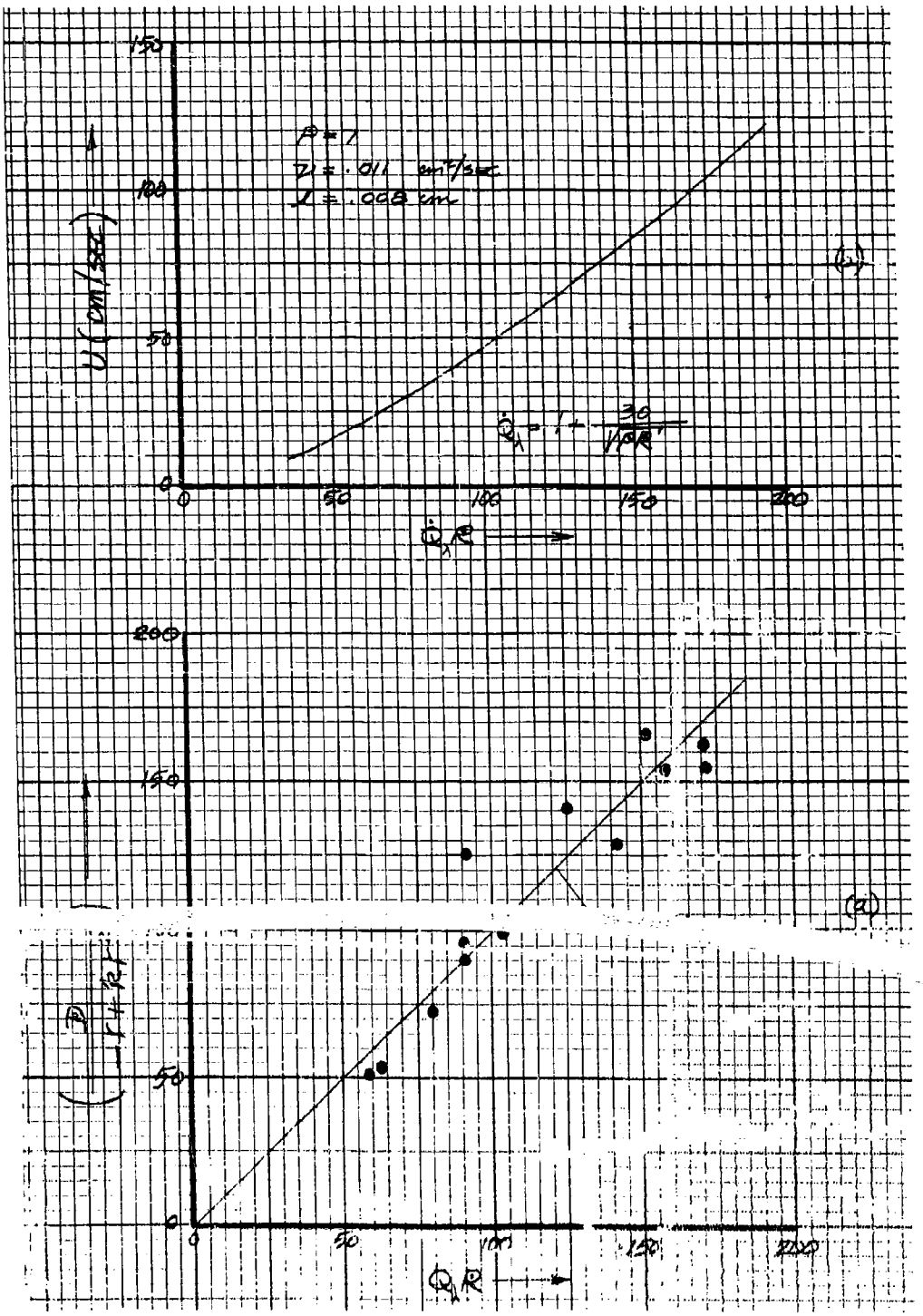

Figure 17.11. Dimensionless Resistance-Power-Velocity Relation

The signal indicated in this Figure represents the fluctuating velocity component of 4 cps bandwidth centered at 100 cps. The change in velocity for the two flow regimes amounts to about 10 %, however, this change occurs abruptly at the transition point and only a slight change in the valves which control the flow is required to trigger this instability. The effectiveness of the measurement is indicated by the signal-to-noise ratio between the two regions of flow which amounts to better than a factor of 100 (40 db). In laminar flow there are, presumably, no velocity or temperature fluctuations in the 100 cps band due to the diffusion damping by the relatively long length of the glass tube.

Output-Input Relation

In a given velocity field, how does the velocity detector output voltage vary with the input voltage to the sensing element? This output/input relation depends, of course, on the fundamental mechanism by which the sensing element is responsible to velocity changes. The importance of an experimental measurement of this relation is that it determines, with the present detector, whether it operates on the basic principle of heating the water by an amount dependent on the water velocity or whether one of the complicated electrochemical processes mentioned in Section 5.2 is operative.

This experiment was performed by exposing the detector to a steady-state turbulent velocity field and observing the magnitude of the random output voltage as the voltage applied to the electrode is varied. The water tunnel was operated steadily at a super critical Reynolds number ($R \approx 5200$) where the flow is turbulent and the rms velocity fluctuations amount to about 4 % of the average velocity (4 knots). For the actual measurements the fluctuations in a narrow band(4 cps at 150 cps), where the spectrum is flat, were recorded on a Sanborn recorder. The average magnitude of the fluctuations was estimated visually from a 30 sec. sample of the recording. This experimental technique of measuring a steady-state turbulent velocity has the advantage that the relatively small changes in resistance do not have to be measured with highly stable dc equipment and water velocity as would be required if the flow velocity was a constant (laminar flow). This is analogous to the advantage of ac amplification over dc amplification.

The expected magnitude of the output follows from the bridge equation for an equal arm resistive bridge (which was used for the test) (Sec. 15.1)

$$\left(\frac{\delta V}{V}\right) = \frac{1}{2}\left(\frac{\delta R}{R}\right) \quad ,$$

where δV is the fluctuating output voltage, and V is the voltage applied to the electrode, and R is the electrode resistance. The relation between the voltage fluctuations, δV, and velocity fluctuations, δU, is derived

as follows. The factor of proportionality, K, between the relative resistance and velocity fluctuations is

$$\left(\frac{\delta R}{R}\right) = K\left(\frac{\delta U}{U}\right)$$

where

$$K = \frac{U}{R}\left(\frac{\partial R}{\partial U}\right) \quad .$$

This derivative is evaluated by means of the expression (assuming constant-power-operation).

$$\frac{\partial R}{\partial U} = \left(\frac{\partial R}{\partial \alpha}\right)\cdot\left(\frac{\partial \alpha}{\partial R}\right)\cdot\left(\frac{\partial R}{\partial U}\right) \quad ,$$

and

$$\left(\frac{R - R_o}{R_o}\right) = -\alpha\left[1 - k\alpha\right] = r$$

$$\alpha = \frac{\mathbb{D}}{QR} \qquad (Q \equiv \dot{Q}_\lambda)$$

$$Q = 1 + \frac{M}{\sqrt{PR}}$$

and

$$R = \frac{U\ell}{\nu} \quad .$$

Performing the indicated derivatives, we find

$$\frac{\partial R}{\partial \alpha} = R_o\left(-1 + 2k\alpha\right)$$

$$-\frac{\partial R}{\partial U} = \frac{\ell}{\nu}$$

$$\frac{\partial \alpha}{\partial R} = -\frac{\mathbb{D}}{QR^2}\left\{1 - \frac{M}{2Q\sqrt{PR}}\right\}.$$

The Prandtl number (P) and kinematic viscosity (ν) are assumed independent of temperature over the temperature range of interest. Defining the fol-

lowing quantities

$$P_0 = \frac{V^2}{R_0} \qquad P = \frac{V^2}{R}$$

$$\mathcal{D}_0 = \frac{\beta P_0 \ell}{2cA\nu} \qquad \mathcal{D} = \frac{\beta P \ell}{2cA\nu}$$

$$g(R) = \frac{1}{Q}\left\{1 - \frac{M}{2Q\sqrt{\mathcal{D}R}}\right\}$$

then

$$\mathcal{D} = \left(\frac{P}{P_0}\right)\mathcal{D}_0 = \left(\frac{R_0}{R}\right)\mathcal{D}_0$$

and

$$K = \left(\frac{R_0}{R}\right)^2 \cdot (1-2k\alpha)\left(\frac{\mathcal{D}_0}{R}\right) g(R) \,.$$

Since

$$\frac{R}{R_0} = 1 - \alpha + k\alpha^2 \,,$$

and defining the function $f(\alpha)$ such that

$$f(\alpha) = \frac{1-2k\alpha}{(1-\alpha+k\alpha^2)^2} \,,$$

we find

$$K = f(\alpha)\, g(R)\left(\frac{\mathcal{D}_0}{R}\right).$$

The quantities α, R and B_0 are interrelated by

$$\alpha\left[1 - \alpha + k\alpha^2\right] = \frac{\mathcal{D}_0}{QR} \,.$$

The functions defined above are plotted in Figure 17.13 over the range of Reynolds number, R, and temperature parameter, α, of interest in most experimental work. The parameter α is limited by boiling in the electrode volume usually to values less than $\alpha = 0.3$. It is observed that for such values, the function $f(\alpha)$ differs only slightly from unity. If this factor is neglected, we find

$$\frac{\delta V}{V} = \frac{1}{2}\, g(R)\, \frac{D_0}{R} \left(\frac{\delta U}{U}\right)$$

Only the number D_0 depends on the applied electrode voltage, V:

$$D_0 = \frac{\ell \beta V^2}{2 C A \nu R_0} \quad ,$$

hence, it follows that the functional behavior of the input-output relation is

$$\delta V \sim V^3 \quad .$$

This is the characteristic behavior of the U-meter which is based on the electrode heating effect. If the velocity dependence of the probe was due to an electrochemical surface process, the above relation would be linear in V instead of cubic.

The observed experimental data is shown in Figure 17.14. The relative output voltage of the velocity detector is plotted against the applied electrode voltage and compares favorably with the expected cubic relation. To get a better indication of how well the output follows the cubic curve, the data is plotted logarithmically in Figure 17.15. A straight line of best fit through the observed points has a slope of 3.2 which is close to the expected value of 3.0. This cubic relation is seen to hold over three orders of magnitude in the output signal.

Turbulence Spectrum

The ability of the velocity detector to measure high frequency, small scale, turbulent velocity fluctuations has been demonstrated by measuring the spectrum of turbulence in pipe flow. This is accomplished by operating the water tunnel at supercritical Reynolds number where the flow is turbulent. The probe is located centrally in the tube, and measures the axial turbulence intensity. The experiment was performed at two Reynolds numbers, one at the maximum capability of the water tunnel ($R = 18{,}600$) and at about 1/3 that value ($R = 6{,}100$). The corresponding axial velocities, including a correction for the shape of the velocity (3), are 730 cm/sec (14.3 knots) and 240 cm/sec (4.7 knots). The spectrum measurements were carried out by means of a General Radio wave analyzer Type 736A which measured the ampli-

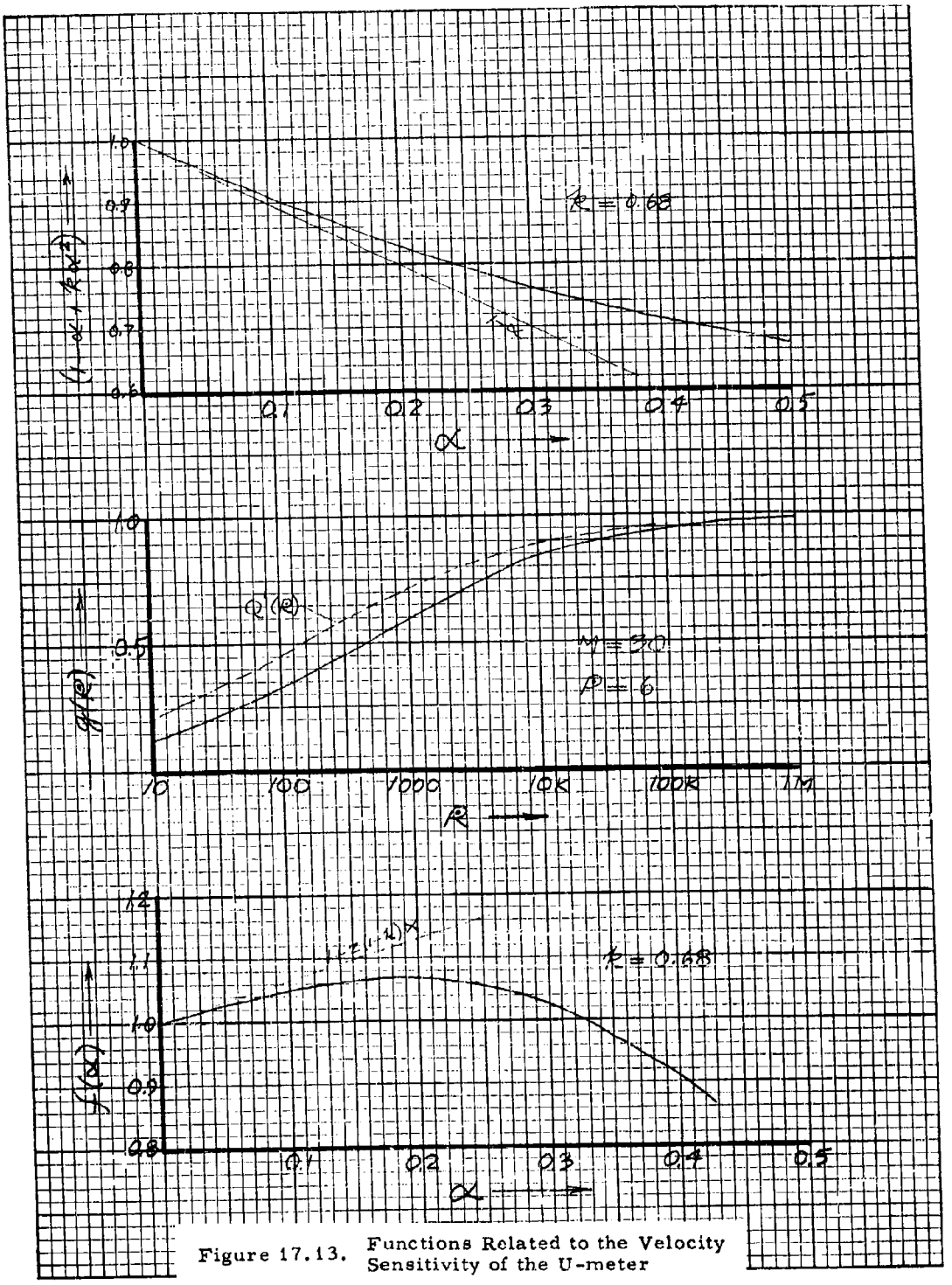

Figure 17.13. Functions Related to the Velocity Sensitivity of the U-meter

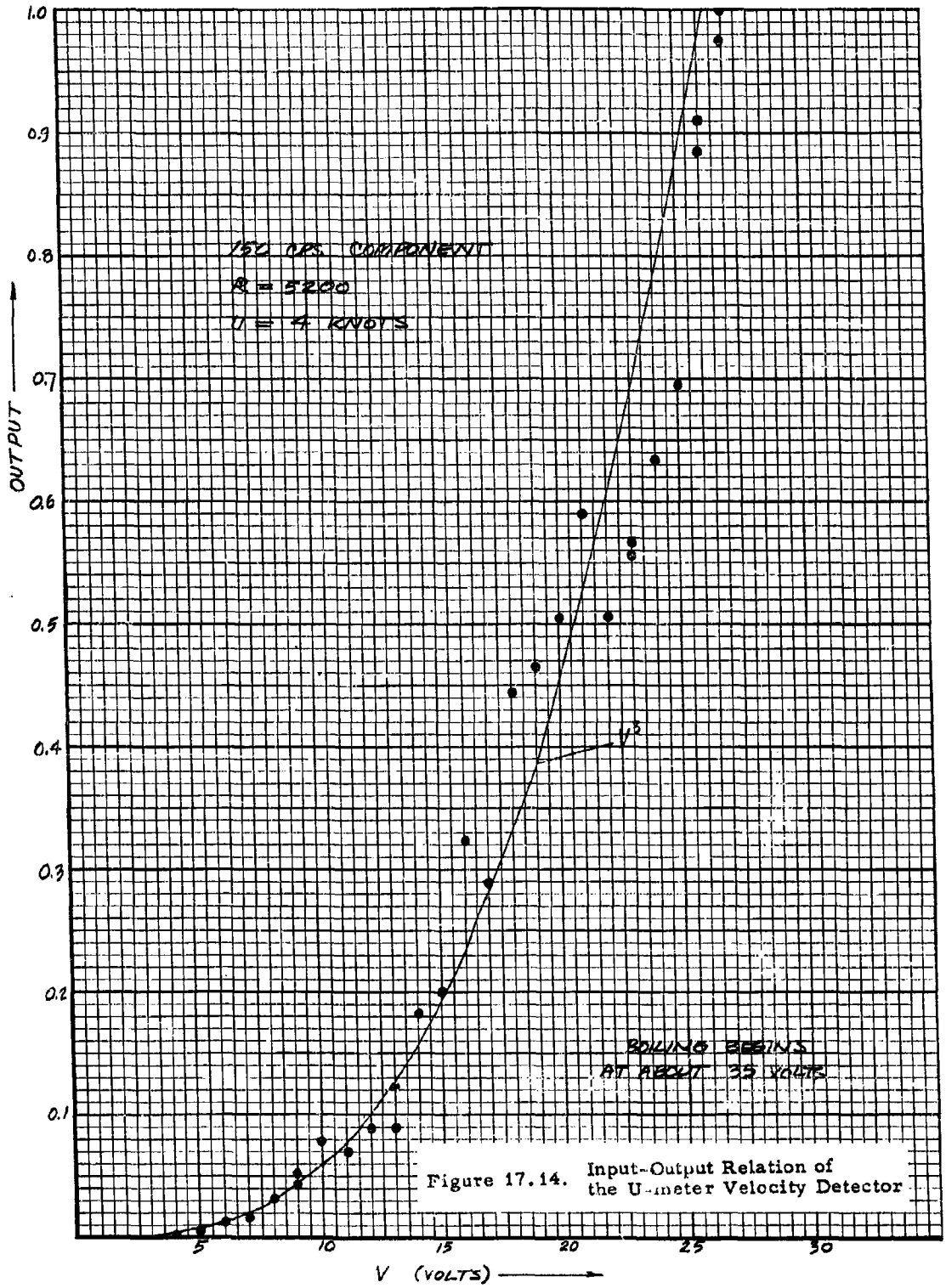

Figure 17.14. Input-Output Relation of the U-meter Velocity Detector

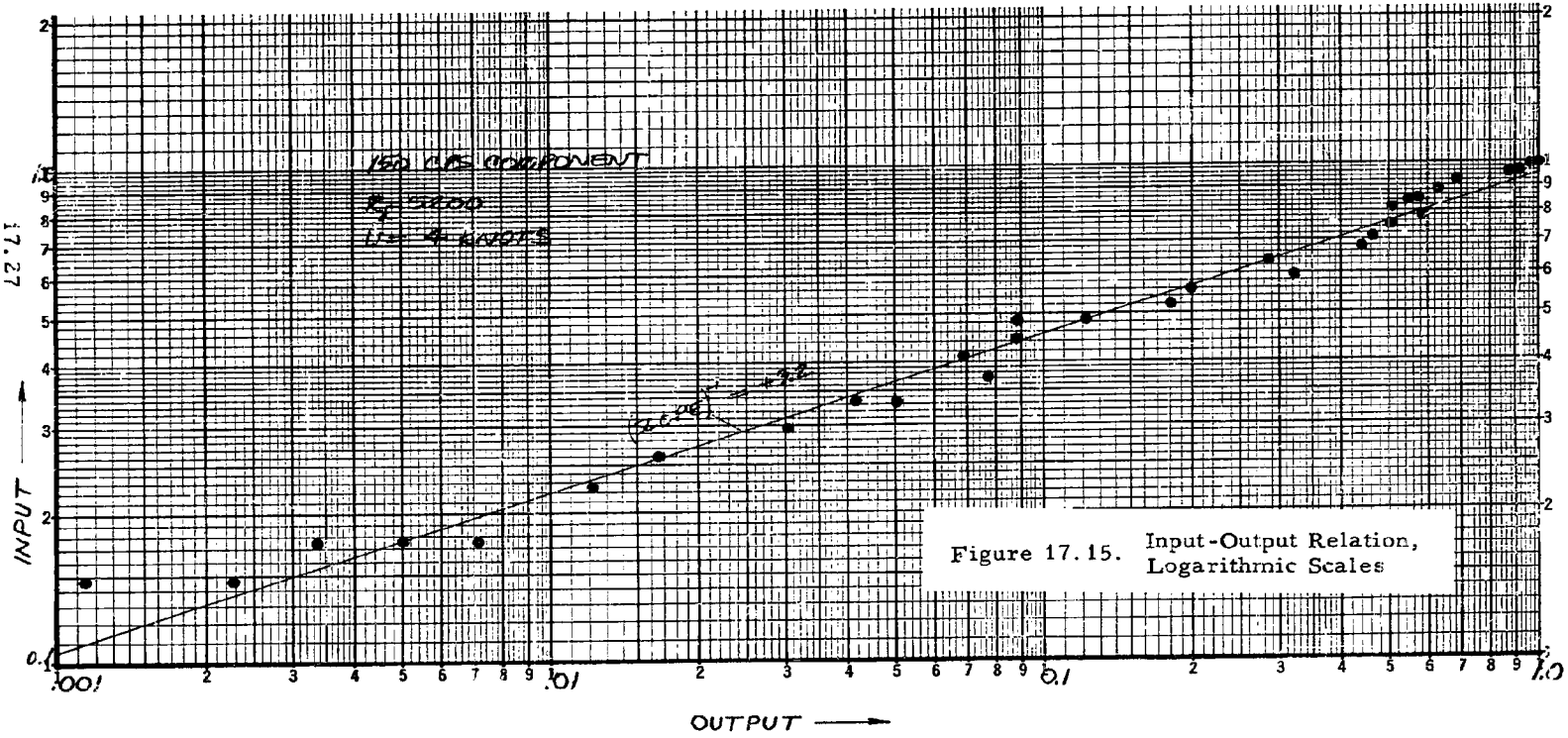

Figure 17.15. Input-Output Relation, Logarithmic Scales

fied signal from the bridge network. The bandwidth of the analyzer is constant and equal to 4 cps. The output of the wave analyzer was measured by a visual judgement of the average meter reading and also by making a visual estimate of the rms amplitude of a 30 sec. sample of the random meter output signal recorded on a Sanborn recorder.

The resulting output rms voltage spectrum vs. frequency of the detector is shown in Figure 17.16. The performance of the velocity sensor is indicated by frequencies involved in these measurements (up to 20 kc) and the low internal noise level observed in the measurements. The turbulent energy spectrum, F(k) is proportional to the square of the data of Figure 17.16, and is replotted in Figure 17.17 as a function of the wavenumber k:

$$k = \frac{2\pi U}{f} \quad ,$$

where U is the water velocity on the axis of the tube, and f the frequency. The diagonal line at the lower left of the graph may be used to convert the linear ordinate to a logarithmic scale. The data for both Reynolds numbers is seen to coincide fairly well with the solid line through the data points. It will be noticed that data is obtained to wavenumbers as high as $k = 250\ cm^{-1}$. The wavenumber corresponding to the tube diameter, d, is $k_d = d^{-1} \approx 2.9\ cm^{-1}$; the wavenumber corresponding to the cutoff response size of the No. 21 gauge needle probe is estimated to be

$$k_c \approx \frac{6}{(\text{gap diameter})} = \frac{6}{.05\ cm} = 120\ cm^{-1} \quad .$$

The dotted curve in Figure 17.17 represents the corrected energy spectrum under the assumption that the probe response falls off at 6 db per octave ($\sim k^{-2}$) over the range of the correction; this is based on the statistical considerations of Section 14.1 and the end of Section 13.1 .

The rms velocity fluctuation, u, on the axis is related to the energy spectrum by

$$\left(\frac{u}{U}\right)^2 = N d \int_0^\infty F(k)\, dk \quad ,$$

where U is the axial velocity, N is a numerical constant, d is the tube diameter and the spectral density is normalized so that F(0) = 1. An estimate of the size of the blobs or lumps of fluid over which the velocity is correlated is given by

$$\int_0^\infty F(k)\, dk = k_T$$

According to the data of Figure 17.17 , we find that

$$dk_T = 10 \pm 2 \quad ,$$

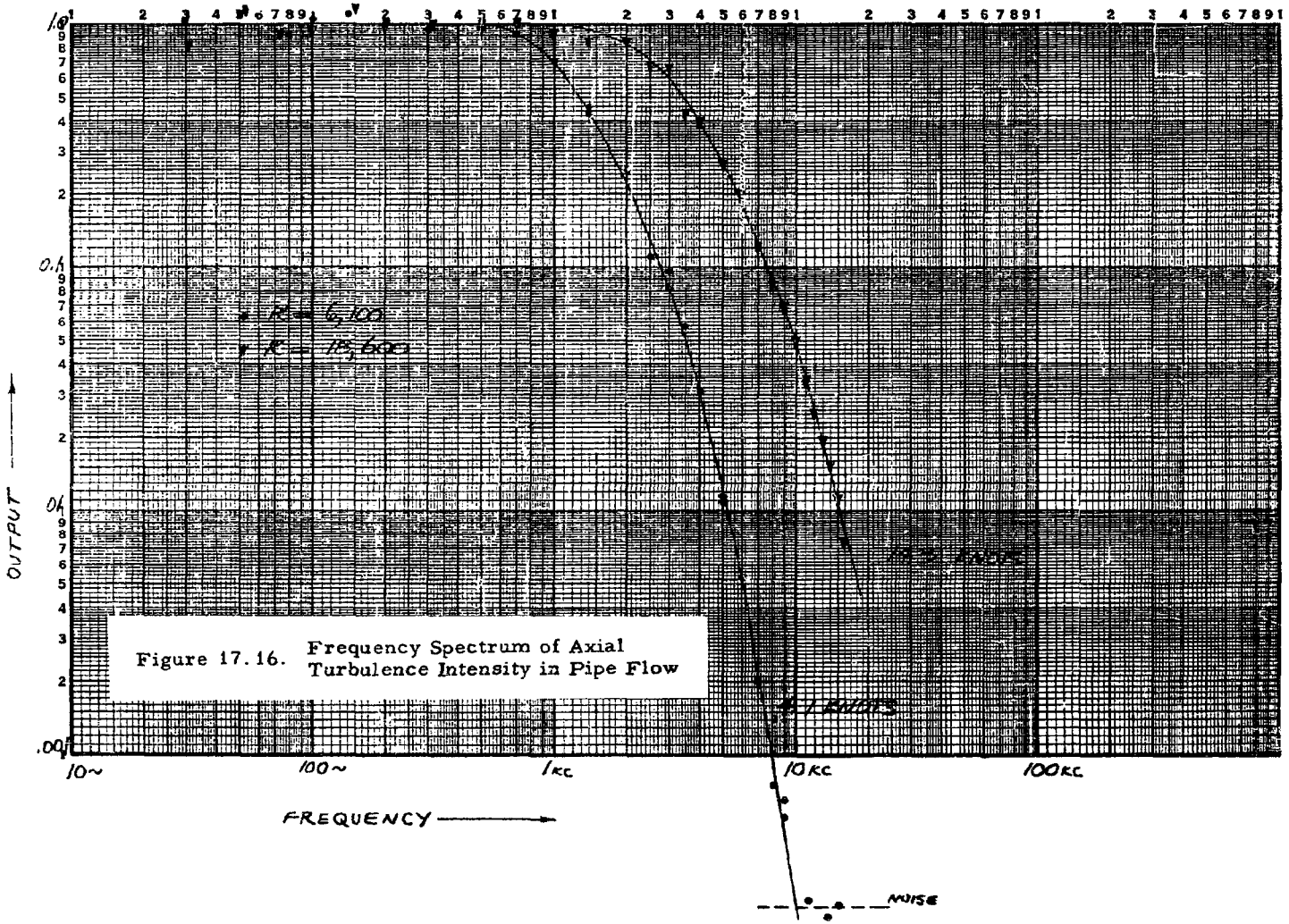

Figure 17.16. Frequency Spectrum of Axial Turbulence Intensity in Pipe Flow

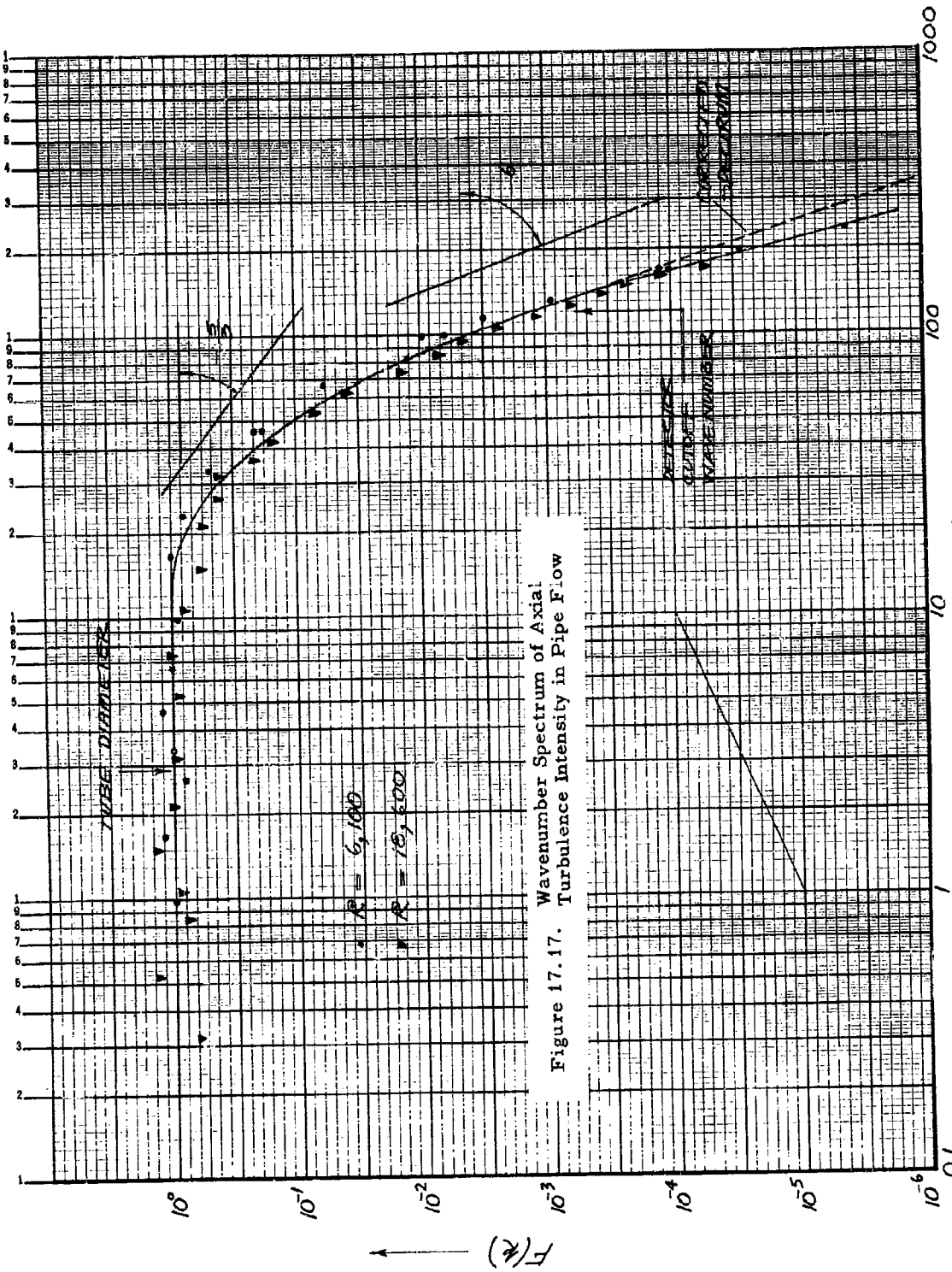

Figure 17.17. Wavenumber Spectrum of Axial Turbulence Intensity in Pipe Flow

that is, the size of the lumps is about 1/10 of the tube diameter. This result is comparable to the mixing length found experimentally for turbulent flow in smooth pipes (4). The constant N depends somewhat on the Reynolds number, particularly for turbulent flow just above the critical Reynolds number. The measurements performed here are not precise enough to make a distinction between the value of N for the two Reynolds numbers used; the approximate value found here is

$$N = \frac{1}{dk_T}\left(\frac{\ell}{U}\right)^2 \approx 4 \times 10^{-4} .$$

The spectral distribution is seen to follow the -5/3-Law only over a limited wavenumber range, and at the highest measured wavenumber range the spectrum falls off as the 6th power of the wavenumber. This behavior is not in disagreement with other measurements of turbulence spectra for fully developed pipe flow (5,6).

Boiling Noise

If sufficient power is dissipated in an electrode in a flowing medium, the fluid is heated to the point where boiling takes place in the electrode volume. This process sets a practical upper limit to the amount of power that may be dissipated in an electrode in the interest of performing sensitive velocity measurements. Experiments have been performed to investigate this process, which constitutes a background noise, with the No. 21 gauge hypodermic needle probe and with the parallel platinum wire probe discussed in Section 9.8 .

The boiling process is characterized by its more or less abrupt beginning once a threshold electrode power has been reached. The noise signal that is observed is due to the random fluctuations in electrode resistance due to the spontaneous formation of bubbles of varying size in the sensitive volume of the electrode. If δR is the rms resistance fluctuation about the average value, R, an expression which fits the observed boiling noise, and which is useful in theoretical analysis, is

$$\left(\frac{\delta R}{R}\right)^2_{rms} = K \left(\frac{P}{P_A}\right)^n ,$$

where P is the electrode power, K is a dimensionless constant, P_A is some reference power level of the order of the threshold value, and n is an exponent with a value between 10 and 25. For a symmetrical bridge network, the voltage fluctuation, δV, at the bridge output is related to the resistance fluctuation, δR, in one of the arms of the bridge by

$$\left(\frac{\delta V}{V}\right) = \frac{1}{2}\left(\frac{\delta R}{R}\right) ,$$

where V is the voltage applied to the element of resistance R. The varia-

tion of δV (rms) with V (rms) is, then,

$$\delta V = \frac{V}{2} K^{\frac{1}{2}} \left(\frac{V^2}{R P_\lambda}\right)^{\frac{n}{2}} \sim V^{n+1}.$$

The measured output signal as a function of electrode voltage in the region where boiling is important is shown in Figure 17.18. This data represents the boiling noise in the 100 cps and 300 cps band and was measured in laminar flow with the platinum parallel wire probe. The theoretical curve with n = 15 is fitted to the 100 cps data. The noise depends on the frequency band under consideration; the total broad band boiling noise increases somewhat faster than the noise in the 100 cps band. Experiments under various conditions indicate that the exponent n assumes values between 10 and 25. It is apparent in Figure 17.18, that the noise fits the theoretical curve only in a narrow region above the boiling threshold, and that as the electrode power is increased appreciably above this point, the noise output levels off. Only the region of sharp rise near the threshold is of interest in connection with the limitation of the detection equipment, since the boiling noise is already very intense for power only a small amount above the threshold power level.

The spectral distribution of boiling noise as a function of frequency is shown in Figure 17.19. The erratic nature of the boiling noise is reflected in the scatter of the data, however, there is an indication that the spectrum shows the 1/f characteristic over the range of the measurements (30 cps - 16 kc).

The constants of the theoretical expression for boiling noise are obtained by comparing the noise to the signal obtained in a velocity field of known turbulence. The resistance variation δR/R (rms) due to velocity fluctuations, δU/U (rms), is

$$\left(\frac{\delta R}{R}\right)_U = \beta \overline{\Delta T} \left(\frac{\delta U}{U}\right) = \alpha \left(\frac{\delta U}{U}\right)$$

where

$$\overline{\Delta T} = \frac{P}{2cAU} .$$

The resistance variation due to boiling noise is

$$\left(\frac{\delta R}{R}\right)_B = K^{\frac{1}{2}} \left(\frac{P}{P_\lambda}\right)^{\frac{n}{2}} .$$

The experimental method of obtaining the constants K and P_λ is to place the probe in the water tunnel in turbulent flow and increase the electrode

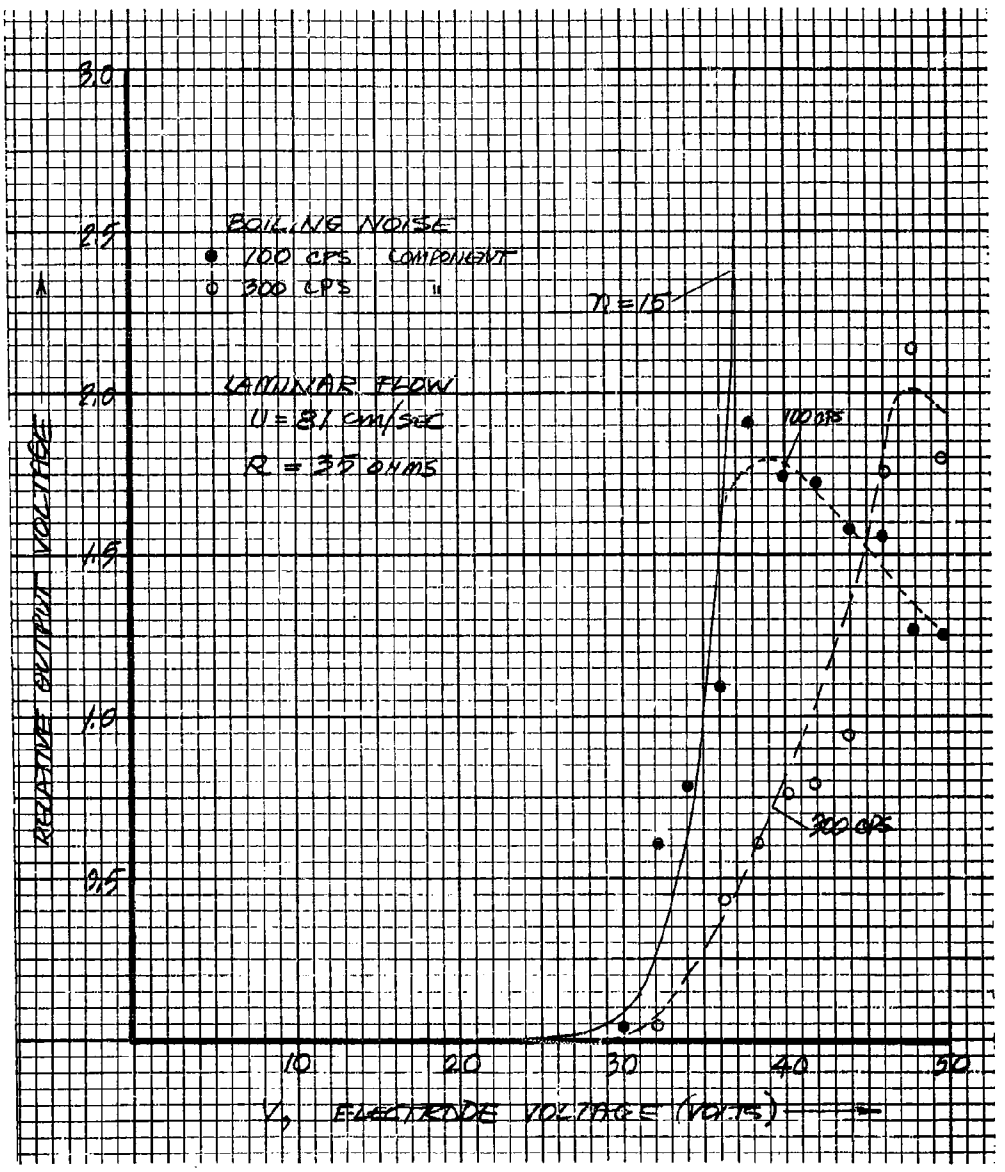

Figure 17.18. Boiling Noise as a Function of Electrode Voltage

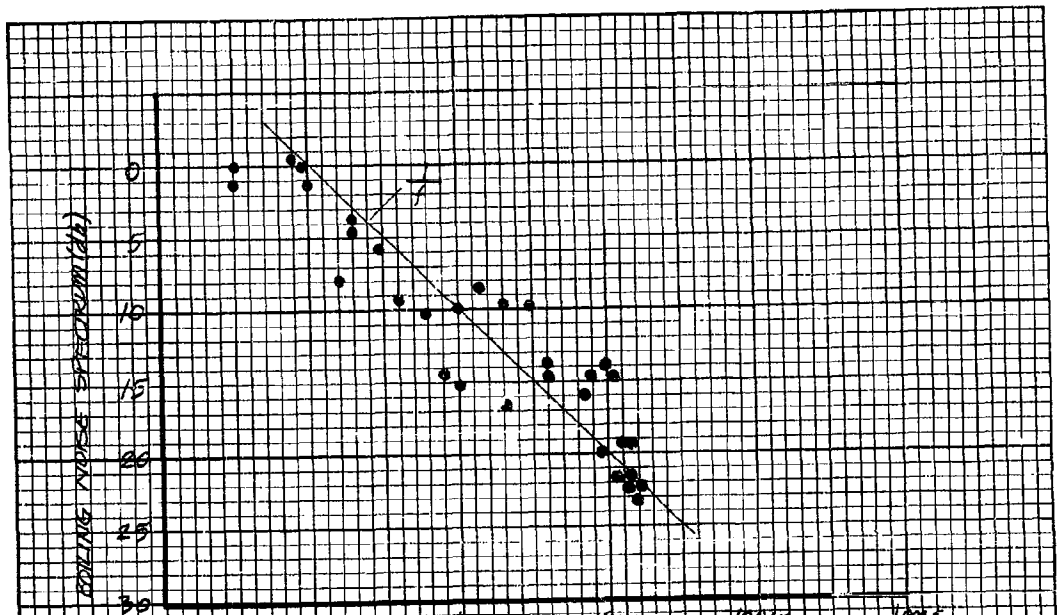

Figure 17.19. Spectral Distribution of Boiling Noise

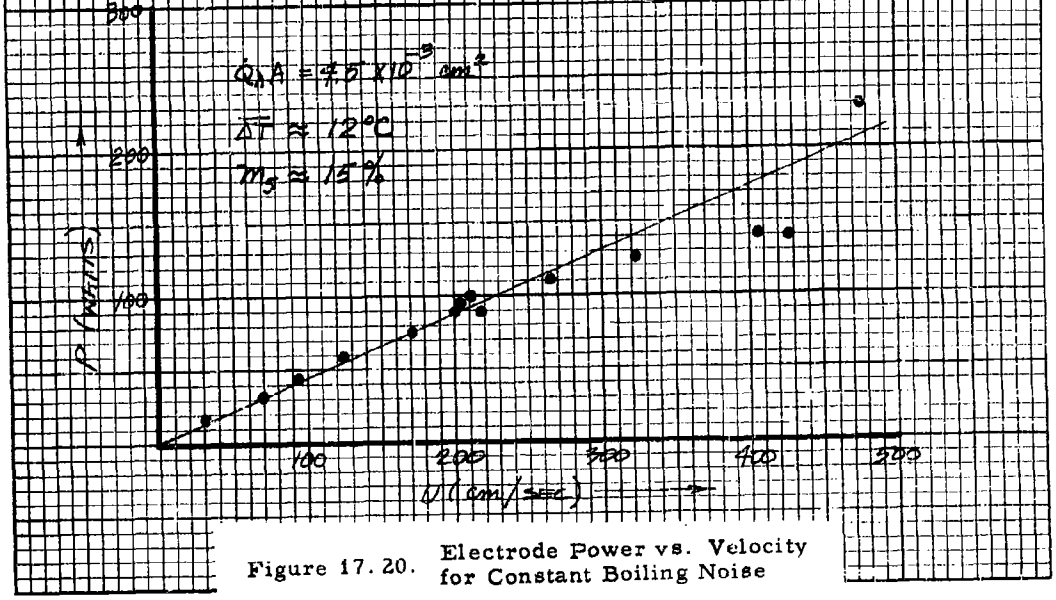

Figure 17.20. Electrode Power vs. Velocity for Constant Boiling Noise

power P until the boiling noise equals the velocity signal. In this case,

$$K^{\frac{1}{2}}\left(\frac{P}{P_\lambda}\right)^{\frac{n}{2}} = \beta\,\overline{\Delta T}\left(\frac{\delta U}{U}\right).$$

For convenience, let us define P_λ to be the electrode power level where this occurs (see Sec. 8.4)

$$P = P_\lambda = P_{VB}$$

then

$$K = \left(\beta\,\overline{\Delta T}_\lambda\right)^2\left(\frac{\delta U}{U}\right)^2 = \alpha_\lambda^2\left(\frac{\delta U}{U}\right)^2.$$

The following values are obtained experimentally,

$$\beta = .0213 \text{ per } {}^\circ C$$

$$\overline{\Delta T}_\lambda = 7\ {}^\circ C$$

$$\alpha_\lambda = 0.15$$

$$\frac{\delta U}{U} = .04$$

and

$$K = 3.6 \times 10^{-5} \quad .$$

It should be pointed out that the value of K is extremely sensitive to the choice of P_λ because of the large value of the exponent n.

The dependence of the electrode power, P, on velocity, U, to produce the same level of boiling noise is shown in Figure 17.20 . The noise was chosen and fixed at a value appreciably larger than the velocity signal produced in turbulent flow. The measurements were performed on the platinum parallel wire probe and the effective frontal area, $A\dot{Q}_\lambda$, was measured by the slope of the resistance vs. power curve (at zero power) and found to be

$$A\dot{Q}_\lambda \simeq 4.5 \times 10^{-3}\ cm^3 \quad .$$

The value agrees with that expected from the physical size of the electrode volume ($\dot{Q}_\lambda \simeq 1$). The average temperature rise at the fixed level of boiling noise in this experiment is $\overline{\Delta T} = 12\ {}^\circ C$. The uniformity of the electrode

in this case (for 20 °C ambient temperature) is

$$m_5 = \frac{\overline{\Delta T}}{\Delta T_{max}} = \frac{12\ ^{\circ}C}{100\ ^{\circ}C - 20\ ^{\circ}C} = 15\ \%\ \text{uniformity} \quad .$$

When boiling noise is large enough to mask the turbulent velocity measurements, no visual manifestation of the boiling process is observed. Although operation at higher power levels than this is of no interest in the detection equipment, it is of interest to observe the locations in the electrode volume where boiling first takes place. The extreme case of boiling effects which are visible was studied by photographic means as illustrated in Figure 17.21a to 17.21d . In the first Figure (a) the electrode power is zero; and in the others it is of the order of 100 watts. Only a small increase in electrode power is required to cause complete boiling once boiling inception has been reached. The flash photos were taken with a time constant of 3×10^{-4} sec.

17.3 Detection Equipment Experiments

The primary function of the detection equipment is to detect extremely small fluctuations in temperature, salinity and velocity of a flowing conducting fluid medium, such as sea water.

Measurements have been made with the detection equipment described in Section 16.1 to determine the conductivity and velocity structure in a tub of thoroughly stirred artificial sea water. The stirring of the water produces the turbulence which is measured and also is effective in removing large scale conductivity structure by mixing the existing temperature and salinity structure. The steady-state temperature and salinity structure which remains is produced by the slow temperature change of the total mass of water, evaporation at the surface of the water, and dissipation of the energy associated with the mechanical stirring of the water. The water is contained in a No. 1 galvanized tub (22 inch diameter, 9 inch depth) and the volume of water is 3.4×10^4 cm^3. Two eye-type electrodes of approximately 30 ohms resistance are used as sensors and are centrally located in the water and separated from each other by a distance of 5 cm. The electrodes are placed in the jet from the propeller for stirring the water where the average velocity is estimated to be about 10 cm/sec. The conductivity structure in the tub is believed to be due primarily to temperature structure rather than salinity structure. This is based on estimates of the expected temperature and salinity structure calculated from the observed rates of change of average water temperature, water depth variation due to evaporation, and power input by the stirring motor.

The magnitude of the temperature and velocity structure is determined by comparing their associated signals with the known internal noise signal of the detection equipment as the electrode power is varied. This method

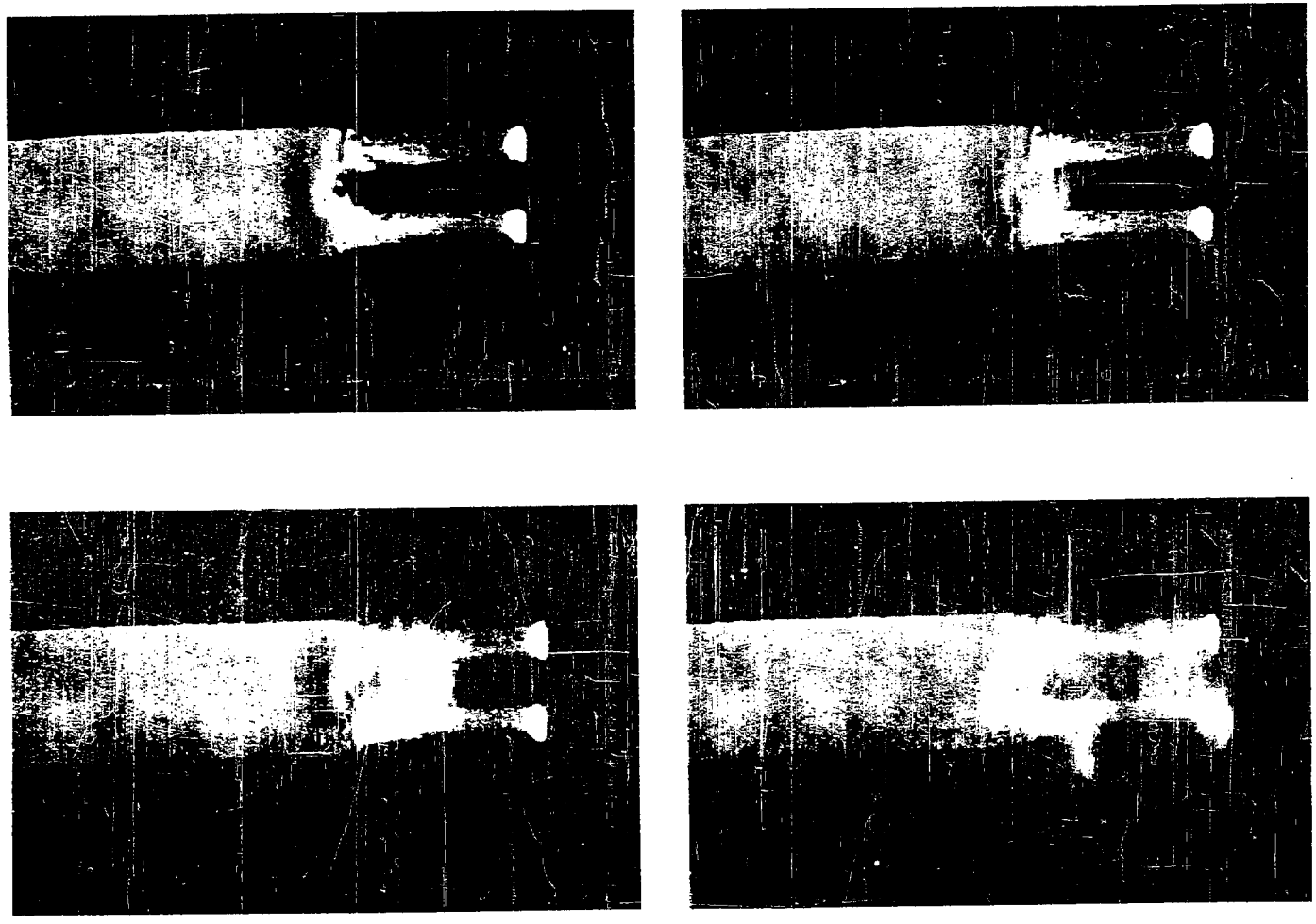

Figure 17.21. Boiling in the Electrode Volume at Electrode High Power

is described in Section 8.5 . The measurements were performed in a narrow band of frequency from 2 to 6 cps which was determined by an adjustable Kronhite Model 330-M filter. An appreciable amount of the measured fluctuations in the properties of the water fall in this band for the existing flow velocity over the electrodes. Let P_1 be the power dissipated in each electrode from the 40 kc source, and P_2 the electrode power from the 3.7 mc heater source. The magnitude of the temperature structure in the passband of interest is determined by observing the detector output as the power P_1 is increased from a small value with $P_2 = 0$. The observed data is shown in Figure 17.22 at very small values of P_1 the output is due exclusively to the internal noise of the detector (Johnson noise), and above a certain value, P_{TN}, the output signal power varies in proportion with the applied electrode power. If Λ denotes the ratio of the detector output power to the noise output power, we find that (Sec. 8.5)

$$\Lambda = 1 + \left(\frac{P_1}{P_{TN}}\right) .$$

This expression is valid provided the electrode power is not high enough to cause appreciable heating in the electrode volume. The value of P_{TN} corresponds to the point where Λ is twice (+3 db) the detector noise. As shown in Figure 17.22 , the value of P_{TN} is found to be 0.25 μw for the 2 - 6 cps passband of the detection equipment.

The measured value of P_{TN} is used to establish the magnitude of the effective temperature structure as follows. When $P_1 = P_{TN}$, the contribution of internal detector noise is equal to that due to temperature, i.e.,

$$(v_n)^2 = \Delta V^2 \text{ (temperature)}$$

or

$$M_3 F 4RkT\Delta f = V^2 M_1 M^2 \beta^2 \delta T^2 ,$$

where these quantities are defined in Section 8.3 . The electrode power, $P_1 = P_{TN}$, is related to the voltage, V, applied to the bridge by

$$P_{TN} = \frac{M_4 V^2}{M_2 R} .$$

Substituting this expression we find

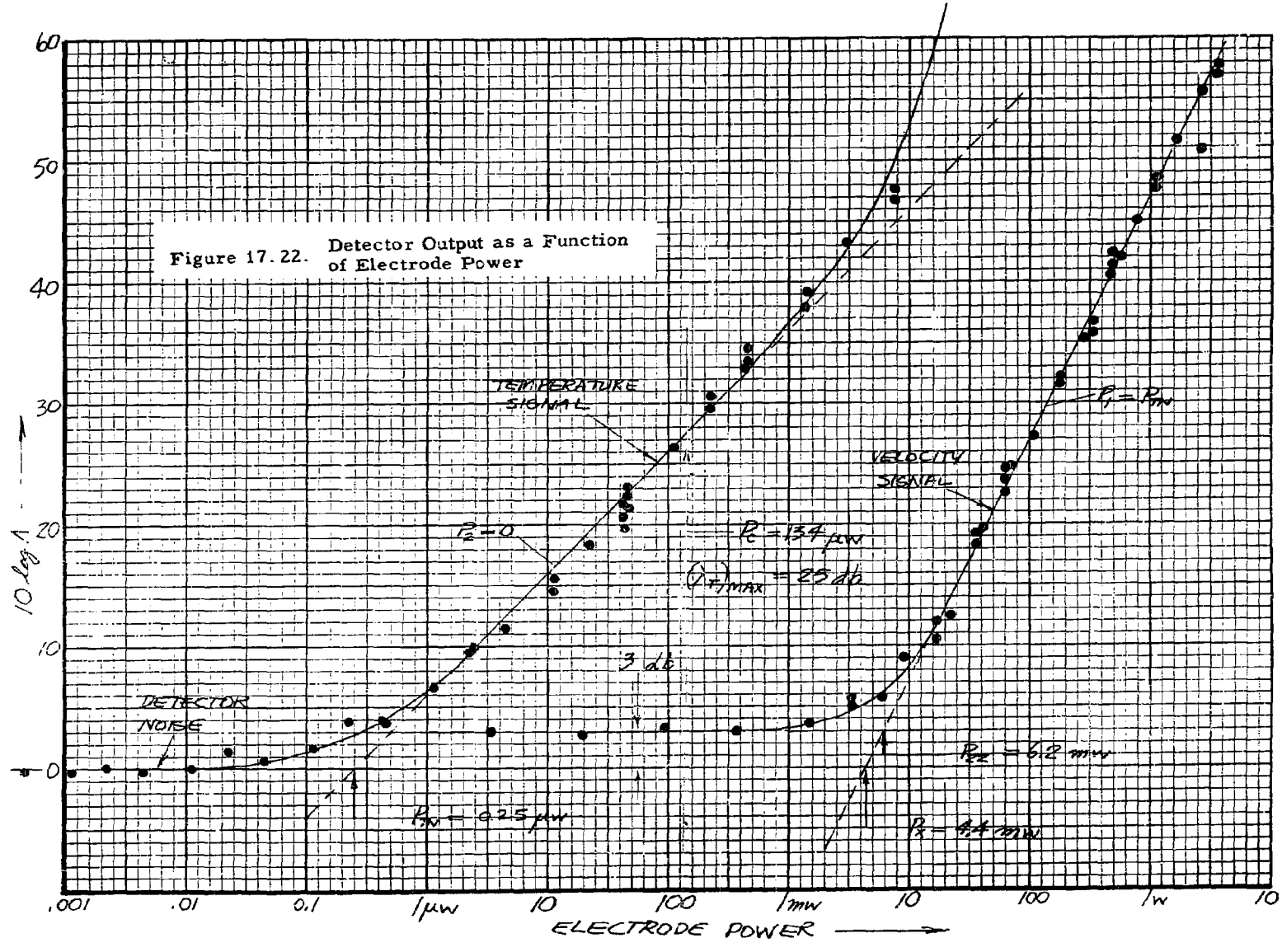

Figure 17.22. Detector Output as a Function of Electrode Power

$$\delta T = \frac{1}{\beta}\left(\frac{4M_3 M_4}{M_1 M_2 M^2}\right)^{1/2}\cdot\left(\frac{FkT\Delta f}{P_{TN}}\right)^{1/2},$$

where δT is the effective temperature structure (rms) of the water over the bandwidth Δf. For an optimum double element differential bridge, this reduces to

$$\delta T = \frac{2.83}{\beta}\left(\frac{FkT\Delta f}{P_{TN}}\right)^{1/2}$$

Substituting the measured values:

$$P_{TN} = 2.5 \times 10^{-7} \text{ watt}$$

$$\Delta f = 4 \text{ cps}$$

$$F = 1.08 \quad (+0.3 \text{ db})$$

and

$$\beta = .0213 \text{ per } {}^{\circ}C$$

$$kT = 4 \times 10^{-21} \text{ joules},$$

then we find

$$\delta T = 36\ \mu\ {}^{\circ}C \quad .$$

The velocity structure is determined by setting the 40 kc power at $P_1 = P_{TN}$ and varying the heater power P_2. The quantity Λ in this case is (Sec. 8.5)

$$\Lambda = 2 + \left(\frac{P_2}{P_x}\right)^2$$

provided $P_2 \gg P_{TN}$. The observed output is also shown in Figure 17.22 and may be used to determine P_x which depends on the magnitude of the velocity structure. The measured value of heater power, $P_2 = P_{22}$, where the output power is doubled ($\Lambda = 4$) occurs at

$$P_{22} = \sqrt{2} \cdot P_x \quad ,$$

which serves to determine P_x which is found to be $P_x = 4.4$ mw for the 2 - 6 cps band of the detection equipment.

The magnitude of the turbulent velocity fluctuations, δU, over this band is found as follows. When $P_2 = P_x$, the temperature and velocity signals are equal

$$\Delta v^2 \text{ (temperature)} = \Delta v^2 \text{ (velocity)}$$

or

$$\delta T = \overline{\Delta T}_x \left(\frac{\delta U}{U}\right)$$

where

$$\overline{\Delta T}_x = \frac{P_x}{2cAU} \qquad (\dot{Q}_\lambda = 1).$$

The value of A and U can be estimated from the experimental conditions, or measured directly as follows. The electrode resistance change, ΔR, is

$$\frac{\Delta R}{R_o} = -\beta \overline{\Delta T} \ ,$$

where R_o is the cold resistance and the average electrode temperature $\overline{\Delta T}$ at electrode power P is

$$\overline{\Delta T} = \frac{P}{2cAU} \ .$$

Differentiating these relations, we find that the rate of change of electrode resistance at zero power is

$$\frac{1}{R_o}\left(\frac{\partial R}{\partial P}\right)_o = \frac{-\beta}{2cAU} \ .$$

The quantities on the left are directly measurable. Substituting this relation in the expression for the rms value of δU, we find

$$\frac{\delta U}{U} = \frac{\delta T}{\overline{\Delta T}_x} = \frac{\beta \delta T}{\frac{P_x}{R_o}\left(\frac{\partial R}{\partial P}\right)_o} = \frac{2cAU\,\delta T}{P_x}$$

where

$$\overline{\Delta T}_x = \frac{P_x}{\beta R_o}\left(\frac{\partial R}{\partial P}\right)_o \ .$$

With the expression for δT involving measured quantities we find

$$\frac{\delta U}{U} = \frac{2.83}{\frac{P_x}{R_o}\left(\frac{\partial R}{\partial P}\right)_o}\left(\frac{FkT\Delta f}{P_{TN}}\right)^{1/2}$$

and for the measured values

$$R_o = 27 \text{ ohms}$$

$$\left(\frac{\partial R}{\partial P}\right)_o = 0.41 \text{ ohm/watt}$$

$$P_x = 4.4 \times 10^{-3} \text{ watts}$$

we find

$$\frac{\delta U}{U} = .012 = 1.2\ \% \quad .$$

This measured value of turbulence over the band of interest is lower than expected, presumably because only a relatively small band of the spectrum of velocity fluctuations has been considered.

The optimum power level, P_c, for detecting the temperature structure over the detector noise and velocity signals is shown in Section 8.4 to be

$$P_c = \left(\frac{P_{TN} P_x^2}{2}\right)^{1/3}$$

and the signal-to-noise ratio at this point is

$$(\lambda_T)_{MAX} = \frac{2}{3}\left(\frac{P_c}{P_{TN}}\right) = 0.53\left(\frac{P_x}{P_{TN}}\right)^{2/3} .$$

For the measured values we find

$$P_c = 134 \text{ } \mu\text{watt}$$

$$(\lambda_T)_{max} = 358 \qquad (25 \text{ db}) \quad .$$

At this point the minimum detectable temperature variation δT_{vo} is

$$\delta T_{vo} = \frac{\delta T}{\sqrt{(\lambda_T)_{MAX}}} = \frac{36\ \mu^\circ C}{19} = 1.9\ \mu^\circ C .$$

Referring to Figure 17.22 , it is observed that the curve with $P_2 = 0$ for measuring the temperature structure deviates from the straight line for electrode power in the region of $P_1 \approx P_x$. This is due to the fact that the electrode power in that region is large enough to cause appreciable heating so that the detector becomes responsive to turbulence. If this effect is included in the expression for Λ , we find

$$\Lambda = 1 + \left(\frac{P_1}{P_{TN}}\right) + \frac{P_1^3}{P_{TN} P_x^2} \quad ,$$

which is the solid curve in Figure 17.22 , and fits the observed temperature data ($P_2 = 0$).

A measurement of the lifetime of salinity structure over the band of interest was performed by dumping a small volume of tap water (about 100 cc) in the tub and observing the resultant detector output. Samples of the signals obtained are shown in Figure 17.23 ; the bottom trace is drawn to show the average build-up and decay of the salinity structure. The decay time constant which fits the data best is about 50 sec. The volume of tap water was injected as far as possible from the propeller and electrodes, so that no signal is observed until after a definite time delay. The injected salinity structure is rather thoroughly mixed by the time it becomes measurable by the sensors. The background signal present in these traces is due to the existing temperature structure in the water (36 μ ^{o}C) which is 25 db above the minimum detectable temperature with this detection equipment (1.9 μ ^{o}C).

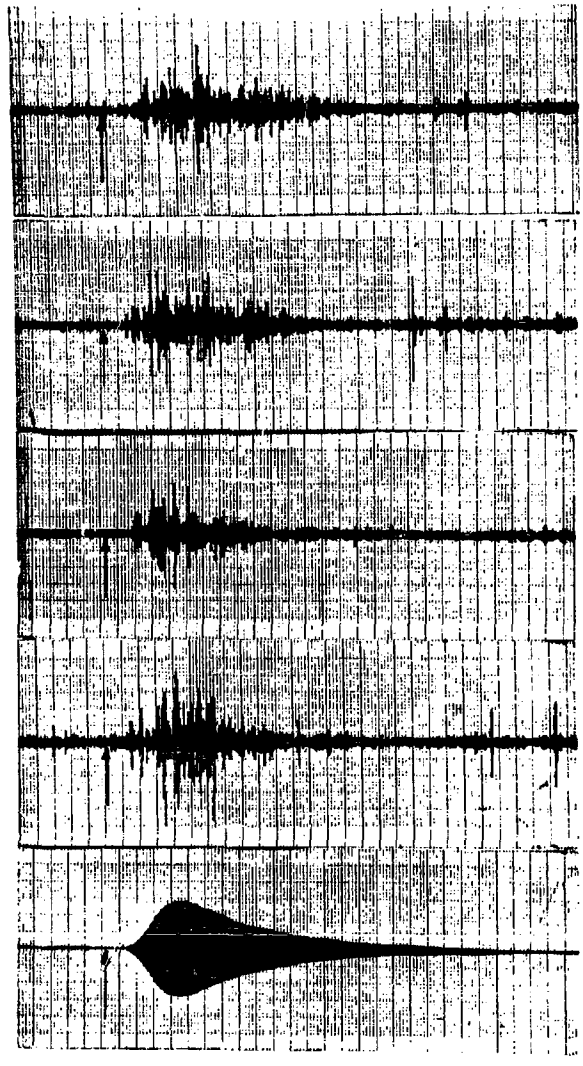

Figure 17.23 . Build-Up and Decay of Salinity Structure

ADDENDUM NO. 1

2nd Order Temperature Coefficient

Let β be the temperature coefficient of conductivity

$$\beta = \beta(T) = \frac{1}{\sigma}\left(\frac{\partial \sigma}{\partial T}\right)$$

where this coefficient is a function of temperature. If h^{-1} is the cell constant of an electrode, the electrode resistance, R, is

$$R = \frac{1}{\sigma h} \quad .$$

Differentiating this expression, we find

$$\frac{1}{R}\left(\frac{\partial R}{\partial T}\right) = -\frac{1}{\sigma}\left(\frac{\partial \sigma}{\partial T}\right) = -\beta$$

and

$$\frac{1}{R}\left(\frac{\partial^2 R}{\partial T^2}\right) = 2\beta^2 - \frac{1}{\sigma}\left(\frac{\partial^2 \sigma}{\partial T^2}\right)$$

$$= \beta^2 - \frac{\partial \beta}{\partial T}$$

where

$$\frac{\partial \beta}{\partial T} = -\beta^2 + \frac{1}{\sigma}\left(\frac{\partial^2 \sigma}{\partial T^2}\right).$$

The expansion of the electrode resistance about ambient temperature is

$$R = R_o\left[1 + aT + \gamma T^2\right] ,$$

where T is the temperature relative to ambient temperature (T = 0).

Differentiating, we find at ambient temperature

$$\frac{1}{R_0}\left(\frac{\partial R}{\partial T}\right) = a$$

and

$$\frac{1}{R_0}\left(\frac{\partial^2 R}{\partial T^2}\right) = 2\gamma .$$

Comparing these expressions with the previous ones, we find

$$a = -\beta$$
$$2\gamma = \beta^2 - \frac{\partial \beta}{\partial T} ,$$

where it is understood that the functions of β on the right are evaluated at T = 0. Define the dimensionless number, k, such that

$$k = \frac{\gamma}{a^2} = \frac{1}{2}\left[1 - \frac{1}{\beta^2}\left(\frac{\partial \beta}{\partial T}\right)\right]$$

and

$$\frac{R - R_0}{R_0} = aT\left[1 + kaT\right] = -\beta T\left[1 - k\beta T\right]$$

$$= aT + \gamma T^2 .$$

The above formulas are used to evaluate k and γ from the data for $\beta(T)$ of Figure 2.7. At 20 ^{o}C in 35 ‰ sea water, we have

$$\beta = +.0212 \text{ per } {}^{o}C$$
$$\frac{\partial \beta}{\partial T} = -3.21 \times 10^{-4} \, {}^{o}C^{-2}$$
$$\gamma = +3.86 \times 10^{-4} \, {}^{o}C^{-2}$$

and

$$k = +0.858 \quad .$$

REFERENCES

Section 2.

(1). Craig, D.N., Electrolytic Resistors for Direct-Current Applications in Measuring Temperatures, U.S. Bur. Stds., J. Res., 21, 225-33, (RP1126), (August 1938).

(2). Prausnitz, J.M. and R.H. Wilhelm, Turbulent Concentration Fluctuations Through Electrical Conductivity Measurements, Rev. Sci. Instru., 27, 1941-43, (November 1956).

(3). Wenner, F., Smith, E.H. and F.M. Soule, Apparatus for the Determination Aboard Ship of the Salinity of Sea Water by the Electrical Conductivity Method, U.S. Bur. Stds., J. Res., 5, 711-32, Research Paper No. 223, (1930).

(4). Schleicher, K.E. and A. Bradshaw, A Conductivity Bridge for Measurement of the Salinity of Sea Water, Conseil perm. int. Explor. Mer, J. du Conseil, 22, 9-20, (1956).

(5). Jacobson, A.W., An Instrument for Recording Continuously the Salinity, Temperature, and Depth of Sea Water, Trans. Am. Inst. Elec. Engrs., 67, 714-22, (1948).

(6). Paquette, R.G., Salinometers, Physical and Chemical Properties of Sea Water, Publication 600, National Academy of Sciences - National Research Council, (1959). pg. 128-31

(7). Paquette, R.G., A Modification of the Wenner-Smith-Soule Salinity Bridge for the Determination of Salinity in Sea Water, University of Washington, Dept. of Oceanography Tech. Rept. No. 61, Ref. No. 58-14, (1958).

(8). Hersey, J.R., Electronics in Oceanography, Advances in Electronics and Electron Physics, Vol. IX, Academic Press, (1957).

(9). Lange, N.A., Handbook of Chemistry, 9th ed., Handbook Publishers, Inc., (1956). pg. 1208-9

(10). Robinson, R.A. and R.H. Stokes, Electrolyte Solutions, 2nd ed., Butterworths Scientific Publications, (1959). pg. 87-98

(11). Thomas, B.D., Thompson, T.G. and C.L. Utterback, The Electrical Conductivity of Sea Water, Conseil Perm. Intern. p. l'Explor. de la Mer, Jour. du Conseil, 9, 28-35, (1934).

(12). Electrolytic Conductivity Measurements, Leeds and Northrup Company, Catalog EN-95, (1953).

Section 3.

(1). Reference Data for Radio Engineers, International Telephone and Telegraph Corp., 4th ed., (1957). pg. 766

(2). Von Hippel, A.R., Dielectrics and Waves, John Wiley and Sons, (1954). pg. 176-77

(3). Saxton, J.A. and J.A. Lane, Electrical Properties of Sea Water, Wireless Engineer, 29, 269-75, (October 1952).

(4). Sverdrup, H.U., Johnson, M.W. and R.H. Fleming, The Oceans, Prentice-Hall, (1942). pg. 142

(5). Siemens, C.W., On the Increase of Electrical Resistance in Conductors with Rise of Temperature Etc., Proc. Roy. Soc. London, 19, 351, (1871).

(6). Callendar, H.L., On the Practical Measurement of Temperature, Phil. Trans., (London), 178, 160, (1887).

(7). Ling, Sung-Ching, Measurements of Flow Characteristics by the Hot-Film Technique, Doctoral Dissertation Series Publication No. 12-905, State University of Iowa, (1955).

(8). Corrsin, S., Extended Applications of the Hot-Wire Anemometer, Rev. Sci. Instru., 18, 469-71, (July 1947).

(9). Hinze, J.O., Turbulence, McGraw-Hill Book Company, (1959). pg. 112-16

(10). Mueller, E.F., Precision Resistance Thermometry, in Temperature - Its Measurement and Control in Science and Industry, Reinhold Publishing Corporation, (1941). pg. 162-79

(11). Lion, K.S., Instrumentation in Scientific Research, McGraw-Hill Book Company, (1959). pg. 154

(12). Eggers, H.R., Brueckenschaltungen zur Temperaturmessung mit Widerstandsthermometern, Archiv. fuer, Tech. Messen, J 222-1, n 117 p T 39-40, (March 1941).

(13). Geyger, W., Arch. Tech. Messen, V 2166-2, (1931).

(14). Schneider, R., Messung kleiner Temperaturdifferenzen mit der Hitzdrahtbrucke, Arch. F. Tecn. Messen V 212-3, Lieferung 237, pg. 217-220, (October 1955).

Section 4.

(1). Eckart, C., An Analysis of the Stirring and Mixing Processes in Incompressible Fluids, J. Marine Research, 7, 266-75, (1948).

(2). Dickson, L.E., New First Course in the Theory of Equations, John Wiley and Sons, (1946).

Section 5.

(1). Thomas, C.C., The Measurement of Gases, J. Franklin Inst., 172, 411-60, (November 1911).

(2). Rein, H., Die Thermo-Stromuhr, Zeit. fur Biologie, 87, 394-418, (1928).

(3). Craig, D.N., Electrolytic Resistors for Direct-Current Applications in Measuring Temperatures, U.S. Bur. Stds., J. Research, 21, 225-33, (RP1126) (August 1938).

(4). Cleverdon, W.S.L., Can the Velocity of Water be Measured by Passing an Electric Current Through It?, Scientific American, Supplement No. 2144, (3 February 1917).

(5). Boyer, M.C., The Measurement of Velocity of Flowing Water by Electrical Methods, Master's Thesis, State University of Iowa, (July 1947).

(6). Boyer, M.C. and E.M. Lonsdale, The Measurement of Low Water Velocities by Electrolytic Means, Proc. 3rd Midwestern Conf. Fluid Mech., Univ. of Minnesota, 455-62, (1953).

(7). Ranz, W.E., Electrolytic Methods for Measuring Water Velocities, AIChE J., 4, 338-342, (September 1958).

(8). Agar, J.N., Diffusion and Convection at Electrodes, in Electrode Processes, Disc. Faraday Soc., Gurney and Jackson, (1947). pg. 26

(9). Levich, B., The Theory of Concentration Polarization, in Electrode Processes, Disc. Faraday Soc., Gurney and Jackson, (1947). pg. 37

(10). Kolthoff, I.M. and J.J. Lingane, Polarography, Interscience Publishers, (1952).

(11). Eskinazi, S., Turbulence Measurement in Electrically Conducting Fluids, Physics of Fluids, 1, 161-62, (1958).

(12). Delahay, P., New Instrumental Methods in Electrochemistry, Interscience Publishers, (1954).

(13). Hinze, J.O., Turbulence, McGraw-Hill Book Company, (1959). pg. 73-122

(14). Kovasznay, L.S.G., Turbulence Measurements, in High Speed Aerodynamics and Jet Propulsion, Vol. 9, Sec. F, 213-85, Princeton Univ. Press, (1954).

(15). Burgers, J.M., Hitzdrahtmessungen, in Handbuch der Experimentalphysik, Vol. 4, Pt. 1, pg. 637-67; Wien-Harms, (1931).

(16). Kovasznay, L.S.G., Turbulence Measurements, Applied Mechanics Reviews, 12, pg. 375-78, (June 1959).

(17). Romano, J.E. and A. Kivnick, Bibliography on Hot-Wire Anemometry, Univ. of Illinois Engineering Experiment Station, TO 11 (1952).

(18). Jacobs, U., Arch. tech. Messen, V 116-3, (January 1954) and V 116-4, (February 1954).

(19). Weber, L., Schriften Naturwiss, Ver. Schleswig-Holstein., 2, 313, (1894).

(20). Oberbeck, A., Ueber die Abkuhlende Wirkung von Luftstromen, Ann. d. Phys. u. Chem., 56, 397, (1895).

(21). King, L.V., On the Convection of Heat from Small Cylinders in a Stream of Fluid, Phil. Trans. Roy. Soc. Lond. (A) 214, 14, 373-432, (1914).

(22). Dryden, H.L. and A.M. Kuethe, The Measurement of Fluctuations of Air Speed in Turbulent Flow, NACA TR No. 329, (1928).

(23). Dryden, H.L. and A.M. Kuethe, The Measurement of Fluctuations of Air Speed by the Hot-Wire Anemometer, NACA TR 320, (1929).

(24). Ziegler, M., The Construction of a Hot-Wire Anemometer with Linear Scale and Negligible Lag, Proc. Koninkl. Ned. Akad. Wetenschap., 15, 3, (1934).

(25). Simmons, F.G., Shielded Hot-Wire Anemometer for Low Speeds, J. Sci. Instru., 26, 407-11, (1949).

(26). Kovasznay, L.S.G., The Hot-Wire Anemometer in Supersonic Flow, J. Aero. Sci., 17, No. 9, (1950).

(27). Richardson, E.G., Two Hot-Wire Viscosimeters, J. Sci. Inst., 6, 337-43, (November 1929).

(28). Ling, Sung-Ching, Measurements of Flow Characteristics by the Hot-Film Technique, Doctoral Dissertation Series Publication No. 12-905, State University of Iowa, (1955).

(29). McAdams, W.H., Heat Transmission, 3rd ed., McGraw-Hill Book Company, (1954). pg. 260 and 267

(30). Kramers, H., Heat Transfer from Spheres to Flowing Media, Physica, 12, 61-80, (June 1946).

(31). Davis, A.H., Convective Cooling of Wires in Streams of Viscous Liquids, Phil. Mag., Series 6, 47, 1057-92, (June 1924).

(32). Richardson (1929). See Reference (27).

(33). Burgers (1931). See Reference (15).

(34). Piret, E.L., James, W. and M.W. Stacy, Heat Transmission from Fine Wires to Water, Ind. Eng. Chem., 39, 1098-103, (1947).

(35). Richardson, E.G., Measurements of Water Flow and Pressure Set Up by Ships in Motion, Trans. North-East Coast Inst. Engrs. and Shipbuilders, Vol. 64, Pt. 6 (discussion), pg. 273-88, (April 1948); also Pt. 7 May/June (1948) p D141-4.

(36). Macovsky, M.S., The Measurement of Turbulence in Water, David Taylor Model Basin Report 670, (October 1948).

(37). Breslin, J.P. and M.S. Macovsky, Effects of Turbulence Stimulation on the Boundary Layer and Resistance of a Ship Model as Detected by Hot Wires, David Taylor Model Basin Report 724, (August 1950).

(38). Middlebrook, G.B. and E.L. Piret, Hot-Anemometry - Solution of Some Difficulties in Measurement of Low Water Velocities, Ind. Eng. Chem., 42, 1511, (1950).

(39). Marui, H. and S. Matsubara, Application of the Hot-Wire Measurement to Water Current, Bull. Fac. Engng., Yokohama Nat. Univ., 2, 15-21, (March 1953).

(40). Richardson, E.G., Appareils a fil Chaud, Institut de Mecanique des Fluides de l'Universite de Paris, (1954).

(41). Hubbard, P.G., Constant Temperature Hot-Wire Anemometry with Application to Measurements in Water, PhD Thesis, University of Iowa, (June 1954).

Section 5.

(42). Ling (1955). See Reference (28).

(43). Stevens, R.G., Borden, A. and P.E. Strausser, The Development of a Hot Wired Turbulence Sensing Element for Use in Water, David Taylor Model Basin Report No. 953, (December 1956).

(44). Ling, S.C. and P.G. Hubbard, The Hot-Film Anemometer: A New Device for Fluid Mechanics Research, J. Aero Sci., 23, 890-1, (September 1956).

(45). Patterson, A.M., Development of a Hot-Wire Instrument for Ocean Turbulence Measurements, Tech. Memo. 57-2, Pacific Naval Lab., Esquimalt, B.C., (December 1957).

(46). Borden, A., Time Constants and Frequency Response of Coated Hot-Wires Used as Turbulence-Sensing Elements, Hydrodynamics Lab., David Taylor Model Basin Report 952, (June 1957).

Section 6.

(1). Lion, K.S., Instrumentation in Scientific Research, McGraw-Hill Book Company, (1959). pg. 120-3

(2). Elrod, H.G., Jr., and R.R. Fouse, An Investigation of Electromagnetic Flowmeters, Trans. ASME, 74, 589, (1952).

(3). Grossman, L.M. and A.F. Charwatt, Measurement of Turbulent Velocity Fluctuations by Method of Electromagnetic Induction, Rev. Sci. Inst., 23, 741-7, (1952).

(4). Creeth, J.M., Electrokinetic Effects, from Electrical Phenomena at Interfaces, J.A. Butler, Ed., Methuen and Co., (1951). pg. 75-101

(5). Harnwell, G.P., Principles of Electricity and Electromagnetism, 2nd ed., McGraw-Hill Book Co., (1949). pg. 106

(6). Delahay, P., New Instrumental Methods in Electrochemistry, Interscience Publishers, Inc., (1954). Chapter 9

(7). Nernst, W., Z. Physik, Chem., 47, 52, (1904).

(8). Agar, J.N., Diffusion and Convection at Electrodes, in Electrode Processes, Disc. Faraday Soc., Gurney and Jackson, (1947). pg. 26

(9). Levich, B., The Theory of Concentration Polarization, in Electrode Processes, Disc. Faraday Soc., Gurney and Jackson, (1947). pg. 37

Section 6.

(10). Harnwell (1949). See Reference (5). pg. 307

(11). Robinson, R.A. and R.H. Stokes, Electrolyte Solutions, 2nd ed., Butterworths Scientific Publications, (1959). pg. 97-9

(12). Thomas, B.D., Thompson, T.G. and C.L. Utterback, The Electrical Conductivity of Sea Water, Conseil Perm. Intern. p. l'Explor. de la Mer, Jour. du Conseil, 9, 28-35, (1934).

(13). Sverdrup, H.U., Johnson, M.W. and R.H. Fleming, The Oceans, Prentice-Hall, (1942). pg. 68

(14). Adams, L.H. and R.E. Hall, The Effect of Pressure on the Electrical Conductivity of Solutions of Sodium Chloride and of Other Electrolytes, J. Physical Chem., 35, 2145-63, (1931).

(15). Fox, F.E., Herzfeld, K.F. and G.D. Rock, The Effect of Ultrasonic Waves on the Conductivity of Salt Solutions, Physical Review, 70, 329-40, (September 1 and 15, 1946).

(16). The Oceans (1942). See Reference (13). pg. 61

(17). The Oceans (1942). See Reference (13). pg. 69

Section 7.

(1). Guggenheim, E.A., Thermodynamics, North Holland Publishing Co., (1950).

(2). Eckart, C., Properties of Water, Part II. The Equations of State of Water and Sea Water at Low Temperatures and Pressures, Amer. Journ. of Sci., 256, 225-40, (April 1958).

(3). U.S. Navy Hydrographic Office, Tables for Sea Water Density, H.O. Pub. No. 615, U.S. Navy Hydrographic Office, (1952).

(4). Sverdrup, H.U., Johnson, M.W. and R.H. Fleming, The Oceans, Prentice-Hall, (1942). Chapter VI

(5). Handbook of Chemistry, 9th ed., Handbook Publishers, Inc., (1956). pg. 804

(6). Bridgeman, P.W., Dimensional Analysis, Rev. Ed., Yale University Press, (March 1931). pg. 36 ff

(7). Dorsey, N.E., Properties of Ordinary Water Substance, Amer. Chem. Soc., Monograph Ser. No. 81, The Reinhold Publishing Corporation, (1940).

(8). Handbook of Chemistry and Physics, Vol. 38, Chemical Rubber Pub. Co., (1956-57).

(9). American Institute of Physics Handbook, McGraw-Hill Book Co., (1957).

(10). Handbook of Chemistry (1956). See Reference (5).

(11). Thomas, B.D., Thompson, T.G. and C.L. Utterback, The Electrical Conductivity of Sea Water, Conseil Perm. Intern. p. l'Explor. de la Mer, Jour. du Conseil, 2, 28-35, (1934).

(12). Pollak, M.J., The Use of Electrical Conductivity Measurements for Chlorinity Determination, J. Marine Research, 13, 228-31, (1954).

(13). The Oceans (1942). See Reference (4). pg. 51

(14). Saxton, J.A. and J.A. Lane, Electrical Properties of Sea Water, Wireless Engineer, 29, 269-75, (October 1952).

(15). National Academy of Sciences-National Research Council, Physical and Chemical Properties of Sea Water, NAS-NRC Publication 600, (1959).

(16). Knudsen, M., Hydrographical Tables, G.E.C. Gad, Copenhagen, (1901).

(17). Cox, R.A. and N.D. Smith, The Specific Heat of Sea Water, Roy. Soc. Proc., 252, 51-62, (August 1959).

(18). The Oceans (1942). See Reference (4). pg. 69

(19). Standard Specifications for Substitive Ocean Water ASTM Designation: D 1141-52, of Manual on Industrial Water and Industrial Waste Water, 2nd ed., (1959). pg. 398

(20). The Oceans (1942). See Reference (4). pg. 185

(21). May and Black, Synthetic Ocean Water, Naval Research Laboratory Report P-2909, (August 1946).

(22). Robinson, R.A. and R.H. Stokes, Electrolyte Solutions, 2nd ed., Butterworths Scientific Publications, (1959). pg. 463, 466, 467

(23). Chambers, J.F., Stokes, J.M. and R.H. Stokes, Conductances of Concentrated Aqueous Sodium and Potassium Chloride Solutions at 25°, Jour. of Physical Chemistry, 60, 985-6, (July 1956).

(24). Chambers, J.F., The Conductance of Concentrated Aqueous Solutions of Potassium Iodide at 25° and of Potassium and Sodium Chlorides at 50°, Jour. of Physical Chemistry, 62, 1136-8, (September 1958).

(25). Shedlovsky, T., The Electrolytic Conductivity of Some Uni-Univalent Electrolytes in Water at 25°, Jour. Amer. Chem Society, 54, 1411-28, (April 1932).

(26). International Critical Tables, Volume VI, (1929). pg. 233

(27). International Critical Tables, Volume III, (1929). pg. 79

(28). Cooper, R., The Electrical Properties of Salt Water Solutions Over the Frequency Range 1-400 Mc/s, Journal of the Institution of Electrical Engineers, 93, Part III, 69-75, (March 1946).

(29). Hasted, J.B., The Dielectric Properties of Water, in Progress in Dielectrics, Vol. 3, Birks, J.B. and J. Hart, Editors, John Wiley and Sons, (1961). pg. 103-49

(30). Von Hippel, A.R., Dielectric Materials and Applications, Published jointly by The Technology Press of M.I.T. and John Wiley and Sons, (1954). pg. 361

(31). International Critical Tables, Volume V, (1929). pg. 67

(32). International Critical Tables, Volume V, (1929). pg. 15

(33). Hasted, J.B., Ritson, D.M. and C.H. Collie, Dielectric Properties of Aqueous Ionic Solutions, J. Chem. Phys., 16, 1, (1948).

(34). International Critical Tables, Volume V, (1929). pg. 229

(35). Robinson and Stokes (1959). See Reference (22). pg. 515

(36). American Public Health Association, Standard Methods for Examination of Water and Waste Water, 11th ed., American Public Health Association, (1960). pg. 34-5, 114-16

(37). Rossum, J.R., Conductance Method for Checking Accuracy of Water Analyses, Analytical Chemistry, 21, 631, (1949).

(38). Wilcox, L.V., Electrical Conductivity, J. American Water Works Association, 42, 775, (1950).

(39). Manual on Industrial Water and Industrial Waste Water, ASTM Special Technical Publication No. 148-D, 2nd ed., (1959), (Tentative Method of Test for Electrical Conductivity of Industrial Water, pg. 365, D 1125-59T).

(40). Robinson and Stokes (1959). See Reference (22). pg. 463-5

(41). Robinson and Stokes (1959). See Reference (22). pg. 457

(42). Handbook of Chemistry and Physics (1956-57). See Reference (8). pg. 1982

(43). Handbook of Chemistry and Physics (1956-57). See Reference (8). pg. 2079

(44). American Institute of Physics Handbook (1957). See Reference (9). pg. 4-70

(45). Saxton, J.A., Electrical Properties of Water, Wireless Engr., 26, 288, (1949).

(46). International Critical Tables, Volume III, (1929). pg. 233

(47). Jones, G. and B.C. Bradshaw, The Measurement of the Conductance of Electrolytes. V. A Redetermination of the Conductance of Standard Potassium Chloride Solutions in Absolute Units, J. Amer. Chem. Soc., 55, 1780, (1933).

(48). International Critical Tables, Volume VI, (1929). pg. 254

(49). The Oceans (1942). See Reference (4). pg. 106 ff, Charts III to IV

(50). The Oceans (1942). See Reference (4). pg. 741

(51). Kuiper, G.P., The Earth as a Planet - The Solar System II, University of Chicago Press, (1954). pg. 215

(52). Eckart, C., An Analysis of the Stirring and Mixing Processes in Incompressible Fluids, J. Marine Research, 7, 266-75, (1948).

(53). Wheelon, A.D., Spectrum of Turbulent Fluctuations Produced by Convective Mixing of Gradients, Physical Review, 105, 1706-10, (March 1957).

(54). Wheelon, A.D., J. Geophys. Res., 63, 854, (1958).

(55). Liebermann, L., The Effect of Temperature Inhomogeneities in the Ocean on the Propagation of Sound, J. Acoustical Soc. of Am., 23, 563-70, (September 1951).

Section 7.

(56). Urick, R.J., Pharo, L.C. and E. Skudrzyk, A New Method for Measuring the Thermal Microstructure of the Sea, Trans. Am. Geophys. Union, 39, 237-40, (April 1958).

(57). Batchelor, G.K., The Theory of Homogeneous Turbulence, Cambridge at the University Press, (1953). Chapter VI

(58). Hinze, J.O., Turbulence, McGraw-Hill Book Co., (1959). pg. 181-204

(59). Proudman, J., Dynamical Oceanography, John Wiley and Sons, (1953).

(60). Knauss, J.A., An Estimate of the Effect of Turbulence in the Ocean on the Propagation of Sound, Jour. Acoustical Society of America, 28, (May 1956).

(61). Pochapsky, T.E., An Estimate of Turbulent Velocities in the Ocean, Hudson Labs., Columbia U. Tech. Rept. No. 67, AD 214 881L, (March 1959).

Section 9.

(1). Morse, P.M. and H. Feshbach, Methods of Theoretical Physics, Part II, McGraw-Hill Book Co., (1953). pg. 1261

(2). Watson, G.N., Bessel Functions, Cambridge University Press, (1922). pg. 390

(3). Byrd, P.F. and M.D. Friedman, Handbook of Elliptic Integrals for Engineers and Physicists, Springer-Verlag/Berlin, (1954). pg. 164, Formula No. 282.01

(4). Smythe, W.R., Static and Dynamic Electricity, McGraw-Hill Book Co., (1950). pg. 203, Prob. No. 39

(5). Morse and Feshbach (1953). See Reference (1). pg. 1300

(6). Smythe (1950). See Reference (4). pg. 121-2

(7). Burfoot, J.C., Probe Impedance in the Electrolytic Tank, Brit. J. Appl. Phys., 6, 67-8, (February 1955).

(8). Hobson, E.W., The Theory of Spherical and Ellipsoidal Harmonics, Cambridge at the University Press, (1931). pg. 451, 433

(9). Bateman, H., Partial Differential Equation of Mathematical Physics, Cambridge University Press, (1959). pg. 461

(10). Morse and Feshbach (1953). See Reference (1). pg. 1261, 1301 (Part II)

(11). Smythe (1950). See Reference (4). pg. 90

(12). Smythe (1950). See Reference (4). pg. 109, Prob. No. 58

(13). Kober, H., Dictionary of Conformal Representations, Dover Publications, (1957).

(14). Smythe (1950). See Reference (4). pg. 114

(15). Harnwell, G.P., Principles of Electricity and Electromagnetism, 2nd ed., McGraw-Hill Book Co., (1949). pg. 42

(16). Morse and Feshbach (1953). See Reference (1). pg. 1210

(17). Eyring, C.F., Mackeown, S.S. and R.A. Millikan, Fields Currents from Points, Physical Review, 31, (May 1928).

(18). Butler, J.A.V. (Ed.), Electrical Phenomena at Interfaces, Methuen, (1951).

(19). Randles, J.E.B., Kinetics of Rapid Electrode Reactions, in Electrode Processes, Disc. Faraday Soc., Gurney and Jackson, (1947). pg. 11

(20). Glasstone, S., Laidler, K.L. and H. Eyring, The Theory of Rate Processes, McGraw-Hill Book Co., (1941).

(21). Grahame, D.C., Electrode Processes and the Electrical Double Layer, Annual Review of Physical Chemistry, 6, 337-58, (1955).

(22). Jones, G. and S.M. Christian, The Measurement of the Conductance of Electrolytes. VI. Galvanic Polarization by Alternating Current, J. Amer. Chem. Soc., 57, 272, (1935).

(23). Robinson, R.A. and R.H. Stokes, Electrolyte Solutions, 2nd ed., Butterworths Scientific Publications, (1959).

(24). Kortum, G. and J.O'M. Bockris, Textbook of Electrochemistry, Vols. I and II, Elsevier Publishing Company, (1951).

(25). Bockris, J.O'M., Modern Aspects of Electrochemistry, New York Academic Press, (1954).

(26). Falkenhagen, H., Electrolytes, Oxford Univ. Press, (1934).

(27). Harned, H.S. and B.B. Owen, The Physical Chemistry of Electrolytic Solutions, 3rd ed., Reinhold Pub. Corp., (1958).

(28). Faraday Society, Electrode Processes, Discussion No. 1, Gurney and Jackson, (1947).

(29). Delahay, P., New Instrumental Methods in Electrochemistry, Interscience Publishers, (1954).

(30). Gupta, S.R. and G.J. Hills, Precision Electrode-Less Conductance Cell for Use at Audiofrequencies, J. Sci. Instru., 33, 313-14, (1958).

(31). Calvert, R., Cornelius, J.A., Griffiths, V.S. and D.I. Stock, The Determination of the Electrical Conductivities of Some Concentrated Electrolyte Solutions by Using a Transformer Bridge, J. Phys. Chem., 62, 47-53, (1958).

(32). Blake, G.G., Conductimetric Analysis at Radio-Frequency, Chemical Publishing Co., (1952).

(33). Delahay (1954). See Reference (29). Part III by C.N. Reilley

(34). Regel, A.R., Electrodeless Method of Measuring Electrical Conductivity and Possibilities for Its Use in Physiochemical Analysis, Zhur. Neorg. Khim., 1, 1271-8, (1956).

(35). Esterson, G.L., The Induction Conductivity Indicator, The Johns Hopkins Univ., Chesapeake Bay Inst. Tech. Rept. XIV, Ref. No. 57-3, (1957).

(36). Harwell, K.E., Radio Frequency Salinity Instrument, Model E, Agric. and Mech. College of Texas, Dept. of Oceanography, Tech. Rept. IV, (1954).

(37). Harwell, K.E. and A.J. Druce, Wien Bridge and Twin-T Salinity Instruments, Agric. and Mech. College of Texas, Dept. of Oceanography, Tech. Rept. V, (1954).

(38). Pritchard, D.W., The In Situ Measurement of "Salinity" With the Induction-Conductivity Indicator, Physical and Chemical Properties of Sea Water, National Academy of Sciences - National Research Council, Pub. 600, (1959). pg. 146-54

(39). Huebner, G.L., Note on Radio Frequency Salinity Measuring Equipment at Texas A. and M. College, Physical and Chemical Properties of Sea Water, National Academy of Sciences - National Research Council, Pub. 600, (1959). pg. 155

(40). Schiemer, E.W. and D.W Pritchard, An Induction Conductivity Temperature Indicator, Tech. Report XXV, Chesapeake Bay Inst., Johns Hopkins Univ., (1961).

(41). Musha, S., Continuous Measurement of the Salinity of Sea Water by a High-Frequency Apparatus, J. Chem. Soc. Japan, Pure Chemistry Section, 77, 140-4, (1956). (In Japanese).

(42). Welsby, V.G., The Theory and Design of Inductance Coils, John Wiley and Sons, (1960).

(43). Lion, K.S., Instrumentation in Scientific Research, McGraw-Hill Book Co., (1959). pg. 120-3

(44). Borden, A., Time Constants and Frequency Response of Coated Hot Wires Used as Turbulence-Sensing Elements, David Taylor Model Basin Report 952, (June 1957).

(45). Evans, U.R., The Corrosion and Oxidation of Metals: Scientific Principles and Practical Applications, Edward Arnold Publishers, (1960).

(46). Wernick, S. and R. Pinner, The Surface Treatment and Finishing of Aluminum and Its Alloys, 2nd ed., Robert Draper Publisher, (1959).

(47). Von Hippel, A.R., Dielectric Materials and Applications, The Technology Press of M.I.T. and John Wiley and Sons, (1954). pg. 181

(48). Reference Data for Radio Engineers, International Telephone and Telegraph Corp., 4th ed., (1957). pg. 62-71

(49). Jones G. and S.M. Christian, The Measurement of the Conductance of Electrolytes. VI. Galvanic Polarization by Alternating Current, J. Amer. Chem. Soc., 57, 272, (1935).

(50). Einstein, P.A., Factors Limiting the Accuracy of the Electrolytic Plotting Tanks, Brit. J. Appl. Phys., 2, 49-55, (1951).

(51). Thiele, R. and J. Himpan, The Choice of Electrode Materials for Field Mapping in Electric Tanks, (in German), Die Telefunkenrohre, Vol. 18, 50-57, (1940).

Section 9.

(52). Shipley, J.W. and C.F Goodeve, The Law of Alternating Current Electrolysis and the Electrolytic Capacity of Metallic Electrodes, Amer Electrochem. Soc., 52, 375-402, (1927).

(53). Jones, G. and G.M. Bollinger, The Measurement of the Conductance of Electrolytes III. The Design of Cells, J. Am. Chem. Soc., 53, 411-451 (1931).

(54). Jones, G. and D.M. Bollinger, The Measurement of the Conductance of Electrolytes. VII. On Platinization, J. Amer. Chem. Soc., 57, 280-4, (1935).

(55). Ives, D.J.G. and J.H. Pryor, The Conductometric Evolution of the Ionization Functions of the Monohalogenoacetic Acids, J. Chem. Soc., pg. 2104-14, (1955).

(56). Feates, F.S. and D.J.G. Ives, Ionization Functions of Cyanoacetic Acid in Relation to the Structure of H_2O and the Hydration of Ions and Molecules, J. Chem. Soc., pg. 2798-812, (1956).

(57). Kuipers, P.G., New Developments in the Field of Electrolytic Conductivity Measurements, in Instruments and Measurements, Vol. 1, Academic Press Publishers, (1961). pg. 420-6

(58). Ellas, L. and H.I. Schiff, J. Phys. Chem., 60, 595, (1956).

(59). Brody, O.V. and R.M. Fuoss, Dipping Electrodes for Precision Conductimetry, J. Phys. Chem., 60, 177, (1956).

Section 10.

(1). Smythe, W.R., Static and Dynamic Electricity, McGraw-Hill Book Co., (1950). pg. 440, 231, 218

(2). Harnwell, G.P., Principles of Electricity and Electromagnetism, 2nd ed., McGraw-Hill Book Co., (1949). pg. 341, 585

(3). Harnwell (1949). See Reference (2). pg. 62

(4). Bateman, H., Partial Differential Equation of Mathematical Physics, Cambridge University Press, (1959). pg. 368, 141

(5). Webster, A.G., Partial Differential Equations of Mathematical Physics, 2nd corr. ed., Dover Publications, (1955). pg. 225

(6). Smythe (1950). See Reference (1). pg. 135

(7). Kellogg, O.D., Foundations of Potential Theory, Dover Publications, (1953). pg. 126

(8). Bateman (1959). See Reference (4). pg. 406

(9). Smythe (1950). See Reference (1). pg. 60

(10). Bateman (1959). See Reference (4). pg. 409

(11). Morse, P.M. and H. Feshbach, Methods of Theoretical Physics, Part II, McGraw-Hill Book Co., (1953). pg. 1206

(12). Morse, P.M. and H. Feshbach, Methods of Theoretical Physics, Part I, McGraw-Hill Book Co., (1953). pg. 766

(13). Watson, G.N., Bessel Functions, Cambridge University Press, (1922). pg. 401, Section 13.4. NOTE: $K(x) = \frac{\pi}{2} F\left(\frac{1}{2}, \frac{1}{2} : 1, x^2\right)$. Differentiate this formula with respect to either constant parameter.

(14). Watson (1922). See Reference (13). pg. 390

(15). Smythe (1950). See Reference (1). pg. 233

(16). Lord Rayleigh, B., The Theory of Sound, Volume II, Dover Publications, (1945). Appendix A, pg. 487-91

(17). Daniell, P.J., The Coefficient of End-Correction (I), Phil. Mag. 30, 137-46, (July 1915).

(18). Daniell, P.J., The Coefficient of End-Correction (II), Phil. Mag. 30, 248-56, (August 1915).

(19). Stratton, J.A., Electromagnetic Theory, McGraw-Hill Book Co., (1941). pg. 205

(20). Milne-Thomson, L.M., Theoretical Hydrodynamics, 4th ed., The MacMillan Co., (1960). pg. 496

(21). Robinson, R.A. and R.H. Stokes, Electrolyte Solutions, 2nd ed., Butterworths Scientific Publications, (1959). pg. 310-13

(22). Wang, J.H., Theory of Self-Diffusion of Water in Protein Solutions. A New Method for Studying the Hydration and Shape of Protein Molecules, J. Amer. Chem. Soc., 76, 4755, (1954).

Section 10.

(23). Fricke, H., The Maxwell-Wagner Dispersion in a Suspension of Ellipsoids, Jour. of Physical Chemistry, 57, 934-7, (December 1953).

(24). Fricke, H., Electric Conductivity of a Suspension of Homogeneous Spheroids, Physical Review, 24, 575-87, (November 1924).

(25). Smythe (1950). See Reference (1). pg. 208, No. 80 to 84

(26). Byrd, P.F. and M.D. Friedman, Handbook of Elliptic Integrals for Engineers and Physicists, Springer-Verlag, (1954).

(27). King, L.V., On the Electrical and Acoustical Conductivities of Cylindrical Tubes Bounded by Infinite Flanges, Philosophical Mag., 21, 140, (1936).

(28). Einstein, P.A., Factors Limiting the Accuracy of the Electrolytic Plotting Tanks, Brit. J. Appl. Phys., 2, 49-55, (1951). The F-factor of this Reference is the inverse of that in this Report.

(29). Jones, G. and S.M. Christian, The Measurement of the Conductance of Electrolytes. VI. Galvanic Polarization by Alternating Current, J. Amer. Chem. Soc., 57, 272, (1935).

(30). Agar, J.N. and T.P. Hoar, The Influence of Change of Size in Electro-Chemical Systems, in Electrode Processes, Disc. Faraday Soc., Gurney and Jackson, (1947). pg. 158

(31). Kupradze, G.D., Polarization Phenomena While Measuring the Resistance of Electrolytic Conductors in Conditions of Nonuniform Symmetrical Electrical Field, (Trudy Gruzin. Politekh. Inst.) 1954, No. 35, 163-8; Referat. Zhur. Khim. 1955, Abstr. No. 54716. (Also Chem. Abs., 5170 i, 52, 1958).

(32). Kagaaner, L.I., Computation of the Current Distribution on Electrodes by Means of Conform Images, (Inst. Soviet Trade, Kharkov), Zhur. Fiz. Khim. Vol. 30, pg. 1760-6, (1956). (Also Chem. Abs., 11127 F, 51, 1957).

Section 11.

(1). Milne-Thomson, L.M., Theoretical Hydrodynamics, 4th ed., MacMillan Company, (1960). pg. 456

(2). Dryden, H.L., Murnaghan, F.P. and H. Bateman, Hydrodynamics, Dover Publications, (1932). pg. 78-83

(3). Milne-Thomson (1960). See Reference (1). pg. 111

(4). Courant, R., Differential and Integral Calculus, Interscience Publishers, Vol. I, (1947). pg. 291

(5). Grobner, W. and N. Hofreiter, Integraltafel, Unbestimmte Integrale, Vol. I, 2nd ed., Springer-Verlag, (1957). pg. 66, No. 241-138

(6). Birkhoff, G. and E.H. Zarantonello, Jets, Wakes, and Cavities, Academic Press, (1957). pg. 7

(7). Von Karman, Th., Berechnung der Druckverteilung an Luftschiffkorpern, Abh. Aerodyn, Inst. Aachen, 6 : 1, (1927), Berlin, Julius Springer. Translated in Nat. Advisory Comm. Aeronautics, Tech. Memo No. 574, (1930) and Berechnung der Druckverteilung an Luftschiff-Korpern, Abh. aus dem Aerodynamischen Inst. der Tech. Hochschulen Aachen. Heft. 7, S 3-17.

(8). Schlichting, H., Boundary Layer Theory, 4th ed., McGraw-Hill Book Co., (1960). pg. 185-7

(9). Frossling, N., Evaporation, Heat Transfer, and Velocity Distribution in Two-Dimensional and Rotationally Symmetrical Laminar Boundary-Layer Flow, NACA TM 1432, (February 1958).

(10). Glauert, M.B. and M.J. Lighthill, The Axisymmetric Boundary Layer on a Long Thin Cylinder, Royal Soc. of London, 230, 188-203, (1955).

(11). Schlichting (1960). See Reference (8). pg. 450-1

(12). Lamb, H., Hydrodynamics, 6th ed., Dover Publications, (1932). pg. 7

(13). Schlichting (1960). See Reference (8). pg. 146-55

(14). Schlichting (1960). See Reference (8). pg. 416

(15). Prandtl, L. and O.G. Tietjens, Applied Hydro- and Aeromechanics, Vol. II, Dover Publications, (1934). pg. 165

(16). Karplus, W.J., Analog Simulation, McGraw-Hill Book Co., (1958). Chapter 6

Section 11.

(17). Pierce, J., Hess, J.L. and A.M.O. Smith, Velocity Distributions and Shapes for Free Streamline Bodies Having Wedge-Shaped Noses, Douglas Aircraft Company Report No. ES 29123, AD 206 842, (August 1958).

(18). Ling, Sung-Ching, Measurements of Flow Characteristics by the Hot-Film Technique, Doctoral Dissertation Series Publication No. 12-905, State University of Iowa, (1955).

(19). Schlichting (1960). See Reference (8). pg. 144

(20). Schlichting (1960). See Reference (8). pg. 412, 455

Section 12.

(1). Bird, R.B., Stewart, W.E. and E.N. Lightfoot, Transport Phenomena, John Wiley and Sons, (1960). pg. 315

(2). Schlichting, H., Boundary Layer Theory, 4th ed., McGraw-Hill Book Co., (1960). pg. 288-92

(3). Carslaw, H.S. and J.C. Jaeger, Conduction of Heat in Solids, 2nd ed., Oxford University Press, (1959).

(4). Morse, P M. and H. Feshbach, Methods of Theoretical Physics, Part II, McGraw-Hill Book Co., (1953). pg. 1264

(5). Ling, S., Measurements of Flow Characteristics by the Hot-Film Technique, Doctoral Diss. Series Publication No. 12-905, State University of Iowa, (1955).

(6). Ford, R., Differential Equations, 2nd ed., McGraw-Hill Book Co., (1955). pg. 77

(7). Schlichting (1960). See Reference (2). pg. 119

(8). McAdams, W.H., Heat Transmission, 3rd ed., McGraw-Hill Book Co., (1954). pg. 230

(9). Drew, T.B., Trans. Am. Inst. Chem. Engrs., 26, 26, (1931).

(10). Toor, H.L., Heat Transfer in Forced Convection with Internal Heat Generation, AIChE J. 4, 319-23, (September 1958).

(11). Topper, L., Chem. Eng. Sci., 5, 13, (1956).

(12). Chambre, P.L., The Laminar Boundary Layer with Distributed Heat Sources or Sinks, Appl. Sci. Res. Section A, 6, 393-401, (1956).

Section 13.

(1). Hinze, J.O., Turbulence, McGraw-Hill Book Co., (1959). pg. 219-38

(2). Batchelor, G.K., The Theory of Homogeneous Turbulence, Cambridge at the University Press, (1953). Chapter 6

(3). Prandtl, L. and O.G. Tietjens, Fundamentals of Hydro-and Aeromechanics, Dover Publications, (1957). pg. 69-77

(4). Davenport, W.B., Jr. and W.L. Root, Random Signals and Noise, McGraw-Hill Book Co., (1958).

(5). Uberoi, M.S. and L.S.G. Kovasznay, On Mapping and Measurement of Random Fields, Quart. Appl. Math., 10, 375, (January 1953)

(6). Tsien, H.S., Engineering Cybernetics, McGraw-Hill Book Co., (1954). pg. 20, 127

(7). Schlichting, H., Boundary Layer Theory, 4th ed., McGraw-Hill Book Co., (1960). pg. 81-3

(8). Kamke, E., Differentialgleichungen Losungsmethoden und Losungen, 3rd ed., Chelsea Publishing Co., (1948). pg. 475

(9). Darwin, C.G., Note on Hydrodynamics, Proc. Camb. Phil. Soc., 49, 342, (1953).

(10). Lighthill, M.J., Drift, Jour. Fluid Mech., 1, 31-53, (1956).

(11). Schlichting (1960). See Reference (7). pg. 116-21

Section 14.

(1). Dryden, H.L. and A.M. Kuethe, The Measurement of Fluctuations of Air Speed by the Hot-Wire Anemometer, NACA TR 320, (1929).

(2). Uberoi, M.S. and L.S.G. Kovasznay, On Mapping and Measurement of Random Fields, Quart. Appl. Math., 10, 375, (January 1953).

(3). Dryden, H.L., Schubauer, G.B., Mock, W.C., Jr., and H.K. Skramstad, Measurements of Intensity and Scale of Wind-Tunnel Turbulence and Their Relation to Critical Reynolds Number of Spheres, NACA No. 581, (1937).

(4). Ziegler, M., A Complete Arrangement for the Investigation, the Measurement and the Recording of Rapid Airspeed Fluctuations with Very Thin and Short Hot Wires, Proc. Koninkl. Ned. Akad. Wetenschap., 34, 663, (1931).

Section 14.

(5). Carslaw, H.S. and J.C. Jaeger, Conduction of Heat in Solids, 2nd ed., Oxford at the Clarendon Press, (1959).

(6). Lighthill, M.J., The Response of Laminar Skin Friction and Heat Transfer to Fluctuations in the Stream Velocity, Proc. Roy. Soc. A, 224, 1-23, (1954).

(7). Rott, N. and M.L. Rosenzweig, On the Response of the Laminar Boundary Layer to Small Fluctuations of the Free-Stream Velocity, J. Aeorspace Sciences, 27, 741-7, (October 1960).

(8). Glauert, M.B., The Laminar Boundary Layer on Oscillating Plates and Cylinders, J. Fluid Mech., 1, 97-110, (1956).

Section 15.

(1). Hague, B., Alternating Current Bridge Methods, 5th ed., Sir Isaac Pitman and Sons, (1957).

(2). Hague (1957). See Reference (1). pg. 75

(3). Hague (1957). See Reference (1). pg. 559-62

(4). Seletzky, A.C. and L.A. Zurcher, Sensitivity of the Four-Arm Bridge, Elec. Eng., 58, 723-8, (1939).

(5). Heaviside, O., On the Best Arrangement of Wheatstone's Bridge for Measuring a Given Resistance with a Given Galvanometer and Battery, Phil. Mag., 45, 114, (1873).

(6). Rayleigh, Lord, On the Sensitiveness of the Bridge Method in its Application to Periodic Electric Currents, Proc. Roy. Soc., 49, 203-17, (1891).

(7). Goodwin, R.D., Design of Simple Resistance Thermometer Bridges for Wide-Range Control at Low Temperatures, Rev. Sci. Instrum., 29, 497-500, (June 1958).

(8). Murray, W.M. and P.K. Stein, Lectures on Strain Gage Techniques, Presented at the Department of Engineering, University of California at Los Angeles, (August 1957).

(9). Freeman, J.J., Principles of Noise, John Wiley and Sons, (1958). pg. 217-23

(10). Van der Ziel, A., Noise, Prentice-Hall, (1954). pg. 29

(11). Hoadley, G.B., The Science of Balancing an Impedance Bridge, Journal Franklin Inst., 228, 733-54, (1939).

(12). Kupfmuller, K., Ueber die Konvergenz der Bruckenmessverfahren, E.U.M., 51, 204-8, (1933).

(13). Hague (1957). See Reference (1). pg. 297-303

(14). Poleck, H., Die Abgleichkonvergenz bei Wechselstrom-Messschaltungen, Arch. f. Tech. Mess., J90-3, pg. 1-4, (October 1951).

(15). Hague (1957). See Reference (1). pg. 585

(16). Friis, H.T., Noise Figures of Radio Receivers, Proc. IRE, 32, 419-22, (July 1944).

(17). Bennett, W.R., Electrical Noise, McGraw-Hill Book Co., (1960). pg. 165-8

(18). Harris, W.A. Fluctuations in Vacuum Tube Amplifiers and Input Systems, RCA Rev., 5, 505-24, (April 1941); 6, 115-24, (July 1941).

(19). Van der Ziel, A., Fluctuation Phenomena in Semi-Conductors, Academic Press Inc., (1959). Chapter 5

(20). Van der Ziel (1954). See Reference (10). pg. 258-61, 209-18

(21). Langford-Smith, F., Radiotron Designer's Handbook, 4th ed., (1953). pg. 694-99

(22). Edson, W.A., Vacuum-Tube Oscillators, John Wiley and Sons, (1953). pg. 374-80

(23). Laurence, J.C. and L.G. Landes, Auxiliary Equipment and Techniques for Adapting the Constant-Temperature Hot-Wire Anemometer to Specific Problems in Air-Flow Measurements, NACA TN 2843, (November 1952).

(24). Ossofsky, E., Constant Temperature Operation of the Hot-Wire Anemometer at High Frequency, Rev. Sci. Instru., 19, 881, (December 1948).

(25). Von Hippel, A.R., Dielectrics and Waves, John Wiley and Sons, (1954). pg. 3

(1). Schlichting, H., Boundary Layer Theory, th ed., McGraw-Hill Co., (1960). pg. 10-11

(2). Schlichting (1960). See Reference (1). pg. 505-6

(3). Schlichting (1960). See Reference (1). pg. 502

(4). Schlichting (1960). See Reference (1). pg. 511

(5). Laufer, J., The Structure of Turbulence in Fully Developed Flow, NACA Report 1174, (1954).

(6). Hinze, J.O., Turbulence, McGraw-Hill Book Co., (1959). pg. 520-33

Best Available Copy